WIRING PRINCIPLES OF CEREBRAL CORTEX

EDITED BY: Julian Budd and Zoltán F. Kisvárday
PUBLISHED IN: Frontiers in Neuroanatomy

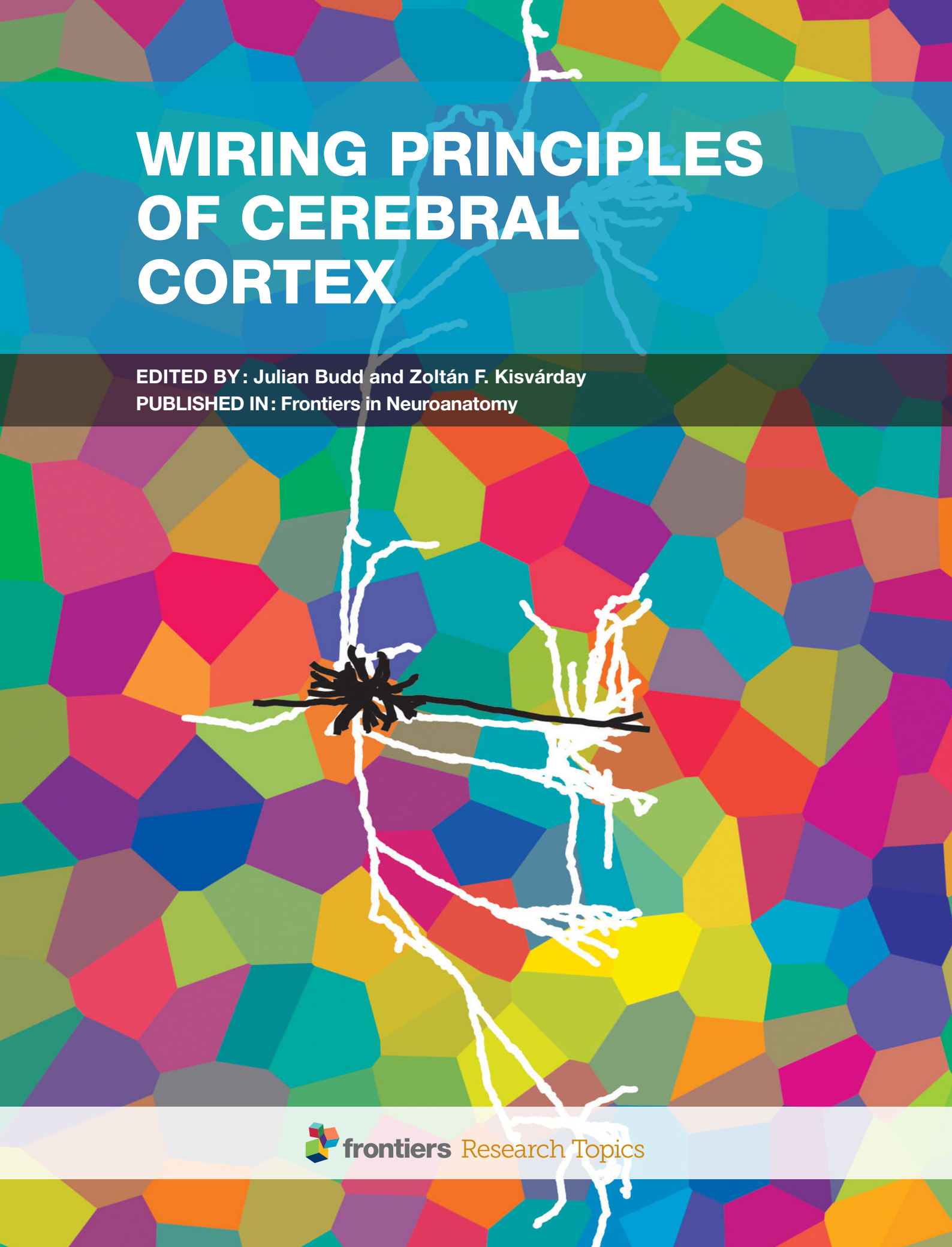

frontiers Research Topics

frontiers

ISSN 1664-8714
ISBN 978-2-88919-692-0
DOI 10.3389/978-2-88919-692-0

About Frontiers

Frontiers is more than just an open-access publisher of scholarly articles: it is a pioneering approach to the world of academia, radically improving the way scholarly research is managed. The grand vision of Frontiers is a world where all people have an equal opportunity to seek, share and generate knowledge. Frontiers provides immediate and permanent online open access to all its publications, but this alone is not enough to realize our grand goals.

Frontiers Journal Series

The Frontiers Journal Series is a multi-tier and interdisciplinary set of open-access, online journals, promising a paradigm shift from the current review, selection and dissemination processes in academic publishing. All Frontiers journals are driven by researchers for researchers; therefore, they constitute a service to the scholarly community. At the same time, the Frontiers Journal Series operates on a revolutionary invention, the tiered publishing system, initially addressing specific communities of scholars, and gradually climbing up to broader public understanding, thus serving the interests of the lay society, too.

Dedication to Quality

Each Frontiers article is a landmark of the highest quality, thanks to genuinely collaborative interactions between authors and review editors, who include some of the world's best academicians. Research must be certified by peers before entering a stream of knowledge that may eventually reach the public - and shape society; therefore, Frontiers only applies the most rigorous and unbiased reviews.
Frontiers revolutionizes research publishing by freely delivering the most outstanding research, evaluated with no bias from both the academic and social point of view.
By applying the most advanced information technologies, Frontiers is catapulting scholarly publishing into a new generation.

What are Frontiers Research Topics?

Frontiers Research Topics are very popular trademarks of the Frontiers Journals Series: they are collections of at least ten articles, all centered on a particular subject. With their unique mix of varied contributions from Original Research to Review Articles, Frontiers Research Topics unify the most influential researchers, the latest key findings and historical advances in a hot research area! Find out more on how to host your own Frontiers Research Topic or contribute to one as an author by contacting the Frontiers Editorial Office: **researchtopics@frontiersin.org**

WIRING PRINCIPLES OF CEREBRAL CORTEX

Topic Editors:
Julian Budd, University of Sussex, UK
Zoltán F. Kisvárday, University of Debrecen, Hungary

To represent the fundamental challenge of understanding the wiring principles of even a single cortical neuron in the relation to cortical function, the cover picture shows a sagittal view of a layer III pyramidal cell's axonal (white lines) and dendritic arbors (black lines) against the background of an idealised stimulus direction of motion map (colour-coded for each direction) obtained in vivo from primary visual cortex.
Image by Zoltán F. Kisvárday

Cerebral cortex is probably the most complex biological network. Here many millions of individual neurons, the functional units of cortex, are interconnected through a massive yet highly organized pattern of axonal and dendritic wiring. This wiring enables both near and distant cells to coordinate their responses and generate a rich variety of cognitions and behaviours. When the wiring is damaged through disease or trauma it may reorganize but this may lead to characteristic pathological behaviours. While there have been significant advances in mapping cortical connectivity, the organizing principles and function of this connectivity are not well understood. On the one hand, there appears to be general design constraints governing cortical wiring, as first recognised by Rámon y Cajal's in his laws of conduction, material, and volume conservation. Yet on the other hand, particular patterns of cortical wiring exist to serve specific functions. There is a wide gap in understanding how the response and connectivity properties of a single neuron contribute to emergent network functions such as in detecting perceptually relevant features. Unravelling this intimate causal relationship represents one of the major challenges in neuroscience.

This Research Topic will examine progress in understanding cortical wiring principles. This Research Topic aims to draw together recent advances in methods and understanding as well as recent challenges to existing ideas about how cerebral cortex is wired. This is particularly timely because new automated techniques may soon yield huge datasets in need of explanation. Recent studies have, for instance, empirically evaluated Rámon y Cajal's conservation laws for cerebral cortex, while others have shown some unexpected connectivity features that may refine the traditional view of how corticocortical connections are organised with regard to functional representations of auditory, somatosensory and visual cortices. Understanding these data will help improve the fidelity of neural models of cerebral cortical function and take into account the diversity of connections at both micro- and mesoscopic scales not seen at such a depth before.

Citation: Budd, J., Kisvárday, Z. F., eds. (2015). Wiring Principles of Cerebral Cortex. Lausanne: Frontiers Media. doi: 10.3389/978-2-88919-692-0

Table of Contents

05 ***How do you wire a brain?***
Julian Budd and Zoltán Kisvárday

08 ***Asymmetrical interhemispheric connections develop in cat visual cortex after early unilateral convergent strabismus: anatomy, physiology, and mechanisms***
Emmanuel Bui Quoc, Jérôme Ribot, Nicole Quenech'Du, Suzette Doutremer, Nicolas Lebas, Alexej Grantyn, Yonane Aushana and Chantal Milleret

37 ***Communication and wiring in the cortical connectome***
Julian M. L. Budd and Zoltán F. Kisvárday

60 ***The dendritic density field of a cortical pyramidal cell***
Hermann Cuntz

66 ***Excitatory neuronal connectivity in the barrel cortex***
Dirk Feldmeyer

88 ***Small-scale module of the rat granular retrosplenial cortex: an example of the minicolumn-like structure of the cerebral cortex***
Noritaka Ichinohe

95 ***Signaling mechanisms in cortical axon growth, guidance, and branching***
Katherine Kalil, Li Li and B. Ian Hutchins

110 ***Wiring of divergent networks in the central auditory system***
Charles C. Lee, Amar U. Kishan, and Jeffery A. Winer

125 ***How the cortex gets its folds: an inside-out, connectivity-driven model for the scaling of mammalian cortical folding***
Bruno Mota and Suzana Herculano-Houzel

139 ***Computing the size and number of neuronal clusters in local circuits***
Rodrigo Perin, Martin Telefont and Henry Markram

149 ***Cognitive consilience: primate non-primary neuroanatomical circuits underlying cognition***
Soren Van Hout Solari and Rich Stoner

frontiers in
NEUROANATOMY

EDITORIAL
published: 28 May 2013
doi: 10.3389/fnana.2013.00014

How do you wire a brain?

Julian Budd[1]* and Zoltán Kisvárday[2]

[1] *Department of Informatics, University of Sussex, Brighton, UK*
[2] *Department of Anatomy, Histology and Embryology, University of Debrecen, Debrecen, Hungary*
**Correspondence: j.m.l.budd@sussex.ac.uk*

Edited by:
Javier DeFelipe, Cajal Institute, Spain

Reviewed by:
Javier DeFelipe, Cajal Institute, Spain

Cerebral cortex is generally thought to provide the neural basis for higher cognitive and perceptual functions (see Gazzaniga et al., 2008). In cerebral cortex, billions of individual neurons, the functional units of cortex, are interconnected via a massive yet highly organized network of axonal and dendritic wiring. This wiring enables both near and distant neurons to coordinate their responses to external stimulation. Specific patterns of cortical activity generated within this network have been found to correlate with cognitive and perceptual functions (see Wang, 2010). If cortical wiring is damaged, through disease or trauma, characteristic behavioral disorders result (e.g., Seeley et al., 2009). Understanding the organizing principles of cortical wiring, therefore, represents a central goal toward explaining human cognition and perception in health and disease. Despite more than a century of endeavor, however, the organizing principles and function of cortical connectivity are not well understood.

This Research Topic presents recent progress and challenges to existing ideas about the principles concerning how cerebral cortex is wired. The publication of this collection of articles comes at a time of great excitement in the field of cortical neuroscience resulting from recent technical advances such as the more rapid tracing of cortical wiring and the ability to more precisely manipulate cortical activity experimentally. The large amount of data these new methods will yield must be tempered by the knowledge that mapping all synaptic connections or *connectome* of an individual brain represents a distant goal (see DeFelipe, 2010). In any case, the main aim of obtaining any map of cortical connectivity is to extract its underlying principles of organization—the subject of this Research Topic.

Although there are many interwoven themes in this collection of articles, we draw attention to five questions which we think will have a major bearing on the direction of future research and discuss how articles here bear on these questions.

WHAT IS THE RELATIONSHIP BETWEEN CORTICAL CONNECTIVITY AND MORPHOLOGY?

Without being able to prove the existence of a synaptic connnection Cajal (1899), and later Lorente de Nó (1949) were able to infer much about brain design and its underlying purpose solely from morphological data. While a number of articles in this Research Topic examine the relationship between morphology and connectivity, we use two articles here to show how this approach continues to prove useful. At the macroscopic level Mota and Herculano-Houzel (2012), propose that cortical folding is driven by white matter connectivity. Specifically, they argue that the mechanical tension generated by the pattern of connectivity of fiber bundles traveling through white matter may account for the observed pattern of cortical surface convolutions. The authors propose the degree of tension, taken as directly proportional to the morphological characteristics of the fiber bundle (i.e., axonal length and average cross-sectional area, and the proportion of efferent neurons), determines how much the cortical surface folds inwards. This model is used to explain how surface convolutions vary with brain size and how gray matter thickness varies. At the single neuron level (Cuntz, 2012), proposes that the "dendritic density field" morphological measure could be used to infer input connectivity. The author suggests dendritic arbor morphology reflects the spatial arrangement of its potential axon inputs relative to the location of its parent cell body. The shape of pyramidal and dentate gyrus granule cell dendritic arbors are explained using this approach. The author also draws attention to the benefits of morphological models for gaining insight into neuronal computation.

WHAT ASPECTS OF CORTICAL CONNECTIVITY ARE UNIVERSAL?

The ability to discover common principles of cortical wiring relies on acquiring a sufficiently diverse set of observations. Comparative data may, for instance, help identify and even rank the precedence of cortical wiring principles. In the context of the auditory system (Lee et al., 2011), examine the use of branched axons (collateralization) as a general wiring principle. The authors record that branched axons are commonly used for divergent processing across species and find this occurs at different levels of cortical organization. For example, they note comparative evidence for horizontal branched axons linking matched functional domains in auditory, somatosensory, and visual cortical areas. But they also report evidence for modality-specific differences in the functional use of branched axons, i.e., between axons of acoustic, somatosensory, and visual systems. To evaluate the existence of a possible multiscale wiring principle in cerebral cortex (Budd and Kisvárday, 2012), examine evidence at single neuron, local circuit, and axon pathway scales of organization. The principle proposes

that to optimize neural communication cortical wiring represents a trade-off between conserving cellular material (wire length) and minimizing conduction delay. The authors find that while there are too little data available to evaluate this hypothetical principle at the local circuit scale, strong evidence for this trade-off exists at the single neuron scale for both dendritic and axonal arbors with weaker support at the axon pathway scale.

HOW ARE THE PRINCIPLES OF CORTICAL WIRING OBSERVED IN THE ADULT BRAIN IMPLEMENTED BY DEVELOPMENTAL MECHANISMS?

Kalil et al. (2011) review how *in vitro* dissociated neuron cultures have been used to isolate the fundamental molecular mechanisms of axon growth and branching. The authors describe recent work demonstrating how molecular guidance cues such as netrin-1 and morphogen Wnt5a alter the morphology of a developing cortical axon via the calcium-mediated reorganization of its cytoskeleton. Relative differences in the frequency of calcium transients between an axon and a branch suggest a competitive push-pull outgrowth mechanism which may underlie selective branch growth and retraction observed during *in vivo* arbor development. The mechanisms of axon branching and outgrowth are relevant to the article of (Bui Quoc et al., 2012), who report on the effects of unilateral convergent strabismus on the development of terminal arbor morphology of cortico-cortical axons linking the primary visual areas of each cerebral hemisphere. This form of abnormal sensory experience leads to the asymmetrical development of callosal terminal arbors with the creation of fewer terminal branches of a specific order in the one hemisphere compared to the other, and hence a decreased overlap between the callosal representations. The authors suggest this asymmetry prevents a unified mapping between visual hemifields required for normal visual development and binocular function. This work underscores the link between changes in the normal organization of cortical wiring and deficits in perceptual function.

DOES A UNIVERSAL CORTICAL COLUMN EXIST AND, IF SO, WHAT FORM DOES IT TAKE?

The answer to this question has considerable importance for determining the dimension of a mesoscopic scale map of the Human Connectome (Bohland et al., 2009). Barrel fields in rodent primary somatosensory cortex have emerged as the *de facto* prototype for a cortical column. These cylindrically-shaped domains, readily identified by variation in cell density, supply a set of morphological coordinates with which to examine the concept of columnar processing. Feldmeyer (2012) provides a thorough review of extrinsic thalamocortical and intrinsic excitatory pathways in rodent barrel cortex. The article describes how separate parallel streams of thalamic signals are processed by the strongly vertical and recurrent excitatory connectivity within a barrel column but also describes connections beyond the column: namely, lateral interactions with neighboring barrel domains and the efferent connections with primary motor and secondary somatosensory areas and feedback to subcortical structures. While acknowledging that the existence of barrel subdomains suggests an individual barrel may not be elementary, the author cautions us not to view connectivity as static because neurons and synaptic connections are dynamically regulated by behavioral state and synaptic plasticity. A similar point is made in (Budd and Kisvárday, 2012). Comparative morphological differences between cortical areas and species also cast doubt on the notion of a universal cortical module or minicolumn (DeFelipe et al., 2002). Ichinohe (2012) describes, for example, how, immunofluorescence labeling has been used to identify the cellular composition of a honeycomb-like minicolumnar structure found in layers 1 and 2 of the rat granular retrosplenial cortex. Tracing has shown how dendritic clusters of specific cell types are grouped or segregated in relation to overlapping cortical, subicular, and thalamic axon terminal patches. The author suggests this type of structure might facilitate rapid and efficient rewiring for learning and memory tasks. What might explain this morphological diversity? Perin et al. (2013) examine theoretically the role of arbor morphology and neuronal density on the emergence of spatially overlapping clusters of recurrently connected cortical neurons. These clusters are generated by repeatedly applying the common neighbor wiring rule until the network structure stabilizes. In this rule the probability of connection between a pair of neurons is proportional to the number of connections they have in common (Perin et al., 2011). The authors report arbor extent limits the size and number of neuronal clusters, which they propose could form innate, elemental cortical groupings. Together, these articles suggest that a more flexible notion of a cortical column rather than a single, fixed dimension might provide a more accurate definition for the mesoscopic scale.

WHAT IS BEST WAY TO ORGANIZE, INTEGRATE, AND VISUALIZE THE INCREASING AMOUNT OF DATA CONCERNING CORTICAL WIRING?

A solution to this Neuroinformatics challenge is important for progressing the discovery of cortical wiring principles. In an ambitious study (Solari and Stoner, 2011), collated, integrated, and visualized the accumulated connectivity data obtained from many published studies of primate cerebral cortex. The results can be interactively accessed on-line (http://www.frontiersin.org/files/cognitiveconsilience/index.html) and via an iPad or iPhone "app." From the results, the authors were able to propose how particular groups of neural pathways centered around cerebral cortex might subserve specific cognitive functions. This article illustrates the importance of a comprehensive neuroanatomical assessment of a complete brain.

Overall, we think this Research Topic demonstrates the complexity and diversity of cortical organization and the wide variety of approaches that can and have been made to understand how we think and perceive. We hope the reader will find something here to stimulate their curiosity concerning a topic of considerable importance to the individual and society.

REFERENCES

Bohland, J. W., Wu, C., Barbas, H., Bokil, H., Bota, M., Breiter, H. C., et al. (2009). A proposal for a coordinated effort for the determination of brainwide neuroanatomical connectivity in model organisms at a mesoscopic scale. *PLoS Comput. Biol.* 5:e1000334. doi: 10.1371/journal.pcbi.1000334

Budd, J. M. L., and Kisvárday, Z. F. (2012). Communication and wiring in the cortical connectome. *Front. Neuroanat.* 6:42. doi: 10.3389/fnana.2012.00042

Bui Quoc, E., Ribot, J., Quenech'Du, N., Doutremer, S., Lebas, N., Grantyn, A., et al. (2012). Asymmetrical interhemispheric connections develop in cat visual cortex after early unilateral convergent strabismus: anatomy, physiology, and mechanisms. *Front. Neuroanat.* 5:68. doi: 10.3389/fnana.2011.00068

Cajal, S. R. Y. (1899). "Histology of the nervous system of man and the vertebrates," in *Chapter 5*, Vol. 1, eds N. Swanson and L. W. Swanson (trans) (New York, NY: Oxford University Press).

Cuntz, H. (2012). The dendritic density field of a cortical pyramidal cell. *Front. Neuroanat.* 6:2. doi: 10.3389/fnana.2012.00002

DeFelipe, J. (2010). From the connectome to the synaptome: an epic love story. *Science* 330, 1198–1201.

DeFelipe, J., Alonso-Nanclares, L., and Arellano, J. I. (2002). Microstructure of the neocortex: comparative aspects. *J. Neurocytol.* 31, 299–316.

Feldmeyer, D. (2012). Excitatory neuronal connectivity in the barrel cortex. *Front. Neuroanat.* 6:24. doi: 10.3389/fnana.2012.00024

Gazzaniga, M. S., Ivry, R. B., and Mangun, G. R. (2008). *Cognitive Neurosciences: The Biology of the Mind, 3rd Edn*. New York, NY: W. W. Norton.

Ichinohe, N. (2012). Small-scale module of the rat granular retrosplenial cortex: an example of the minicolumn-like structure of the cerebral cortex. *Front. Neuroanat.* 5:69. doi: 10.3389/fnana.2011.00069

Kalil, K., Li, L., and Hutchins, B. I. (2011). Signaling mechanisms in cortical axon growth, guidance, and branching. *Front. Neuroanat.* 5:62. doi: 10.3389/fnana.2011.00062

Lee, C. C., Kishan, A. U., and Winer, J. A. (2011). Wiring of divergent networks in the central auditory system. *Front. Neuroanat.* 5:46. doi: 10.3389/fnana.2011.00046

Lorente de Nó, R. (1949). "Cerebral cortex: architecture, intracortical connections, motor projections," in *Physiology of the Nervous System, 3rd Edn*, ed J. F. Fulton (Oxford: Oxford University Press), 288–330.

Mota, B., and Herculano-Houzel, S. (2012). How the cortex gets its folds: an inside-out, connectivity-driven model for the scaling of mammalian cortical folding. *Front. Neuroanat.* 6:3. doi: 10.3389/fnana.2012.00003

Perin, R., Berger, T. K., and Markram, H. (2011). A synaptic organizing principle for cortical neuronal groups. *Proc. Natl. Acad. Sci. U.S.A.* 108, 5419–5424.

Perin, R., Telefont, M., and Markram, H. (2013). Computing the size and number of neuronal clusters in local circuits. *Front. Neuroanat.* 7:1. doi: 10.3389/fnana.2013.00001

Seeley, W. W., Crawford, R. K., Zhou, J., Miller, B. L., and Greicius, M. D. (2009). Neurodegenerative diseases target large-scale human brain networks. *Neuron* 62, 42–52.

Solari, S. V. H., and Stoner, R. (2011). Cognitive consilience: primate non-primary neuroanatomical circuits underlying cognition. *Front. Neuroanat.* 5:65. doi: 10.3389/fnana.2011.00065

Wang, X.-J. (2010). Neurophysiological and computational principles of cortical rhythms in cognition. *Physiol. Rev.* 90, 1195–1268.

Received: 06 May 2013; accepted: 08 May 2013; published online: 28 May 2013.
Citation: Budd J and Kisvárday Z (2013) How do you wire a brain? Front. Neuroanat. 7:14. doi: 10.3389/fnana.2013.00014

frontiers in
NEUROANATOMY

ORIGINAL RESEARCH ARTICLE
published: 11 January 2012
doi: 10.3389/fnana.2011.00068

Asymmetrical interhemispheric connections develop in cat visual cortex after early unilateral convergent strabismus: anatomy, physiology, and mechanisms

Emmanuel Bui Quoc[1,2,3†], Jérôme Ribot[1,2†], Nicole Quenech'Du[1,2], Suzette Doutremer[1,2], Nicolas Lebas[1,2], Alexej Grantyn[1,2], Yonane Aushana[1,2] and Chantal Milleret[1,2]*

[1] *Laboratoire de Physiologie de la Perception et de l'Action, Collège de France, Paris, France*
[2] *Laboratoire de Physiologie de la Perception et de l'Action, CNRS UMR 7152, Paris, France*
[3] *Service d'Ophtalmologie, Hôpital Robert Debré, Paris, France*

Edited by:
Zoltan F. Kisvarday, University of Debrecen, Hungary

Reviewed by:
Alino Martinez-Marcos, Universidad de Castilla, Spain
Zoltan F. Kisvarday, University of Debrecen, Hungary

***Correspondence:**
Chantal Milleret, Laboratoire de Physiologie de la Perception et de l'Action, Collège de France, CNRS UMR 7152, 11 Place Marcelin Berthelot, 75005 Paris, France.
e-mail: chantal.milleret@college-de-france.fr

†*Emmanuel Bui Quoc and Jérôme Ribot have contributed equally to this work.*

In the mammalian primary visual cortex, the corpus callosum contributes to the unification of the visual hemifields that project to the two hemispheres. Its development depends on visual experience. When this is abnormal, callosal connections must undergo dramatic anatomical and physiological changes. However, data concerning these changes are sparse and incomplete. Thus, little is known about the impact of abnormal postnatal visual experience on the development of callosal connections and their role in unifying representation of the two hemifields. Here, the effects of early unilateral convergent strabismus (a model of abnormal visual experience) were fully characterized with respect to the development of the callosal connections in cat visual cortex, an experimental model for humans. Electrophysiological responses and 3D reconstruction of single callosal axons show that abnormally asymmetrical callosal connections develop after unilateral convergent strabismus, resulting from an extension of axonal branches of specific orders in the hemisphere ipsilateral to the deviated eye and a decreased number of nodes and terminals in the other (ipsilateral to the non-deviated eye). Furthermore this asymmetrical organization prevents the establishment of a unifying representation of the two visual hemifields. As a general rule, we suggest that crossed and uncrossed retino-geniculo-cortical pathways contribute successively to the development of the callosal maps in visual cortex.

Keywords: strabismus, visual interhemispheric integration, cerebral asymmetry, higher mammals

INTRODUCTION

In adult mammals, the left and right halves of the visual field project to the opposite hemispheres. Continuity is ensured in primary visual cortex by interhemispheric callosal connections (CC) which mediate representations of the central vertical meridian (CVM) and its vicinity (Berlucchi et al., 1967; Hubel and Wiesel, 1967; Berlucchi and Rizolatti, 1968; Leporé and Guillemot, 1982; Payne, 1990a,b, 1991; Payne and Siwek, 1991; Milleret and Buser, 1993; Milleret et al., 1994, 2005; Nakamura et al., 2008; cf. **Figure 1**). Anatomical and functional data from cat visual cortex indicate that the development of CC occurs progressively from birth (Innocenti et al., 1977; Elberger, 1993; Aggoun-Zouaoui and Innocenti, 1994; Milleret et al., 1994; Aggoun-Zouaoui et al., 1996), and depends on postnatal visual experience. However, the latter data are sparse and incomplete (e.g., Innocenti and Frost, 1979; Olavarria, 1995; Schmidt et al., 1997; Milleret and Houzel, 2001; Tagawa et al., 2008; Alekseenko et al., 2009). Thus, the consequences of abnormal postnatal visual experience on the development of CC and on their role in unifying both hemifields remain unclear. The present study addresses this issue by using early unilateral convergent strabismus as a model of abnormal experience. Subsequent development of CC in cat visual cortex was investigated at the level of callosal terminals by combining electrophysiology and tracer injection techniques. Although controversial, some anatomical data in the literature have already suggested that procedure this may lead to asymmetric callosal connections in one hemisphere and the other in adulthood (Lund and Mitchell, 1979; Berman and Payne, 1983; but see Elberger et al., 1983; Bourdet et al., 1996).

The idea that CC in cat visual cortex contribute to unifying the representation of both visual hemifields has emerged progressively over the years. Early studies showed that callosal fibers transmit signals originating from the CVM and its vicinity (Berlucchi et al., 1967; Hubel and Wiesel, 1967), and that units recorded simultaneously in the callosal zone of each hemisphere display overlapping spatial distributions of their receptive fields (RFs; Leicester, 1968; Payne, 1990a,b, 1991, 1994; Payne and Siwek, 1991). However, a direct proof was only made possible by using the split-chiasm preparation (Berlucchi and Rizolatti, 1968;

Abbreviations: Az_1, Az_2, and Az_3, medial-most, center, and lateral-most limits of the receptive fields respectively; CC, corpus callosum or callosal connections; CVM, central vertical meridian of the visual field; GC, geniculo-cortical; LH and RH, left and right hemisphere respectively; *m*, mean; NR, normally reared; OI, overlap index; RF, receptive field; S and NS, selective and non-selective cells for orientation; TC, transcallosal; WM, white matter.

Leporé and Guillemot, 1982; Milleret and Buser, 1993; Milleret et al., 1994, 2005; Rochefort et al., 2007; **Figure 1**). This surgery allows direct activation of the transcallosal (TC) pathway by stimulating the eye contralateral to the explored cortex, as well as direct activation of the geniculo-cortical (GC) pathway by stimulating the ipsilateral eye. This showed that TC units are situated mainly in layers II/III of the transition zone between A17 and A18 (17/18 TZ), with RFs distributed along the CVM, between 13° in the ipsilateral hemifield to the explored cortex to 6° in the contralateral hemifield (Milleret et al., 2005). Their spatial distribution in the left and the right hemifields, corresponding to the "callosal visual field," mirror one another. Such TC units were also revealed to be binocular, with TC- and GC-RFs encoding similar orientation selectivity and substantially overlapping. But couples of RFs displayed position disparity ($m \approx 5°$), mainly of the crossed type. This suggests that under normal conditions the CC are mainly involved in coarse depth perception in front of the fixation plane. Anatomical studies have further shown that CC in cat visual cortex display a non-mirror-symmetric organization between the two hemispheres (Olavarria, 1996, 2001). Callosal-projecting neurons are found within rather large portions of A17 and A18. On the other hand, most of the terminals in the other hemisphere are located around the 17/18 TZ, except caudally where they also invade substantial portions of both A17 and A18 (Innocenti and Fiore, 1976; Payne and Siwek, 1991; Houzel et al., 1994; e.g., Innocenti, 1986 for review). Finally, both neurons and callosal terminals are found mainly within cortical layers II and III (Innocenti and Fiore, 1976; Payne, 1990a,b; Houzel et al., 1994).

During normal development, the CC's contribution to unifying the split representation of the visual field develops progressively during the first four postnatal months, i.e., during the critical period (Hubel and Wiesel, 1970). Two weeks after birth (i.e., around eye opening in cats), TC units display tangential and radial distributions similar to the case in adults, with RFs located in the 17/18 TZ, mainly in supra-granular layers (Milleret et al., 1994). However, their functional properties are still immature. Their RFs are located on the CVM, as well as in a large portion of the ipsilateral hemifield (as far as 20°). Position disparity between TC- and GC-RFs for binocular units is about 16° at 21 postnatal days (PND) and thus exceeds the value of 5° found in adult animals.

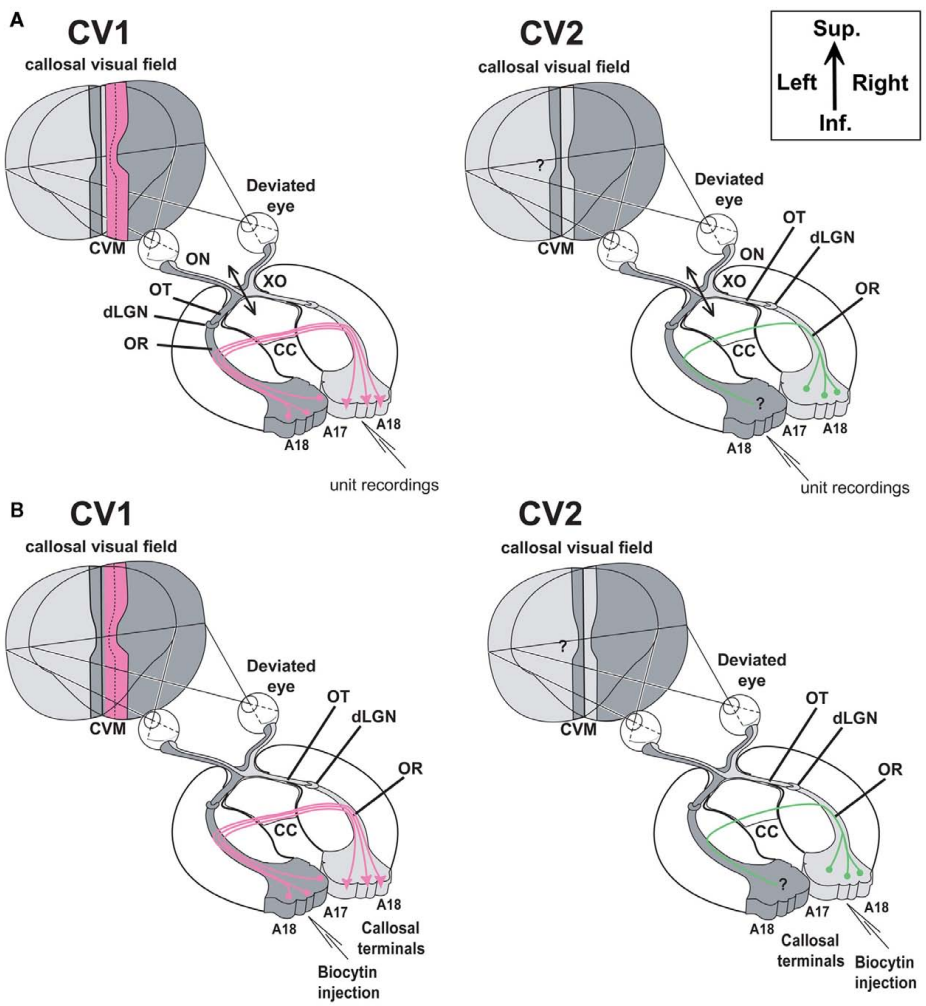

FIGURE 1 | Continued

FIGURE 1 | Experimental designs. (A) Electrophysiological characterization of visual callosal transfer in the CV_1 and CV_2 groups. Diagrams are based on the normal organization of the cat visual system. Each visual hemifield is represented in the contralateral hemisphere (in light and dark gray, respectively). Continuity is however ensured by "symmetric" cortical representations of the central vertical meridian (CVM) and its vicinity in each visual cortex (A17 and A18) that are reciprocally connected by interhemispheric callosal connections (CC). In addition to the convergent deviation of their right eye, the optic chiasm was sectioned midsagitally 3 days before cortical recordings (XO, double arrow). Thus, crossed fibers originating from both nasal retinas were severed while uncrossed fibers originating from both temporal retinas remained intact and projected to the ipsilateral visual cortex *via* the optic nerve (ON), the optic tract (OT), the dorsal lateral geniculate nucleus (dLGN) and the optic radiations (OR). *In the CV_1 group*, previously to the present study (cf. Milleret and Houzel, 2001), single units were recorded in the right hemisphere, thus ipsilaterally to the deviated eye. Stimulating the non-deviated (left) eye activated the transcallosal pathway (in pink color) while the stimulation of the deviated (right) eye activated the ipsilateral retino-geniculo-cortical pathway. This allowed establishing that callosal terminals in this group are exuberant compared to normal. We also demonstrated that the "callosal visual field" seen through these terminals is larger than normal (dotted vertical line) and looses any contact with the central vertical meridian (CVM) of the visual field while it has some normally (see text for further details). *In our CV_2 group here*, in order to characterize a possible asymmetry, we made the reverse exploration. Single unit were recorded in the left hemisphere, thus ipsilaterally to the non-deviated eye. Stimulating the deviated (right) eye activated the transcallosal pathway while the stimulation of the non-deviated (left) eye activated the ipsilateral retino-geniculo-cortical pathway. How callosal terminals in visual cortex and "callosal visual field" (here in "green") develop in this case is the present question. **(B,C)** Anatomical characterization of callosal terminals in visual cortex of strabismic cats (CV_1 and CV_2 groups). **(B)** In contrast to **(A)** the optic chiasm was not sectioned here. In the CV_1 group, biocytin was injected in the left visual cortex in order to label terminals of single callosal axons in the right visual cortex, ipsilateral to the deviated eye. On the basis of previously obtained functional data (Milleret and Houzel, 2001), the expected anatomical data are summarized in pink. After strabismus, both callosally projecting neurons in the left hemisphere and callosal terminals in the right would display exuberant distributions compared to normal. In the CV_2 group, to identify a possible asymmetry of the callosal connections between the hemispheres because of strabismus, biocytin was injected in the right visual cortex in order to label terminals of single callosal axons in the left visual cortex, ipsilateral to the non-deviated eye. Callosally projecting cells are known to display a larger distribution than normal (see Text); our study aims to quantify the extent of these terminals (in green). **(C)** Examples of injection sites (zones in dark) in the left and right hemispheres (from CV_1 and CV_2 groups respectively). Section thickness was 75 μm; at left, the section was additionally colored with the Nissl method to identify cortical layers. Sup, superior; Inf, inferior.

Finally, spontaneous activity, response strength, orientation selectivity, and response to slits moving at middle-range velocities are also low compared to adult animals. Anatomical studies have also shown that the specific organization of the callosal connections found in adult cats is not innate, but rather is refined during the critical period. In kittens, callosal neurons are initially located in extensive portions of A17 and A18 (Innocenti et al., 1977). Their callosal terminals are initially exuberant, although restricted to the 17/18 TZ when entering the contralateral cortex (Innocenti, 1981; Innocenti and Clarke, 1984; Innocenti et al., 1986; but see Elberger, 1993). The number of callosal axons is also much greater than in adults, and is considerably reduced during development (Berbel and Innocenti, 1988). Nevertheless, synapses are already predominant in supra-granular layers of the 17/18 TZ (Aggoun-Zouaoui and Innocenti, 1994; Aggoun-Zouaoui et al., 1996).

The development of callosal connections in visual cortex of higher mammals is highly dependent on postnatal visual experience. For example, we have previously shown that early convergent strabismus induced at PND 6 leads to functional abnormalities of CC in adulthood in the hemisphere ipsilateral to the deviated eye (Milleret and Houzel, 2001; "CV_1 group," **Figure 1A**). Contrary to normal animals, numerous TC units can be recorded outside of the 17/18 TZ, both in A17 and in A18, but also in the white matter (WM). TC units exhibit additional functional deficits usually associated with strabismus, such as decreased binocularity, ability to respond to fast-moving stimuli, or increased RF sizes. Many units also exhibit reduced orientation selectivity and increased position disparity. Most importantly, the location of the TC-RFs falls within the hemifield ipsilateral to the explored cortex, with almost no contact with the CVM, suggesting that the role of the CC in unifying both hemifields is likely to be disturbed. Our goal here is to test this by characterizing the region of the visual field "seen" by TC units in the hemisphere contralateral to the deviated eye ("CV_2 group"; **Figure 1A**).

The few studies anatomically characterizing callosal connections in strabismic cats are highly diverse, precluding an overall

view. Experimental conditions often vary from one study to another, and can be imprecise, dealing with monocular and binocular strabismus, or convergent and divergent deviations. In cases of monocular strabismus, there was often no mention of which hemisphere was studied with respect to the deviated eye. At the present time, some authors claim that strabismus leads to extended distribution of cell bodies of callosal neurons in one or both hemispheres through the stabilization of juvenile exuberant ones (Innocenti and Frost, 1979; Berman and Payne, 1983; Elberger et al., 1983). But other authors do not agree with this view (Lund et al., 1978; Bourdet et al., 1996). The same conclusion has also been proposed for callosal terminals (Lund et al., 1978; Lund and Mitchell, 1979; Berman and Payne, 1983). Such discrepancies could be explained by an asymmetrical development of callosal connections between the hemispheres after early unilateral strabismus. Some data in the literature support such a hypothesis (cf. Lund and Mitchell, 1979; Berman and Payne, 1983 for details), but it has never been studied with precision.

In this study, for the first time, we fully characterize the effects of an early unilateral convergent strabismus on the development of the callosal connections in cat visual cortex, from the right hemisphere (RH) to the left one and conversely. For this purpose, functional and anatomical approaches were combined. Our results show that asymmetrical callosal connections do develop after unilateral convergent strabismus. Two complementary mechanisms are proposed to explain such a development. We also demonstrate that such asymmetric organization prevents the CC from properly unifying representation of the two visual hemifields.

MATERIALS AND METHODS

Thirteen adult cats, born from different litters in our colony, were used in this study. All were in good health and had no apparent malformations or pathologies. All experiments were performed in accordance with the relevant institutional and national guidelines and regulations including the Collège de France, the CNRS and the DDPP (JO 87–848, consolidated after revision on May 30, 2001, Certificate *n°* 75–337, French "Ministère de l'Agriculture et de la Pêche"). They also conformed to the relevant regulatory standards recommended by the European Community (Directive 2010/63/UE) and the US National Institutes of Health.

FUNCTIONAL APPROACH

Seven cats were included in the functional experiments [CV_2 group: cats CVA(3), CVE5, CVE6, CVE9, CVE10, CVE11, CVE12]. The protocol was very similar to that used previously for the CV_1 group (cf. Milleret and Houzel, 2001) in order to facilitate comparisons between the two groups.

Induction of convergent strabismus

At PND 6, i.e., a few days before natural eye opening and while callosal projections are still exuberant (Innocenti et al., 1977), the *right eye* (RE) of each animal was made esotropic under Saffan anesthesia® (Schering-Plough Animal Health, Welwyn Garden City, AL7 1TW, UK), with a posology of 1.2 ml/kg i.m. The rectus lateralis muscle was removed surgically as completely as possible. A single i.m. injection of antibiotics was given at the end of the surgery (Extencilline, 1 MU/kg, Specia Rhône-Poulenc Rorer, France). Local antibiotics were also administered three times a day during 1 week: Neomycin® eye drops (3,50,000 UI/ml, Roussel Diamant, France) and Rifamycine® eye drops (10 mg/ml, MSD-Chibret, France). All kittens recovered rapidly, showed no sign of pain or discomfort, and developed a manifest convergent squint. At adulthood (10 months of age and older), strabismus was assessed using the corneal reflex method (Sherman, 1972) and was ranged between 3.5° and 13.5° across animals.

Section of the optic chiasm

Chiasmotomy was performed to suppress responses from crossed retinal fibers originating mainly from the nasal retina. This surgery allows selective activation of the callosal pathway or the GC pathway converging onto the same visual cortex depending on the stimulated eye (Berlucchi and Rizolatti, 1968; cf. **Figure 1A**). Anesthesia was induced and maintained with Saffan® (initial, i.m., 1.2 mg/kg as above; supplements, 1:1 in saline, i.v. *ad libitum*). Each cat was installed supine in a Horsley–Clarke stereotaxic apparatus. The electrocardiogram and the rectal temperature were continuously monitored. While the mouth was maintained open, the soft palate was cut along the midline. The exposed bony palate was treated with a local anesthetic (Xylocaine 2%, AstraZeneca, Rueil-Malmaison, France) and drilled to expose the dura. This dura was incised and the underlying optic chiasm was cut totally in the midsagittal plane. Antibiotics were applied both locally (Cébénicol®, 80 mg/ml, Chauvin-Bausch and Lomb, Montpellier, France) and i.m. Extencilline® 1 MU/kg, Aventis, France). Finally, the soft palate was sutured and an oral analgesic was administrated (Metacam®, 0.1 mg/kg, Boehringer Ingelheim). Completeness of the optic chiasm section was verified systematically postmortem using gold-chloride staining (Schmued, 1990) on 50 μm sections.

Electrophysiological recordings

Single unit electrophysiological recordings in the *left hemisphere, ipsilateral to the non-deviated eye* (**Figure 1A**, CV_2) revealed functional properties of transcallosally activated neurons. This was performed on anesthetized and paralyzed adult cats 3 days after acute section of the optic chiasm since primary visual cortical responsiveness and RF size can change rapidly after chiasmotomy in adult cats (Milleret and Buser, 1984).

On the day of the experiment, animals were re-anesthetized with Saffan® as described earlier. After tracheal and venous cannulation, electrocardiogram, temperature, and expired CO_2 probes were placed for continuous monitoring. Animals were installed in the Horsley–Clarke stereotaxic frame and prepared for acute electrophysiological recordings. The scalp was incised in the sagittal plane, and a large craniotomy was performed overlying areas 17 and 18. The nictitating membranes were then retracted with neosynephrine eye drops (Neosynephrine® 5%, Ciba Vision Ophthalmics, France) and the pupils dilated with atropine eye drop (Atropine 1%, MSD-Chibret, France). Scleral lenses (PMMA, Polymethyl Methacrylate) were placed to protect the cornea and focus the eyes on a screen placed 57 cm away. Their size was adapted to the eye of each cat; between the lens and the cornea, their geometry creates a space filled with liquid which protects the cornea. Animals were then paralyzed with an infusion of Pavulon (0.2 ml/kg, i.e., 0.4 mg/kg i.v.) and breathing was assisted

artificially through a tracheal cannula. The breathing was adjusted to a frequency of 10–12/min and the volume adapted to the ratio of exhaled CO_2 (PCO_2 was maintained at 4%). Anesthesia and paralysis were maintained throughout the experiment by continuous infusion of a mixture of Saffan® (3.6 mg/kg/h) and Pavulon (0.1 ml/kg/h) diluted in glucose (5%) and NaCl (0.9 g/l).

Each cat had two to three electrode penetrations in the coronal plane and angled toward the midline, with 20–40° of inclination relative to the vertical. The standard stereotaxic coordinates were P4 to A12 and L1 to L4 in order to explore the representation of the center and the lower quadrant (down to −30°) of the visual field within A17 and A18, according to a published description of the retinotopic maps of the cortex of the cat (Tusa et al., 1978, 1979). They consisted in sampling multiunit extracellular activity using tungsten micro-electrodes (1–2 MΩ at 1 kHz) after amplification and band-pass filtering the signal between 300 Hz and 3 kHz. Single-cell spike activity was selected with a window discriminator and audio-monitored on a second channel. Single units were recorded at regular intervals of 100 μm, over a total course of 1500–4000 μm. Finally, two small electrolytic lesions (cathodal current, 10 μA DC, 15 s) were made along each track for subsequent reconstruction.

Analysis of the properties of the visual responses

To analyze the visual responses of units, the surrounding environment displayed a mesopic luminance (∼5 Cd/m^2). Visual stimuli (50 Cd/m^2) of various shapes, sizes, and velocities were projected manually onto the faintly illuminated tangent translucent screen (13 Cd/m^2) facing the animal. The position of each optic disk was also projected onto the screen with an ophthalmoscope (further details below).

Visual stimuli were systematically presented to each eye in succession. This allowed comparison of the properties of the visual responses of each cortical cell when activated through either the interhemispheric pathway by stimulating the right (deviated) eye or through the retino-GC pathway by stimulating the left (non-deviated) eye (Berlucchi and Rizolatti, 1968; cf. **Figure 1A**). Note that a section of the corpus callosum in such strabismic animals totally abolishes any transfer of visual information from one hemisphere to the other (Milleret and Houzel, 2001).

Several functional properties were examined for each recorded unit: (1) Response strength was rated into four classes of increasing discharge levels: 1 (irregular and poor), 2 (clear and reproducible), 3 (strong), and 4 (extremely vigorous); (2) Ocular dominance was determined by comparing the strength of the responses to visual stimulation of each eye successively. Classically, units were assigned to one of the five following classes: "*c*," "$c > i$," "$i = c$," $i > c$, or "*i*," with "*c*" and "*i*" signifying the contralateral and the ipsilateral eye respectively; (3) Orientation selectivity was assessed by comparing responses to light bars of different orientations. Units were classified as orientation selective (S) or non-selective (NS); (4) Precise limits of the RFs were mapped as the "minimum response field"; (5) Spatial location of each RF within the visual field was inferred *off line* from the most recent determination of the positions of the projection of both the optic disk and the area centralis of the stimulated eye (these were verified systematically once per 2 h all during each experiment as well as when significant changes in spatial position occurred while mapping RFs of successive recorded units; Vakkur et al., 1963; Milleret et al., 1988a). Possible eye cyclo-rotation was eliminated by superimposing the projections of the area centralis from both eyes and by aligning the projections of their optic disks. We also verified the lack of significant asymmetry in the positions of paired landmarks from the two retinas each time they were projected onto the screen; the retinal vessels proximal to these landmarks were also used as indices. The spatial location of each RF was then quantified by measuring the angular distance separating its medial edge (Az_1), its center (Az_2), and its lateral edge (Az_3) from the visual midline; (6) RF size (in degrees^2) was derived from plots carefully drawn on the tangent screen. Measurements related to the latter two analyses were rather easy because, when the distance between the screen and the eyes of the animal is 57 cm, 10 cm on the screen represent 10° of the visual field; (7) For each binocular unit, the difference in position between pairs of RFs was evaluated as the angular distance between the centers of the two RFs; (8) Finally, the RF overlap index (OI) was calculated using the formula: $[B/(I + C - B)] \times 100$, where I and C are the size of the ipsilateral and the contralateral RF of a given binocular unit, respectively, and B is the visual field are common to both RFs.

Histological procedure

After the recording session, the anesthetized animal was perfused through the heart with 1 l of Ringer solution followed by 1 l of a fixative (2.5% paraformaldehyde and sucrose 4% in 0.1 M phosphate buffer). The stereotaxically blocked brain was frozen, cut in 75 μm thick sections and processed alternately to reveal Nissl substance or cytochrome oxydase activity (Wong-Riley, 1979). The areal and laminar locations of each recording site were determined from the reconstructed tracks. As in normal animals, 17/18 TZ appeared as a cortical ribbon elongated in a roughly parasagittal direction of about 1 mm wide. Electrophysiological criteria such as RF size, RF position, and neuronal responsiveness to moving stimuli indicated the identity of the recording site (A17, A18, or 17/18 TZ). More accurate cytoarchitectonic and histochemical criteria were then used based on Nissl (Otsuka and Hassler, 1962) and cytochrome oxydase activity staining (Price, 1985; Kageyama and Wong-Riley, 1986a,b; Payne, 1990b) of adjacent sections. The boundaries of cortical layers were first examined in both A17 and A18. Layer I appeared as a cell-poor region with low cytochrome oxydase activity; its lower border was marked by high cytochrome activity staining. We did not differentiate layer II from layer III. The lower limit of layer III was identified by its typical pyramidal cells; cytochrome oxydase activity was not considered in this case because of disagreement in the literature, although we could confirm its presence in the deepest parts of layer III in both A17 and A18, as reported by Payne (1990b). Layer IV was characterized by high granular cell density and strong cytochrome oxydase activity. In contrast the latter was very weak in layer V, which contained sparse pyramidal cells. Finally, layer VI displayed a higher cell density and moderate, but significant cytochrome oxydase activity. The 17/18 TZ was then analyzed, using variations in the relative thickness of some cortical layers: when passing from A17 to A18, the width of layers II/III increases whereas the width of layer VI decreases (cf. Payne, 1990a; Milleret et al., 1994).

Statistical analyses

Measurements were indicated as the mean, $m \pm$ standard mean deviation (SMD, where: SMD $= \sigma/\sqrt{N}$; N is the sample size; σ is the SD). Statistical tests were done with the χ^2 test with Yates correction. But when this could not be used because of the small sample size numbers, statistics were done with the Fischer exact test.

ANATOMICAL APPROACH

Six other cats that had the same early induced convergent strabismus of the RE were injected 6–12 months later (as adults) with the anterograde tracer biocytin in the visual cortex to examine callosal axons (cf. **Figure 1B**). The protocol was the same one we previously used to label callosal axons from visual cortex of normal adult cats (cf. Houzel et al., 1994). This allowed the data from normal cats (NR group) to serve as a reference here. Thus this protocol will only be briefly summarized.

Experimental groups

In order to correlate functional and anatomical data obtained in visual cortex after early strabismus, two experimental groups, CV_1 and CV_2, were distinguished here. In the CV_1 group, experiments characterized the callosal terminal zone within the (right) visual cortex, ipsilateral to the surgically deviated eye, while study of the CV_2 group concerned the contralateral (left) visual cortex, ipsilateral to non-deviated eye (**Figure 1B**). The CV_1 group included cats BCV7, BCV9, CV13, and CV14 while CV_2 group included CVE4 and CVE7.

Tracer injections, staining method, and 3D reconstruction of callosal terminals

On the day of the experiment, anesthesia was induced and maintained and surgical preparation proceeded as above. In both groups, callosal axons were anterogradely labeled with pressure injected biocytin (Sigma, at 5% in 0.05 M tris buffer, pH 8). Labeling and visualization procedures were as described previously (Houzel et al., 1994). In brief, in the CV_1 group, biocytin was injected in the *left hemisphere*, i.e., ipsilateral to the non-deviated eye while in the CV_2 group, biocytin was injected in the RH, i.e., ipsilateral to the deviated eye (**Figure 1B**). In each injection site, two or three 0.2–0.5 µl of tracer was pressure injected through a micropipette, separated by ∼800 µm from one another, between 500 and 1500 µm below the cortical surface. This produced injections spanning layers I through VI, with diameters ranging between 1500 and 2000 µm medio-laterally and 600 and 1650 µm antero-posteriorly (**Figure 1C**). Injections were made in 17/18 TZ at Horsley–Clarke stereotaxic coordinates between P_2L_4 and A_7L_1 in the CV_1 group (cats CV_{14} and BCV_9) and between $A_{5.5}L_2$ and A_8L_3 in CV_2 group (cats CVE4 and CVE7). Then, injections were made more medially within area 17 (A17) at Horsley–Clarke coordinates P_7L_1 or A_0L_1 in CV_1 group (cats CV13 and BCV7 respectively) and between P_4L_3 and P_2L_2 in CV_2 group (cats CVE7 and CVE4). In one animal of the CV_1 group (cat CV13), a more lateral injection was also made within A18 at Horsley–Clarke coordinates $A_9L_{2.5}$. After tracer injections, an antibiotic was administered i.m. (Extencilline, 1 MU/kg, Avantis, France).

Histological procedures were then applied to both hemispheres to obtain 75 µm thick frontal serial sections of brain. Sixty hours after the intra-cortical injections of the tracer, the animals were again deeply anesthetized with Saffan (1.2 ml/kg). Then, they were perfused transcardially first with 0.1 M PBS at pH 7.4, second with a mixture of 4% paraformaldehyde in PBS and 0.3% glutaraldehyde. Brains were post-fixed during 4 h in cold (4°C) in paraformaldehyde 4%, stored for 48 h in 30% sucrose solution for cryoprotection, frozen sectioned, and then incubated at room temperature for 12 h in an avidin peroxydase complex (ABC kit, 1/200 dilution into PBS solution with 1% of Triton-X100). A second incubation was performed in diaminobenzidine solution amplified with nickel sulfate to stain peroxydase. Alternate frontal sections were Nissl stained for identification of A17, A18, and the 17/18 TZ by differences in thickness of respective cortical layers (Payne, 1990a; Milleret et al., 1994).

Finally, the 3D morphology of individual callosal axons was reconstructed from the midline to their terminals at high magnification (1000×, with oil immersion) with the Neurolucida® tracing system (Microbrightfield Inc.). Detailed methods regarding the 3D reconstruction and the quantification of morphology have been described previously (Houzel et al., 1994). Histological procedures such as fixation, cryogenation, deflating, and mounting on slides generally induce a 35–40% isotropic shrinkage along the x and y and w axes. Compression of the tissue also occurs perpendicular to the cut surface of sections, reducing section thickness by ∼1/3 of its value at the time of sectioning. These were compensated for in quantitative analyses (incrementing by 35 and 33% for shrinkage and compression respectively; cf. Innocenti et al., 1994 for details).

Axonal morphology

The morphology of each callosal axon was characterized on the basis of previously described criteria (Houzel et al., 1994) facilitating the comparison between CV and NR groups. In summary (see **Figure 2A**), the *trunk* was identified as that part of the axon proximal to the first branching point (*node*) in the hemisphere contralateral to the injection. The part of the axon located distal to the first node was called the *terminal arbor*. Axonal branches were then identified by their topological order. Thus *first order* (or *primary*) branches originated from the first node and that gave rise to the *second order* (or *secondary*) branches; the latter gave rise to *third-order* (or *tertiary*) branches, etc. Branches which were particularly conspicuous by their length and/or thickness were designated as *main branches*. *Pre-terminal branche*s carried (presumably synaptic) boutons. The latter could be *terminal boutons*, characterized by the presence of a connecting stalk or "*en passant*" *boutons*, i.e., swellings along the pre-terminal branch. In the gray matter, axons might end with one or several *tufts*. A *tuft* was a part of an arbor characterized by densely ramified and tightly distributed high-order and pre-terminal branches originating from a common stem. In addition, these tufts might have some modest *collaterals*. Tufts and/or collaterals of one axon might terminate in segregated volumes of cortex including one of several cortical layers. Hereafter we shall call these volumes *terminal columns*. The characterization of a terminal column required the identification of distinct *clusters* of *pre-terminal branches* and *boutons* in a view perpendicular to the cortical surface (**Figure 2B**).

Architecture of individual terminal arbors

Axons may vary in the complexity and spatial organization of their terminal arbors. We distinguished here only two types of architectures: (a) *A simple architecture:* the axon terminates with a single tuft within an approximately conical volume (see for example **Figure 8A**); (b) *A multiple clustered architecture:* the axon is characterized by a trunk which divides into first- and/or higher-order branches. Then, it terminates with several columns and several tufts in the cortex which are generally clearly separated (see for example **Figure 8B**).

Laminar distribution of the terminal boutons

The various laminar distributions of the terminal boutons encountered here were also classified on the basis of criteria used previously for the NR group: (a) when boutons were restricted to supra-granular layers II and III and often included layer 1 (and in some cases also layer IV), this pattern of distribution was described as *supra-granular*; (b) when the highest density of boutons was still in the supra-granular layers and others were located in infragranular layers (with no or very few boutons in layer IV), this pattern of distribution was described as *bi-laminar*; (c) when boutons were all located in the granular layer IV, as expected, the distribution was described as *granular*; (d) the fourth pattern was characterized by boutons distributed across both the supra and infragranular layers, including layer IV (*trans-granular* distribution); (e) finally, if boutons were only located in infragranular layers, the distribution is described as *infragranular*.

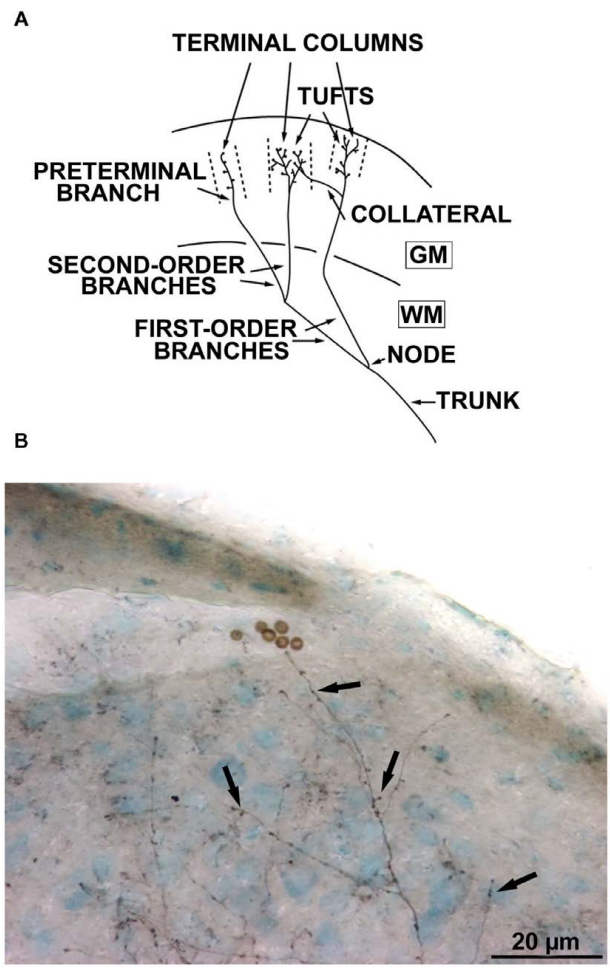

FIGURE 2 | Architecture of the callosal axons. (A) Schematic drawing of a terminal arbor in the cerebral cortex (WM = white matter, GM = gray matter) and illustrating the nomenclature employed. "Terminal columns" refer to the volumes delineated by interrupted lines; each column is supplied by an isolated pre-terminal branch. For further details, see text (Reproduced with permission, from Houzel et al., 1994). **(B)** A callosal axon labeled with biocytin, with its terminal boutons (arrows).

Statistical analyses

The morphology of each callosal axon was quantified classically using the Neuroexplorer program by measuring the diameter of the trunk, the number of nodes, the length of branches (first to fifth order), the number of terminals, and the number of boutons. A Wilcoxon rank sum test (two-sided for independent unequal-sized samples) compared the CV_1, CV_2, and NR groups in a pair wise manner (Hollander and Wolfe, 1973; Gibbons, 1985).

RESULTS

FUNCTIONAL DATA

In the CV_2 group ($n = 7$), 457 units were recorded in the left hemisphere LH (ipsilateral to the non-deviated eye) and 70 responded to visual stimulation through the TC pathway (**Table 1**). Other units were either exclusively responsive to stimulation through the GC pathway ($n = 307$), or were visually unresponsive ($n = 83$). We only examined the distribution and functional characteristics of units that responded to TC stimulation ("TC units"). Data have been compared to those previously obtained in the RH, ipsilateral to the deviated eye (CV_1 group from Milleret and Houzel, 2001), and those obtained in normally reared (NR) cats (Milleret et al., 1994, 2005; Milleret and Houzel, 2001). Such comparisons were possible because we explored similar cortical regions in all cases, corresponding to comparable portions of the visual field (further details in Receptive Field Characteristics of the Transcallosally Activated Units).

Table 1 | Number of cortical units recorded in areas 17 and 18 of the left hemisphere in the CV_2 group.

Cat	Number of recorded cells			
	TC	I	NV	Total
CVA(3)	20	54	7	81
CVE5	0	45	24	69
CVE6	15	44	6	65
CVE9	19	45	5	69
CVE10	16	45	2	63
CVE11	0	45	23	68
CVE12	0	26	16	42
Total	70	307	83	457

TC, transcallosally activated units; I, ipsilaterally activated units; NV, non-responsive cells.

Location of the transcallosally driven units

In the CV_2 group, almost all TC units (69/70) were located within the gray matter (**Table 2**). Within 17/18 TZ, 78% (60/77) of units responded to TC stimulation, but only 3% (7/212) did so in A17 and 1% (2/151) in A18. TC units could be located as far as 3600 μm from 17/18 TZ in A17 and 1200 μm from 17/18 TZ in A18 (**Figure 3A**). Within 17/18 TZ, TC units were numerous in all cortical layers (**Figure 3B**). Within A17 and A18, they were not numerous enough to test their distribution (**Figure 3B**).

These results were different from those established previously in the CV_1 group (see **Table 2** and **Figure 3**). The first major difference was in the tangential distribution of the TC units: they were almost exclusively located in the 17/18 TZ in the CV_2 group, whereas they also included extended portions of A17 and A18 in the CV_1 group. In addition, in the CV_2 group, the proportion of the TC units within the 17/18 TZ was higher than in the CV_1 group, with 78 vs. 46.5% respectively (χ^2 test with Yates correction, $P < 0.0001$). The radial distributions of the TC units also differed: whereas the TC units of the 17/18 TZ were distributed in all cortical layers (from layer I to layer VI) in the CV_2 group, they were mainly located in infragranular layers in the CV_1 group. Finally, in both groups, some TC units could be recorded in the WM, although the proportion was higher in the CV_1 group than in the CV_2 group (9/54 units and 1/17 unit respectively).

Results in the CV_2 group also differed from those obtained in the NR group (c.f. **Table 2** and **Figure 3**). However, these differences were minor compared to those observed between the CV_1 and CV_2 groups. In both groups, almost all TC units were recorded within the 17/18 TZ. Still, within the 17/18 TZ, the proportion of TC units in the CV_2 group was significantly higher than that in the NR group (78 vs. 51%; χ^2 test with Yates correction, $P = 0.0012$). The radial distributions of the TC units in the 17/18 TZ also varied greatly between groups, with an almost equal repartition of TC units within the different cortical layers in the CV_2 group and a strong bias in favor of the supra-granular layers in the NR group. Finally, no TC unit was recorded in the WM of cats in this latter group.

Strength of transcallosal responses

The strength of TC responses in the CV_2 group varied greatly (**Figure 3B**): class 1 ($n = 31$, i.e., 44.3%), class 2 ($n = 25$, i.e., 35.7%), class 3 ($n = 13$, i.e., 18.6%), class 4 ($n = 1$, i.e., 1.4%). But some differences appeared depending on the cortical region. All responses recorded in A17, A18, or the WM were poor (class 1: 7/7 in A17, 2/2 in A18, and 1/1 in the WM). On the other hand, responses in the 17/18 TZ were more vigorous: class 2 (25/60, i.e., 41.6%), class 3 (12/60, i.e., 20%), and class 4 (2/60, i.e., 3.3%).

These observations indicate that visual interhemispheric transfer to the 17/18 TZ in the CV_2 group can lead to rather vigorous post-synaptic responses. Such data are similar to those obtained for the CV_1 group (class 2, 55% of the TC units; class 3, 30%). Surprisingly, response strength in the 17/18 TZ in CV groups was even significantly higher than in the NR group, since only class 1 and 2 responses occurred in the latter (χ^2 test with Yates's correction, $P < 0.05$).

Ocular dominance of the transcallosal units

In the CV_2 group, the global ocular dominance distribution of the TC units was *U*-shaped with a strong bias favoring the contralateral eye (TC pathway). About half of TC units (37/70, i.e., 53%) were even exclusively activated through the stimulation of the right (deviated) eye, contralateral to the explored cortex (**Figure 4A**), while the others were binocular, also activated through the GC pathway. These units displayed the following distribution according to their ocular dominance: $c > i$, 9/70 (13%); $i = c$, 8/70 (11%); $i > c$, 16/70 (23%). Because numbers of TC units were low in A17, A18, and WM (7, 2, and 1 units respectively), this distribution reflects mainly the ocular dominance distribution in the 17/18 TZ.

The ocular dominance distribution in the 17/18 TZ of CV_2 group resembled that of the CV_1 group: there was a strong bias toward the contralateral eye Nevertheless, many units also responded to stimulation of the ipsilateral eye. That difference between the CV_2 and CV_1 groups with regard to the proportion of binocular units did not reach significance (33/70 in CV_2 group vs. 63/108 in CV_1 group; χ^2 test with Yates correction, $P = 0.2144$). On the contrary, both strabismic groups differed greatly from the NR group, where ocular dominance was strongly biased in favor of the ipsilateral eye. Note that the proportion of binocular units in the CV_2 group (33/70, i.e., 47.1%) was lower than in the NR group (75/79, i.e., 95%; Fisher exact test, $P < 0.0001$). Such data merely reflect the well known effects of strabismus on the ocular dominance of the overall population of cortical neurons of primary visual cortical areas (cf. Boothe et al., 1985; Milleret, 1994a,b; Kiorpes and McKee, 1999 for review).

Table 2 | Incidence of the different types of units recorded contralaterally to the deviated eye in the CV_2 group.

	Area 17			17/18 TZ (17/18 border)			Area 18			White matter			Total
	TC	I	NV	TC	I	NV	TC	I	NV	TC	I	NV	
CV_2 group N cells	7	157	48	60	14	3	2	120	29	1	13	3	457
%TC		3% (7/212)			78% (60/77)			1% (2/151)			6% (1/17)		
CV_1 group N cells	23	79	40	47	37	17	29	63	17	9	32	13	406
%TC		16% (23/142)			46.5% (47/101)			27% (29/109)			17% (9/54)		
NR group N cells	1	105	19	78	49	25	0	49	2	0	11	2	341
%TC		1% (1/125)			51% (78/152)			0% (0/51)			0% (0/13)		

Data are compared to previous ones obtained in the CV_1 and NR groups (see text for further details). TC, I, NV have respectively the same signification as in ***Table 1****.*

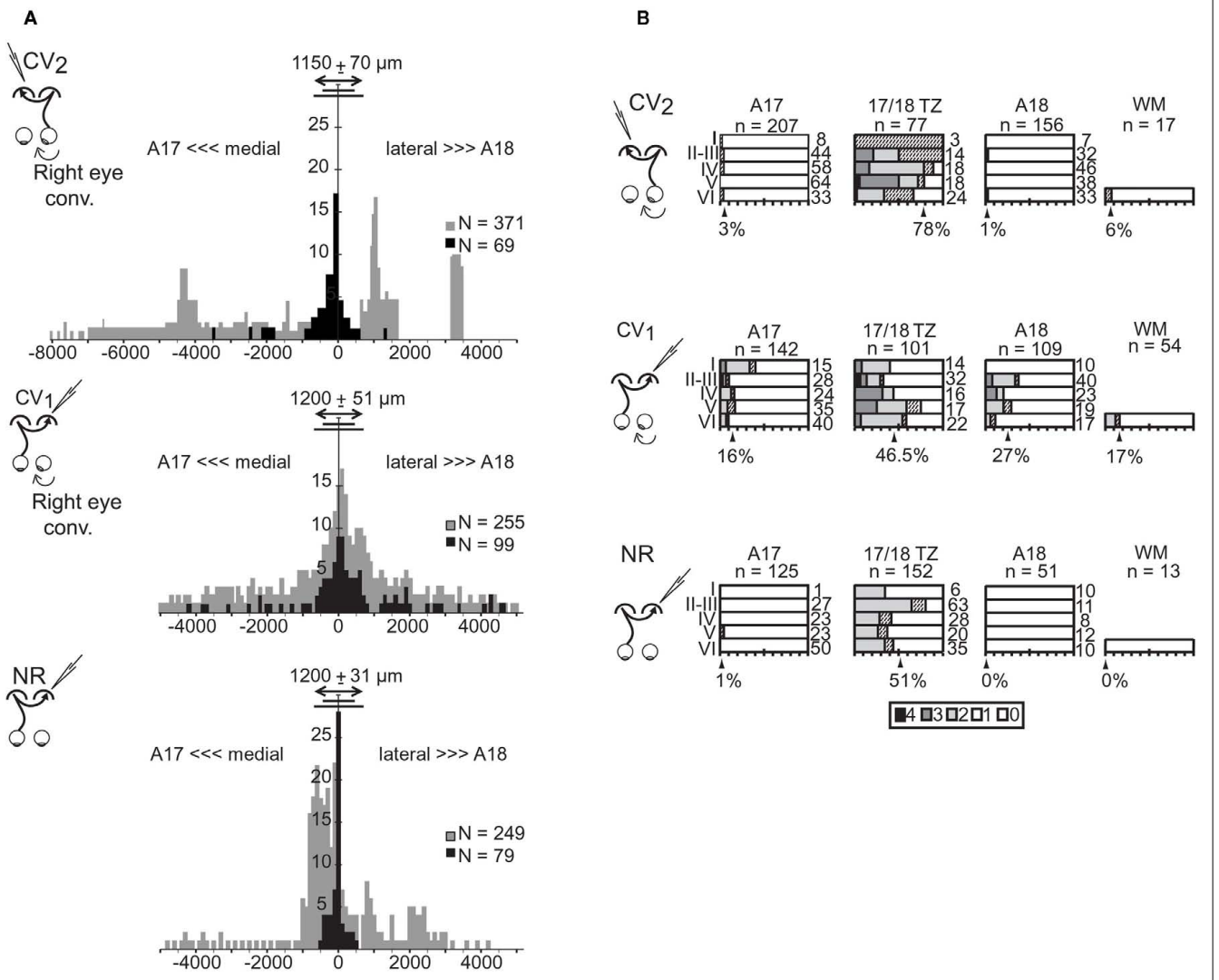

FIGURE 3 | Cortical distributions of the transcallosally activated units in visual cortex of strabismic (CV_1 and CV_2) and normal (NR) cats. **(A)** Tangential distribution of the cortical units activated (in black) or non-activated (in gray) through the transcallosal pathway. Abscissa, tangential distance (in µm) of the recorded cortical units from the center of the transition zone between A17 and A18 (17/18 TZ); negative values correspond to more medial locations in A17 while positive values correspond to more lateral locations in A18. Ordinates, number of units in samples. Double-headed arrow, short and long lines indicate mean, minimum, and maximum width of the 17/18 TZ, respectively. *n*: Number of units in samples. **(B)** Radial distribution of the transcallosally activated units (TC units) with respect to area and laminar location. For each cortical layer (I–VI), bars indicate the percentage of TC units relative to the total number of recorded units indicated on the right. Shading represents response strength (scale: 0–4). Arrowheads indicate the mean percentage of TC units in each region indicated below. WM, white matter in samples. *n*, number of cells. Data from the CV_1 and the NR group have been reproduced with permission from Milleret and Houzel (2001).

Orientation selectivity of the transcallosal units

In the CV_2 group, 44% of TC units were selective for the orientation of the stimulus (S) whereas the others were non-selective (NS, **Figure 4B**). Again, this proportion mainly resulted from TC units in the 17/18 TZ (48% of S units; 52% of NS units). In the other areas, both S and NS units also co-existed but their respective numbers were too low to draw any significant conclusion (A17: 6 S, 1 NS; A18: 1 S, 1 NS; WM: 1 NS).

These observations are similar to those of the CV_1 group (58% S units). The difference in incidence of S units between these two experimental groups did not reach significance (χ^2 test with Yates correction, $P = 0.1$). In contrast, the proportions of S units in the CV groups were significantly lower than that of the NR group (96%; Fisher exact test, $P < 0.0001$). Thus, strabismus alters the development of orientation selectivity of transcallosal units, and this is equivalent regardless of the eye being stimulated. Again, such data merely reflect the well known effects of strabismus on the orientation selectivity of the overall population of cortical neurons of primary visual cortical areas (cf. Boothe et al., 1985; Milleret, 1994a,b; Kiorpes and McKee, 1999 for review).

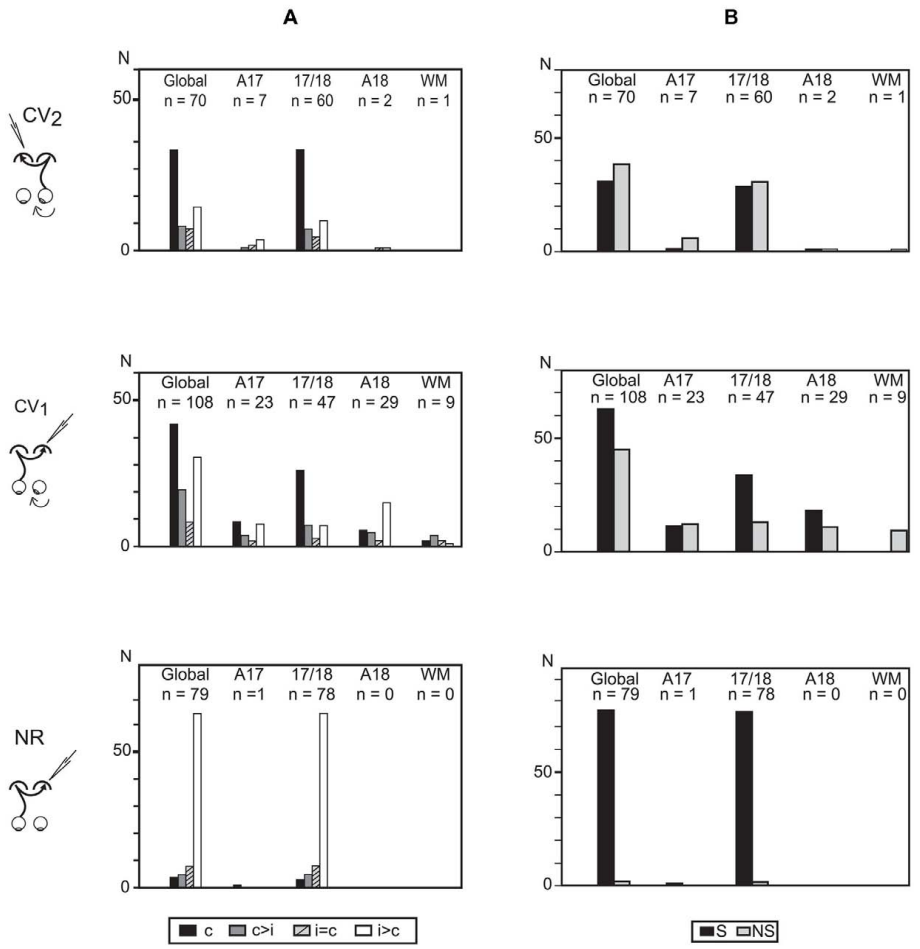

FIGURE 4 | Ocular dominance and orientation selectivity of the transcallosally activated units recorded in visual cortex of strabismic (CV_1 and CV_2) and normal (NR) cats. (A) Ocular dominance of transcallosal units recorded in A17, 17/18 TZ, A18, and the white matter (WM). Units were ranked into four classes according to the relative strength of response to contralateral (*c*) and ipsilateral (*i*) eye stimulation: *c*, units activated only through the stimulation of the contralateral eye; $c > i$, units activated preferentially through the contralateral eye; $c = i$, units activated equally through both eyes; $i > c$, units activated preferentially through the ipsilateral eye. Global, all units pulled together. *n*, number of units. **(B)** Orientation selectivity of transcallosal units recorded in A17, 17/18 TZ, A18, and WM. Orientation selective (S) and non-orientation selective (NS) units were distinguished. Global, all units pulled together, whatever their cortical location. *n*, number of units. Data from the CV_1 and the NR group have been reproduced with permission from Milleret and Houzel (2001).

Receptive field characteristics of the transcallosally activated units As described above, in group CV_2, some TC units received exclusively transcallosal inputs from the stimulation of the right (deviated) eye, while others received additional ipsilateral retino-GC inputs from the left (non-deviated) eye (cf. **Figure 1**). Their RFs will therefore be referred as TC-RFs or GC-RFs depending on the pathway stimulated to map them.

Size of the transcallosal and retino-geniculo-cortical receptive fields. In the CV_2 group, 58 TC-RFs could be mapped (**Figure 5A**). Their size varied greatly, ranging from 2 to 314 degrees^2, with a mean area of 64.4 ± 8.9 degrees^2. Within the 17/18 TZ (where most TC units were recorded), mean area was 70.2 ± 9.8 degrees^2. In contrast, the mean RF size for TC units recorded in the 17/18 TZ in group CV_1 was much lower (37.9 ± 7.2 degrees^2; **Figure 5B**). Therefore, the deviated (right) eye in the CV_2 group activated larger TC-RFs than the non-deviated (left) eye in the CV_1 group. Still, mean RF sizes in CV groups remained much larger that of the NR group (11 ± 1.5 degrees^2; **Figure 5C**).

Of the 33 binocular TC units recorded in the CV_2 group, it was possible to also map the GC-RFs of 31 units (7 in A17, 22 in the 17/18 TZ, 1 in A18, and 1 in the WM). Globally, the areas of these RFs also varied greatly (ranging from 2 to 615 degrees^2). The mean area was 74.1 ± 21.6 degrees^2 (67.8 ± 15.7 degrees^2 within the 17/18 TZ), very similar to that of the TC-RFs (64.4 ± 8.4 degrees^2). The same observation has been previously made in both CV_1 and NR groups (Milleret et al., 1994, 2005; Milleret and Houzel, 2001).

Spatial distribution of the TC-RFs. Globally, the elevations of TC-RFs in the CV_2 group ranged from $+5^\circ$ to -25° along the CVM (**Figure 6A**). We focused more specifically on TC-RFs within

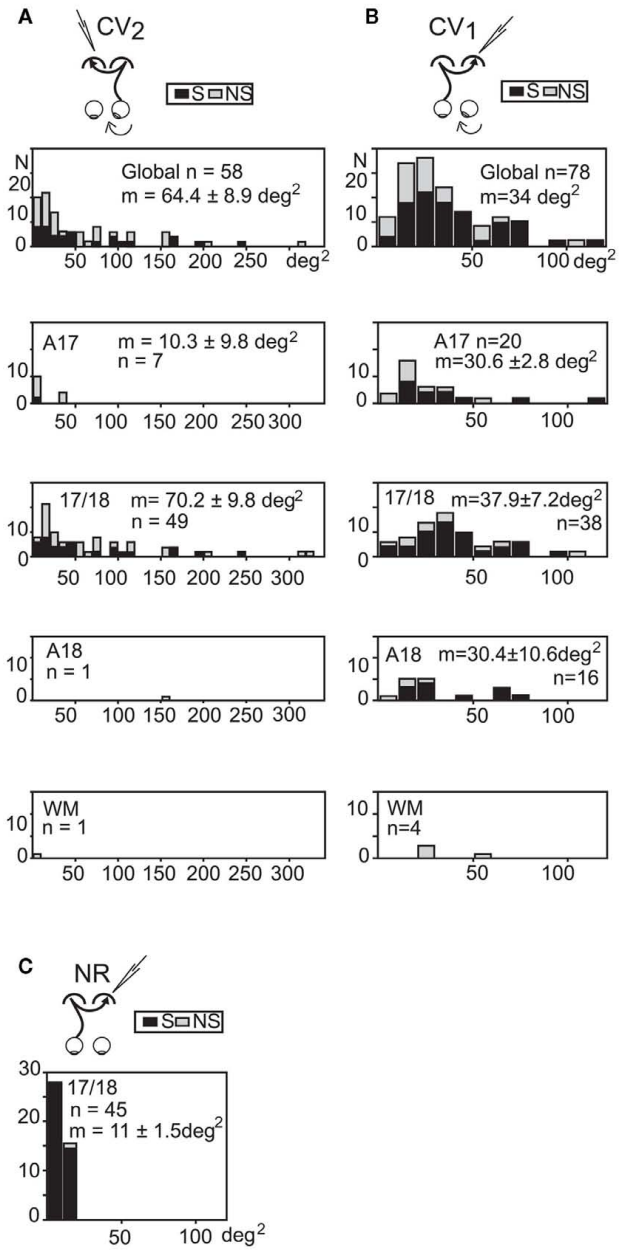

FIGURE 5 | Distribution of the sizes of the "transcallosal" receptive fields in the various explored cortical areas of strabismic and normally reared cats. (A,B) In each strabismic group, units were recorded from A17, A18, the 17/18 TZ (17/18) and the white matter (WM). Global, units from all areas. **(C)** TC units in the NR group were only found in the 17/18 TZ. S: orientation selective units; NS: units with no orientation selectivity. *m*: mean receptive field size ±SD. *n*: number of units. Bin width, 10 degrees^2. Data from the CV_1 and the NR group have been reproduced with permission from Milleret and Houzel (2001). See text for further details.

the 17/18 TZ, where the number of recorded units was sufficient to draw significant conclusions. The medial-most limit (Az_1) and lateral-most limit (Az_3) of the TC-RFs were, respectively, localized at $+7^\circ$ and -20° of azimuth, apart from the CVM (mean $Az_1 = -3.1^\circ \pm 0.5^\circ$; mean $Az_3 = -12.3^\circ \pm 0.5^\circ$); the azimuth of the centers (Az_2) of the TC-RFS ranged from -4° to -14.5° (mean $Az_2 = -7.6^\circ \pm 0.4^\circ$). As a result, the callosal visual field, i.e., the portion of visual field transferred to the target hemisphere through the CC, spanned a global width as large as 27°. It intersected the CVM but extended substantially within the hemifield ipsilateral to the explored cortex.

Comparing the CV_2 group to the CV_1 group revealed that both the width and the spatial location of their callosal visual fields differed markedly. In the CV_1 group, for units recorded in the 17/18 TZ, the Az_1, and Az_3 of the TC-RFs were $+2^\circ$ and $+19^\circ$, and the mean Az_2 was $9.5^\circ \pm 0.3$. Therefore, the width of their callosal visual field (17°) was 10° less than in the CV_2 group. Similar to CV_2, it mainly extended in the hemifield ipsilateral to the explored cortex but it no longer contacted the CVM, missing it by a few degrees. Note that, in the CV_1 group, numerous TC-RFs were additionally mapped in A17 and A18. The Az_1 and Az_3 of their TC-RFs were located at $(-1^\circ, +15^\circ)$ and $(-1^\circ, +14^\circ)$ respectively. When taken into account, the width of the global callosal visual field in CV_1 group became 20° ($-1^\circ/+19^\circ$), which was still narrower than the width in CV_2 group. Thus the two respective callosal visual fields do not occupy the same location in space.

The CV_2 and NR groups also differed slightly. In the NR group, within the 17/18 TZ, the Az_1, and Az_3 of the TC-RFs were $-6^\circ/+13^\circ$ (Milleret et al., 2005). The width of the callosal visual field in the NR group (19°) was therefore smaller than in the CV_2 one (27°). The mean Az_2 was $2.4^\circ \pm 0.6^\circ$ in the NR, indicating a substantial extent of the TC-RFs within the hemifield ipsilateral to the explored cortex. But this extent was smaller than that of CV_2 ($-7.6^\circ \pm 0.4$). Importantly, the callosal visual field abutted or intersected the CVM in both experimental groups, which is very different from the CV_1 group.

Spatial distribution of the GC-RFs. Globally, GC-RFs of TC units in the CV_2 group appeared at elevations ranging from $+5^\circ$ to -25° elevation (**Figure 6B**). Within the 17/18 TZ, the Az_1, and Az_3 of the GC-RFs were respectively localized at -5° and $+16.5^\circ$ distance from the CVM ($m\,Az_1 = 0.8^\circ \pm 0.8^\circ$; $m\,Az_3 = 9.2^\circ \pm 1.0^\circ$); the Az_2 of the GC-RFs ranged between 0° and $+5^\circ$ ($m\,Az_2 = 5.0^\circ \pm 0.9^\circ$). Thus, the width of the portion of visual field signaled by the GC-RFs was 21.5°. It intersected the CVM and extended substantially within the hemifield contralateral to the explored cortex.

Comparisons between the CV_2 and the CV_1 groups revealed similarities and differences (cf. **Figure 6B**). Within the 17/18 TZ, the Az_1, and Az_3 of the GC-RFs in the CV_1 group were -16° and $+3^\circ$. Therefore, as in the CV_2 group, GC-RFs in CV_1 are mainly located within the hemifield contralateral to the explored cortex. They occupy similar extents of visual field in both groups (19° vs. 21.5°), with some contact with the CVM. However, the mean Az_1, Az_2, and Az_3 of the GC-RFs differed greatly ($m\,Az_1$, $0.8^\circ \pm 0.8^\circ$ vs. $-4.3^\circ \pm 1.7^\circ$; $m\,Az_2$, $5.0^\circ \pm 0.9^\circ$ vs. $-7.2^\circ \pm 0.8^\circ$; $m\,Az_3$, $9.2^\circ \pm 1.0^\circ$ vs. $-13.7^\circ \pm 0.6^\circ$). The same observations held true when considering GC-RFs recorded in A17 of the CV_1 group (the Az_1 and Az_3 of the GC-RFs were -16° and $+9^\circ$ respectively, leading to a width of 25°, but $m\,Az_1 = -3.6^\circ \pm 1.2^\circ$, $m\,Az_2 = -6^\circ \pm 1.4^\circ$, and $m\,Az_3 = -8.4^\circ \pm 2.1^\circ$). The main difference between groups came from the GC-RFs of the TC units recorded in A18 of the CV_1 group. Indeed, with the Az_1 of the GC-RFs at -3.5°, none displayed any

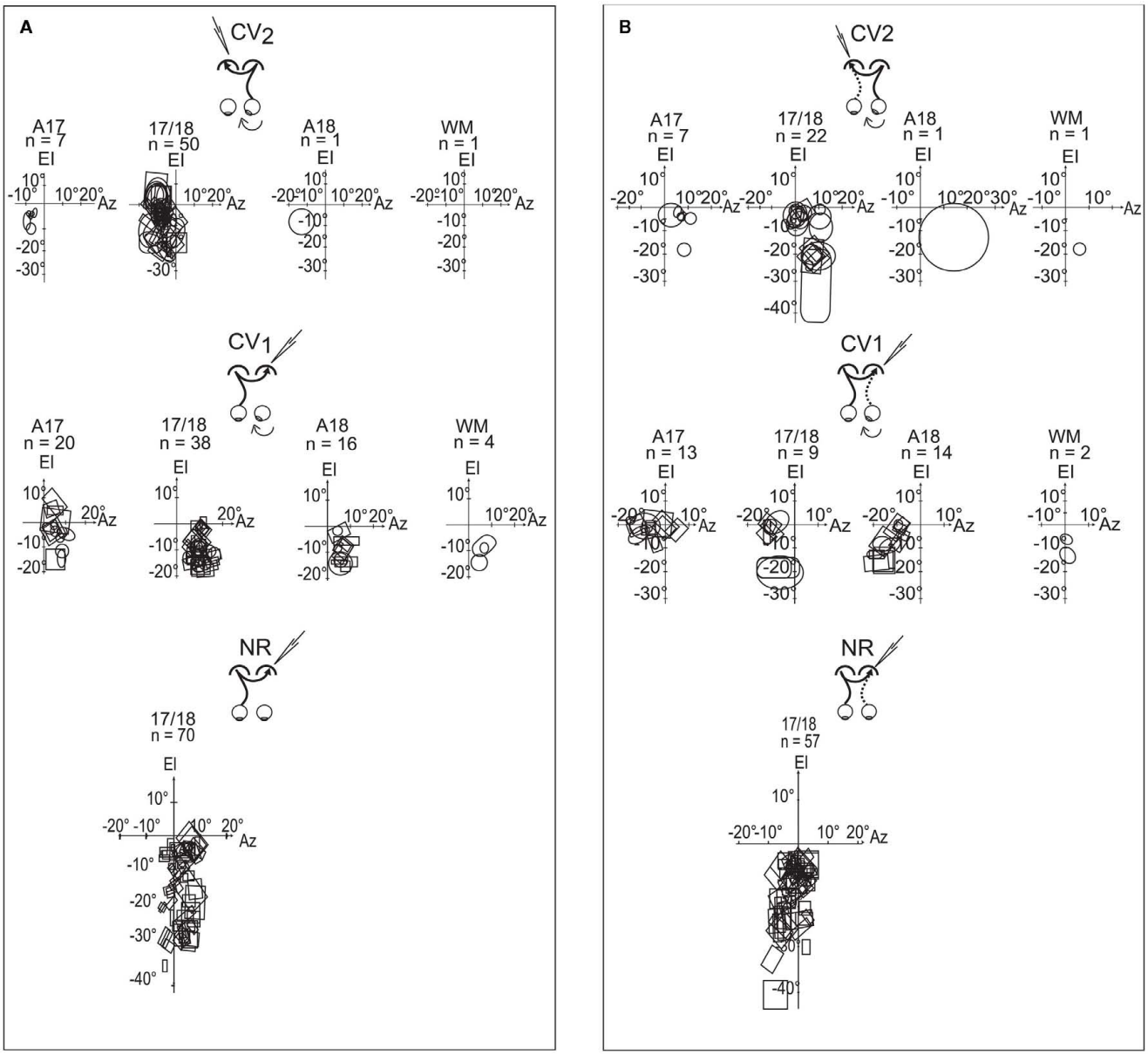

FIGURE 6 | Spatial distributions of the transcallosal receptive fields (TC-RFs) and the geniculo-cortical receptive fields (GC-RFs) of the transcallosally activated units of all strabismic and normally reared cats. (A) Spatial distribution of the TC-RFs mapped through visual stimulation of the eye contralateral to the explored cortex. **(B)** Spatial distribution of the GC-RFs mapped through visual stimulation of the eye ipsilateral to the explored cortex. In common to **(A,B)** the explored areas were A17, 17/18 border, A18 and WM below visual cortex; El is the elevation axis (central vertical meridian of the visual field); Az is the azimuth axis; rectangles and circles are contours of the minimum response fields of orientation selective and non-selective transcallosally activated units, respectively; *n* is the number of units. Data from the CV_1 and the NR group have been reproduced with permission from Milleret and Houzel (2001).

contact with the CVM. With the Az_3 at −23°, they extended more laterally within the hemifield contralateral to the explored cortex than GC-RFs in A17 and 17/18 TZ. Finally, with *m* Az_1, *m* Az_2, and *m* Az_3 at −8.7° ± 1.1°, −12.6° ± 1.1°, and 16.5° ± 1.3° respectively, the spatial distribution of the GC-RFs in the CV_1 group differed strongly from that of the CV_2 one.

The CV_1 group is already known to be highly abnormal (cf. Milleret and Houzel, 2001). In contrast, the comparison between the CV_2 group and the NR one revealed strong similarities. Within the 17/18 TZ, the Az_1, and Az_3 of the GC-RFs were −5° and +16.5° in the CV_2 group, and −7° and +13° in the NR group. The widths of the spatial distribution of these RFs were thus similar: 21.5° (CV_2) vs. 20° (NR). The GC-RFs also occupied similar positions in the visual field, extending substantially in the hemifield contralateral to the explored cortex in both cases, contacting the CVM. Some subtle differences existed, however, as revealed when

comparing the mean Az_1, Az_2, and Az_3 of the GC-RFs in both the CV_2 and the NR groups: *m* Az_1, $0.8^\circ \pm 0.8^\circ$ vs. $+1^\circ \pm 0.3^\circ$; *m* Az_2, $5.0^\circ \pm 0.9^\circ$ vs. $+0.9^\circ \pm 0.7^\circ$; *m* Az_3, $9.2^\circ \pm 1.0^\circ$ vs. $+1^\circ \pm 1^\circ$. It is clear that the mean values of Az_2 and Az_3 are higher in CV_2 group than in NR group, but *m* Az_1 are very similar.

Position disparity of the receptive fields of binocular units. As expected from the global spatial distributions described above, the position of TC-RFs and the GC-RFs of binocular TC units in the CV_2 group generally did not match. This held true while both eyes were in their "paralyzed" position, without any correction for strabismic angle (data not shown). This also held true after correction of the data for strabismus angle by superimposing the projections of both *areas centrales*. In this condition, the TC-RFs were always located in the hemifield ipsilateral to the explored cortex, whereas the GC-RFs were always located in the hemifield contralateral to the explored cortex. This resulted in a systematic crossed position disparity between pairs of RFs of binocular units, whose amplitude varied from cell to cell, even within the course of a single recording track (**Figure 7A**). Within the 17/18 TZ, 21 pairs of RFs could be mapped. The mean position disparity between couples of RFs was $13.9^\circ \pm 5.6^\circ$, with a minimum of 7° and a maximum of 29°. The small numbers of pairs of RFs in each animal precluded tests of correlation of angle of disparity with the angle of strabismus. Only one unit exhibited an overlap between TC- and GC-RFs, and its OI was poor (OI = 4.6%).

Comparing the CV_2 and CV_1 groups for the 17/18 TZ revealed similarities with only crossed disparities in both groups and a null OI in almost all cases (**Figure 7B**). The mean position disparity in CV_1 group ($18.7^\circ \pm 0.4$) was only slightly higher than in CV_2 group.

In contrast, comparison between the CV groups and the NR group revealed major differences (**Figure 7B**). In the NR group, position disparities could be crossed type, but also null or uncrossed. Moreover, because position disparities are small in the NR group ($5.4^\circ \pm 0.4^\circ$), the OI is far from null (22%). Therefore, strabismus greatly alters this overlap between TC- and GC-RFs. Altogether, this indicates that strabismus leads to some distortions in the fine organization of the TC and/or the GC retinotopic maps in visual cortex.

ANATOMY OF TRANSCALLOSAL AXONAL ARBORIZATIONS

The functional data described above demonstrate electrophysiologically that an asymmetrical interhemispheric transfer of visual information develops between visual cortical areas in early unilateral strabismic cats. Here we present the anatomical structure underlying this asymmetry from biocytin injections in the hemisphere *contralateral* or *ipsilateral* to the deviated eye (CV_1 and CV_2 groups respectively). Eight callosal axons were reconstructed in 3D in the CV_1 group (cf. **Figure 8B**). Four of these originated from A17, three from the 17/18 TZ, and one from A18. In the CV_2 group, nine callosal axons were reconstructed, originating from A17 ($n = 4$) or 17/18 TZ ($n = 5$); cf. **Figure 8A**). Morphological characteristics of these axons are fully described in **Tables A1** and **A2** in Appendix. Callosal axons in NR animals serve as references (from Houzel et al., 1994).

Global organization of the CV callosal axons

Five parameters are used to describe the global organization of the CV callosal axons: the localization of the first node, the general architecture of the axons, the tangential distribution of the terminal arbors as well as the terminal boutons and finally the radial distribution of the terminal boutons.

Localization of the first node of the callosal axons. Callosal axons in the CV animals could branch first at one of the three following positions: very deep in the WM below cortex (including when just exiting the CC), just below cortex or within the visual cortex itself (cf. **Figures 8B** and **9A**). But callosal axons branching first *very deep* below cortex were clearly the most numerous (CV_1 group, 4/8; CV_2 group, 5/9; cf. **Table A4** in Appendix). Most often, they branched as deep as the fundus of the splenium sulcus or the cingular sulcus, depending of the antero-posterior position (see for examples axons BCV7, BCV9, CV14-V in the CV_1 group and axons CVE4-1, CVE4-2, and CVE4-A in the CV_2 group in **Figures 8** and **9A**). Notice that these characteristics have also been found in early monocularly deprived animals (through monocular occlusion), within the hemisphere ipsilateral to the deprived eye (Foubert et al., 2010), suggesting that this might occur systematically after a monocular alteration of vision occurring early in life (see also Discussion).

In comparison, in the NR adults, only one callosal axon branched first rather deep in the WM (axon 16E in **Figure 9A**; **Table A4** in Appendix). For the 16 remaining axons, the first node was systematically located near the visual cortex, either between the fundus of the lateral sulcus and the convexity of the lateral and post-lateral gyri, often beneath A18, or within the cortex itself. Thus the morphology of the callosal axons is different in strabismic and NR animals with respect to this parameter.

Architecture of callosal terminal axons. On the basis of our classification (see Materials and Methods), out of the eight callosal axons that were reconstructed in 3D in the CV_1 group, three displayed a *simple* architecture (37.5%) while all the remaining ones displayed a *multiple clustered architecture* (62.5%). Each axon had one to three branches, and one to eight columns (cf. **Table A1** in Appendix). In the CV_2 group, out of the nine callosal axons that were 3D reconstructed, most axons also displayed architecture or the other: four displayed a *simple* architecture (44%) while four others displayed a *multiple clustered architecture* (44%). Similar to the CV_1 Group, their number of branches ranged from 1 to 3 and the number of columns from 1 to 8. One exception however was found with axon CVE4-A which divided into three main branches in the WM but did not enter the visual cortex (cf. **Table A2** in Appendix).

Globally, most of the architectures described for NR animals also existed in the CV groups. Overall, no difference could be found between groups (see **Table A4** in Appendix, second row). One atypical axon was however found in the CV_2 group, with branches in the WM but no terminals in visual cortex. Since all other axons in the same cat with similar trunk diameters could be reconstructed in 3D up to their terminals (cf. axons CVE4-1 and CVE4-2 in **Table A2** in Appendix), one interpretation is that this

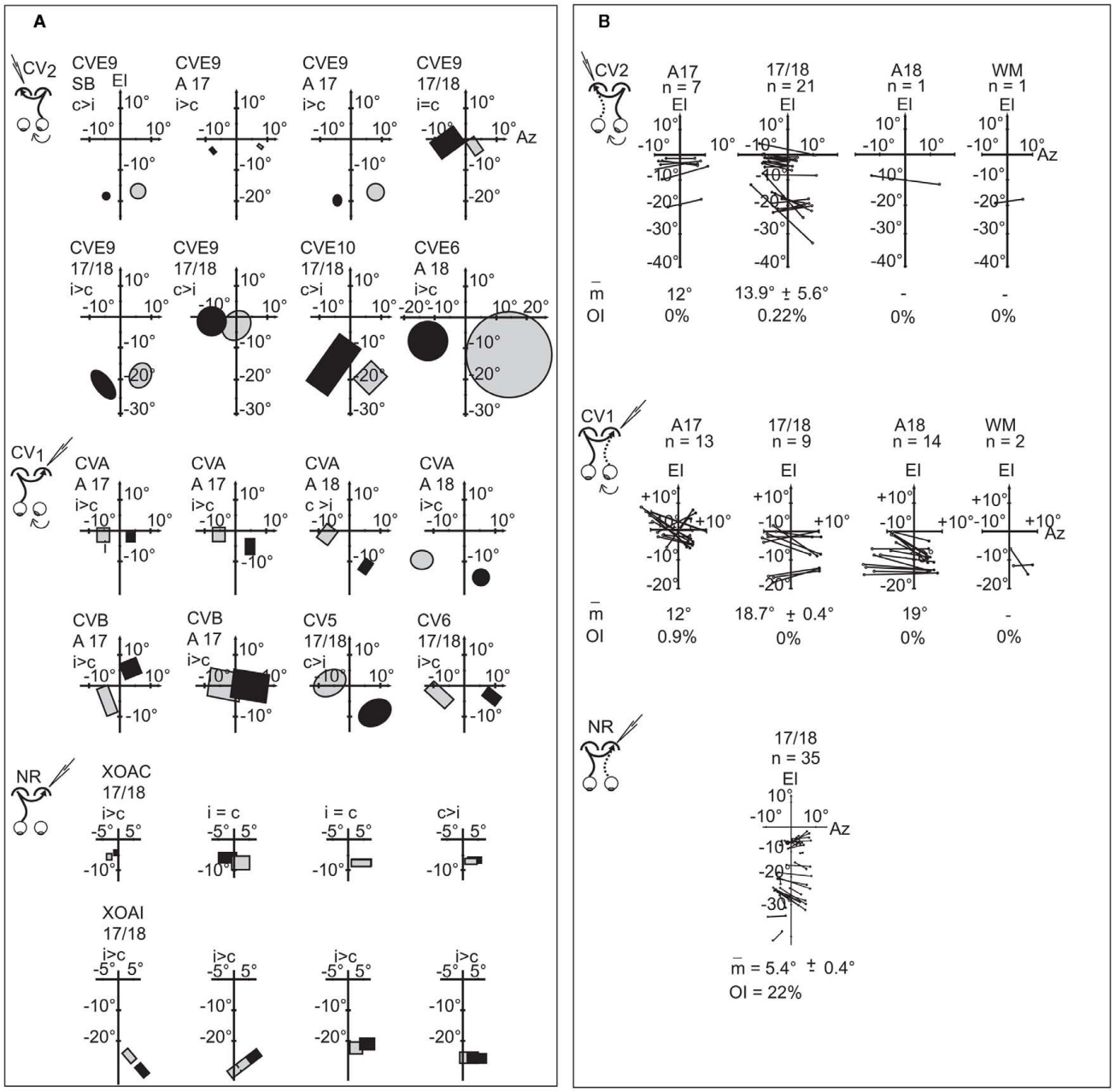

FIGURE 7 | Position disparity between pairs of receptive fields of the binocular transcallosally activated units after off line realignment of the eyes in convergent strabismics. (A) Geniculo-cortical receptive fields (in gray) and corresponding transcallosal receptive fields (in black) of a few representative binocular TC units recorded in different animals of each experimental group (CV9, CV10, and CVE6 in the CV_1 group; CVA, CVB, CV5, and CV6 in the CV_2 group; XOAC and XOAI in the NR group). Rectangles and circles, contours of the minimum response field of orientation selective and non-selective TC units, respectively. *c*, $i > c$, $i = c$ and $c > i$ indicate the ocular dominance of each unit as in **Figure 5**. **(B)** Spatial distributions of pairs of receptive fields of binocular TC units. Lines connect centers of couples of RFs observed for individual cells and indicate position disparity. *m*, mean position disparity value ± SEM (in deg); OI, overlap index (in %). El and Az, elevation and azimuth axes; *n*, number of units. Data from the CV_1 and the NR group have been reproduced with permission from Milleret and Houzel (2001).

growing axon could not reach visual cortex before the end of the critical period.

Areal distribution of callosal terminal arbors. As summarized in both **Table A1** in Appendix axon per axon and **Figure 9B** (all axons together), in the CV_1 group, callosal terminal arbors originating from the 17/18 TZ terminated mostly in A18. However, a few additional terminal branches could be also found in A17, 17/18 TZ, and even in A19. Those originating from A17 mostly terminated in the 17/18 TZ and A18, with a few branches also in A17. The only axon

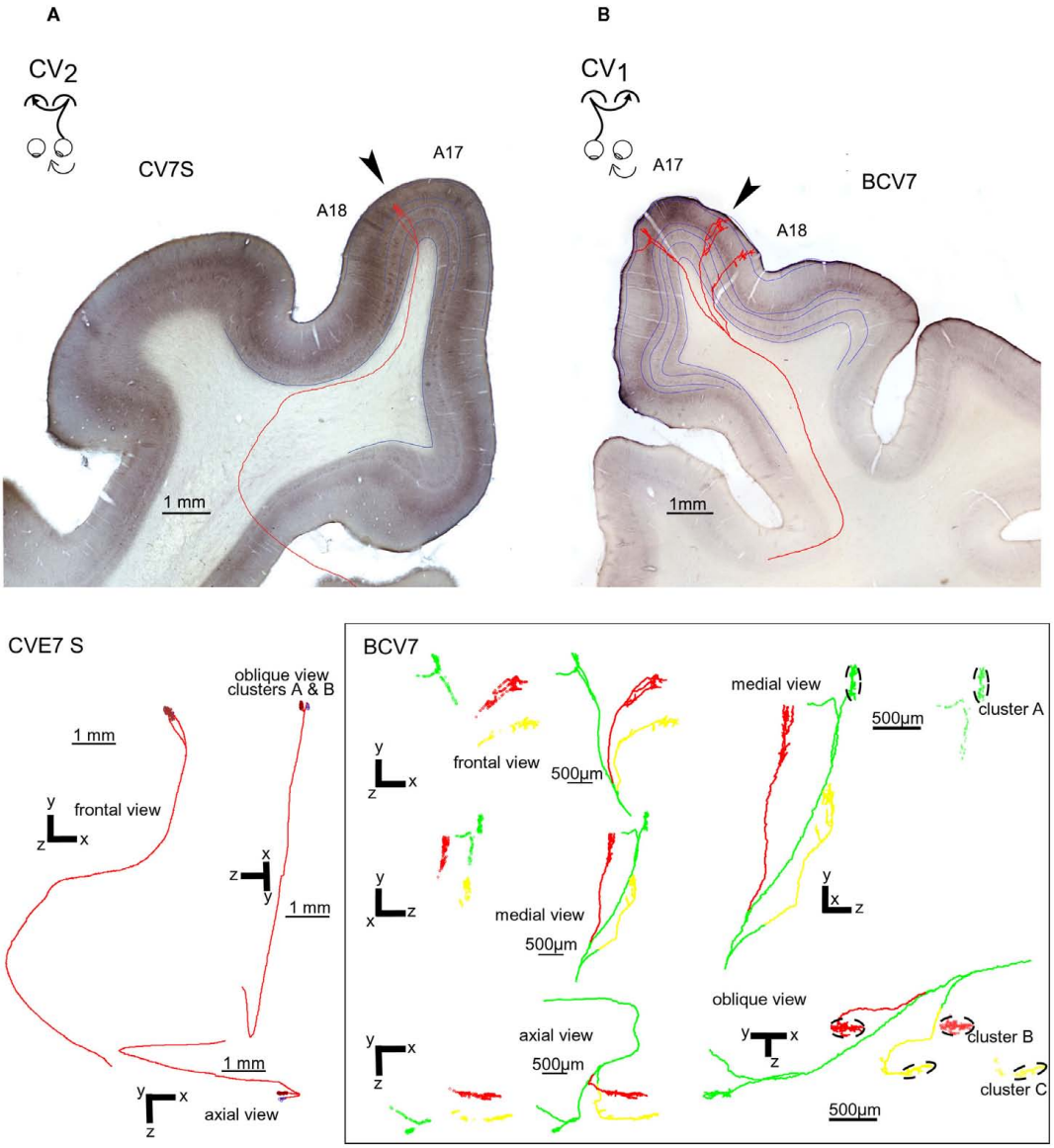

FIGURE 8 | Representative callosal terminals of the CV_1 and CV_2 groups after biocytin injection in the contralateral hemisphere and reconstruction in 3D. (A) Callosal terminal from the CV_2 group (named "CV7S," i.e., axon "S" from cat CV7). The axon originated from A17 in the right hemisphere, at stereotaxic coordinate P4. The trunk of this axon has a diameter of 0.6 µm and its total length from the midline was 15.52 mm. It ended in the 17/18 TZ (arrow) in the left hemisphere at P3–P4. Its architecture was "simple." As represented below, its main branch divided in the gray matter to form two clusters in the lateral gyrus. Altogether, its antero-posterior and medio-lateral extensions were 175 and 249 µm respectively. It also displayed a total of 93 boutons and their distribution was supra-granular. **(B)** Callosal terminal from the CV_1 group (named "BCV7," i.e., axon 7 from cat BCV). It originated from A17 in the left hemisphere, at stereotaxic coordinate AP0. The diameter of its trunk was only 0.4 µm and its total length was 32.23 mm. It also ended in the right hemisphere at antero-posteriority AP0. It displayed a multiple clustered architecture. Its terminal formed three different tufts which were very distant from each other in the marginal and in the lateral gyrus. They were located respectively in A17, A18, and in the 17/18 TZ (arrow). As a consequence, this axon had a rather large frontal extent (3789 µm) whereas it ranged antero-posteriorly over only 750 µm. This axon had a total of 1056 boutons ending for the vast majority in layer II/III (76%) and V (15%). The tuft ending in A17 divided itself in layer VI in two branches: one of them formed a terminal cluster of 231 boutons, 230 of them being located in layer II/III (cluster A). The other branch formed 88 "en passant" boutons, with 50 of them being located in layer II/III. The tufts ending in A18 and in the 17/18 TZ formed each several branches and two separate clusters: one in the 17/18 TZ (cluster B) and one in A18 (cluster C). The laminar distribution of BCV7 was supra-granular (see details about branches and clusters in the lowest part of the figure).

originating from A18 terminated strictly in A18. Differences in stereotaxic coordinates could be observed between the injection site and the callosal terminal zone (cf. for example axons CV13-A, CV13-B, CV13-C, and axon BCV9 in **Table A1** in Appendix; cf. also **Figure 9B**). Thus, globally, the CV_1 group seemed to preserve the "non-mirror" organization of the interhemispheric callosal

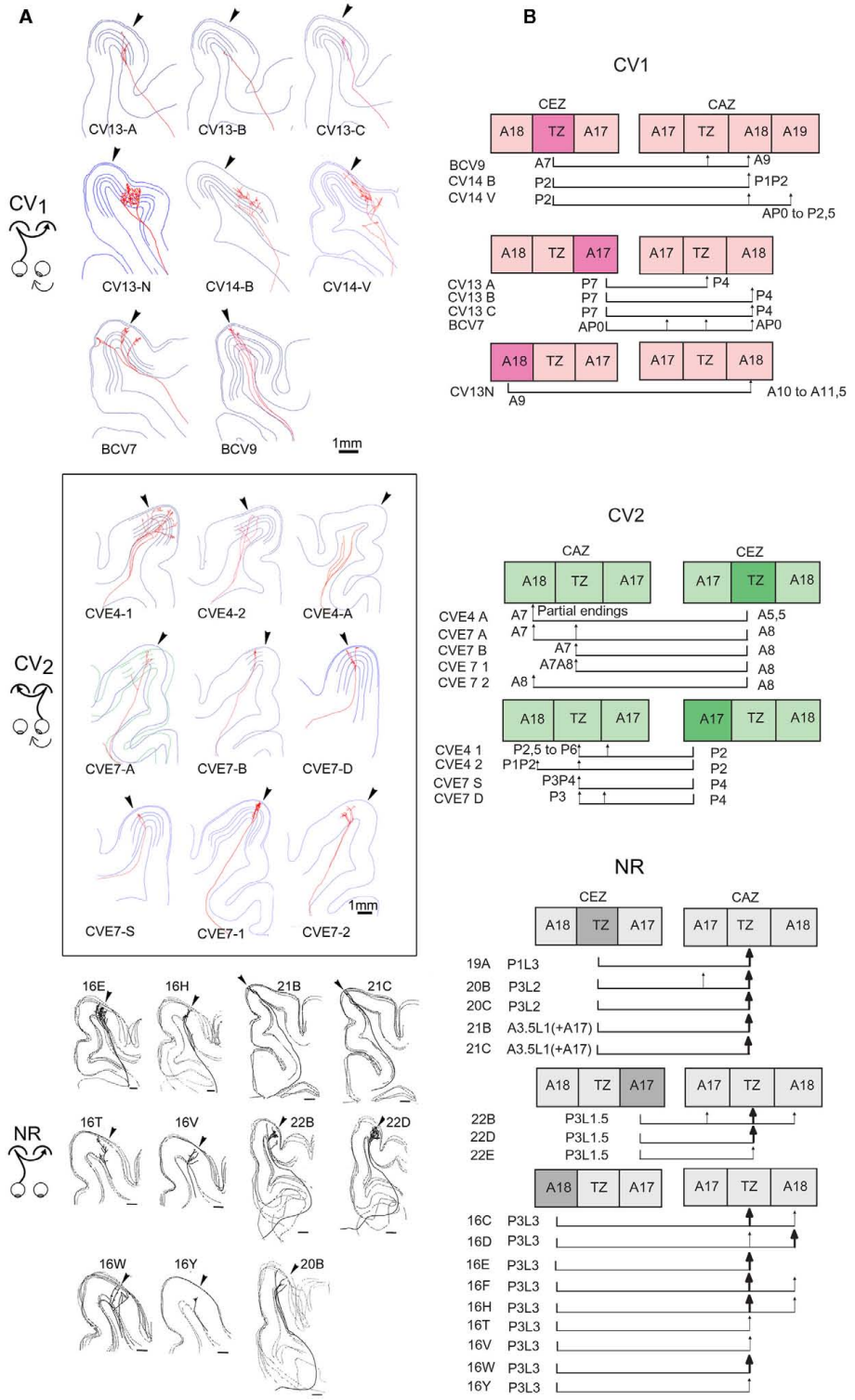

FIGURE 9 | Comparing the tangential distributions of the callosal terminals in the respective groups as a function of their origin. **(A)** Frontal representation of all the individual callosal axons that were reconstructed in 3D from serial sections of visual cortex in each experimental group. Arrow, transition zone between A17 and A18 (TZ). **(B)** Tangential distribution of the terminals of each callosal axon as a function of their origin (TZ, A17, or A18), with corresponding stereotaxic coordinates. CEZ, callosal efferent zone; CAZ, callosal afferent zone. Data from NR group have been reproduced with permission from Houzel et al. (1994).

connections that has been described in the NR animals (see Introduction for further details and **Figure 9**). But connections were heterotopic instead of being homotopic. In addition, the callosal terminal arbors in the CV_1 group were not restricted to the 17/18 TZ as observed in NR animals, but rather extended additionally to A17 and A18. This also held true at the level of single neurons: as indicated in **Table A1** in Appendix, single callosal terminal arbors could extend from 50 to 950 μm along the antero-posterior axis ($m = 475$ μm) and from 40 to 3789 μm along the medio-lateral one ($m = 1612$ μm). These values were much greater than those found in NR cats, for which callosal terminal arbors occupied only 0.5–2.5 mm^2 in the 17/18 TZ, and extended maximally from 200 to 2000 μm.

The axon distribution in the CV_2 group (cf. **Table A2** in Appendix and **Figure 9B**) was different from that observed for the CV_1 group. Callosal terminals originating from 17/18 TZ also terminated preferentially in 17/18 TZ and A18. Those originating from A17 terminated mainly in 17/18 TZ and A17 with a few branches in A18. But the stereotaxic coordinates of both the injection site and the terminals branches were similar. Thus here, at least globally, both the callosal connections between primary visual cortices and the callosal terminal arbors displayed apparently normal characteristics. Callosal terminals were also mostly located in 17/18 TZ like in NR animals. Some abnormalities could however be found at the level of single callosal terminals, which extended from 50 to 1000 μm along the antero-posterior axis ($m = 453$ μm) and from 235 to 4353 μm along the medio-lateral one ($m = 1321$ μm). These values were thus, as in the CV1 group, greater than the ones found in NR animals.

Areal distributions of the synaptic boutons. In the CV_1 group, the number of boutons per axon varied from 38 to 1056 (cf. **Table A1B** in Appendix). More than half of them were located in A18 (57%, **Table A3A** in Appendix) while others were distributed in the 17/18 TZ (31%) or in A17 (12%). Thirty boutons were also located in the WM, either below A17 ($n = 9$) or below A18 ($n = 21$). In comparison, the percentages of the synaptic boutons of the callosal axons in the NR adult animals were 78% in the 17/18 TZ, 1% in A17, and 21% in A18. Therefore, the areal distribution of the synaptic boutons of the callosal terminals in the CV_1 group is far from being normal (χ^2 with Yates correction, $P < 0.01$).

In the CV_2 group, data were again different (cf. **Table A2B** and **Table A3B** in Appendix). The number of boutons per axon could vary from none to 602. For recall, the axon with no bouton did not enter the cortex likely because the critical period ended before (cf. axon CVE4-A in Architecture of Callosal Terminal Axons). The areal distribution of the synaptic boutons resembled that found in the NR adults. In particular, a majority of boutons were located in the 17/18 TZ (68.5%). Still, this distribution was different from the one obtained in NR, with additionally 10.5% boutons in A18 and 21% of boutons in A17 (χ^2 with Yates correction, $P < 0.01$). Evidently, the difference between CV_1 group and CV_2 group is significant (χ^2 with Yates correction, $P < 0.01$).

Although this will not be developed here, the synaptic boutons of callosal axons in both CV_1 and CV_2 groups formed clusters (or "columns"). Similarly to the NR group, their number ranged from 1 to 8 according to the axon (cf. **Table A1A** and **Table A2A** in Appendix).

Laminar distributions of the synaptic boutons. In the CV_1 group, the laminar distributions of the synaptic boutons were supra-granular ($n = 2$), bi-laminar ($n = 3$), granular ($n = 1$), trans-granular ($n = 1$), or infragranular ($n = 1$). Thus, every type of distribution was represented although the supra-granular and the bi-laminar distributions seemed to be more common (**Table A1B** in Appendix). In the CV_2 group, by contrast, only two configurations were found: supra-granular ($n = 5$) and trans-granular ($n = 3$); cf. **Table A2B** in Appendix. This resembles the NR group, with most callosal axons displaying a supra-granular distribution of their synaptic boutons.

In both strabismic groups, most callosal synaptic boutons were found in layers II/III (71% in the CV_1 group and 67% in the CV_2 group) while the remaining ones were distributed in all other cortical layers (cf. **Tables A3A,B** in Appendix). This held true for terminals located in A17, A18, or in 17/18 TZ. Surprisingly, this is similar to the data of the NR animals where on average 70% of the callosal synaptic boutons were located in the supra-granular layers (A17: 86%, 17/18 TZ: 72%; A18: 62%); cf. **Table A3C** in Appendix. The strabismics were not significantly different from normals (CV_1 vs. NR: χ^2 with Yates correction, $P > 0.05$; CV_2 vs. NR: χ^2 with Yates correction, $P > 0.05$; cf. **Table A3D** in Appendix). But a significant difference was found between CV_1 and CV_2 distributions (χ^2 test with Yates correction, $P < 0.05$).

Note that, in contrast with NR adult animals, a few additional callosal synaptic boutons appeared in the WM of both strabismic groups, just below A17, A18, and 17/18 TZ (cf. **Tables A3A,B** in Appendix). Thus, strabismus seemed to increase their incidence in this particular part of the cortex (cf. **Table A1B** and **Table A2B** in Appendix).

Quantitative analysis of the CV callosal axons

This section quantifies parameters characterizing the morphology of callosal axons: mean trunk diameter, mean diameter of first order branches, mean lengths of first to fifth order branches, and mean numbers of nodes, terminals, and synaptic boutons (cf. **Table A4** in Appendix). Each parameter tested for differences between the three experimental groups and only the three parameters found to be significantly different among groups are described.

Mean lengths of the first to the fifth order branches of the callosal axons. In the CV_1 group, the mean length of the first to fifth order branches were respectively: 1417 ± 1341, 695 ± 865, 452 ± 244, 247 ± 104, and 141 ± 68 μm. In the CV_2 group, the mean lengths of the first to fifth order branches were respectively: 2356 ± 1214, 1058 ± 1315, 342 ± 342, 263 ± 280, and 115 ± 86 μm (cf. **Table A4** in Appendix). For comparison, in the NR animals, the mean lengths of these various branches were respectively: 1599 ± 1366, 433 ± 494, 253 ± 236, 132 ± 76, and 79 ± 39 μm.

Statistical analysis (see **Table A4** in Appendix) revealed no difference between the lengths of the first and of the second order branches. By contrast, the branches of superior orders were all significantly longer in the CV_1 group compared to the NR

group. Note, however, that no significant difference could be found between the CV_1 and the CV_2 groups.

Mean numbers of nodes of the callosal axons. The mean number of nodes per axon was 61 ± 50 in the CV_1 group (range: 2–88), 31 ± 30 in the CV_2 group (range: 2–90), and 124 ± 88 in the NR group (range: 18–299). The mean numbers of nodes for both CV groups were therefore systematically lower than the one observed for the NR group. However, only a significant difference could be found between the CV_2 group and the NR group (Wilcoxon test, $P = 0.003$, $Z = 2.9713$; cf. **Table A4** in Appendix).

Mean numbers of terminals of the callosal axons. The mean number of terminals per axon was 62 ± 50 in the CV_1 group (range: 3–90) and 34 ± 30 in the CV_2 group (range: 3–92). These values were lower than that found in the NR group (125 ± 88; range: 19–300). However, statistical differences could only be found between the CV_2 group and the NR (Wilcoxon test, $P = 0.0033$, $Z = 2.94$).

DISCUSSION

While previous data in the literature were sparse and controversial (cf. Introduction), this study demonstrates unequivocally for the first time that early unilateral convergent strabismus does lead to the development of asymmetrical interhemispheric connections through the corpus callosum (CC) in cat primary visual cortex. Differences in functional characteristics of the visual interhemispheric transfer within each hemisphere were identified first. Asymmetry between the hemispheres was confirmed anatomically, after labeling and reconstructing in 3D single callosal axons. Such asymmetry resulted from specific anatomo-functional abnormalities in each hemisphere (**Figure 10**). Consequently, the CC is no longer able to properly unify the two visual hemifields. Two new general mechanisms are proposed to explain this abnormal development of the CC.

ASYMMETRICAL CALLOSAL CONNECTIONS DO DEVELOP AFTER EARLY UNILATERAL CONVERGENT STRABISMUS IN CAT VISUAL CORTEX

In NR adult cats, the transfer of visual information from RH to LH is similar to that from LH to RH. This is because both the callosal neurons and their terminals are distributed equally in each hemisphere (e.g., Leicester, 1968; Innocenti and Fiore, 1976; Payne, 1990a,b; Payne and Siwek, 1991; Houzel et al., 1994; Olavarria, 1996, 2001). One may say that callosal connections are organized *symmetrically* between the hemispheres (**Figure 10B**). By contrast, as assessed by the functional and the anatomical data we report here, callosal connections after an early unilateral convergent strabismus are abnormal and develop *asymmetrically* (**Figure 10A**).

Comparing first the distribution of the TC units established here in the CV_2 group to the one we have established previously in the CV_1 group (Milleret and Houzel, 2001), we found that they differed markedly in LH and RH of strabismics. The most marked result was a clear difference in the tangential distribution of TC units: it was almost normal in the hemisphere ipsilateral to the non-deviated eye (LH of CV_2 group), in contrast with the exuberance in the hemisphere ipsilateral to the deviated eye (RH of CV_1 group). In the latter group, the location of TC units extended to both in A17 and A18, thus much further than the 17/18 TZ. The observation of a functional asymmetry is reinforced by the differences in the percentages of TC units within each cortical region. Within the 17/18 TZ, which was the main location of the TC units in both experimental groups, the proportion of the TC units was significantly higher in the CV_2 group than in the CV_1 one (78 vs. 46.5%). In contrast, the proportion of TC units within A17 and A18 was significantly lower in the CV_2 group than in the CV_1 one (3 vs. 16% and 1 vs. 27% respectively). The comparison between the laminar distributions of the TC units in both CV groups also showed asymmetry. Focusing on the 17/18 TZ, where TC units were numerous for each experimental group, those recorded in the CV_2 group (LH) were found in all cortical layers and their radial distribution did not exhibit any specific bias. In contrast in RH of the CV_1 group, TC units were predominantly located in infragranular layers.

The anatomical study supports these functional results, but characterizes this asymmetry in greater detail by analyzing the morphological differences between single callosal axons of each hemisphere. This shows that both the tangential and the radial distributions of the terminals of these axons differed markedly between hemispheres. Furthermore the tangential distribution of their synaptic boutons differed bilaterally. Overall, both qualitative and quantitative analyses indicate that the asymmetry results from a profound but different reshaping of the morphology of single callosal axons within each hemisphere, which is reflected in the functional responses. Such data are in agreement with two early studies which suggested that an exuberant distribution of callosal terminals was present in the hemisphere ipsilateral to the deviated eye while a rather normal distribution was present in the hemisphere ipsilateral to the non-deviated eye after unilateral convergent strabismus (Lund and Mitchell, 1979; Berman and Payne, 1983).

Of interest, this asymmetry reflects anomalies in both hemispheres compared to the normal situation. But the most important abnormalities were systematically found in RH, i.e., in the hemisphere ipsilateral to the deviated eye (CV_1 group). As developed below, this is particularly important to explain the origin of the functional asymmetry that develops in visual cortex after unilateral strabismus. Functionally, in the NR group, almost all TC units are located in the 17/18 TZ. In contrast, in the CV_1 group (RH), a substantial proportion of TC units were abnormally present in A17 and A18 as well as in the WM. On the other hand, in the CV_2 group (LH), the tangential distribution of the TC units was closer to normal, but the proportion of TC units in the 17/18 TZ was significantly higher than normal. In addition, a few TC units were abnormally located at rather eccentric portions of A17 and A18 as well as in the WM. The same holds true when considering the radial distribution of the TC. Comparison of anatomical data between strabismic and normal animals also revealed abnormalities in both hemispheres after unilateral strabismus, with the most important abnormalities in RH, even if both RH and LH exhibited an areal distribution respecting the normal "non-mirror" organization of the interhemispheric callosal connections (cf. Introduction). Callosal terminals within RH were mostly heterotopic, while those in LH were mostly homotopic as in normal. The tangential distribution

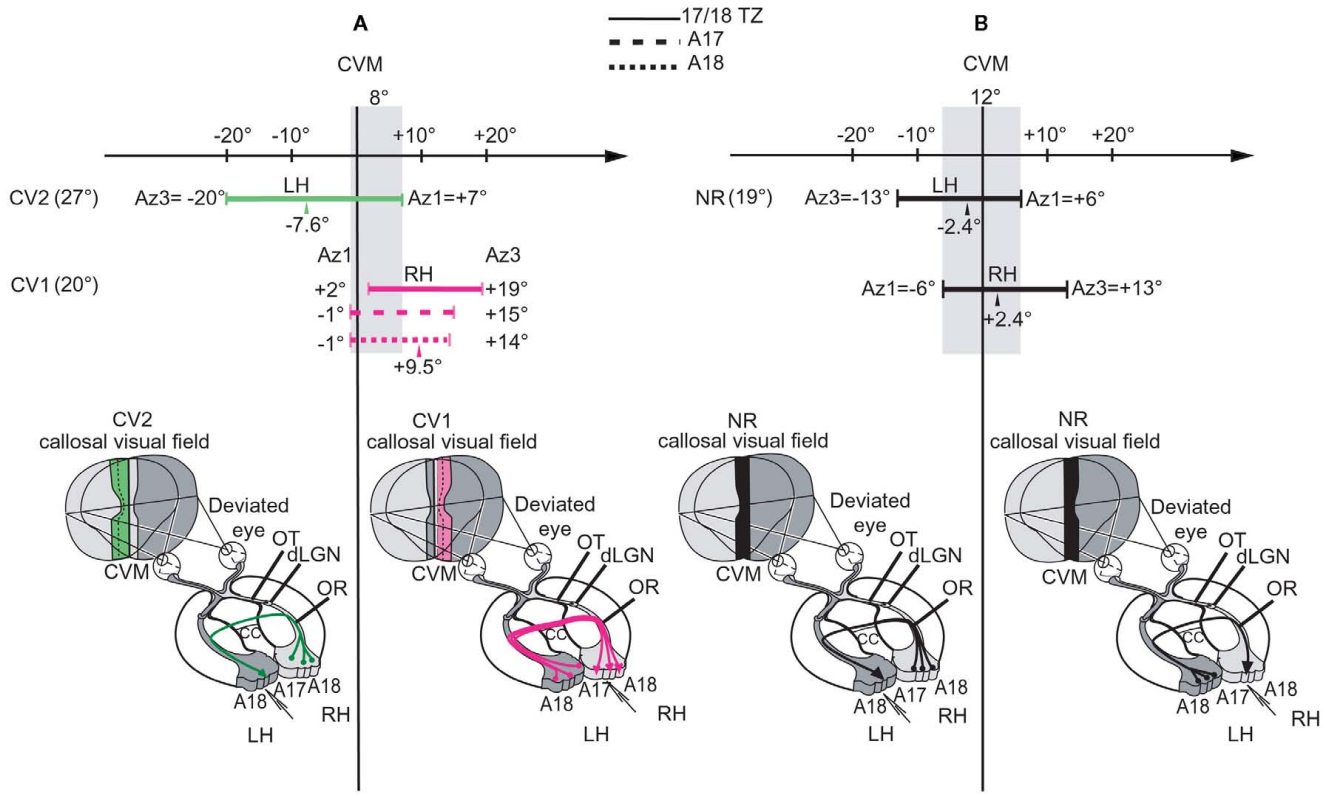

FIGURE 10 | Summary of the organization of the callosal connections and spatial characteristics of the "callosal visual field" in the CV_1 and CV_2 groups compared to NR. The lowest part of each panel summarizes the location of both the callosal neurons (filled circles at bases of colored lines) and their terminals (arrows) in LH and RH. It also summarizes the spatial distribution of the receptive fields of the transcallosally activated units (TC-RFs) that were mapped while exploring 17/18 TZ, i.e., the callosal visual field corresponding to this specific region (in pink, green, or black depending on the experimental group). For more precision about it, in the upper part of each panel, we have additionally reported the exact values of the azimuths (in degrees) of the medial-most (Az_1) and the lateral-most (Az_3) borders of the TC-RFs mapped through recordings 17/18 TZ as well as A17 and A18 (cf. at top of the figure for their respective representations). This allows defining the width of the "callosal visual field" encoded by each of these cortical regions. In each case, the arrow indicates the mean azimuth of the center of the TC-RFs ($m\,Az_2$). At left, the maximum width of the "callosal visual field" is also indicated. **(A)** Illustration of the asymmetrical organization of both the callosal connections and the callosal visual field in the strabismic cats. In the CV_1 group (in pink), callosal neurons (in LH), and callosal terminals (in RH) are distributed in A17, A18, and 17/18 TZ. The callosal visual field encoded in the 17/18 TZ extends within the hemifield ipsilateral to the explored cortex (RH) and does not contact the CVM while the callosal visual fields encoded in A17 and A18 have only a very limited contact with it. In the CV_2 group (in green), callosal neurons are distributed in A17, A18, and 17/18 TZ but callosal terminals are almost restricted to the 17/18 TZ. The callosal visual field also extends widely in the hemifield ipsilateral to the explored cortex (LH) but, this time, it overlaps substantially the CVM. Altogether, the overlap between the callosal representations along the CVM in LH and RH of strabismics thus does not exceed 8° (i.e., from −1° to +7°, as represented by the vertical shaded area along the CVM). **(B)** Illustration of the symmetry in NR group (in black). There are reciprocal and equivalent callosal connections from RH to LH and from LH to RH. In all cases, the callosal neurons are mainly located in the 17/18 TZ while some are also located in A17 and A18 near the 17/18 TZ, but the callosal terminals are almost restricted to the 17/18 TZ. Thus, the callosal visual fields encoded in LH and RH (i.e., the callosal representations in LH and RH) display both the same width but mirror exactly each other. Both overlap the CVM, with a substantial part in the hemifield ipsilateral to the explored cortex and a more restricted part in the contralateral hemifield, sharing this time as much as 12° (vertical shaded area from −6° to +6°).

of the callosal terminals in RH was also wider than normal, while in LH this was rather normal although a few abnormal terminals were found in A17 and A18. Finally, the distribution of the synaptic boutons in RH of strabismics was also very different from normal while the one in LH of strabismics was closer to normal.

EFFECT OF STRABISMUS ON THE CONTRIBUTION OF THE CORPUS CALLOSUM TO UNIFY THE TWO VISUAL HEMIFIELDS

In NR adult cats, as with the other functional properties, the spatial distribution of the TC-RFs in RH, i.e., the "callosal visual field" in this hemisphere is similar to that from LH, even if they mirror one another (e.g., Payne, 1990a,b; cf. **Figure 10B**, in black). Again, one may say that they are represented *symmetrically* between the hemispheres. Within RH, their extreme limits are at −6° in the left hemifield and +13° in the right hemifield, with a mean azimuth of their centers at +2.4° ± 0.6°; in LH, they are at +6° in the right hemifield and −13° in the left one, with a mean azimuth of their centers at −2.4° ± 0.6° (Milleret et al., 2005; **Figure 10B**). Thus, globally, callosal visual fields of both hemispheres in NR animals share 6° on each side of the CVM, i.e., 12°.

By contrast, after strabismus, the spatial distribution of the TC-RFs in RH (CV_1 group; cf. Milleret and Houzel, 2001) is rather different to that from LH (CV_2 group). Thus, the "callosal visual fields" develop abnormally and *asymmetrically* between the hemispheres (**Figure 10A**). In RH, i.e., the hemisphere ipsilateral to the deviated eye (CV_1 group), the TC-RFs were almost all shifted by several degrees away from the CVM, within the hemifield ipsilateral to the explored cortex. In the 17/18 TZ, with their extreme limits being located at +2° and +19° in the hemifield ipsilateral to the explored cortex, the maximum width of their distribution was 17° and TC-RFs did not have any contact with the CVM. In A17 and A18, with extreme values at −1°/+15° and −1°/+14° respectively, they only kept a very restricted contact with the CVM. By contrast, in LH, i.e., the hemisphere ipsilateral to the non-deviated eye (CV_2 group), the TC-RFs in the 17/18 TZ extended substantially in the hemifield ipsilateral to the explored cortex but almost systematically abutted or intersected the CVM. With their extreme limits extended at +7° in the hemifield contralateral to the explored cortex and −20° in the ipsilateral one respectively, the maximum width of their distribution reached 27°. As a consequence, the "callosal visual fields" in RH and LH of CV animals share a smaller angle than normal (8° instead of 12°, cf. the vertical shaded area in **Figure 10A**). In other words, the overlap between the callosal representation along the CVM in LH and RH decreased after strabismus compared to normal. This common part in the visual field is also no longer distributed symmetrically on each side of the CVM, with 7° in the right hemifield and 1° in the left. Again, note that asymmetry resulted from abnormalities in both hemispheres because of strabismus, with most located in RH, i.e., in the hemisphere ipsilateral to the deviated eye (CV_1 group). *Altogether, this leads to the important conclusion that the capacity of the CC to unify both hemifields is greatly impaired after early unilateral convergent strabismus.* (**Figure 10A**).

EFFECT OF STRABISMUS ON THE IPSILATERAL RETINO-GENICULO-CORTICAL PATHWAY

Interestingly, different spatial distributions of the GC-RFs of the TC units were also found in each hemisphere of strabismics (cf. Spatial Distribution of the GC-RFs for details). As before, such asymmetry is related to abnormalities in both hemispheres because of strabismus (cf. **Figure 6B**). *But those in RH, i.e., within the hemisphere ipsilateral to the deviated eye* (*CV_1 group*), *are again the greatest.* In brief, compared to normal, the spatial distribution of the GC-RFs in RH (CV_1 group) was shifted toward the hemifield contralateral to the explored cortex by several degrees, losing most of its contact with the CVM. In addition, it was substantially wider than normal (32° instead of 20°). By contrast, in LH (CV_2 group), the spatial distribution of the GC-RFs resembles that of normals. Still, the mean values of Az_2 and Az_3 values were larger in the CV_2 group than in the NR group. *Globally, this indicates that the retino-*GC *pathway which projects in the hemisphere ipsilateral to the deviated eye is also globally more affected by strabismus than the hemisphere ipsilateral to the non-deviated eye. Again, this is of particular importance to explain the origin of the brain asymmetry that develops in visual cortex after unilateral strabismus* (*see next paragraph*).

TWO POSSIBLE MECHANISMS OF HOW INTERHEMISPHERIC CONNECTIONS BECOME ASYMMETRIC AFTER EARLY UNILATERAL CONVERGENT STRABISMUS

A first mechanism provided directly from the data reported here

First, considering the morphology of single callosal axons, in RH (i.e., CV_1 group), we found that the mean lengths of the third to fifth order branches were significantly longer than normal (by at least a factor of 2). In contrast, in LH (i.e., the CV_2 group), we found that the mean number of nodes and terminals were significantly lower than normal. *We propose that the lengthening of the third to fifth order callosal branches in the hemisphere ipsilateral to the deviated eye and the decrease in numbers of nodes and terminals in the hemisphere ipsilateral to the non-deviated eye is one of the main mechanisms to account for the development of asymmetrical callosal connections between the hemispheres after unilateral strabismus.*

Surprisingly, our recent data suggest that *this mechanism might be generalized to any unilateral alteration of vision occurring early in life.* Indeed, we have recently shown that, after early monocular deprivation, exuberant callosal terminals can also be found at adulthood within the hemisphere ipsilateral to the deprived eye compared to normal. Moreover, the lengths of the fourth and the fifth order branches of the callosal axons within this hemisphere are significantly longer than normal (multiplied by a factor of at least 3, Foubert et al., 2010). These data fit with the idea that the lengthening of callosal branches of superior order occurs systematically within the hemisphere ipsilateral to the altered eye. Whether the numbers of nodes and terminals are also decreased in the hemisphere ipsilateral to the non-deprived eye remains unknown.

What general rules govern the development of asymmetrical callosal connections in visual cortex?

Our data demonstrate that callosal connections between visual cortices develop asymmetrically after unilateral convergent strabismus because of the sprouting of some specific callosal branches in one hemisphere and the decreased number of nodes and terminals in the other hemisphere. But, presently, the rules that govern the development of such asymmetry are not known. Although some hypotheses have been proposed (Lund and Mitchell, 1979; Berman and Payne, 1983), they are not supported by the obtained experimental data using both the anatomical and the functional approaches.

The hypothesis we propose here is based upon several rather well established general rules governing the development of connectivity in cat visual cortex: (a) At birth all pathways are immature: the crossed retino-GC pathways originating mainly from the nasal retinas (cRGC), the uncrossed ones originating mainly from both temporal retinas (iRGC) as well as the CC (e.g., Berbel and Innocenti, 1988; Aggoun-Zouaoui and Innocenti, 1994; Milleret et al., 1994; Aggoun-Zouaoui et al., 1996; Crair et al., 1998, 2001; Katz and Crowley, 2002); (b) Their respective anatomo-functional development is highly dependent on postnatal visual experience (e.g., Innocenti, 1986; Crair et al., 1998; Foubert et al., 2010); (c) The cRGC pathways are functionally active before the iRGC pathways (e.g., Milleret et al., 1988b; Crair et al., 1998, 2001); (d) Callosal connections develop after both the cRGC and the iRGC pathways have established functional synapses in visual cortex

(e.g., Innocenti, 1981; Milleret et al., 1994; Crair et al., 2001; Katz and Crowley, 2002). Thus, any abnormality in the development of the cRGC and the iRGC pathways resulting from an abnormal postnatal visual experience may alter the development of callosal connections; (e) The deviation of one eye early in life alters the anatomo-functional characteristics of both the cRGC and the iRGC pathways originating from that eye (e.g., Hubel and Wiesel, 1963; Ikeda et al., 1977, 1978); (f) Early convergent strabismus may lead to the stabilization of juvenile exuberant callosal neurons (e.g., Innocenti and Frost, 1979; Berman and Payne, 1983; Elberger et al., 1983) and to the sprouting of callosal terminals during postnatal development (e.g., Lund et al., 1978; Lund and Mitchell, 1979; Berman and Payne, 1983; Milleret and Houzel, 2001).

On the basis of these rules, we postulate that both the cRGC and the iRGC pathways contribute to the postnatal development of the callosal connections in cat visual cortex. We hypothesize that these contributions occur in succession over time. First, both the left and the right cRGC pathways would determine the characteristics of the callosal efferent zones, i.e., the zones where the cell bodies of the callosal neurons are located. Then, both the left and the right iRGC pathways would determine the characteristics of the callosal afferent zones, i.e., the cortical zones where the callosal terminals are located. As a result, a RGC pathway (whether cRGC or iRGC) developing in normal viewing conditions would then lead to a normal organization of the related callosal zone. By contrast, an abnormal RGC pathway developing in abnormal viewing conditions would lead to an abnormal organization of the related callosal zone, i.e., a wider extension than normal.

Such a mechanism would explain the asymmetrical organization of callosal connections shown here in the adult following early convergent strabismus of the RE (cf. **Figure 10A**). For the CV_1 group, vision through the deviated RE would first alter the development of the cRGC pathway projecting to LH. As a consequence, some juvenile exuberant callosal neurons would be stabilized in this hemisphere, leading to an abnormally large distribution of the callosal neurons. Several studies support such an interpretation (Innocenti and Frost, 1979; Berman and Payne, 1983; Elberger et al., 1983). Such an increase in callosal neurons would then lead to an increase of callosal axons in the CC compared to normal. Then, vision through this same deviated RE would alter the development of the iRGC pathway projecting to the RH. As a consequence, some exuberant callosal axons would enter the visual cortex through sprouting, leading to an abnormally large distribution of the callosal terminals in this hemisphere. Results from the CV_1 group support this view. This is also in agreement with previous anatomical data reported in the literature (Lund and Mitchell, 1979; Berman and Payne, 1983).

In contrast, according to this mechanism, the development of both the cRGC and the iRGC pathways originating from the left (non-deviated) eye (LE) would be expected to be close to normal. Therefore, in the CV_2 group, both the distribution of the callosal neurons in RH and that of the callosal terminals in LH are predicted to be comparable to those in normal animals. This is partially true. From the literature, it is known that the distribution of callosal neurons is slightly larger than normal (Berman and Payne, 1983; Elberger et al., 1983). Moreover, we found here that callosal terminals in LH exhibit a distribution that is also slightly larger than normal. However, these differences were much weaker than the ones evoked through the deviated eye, and may account to the ability of the non-deviated eye in unilateral strabismics to also evoke some abnormalities in visual cortex (Chino et al., 1983, 1988; Levi and Klein, 1985; Leguire et al., 1990).This view is supported by data from the CV_2 group. For example, the spatial distribution of the GC-RFs of the TC units in this group is close to normal but not identical, suggesting that some subtle changes in the retinotopic map may occur.

These rules may apply more generally to the development of callosal connections in case of any monocular alteration of vision occurring early in life (for example a monocular occlusion or a monocular enucleation). Furthermore, it also works for other mammal species, including rat, hamster, and cat (e.g., Rhoades and Dellacroce, 1980; Olavarria et al., 1987; O'Brien and Olavarria, 1995; Foubert et al., 2010).

ETIOLOGY OF STRABISMUS AND CALLOSAL CONNECTIONS

In humans, it is well known that early strabismus generally occurs during the first postnatal months. Mostly convergent, its characteristics are remarkable: crossed fixation, latent nystagmus, dissociated vertical deviation (Bui Quoc and Espinasse-Berrod, 2004; Thouvenin, 2004). It systematically leads to a loss of 3D perception. It may also be responsible for unilateral amblyopia. From studies on animal models, the perceptual deficits associated with strabismus likely result from abnormal development of the visual system, in particular at the level of the primary visual cortex (cf. Boothe et al., 1985; Milleret, 1994a,b; Kiorpes and McKee, 1999; Löwel and Engelmann, 2002). The anatomical and functional data reported here about callosal connections are coherent with this abnormal cortical development.

By contrast, the etiology of strabismus is still poorly understood, though it is clear that heredity as well as acquired factors such as premature birth is associated with early strabismus (Von Noorden, 1988). Some hypotheses may however be proposed.

First, strabismus could have a *peripheral* origin such as abnormalities at the level of the proprioceptive receptors of the extraocular muscles. Abnormal signals in the extraocular proprioceptive afferents projecting centrally would then alter the development of visual cortex (e.g., Buisseret, 1995 for review). The activity of the oculomotor neurons may also be greater or smaller than normal because of potential dysfunctions of the oculomotor circuitry (Miller, 2003). But there is no reason to favor one hypothesis over another. Note however that, whatever the peripheral palliative treatment is clinically performed in humans, regardless of age, early strabismus results in severe alteration of binocular vision, even if realignment of eyes is obtained. Very early surgery during the first year of life, the use of prismatic glasses, and early injection of botulinum toxinum in the muscles have not proven their efficacy in restoring normal binocular vision in early strabismus.

The hypothesis of a *central* origin of strabismus may explain such difficulties, at least in some cases. Almost a century ago, Worth (1915) suggested the existence of a "center of binocular vision" that would be initially impaired in strabismics. If so, the absence of binocular vision would be responsible for the deviation of the eyes, although the precise mechanism for this remains unclear

(Hutcheson, 2004). The callosal projection pathways would be a principal element of such a "center of binocular vision." This leads to the hypothesis that abnormal development of visual interhemispheric transfer and the related abnormal binocular activation of callosal connections (cf. **Figure 7**) would be responsible for abnormal binocular vision in humans. Consequently, as suggested by Worth, this absence of normal binocular vision would induce early strabismus in humans. This is consistent with the observation that binocular vision remains abnormal even if eye realignment is achieved. Supporting this, failure of development of the corpus callosum in humans or even a pathological development of corpus callosum is often associated with abnormal eye movements and strabismus (e.g., Goyal et al., 2010).

ACKNOWLEDGMENTS

The authors thank Murielle Bourge for animal care. France Maloumian for assistance in preparing of some of the figures. We also thank Drs. S. Wiener and S. Sara for useful comments on the manuscript, European Journal of Neuroscience publisher for permitting reproducing Figures 2, 4, 11–13 from Houzel et al. (1994) and Figures 2, 3, 5, 6, 8–12 from Milleret and Houzel (2001) as well as Visual Neuroscience for permitting reproducing part of Figures 5 and 9 from Milleret et al. (2005). This work was supported by the MENSER (ACI "Neurosciences Integratives and Computationelles") to C. Milleret, the "Fondation pour la Recherche Médicale" to E. Bui Quoc and the European Grant "Marie Curie IRG" (N° 210459) to J. Ribot.

REFERENCES

Aggoun-Zouaoui, D., and Innocenti, G. M. (1994). Juvenile visual callosal axons in kittens display origin- and fate-related morphology and distribution of arbors. *Eur. J. Neurosci.* 6, 1846–1863.

Aggoun-Zouaoui, D., Kiper, D. C., and Innocenti, G. M. (1996). Growth of callosal terminal arbors in primary visual areas of the cat. *Eur. J. Neurosci.* 8, 1132–1148.

Alekseenko, S. V., Toporova, S. N., and Shkorbatova, P. Y. (2009). Interhemispheric connections of eye dominance columbs in the cat visual cortex in conditions of impaired binocular vision. *Neurosci. Behav. Physiol.* 39, 489–495.

Berbel, P., and Innocenti, G. M. (1988). The development of the corpus callosum in cats: a light- and electron-microscopic study. *J. Comp. Neurol.* 2, 242–259.

Berlucchi, G., Gazzaniga, M. S., and Rizzolatti, G. (1967). Microelectrode analysis of transfer of visual information by the corpus callosum. *Arch. Ital. Biol.* 105, 583–596.

Berlucchi, G., and Rizolatti, G. (1968). Binocular driven neurons in the visual cortex of split-chiasm cats. *Science* 159, 308–310.

Berman, N. E., and Payne, B. (1983). Alterations in connections of the corpus callosum following convergent and divergent strabismus. *Brain Res.* 274, 201–212.

Boothe, R. G., Dobson, V., and Teller, D. (1985). Postnatal development of vision in humans and non human primates. *Annu. Rev. Neurosci.* 8, 495–545.

Bourdet, C., Olavarria, J. F., and Van Sluyters, R. C. (1996). Distribution of visual callosal neurons in normal and strabismic cats. *J. Comp. Neurol.* 366, 259–269.

Bui Quoc, E., and Espinasse-Berrod, M.-A. (2004). Strabisme chez l'enfant. *Encyclopédie Médico-Chirurgicale, Pédiatrie,* 4-120-D-10, Paris.

Buisseret, P. (1995). Influence of extraocular muscle proprioception on vision. *Physiol. Rev.* 75, 323–338.

Chino, Y. M., Ridder, W. H., and Czora, E. A. (1988). Effects of convergent strabismus on spatio-temporal properties of neurons in cat area 18. *Exp. Brain Res.* 72, 264–278.

Chino, Y. M., Shansky, M. S., Jankowski, W. L., and Banser, F. A. (1983). Effects of rearing kittens with convergent strabismus on development of receptive field properties in striate cortex neurons. *J. Neurophysiol.* 50, 265–286.

Crair, M. C., Gillespsie, D. C., and Stryker, M. P. (1998). The role of visual experience in the development of columns in cat visual cortex. *Science* 279, 586–570.

Crair, M. C., Horton, J. C., Antonini, A., and Stryker, M. (2001). Emergence of ocular dominance columns in cat visual cortex by 2 weeks of age. *J. Comp. Neurol.* 430, 235–249.

Elberger, A. (1993). Distribution of transitory corpus callosum axons projecting to developing cat visual cortex revealed by Dii. *J. Comp. Neurol.* 333, 326–342.

Elberger, A., Smith, E. L. III, and White, J. M. (1983). Spatial dissociation of visual inputs alters the origin of the corpus callosum. *Neurosci. Lett.* 35, 19–24.

Foubert, L., Bennequin, D., Thomas, M. A., Droulez, J., and Milleret, C. (2010). Interhemispheric synchrony in visual cortex and abnormal postnatal visual experience. *Front. Biosci.* 15, 681–707.

Gibbons, J. D. (1985). *Nonparametric Statistical Inferences*, 2nd Edn. New York: M. Dekker.

Goyal, R., Watts, P., and Hourihan, M. (2010). Ocular findings in pediatric patients with partial agenesis of corpus callosum. *J. Pediatr. Ophthalmol. Strabismus* 47, 236–241.

Hollander, M., and Wolfe, D. A. (1973). *Nonparametric Statistical Methods.* New York: John Wiley and Sons.

Houzel, J.-C., Milleret, C., and Innocenti, G. (1994). Morphology of callosal axons interconnecting areas 17 and 18 of the cat. *Eur. J. Neurosci.* 6, 898–917.

Hubel, D. H., and Wiesel, T. N. (1963). Binocular interaction in straite cortex of kittens reared with artificial squint. *J. Neurophysiol.* 28, 1041–1059.

Hubel, D. H., and Wiesel, T. N. (1967). Cortical and callosal connections concerned with the vertical meridian of visual fields in the cat. *J. Neurophysiol.* 30, 1561–1573.

Hubel, D. H., and Wiesel, T. N. (1970). The period of susceptibility to the physiological effects of unilateral eye closure in kittens. *J. Physiol. (Lond.)* 206, 419–436.

Hutcheson, K. A. (2004). Childhood esotropia. *Curr. Opin. Ophthalmol.* 15, 444–448.

Ikeda, H., Plant, G. T., and Tremain, K. E. (1977). Nasal field loss in kittens reared with convergent squint: neurophysiological and morphological studies on the lateral geniculate nucleus. *J. Physiol. (Lond.)* 270, 345–366.

Ikeda, H., Tremain, K. E., and Einon, G. (1978). Loss of spatial resolution of lateral geniculate nucleus neurons in kittens raised with convergent squint produced at different stages in development. *Exp. Brain Res.* 31, 207–220.

Innocenti, G. M. (1981). Growth and reshaping of axons in the establishment of visual callosal connections. *Science* 212, 824–827.

Innocenti, G. M. (1986). "General organization of callosal connections in the cerebral cortex," in *Cerebral Cortex*, eds A. Peters and E. G. Jones (New York: Plenum), 291–353.

Innocenti, G. M., and Clarke, S. (1984). The organization of immature callosal connections. *J. Comp. Neurol.* 230, 287–309.

Innocenti, G. M., Clarke, S., and Kraftsik, R. (1986). Interchange of callosal and association projections in the developing visual cortex. *J. Neurosci.* 6, 1384–1409.

Innocenti, G. M., and Fiore, L. (1976). Morphological correlates of visual field transformation in the corpus callosum. *Neurosci. Lett.* 2, 245–252.

Innocenti, G. M., Fiore, L., and Caminiti, R. (1977). Exuberant projection into the corpus callosum from the visual cortex of newborns cats. *Neurosci. Lett.* 4, 237–242.

Innocenti, G. M., and Frost, D. (1979). Effects of visual experience on the maturation of the efferent system to the corpus callosum. *Nature* 280, 231–234.

Innocenti, G. M., Lehmnn, P., and Houzel, J. C. (1994). Computational structure of visual callosal axons. *Eur. J. Neurosci.* 6, 918–935.

Kageyama, G. M., and Wong-Riley, M. (1986a). The localization of cytochrome oxidase in the LGN and striate cortex of postnatal kittens. *J. Comp. Neurol.* 243, 182–194.

Kageyama, G. M., and Wong-Riley, M. (1986b). Laminar and cellular localization of cytochrome oxidase in the cat striate cortex. *J. Comp. Neurol.* 245, 137–159.

Katz, L. C., and Crowley, J. C. (2002). Development of cortical circuits: lessons from ocular dominance columns. *Nature* 3, 34–42.

Kiorpes, L., and McKee, S. P. (1999). Neural mechanisms underlying amblyopia. *Curr. Opin. Neurobiol.* 9, 480–486.

Leguire, L. E., Rogers, G. L., and Bremer, D. L. (1990). Amblyopia: the normal eye is not normal. *J. Pediatr. Ophthalmol. Strabismus* 27, 32–38.

Leicester, J. (1968). Projection of the visual vertical meridian to cerebral cortex of cat. *J. Neurophysiol.* 31, 371–382.

Leporé, F., and Guillemot, J. P. (1982). Visual receptive field properties of cells innervated through the corpus callosum in the cat. *Exp. Brain Res.* 46, 413–424.

Levi, D. M., and Klein, S. A. (1985). Vernier acuity, crowding and amblyopia. *Vision Res.* 25, 979–991.

Löwel, S., and Engelmann, R. (2002). Neuroanatomical and neurophysiological consequences of strabismus: changes in the structural and functional organization of the primary visual cortex in cats with alternating fixation and strabismic amblyopia. *Strabismus* 10, 95–105.

Lund, R. D., and Mitchell, D. E. (1979). Asymmetry in the visual callosal connections of strabismic cats. *Brain Res.* 167, 176–179.

Lund, R. D., Mitchell, D. E., and Henry, G. H. (1978). Squint-induced modification of callosal connections in cats. *Brain Res.* 144, 169–172.

Miller, J. (2003). No oculomotor plant, no final common path. *Strabismus* 11, 205–211.

Milleret, C. (1994a). Physiopathogénie de l'amblyopie strabique. Editions techniques. *Encyclopedia Méd Chir, Ophtalmologie*, 21-595-A-05, Paris.

Milleret, C. (1994b). Visual callosal connections and strabismus. *Behav. Brain Res.* 64, 85–95.

Milleret, C., and Buser, P. (1984). Receptive fields sizes and responsiveness to light in area 18 of the adult cat after chiasmotomy. Postoperative evolution; role of visual experience. *Exp. Brain Res.* 57, 73–81.

Milleret, C., and Buser, P. (1993). Reorganization processes in the visual cortex also depend on visual experience in the adult cat. *Prog. Brain Res.* 95, 257–269.

Milleret, C., Buser, P., and Watroba, L. (2005). Unilateral paralytic strabismus in the adult cat induces plastic changes in interocular disparity along the visual midline: contribution of the corpus callosum. *Vis. Neurosci.* 22, 325–343.

Milleret, C., Gary-Bobo, E., and Buisseret, P. (1988a). Area centralis position relative to the optic disc projection in kittens as a function of age. *Invest. Ophthalmol. Vis. Sci.* 29, 1299–1305.

Milleret, C., Gary-Bobo, E., and Buisseret, P. (1988b). Comparative development of cell properties in cortical area 18 of normal and dark-reared kittens. *Exp. Brain Res.* 71, 8–20.

Milleret, C., and Houzel, J. C. (2001). Visual interhemispheric transfer to areas 17 and 18 in cats with convergent strabismus. *Eur. J. Neurosci.* 13, 137–152.

Milleret, C., Houzel, J. C., and Buser, P. (1994). Pattern of development of the callosal transfer of visual information to cortical areas 17 and 18 in the cat. *Eur. J. Neurosci.* 6, 193–202.

Nakamura, H., Chaumon, M., Klijn, F., and Innocenti, G. M. (2008). Dynamic properties of the representation of the visual field midline in the visual areas 17 and 18 of the ferret (*Mustela putorius*). *Cereb. Cortex* 18, 1941–1950.

O'Brien, B. J., and Olavarria, J. F. (1995). Anomalous patterns of callosal connections develop in visual cortex of monocularly enucleated hamsters. *Biol. Res.* 28, 211–218.

Olavarria, J., Malach, R., and Van Sluyters, R. C. (1987). Development of visual callosal connections in neonatally enucleated rats. *J. Comp. Neurol.* 260, 321–348.

Olavarria, J. F. (1995). The effects of visual deprivation on the number of callosal cells in the cat is less pronounced in extrastriate cortex than in the 17/18 border region. *Neurosci. Lett.* 195, 147–150.

Olavarria, J. F. (1996). Non-mirror-symmetric patterns of callosal linkages in areas 17 and 18 in cat visual cortex. *J. Comp. Neurol.* 366, 643–655.

Olavarria, J. F. (2001). Callosal connections correlate preferentially with ipsilateral cortical domains in cat areas 17 and 18, and with contralateral domains in the 17/18 transition zone. *J. Comp. Neurol.* 433, 441–457.

Otsuka, R., and Hassler, R. (1962). Uber Aufbau und Gliederung der corticalen Sehsphäre bei der Katze. *Arch. Psychiatr. Z. Gesamte Neurol.* 203, 203–212.

Payne, B. (1990a). Function of the corpus callosum in the representation of the visual field in cat visual cortex. *Vis. Neurosci.* 5, 205–211.

Payne, B. (1990b). Representation of the ipsilateral visual field in the transition zone between areas 17 and 18 of the cat's cerebral cortex. *Vis. Neurosci.* 4, 445–474.

Payne, B. (1991). Visual-field map in the transcallosal sending zone of area 17 in the cat. *Vis. Neurosci.* 7, 201–219.

Payne, B. (1994). Neuronal interactions in cat visual cortex mediated by the corpus callosum. *Behav. Brain Res.* 64, 55–64.

Payne, B., and Siwek, D. F. (1991). Visual-field map in the callosal recipient zone at the border between areas 17 and 18 in the cat. *Vis. Neurosci.* 7, 221–236.

Price, D. J. (1985). Pattern of cytochrome oxidase activity in areas 17, 18 and 19 of the visual cortex of cats and kittens. *Exp. Brain Res.* 58, 125–133.

Rhoades, R. W., and Dellacroce, D. D. (1980). Neonatal enucleation induces an asymmetric pattern of visual callosal connections in hamsters. *Brain Res.* 202, 189–195.

Rochefort, N. L., Buzas, P., Kisvárday, Z. K., Eysel, U. U., and Milleret, C. (2007). Layout of transcallosal activity in cat visual cortex revealed by optical imaging. *Neuroimage* 36, 804–821.

Schmidt, K. E., Kim, D. S., Singer, W., Bonhoeffer, T., and Löwel, S. (1997). Functional specificity of long-range intrinsic and interhemispheric connections in the visual cortex of strabismic cats. *J. Neurosci.* 17, 5480–5492.

Schmued, L. C. (1990). A rapid, sensitive histochemical stain for myelin in frozen brain sections. *J. Histochem. Cytochem.* 38, 717–720.

Sherman, S. M. (1972). Development of interocular alignment in cats. *Brain Res.* 37, 187–203.

Tagawa, Y., Mizuno, H., and Hirano, T. (2008). Activity-dependent development of interhemispheric connections in the visual cortex. *Rev. Neurosci.* 19, 19–28.

Thouvenin, D. (2004). "Strabisme précoce," in *Strabologie: approches diagnostique et thérapeutique*, ed M.-A. Espinasse-Berrod (Atlas en Ophtalmologie, Elsevier), 87–95.

Tusa, R. J., Palmer, L. A., and Rosenquist, A. C. (1978). The retinotopic organisation of area 17 (striate cortex) in the cat. *J. Comp. Neurol.* 177, 213–236.

Tusa, R. J., Palmer, L. A., and Rosenquist, A. C. (1979). The retinotopic organisation of area 18 and 19 in the cat. *J. Comp. Neurol.* 185, 657–678.

Vakkur, G. J., Bishop, P. O., and Kozak, W. (1963). Visual optics in the cat, including posterior nodal distance and retinal landmarks. *Vision Res.* 61, 289–314.

Von Noorden, G. K. (1988). Bowman lecture. Current concepts of infantile esotropia. *Eye* 2, 343–357.

Wong-Riley, M. (1979). Changes in the visual system of monocularly sutured or enucleated cats demonstrated with cytochrome oxidase histochemistry. *Brain Res.* 171, 11–28.

Worth, C. (1915). *Squint: Its Causes, Pathology and Treatment*, 4th Edn. London: John Bale and Danielson.

Conflict of Interest Statement: The authors declare that the research was conducted in the absence of any commercial or financial relationships that could be construed as a potential conflict of interest.

Received: 19 September 2011; paper pending published: 11 October 2011; accepted: 19 December 2011; published online: 11 January 2012.

Citation: Bui Quoc E, Ribot J, Quenech'Du N, Doutremer S, Lebas N, Grantyn A, Aushana Y and Milleret C (2012) Asymmetrical interhemispheric connections develop in cat visual cortex after early unilateral convergent strabismus: anatomy, physiology, and mechanisms. Front. Neuroanat. ***5****:68. doi: 10.3389/fnana.2011.00068*

APPENDIX

Table A1 | Morphological characteristics of each of the eight callosal axons reconstructed in 3D in the CV_1 group.

A

Axon code	Origin area/ antero post	Trunk diameter (μm)	Architecture	Number of nodes	Ant/post ext (μm)	Frontal extension (μm)	Branches	Columns (or clusters)	Termination area/antero post
INJECTION IN A17									
CV13-A	A17 (P7)	1.22	Multiple clustered	16	150	1168	Single branch	A	TZ (P4)
								B	TZ (P4)
CV13-B	A17 (P7)	1.31	Simple	2	50	40	Single branch	A	A18 (P4)
CV13-C	A17 (P7)	1.21	Simple	3	50	440	Single branch	A	A18 (P4)
								En passant boutons	A18 (P4)
BCV7	A17 (AP0)	0.4	Multiple clustered	101	750	3789	1st main branch	A	A17 (AP0)
								En passant boutons	A17 (AP0)
							2nd main branch	B	TZ (AP0)
								En passant boutons	TZ (AP0)
							3rd main branch	C	A18 (AP0)
								En passant boutons	A18 (AP0)
INJECTION IN TZ									
CV14-V	TZ (P2)	1.37	Multiple clustered	118	950	2833	1st main branch	A	A19 (P2.5)
							2nd main branch	B	A18 (P1.5)
								C	A18 (P1.5)
								D	A18 (P1.5)
								E	A18 (P1.5)
								F	A18 (P1.5)
								G	A18 (P1.5)
								H	A18 (AP0)
								Other boutons	A18 (P1.5)
CV14-B	TZ (P2)	1.27	Simple	88	500	1971	Two main branches ; the secondary branches are entangled and end in several clusters	A	A18 (P2)
								B	A18 (P2)
								C	A18 (P2)
								D	A18 (P2)
								E	A18 (P2)
								F	A18 (P0.5)
								G	A18 (P0.5)
								Other boutons	A18 (P0.5)
BCV9	TZ (A7)	1.62	Multiple clustered	46	550	1747	1st main branch	En passant boutons	A17 (A9)
							2nd main branch	A	TZ (A9)
							3rd main branch	B	TZ (A9)
INJECTION IN A18									
CV13-N	A18 (A9)	1.57	Multiple clustered	111	800	909	1st main branch	A	A18 (A10)
							2nd main branch	B	A18 (A11.5)

(Continued)

Table A1 | Continued

B

Axon code	Origin area/ antero post	Termination area/antero post	Cortical layers						Total number of boutons	Type of laminar distribution of the boutons	Number of boutons per area
			I	II/III	IV	V	VI	WM			
INJECTION IN A17											
CV13-A	A17 (P7)	TZ (P4)	0	22	6	20	36	0	156	Bi-laminar	TZ 156
		TZ (P4)	0	0	0	59	13	0			
CV13-B	A17 (P7)	A18 (P4)	0	0	0	0	19	21	40	Infragranular	A18 40
CV13-C	A17 (P7)	A18 (P4)	0	0	37	0	0	0	38	Granular	A18 38
		A18 (P4)	0	0	0	1	0	0			
BCV7	A17 (AP0)	A17 (AP0)	0	230	1	0	0	0	1056	Bi-laminar	A17 319
		A17 (AP0)	0	50	5	18	15	0			
		TZ (AP0)	9	343	36	111	9	0			TZ 509
		TZ (AP0)	0	0	0	0	1	0			
		A18 (AP0)	3	180	0	0	0	0			A18 328
		A18 (AP0)	0	1	2	30	12	0			
INJECTION IN TZ											
CV14-V	TZ (P2)	A19 (P2.5)	0	8	14	0	0	0	525	Supra-granular	A19 22
		A18 (P1.5)	0	116	32	7	0	0			A18 503
		A18 (P1.5)	0	210	0	0	0	0			
		A18 (P1.5)	0	25	0	0	0	0			
		A18 (P1.5)	0	18	0	0	0	0			
		A18 (P1.5)	0	17	0	0	0	0			
		A18 (P1.5)	0	53	0	0	0	0			
		A18 (AP0)	9	0	0	0	0	0			
		A18 (P1.5)	0	16	0	0	0	0			
CV14-B	TZ (P2)	A18 (P2)	0	17	0	0	0	0	257	Supra-granular	A18 257
		A18 (P2)	0	16	0	0	0	0			
		A18 (P2)	0	17	0	0	0	0			
		A18 (P2)	0	14	0	0	0	0			
		A18 (P2)	0	55	0	0	0	0			
		A18 (P0.5)	0	31	0	0	0	0			
		A18 (P0.5)	0	54	0	0	0	0			
		A18 (P0.5)	3	46	2	2	0	0			
BCV9	TZ (A7)	A17 (A9)	0	0	0	3	12	9	211	Bi-laminar	A17 24
		TZ (A9)	0	41	0	0	11	0			TZ 187
		TZ (A9)	0	125	10	0	0	0			
INJECTION IN A18											
CV13-N	A18 (A9)	A18 (A10)	0	121	31	77	13	0	528	Trans-granular	A18 528
		A18 (A11.5)	0	135	23	21	107	0			

General and detailed descriptions are represented in A and B respectively (Cf. text for details). TZ, 17/18 TZ.

Table A2 | Morphological characteristics of each of the nine callosal axons that were reconstructed in 3D in the CV_2 group.

A

Axon code	Origin area/ antero post	Trunk diameter (μm)	Architecture	Number of nodes	Ant-post extension (μm)	Frontal extension (μm)	Branches	Columns (= clusters)	Termination area/antero post
INJECTION IN A17									
CVE4-1	A17 (P2)	1.47	Multiple clustered	90	1000	4353	1st main branch	A "En passant" boutons	TZ (P3) A17 (P2.5)
							2nd main branch	E	A17 (P3/4)
								F	A17 (P2.5)
								H	A17 (P2.5)
							3rd main branch	B	TZ (P4)
								C	A17 (P2.5)
								D	A17 (P5/6)
								G	A17 (P3/4)
							Merging of secondary branches coming from branches 2 and 3	I	A17 (P2.5)
CVE4-2	A17 (P2)	1.27	Multiple clustered	15	900	1768	1st main branch	A	TZ (P1)
								B	A18 (P1)
								C	TZ (P1)
								D	TZ (P2)
							2nd main branch	E	A18 (P2)
CVE7-D	A17 (P4)	0.6	Multiple clustered	12	300	887	1st main branch	A	TZ (P3)
							2nd main branch	B	A17 (P3)
CVE7-S	A17 (P4)	0.6	Simple	18	175	249	2 branches ending each in one cluster	A	TZ (P3/4)
								B	TZ (P3/4)
INJECTION IN TZ									
CVE4-A	TZ (A5.5)	1.54		2	800	NC	3 main branches	No cluster	Toward A18 (A7)
CVE7-A	TZ (A8)	1.75	Simple	20	100	1013	3 branches; only one ends in clusters	A	TZ (A7)
								B	A18 (A7)
CVE7-B	TZ (A8)	1.12	Multiple clustered	11	50	235	2 branches merging in one cluster	A	TZ (A7)
CVE7-1	TZ (A8)	1.11	Simple	61	125	474	2 branches merging in one cluster	A	TZ (A7/8)
CVE7-2	TZ (A8)	1.11	Multiple clustered	32	175	1590	1st main branch	A	A18 (A8)
							2nd main branch	B	A18 (A8)
							Merging of secondary branches coming from main branches 1 and 2	Cluster C	A18 (A8)

(Continued)

Table A2 | Continued

B

Axon code	Origin area/ (antero post)	Termination area/(antero post)	Cortical layers						Total number of boutons	Type of laminar distribution of the boutons	Number of boutons per area
			I	II/III	IV	V	VI	WM			
INJECTION IN A17											
CVE4-1	A17 (P2)	TZ (P3)	0	0	1	3	3	7	445	Supra-granular	A17 326
		A17 (P2.5)	3	6	0	0	0	0			
		A17 (P3/4)	26	40	0	0	0	3			TZ 119
		A17 (P2.5)	0	9	0	0	0	0			
		A17 (P2.5)	20	89	0	5	0	0			
		TZ (P4)	33	72	0	0	0	0			
		A17 (P2.5)	0	9	0	0	0	0			
		A17 (P5/6)	10	43	0	0	0	0			
		A17 (P3/4)	29	27	0	0	0	0			
		A17 (P2.5)	0	7	0	0	0	0			
CVE4-2	A17 (P2)	TZ (P1)	0	43	0	0	0	0	63	Supra-granular	TZ 55
		A18 (P1)	0	0	2	0	0	0			
		TZ (P1)	0	5	2	0	0	0			A18 8
		TZ (P2)	0	3	0	2	0	0			
		A18 (P2)	0	6	0	0	0	0			
CVE7-D	A17 (P4)	TZ (P3)	0	14	22	17	41	0	113	Trans-granular	TZ 94
		A17 (P3)	0	19	0	0	0	0			A17 19
CVE7-S	A17 (P4)	TZ (P3/4)	0	47	38	0	0	0	93	Supra-granular	TZ 93
		TZ (P3/4)	0	7	1	0	0	0			
INJECTION IN TZ											
CVE4-A	TZ (A5.5)	Toward A18 (A7)	0	0	0	0	0	0	0	–	–
CVE7-A	TZ (A8)	TZ (A7)	0	0	7	12	0	0	48	Trans-granular	TZ 19
		A18 (A7)	0	27	2	0	0	0			A18 29
CVE7-B	TZ (A8)	TZ (A7)	6	113	37	7	0	0	163	Supra-granular	TZ 163
CVE7-1	TZ (A8)	TZ (A7/8)	0	443	48	34	77	0	602	Trans-granular	TZ 602
CVE7-2	TZ (A8)	A18 (A8)	0	3	11	0	0	0	140	Supra-granular	A18 140
		A18 (A8)	0	35	2	3	7	0			
		A18 (A8)	0	46	30	0	3	0			

General and detailed descriptions are represented in A and B respectively (Cf. text for details). TZ, 17/18 TZ.

Table A3 | Global distributions of the callosal terminal boutons (percentages and numbers) in the CV_1, CV_2, and NR groups, in cortical areas 17/18 TZ, A17, and A18, and among the cortical layers (I–VI).

Number of boutons	I	II/III	IV	V	VI	Total
A: CV_1 GROUP						
17/18 TZ	1% (9)	63% (531)	6% (52)	22% (190)	8% (70)	31% (852)
A17	0% (0)	84% (280)	2% (6)	6% (21)	8% (27)	12% (334)
A18	1% (15)	73% (1142)	8% (127)	9% (138)	9% (151)	57% (1573)
Total	1% (24)	71% (1953)	7%(185)	12% (349)	9% (248)	100% (2759)
B: CV_2 GROUP						
17/18 TZ	3.5% (39)	65.5% (747)	14% (156)	6.5% (75)	10.5% (121)	68.5% (1138
A17	26% (88)	73% (249)	0% (0)	1% (5)	0% (0)	21% (342)
A18	0% (0)	66% (117)	26.5% (47)	2% (3)	5.5% (10)	10.5% (177)
Total	8% (127)	67% (1113)	12% (203)	5% (83)	8% (131)	100% (1657)
C: NR GROUP						
17/18 TZ	4% (189)	72% (2930)	9% (357)	7% (270)	8% (325)	78% (4071)
A17	14% (2)	86% (12)	0% (0)	0% (0)	0% (0%)	1% (14)
A18	1% (12)	62% (708)	4% (45)	16% (185)	17% (199)	21% (1149)
Total	4% (203)	70% (3650)	8%(402)	8% (455)	10% (524)	100% (5234)
		Cortical layers (I, II/III, IV, V, VI)			**Cortical areas (17/18 TZ, A17, A18)**	
D: CHI SQUARED TEST						
CV1 vs. NR		P-value $= 0.605 \gg 0.05$			P-value $= 9.33.10^{-11} \ll 0.01$	
CV2 vs. NR		P-value $= 0.539 \gg 0.05$			P-value $= 1.44.10^{-5} \ll 0.01$	
CV1 vs. CV2		P-value $= 0.044 < 0.05$			P-value $= 2.77.10^{-11} \ll 0.01$	

Data are presented in panels A to C. In D, the χ^2 test (with Yates correction) identified some significant differences between these distributions (in red). Note that some boutons were also found within the white matter of both CV groups: CV_1 group: 7, 3, 0; CV_2 group: 0, 9, 21 below 17/18 TZ, A17, and A18 respectively. Twenty-two boutons were also found in A19 of the CV_1 group.

Table A4 | Quantitative analysis of the callosal terminal arbors in the CV_1, CV_2, and NR groups.

Experimental groups		CV1	CV2	NR	Stat CV1/NR	Stat CV2/NR	Stat CV1/CV2
N axons		7–8	6–9	17	–	–	–
Architectures of the callosal terminals	Axon branching first very low beyond the cortex	4 out of 8	5 out of 9	1 out of 17			
	Simple	3	4	2	NS	NS	NS
	Parallel	3	5	7	$P = 0.6250$	$P = 0.6250$	$P = 1$
	Serial	0	0	2			
	Mixed	2	0	4			
Mean diameter (μm)	Trunk	1.24	1.17	1.25	NS	NS	NS
SD		0.41	0.42	0.36	$P = 0.2554$	$P = 0909$	$P = 0.219$
Min–max		0.4–1.62	0.6–1.75	0.65–2.02	Z-val = 1.1373	Z-val = 1.6907	Z-val = N.A
	1st order branches thinner than the trunk	−50%	−34%	−33%			
Mean length of the branches (μm)	1st order	1417	2356	1599	NS	NS	NS
SD		1341	1214	1366	$P = 0.8303$	$P = 0.2093$	$P = 0.3282$
Min–max		214–3476	528–3598	42–4866	Z-val = −0.2143	Z-val = 1.2554	Z-val = N.A
Mean length of the branches (μm)	2nd order	695	1058	433	NS	NS	NS
SD		865	1315	494	$P = 0.4813$	$P = 0.2573$	$P = 0.5737$
Min–max		61–2648	50–4045	47–1976	Z-val = 0.7042	Z-val = 1.1329	Z-val = N.A
Mean length of the branches (μm)	3rd order	452	342	253	S	NS	NS
SD		244	342	236	$P = 0.0416$	$P = 0.6163$	$P = 0.3176$
Min–max		159–884	34–1022	27–794	Z-val = 2.0379	Z-val = 0.5011	Z-val = N.A
Mean length of the branches (μm)	4th order	247	263	132	S	NS	NS
SD		104	280	76	$P = 0.0356$	$P = 0.3004$	$P = 0.4452$
Min–max		150–405	64–853	31–269	Z-val = 2.101	Z-val = 1.0356	Z-val = N.A
Mean length of the branches (μm)	5th order	141	115	79	S	NS	NS
SD		68	86	39	$P = 0.0296$	$P = 0.4423$	$P = 0.2949$
Min–max		65–264	44–295	20–152	Z-val = 2.1748	Z-val = 0.7684	Z-val = N.A
Mean number of nodes		61	31	124	NS	S	NS
SD		50	30	88	$P = 0.0809$	$P = 0.003$	$P = 0.3417$
Min–max		2–088	2–090	18–299	Z-val = −1.7453	Z-val = −2.9713	Z-val = N.A
Mean number of terminals		62	34	125	NS	S	NS
SD		50	30	88	$P = 0.0863$	$P = 0.0033$	$P = 0.3417$
Min–max		3–090	3–092	19–300	Z-val = −1.715	Z-val = −2.94	Z-val = N.A
Mean number of terminal boutons		351	194	307	NS	NS	NS
SD		342	214	247	$P = 0.9756$	$P = 0.3122$	$P = 0.3823$
Min–max		38–1056	0–602	33–864	Z-val = 0.0306	Z-val = −1.0106	Z-val = N.A

For statistical analysis ("Stat" columns), we used a Wilcoxon rank sum test which performs a two-sided rank sum test for two independent unequal-sized samples (Hollander and Wolfe, 1973; Gibbons, 1985). In red, significant differences between groups.

frontiers in
NEUROANATOMY

REVIEW ARTICLE
published: 16 October 2012
doi: 10.3389/fnana.2012.00042

Communication and wiring in the cortical connectome

***Julian M. L. Budd*[1]* and *Zoltán F. Kisvárday*[2]**

[1] *Department of Informatics, University of Sussex, Falmer, East Sussex, UK*
[2] *Laboratory for Cortical Systems Neuroscience, Department of Anatomy, Histology and Embryology, University of Debrecen, Debrecen, Hungary*

Edited by:
Kathleen S. Rockland, Massachusetts Institute of Technology, USA

Reviewed by:
Kathleen S. Rockland, Massachusetts Institute of Technology, USA
Richard J. Weinberg, University of North Carolina, USA

***Correspondence:**
Julian M. L. Budd, Department of Informatics, University of Sussex, Falmer, East Sussex, BN1 9RH, UK.
e-mail: j.m.l.budd@sussex.ac.uk

In cerebral cortex, the huge mass of axonal wiring that carries information between near and distant neurons is thought to provide the neural substrate for cognitive and perceptual function. The goal of mapping the connectivity of cortical axons at different spatial scales, the cortical connectome, is to trace the paths of information flow in cerebral cortex. To appreciate the relationship between the connectome and cortical function, we need to discover the nature and purpose of the wiring principles underlying cortical connectivity. A popular explanation has been that axonal length is strictly minimized both within and between cortical regions. In contrast, we have hypothesized the existence of a multi-scale principle of cortical wiring where to optimize communication there is a trade-off between spatial (construction) and temporal (routing) costs. Here, using recent evidence concerning cortical spatial networks we critically evaluate this hypothesis at neuron, local circuit, and pathway scales. We report three main conclusions. First, the axonal and dendritic arbor morphology of single neocortical neurons may be governed by a similar wiring principle, one that balances the conservation of cellular material and conduction delay. Second, the same principle may be observed for fiber tracts connecting cortical regions. Third, the absence of sufficient local circuit data currently prohibits any meaningful assessment of the hypothesis at this scale of cortical organization. To avoid neglecting neuron and microcircuit levels of cortical organization, the connectome framework should incorporate more morphological description. In addition, structural analyses of temporal cost for cortical circuits should take account of both axonal conduction and neuronal integration delays, which appear mostly of the same order of magnitude. We conclude the hypothesized trade-off between spatial and temporal costs may potentially offer a powerful explanation for cortical wiring patterns.

Keywords: axon, cerebral cortex, communication, connectome, dendrite, networks, optimization, Ramón y Cajal

INTRODUCTION

> "That apparent disorder of the cerebral jungle, so different from the regularity and symmetry of the spinal cord and of the cerebellum, conceals a profound organization of the utmost subtility which is at present inaccessible"
>
> (p. 395, Cajal, 1937).

Communication has been defined as the flow of information between a transmitter, generating a signal, and a receiver, reconstructing a signal after its passage through a noisy channel (Shannon, 1948). In his theory of dynamic polarity, Cajal (1899) had correspondingly divided a neuron, the fundamental unit of the brain, into three functional compartments: a receptor apparatus (soma and dendrites), an emission apparatus (axon), and a distribution apparatus (terminal axon arbor). Significantly, Cajal's inferences about how axonal and dendritic wiring are used to communicate derived from anatomical data only. Physiological experiments confirmed Cajal's inferences concerning neural communication: an action potential (signal) generated by one neuron propagates along its axon and via a noisy synaptic connection (channel) induces a response in the soma and dendrites of other neurons (see Purves et al., 2007). The notion of individual neuron polarity, though modified, remains a foundation of our understanding of neural communication in cerebral cortex (see DeFelipe, 2010). Mapping cortical connectivity is, therefore, vital to defining the channels of information flow underlying cortical function in both health and disease.

Recent technical advances now offer significant improvements in mapping the apparent disorder of the "cerebral jungle" across a range of spatial scales. Large-scale serial electron microscopy (EM) of gray matter volumes ($<1\,mm^3$) can be used to map the fine structure of cerebral cortex (Mishchenko et al., 2010; Bock et al., 2011). Trans-synaptic viral tracing methods now make it possible to visualize multiple stages of synaptic connectivity (Wickersham et al., 2007). Combinatorial fluorescent protein labeling methods are used to separately color the processes of many individual neurons simultaneously to aid multiple axon tracing (Lichtman et al., 2008). Combined magnetic resonance imaging (MRI) techniques are now used to reconstruct the whole cortico-cortical pathway network for an individual brain *in vivo* (Hagmann et al., 2010). Thus, the future promises to yield far more mapping data concerning cerebral cortex.

Yet mapping cortical connectivity will not in itself tell us how cerebral cortex works (see Douglas and Martin, 2011). Indeed, even with these technical advances, the huge number of neurons and synapses per cortical hemisphere make constructing a whole map of synaptic connections or *connectome* impractical (Lichtman et al., 2008; DeFelipe, 2010). From available mapping data we need to discover the general organizing principles of the "cerebral jungle" and to infer what purpose these principles may serve in terms of cortical function.

To explain brain design, Cajal (1899) proposed that neuronal morphology was regulated by distinct organizing principles that sought to separately conserve cellular material ("wire"), conduction delay, and brain volume. Contemporary research on brain design has focussed predominantly on the wiring minimization principle (Mitchison, 1991; Cherniak, 1994; Chklovskii et al., 2002). Strong claims have been made that this organizing principle alone can explain, for example, the intracortical wiring underlying functional maps (Koulakov and Chklovskii, 2001). Recent studies suggest, however, that individual cortical neuron morphology (Budd et al., 2010; Cuntz et al., 2010) and neural networks are not organized by wire minimization only (Ahn et al., 2006; Kaiser and Hilgetag, 2006; Bassett et al., 2010).

We have previously proposed a multi-scale wiring principle for optimizing neuronal network communication in cerebral cortex (Budd et al., 2010). This hypothesis states that the conservation of cellular material (construction cost) is traded-off against the need to minimize conduction delay (routing cost). Indeed, for a modest excess of cellular material, this trade-off promotes precise and rapid communication in cerebral cortex, which has implications for our understanding of neural coding and synchrony (see Uhlhaas et al., 2009).

The main purpose of this article is to critically review recent evidence to discover how well this hypothetical wiring principle may explain cortical connectivity across different spatial scales. The article is not intended as a review of the cortical connectome approach *per se* but it does examine the utility of this framework to help evaluate this and other hypothetical wiring principles. We begin with a brief introduction to spatial networks and its application to different levels of cortical organization before evaluating evidence relating to the hypothesis.

SPATIAL CORTICAL NETWORKS: NEURONS, CIRCUITS, AND PATHWAYS

Graph theory is a powerful technique for the mathematical abstraction of real world problems (see Newman, 2010). **Box 1** offers a short introduction to relevant graph theory concepts and notation. Briefly, in a *network* each distinct entity of a given system is represented by a single *vertex* and the pairwise relations and processes between these entities is represented by an *edge* (see **Box 1**; for further details, see Cormen et al., 2001). The network configuration describes all possible paths of information flow within the system. A graph theoretic approach is applicable, therefore, if a system can be viewed as a collection of distinct yet inter-related objects.

Neural systems can be decomposed into distinct objects and pairwise relations. For example, pre- and post-synaptic neurons are related yet distinct objects in a neural system as are, at a more basic level, the individual branches of a neuron's axonal or dendritic tree. But applying graph theory to model a neural system naturally requires assumptions to be made about the system's architecture. Characterizing an entire axonal pathway by a single edge, for instance, does not capture how information is distributed by the divergence/convergence of presynaptic axons in the target structure. Hence, it is important to be mindful of model assumptions and granularity when making inferences about cortical function from network models.

To construct a realistic biological network, the entities and pairwise relations in the biological system must be mathematically defined using available empirical evidence. When existing knowledge is insufficient or conflicting, however, it is necessary to either exclude certain system properties from consideration or make explicit assumptions regarding the system to resolve the issue. Once constructed, measures can be taken to describe the characteristics of the biological network and the results compared with those of artificial networks generated using hypothesized principles of organization. The degree of similarity between artificial and biological network characteristics can then be used to determine whether the hypothesized organizing principle merits further investigation, requires modification, or should be rejected. Here, we focus on spatial cortical networks, where vertices and edges have a physical correspondence to the anatomy of cerebral cortex. While not ignoring the importance of other relevant parameters, for reasons of available data we concentrate on two main costs in neuronal communication: conduction delay and cellular material.

SPATIAL NETWORKS

A *spatial network* is a graph whose vertices have spatial coordinates and where measurements are taken with respect to their physical space (Barthélemy, 2011). In spatial cortical networks, each vertex represents a distinct neural feature in cerebral cortex with anatomical coordinates and each edge represents an uninterrupted path of communication between a vertex pair.

In an unweighted spatial network, analysis is directed toward understanding the relationship between space and topology in a given system, e.g., what connectivity patterns exist between particular groups of neurons? In the last decade or so, networks whose topology is neither entirely regular nor entirely random—*complex networks*—have generated considerable interest because of their ability to account for the organization of large-scale biological, physical, and social system using simple connectivity rules (Newman, 2010). In s*mall world* complex networks, for instance, the average path length between any given vertex pairs is reduced by incorporating a small percentage of long-distance connections in a network of mostly short-range regular connections (Watts and Strogatz, 1998). In *scale-free* complex networks, the vertex degree (see **Box 1**) distribution is described by a power law in which there are a small fraction of highly connected vertices called *hubs* (Barabási and Albert, 1999). Analyzing network partitions, *subgraphs*, may reveal further structural complexity. The conditional probability of a vertex pair being additionally connected to a third vertex is termed *clustering*, which is high in complex but low in random networks (Watts and Strogatz, 1998). Relatedly, when a given set of vertices has more connections in common

Box 1 | Graph Theory.

Network Structure

A **network** is a graph (G) consisting of a set of vertices (V) and a set of edges (E) connecting those vertices, $G = (V,E)$, e.g. a neural circuit.

A **vertex**, v, represents a distinct object, e.g. a neuron's cell body.

An **edge**, e, represents an uninterrupted path of communication between a vertex pair (u,v), e = (u,v), e.g. an axon connecting a pair of neurons.

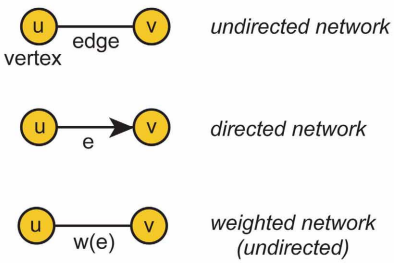

Network edges (see above) may communicate in both directions (**undirected**) or one direction only (**directed**); and may additionally be assigned a **weight** or **cost**, w(e), such as the spatial distance between connected vertex pairs.

Network connectivity (topology) is defined in the **adjacency matrix**, where each matrix element records the presence (non-zero value) or absence (zero value) of an edge.

Example 1 **Adjacency Matrix**

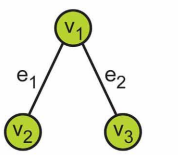

acyclic network (tree)

	v_1	v_2	v_3
v_1	0	1	1
v_2	1	0	0
v_3	1	0	0

adjacency matrix

A network of three vertices $V = \{v_1, v_2, v_3\}$, that is $|V| = 3$, and two edges $E = \{e_1, e_2\}$, so $|E| = 2$.

Here, vertex #2 (row 2) is directly connected to vertex #1 (column 1) but not directly connected to vertex #3 (column 3).

Degree is the number of edges incident on a vertex.

Networks are termed **sparse** when most elements of the adjacency matrix are zero (i.e. $|E| << |V|^2$) and **dense** when most are non-zero (i.e. $|E| \sim |V|^2$).

Path Length

A **path**, p, is an ordered sequence of k vertices connecting a given pair of vertices (u,v), where $k = |p|$.

Path length is measured differently depending on whether the type of network is unweighted or weighted.

In unweighted networks (see Example 1), path length is measured by the number of intermediate vertices (k-2) or '**hops**', or the number of edges (k-1) traversed along the path. In Example 1, the shortest path from vertex #2 to vertex #3 takes one hop (i.e. $p = <v_2, v_1, v_3>$, k-2 = 1) and two edges (i.e. k-1 = 2).

In weighted networks (see Example 2), path length is measured by the sum of weighted edges traversed, w(p).

A **cost or weight matrix** stores the value of each edge's cost/weight. When no edge exists, an infinite ('inf') cost is recorded.

Example 2 **Weight Matrix**

The goal is to find the shortest length path between vertex pair (v_1, v_4) in the weighted network below.

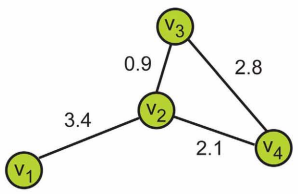

cyclic network

	v_1	v_2	v_3	v_4
v_1	inf	3.4	inf	inf
v_2	3.4	inf	0.9	2.1
v_3	inf	0.9	inf	2.8
v_4	inf	2.1	2.8	inf

cost or weight matrix

Here, two possible shortest paths exist:
$p_1 = <v_1, v_2, v_4>$, and
$p_2 = <v_1, v_2, v_3, v_4>$.

Path p_1 is shortest because $w(p_1) < w(p_2)$:
$w(p_1) = 3.4 + 2.1 = 5.5$.
$w(p_2) = 3.4 + 0.9 + 2.8 = 7.1$.

Notation: symbol |x| means size of set x.

than with other vertices, the subgraph is considered a (vertex) *community* or *module* (Girvan and Newman, 2002). Subgraphs with frequently repeating patterns of connectivity are termed *network motifs* (Milo et al., 2002).

In a weighted spatial network, analysis is focused on the relationships among cost, space, and topology, e.g., how much does a specific spatial and/or topological arrangement of neural features cost? Global network metrics are often used to address such questions. The total cost of the network is equal to the sum of all weighted network edges. For example, when edge cost is proportional to the Euclidean distance between a vertex pair the total cost gives the spatial *construction cost* of the network. In this article, distance will refer to Euclidean distance unless otherwise stated. A complementary metric is global *routing cost*, which is the average or total path length of a network. There are two alternative measures of routing cost. Latora and Marchiori (2001) have defined network *efficiency* as the inverse of the shortest path length and the average efficiency over all vertex pairs as a measure of global efficiency. Gastner and Newman (2006) have proposed *route factor* as a measure of efficiency for trees, the mean of metric path length divided by radius from root to all vertices.

How a system is represented graphically influences what can be inferred about its communication or processing characteristics. **Figure 1** illustrates this point by comparing the shortest path length in unweighted (**Figure 1A**) and weighted network representations (**Figure 1B**) for the same toy problem. Recall that path length is measured differently between weighted and unweighted networks (see **Box 1**). In the unweighted representation, the use of directional edges removes one of two possible paths connecting vertex A to vertex D (**Figure 1C**). So if the directions of information flow were known for the system but not incorporated in the network model, inferences concerning the directness of communication would be distorted; the undirected network would allow information to flow along paths that were impossible in the real system. Similarly, the shortest length path in the unweighted network representation (**Figure 1A**, left) is the one with the fewest hops whereas in the weighted network representation of the same system (**Figure 1B**) it is the path with the lowest total cost (see **Figure 1C**). This means that the choice of graphical representation can for the same system identify different shortest paths, though this choice may be dictated by available data.

In network design, simultaneously minimizing both construction and routing costs is considered an intractable (NP-hard) optimization problem because these are conflicting objective functions (Hu, 1974; Alpert et al., 1995; Khuller et al., 1995; Wu et al., 2002; Gastner and Newman, 2006). **Figure 2** illustrates how a trade-off between these conflicting objective functions affects the structure of a spatial network. Here, optimizing total weight (construction cost) only leads to a *minimum spanning tree* (**Figure 2A,** left) or, if additional vertices are inserted, a *Steiner minimal tree* design (Garey and Johnson, 1979). In

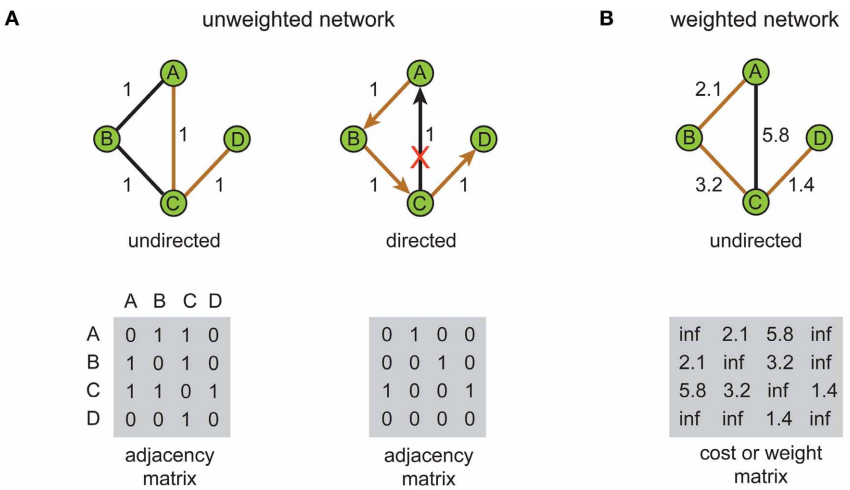

C

Path			
A-B-C-D	2 hops or 3 edges	**2 hops or 3 edges**	**6.7 cost units**
A-C-D	**1 hop or 2 edges**	invalid path (x)	7.2 cost units

FIGURE 1 | Shortest path for the same problem can be different depending on the type of network representation used. An example network consists of four labeled vertices A, B, C, and D. The aim is to find shortest path between vertex A to vertex D. **(A)** Unweighted network representation. The topology of undirected (left) and directed versions (right) is shown graphically (top) with their corresponding adjacency (connectivity) matrices below (bottom). Brown lines show shortest paths. Red cross indicates a counter-directional edge, which creates an invalid path from vertex A to vertex D. **(B)** Weighted network representation. Graphical representation (top) of an undirected weighted graph with values of weights (distance) shown next to edges and recorded in the cost or weight matrix below (bottom). Note in the cost or weight matrix the absence of an edge is recorded as an infinite cost ("inf") while in adjacency matrix it is recorded as zero. **(C)** Summary table for path length results corresponding to each type of network. Shortest paths are shown in bold brown text.

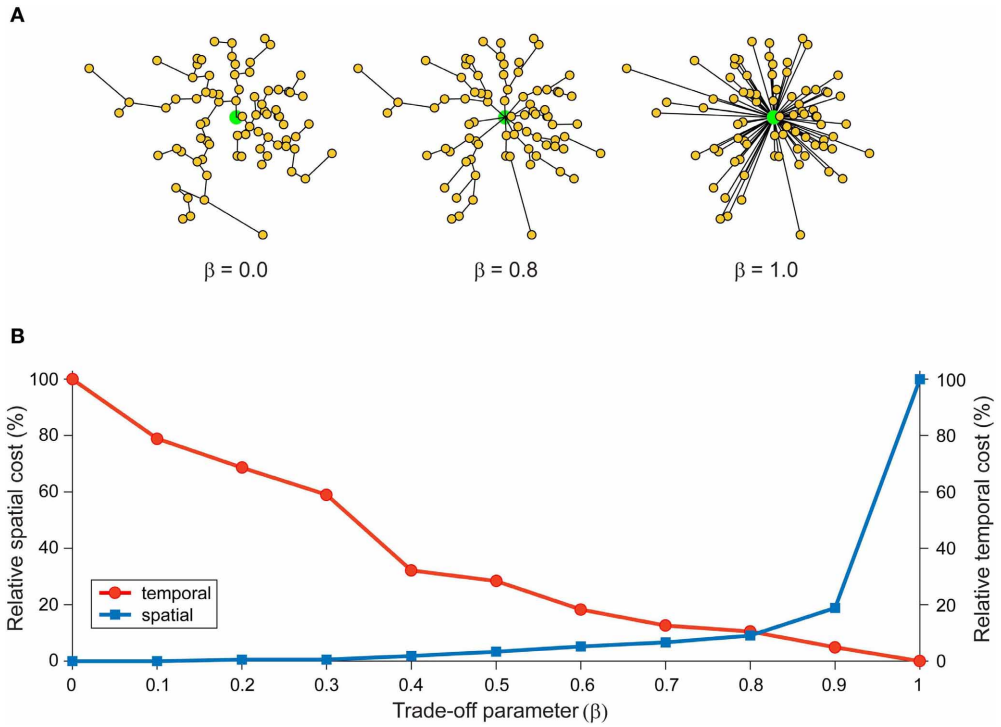

FIGURE 2 | Spatial and temporal cost trade-off alters arbor morphology. An example network consists of 80 labeled vertices (small yellow filled circles) plus a root vertex (large green filled circle). Here, total wiring cost = spatial cost + (β × temporal cost), where the parameter β, which varies between 0 and 1, is used to trade-off spatial construction cost against temporal routing cost. **(A)** Artificial arbor structures optimized for different values of a cost trade-off parameter, β = 0.0 (spatial cost optimization, left), 0.8 (mixed cost optimization, middle), and 1.0 (temporal cost optimization, right). **(B)** Relative communication costs vary as a function of the trade-off parameter. Relative spatial cost (wire length) increases with β rapidly when β > 0.8, while relative temporal cost (path length) steadily decreases with β. Costs at equilibrium around β = 0.8. Artificial arbors were generated using Gastner and Newman (2006) algorithm.

contrast, optimizing average/total path length only (routing cost) generates a *star tree* (**Figure 2A,** right), where there is direct connection from a central hub to each remaining vertex to create a hub-and-spoke design. Instead, a suboptimal minimization of construction cost permits a low routing cost (**Figure 2A,** middle). **Figure 2B** shows the relative change in communication costs in this spatial network for different values of β, a parameter that trade-offs spatial construction cost against temporal routing cost. When β = 0 then spatial cost is minimized and temporal cost maximized. Whereas when β = 1, the situation is reversed. Between these extremes, temporal cost decreases monotonically with increasing β while simultaneously spatial cost increases slowly until after the equilibrium point (β = 0.79) when it increases rapidly.

Here, the purpose of network analysis is to generate experimentally testable hypotheses to help advance our understanding of cortical organization and dynamics in health and disease (Bassett and Bullmore, 2009; Sporns, 2011; Leergaard et al., 2012—see *Frontiers in Neuroinformatics* Research Topic "Mapping the connectome: Multi-level analysis of brain connectivity"). To date, all network analysis suggests cortical connectivity has non-random, complex network characteristics (Sporns, 2011). In the following parts, we will discuss results obtained with multi-scale spatial analysis of cortical organization.

SPATIAL SCALES OF CORTICAL ORGANIZATION

A *connectome* is a graph theoretic construct used to describe neural architecture at different spatial scales in terms of neural elements (vertices) and neural connections (edges) (see Sporns et al., 2005). Ideally, each edge should be annotated with a range of associated properties to completely describe its anatomical and physiological connection characteristics including axonal length and conduction delay. In the Human Connectome proposal, Sporns et al. (2005) argued that the organization of cerebral cortex could be viewed at three distinct spatial scales: *microscopic* (micron spatial resolution of the processes of individual neurons and synapses), *mesoscopic* (hundreds of micrometers spatial resolution of cortical columns and local circuits), and *macroscopic* (millimeter spatial resolution of brain regions and pathways). This framework elegantly utilizes the generality of graph theory to abstract anatomical entities and their relationships at different spatial scales of cortical organization. To understand brain structure as a whole, DeFelipe (2010) argues we need to possess connectomes for each spatial scale.

But the term "connectome" may be used too loosely (Kasthuri and Lichtman, 2007; DeFelipe, 2010). EM is required to confirm the presence of a synaptic connection (Peters et al., 1991) otherwise putative synaptic connectivity can only be inferred from the close spatial proximity such as axonal-dendritic

membrane apposition (microscopic scale) or regional termination pattern (macroscopic scale) as is done in most studies using confocal microscopy. Consequently, a connectivity (adjacency) matrix constructed from axonal tracing but lacking ultrastructural confirmation might more accurately be referred to as a "projectome" (Kasthuri and Lichtman, 2007). Additionally, a connectome whose connectivity has been confirmed by EM might better be called a "synaptome" (DeFelipe, 2010). For the sake of simplicity, we use the term "connectome" here to mean the accurate structural description of connected neural elements.

The Human Connectome scheme has some degree of correspondence with the Levels of Brain Organization approach (Shepherd, 1990). In this the top level is concerned with mapping *systems and pathways level*, which relates directly with the macroscopic scale. The next level describes the *local circuit level*, defined as regional groups of interconnected neurons, which matches with the microscopic scale. However, the correspondence breaks down because the levels approach appears to lack a mesoscopic scale and the Connectome scheme lacks both a *neuron level*—discrete nerve cells as morphological entities with integrative properties—and a *microcircuit level*—stereotyped patterns of synaptic connections forming neuronal subunits. While the advantages of having a well-defined mesoscopic scale in cerebral cortex are clear (Bohland et al., 2009), no precise, and universal defintion currently exists (Horton and Adams, 2005; da Costa and Martin, 2010; Rockland, 2010). Here the problem lies in the fact that there is no consensus what should be the measure of dimension of mesoscopic connections.

COMMUNICATION COSTS AT DIFFERENT SPATIAL SCALES

To evaluate the proposed multi-scale wiring principle, we now examine the results from the analyses of graphical representations of cortical organization at three different spatial scales (see **Figure 3**): neuron, local circuit, and pathway scales. The reason for choosing these scales is that they offer a simple hierarchical organization of cerebral cortex into individual functional elements, connectivity within a cortical region, and connectivity between cortical regions, respectively. Local circuit (microscopic) and pathway (macroscopic) scales are represented in both approaches discussed in the previous section. But this scheme includes a neuron scale, which is absent in the Human Connectome proposal, because we are interested in how communication costs may have shaped neuronal morphology as well as cortical circuits. We recognize that this scheme limits our consideration to specific spatial scales and so may neglect subtle intermediate-scale wiring strategies.

NEURON SCALE

To explain qualitative observations made from Golgi impregnated neurons, Ramón y Cajal proposed that neuronal morphology is controlled by laws separately conserving cellular material ("wire"), conduction delay (time), and brain volume (Cajal, 1899). Cajal did not attempt to quantify these relationships nor explain how they might interact. But he noted that in some cases the conservation laws might conflict "sacrificing economy of matter in favor of economy of time" (Cajal, 1899), which

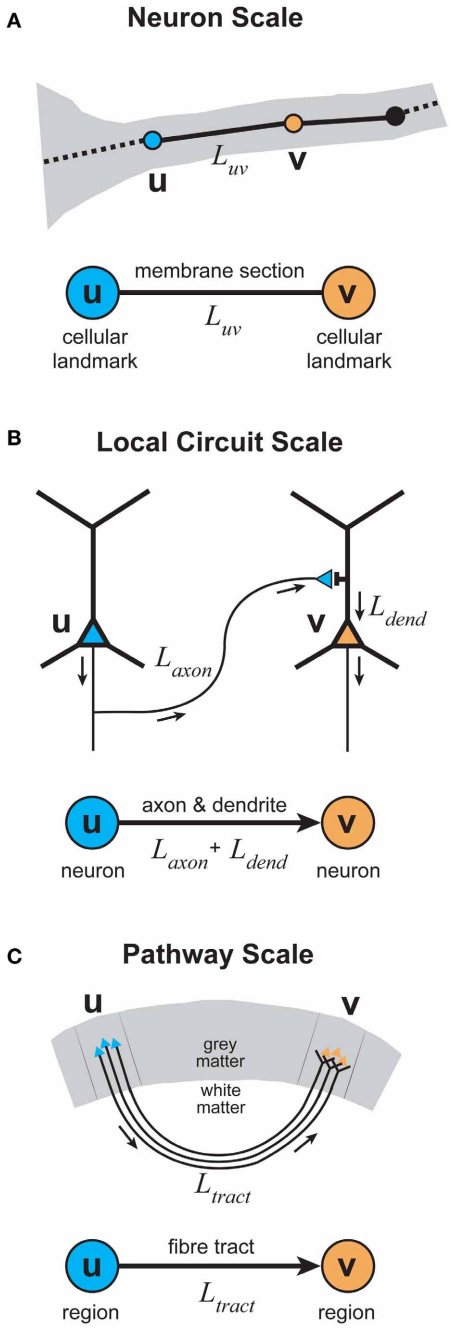

FIGURE 3 | Elementary graphical representations of cortical organization at different spatial scales. (A) *Neuron scale.* Each vertex represents the location of a cellular landmark obtained from the 3D reconstruction of individual axonal or dendritic arbors (e.g., location of the presynaptic terminal boutons) with an undirected edge representing the section of membrane linking these vertices either by the actual path length or the direct distance between a vertex pair. **(B)** *Local Circuit scale.* Each vertex represents the somatic location of a single neuron with a directed (or undirected) edge representing the sum of the axonal and dendritic lengths connecting a pair of neuronal somata. **(C)** *Pathway scale.* Each vertex represents a distinct cortical brain region in grey matter with a directed (or undirected) edge representing the axonal fiber tract connecting a pair of cortical regions, where its length describes the actual path or direct distance of its course within white matter.

pre-dates observations made regarding cost trade-offs in network design (Section "Spatial Networks").

To explain features of neuronal morphology and synaptic connectivity, research initially focussed almost exclusively on the role of conserving cellular material or wire length—the wiring minimization principle (Mitchison, 1991; Cherniak, 1994; Chklovskii et al., 2002). The ability of this solitary principle to explain connectivity has been highly influential in shaping thinking about brain design and explaining CNS connectivity (Chklovskii and Koulakov, 2004). For example, it was claimed that the wiring minimization principle could completely explain the wiring pattern of the roundworm *C. elegans* (Cherniak, 1994), the only fully mapped CNS connectome.

In recent years, however, a steady accumulation of evidence has eroded the over-riding importance of wire length minimization. In particular, the wiring pattern of *C. elegans* connectome is not strictly minimized for wire length because of the existence of long-range connections, which runs counter to the wiring minimization principle (Ahn et al., 2006; Kaiser and Hilgetag, 2006). The dominance of the wiring minimization principle, however, resulted in less attention being given to the other conservation laws of conduction delay and volume minimization and to understanding how these distinct laws interact. To redress the balance, two recent studies independently investigated Cajal's laws of material and conduction delay conservation in relation to the axonal and dendritic arbors of individual neocortical neurons, respectively.

Axon arbors

To analyze the wiring characteristics of single intracortical axon arbors, Budd et al. (2010) applied a range of graph theory optimization techniques to 19 *in vivo* reconstructions of excitatory spiny (pyramidal and spiny stellate) and inhibitory basket cells (Buzás et al., 2001; Kisvárday et al., 2002; Buzás et al., 2006). A 3D graphical representation was constructed for each axon arbor (see **Figure 3A**). Here, each fixed vertex corresponded to one of the thousands of putative presynaptic axonal boutons associated with the arbor plus a root vertex to represent the axon origin. The edges linking these vertices represented the arrangement of axon branches and collaterals in the arbor reconstructions. Edge weight was determined from the distance between the locations of connected vertex pairs. Total axonal wire length and average path length metrics were used to compare biological axon arbors against cost optimized artificial arbors.

Neocortical axon arbors were not strictly minimized for either total axonal length or average path length; arbors used approximately 10–20% more axonal length than strictly necessary (Budd et al., 2010). Axon arbors used this excess wire to substantially improve average path length from axon origin to axonal boutons (**Figure 4A**). Strictly minimizing wire length only generated artificial arbors with a tortuous morphology and poorer average path lengths. In contrast, when artificial arbors were strictly minimized for path length only, they used a huge amount of axonal wire. Excess axonal wire in biological arbors was associated with branching close to the parent cell body and internodal axon segments lacking any boutons, which were often found between terminal branch clusters. Extrapolating from reported intracortical axon conduction velocity values (e.g., Luhmann et al., 1990), axonal path length distributions in this study suggested a narrow temporal dispersion of axonal latency within an arbor and a tight relationship between axonal latency and cortical distance (Budd et al., 2010). This prediction receives some support from the strong correlation between EPSP latency and cortical distance in the connections from layer 4 spiny neurons to layer 2/3 interneurons observed *in vitro* (see **Figure 3C** in Helmstaedter et al., 2008). Due to their greater branching complexity, the estimated axonal latencies of inhibitory basket cell were less dispersed than those of excitatory spiny cell axons. Thus, as expected for spatial networks generally (see "Spatial Networks"), neocortical axon arbors appear to trade-off communication costs using a small amount of extra axonal wire to ensure rapid and temporally precise signal propagation.

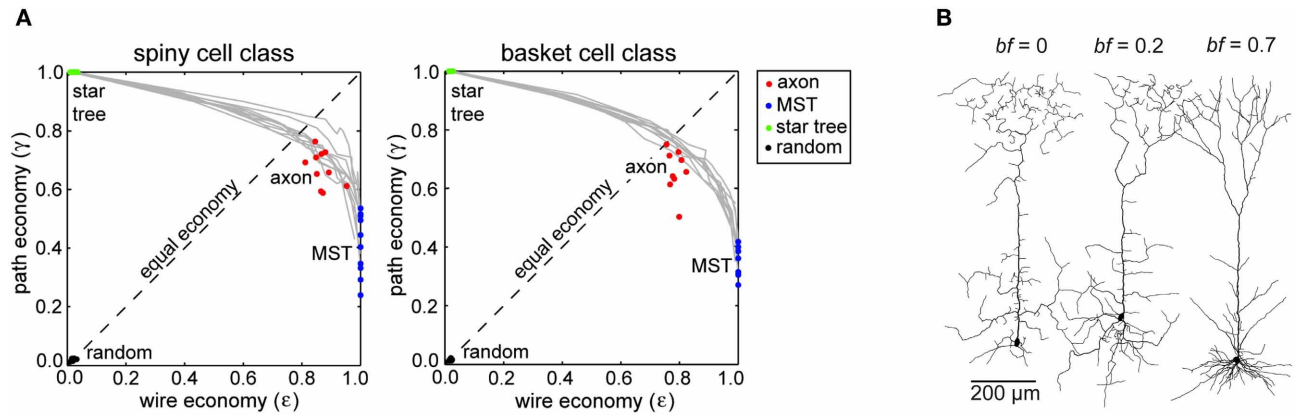

FIGURE 4 | Communication cost trade-off at Neuron scale of cortical organization. (A) Similar degree of trade-off between path length and wire length economy of intracortical spiny (left) and basket cell axon arbors (right) between corresponding path length optimized star trees and wire length optimized minimal spanning trees (MST), which were all more economical than random arbors (Reprinted from Budd et al., 2010). **(B)** Examples of spiny pyramidal cell dendritic arbors generated using different trade-off balancing factor (*bf*) values show that the most realistic looking arbor was obtained for $bf = 0.7$ (Reprinted from Cuntz et al., 2010). Note *bf* parameter is equivalent to β parameter in **Figure 2**.

It should be mentioned that little is known about the trade-off across different species and neuronal types. The above study examined intracortical axons from adult cat primary visual cortex only and did not examine other neuronal types accounting for 10–15% of all neocortical neurons (see Budd et al., 2010). It would be interesting to know whether the communication cost trade-off extends universally to other neuronal types (typically short-axon types), cortical areas and species. In addition, axon diameter was not considered as an optimizing parameter in this study for reasons of computational complexity and measurement accuracy (see "Cortical Network Design Problem"). Finally, like other structural analyses, this study extrapolated temporal characteristics from published estimates of axonal conduction velocity. This general limitation of structural network analyses is examined in more detail later (see "Physiological Considerations").

Dendritic arbors

To investigate how Cajal's principles might shape dendritic arbor morphology, Cuntz et al. (2010) "grew" artificial arbors starting from a single root vertex and then incrementally added edges to connect a set of sample (carrier) points. These sample points were selected uniformly at random from a 3D probability density distribution of branch and terminal points derived from multiple morphological reconstructions of actual pyramidal cell dendritic arbors in a specific cortical layer. At each iteration, a minimal spanning tree (MST) algorithm connected the existing arbor to the carrier point with the next lowest total cost until all points were connected to the tree (Cormen et al., 2001). Total cost was equal to the total wire length plus path length cost, which was multiplied by a balancing factor, *bf* (equivalent to β in **Figure 2**). For $bf = 1$, wire length and path length costs were treated equally; when $bf = 0$ then path length cost was ignored, minimizing wire length only. This approach has been previously applied to spatial network design problems outside neuroscience (Alpert et al., 1995; Gastner and Newman, 2006). Spatial jitter was randomly added to the artificial arbor vertices to mimic branch tortuosity in the neuropil. To estimate neuronal electrotonic cable properties, Cuntz et al. (2010) applied a radius-dependent dendritic diameter-tapering rule to the edges of the final artificial arbor to obtain the average electrotonic compartment size. Artificial arbors were morphologically compared with biological arbors using branch order and path length distributions and Sholl analysis descriptive statistics (Sholl, 1953).

Pyramidal cell dendritic arbors, regardless of cortical lamina, were best approximated by artificial arbors with a balancing factor of around 0.7 (**Figure 4B**). With a lower balancing factor, dendritic morphology was more tortuous and had a much greater average compartment size than observed in corresponding biological arbors. But Cuntz et al. (2010) noted pyramidal dendritic arbors had greater variability than dendritic trees in other neural structures. Interestingly, with a forest of growing arbors competing for carrier points, Cuntz et al. (2010) were able, by making each carrier point exclusive to the first arbor to which it became attached, to reproduce realistic individual artificial arbors and spatial tiling at the same time. These simulations demonstrate for the first time how balancing individual arbor communication costs may also conform to Cajal's law of brain volume conservation.

This study is, however, open to a number of criticisms. First, while artificial and biological pyramidal dendritic arbors visually appeared highly similar, no statistical tests for the degree of fit were reported. Second, to replicate the morphology of whole arbors the algorithm had to grow the apical tuft of an artificial neuron separately from its basal dendritic tree (see Cuntz et al., 2010). This suggests that the current algorithm might find it difficult to automatically reproduce more sparsely connected structures such as large axon arbors (e.g., Buzás et al., 2006). Third, the study was restricted to reproducing the morphological charcteristics of pyramidal cell dendritic trees neglecting those of other cortical neuronal types, notably aspiny or smooth type cortical neurons. Finally, it is not clear what biological mechanism could reproduce the results of the growth algorithm that appears to require global knowledge of vertex positions to compute total cost.

Arbor self-similarity

Relatedly, the morphology of neocortical axon and dendritic arbors have been separately described as possessing statistical self-similarity (e.g., Tettoni et al., 1998; Binzegger et al., 2005; Rothnie et al., 2006; Wen et al., 2009), implying common principles of arbor construction across a range of spatial scales.

To gain insight into the morphological diversity of afferent axon arbors innervating cerebral cortex, Tettoni et al. (1998) examined the metric and topological characteristics of 3D reconstructions of twenty-two callosal afferent axons from the area 17/18 border of cat visual cortex and seventeen thalamocortical afferent axons projecting from mouse ventrobasal thalamic nucleus to primary somatosensory cortex. Although these visually distinct axons derived from different species and represented different arbor types, they were similar metrically and topologically. Metrically, arbor types did not differ significantly in total axonal length, total number of branches, or branching angles. The topology of the two types of arbor proved highly similar when compared for maximal branching order (centripetal ordering scheme) and the distribution of branch order per arbor. However, arbor types were distinguishable in at least two respects. First, single thalamocortical arbors had on average five times more boutons with a higher proportion of branches with boutons than callosal arbors. Second, arbor types differed in their relationship between branch order and branch length: as branch order increased (distal to proximal direction), the individual branches of callosal axons tended to lengthen while thalamocortical axon branches shortened. Although there was individual arbor variability, this study suggests that corticocortical and corticothalamic afferent axons may share a common topology and differ only in a few metric parameters.

In a complementary study, Binzegger et al. (2005) systematically investigated the metric, topological, and fractal self-similarities of 3D reconstructions of spiny, smooth, and thalamic axon arbors intracellularly labeled in adult cat visual cortex ($n = 39$ axons). Here, each axon arbor was represented graphically with its edges corresponding to the axon's branch collaterals. Each edge was assigned a length corresponding to the length of the branch

collateral and labeled to denote its topological order according to the Strahler centripetal scheme (see MacDonald, 1983). Arbor complexity was measured using the fractal box-counting dimension (see Addison, 1997). Binzegger et al. (2005) found that while smooth cell axon arbors branch more frequently than spiny cell axons (see also Budd et al., 2010) these arbors have similar branch length distributions. In addition, they reported the morphological diversity amongst arbor types masked a highly similar branching topology and statistical self-similarity (1.2–1.9 average fractal dimension). Smooth cell axons tended to exhibit greater complexity than either spiny or thalamocortical arbors. Although the majority of arbors showed statistical self-similarity, it remains unexplained why nearly 18% of arbors studied did not appear fractal-like. Together, the results of Tettoni et al. (1998) and Binzegger et al. (2005) imply a common principle of construction for thalamocortical and both extrinsic and intrinsic corticocortical axon arbors, where arbor topology is type-invariant but metric parameter values vary to alter axon branching patterns and synaptic bouton density.

In analyzing the basal dendritic arbors of pyramidal cells, Wen et al. (2009) reported evidence of a statistical self-similarity in the shape of 3D arbor reconstructions from cat visual cortex and a scaling correlation between arbor radius and dendritic length for these and more than two thousand 2D arbor images from primate neocortex. To explain these results, Wen et al. (2009) initially hypothesized that dendritic arbors sought only to maximize the number of different combinations of potential synapses, axon and dendritic appositions within a dendritic spine's length (Stepanyants and Chklovskii, 2005). Yet this unconstrained objective function (entropy maximization) generated space-filling artificial arbors with a tortuous morphology, because the branches sought both to maximize total arbor volume and spread out to avoid receiving multiple potential synapse from the same axon. When the objective function was constrained by path length cost (conduction delay), however, the less tortuous artificial arbor morphology was more realistic. This result highlights the importance of conduction delay conservation as a constraint on neuronal arbor design and communication.

In a bold unifying approach, Snider et al. (2010) proposed that all axonal and dendritic arbor types could be described by a single truncated Gaussian spatial density function (envelope of averaged arbor branching density). Yet a unimodal kernel cannot, for instance, properly portray the spatial clustering of axon terminals observed within the extent of long-range basket and pyramidal cell axon arbors (e.g., Kisvárday et al., 2002; Binzegger et al., 2005, 2007; Budd et al., 2010). Moreover, this approach had to describe separately the apical and basal dendritic trees of the same pyramidal neuron (Snider et al., 2010). Although Snider et al. (2010) acknowledged their approach was not directly concerned with branching topology, this work does emphasise the universality of dense arbor branching close to the parent cell body, identified as a source of excess wire length that helps reduce average axon path length (Budd et al., 2010).

Summary

Structural evidence for balanced communication costs in single cortical axons and dendritic arbors appears compelling, though it remains to be seen whether this wiring principle is universal across all neuronal types, cortical regions, and species. To test structural predictions, *in vivo* two-photon calcium imaging microscopy might be used to reconstruct the morphology of single cortical axon and dendritic arbors and then measure the latency of signal propagation at various arbor locations (e.g., Katona et al., 2011). However, as the field of view of two-photon microscopy is currently limited to less than 1 mm it would provide only a partial test for axon arbors (Katona et al., 2011).

Importantly, the results together suggest intracortical axon and dendritic arbors may well follow the same wiring principle. If so this principle has at least three advantages for efficient cortical design. First, it may provide the basis for arbor scaling because it will, unlike wire length minimization, allow for the addition of branches without significantly degrading communication. Second, time and distance in cerebral cortex will be strongly and positively correlated to promote temporal coherence between simultaneously excited but equidistant sources. Third, it implies a highly efficient genetic encoding of morphological neuronal differentiation may account for neuronal diversity though variation in the expression of relatively few molecular factors (see Dent et al., 2011). We next consider whether this wiring principle applies at larger spatial scales of cortical organization.

LOCAL CIRCUIT SCALE

Although individual axonal and dendritic arbors may separately trade-off structural communication costs, it cannot be assumed that these necessary conditions are together sufficient for local cortical circuits to also trade-off communication costs. When constructing graphical representations of local cortical circuits, edge lengths must combine both the axonal path length from presynaptic cell body and dendritic path length from synapse to postsynaptic cell body (see **Figure 3B**). This means that axosomatic or axoaxonic connections should tend to be less costly than axodendritic synapses, which are by far the most common variety of cortical synapse (Beaulieu and Colonnier, 1985; Schüz and Palm, 1989; Beaulieu et al., 1992). Somatic size limits the number of axosomatic connections to at most a few hundred (Fariñas and DeFelipe, 1991). Nonetheless these synaptic inputs probably have a robust influence on firing due to the closeness of their synapses to the action potential initiation zone, such as inhibitory basket cell axons and axoaxonic cell contacts regulating the phase of oscillatory firing (e.g., Cobb et al., 1995; Klausberger et al., 2003). On the other hand, the spatially extended dendritic arbors allow cortical neurons to each receive thousands of synaptic inputs (Feldman, 1984; Larkman, 1991). In deciding whether communication costs have been optimized in local cortical circuits, however, we need to know whether particular types of axon are constrained to target subcellular domains of dendritic arbors in cerebral cortex (see Somogyi et al., 1998). If so then a fixed offset should be subtracted from the edge length to compensate for this constraint. Yet the evidence that different types of axonal pathways innervate distinct subcellular domains of postsynaptic neurons is not clear-cut, e.g., thalamocortical axons (Ahmed et al., 1994; Bagnall et al., 2011 cf. da Costa and Martin, 2011).

Due to the lack of morphologically reconstructed local cortical circuits, there have to our knowledge been no published

empirical studies of structural communication costs in cerebral cortex at this scale. Instead we will focus on what is known about the network topology of perhaps the most studied subcircuit of neocortex.

Layer 5 networks

To investigate the topology of local circuits, network analysis has been applied to data obtained from multiple simultaneous *in vitro* electrophysiological recordings of thick tufted layer 5 (TTL5) pyramidal cells taken from immature rat neocortical slice preparations (Song et al., 2005, postnatal day, P12–20; Perin et al., 2011, P14–16). Using differential infra-red microscopy, this cell type is readily identifiable for recording because of its relatively large cell body (Markram et al., 1997). Consequently, the electrophysiology, morphology, and synaptic properties of TTL5 neurons have been studied extensively *in vitro* (Chagnac-Amitai and Connors, 1989; Larkman, 1991; Markram et al., 1997). TTL5 pyramidal cell networks, which are sparsely interconnected via recurrent collaterals (∼10%) (Markram et al., 1997), are of interest because they may be able to generate coherent theta-band oscillatory activity in neocortex (Chagnac-Amitai and Connors, 1989; Budd, 2005).

To investigate the degree of randomness in local cortical circuit connectivity, Song et al. (2005) analyzed quadruple whole-cell recordings of over 800 TTL5 pyramidal neurons in visual cortex obtained in a previous study (Sjöström et al., 2001). In these quadruple recordings, action potentials were evoked in each neuron in turn while recording the strength of any excitatory postsynaptic response in the remaining cells. Song et al. (2005) used these data to construct directed graphs for each quadruple recording group. They concentrated their analysis on three neuron groups for which there are 16 topologically distinct possible subgraph configurations. By generating random networks using their own estimates of unidirectional and reciprocal connection probabilities, Song et al. (2005) reported the existence of a number of three neuron motifs, subgraphs that occur more frequently than expected by chance, but only two of these achieved levels of statistical significance. Importantly, Song et al. (2005) found the more interconnected motifs tended to have stronger excitatory connections, from which they inferred a general network architecture consisting of a skeleton of strongly interconnected motifs surrounded by weaker and less connected neuronal motifs. They concluded the connectivity of TTL5 pyramidal cell networks were highly non-random.

Following a similar approach in somatosensory cortex, Perin et al. (2011) recorded from up to 12 pyramidal cells at a time for a total of over 1300 neurons. Like Song et al. (2005) they too discovered specific three- and, in addition, four-neuron motifs that were over-represented but obtained statistical significance only when recording groups contained six or more neurons. This confirmation of TTL5 pyramidal network structure suggests local cortical circuits may be composed of repeated elementary subnetworks, where each type of network motif serves a specific computational function (see Milo et al., 2002).

In addition, Perin et al. (2011) observed that the connection probability for a given neuron pair rose linearly with the number of connections they shared with other neurons—"*common neighbour*" rule. This relationship was stronger for shared input rather than output connections. This observation was independent of the intersomatic separation distance within the slice (up to 0.3 mm). Note the term "common" here does not necessarily imply neurons were spatially close. Perin et al. (2011) found neurons participating in a given motif which were often spread out spatially (100–125 μm).

Using the common neighbor rule and empirically based estimates of first-order distance-dependent connection probabilities, Perin et al. (2011) generated and analyzed an artificial network of 2000 point neurons. In this model, they identified nearly 40 spatially interlaced neuronal clusters, each of around 50 neurons. The model topology lacked the characteristics of scale-free, random, or regular networks but instead demonstrated small world clustering; the average shortest path length (unweighted) between any two neurons within a cluster was 1.9 hops, which is equivalent to 2.9 edges (synapses); hop count is the number of intermediate vertices (neural elements) that must be "hopped over" in a given path (see **Box 1**). This pattern of connectivity suggests a neuron may communicate more easily with others within a cluster regardless of its spatial location but less well with cells in other clusters even when they are spatially adjacent.

These two studies are significant because they hint at a local circuit topology that favors a high degree of clustering (small worldness) and emphasize the importance of higher-order statistics to determine connection probabilities. These higher-order statistics indicate that to understand local circuit connectivity requires more information than can be obtained from paired cell recordings.

Yet as neither study reconstructed and traced the processes connecting individual neurons, we cannot determine whether these local circuits were optimized for structural communication costs. We are unable to infer this, for instance, from electrode spatial locations, typically around 0.05 mm (e.g., Song et al., 2005), because these can these only give intersomatic distances between cell pairs. The intersomatic distance ignores the length of axon connecting a cell pair and the intracellular distance from dendritic synaptic input location to cell body, which alone is generally greater than the electrode separation distance (0.08–0.58 mm, Markram et al., 1997). To obtain the necessary data on whether the communication trade-off hypothesis holds at the local circuit scale of cerebral cortical organization, therefore, requires a reconstruction of the neuronal processes and tracing the connections of many individual neurons participating in a local cortical circuit—a formidable task for future studies.

Mapping morphology in local circuits

To help reconstruct local circuits, large-scale volume serial-section EM is now being used to map the fine structure of the cortical neuropil (e.g., Mishchenko et al., 2010; Bock et al., 2011). Manual annotation and tracing requirements of the very many EM images involved, however, severely limits progress. For example, Bock et al. (2011) examined a relatively small volume of mouse visual cortex (0.008 mm^3), containing large portions of around 1500 upper layer neurons, but manually mapped only a tiny fraction of all synapses (∼0.003%, 250 synapses out of 1×10^9 total synapses per mm^3 reported in Schüz and Palm, 1989). To completely survey even relatively small cortical volumes within a

reasonable time scale, automated or semi-automated annotation, and tracing methods under development (e.g., Chothani et al., 2011; Helmstaedter et al., 2011) will need to improve productivity by many orders of magnitude without endangering quality. Mapping small cortical volumes though will not account for the significant fraction of intrinsic connections originating from outside the local neuropil volume (Stepanyants et al., 2009) without the use of additional labeling techniques. The productivity gains achieved in the history of Genome mapping, however, does give cause for optimism (see Lichtman and Sanes, 2008).

The current Human Connectome framework (Sporns et al., 2005) does not appear to explicitly incorporate morphological descriptions of neuronal processes. Yet to evaluate structural hypotheses at the local circuit level, morphological descriptions are required. The morphology of an axonal or dendritic arbor cannot be recovered from a connectivity matrix alone because of non-uniqueness. Specifically, for a neuron forming N synaptic connections, the connectivity matrix data could be accounted for by any one of $N^{(N-2)}$ possible distinct tree configurations (Cayley's formula, Cormen et al., 2001). Reconstrucing a neuron's morphology is not only essential to estimate communication costs in cortical circuits but vital for understanding signal integration and distribution. In dendritic trees, for example, synaptic integration is shaped by arbor geometry, synaptic motifs, and the spatiotemporal pattern of dendritic stimulation (see Sjöström et al., 2008; Branco et al., 2010). On the positive side, however, incorporating an explicit 3D morphological description into the Human Connectome framework should not involve much additional computational cost. This is because to construct a connection matrix the paths of neuronal processes connected to a synapse must be traced back to the respective presynaptic and postsynaptic neurons (e.g., Mishchenko et al., 2010).

Summary

The absence of sufficient data for estimating structural communication costs at the local cortical circuit is a major hurdle in evaluating the multi-scale hypothesis. It is probable that soon fragments of a canonical cortical circuit will be reconstructed to permit the estimation of structural communication costs. In the meantime, progress in evaluating the hypothesis might be made by examining whether any trade-off between communications costs varies as the number of neurons per network motif increases.

PATHWAY SCALE

Cortical regions are connected via fiber tracts, bundles of efferent axons of various calibers and mostly myelinated, that course through white matter to their target cortical region (see Salin and Bullier, 1995). On entering gray matter, each axon ramifies to produce one or more terminal arbors that synapse with many postsynaptic neuronal processes in a characteristic laminar-specific pattern (Salin and Bullier, 1995). Individual axonal pathways may be classified as feedforward (traveling away from primary sensory areas), feedback (traveling toward primary sensory areas) or lateral (Rockland and Pandya, 1979; Felleman and Van Essen, 1991; Rockland, 1997). Based on the differential laminar termination patterns and physiological effect of afferent axons, feedforward pathways are thought to drive neuronal activity while feedback pathways act to modulate neuronal gain (Johnson and Burkhalter, 1996, 1997; Budd, 1998; Larkum et al., 2004; Rothman et al., 2009). Macroscopic cortico-cortical networks may be constructed by mapping fiber tracts to their end points to define regional vertex positions and using the tract itself to define the connecting edge (see **Figure 3C**). Edge costs can be defined according to tract morphological properties such as fiber length and fiber density/number.

Tracer-derived networks

By injecting molecular labeling agents such as biocytin or *Phaseolus vulgaris*-leucoagglutinin (PHA-L) into anatomically identified cortical regions, the origin or termination sites of individual cortical axons can be traced over long-distances (Rockland, 2004). Individual axons can have quite convoluted trajectories (Rockland, 1997) and may diverge to terminate in more than one cortical area (Schwartz and Goldman-Rakic, 1982; Bullier et al., 1984). By combining results from different laboratories for a variety of tracer agents, it has been possible to construct draft qualitative adjacency matrices of inter-areal cortical connectivity (Felleman and Van Essen, 1991; Scannell et al., 1995), of which some are publicly available, e.g., CoCoMac database for macaque cerebral cortex (http://cocomac.g-node.org/drupal/, Stephan et al., 2001; Kötter, 2004). An example is shown in **Figure 5A**. Analyses of these draft connectivity matrices have proved useful in, for example, establishing the high incidence of reciprocal pathways in macaque cortex (Felleman and Van Essen, 1991), offering an anatomical basis for separate ventral and dorsal functional streams in visual cortex (Young, 1992), and discovering "nearest-neighbour" and "next-nearest-neighbour" connectivity rules between cortical areas (Felleman and Van Essen, 1991; Young, 1992). But in the latter case these rules only partly explain the full connectivity matrix (Scannell et al., 1995; Costa et al., 2007).

To discover whether cerebral cortex macroscopic networks were minimized for wire length, Kaiser and Hilgetag (2006) used CoCoMac data to construct a 3D spatial network. This network comprised 95 vertices, where each vertex represented the 3D centre-of-gravity of a distinct cortical area or subarea obtained from a standardized cortical parcellation surface map, and 2402 edges, where each edge represented a pathway revealed by tracer injections. Edge cost was estimated from the distance between the 3D positions of vertex pairs rather than the actual length of the fiber tract. Kaiser and Hilgetag (2006) found the macaque cortico-cortical network does not appear to be strictly minimized for wire length. Optimization algorithms were able to significantly shorten the total wire length of the original macaque network ($>30\%$) mainly by reducing the number of long-distance connections (Kaiser and Hilgetag, 2006), though this significantly increased the average path length (hops) between cortical areas (**Figure 5B**). Kaiser and Hilgetag (2006) concluded that the excess wire associated with long-range pathways introduced shortcuts to reduce the number of "processing steps" between cortical areas. This conclusion is consistent with the results from the optimization analysis of single intrinsic axon and dendritic arbors (Budd et al., 2010; Cuntz et al., 2010).

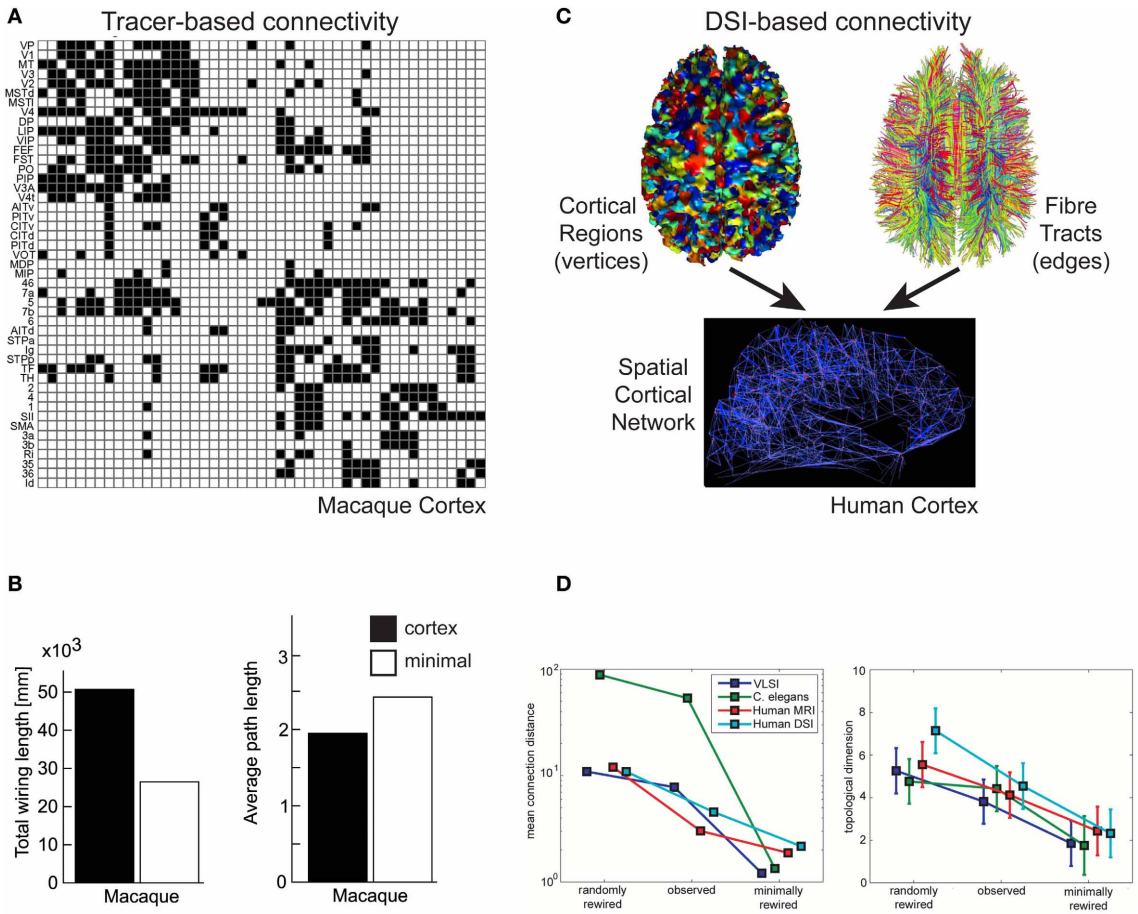

FIGURE 5 | Communication cost trade-off at Pathway scale of cortical organization. (A,B) Macaque tracer-derived pathway connectivity. **(A)** Example of directed connectivity (adjacency) matrix of visual and somatomotor macaque cerebral cortex (Reprinted from Sporns et al., 2007), where black squares indicate evidence supporting a axonal pathway connection between areas (matrix rows as sources and columns as target cortical regions). **(B)** Macaque cerebral cortical network is suboptimal for total axonal length (left) but minimal length network increased averaged path length (right) (Reprinted from Kaiser and Hilgetag, 2006). **(C,D)** Human DSI-derived pathway connectivity. **(C)** An undirected spatial cortical network (bottom) is constructed from vertices of cortical regions (top, left) and edges determined from the probability of fiber tracts existing between corresponding pairs of cortical regions based on tractography tracing algorithms (top, right) (Reprinted from Hagmann et al., 2008). **(D)** Human DSI network is suboptimal for wire length (left) but minimal length network has lower topological dimension than observed cortical network (right) (Reprinted and partly redrawn from Bassett et al., 2010). Topological dimension here is a fractal measure of a network's degree of internal connectedness.

Does it matter that this study assumed straight-line fiber trajectories? Kaiser and Hilgetag (2006) acknowledged their assumption underestimated pathway length, though in fairness, there is insufficient actual fiber length data available. This issue may not be a significant problem provided tract curvature is relatively constant, i.e., if pathways are all similarly curved. In primate prefrontal cortex, for example, around 55% of the fiber tract trajectories measured were approximately straight though the remainder had some degree of curvature with denser tracts tending to be straighter than sparse ones (Hilgetag and Barbas, 2006). Moreover, these measurements are not easy to make because initially compact fibers bundles can splay and divide so that fibers may take different trajectories through white matter (Hilgetag and Barbas, 2006). This uncertainty about the effect of tract length on communication costs makes it important to investigate this issue further.

In general, network analysis based on tracer study data has been impeded by the absence of a systematic quantification of axonal pathways properties such as axon length or axon (connection) density (see Salin and Bullier, 1995). The CoCoMac database, for example, provides a limited integer rating of connection density/strength but no information on pathway length (Stephan et al., 2001; Sporns et al., 2007). There are understandable reasons for the absence of these data. Tracer label may not fill all axonal branches especially when it is of a fine caliber ($<1\,\mu m$) and plotting the trajectory of long, fine cortical axons, and measuring their structural parameters is hugely time-consuming (Salin and Bullier, 1995; Rockland, 2002). Moreover, tracer studies report considerable between-individual variability in the fiber density of specific cortio-cortical pathways (e.g., Scannell et al., 2000). Even when the labeling methodology is carefully controlled, Markov et al. (2011) found, as well as discovering

previously unreported pathways to well-studied visual cortical areas, that connection density could vary upto five-fold between individuals. But caution should be used in assuming that pathways of equal axon number have an equal postsynaptic effect on target neurons, especially when one may be feedforward and the other feedback (Johnson and Burkhalter, 1997). Moreover, connectivity matrices derived from the composite results of tracer injection studies tacitly assume that network topology is the same for all individuals of the same species. It is unclear whether this assumption is secure.

MRI-derived networks

Axonal tracer studies can only be used map relatively few fiber tracts per animal (see Salin and Bullier, 1995) making them ill-suited to map all extrinsic cortico-cortical pathways in an individual brain. Recently, by combining two complementary *in vivo* MRI techniques whole macroscopic cortico-cortical networks can be mapped non-invasively for an individual brain. An example is shown in **Figure 5C**. This approach offers the possibility to study individual differences in health and disease (Bassett and Bullmore, 2009; Hagmann et al., 2010).

In the first stage, structural MRI is used to construct a 3D surface model of the cerebral hemispheres at the boundary where fibers enter and leave cortical gray matter. A standardized parcellation template is applied to the surface model to identify cortical areas in each subject, after which these areas are subdivided into distinct, equally sized regions of interest (ROI), typically $\sim$cm^2 of surface area (Hagmann et al., 2008; Echtermeyer et al., 2011). Each network vertex corresponds to a distinct ROI (**Figure 5C**, top, left).

In the second stage, to help construct network topology, diffusion MRI (diffusion spectrum imaging, DSI) is used to trace fiber tracts to and from ROIs. Fiber tracts are identified and traced from the anisotropic diffusion of water molecules along their length (Moseley et al., 1990; Conturo et al., 1999; Wedeen et al., 2012). Tractography algorithms trace paths of maximal diffusion coherence (correlation) to generate a connection probability of each pseudo-fiber (see Hagmann et al., 2010; **Figure 5C**, top, right). Tract density and length may also be estimated from pseduo-fiber constructions (Hagmann et al., 2008), though fibers cannot be traced once they enter gray matter with this method because of the relative lack of anisotropic water diffusion here (Conturo et al., 1999). To decide whether to add an undirected edge to the network, a threshold is typically applied to the raw connection probability matrix (see Rubinov and Sporns, 2010; **Figure 5C**, bottom). Validation of DSI tractography for human cortex using tracer methods is not possible for obvious ethical reasons and dissection approaches are considered unreliable at this level of detail (Hagmann et al., 2010). However, the postmortem application of tract tracing histological tools (e.g., lipophilic tracer, DiI, Galuske et al., 2000) can be envisaged. Recently, Axer et al. (2011) have shown 3D-polarized light imaging applied to postmortem tissue can trace fiber tracts in white matter at a sub-millimeter resolution though it cannot yet follow individual fine caliber ($<1\,\mu$m) axons.

To date, two studies have investigated the communication costs in human MRI-derived large-scale cortical networks (Hagmann et al., 2008; Bassett et al., 2010). Analyses of networks constructed from functional MRI data report similar results (e.g., Achard and Bullmore, 2007) though are not discussed here.

To non-invasively map inter-regional connectivity in human cerebral cortex, Hagmann et al. (2008) constructed and analyzed networks each of 998 ROI vertices for five healthy human subjects. An edge was inserted if at least one pseudo-fiber identified by DSI connected an ROI pair. In some versions of the network, edges were weighted with a length, l(e), based on the average length of pseudo-fiber trajectories, and a density, w(e), based on the number of pseudo-fibers per mm^2. From their analysis, Hagmann et al. (2008) identified a network core consisting of a relatively small number of highly interconnected cortical hubs. By virtue of having low average path lengths to all other cortical regions, the network had high local efficiency. Six main modules were related to these hubs. The study reported a good but imperfect correspondence between the gross cortical pathways of macaque and human brains. The study did not, however, investigate whether network communication costs were optimized.

To investigate topology and wiring costs in human cortical macroscopic networks, Bassett et al. (2010) analyzed a modified version of the Hagmann et al. (2008) DSI network for single human subjects and, for comparison, a network derived on gray matter volumes covariation (GMC). GMC is an indirect anatomical marker for connectivity (He et al., 2007) obtained from averaging over many human subjects. In contrast to Hagmann et al. (2008), network topology was determined by thresholding connection probabilities between ROI pairs. Moreover, while edges were assigned a length cost, based on the distance between ROI pairs instead of pseudo-fiber length, they were not given a density parameter. Bassett et al. (2010) acknowledged this is likely to underestimates actual fiber length but they judged pseudo-fiber measurements unreliable (see later). Bassett et al. (2010) reported evidence of network modularity over a range of scales, consistent with statistically self-similar connectivity. This hierarchical modularity or "modules within modules" architecture (Simon, 1962) was more clearly defined in DSI than GMC networks. The "modules within module" architecture offers a high degree of network efficiency (see "Spatial Networks") because in general fewer vertices are traversed to reach a target vertex than in regular or random architectures (Simon, 1962). Importantly, Bassett et al. (2010) found human cortical networks were not strictly minimized for wire length (**Figure 5D**, left). Indeed, strictly minimizing wire length reduced or eliminated hierarchical modularity, which in turn reduced the cost-efficiency of balancing topological complexity within available physical space (Bassett et al., 2010; **Figure 5D**, right). Topological complexity here was reported using a fractal measure of the network's topological dimension, its degree of internal connectedness. These findings agree with the conclusions of Kaiser and Hilgetag (2006) regarding the balancing of communication costs in macroscopic networks.

Networks constructed using DSI are, however, subject to limitations. First, diffusional MRI fiber tracing suffers from a distance bias. Long-range fibers may not be reliably traced because of an exponential decrease in coherent diffusion with distance and short tracts may not be detectable due to the spatial sampling limitations of MRI (Hagmann et al., 2007; Gigandet et al., 2008).

Second, tractography algorithms have difficulties segmenting proximal fiber tracts such as distinguishing "kissing" from crossing fiber bundles because MRI lacks the spatial detail of tracer studies, which may also mean that splaying fiber tracts are underrepresented (Schmahmann et al., 2007; Gigandet et al., 2008; Hagmann et al., 2010). *In vivo* MRI spatial resolution is limited to at best a few hundred microns (e.g., Schmahmann et al., 2007). Third, ROI size choice affects network topology (Hagmann et al., 2007; Echtermeyer et al., 2011) with implications for drawing robust inferences about network properties such as motif distributions (Echtermeyer et al., 2011). Fourth, unlike tracer studies, diffusional MRI cannot provide information concerning the laminar origin or termination of tract axons in gray matter (Conturo et al., 1999). Hence, MRI-derived networks cannot currently employ directed edges. The use of undirected edges, however, tacitly assume that communication has an equal (postsynaptic) impact in either direction when, as mentioned earlier, there are reasons for believing this may not be the case, e.g., feedforward vs. feedback cortical afferent pathways (Rockland and Pandya, 1979; Felleman and Van Essen, 1991; Johnson and Burkhalter, 1996, 1997; Rockland, 1997; Budd, 1998; Larkum et al., 2004; Rothman et al., 2009). In addition, while in primate cerebral cortex most axonal pathways between cortical areas are reciprocal it appears some are not (Felleman and Van Essen, 1991). Finally, thresholding connection probabilities to determine whether an edge exists necessarily generates different network topologies for the same dataset: high thresholds lead to sparsely connected networks that may accidentally eliminate weak but actual pathways, while low thresholds may result in densely connected networks including erroneous edges generated by noise.

Summary

Evidence from two studies, one based on a composite network of axonal tracer data of macaque cortex (Kaiser and Hilgetag, 2006) and the other from individual MRI-based human corticocortical networks (Bassett et al., 2010), offer support for the main hypothesis. Both studies concluded that, like single intracortical axonal (Budd et al., 2010) and dendritic arbors (Cuntz et al., 2010), cortical wiring is not strictly length-minimized with excess wire used to promote rapid communication. To better understand corticocortical communication costs at this scale, however, future research will need to incorporate the density of connection and postsynaptic effect of fiber tracts into network models. Given such a wide range of individual differences in connection density (e.g., Scannell et al., 1995; Markov et al., 2011), it seems improbable that this variation has a negligible influence on information flow.

PHYSIOLOGICAL CONSIDERATIONS

What is the justification for inferring temporal cost (delay) from path length in spatial networks? The total signaling delay of a stimulus in a cortical network, t_{total}, may be separated into two main components (Nowak and Bullier, 1997): a presynaptic component, axonal conduction delay, and a postsynaptic component, neuronal integration delay (see **Figure 6**). We now examine these distinct components and consider how they should be used in estimating temporal cost in cortical networks at different spatial scales.

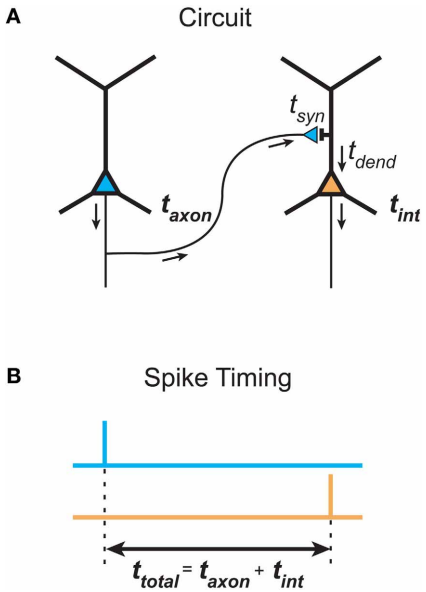

FIGURE 6 | Total communication delay between neurons separable into a presynaptic axonal conduction delay and a postsynaptic neuronal integration delay. (A) Schematic circuit diagram shows the time taken by an action potential generated in the presynaptic neuron (left neuron, blue) to propagate along the axon to a presynaptic terminal, where it causes the release of neurotransmitter into the synaptic cleft, defines the axonal conduction delay (t_{axon}). The postsynaptic neuronal integration delay (t_{int}) is the sum of the time taken for neurotransmitter molecules to induce a local postsynaptic response (synaptic delay, t_{syn}) and the latency for this response to propagate down the dendritic tree to the axon initial segment, where its integration produces an action potential in the postsynaptic neuron (right neuron, orange) (dendritic delay, t_{dend}). **(B)** Total delay (t_{total}) between the timing of a presynaptic spike occuring (top, blue line) and the generation of a postsynaptic spike (bottom, orange line) is determined by the sum of presynaptic and postsynaptic delay components.

PRESYNAPTIC TEMPORAL COST

Presynaptic axonal conduction delay (t_{axon}) is the time taken for an action potential to propagate from its initiation site at the axon initial segment (AIS) or axon hillock (Stuart et al., 1997) along the axon arbor to a given presynaptic terminal (see **Figure 6A**).

Axonal conduction delay may be estimated from the product of the weighted path length between axon origin and presynaptic terminal and the average conduction velocity along this path (see L_{axon}, **Figure 3B**). Weighted path length is thought to be the major determinant of conduction delay for intracortical axon arbors (Manor et al., 1991). Conduction velocity increases with axon diameter and in the presence of myelination but may be reduced when branch points and axon varicosities are encountered (see Debanne et al., 2011). Intrinsic corticocortical axons have a narrow, positively skewed diameter distribution (0.1–1.0 μm) with the majority of their arbor length composed of unmyelinated branches, as so far reported (e.g., Haug, 1968; Braitenberg and Schüz, 1991; Peters and Sethares, 1996). In contrast, extrinsic corticocortical axons, though with a similarly shaped diameter distribution, tend to be thicker (e.g., ∼1–3 μm in macaque) and most are myelinated along their length until

arborization (e.g., Houzel et al., 1994; Anderson and Martin, 2002; Wang et al., 2008). Correspondingly, the conduction velocity of intracortical axons is generally reported as slower (0.1–0.6 m/s, Komatsu et al., 1988; Luhmann et al., 1990; Hirsch and Gilbert, 1991; Lohmann and Rörig, 1994; Feldmeyer et al., 2002) than extrinsic corticocortical pathway axons (>1 m/s, Harvey, 1980; Girard et al., 2001). Typically axonal pathways are heterogeneous, composed of axons with a range of calibers (e.g., Anderson and Martin, 2002; Wang et al., 2008) and conduction velocities (Harvey, 1980; Girard et al., 2001). Interestingly, conduction latency distributions between reciprocally connected cortical areas overlap (Raiguel et al., 1989; Girard et al., 2001). In general, action potentials are reliably transmitted throughout cortical axon arbors (Cox et al., 2000) even along thin varicose branches at least up to 100 Hz (Raastad and Shepherd, 2003). However, propagation failures can occur under certain circumstances such as spike bursting (Raastad and Shepherd, 2003; see Debanne et al., 2011). Short-term spiking history can induce a modest change in conduction velocity in some types of cortical axon (2–22%, Swadlow et al., 1978; Shlosberg et al., 2008). Overall, these findings suggest that when mean conduction velocity is known it is not unreasonable to estimate presynaptic axonal conduction delay from weighted path length.

POSTSYNAPTIC TEMPORAL COST

Postsynaptic neuronal integration delay (t_{int}) is the time taken for postsynaptic depolarization arising from a given presynaptic axon to generate one or more action potentials in response (see **Figure 6A**). We divide this delay into two subcomponents.

First, there is a synaptic delay (t_{syn}), the time taken for neurotransmitter molecules released presynaptically to activate postsynaptic receptors, which for glutamate and GABA fast transmission at central synapses is thought to be brief (<0.5 msec, Sabatini and Regehr, 1996; Markram et al., 1997). The amplitude and width of the presynaptic action potential, however, can affect the degree of synaptic delay (Boudkkazi et al., 2007, 2011).

Second, there is a dendritic delay (t_{dend}), the time taken for the local postsynaptic dendritic depolarization to induce one or more action potentials following its propagation to and integration at the AIS. The dendritic propagation delay depends on dendritic path length (L_{dend}, see **Figure 3B**) and the mean dendritic conduction velocity along this path. Dendritic conduction velocity depends on the electrical properties of these dendritic branches, which is in turn influenced by arbor geometry such as branching ratio and dendritic diameter and, importantly, whether the signal is conducted actively or passively along the dendritic branch (see London and Häusser, 2005; Spruston, 2008). Morphologically, a pyramidal cell dendritic arbor, for example, is typically composed of a largely spherical basal dendritic arbor around the cell body and a main apical dendritic trunk, oriented toward the pia, which emits a number of proximal oblique branches before bifurcating to produce a densely branched distal apical tuft (Feldman, 1984). Passively conducting EPSPs in the basal and oblique apical branches conduct rapidly to the soma (at most a few milliseconds) but EPSPs from distal apical tuft can take longer (up to 10 msec or more) (Agmon-Snir and Segev, 1993; Markram et al., 1997; Ulrich and Stricker, 2011). The synaptic activation of voltage- and calcium-dependent dendritic spiking amplifies and more rapidly conducts dendritic EPSPs to the soma from all locations of the pyramidal dendritic tree (Yuste et al., 1994; Larkum et al., 1999; Schiller et al., 2000; Nevian et al., 2007; Larkum et al., 2009). *In vivo*-like spontaneous synaptic background activity, observed in neuronal recordings of awake animals, differentially reduces the delay of distal compared with proximal dendritic EPSPs (Rudolph and Destexhe, 2003a). The higher conductance state decreases the effective membrane time constant that regulates the rate of temporal integration, so the neuron responds more readily to sharp fluctuations in membrane conductance than slowly changing dendritic signals (Rudolph and Destexhe, 2003b). However, intrinsic delayed potassium currents in cortical neurons may defer spiking (Storm, 1988; Beggs et al., 2000). Hence, there is more scope for variability in the postsynaptic than the presynaptic component of total signaling delay.

Based on *in vivo* electrophysiological recordings following sensory stimulation, Nowak and Bullier (1997) estimated that the minimum neuronal integration delay for quiescent (low conductance state) cortical neurons was 5–10 ms but faster at 1–5 ms for already depolarized neurons (high conductance state). This suggests the level of spontaneous synaptic background activity may regulate neuronal integration delay. Based mostly on cat and monkey data, the minimum total signaling delay between cortical areas is thought to be around 10 msec (see Nowak and Bullier, 1997), though it might be different in other species such as rodents.

ESTIMATING TEMPORAL COST IN NETWORKS

Figure 1 illustrated that the shortest path length between a given pair of vertices in the same network may be different depending on whether path length was measured using the number of edges/hops (unweighted path length) or the sum of edge lengths (weighted path length). While weighted path length only was used to estimate temporal cost in intrinsic axonal and dendritic cortical arbors (Budd et al., 2010; Cuntz et al., 2010), both measures have been used for local cortical circuits and large-scale extrinsic cortico-cortical networks (Kaiser and Hilgetag, 2006; Bassett et al., 2010; Perin et al., 2011).

So which path length measure is the most appropriate to use to estimate temporal cost at each spatial scale of cortical organization? At the single neuron scale, temporal cost is isolated from the network in which it is embedded. Hence, temporal costs estimated from either axonal or dendritic weighted path length can assume average levels of activity. Yet for local or large-scale cortical networks scales we are interested in combined presynaptic and postsynaptic delays, which will vary according to the conductance state of each neuron traversed in a path.

There are three main parameter regimes to consider here. First, when presynaptic axonal conduction delays are much longer than the postsynaptic neuronal integration delays ($t_{\text{axon}} >> t_{\text{int}}$) then weighted path length dominates total signaling delay estimates. This regime operates when, relative to the other source of delay, axons are long or integration delays brief. Second, when presynaptic conduction delays are much shorter than postsynaptic neuronal integration delays ($t_{\text{axon}} << t_{\text{int}}$) then hop count

becomes a more representative measure of total signaling delay. This regime occurs when axons are relatively short or integration delays long. Third, when the presynaptic conduction delay is of a similar order of magnitude to the postsynaptic neuronal integration delay ($t_{axon} \sim t_{int}$) then a combined measure should be used to estimate total signaling delay.

To examine under which parameter regime local and circuit macroscopic pathway scale networks may operate, we calculated what percentage of estimated axonal delays (presynaptic component) fell within an order of magnitude of the minimum neuronal integration delay (postsynaptic component) (1–5 ms for high- and 5–10 ms for low-conductance or quiescent states; see Nowak and Bullier, 1997). We estimated axonal conduction delays based on empirical distributions of path length in individual spiny neuron axons from cat visual cortex ($n = 22{,}001$ paths, Budd et al., 2010) and fiber tract lengths estimated for macaque cerebral cortex (Kötter, 2004; Kaiser and Hilgetag, 2006; $n = 2390$ tracts; see www.biological-networks.org). To estimate axonal conduction delay, intrinsic spiny axon path lengths were divided by a realistic range of mean conduction velocities for intrinsic cortical axons (0.1–0.6 m/s, Komatsu et al., 1988; Luhmann et al., 1990; Hirsch and Gilbert, 1991; Lohmann and Rörig, 1994; Feldmeyer et al., 2002), while extrinsic fiber tract lengths were divided by a realistic range of mean conduction velocities for extrinsic cortical axons (1–10 m/s, Miller, 1975; Swadlow et al., 1978; Harvey, 1980; Girard et al., 2001).

Figure 7 shows the results for both single intrinsic axon and extrinsic fiber tract data were quite similar. For the low-conductance state, virtually all axonal conduction delays were within an order of magnitude of neuronal integration delay almost regardless of mean conduction velocity (**Figures 7A,B**, square symbols). For the high-conductance state, except at the very lowest conduction velocities, the majority of the conduction delays were comparable to integration delays (**Figures 7A,B**, circle symbols). These results suggest that in both local and macroscopic cortical networks presynaptic axonal conduction delays may be mostly of a similar order of magnitude as postsynaptic neuronal integration delays (i.e., $t_{axon} \sim t_{int}$). To determine the shortest path length between a pair of neural elements, therefore, it is important to take into account both the number of neural elements in the path as well as its physical length estimated from measuring axonal and/or dendritic processes. It is unclear whether assigning a cost for each vertex as well as each edge would significantly affect the results for cortical networks previously analyzed (Kaiser and Hilgetag, 2006; Bassett et al., 2010).

DISCUSSION

OVERVIEW

Although cerebral cortex appears a jungle of axonal and dendritic wiring, as we explore deeper into its structure we find an order to its organization that helps explain how, in a vast network composed of billions of highly interconnected yet spatially distributed neurons, information is processed accurately and rapidly. In this article, we critically examined an hypothesis to help at least partially explain cortical wiring and connectivity at multiple scales of organization in terms of a trade-off between spatial and temporal communication costs (Budd et al., 2010). This hypothesis is grounded in Cajal's laws of conservation for cellular material and conduction delay (Cajal, 1899). We found supporting evidence for the hypothesis from studies applying network analysis at single neuron and macroscopic pathway network spatial scales. But a lack of available structural data prevented any meaningful evaluation at the local circuit scale. To progress this evaluation, we have identified the need for a more detailed morphological component in the Human Connectome framework. Recent advances in high-resolution cortical connectivity mapping (Mishchenko et al., 2010; Bock et al., 2011) make it timely to consider how morphological data should be recovered and suitably databased to aid analysis and modeling (e.g., Ascoli, 2007). To better estimate temporal cost in local circuit and macroscopic (pathway) scale networks, we suggest combining edge (axonal conduction) and vertex (neuronal integration) delays.

LIMITATIONS OF GRAPH THEORY

Network descriptions, like other types of model, provide a simplified representation of a real world system. Yet there is a risk that viewing cerebral cortex simply in terms of discretely interconnected neural elements may blinker us to what Cajal (1937) referred to as "the utmost subtleties" of its structure. To gain insight into a phenomenon, the process of abstraction necessarily involves discarding some details considered less important though this risks leaving out key elements to its understanding. We now consider the appropriateness of applying graph theory to understanding cortical wiring.

Here, the abstraction of neural architecture into vertices (neural elements) and edges (neural connections) is most straightforward when there is a direct physical correspondence with distinct anatomical features. At the single neuron level, axon and dendritic arbors are easily identified from the visualized processes of neurons. In contrast, defining precisely what a vertex represents at the mesoscopic scale has proved problematic. The mesoscopic appears inextricably linked with the cortical column concept (Horton and Adams, 2005; Rockland, 2010; da Costa and Martin, 2010), where considerable controversy exists regarding its spatio-functional dimensions. While pathways may be easily identified, there is, however, no universally accepted scheme regarding how to divide cerebral cortex into regions (Van Essen et al., 2012a,b), which means there is no standard vertex set. Moreover, edge definitions can be more complicated at this scale. Modeling a reciprocally connected pair of cortical regions by a single edge (Hagmann et al., 2008; Bassett et al., 2010) ignores differences that may exist between feedforward and feedback pathways in the laminar termination pattern of their afferent axons and likely postsynaptic effect (Johnson and Burkhalter, 1996, 1997; Rockland, 1997; Budd, 1998; Larkum et al., 2004; Rothman et al., 2009). Ideally, each of pair of pathways should each be represented by a pair of directed edges and weighted in some way to record their relative influence on the flow of information. This is problematic for human cerebral cortex where these data are wholly absent. In addition, there is a tacit assumption that a single edge represents a fairly homogeneous fiber system whereas, like callosal pathways, it may be composed of a diverse range of myelinated and unmyelinated axons of various calibers (Houzel et al., 1994; Wang et al., 2008; Caminiti et al., 2009).

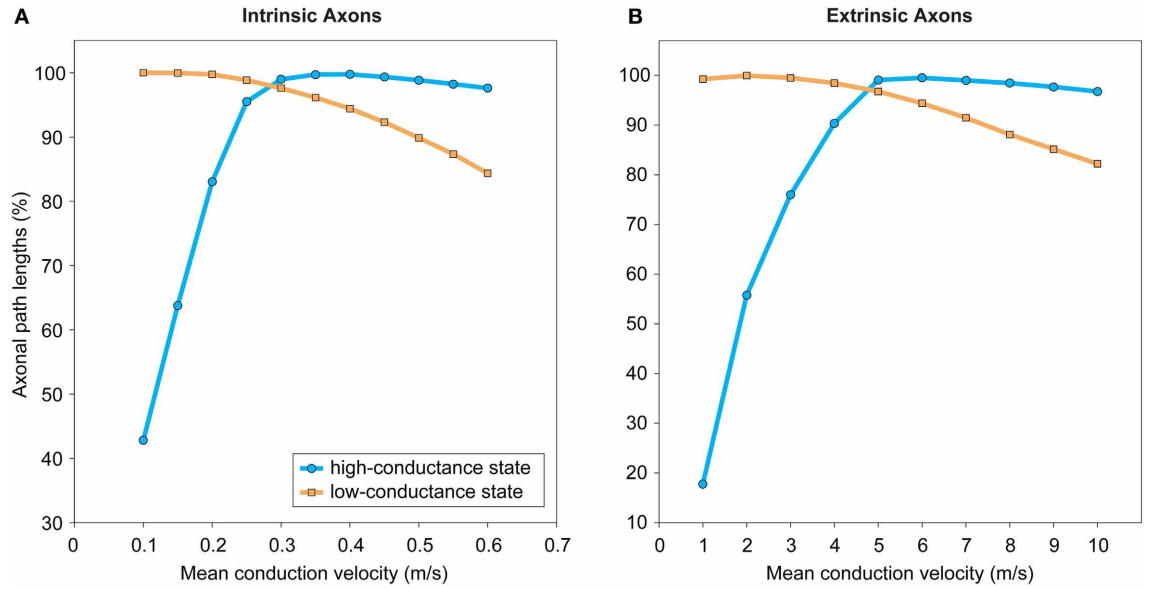

FIGURE 7 | Most estimated intrinsic and extrinsic axonal conduction delays are within an order of magnitude of neuronal integration delays apart from when axons conduct at their slowest rate and neurons operate in a high-conductance state. (A) Intrinsic axon path lengths of spiny neuron within gray matter in adult cat cerebral cortex ($n = 22{,}001$ paths from 19 neuron reconstructions). Data taken from Budd et al. (2010). **(B)** Extrinsic axonal fiber tract lengths in adult macaque cerebral cortex ($n = 2309$ pathways). Data taken from Kaiser and Hilgetag (2006).

A heterogeneous pathway may reflect the existence of a number of parallel functional streams that selectively target separate neuronal groups and/or at different conduction velocities, e.g., the pathway between area V1 to V2 in macaque monkey visual cortex (e.g., Sincich et al., 2010). To represent heterogeneous pathways, therefore, it might be more accurate to use multiple edges connecting a pair of distinct cortical regions, each assigned different properties. Finally, other forms of communication should not be forgotten such as local ephaptic interactions between neigboring neurons (Anastassiou et al., 2011) and cortical inhibition without direct synaptic connections (Oláh et al., 2009), as well as global extrasynaptic neuromodulation that can alter neuronal state (see Bargmann, 2012).

Despite these limitations, this review has provided ample evidence of the utility of graph theory abstractions to help gain insight into cortical design and concomitantly wiring economy. It should be borne in the mind that the success of such models depends not on their fidelity in replicating the physical features of the biological system but on the accuracy of their predictions and what insight this offers into the system studied.

CORTICAL NETWORK DESIGN PROBLEM

Natural selection as a designing agent is a unifying concept in biology (Maynard Smith, 1978). It follows from this notion that the characteristics of brain architecture and function have adapted to improve an organism's survival in its environment (e.g., Kaas, 1989). Here, a cost function can be viewed as an hypothesis about what selective forces are responsible for cortical network design. A test of this hypothesis is how well cost optimization explains the characteristics of brain structure and function. In this article, we have focussed on two known costs concerning the cortical network design problem but clearly there are others. We now evaluate how well the wire length metric approximates spatial cost (cellular material) and consider the influence of other costs on cortical network design. Path length as an approximation for temporal cost was evaluated earlier (see "Physiological Considerations").

Almost all optimization studies discussed in this review have approximated Cajal's conservation of cellular material to minimizing wire length (Mitchison, 1991; Cherniak, 1994; Koulakov and Chklovskii, 2001; Kaiser and Hilgetag, 2006; Wen et al., 2009; Bassett et al., 2010; Budd et al., 2010). The main assumptions underlying this approach are: (1) wire length is directly proportional to the amount of cellular material used; and, (2) distance traveled is directly proportional of the degree of conduction delay (Cajal, 1899; see Chklovskii and Koulakov, 2004). Although both assumptions are valid, this approach does not take account of other characteristics of neuronal processes that have a bearing on cellular material and conduction delay conservation, in particular axonal and dendritic diameter, which we now discuss.

Axonal and dendritic diameter regulates the rate of ionic diffusion per unit length responsible for the conduction velocity of electrochemical signals (see Debanne et al., 2011). Doubling the diameter of a myelinated axon, for instance, would be expected to halve the conduction time for a given length of axon because of the approximately linear relationship between axon diameter and conduction velocity (Hursh, 1939; Waxman and Bennett, 1972). However, for an unmyelinated axon the conduction time differential would be less because conduction velocity is proportional to the square root of axon diameter (Rushton, 1951; Hodgkin, 1954).

Hence, an increase in axon or dendritic diameter causes a squared expansion in the volume of cellular material while conduction velocity increases, at best, linearly.

Currently, a lack of data prevents an optimization analysis combining axon diameter and length. Because of the spatial resolution limits of light microscopy (LM), EM is needed to accurately measure the finest caliber axons found in both extrinsic and intrinsic corticocortical axon pathways (see Peters et al., 1991). To control for morphological irregularities such as swellings, multiple sample points are needed to obtain the average diameter of an axon branch. Hence, for a single axon arbor hundreds of diameter measurements under EM might be required. Population axon diameter distribution data does exist but only for a fraction of the hundreds of extrinsic corticocortical pathways; the callosal pathway is probably the most studied in this regard (e.g., Houzel et al., 1994; Wang et al., 2008). In contrast, axonal length is readily measured from LM reconstructions typically by the piecewise linear approximation of curvilinear axon trajectories.

In this article, construction cost has referred to the cost of the mature and stable cortical network. So we have not discussed the developmental cost of constructing the mature network or the plasticity cost of remodeling connections of the mature network in response to environmental changes in the adult brain. The task of arranging billions of connections efficiently using developmental mechanisms of axonal and dendritic outgrowth, guidance, branching, and remodeling is immense and appears to require a sophisticated orchestration of molecular cues and gradients as well as activity-dependent modification (Price et al., 2006).

We do not yet know enough about cortical development to determine which cost factors most influence the construction of cortical networks. Developmental chronology may, however, offer some clues. For instance, astroctye and oligodendrocyte cell differentiation lag intrinsic axonal development (Müller, 1992; Bandeira et al., 2009) while the cortical capillary blood supply co-develops with intrinsic axons, most probably guided by common molecular cues (Ben Hamida et al., 1983; Risau, 1997; Tieman et al., 2004). These observations suggest glia and blood vessels may act primarily as supportive rather than strongly constraining factors in the development of cortical networks. The role of oligodendroctyes is of special interest here because their signals are necessary to induce local axon caliber expansion (e.g., Sánchez et al., 1996) yet their number is thought to be regulated by regional axon-derived signals (e.g., Barres and Raff, 1993). Taken together with the developmental chronology, we might infer from this that as axons extend toward their most distant targets it is important to conserve the amount of cellular material used. But later, once axons have reached their targets and are remodeled, thickening selected axonal branches may become more important in order to significantly reduce conduction delays within the network. This example of developmental chronology suggests that the relative influence of cost factors in cortical network formation may vary during development.

Metabolic cost is widely considered as a unifying influence on brain design and function because it is a limited resource essential to an organism's survival (Laughlin and Sejnowski, 2003). A significant proportion of the energy budget is expended on maintaining ionic equilibrium and communicating signals between cortical neurons (e.g., Attwell and Laughlin, 2001). Both construction and routing costs can be defined in energetic terms. The energy required to maintain ionic equilibrium is proportional to the amount of cellular material. The energy required to propagate action potentials and subthreshold signals is related to the path distance a signal must travel along an axon or dendrite from its source to each target.

In summary, we suggest that understanding of the cortical network design problem has been improved by considering construction and routing costs together rather than either by itself. However, a more complete appreciation of cortical network design will require the consideration of other important cost factors such as axon diameter (see Perge et al., 2012).

ROLE OF CORTICAL DYNAMICS

In this article, we have considered structural communication costs at different scales of cortical organization. But we are keen not to give the impression that we consider dynamics unimportant—clearly signals do not flow unaltered through cortical circuitry and network structure and cortical dynamics are inextricably linked (e.g., Sporns et al., 2000). To generate hypotheses concerning function, structural network analysis examines how information may *potentially* be communicated. Given the considerable complexity of neuronal and synaptic dynamics (Herz et al., 2006), let alone when combined in cortical circuits, structural network analysis offers a simpler alternative for gaining insight into cortical function by generating experimentally testable hypotheses such as the one examined here. It should be remembered that Cajal (1899) made considerable progress in understanding neural communication without being able to record the electrochemical dynamics of the Golgi-stained neurons he studied.

SCALABLE BRAIN ARCHITECTURE

Mammalian brains vary greatly in size (see Kaas, 2000). For example, the surface area of primary visual area V1 in humans (2134 mm^2, Adams et al., 2007) is more than 1500 times larger than that of the mouse (1.40 mm^2, McCurry et al., 2010). Yet anatomically the substance of cerebral cortex appears similar in many respects. First, neocortical neuronal types such as spiny pyramidal and smooth basket cells are conserved across species (Tyler et al., 1998) though some differences may exist between cortical areas (e.g., Elston, 2003) and between species (e.g., DeFelipe et al., 2003). Second, the ratio of white matter to gray matter volumes of cerebral cortex appears constant across species (Zhang and Sejnowski, 2000). Third, changes in axon diameter and myelination help preserve latency across brain size in corticocortical pathways such as corpus callosum (Wang et al., 2008; Caminiti et al., 2009). Therefore, it is a puzzle how cortical design appears to remain invariant over these dramatic changes of spatial scale (Kaas, 2000; Clark et al., 2001; Stevens, 2001).

The hypothetical principle examined here is consistent with the notion of a scaleable cortical architecture because the trade-off between minimizing spatial and temporal costs should be scale-invariant. In the case of intrinsic axon arbors, for instance, the addition of neuronal branches to increase connectivity would do so without destroying its communication capabilities

(see "Axon Arbors"). However, a central issue is whether the balance between communication costs in cortical design is relatively constant, that is, universal or varies according to the particular processing demands of a cortical region or particular niche environment of a species.

CONCLUSIONS

In this article, we reviewed current evidence to evaluate the hypothesis that to optimize communication spatial (construction) and temporal (routing) wiring costs are traded-off across different scales of cortical organization (Budd et al., 2010). We conclude the following:

- At the single neuron scale, a trade-off between spatial and temporal communication costs appears to capture the core morphological structure of axonal and dendritic trees of the most common neuronal types, though this conclusion may not apply for all intrinsic and afferent arbor types. The predictions of the hypothesis can at least be partly validated using existing physiological techniques.
- At the local circuit scale, higher-order statistics obtained from multiple electrode recordings seem to provide a better explanation of network design than those derived from paired recordings. In the absence of complete anatomical reconstructions of local circuits, however, it has not been possible to estimate structural communication costs and test the hypothesis at this scale. Nevertheless, the predictions of the hypothesis might be investigated using fragmentary circuit reconstructions.
- At the pathway scale, corticocortical fiber tracts may also trade-off spatial and temporal communication costs. However, network analysis at this scale is more complicated because there is no standard parcellation scheme and considerable individual variation in corticocortical pathway properties (e.g., fiber density/number and postsynaptic effect on target regions).
- When estimating temporal cost in local circuit and pathway level networks account should be taken of both presynaptic axonal delay and postsynaptic neuronal integration delay, which may be of a similar order of magnitude.
- Recent technical advances in cellular tracing will soon yield massive volumes of data to help evaluate wiring principles of cerebral cortex. To aid hypothesis testing of wiring principles, however, the connectome framework needs to incorporate more morphological data into its description of cortical connectivity.

ACKNOWLEDGMENTS

Supported by FP7-ICT-2011-7/287701 (BrainScaleS-enlargEU), MTA-TKI-355/11008 and TÁMOP-4.2.1/B-09/1/KONV-2010-0007 to Zoltán F. Kisvárday.

REFERENCES

Achard, S., and Bullmore, E. (2007). Efficiency and cost of economical brain functional networks. *PLoS Comput. Biol.* 3:e17. doi: 10.1371/journal.pcbi.0030017

Adams, D. L., Sincich, L. C., and Horton, J. C. (2007). Complete pattern of ocular dominance columns in human primary visual cortex. *J. Neurosci.* 27, 10391–10403.

Addison, P. S. (1997). *Fractals and Chaos: An Illustrated Course.* CRC Press. Available online at: http://books.google.com/books?id=l2E4ciBQ9qECandpgis=1

Agmon-Snir, H., and Segev, I. (1993). Signal delay and input synchronization in passive dendritic structures. *J. Neurophysiol.* 70, 2066–2085.

Ahmed, B., Anderson, J. C., Douglas, R. J., Martin, K. A., and Nelson, J. C. (1994). Polyneuronal innervation of spiny stellate neurons in cat visual cortex. *J. Comp. Neurol.* 341, 39–49.

Ahn, Y.-Y., Jeong, H., and Kim, B. J. (2006). Wiring cost in the organization of a biological neuronal network. *Physica A* 367, 531–537.

Alpert, C. J., Hu, T. C., Huang, J. H., Kahng, A. B., and Karger, D. (1995). Prim-Dijkstra tradeoffs for improved performance-driven routing tree design. *IEEE Trans. Comput. Aided Des. Integr. Circuits Syst.* 14, 890–896.

Anastassiou, C. A., Perin, R., Markram, H., and Koch, C. (2011). Ephaptic coupling of cortical neurons. *Nat. Neurosci.* 14, 217–223.

Anderson, J. C., and Martin, K. A. C. (2002). Connection from cortical area V2 to MT in macaque monkey. *J. Comp. Neurol.* 443, 56–70.

Ascoli, G. A. (2007). Successes and rewards in sharing digital reconstructions of neuronal morphology. *Neuroinformatics* 5, 154–160.

Attwell, D., and Laughlin, S. B. (2001). An energy budget for signaling in the grey matter of the brain. *J. Cereb. Blood Flow Metab.* 21, 1133–1145.

Axer, M., Grässel, D., Dammers, J., Hütz, T., Eiben, B., Pietrzyk, U., et al. (2011). High-resolution fiber tract reconstruction in the human brain by means of three-dimensional polarized light imaging. *Front. Neuroinform.* 5:34. doi: 10.3389/fninf.2011.00034

Bagnall, M. W., Hull, C., Bushong, E. A., Ellisman, M. H., and Scanziani, M. (2011). Multiple clusters of release sites formed by individual thalamic afferents onto cortical interneurons ensure reliable transmission. *Neuron* 71, 180–194.

Bandeira, F., Lent, R., and Herculano-Houzel, S. (2009). Changing numbers of neuronal and non-neuronal cells underlie postnatal brain growth in the rat. *Proc. Natl. Acad. Sci. U.S.A.* 106, 14108–14113.

Barabási, A.-L., and Albert, R. (1999). Emergence of scaling in random networks. *Science* 286, 509–512.

Bargmann, C. I. (2012). Beyond the connectome: how neuromodulators shape neural circuits. *Bioessays* 34, 458–465.

Barres, B. A., and Raff, M. C. (1993). Proliferation of oligodendrocyte precursor cells depends on electrical activity in axons. *Nature* 361, 258–260.

Barthélemy, M. (2011). Spatial networks. *Phys. Rep.* 499, 1–101.

Bassett, D. S., and Bullmore, E. T. (2009). Human brain networks in health and disease. *Curr. Opin. Neurol.* 22, 340–347.

Bassett, D. S., Greenfield, D. L., Meyer-Lindenberg, A., Weinberger, D. R., Moore, S. W., and Bullmore, E. T. (2010). Efficient physical embedding of topologically complex information processing networks in brains and computer circuits. *PLoS Comput. Biol.* 6:e1000748. doi: 10.1371/journal.pcbi.1000748

Beaulieu, C., and Colonnier, M. (1985). A laminar analysis of the number of round-asymmetrical and flat-symmetrical synapses on spines, dendritic trunks, and cell bodies in area 17 of the cat. *J. Comp. Neurol.* 231, 180–189.

Beaulieu, C., Kisvarday, Z., Somogyi, P., Cynader, M., and Cowey, A. (1992). Quantitative distribution of GABA-immunopositive and -immunonegative neurons and synapses in the monkey striate cortex (area 17). *Cereb. Cortex* 2, 295–309.

Beggs, J. M., Moyer, J. R., McGann, J. P., and Brown, T. H. (2000). Prolonged synaptic integration in perirhinal cortical neurons. *J. Neurophysiol.* 83, 3294–3298.

Ben Hamida, C., Bisconte, J. C., and Margules, S. (1983). Postnatal maturation of the vascularisation of the suprasylvian gyrus of the cat. *J. Anat.* 137(Pt 2), 371–385.

Binzegger, T., Douglas, R. J., and Martin, K. A. C. (2005). Axons in cat visual cortex are topologically self-similar. *Cereb. Cortex* 15, 152–165.

Binzegger, T., Douglas, R. J., and Martin, K. A. (2007). Stereotypical bouton clustering of individual neurons in cat primary visual cortex. *J. Neurosci.* 27, 12242–12254.

Bock, D. D., Lee, W.-C. A., Kerlin, A. M., Andermann, M. L., Hood, G., Wetzel, A. W., et al. (2011). Network anatomy and *in vivo* physiology of visual cortical neurons. *Nature* 471, 177–182.

Bohland, J. W., Wu, C., Barbas, H., Bokil, H., Bota, M., Breiter, H. C., et al. (2009). A proposal for a

coordinated effort for the determination of brainwide neuroanatomical connectivity in model organisms at a mesoscopic scale. *PLoS Comput. Biol.* 5:e1000334. doi: 10.1371/journal.pcbi.1000334

Boudkkazi, S., Carlier, E., Ankri, N., Caillard, O., Giraud, P., Fronzaroli-Molinieres, L., et al. (2007). Release-dependent variations in synaptic latency: a putative code for short- and long-term synaptic dynamics. *Neuron* 56, 1048–1060.

Boudkkazi, S., Fronzaroli-Molinieres, L., and Debanne, D. (2011). Presynaptic action potential waveform determines cortical synaptic latency. *J. Physiol.* 589, 1117–1131.

Braitenberg, V., and Schüz, A. (1991). *Anatomy of the Cortex: Statistics and Geometry*. Springer-Verlag. Available online at: http://books.google.com/books?id=zgxrAAAAMAAJandpgis=1

Branco, T., Clark, B. A, and Häusser, M. (2010). Dendritic discrimination of temporal input sequences in cortical neurons. *Science* 329, 1671–1675.

Budd, J. M. (1998). Extrastriate feedback to primary visual cortex in primates: a quantitative analysis of connectivity. *Proc. Biol. Sci.* 265, 1037–1044.

Budd, J. M. L. (2005). Theta oscillations by synaptic excitation in a neocortical circuit model. *Proc. Biol. Sci.* 272, 101–109.

Budd, J. M. L., Kovács, K., Ferecskó, A. S., Buzás, P., Eysel, U. T., and Kisvárday, Z. F. (2010). Neocortical axon arbors trade-off material and conduction delay conservation. *PLoS Comput. Biol.* 6:e1000711. doi: 10.1371/journal.pcbi.1000711

Bullier, J., Kennedy, H., and Salinger, W. (1984). Branching and laminar origin of projections between visual cortical areas in the cat. *J. Comp. Neurol.* 228, 329–341.

Buzás, P., Eysel, U. T., Adorján, P., and Kisvárday, Z. F. (2001). Axonal topography of cortical basket cells in relation to orientation, direction, and ocular dominance maps. *J. Comp. Neurol.* 437, 259–285.

Buzás, P., Kovács, K., Ferecskó, A. S., Budd, J. M. L., Eysel, U. T., and Kisvárday, Z. F. (2006). Model-based analysis of excitatory lateral connections in the visual cortex. *J. Comp. Neurol.* 499, 861–881.

Cajal, S. R. Y. (1899). "Histology of the nervous system of man and the vertebrates," Vol. 1, Chapter 5, eds N. Swanson and L. W. Swanson (trans) (New York, NY: Oxford University Press).

Cajal, S. R. Y. (1937). "Recollections of my life," Chapter 15, eds E. H. Craigie, W. M. Cowan, and J. Cano (Cambridge, MA: MIT Press).

Caminiti, R., Ghaziri, H., Galuske, R., Hof, P. R., and Innocenti, G. M. (2009). Evolution amplified processing with temporally dispersed slow neuronal connectivity in primates. *Proc. Natl. Acad. Sci. U.S.A.* 106, 19551–19556.

Chagnac-Amitai, Y., and Connors, B. W. (1989). Synchronized excitation and inhibition driven by intrinsically bursting neurons in neocortex. *J. Neurophysiol.* 62, 1149–1162.

Cherniak, C. (1994). Component placement optimization in the brain. *J. Neurosci.* 14, 2418–2427.

Chklovskii, D. B., and Koulakov, A. A. (2004). Maps in the brain: what can we learn from them? *Annu. Rev. Neurosci.* 27, 369–392.

Chklovskii, D. B., Schikorski, T., and Stevens, C. F. (2002). Wiring optimization in cortical circuits. *Neuron* 34, 341–347.

Chothani, P., Mehta, V., and Stepanyants, A. (2011). Automated tracing of neurites from light microscopy stacks of images. *Neuroinformatics* 9, 263–278.

Clark, D. A., Mitra, P. P., and Wang, S. S.-H. (2001). Scalable architecture in mammalian brains. *Nature* 411, 189–193.

Cobb, S. R., Buhl, E. H., Halasy, K., Paulsen, O., and Somogyi, P. (1995). Synchronization of neuronal activity in hippocampus by individual GABAergic interneurons. *Nature* 378, 75–78.

Conturo, T. E., Lori, N. F., Cull, T. S., Akbudak, E., Snyder, A. Z., Shimony, J. S., et al. (1999). Tracking neuronal fiber pathways in the living human brain. *Proc. Natl. Acad. Sci. U.S.A.* 96, 10422–10427.

Cormen, T. H., Leiserson, C. E., and Rivest, R. L. (2001). *Introduction to Algorithms*. MIT Press. Available online at: http://books.google.com/books?hl=enandlr=andid=NLngYyWFl_YCandpgis=1

Costa, L. da F., Kaiser, M., and Hilgetag, C. C. (2007). Predicting the connectivity of primate cortical networks from topological and spatial node properties. *BMC Syst. Biol.* 1, 16.

Cox, C. L., Denk, W., Tank, D. W., and Svoboda, K. (2000). Action potentials reliably invade axonal arbors of rat neocortical neurons. *Proc. Natl. Acad. Sci. U.S.A.* 97, 9724–9728.

Cuntz, H., Forstner, F., Borst, A., and Häusser, M. (2010). One rule to grow them all: a general theory of neuronal branching and its practical application. *PLoS Comput. Biol.* 6:e1000877. doi: 10.1371/journal.pcbi.1000877

da Costa, N. M., and Martin, K. A. C. (2010). Whose cortical column would that be? *Front. Neuroanat.* 4:16. doi: 10.3389/fnana.2010.00016

da Costa, N. M., and Martin, K. A. C. (2011). How thalamus connects to spiny stellate cells in the cat's visual cortex. *J. Neurosci.* 31, 2925–2937.

Debanne, D., Campanac, E., Bialowas, A., and Carlier, E. (2011). Axon physiology. *Physiol. Rev.* 555–602.

DeFelipe, J. (2010). From the connectome to the synaptome: an epic love story. *Science* 330, 1198–1201.

DeFelipe, J., Alonso-Nanclares, L., and Arellano, J. I. (2003). Microstructure of the neocortex: comparative aspects. *J. Neurocytol.* 31, 299–316.

Dent, E. W., Gupton, S. L., and Gertler, F. B. (2011). The growth cone cytoskeleton in axon outgrowth and guidance. *Cold Spring Harb. Perspect. Biol.* 3, a001800.

Douglas, R. J., and Martin, K. C. (2011). What's black and white about the grey matter? *Neuroinformatics* 9, 167–179.

Echtermeyer, C., Han, C. E., Rotarska-Jagiela, A., Mohr, H., Uhlhaas, P. J., and Kaiser, M. (2011). Integrating temporal and spatial scales: human structural network motifs across age and region of interest size. *Front. Neuroinform.* 5:10. doi: 10.3389/fninf.2011.00010

Elston, G. N. (2003). Cortex, cognition and the cell: new insights into the pyramidal neuron and prefrontal function. *Cereb. Cortex* 13, 1124–1138.

Fariñas, I., and DeFelipe, J. (1991). Patterns of synaptic input on corticocortical and corticothalamic cells in the cat visual cortex. I. The cell body. *J. Comp. Neurol.* 304, 53–69.

Feldman, M. L. (1984). "Morphology of the neocortical pyramidal neuron," in *Cerebral Cortex, Vol. 1, Cellular Components of the Cerebral Cortex,* eds A. Peters and E. G. Jones (New York, NY: Plenum), 123–200.

Feldmeyer, D., Lübke, J., Silver, R. A., and Sakmann, B. (2002). Synaptic connections between layer 4 spiny neurone-layer 2/3 pyramidal cell pairs in juvenile rat barrel cortex: physiology and anatomy of interlaminar signalling within a cortical column. *J. Physiol.* 538, 803–822.

Felleman, D. J., and Van Essen, D. C. (1991). Distributed hierarchical processing in the primate cerebral cortex. *Cereb. Cortex* 1, 1–47.

Galuske, R. A. W., Schlote, W., Bratzke, H., and Singer, W. (2000). Interhemispheric asymmetries of the modular structure in human temporal cortex. *Science* 289, 1946–1949.

Garey, M. R., and Johnson, D. S. (1979). *Computers and Intractability: A Guide to the Theory of NP-Completeness*. San Francisco, CA: WH Freeman.

Gastner, M. T., and Newman, M. E. J. (2006). Shape and efficiency in spatial distribution networks. *J. Stat. Mech. Theory Exp.* 2006, P01015–P01015.

Gigandet, X., Hagmann, P., Kurant, M., Cammoun, L., Meuli, R., and Thiran, J.-P. (2008). Estimating the confidence level of white matter connections obtained with MRI tractography. *PLoS ONE* 3:e4006. doi: 10.1371/journal.pone.0004006

Girard, P., Hupé, J. M., and Bullier, J. (2001). Feedforward and feedback connections between areas V1 and V2 of the monkey have similar rapid conduction velocities. *J. Neurophysiol.* 85, 1328–1331.

Girvan, M., and Newman, M. E. J. (2002). Community structure in social and biological networks. *Proc. Natl. Acad. Sci. U.S.A.* 99, 7821–7826.

Hagmann, P., Cammoun, L., Gigandet, X., Gerhard, S., Grant, P. E., Wedeen, V., et al. (2010). MR connectomics: principles and challenges. *J. Neurosci. Methods* 194, 34–45.

Hagmann, P., Cammoun, L., Gigandet, X., Meuli, R., Honey, C. J., Wedeen, V. J., et al. (2008). Mapping the structural core of human cerebral cortex. *PLoS Biol.* 6:e159. doi: 10.1371/journal.pbio.0060159

Hagmann, P., Kurant, M., Gigandet, X., Thiran, P., Wedeen, V. J., Meuli, R., et al. (2007). Mapping human whole-brain structural networks with diffusion MRI. *PLoS ONE* 2:e597. doi: 10.1371/journal.pone.0000597

Harvey, A. R. (1980). A physiological analysis of subcortical and commissural projections of areas 17 and 18 of the cat. *J. Physiol.* 302, 507–534.

Haug, H. (1968). Quantitative examinations of electromicrographs on the structure of the myelinated fibers in cat's visual cortex. *Brain Res.* 11, 65–84.

He, Y., Chen, Z. J., and Evans, A. C. (2007). Small-world anatomical networks in the human brain revealed by cortical thickness from MRI. *Cereb. Cortex* 17, 2407–2419.

Helmstaedter, M., Briggman, K. L., and Denk, W. (2011). High-accuracy neurite reconstruction for high-throughput neuroanatomy. *Nat. Neurosci.* 14, 1081–1088.

Helmstaedter, M., Staiger, J. F., Sakmann, B., and Feldmeyer, D. (2008). Efficient recruitment of layer 2/3 interneurons by layer 4 input in single columns of rat somatosensory cortex. *J. Neurosci.* 28, 8273–8284.

Herz, A. V. M., Gollisch, T., Machens, C. K., and Jaeger, D. (2006). Modeling single-neuron dynamics and computations: a balance of detail and abstraction. *Science* 314, 80–85.

Hilgetag, C. C., and Barbas, H. (2006). Role of mechanical factors in the morphology of the primate cerebral cortex. *PLoS Comput. Biol.* 2:e22. doi: 10.1371/journal.pcbi.0020022

Hirsch, J. A., and Gilbert, C. D. (1991). Synaptic physiology of horizontal connections in the cat's visual cortex. *J. Neurosci.* 11, 1800–1809.

Hodgkin, A. L. (1954). A note on conduction velocity. *J. physiol.* 125, 221–224.

Horton, J. C., and Adams, D. L. (2005). The cortical column: a structure without a function. *Philos. Trans. R. Soc. Lond. B Biol. Sci.* 360, 837–862.

Houzel, J. C., Milleret, C., and Innocenti, G. (1994). Morphology of callosal axons interconnecting areas 17 and 18 of the cat. *Eur. J. Neurosci.* 6, 898–917.

Hu, T. C. (1974). Optimum communication spanning trees. *SIAM J. Comput.* 3, 188–195.

Hursh, J. B. (1939). Conduction velocity and diameter of nerve fibers. *Am. J. Physiol.* 127, 131–139.

Johnson, R. R., and Burkhalter, A. (1996). Microcircuitry of forward and feedback connections within rat visual cortex. *J. Comp. Neurol.* 368, 383–398.

Johnson, R. R., and Burkhalter, A. (1997). A polysynaptic feedback circuit in rat visual cortex. *J. Neurosci.* 17, 7129–7140.

Kaas, J. H. (1989). The evolution of complex sensory systems in mammals. *J. Exp. Biol.* 146, 165–176.

Kaas, J. H. (2000). Why is brain size so important: design problems and solutions as neocortex gets biggeror smaller. *Brain Mind* 1, 7–23.

Kaiser, M., and Hilgetag, C. C. (2006). Nonoptimal component placement, but short processing paths, due to long-distance projections in neural systems. *PLoS Comput. Biol.* 2:e95. doi: 10.1371/journal.pcbi.0020095

Kasthuri, N., and Lichtman, J. W. (2007). The rise of the "projectome". *Nat. Methods* 4, 307–308.

Katona, G., Kaszás, A., Turi, G. F., Hájos, N., Tamás, G., Vizi, E. S., et al. (2011). Roller coaster scanning reveals spontaneous triggering of dendritic spikes in CA1 interneurons. *Proc. Nat. Acad. Sci. U.S.A.* 108, 2148–2153.

Khuller, S., Raghavachari, B., and Young, N. (1995). Balancing minimum spanning trees and shortest-path trees. *Algorithmica* 14, 305–321.

Kisvárday, Z. F., Ferecskó, A. S., Kovács, K., Buzás, P., Budd, J. M. L., and Eysel, U. T. (2002). One axon-multiple functions: specificity of lateral inhibitory connections by large basket cells. *J. Neurocytol.* 31, 255–264.

Klausberger, T., Magill, P. J., Márton, L. F., Roberts, J. D. B., Cobden, P. M., Buzsáki, G., et al. (2003). Brain-state- and cell-type-specific firing of hippocampal interneurons *in vivo*. *Nature* 421, 844–848.

Komatsu, Y., Nakajima, S., Toyama, K., and Fetz, E. E. (1988). Intracortical connectivity revealed by spike-triggered averaging in slice preparations of cat visual cortex. *Brain Res.* 442, 359–362.

Kötter, R. (2004). Online retrieval, processing, and visualization of primate connectivity data from the CoCoMac database. *Neuroinformatics* 2, 127–144.

Koulakov, A. A., and Chklovskii, D. B. (2001). Orientation preference patterns in mammalian visual cortex: a wire length minimization approach. *Neuron* 29, 519–527.

Larkman, A. U. (1991). Dendritic morphology of pyramidal neurones of the visual cortex of the rat: III. Spine distributions. *J. Comp. Neurol.* 306, 332–343.

Larkum, M. E., Nevian, T., Sandler, M., Polsky, A., and Schiller, J. (2009). Synaptic integration in tuft dendrites of layer 5 pyramidal neurons: a new unifying principle. *Science* 325, 756–760.

Larkum, M. E., Senn, W., and Lüscher, H.-R. (2004). Top-down dendritic input increases the gain of layer 5 pyramidal neurons. *Cereb. Cortex* 14, 1059–1070.

Larkum, M. E., Zhu, J. J., and Sakmann, B. (1999). A new cellular mechanism for coupling inputs arriving at different cortical layers. *Nature* 398, 338–341.

Latora, V., and Marchiori, M. (2001). Efficient behavior of small-world networks. *Phys. Rev. Lett.* 87. Available online at: http://prl.aps.org/abstract/PRL/v87/i19/e198701

Laughlin, S. B., and Sejnowski, T. J. (2003). Communication in neuronal networks. *Science* 301, 1870–1874.

Leergaard, T. B., Hilgetag, C. C., and Sporns, O. (2012). Mapping the connectome: multi-level analysis of brain connectivity. *Front. Neuroinform.* 6:14. doi: 10.3389/fninf.2012.00014

Lichtman, J. W., Livet, J., and Sanes, J. R. (2008). A technicolour approach to the connectome. *Nat. Rev. Neurosci.* 9, 417–422.

Lichtman, J. W., and Sanes, J. R. (2008). Ome sweet ome: what can the genome tell us about the connectome? *Curr. Opin. Neurobiol.* 18, 346–353.

Lohmann, H., and Rörig, B. (1994). Long-range horizontal connections between supragranular pyramidal cells in the extrastriate visual cortex of the rat. *J. Comp. Neurol.* 344, 543–558.

London, M., and Häusser, M. (2005). Dendritic computation. *Annu. Rev. Neurosci.* 28, 503–532.

Luhmann, H. J., Greuel, J. M., and Singer, W. (1990). Horizontal interactions in cat striate cortex: II. A current source-density analysis. *Eur. J. Neurosci.* 2, 358–368.

MacDonald, N. (1983). *Trees and Networks in Biological Models*. Chichester, UK: Wiley and Sons.

Manor, Y., Koch, C., and Segev, I. (1991). Effect of geometrical irregularities on propagation delay in axonal trees. *Biophys. J.* 60, 1424–1437.

Markov, N. T., Misery, P., Falchier, A., Lamy, C., Vezoli, J., Quilodran, R., et al. (2011). Weight consistency specifies regularities of macaque cortical networks. *Cereb. Cortex* 21, 1254–1272.

Markram, H., Lübke, J., Frotscher, M., Roth, A., and Sakmann, B. (1997). Physiology and anatomy of synaptic connections between thick tufted pyramidal neurones in the developing rat neocortex. *J. Physiol.* 500, 409–440.

Maynard Smith, J. (1978). Optimization theory in evolution. *Annu. Rev. Ecol. Syst.* 9, 31–56.

McCurry, C., Shepherd, J., and Tropea, D. (2010). Loss of arc renders the visual cortex impervious to the effects of sensory experience or deprivation. *Nat. Neurosci.* 13, 450–457.

Miller, R. (1975). Distribution and properties of commissural and other neurons in cat sensorimotor cortex. *J. Comp. Neurol.* 164, 361–373.

Milo, R., Shen-Orr, S., Itzkovitz, S., Kashtan, N., Chklovskii, D., and Alon, U. (2002). Network motifs: simple building blocks of complex networks. *Science* 298, 824–827.

Mishchenko, Y., Hu, T., Spacek, J., Mendenhall, J., Harris, K. M., and Chklovskii, D. B. (2010). Ultrastructural analysis of hippocampal neuropil from the connectomics perspective. *Neuron* 67, 1009–1020.

Mitchison, G. (1991). Neuronal branching patterns and the economy of cortical wiring. *Proc. Biol. Sci.* 245, 151–158.

Moseley, M. E., Cohen, Y., Kucharczyk, J., Mintorovitch, J., Asgari, H. S., Wendland, M. F., et al. (1990). Diffusion-weighted MR imaging of anisotropic water diffusion in cat central nervous system. *Radiology* 176, 439–445.

Müller, C. M. (1992). Astrocytes in cat visual cortex studied by GFAP and S-100 immunocytochemistry during postnatal development. *J. Comp. Neurol.* 317, 309–323.

Nevian, T., Larkum, M. E., Polsky, A., and Schiller, J. (2007). Properties of basal dendrites of layer 5 pyramidal neurons: a direct patch-clamp recording study. *Nat. Neurosci.* 10, 206–214.

Newman, M. (2010). *Networks: An Introduction*. Oxford: Oxford University Press. Available online at: http://dl.acm.org/citation.cfm?id=1809753

Nowak, L. G., and Bullier, J. (1997). "The timing of information transfer in the visual system," in *Cerebral Cortex Cerebral Cortex, Vol. 12, Extrastriate Cortex in Primates,* eds K. S. Rockland, J. H. Kaas, and A. Peters (New York, NY: Plenum), 205–233.

Oláh, S., Füle, M., Komlósi, G., Varga, C., Báldi, R., Barzó, P., et al. (2009). Regulation of cortical microcircuits by unitary GABA-mediated volume transmission. *Nature* 461, 1278–1281.

Perge, J. A., Niven, J. E., Mugnaini, E., Balasubramanian, V., and Sterling, P. (2012). Why do axons differ in caliber? *J. Neurosci.* 32, 626–638.

Perin, R., Berger, T. K., and Markram, H. (2011). A synaptic organizing principle for cortical neuronal groups. *Proc. Natl. Acad. Sci. U.S.A.* 108, 5419–5424.

Peters, A., Palay, S. F., and deF Webster, H. (1991). *The Fine Structure of the Nervous System: Neurons and Their Supporting Cells*. 3rd Edn. New

York, NY, USA: Oxford University Press.

Peters, A., and Sethares, C. (1996). Myelinated axons and the pyramidal cell modules in monkey primary visual cortex. *J. Comp. Neurol.* 365, 232–255.

Price, D. J., Kennedy, H., Dehay, C., Zhou, L., Mercier, M., Jossin, Y., et al. (2006). The development of cortical connections. *Eur. J. Neurosci.* 23, 910–920.

Purves, D., Augustine, G. J., Fitzpatrick, D., Hall, W. C., LaMantia, A.-S., McNamara, J. O., et al. (2007). *Neuroscience*. 4th Edn. Sunderland, MA: Sinauer Associates.

Raastad, M., and Shepherd, G. M. G. (2003). Single-axon action potentials in the rat hippocampal cortex. *J. Physiol.* 548, 745–752.

Raiguel, S. E., Lagae, L., Gulyàs, B., and Orban, G. A. (1989). Response latencies of visual cells in macaque areas V1, V2 and V5. *Brain Res.* 493, 155–159.

Risau, W. (1997). Mechanisms of angiogenesis. *Nature* 386, 671–674.

Rockland, K. S. (1997). "Elements of cortical architecture: hierarchy revisited," in *Cerebral Cortex, Vol. 12, Extrastriate Cortex in Primates*, eds K. S. Rockland, J. H. Kaas, and A. Peters (New York, NY: Plenum), 243–293.

Rockland, K. S. (2002). Visual cortical organization at the single axon level: a beginning. *Neurosci. Res.* 42, 155–166.

Rockland, K. S. (2004). Connectional neuroanatomy: the changing scene. *Brain Res.* 1000, 60–63.

Rockland, K. S. (2010). Five points on columns. *Front. Neuroanat.* 4:22. doi: 10.3389/fnana.2010.00022

Rockland, K. S., and Pandya, D. N. (1979). Laminar origins and terminations of cortical connections of the occipital lobe in the rhesus monkey. *Brain Res.* 179, 3–20.

Rothman, J. S., Cathala, L., Steuber, V., and Silver, R. A. (2009). Synaptic depression enables neuronal gain control. *Nature* 457, 1015–1018.

Rothnie, P., Kabaso, D., Hof, P. R., Henry, B. I., and Wearne, S. L. (2006). Functionally relevant measures of spatial complexity in neuronal dendritic arbors. *J. Theor. Biol.* 238, 505–526.

Rubinov, M., and Sporns, O. (2010). Complex network measures of brain connectivity: uses and interpretations. *Neuroimage* 52, 1059–1069.

Rudolph, M., and Destexhe, A. (2003a). A fast-conducting, stochastic integrative mode for neocortical neurons *in vivo*. *J. Neurosci.* 23, 2466–2476.

Rudolph, M., and Destexhe, A. (2003b). Tuning neocortical pyramidal neurons between integrators and coincidence detectors. *J. Comput. Neurosci.* 14, 239–251.

Rushton, W. A. H. (1951). A theory of the effects of fibre size in medullated nerve. *J. Physiol.* 115, 101–122.

Sabatini, B. L., and Regehr, W. G. (1996). Timing of neurotransmission at fast synapses in the mammalian brain. *Nature* 384, 170–172.

Salin, P. A., and Bullier, J. (1995). Corticocortical connections in the visual system: structure and function. *Physiol. Rev.* 75, 107–154.

Sánchez, I., Hassinger, L., Paskevich, P. A., Shine, H. D., and Nixon, R. A. (1996). Oligodendroglia regulate the regional expansion of axon caliber and local accumulation of neurofilaments during development independently of myelin formation. *J. Neurosci.* 16, 5095–5105.

Scannell, J. W., Blakemore, C., and Young, M. P. (1995). Analysis of connectivity in the cat cerebral cortex. *J. Neurosci.* 15, 1463–1483.

Scannell, J. W., Grant, S., Payne, B. R., and Baddeley, R. (2000). On variability in the density of corticocortical and thalamocortical connections. *Philos. Trans. R. Soc. Lond. Ser. B Biol. Sci.* 355, 21–35.

Schiller, J., Major, G., Koester, H. J., and Schiller, Y. (2000). NMDA spikes in basal dendrites of cortical pyramidal neurons. *Nature* 404, 285–289.

Schmahmann, J. D., Pandya, D. N., Wang, R., Dai, G., D'Arceuil, H. E., de Crespigny, A. J., et al. (2007). Association fibre pathways of the brain: parallel observations from diffusion spectrum imaging and autoradiography. *Brain J. Neurol.* 130, 630–653.

Schüz, A., and Palm, G. (1989). Density of neurons and synapses in the cerebral cortex of the mouse. *J. Comp. Neurol.* 286, 442–455.

Schwartz, M. L., and Goldman-Rakic, P. S. (1982). Single cortical neurones have axon collaterals to ipsilateral and contralateral cortex in fetal and adult primates. *Nature* 299, 154–155.

Shannon, C. E. (1948). A mathematical theory of communication. *Bell Syst. Tech. J.* 27, 379–423.

Shepherd, G. M. (1990). *The Synaptic Organization of the Brain*. 3rd Edn. New York, NY: Oxford University Press.

Shlosberg, D., Abu-Ghanem, Y., and Amitai, Y. (2008). Comparative properties of excitatory and inhibitory inter-laminar neocortical axons. *Neuroscience* 155, 366–373.

Sholl, D. A. (1953). Dendritic organization in the neurons of the visual and motor cortices of the cat. *J. Anat.* 87, 387–406.

Simon, H. (1962). The architecture of complexity. *Proc. Am. Philos. Soc.* 106, 467–482.

Sincich, L. C., Jocson, C. M., and Horton, J. C. (2010). V1 interpatch projections to V2 thick stripes and pale stripes. *J. Neurosci.* 30, 6963–6974.

Sjöström, P. J., Rancz, E. A., Roth, A., and Häusser, M. (2008). Dendritic excitability and synaptic plasticity. *Physiol. Rev.* 88, 769–840.

Sjöström, P. J., Turrigiano, G. G., and Nelson, S. B. (2001). Rate, timing, and cooperativity jointly determine cortical synaptic plasticity. *Neuron* 32, 1149–1164.

Snider, J., Pillai, A., and Stevens, C. F. (2010). A universal property of axonal and dendritic arbors. *Neuron* 66, 45–56.

Somogyi, P., Tamás, G., Lujan, R., and Buhl, E. H. (1998). Salient features of synaptic organisation in the cerebral cortex. *Brain Res. Rev.* 26, 113–135.

Song, S., Sjöström, P. J., Reigl, M., Nelson, S., and Chklovskii, D. B. (2005). Highly nonrandom features of synaptic connectivity in local cortical circuits. *PLoS Biol.* 3:e68. doi: 10.1371/journal.pbio.0030068

Sporns, O. (2011). The non-random brain: efficiency, economy, and complex dynamics. *Front. Comput. Neurosci.* 5:5. doi: 10.3389/fncom.2011.00005

Sporns, O., Honey, C. J., and Kötter, R. (2007). Identification and classification of hubs in brain networks. *PLoS ONE* 2:e1049. doi: 10.1371/journal.pone.0001049

Sporns, O., Tononi, G., and Edelman, G. M. (2000). Connectivity and complexity: the relationship between neuroanatomy and brain dynamics. *Neural Netw.* 13, 909–22.

Sporns, O., Tononi, G., and Kötter, R. (2005). The human connectome: a structural description of the human brain. *PLoS Comput. Biol.* 1:e42. doi: 10.1371/journal.pcbi.0010042

Spruston, N. (2008). Pyramidal neurons: dendritic structure and synaptic integration. *Nat. Rev. Neurosci.* 9, 206–221.

Stepanyants, A., and Chklovskii, D. B. (2005). Neurogeometry and potential synaptic connectivity. *Trends Neurosci.* 28, 387–94.

Stepanyants, A., Martinez, L. M., Ferecskó, A. S., and Kisvárday, Z. F. (2009). The fractions of short- and long-range connections in the visual cortex. *Proc. Natl. Acad. Sci. U.S.A.* 106, 3555–60.

Stephan, K. E., Kamper, L., Bozkurt, A., Burns, G. A., Young, M. P., and Kötter, R. (2001). Advanced database methodology for the Collation of Connectivity data on the Macaque brain (CoCoMac). *Philos. Trans. R. Soc. Lond. Ser. B Biol. Sci.* 356, 1159–1186.

Stevens, C. F. (2001). An evolutionary scaling law for the primate visual system and its basis in cortical function. *Nature* 411, 193–195.

Storm, J. F. (1988). Temporal integration by a slowly inactivating K+ current in hippocampal neurons. *Nature* 336, 379–81.

Stuart, G., Schiller, J., and Sakmann, B. (1997). Action potential initiation and propagation in rat neocortical pyramidal neurons. *J. Physiol.* 505, 617–632.

Swadlow, H. A., Waxman, S. G., and Rosene, D. L. (1978). Latency variability and the identification of antidromically activated neurons in mammalian brain. *Exp. Brain Res.* 32, 439–443.

Tettoni, L., Gheorghita-Baechler, F., Bressoud, R., Welker, E., and Innocenti, G. M. (1998). Constant and variable aspects of axonal phenotype in cerebral cortex. *Cereb. Cortex* 8, 543–552.

Tieman, S. B., Möllers, S., Tieman, D. G., and White, J. (2004). The blood supply of the cat's visual cortex and its postnatal development. *Brain Res.* 998, 100–112.

Tyler, C. J., Dunlop, S. A., Lund, R. D., Harman, A. M., Dann, J. F., Beazley, L. D., et al. (1998). Anatomical comparison of the macaque and marsupial visual cortex: common features that may reflect retention of essential cortical elements. *J. Comp. Neurol.* 400, 449–68.

Uhlhaas, P. J., Pipa, G., Lima, B., Melloni, L., Neuenschwander, S., Nikoliæ, D., et al. (2009). Neural synchrony in cortical networks: history, concept and current status. *Front. Integr. Neurosci.* 3:17. doi: 10.3389/neuro.07.017.2009

Ulrich, D., and Stricker, C. (2011). Dendrosomatic voltage and charge transfer in rat neocortical pyramidal cells *in vitro* temperatures dendrosomatic voltage and charge transfer in rat neocortical pyramidal cells *in vitro*. *J. Neurophysiol.* 84, 1445–1452.

Van Essen, D. C., Glasser, M. F., Dierker, D. L., and Harwell, J. (2012a). Cortical parcellations of the macaque monkey analyzed on

surface-based atlases. *Cereb. Cortex* 22, 2227–2240.

Van Essen, D. C., Glasser, M. F., Dierker, D. L., Harwell, J., and Coalson, T. (2012b). Parcellations and hemispheric asymmetries of human cerebral cortex analyzed on surface-based atlases. *Cereb. Cortex* 22, 2241–2262.

Wang, S. S.-H., Shultz, J. R., Burish, M. J., Harrison, K. H., Hof, P. R., Towns, L. C., et al. (2008). Functional trade-offs in white matter axonal scaling. *J. Neurosci.* 28, 4047–4056.

Watts, D. J., and Strogatz, S. H. (1998). Collective dynamics of "small-world" networks. *Nature* 393, 440–442.

Waxman, S. G., and Bennett, M. V. L. (1972). Relative conduction velocities of small myelinated and non-myelinated fibres in the central nervous system. *Nat. New Biol.* 238, 217–219.

Wedeen, V. J., Rosene, D. L., Wang, R., Dai, G., Mortazavi, F., Hagmann, P., et al. (2012). The geometric structure of the brain fiber pathways. *Science* 335, 1628–1634.

Wen, Q., Stepanyants, A., Elston, G. N., Grosberg, A. Y., and Chklovskii, D. B. (2009). Maximization of the connectivity repertoire as a statistical principle governing the shapes of dendritic arbors. *Proc. Natl. Acad. Sci. U.S.A.* 106, 12536–12541.

Wickersham, I. R., Lyon, D. C., Barnard, R. J. O., Mori, T., Finke, S., Conzelmann, K.-K., et al. (2007). Monosynaptic restriction of transsynaptic tracing from single, genetically targeted neurons. *Neuron* 53, 639–647.

Wu, B. Y., Chao, K.-M., and Tang, C. Y. (2002). Light graphs with small routing cost. *Networks* 39, 130–138.

Young, M. P. (1992). Objective analysis of the topological organization of the primate cortical visual system. *Nature* 358, 152–155.

Yuste, R., Gutnick, M. J., Saar, D., Delaney, K. R., and Tank, D. W. (1994). Ca2+ accumulations in dendrites of neocortical pyramidal neurons: an apical band and evidence for two functional compartments. *Neuron* 13, 23–43.

Zhang, K., and Sejnowski, T. J. (2000). A universal scaling law between gray matter and white matter of cerebral cortex. *Proc. Natl. Acad. Sci. U.S.A.* 97, 5621–5626.

Conflict of Interest Statement: The authors declare that the research was conducted in the absence of any commercial or financial relationships that could be construed as a potential conflict of interest.

Received: 07 February 2012; accepted: 24 September 2012; published online: 16 October 2012.

Citation: Budd JML and Kisvárday ZF (2012) Communication and wiring in the cortical connectome. Front. Neuroanat. ***6****:42. doi: 10.3389/fnana.2012.00042*

frontiers in
NEUROANATOMY

PERSPECTIVE ARTICLE
published: 01 February 2012
doi: 10.3389/fnana.2012.00002

The dendritic density field of a cortical pyramidal cell

Hermann Cuntz [1,2] *

[1] Institute of Clinical Neuroanatomy, Goethe-University, Frankfurt am Main, Germany
[2] Ernst Strüngmann Institute in Cooperation with Max Planck Society, Max-Planck Institute, Frankfurt am Main, Germany

Edited by:
Julian Budd, University of Sussex, UK

Reviewed by:
Armen Stepanyants, Northeastern University, USA
Guy Elston, International Brain Research Organization, Switzerland

***Correspondence:**
Hermann Cuntz, Institute of Clinical Neuroanatomy, Goethe-University, Theodor-Stern-Kai 7, D-60590 Frankfurt am Main, Germany.
e-mail: hermann.neuro@gmail.com

Much is known about the computation in individual neurons in the cortical column. Also, the selective connectivity between many cortical neuron types has been studied in great detail. However, due to the complexity of this microcircuitry its functional role within the cortical column remains a mystery. Some of the wiring behavior between neurons can be interpreted directly from their particular dendritic and axonal shapes. Here, I describe the dendritic density field (DDF) as one key element that remains to be better understood. I sketch an approach to relate DDFs in general to their underlying potential connectivity schemes. As an example, I show how the characteristic shape of a cortical pyramidal cell appears as a direct consequence of connecting inputs arranged in two separate parallel layers.

Keywords: modeling, dendrite, axon, pyramidal cell, Ramón y Cajal

> *The laws of time, space, and material conservation, which must be considered the final cause of all variations in the shape of neurons, should in our view be immediately obvious to anyone thinking about or trying to verify them, and ought to constitute the final proof of our axopetal polarity theory. All that remains is to substantiate the influence of these laws on the conformation of particular neurons.*
> *(Ramón y Cajal, 1909)*

Cortical circuits are modular and subdivide functionally into cortical columns (Mountcastle, 1957; Hubel and Wiesel, 1962). While it remains controversial as to how stringent this organizational principle is (Horton and Adams, 2005) and the advantages for such an organization remain largely unknown (Malach, 1994), the importance of understanding the columnar organization of the cortex is undisputed. In order to understand the computation occurring in the single column, the principles underlying its local circuitry need to be fully understood. Physiological analyses (e.g., through multiple simultaneous recordings) in combination with anatomical characterizations of the individual neurons involved were successful in unraveling many details of local cortical connectivity (e.g., Szentágothai, 1975; Douglas and Martin, 2004; Lübke and Feldmeyer, 2007). Anatomically, evidence exists that neurons send out their dendrites to allow potential connections (points of anatomical proximity; Stepanyants and Chklovskii, 2005) to the axons of all neurons of their particular target neuron types within their column (Lübke et al., 2003; Douglas and Martin, 2004; Kalisman et al., 2005). To which degree neurons in the cortical column form such an anatomical substrate which allows for all combinations of functional connections remains the subject of debate (e.g., DeFelipe et al., 2002; Shepherd et al., 2005). Whether anatomical connections target specific individual cells probably depends on the neuron type (Stepanyants et al., 2004). Functionally then, only subsets of the anatomical potential connections are in use and highly non-random features have been observed in the corresponding functional connectivity map (Song et al., 2005). Selecting functional synapses among anatomical potential connection sites may happen through spine rearrangement, a rewiring which does not require reshaping entire dendritic branches (e.g., Stepanyants et al., 2002; Chklovskii et al., 2004).

Are dendrites and axons then ideally matched to anatomically maximize connections to their potential connection partners? Theoretical predictions from optimality criteria are indeed in line with this idea (Wen et al., 2009). For dendrites and axons, wiring principles and branching patterns are certainly intertwined (Chklovskii, 2004; Cuntz et al., 2007; Wen and Chklovskii, 2008; Budd et al., 2010). Moreover, branching patterns can actually be predicted based predominantly on wiring principles (Cuntz et al., 2010). Simulation approaches such as these deepen our insights by testing whether the theoretical predictions are valid under realistic conditions. In order to simulate anatomical connections between neurons, model assumptions for both dendrite and axon morphologies are required. One approach is to estimate synaptic connectivity based on anatomical neuron models obtained from neuron reconstructions (Lübke et al., 2003; Douglas and Martin, 2004; Fares and Stepanyants, 2009) or by simulating the mechanisms of dendrite and axon growth (Koene et al., 2009; van Pelt et al., 2010). The second approach is to predict dendrite and axon morphologies according to the optimal implementation of a particular connectivity scheme and compare the results with biological data. In the following, I will briefly describe the method of morphological modeling (Cuntz et al., 2008, 2010) which follows this second strategy. From there I will make a direct link between a specific connectivity pattern and the corresponding dendritic tree. In the process I will show how the dendritic density field (DDF) can be estimated on the basis of this link.

THE DENDRITIC DENSITY FIELD AND MORPHOLOGICAL MODELING

We have shown previously that by extending the minimum spanning tree (MST) algorithm it is possible to connect a set of point

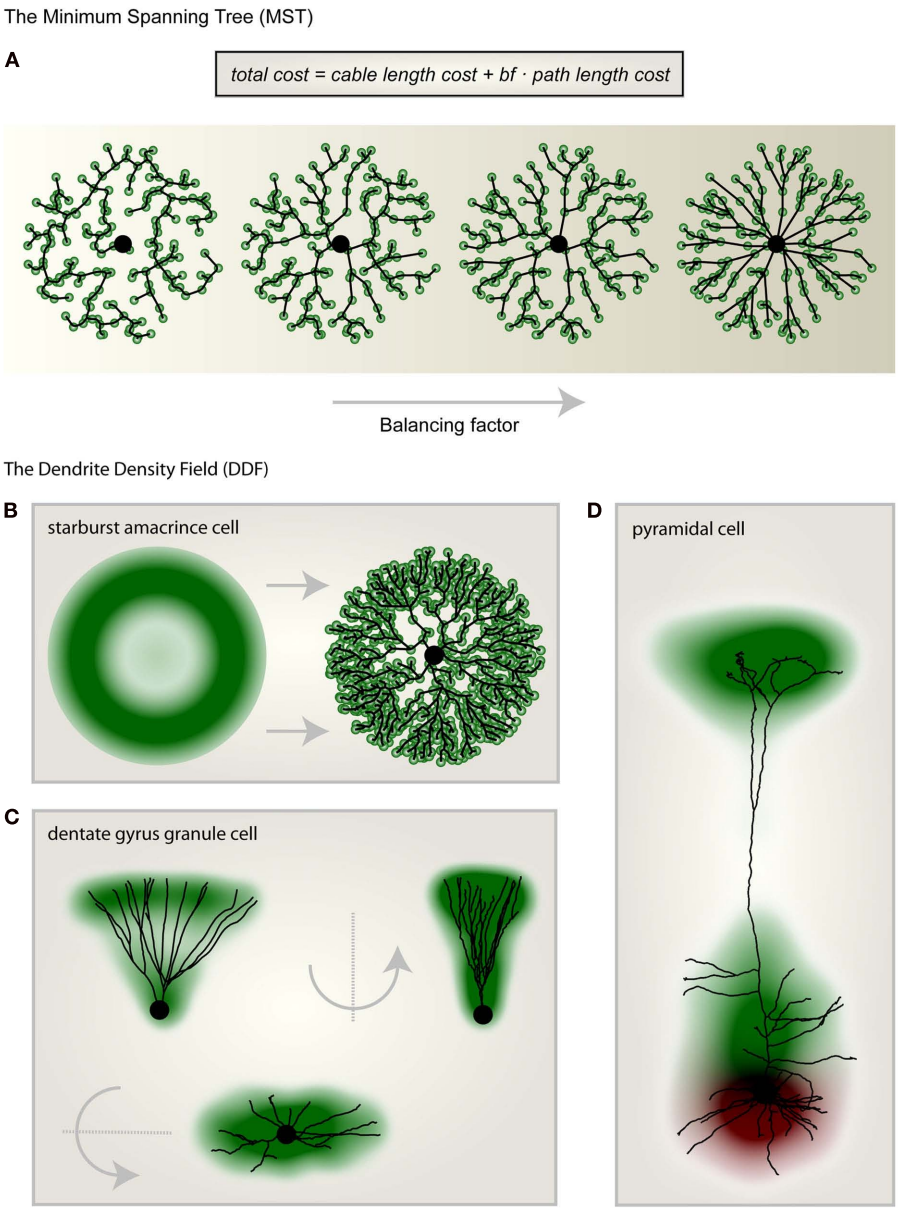

FIGURE 1 | Morphological modeling and the dendritic density field (DDF). (A) From left to right the same set of unconnected target points (green) were connected to a starting point (large black dot) according to the minimum spanning tree (MST) algorithm with increasing balancing factor *bf* between the two wiring costs: total cable length and sum of all paths. **(B)** Geometric description of the DDF of a starburst amacrine cell (left). By randomly selecting target points according to the DDF and subsequently connecting them using the MST algorithm (right) to a starting node (large black dot), a synthetic starburst amacrine cell dendrite can be generated. **(C)** The DDF obtained directly from reconstructions of dentate gyrus granule cells with its characteristic cone-like shape. A representative real morphology is shown. **(D)** Separate DDFs for L5 cortical pyramidal cell basal trees (red) and apical trees (green). One representative real morphology is shown. Parts of the figure were adapted from Cuntz et al. (2010).

targets which are distributed in space to satisfy biological optimization costs of dendritic trees (Cuntz et al., 2007). The required cost function is composed of two individual costs (**Figure 1A**): the total amount of wiring (cable length cost) and the cost of signal conduction (path length cost: the sum of the length of all paths along the tree from any target point to the root) corresponding well with costs originally proposed by Ramón y Cajal (1909). When a set of target points is adequately selected, any dendritic tree morphology can be reproduced after connecting the target points to a tree using the MST algorithm. This approach represents a method of morphological modeling useful for generating realistic synthetic dendritic trees (Cuntz et al., 2010). The sketch in **Figure 1B** shows

a synthetic starburst amacrine cell which was generated by distributing target points stochastically according to a geometrical arrangement of densities. Target points are then connected to a tree structure whilst observing the wiring costs mentioned above. This simple procedure highlights the usefulness of a DDF, here representing the density of target points per area, to describe a dendrite's morphology. The DDF and the one parameter balancing the two costs for wiring mentioned above are thereby sufficient to describe the dendrite type. In fact, we have previously shown that for fly interneurons the spanning field is the most informative element for classifying dendritic trees into their respective cell types (Cuntz et al., 2008). In some cases, DDFs can be obtained directly from reconstructions of real neurons. By superimposing their soma locations and rotating them such that they lie symmetrically around the y-axis and then scaling their width, height, and depth, a set of reconstructions of dentate gyrus granule cell (data from Rihn and Claiborne, 1990) dendrites are brought into a common context. An appropriate approximation of the DDF is then obtained directly from the density of branch and termination points from the reconstructions (**Figure 1C**). When apical and basal dendrites are considered separately, the DDFs of pyramidal cells can be calculated in a similar way (L5 PCs, **Figure 1D**; data from Wang et al., 2002).

PREDICTING THE DENDRITIC DENSITY FIELD FROM INPUT AXON CONFIGURATIONS

While the dendrites of starburst amacrine cells, dentate gyrus granule cells, and many other neurons exhibit complex DDFs, some simpler ones such as pyramidal cell basal dendrites observe basic principles which can be characterized by studying the statistical moments of their density distributions (Snider et al., 2010). Stevens and colleagues have shown that the cable density distributions in dendrites roughly follow separate Gaussian distributions for each dimension in space which are cut off at 2 standard deviation. What determines this particular density profile? In synthetic dendrites generated using the MST, homogenously distributed carrier points lead to a homogeneous cable density. The MST alone can therefore not be responsible for the observed Gaussian cable density distribution. Intuitively, the shape of a DDF should be determined by the set of axons which are a dendrite's potential, i.e., anatomical connection partners. This simple intuition can provide direct explanations for basic features of DDFs.

When input target points were distributed along one dimension, the MST was simply a straight line connecting these points (**Figure 2A**). When these target points were extended to parallel lines as in **Figure 2B**, and the MST was set to connect to each axon once, the resulting synthetic dendrite was not changed. Out of cable and conduction time minimization, a straight and direct connection remained ideal. When more axons were added and noise was introduced to their trajectories (**Figure 2C**), the MST dendrite started to branch out. In a similar but more realistic setting, a dendrite connecting to a set of parallel axons traversing space was flat according to the MST (**Figure 2D**). A flat dendrite which lies perpendicular to a set of parallel axons was shown to be the overall ideal geometrical arrangement given Cajal's wiring costs (Wen and Chklovskii, 2008). It is therefore not surprising that the MST approach reproduces this intuition. Such a planar dendritic structure can be observed in cerebellar Purkinje cells for example which reach out to the molecular layer to collect their parallel fiber inputs. These being arranged entirely in parallel the dendrite must grow in a planar way perpendicular to the parallel fibers to connect to them most efficiently.

Most neural systems however are not entirely optimized for the connection between only one set of axons and one dendrite type. Axon distributions are therefore more complex. In order to illustrate the potential of this constructive approach, I demonstrate in the following how a few sample input axon sets would impact on the resulting MST dendrites and therefore on their average DDF. The first case scenario that I chose exhibits a set of axons which were located in parallel neighboring planes forming a neuronal layer. Within their respective planes, the axons were isotropically oriented and the starting point, the root of the dendrite, was positioned below the layer of axons. Only the axons passing in close vicinity with a cutoff at half of the thickness of the layer were considered (**Figure 2E**). In such a configuration the distribution of axons was homogeneous. However, the resulting MST dendrite grew a shape reminiscent of dentate gyrus granule cell dendrites and exhibited an inhomogeneous DDF (**Figure 2F**). When the starting point was moved to the center of the axonal layer, this resulted in an isotropic DDF similar to a pyramidal cell basal dendritic density profile (**Figure 2G**). It is possible that such a DDF follows similar features as the dendritic cable densities measured previously (Snider et al., 2010; Teeter and Stevens, 2011). Note that the precise relation between density of topological points in a dendrite and dendrite cable density has yet to be studied in detail. In any case, it will be possible to find the type of arrangement of input axons which generally reproduces their measures, thereby unveiling general principles of axon arrangements and connectivity patterns. To finish, I would like to suggest a last sample configuration in which two separate layers of axons similar to the one previously described were both connected to a single starting point located in the middle of the lower of the two layers (**Figure 2H**). Under these conditions, the natural shape of a pyramidal cell, including its apical dendrite and its two separate DDFs (**Figure 2I**) were a natural consequence. When biological jitter and diameter values were mapped onto the corresponding tree structure (as in Cuntz et al., 2010), this resulted in a biologically realistic pyramidal cell (**Figure 2J**).

OUTLOOK

I have shown that morphological models can provide more than just anatomical profiles for realistic neural network simulations. They can also be a tool to understand how dendrite morphology comes about and a tool to test our knowledge about the local connectivity in the brain. This short exercise provides once more evidence that the major determinant for a dendrite's morphology is its role in the connectivity. It is well known that morphology particularly in cortical pyramidal cells plays a role for the intrinsic computation that a single neuron performs on its inputs (Vetter et al., 2001; Polsky et al., 2004; Sjöström and Häusser, 2006; Branco et al., 2010). The role of morphology on single neuron computation, and vice versa, can also be studied using morphological modeling. In the morphological model, neuronal computation is affected in various ways. The main morphological

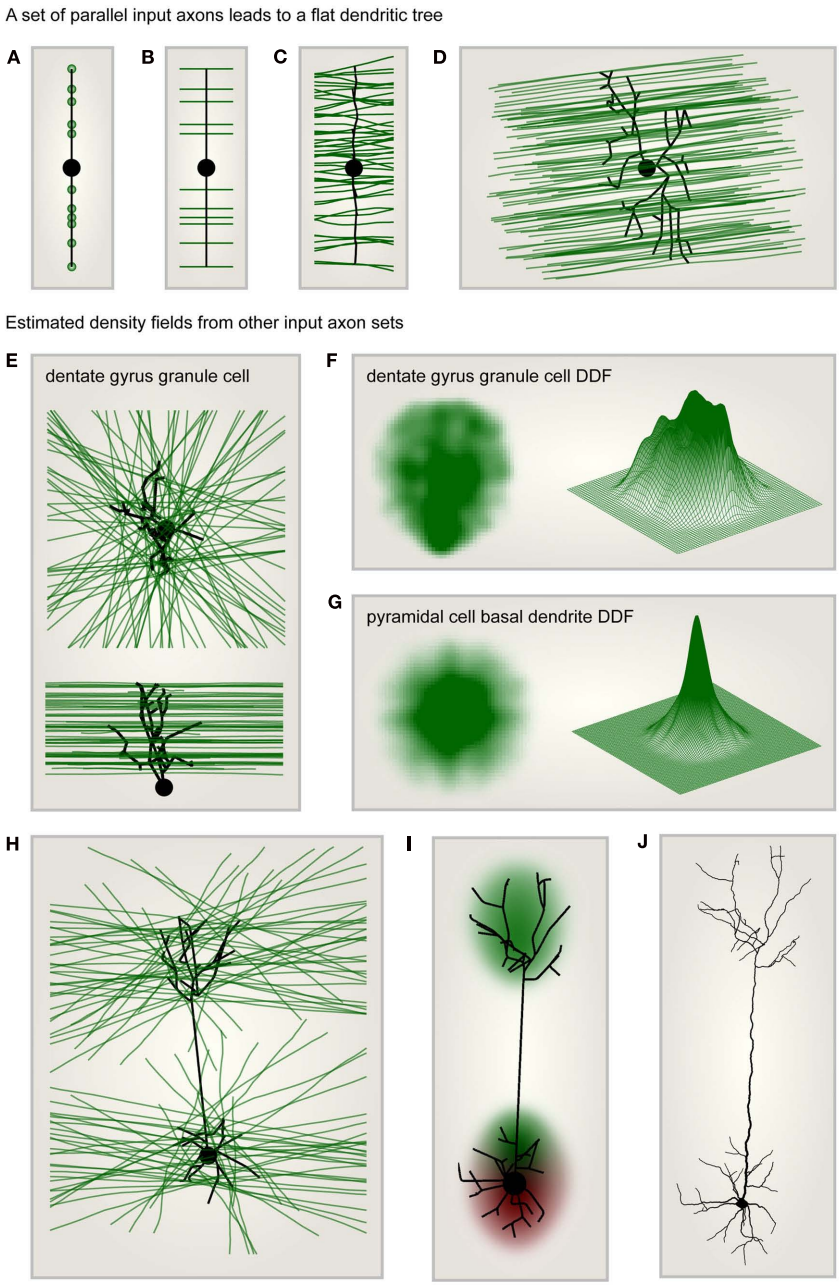

FIGURE 2 | Dendritic density field (DDF) estimation directly from input axon distributions. (A) Target points (green) lying on one line are connected to a starting node (large black dot) using the MST algorithm. This leads to a dendrite consisting of a single line. **(B)** Same as in **(A)** but targets are parallel lines (axons, green) rather than points. The optimal dendrite connecting to these axons is the same as in **(A)**. **(C)** Same as in **(B)** but the number of target axons is increased and the axon trajectories are slightly jittered: the MST is slightly jittered and a few branch points appear. **(D)** Synthetic dendrite (black) connecting a starting point (large black dot) in 3D space to a set of parallel axons (green): the resulting MST is flat. **(E)** Target axons (green) are arranged in parallel planes but are of isotropic orientation within these planes. The axons are connected using MST (black tree) to a starting point (large black dot) located below the layer of axons. Top: view from the top; bottom: view from the side. The result is a typical dentate gyrus granule cell morphology. **(F)** DDF of 50 synthetic granule cells grown as in **(E)**; compare with **Figure 1C**. Left: side view of density profile; right: mesh representation of the same density distribution. **(G)** Same as in **(F)** but the starting point was moved to the center of the layer to reproduce the characteristic shape of the basal tree of a cortical pyramidal cell. **(H)** Same as in **(E)** but the MST connects to axons located in two parallel layers. The starting point is located in the middle of the lower layer. The result is a characteristic pyramidal cell shape. **(I)** DDF of 100 synthetic pyramidal cells grown as in **(H)**; compare with **Figure 1D**. **(J)** One such synthetic pyramidal cell where diameter values were mapped onto the dendritic segments and spatial jitter was added along the dendrite.

parameter which impacts neuronal computation is the balancing factor *bf* between the two wiring costs (**Figure 1A**). We have previously shown that a large *bf* promotes a higher electrotonic compartmentalization of the resulting synthetic dendritic tree (Cuntz et al., 2010). This adds to the natural increase in conduction time speeds which is favored with increasing *bf* to the detriment of wiring economy. Secondly, dendritic diameters play a role in dendritic signal integration. We have previously attributed diameter tapering to synaptic democracy. However, only electron microscopy reconstructions (e.g., Kubota et al., 2011) will resolve the precise role of diameter distributions on the electrotonic properties of a dendrite. Lastly, to implement a given computation, the single neuron can select a subset out of a large variety of possible ion channel combinations which may be adapted to suit the underlying morphological template (Prinz et al., 2003). Interestingly, the toy model of a pyramidal cell presented here does not build on any functional differences between the two layers that it connects. The location of the starting point alone determines which of the layers will yield an apical dendrite and which one a basal dendrite. This dendrite root corresponds to the summation point of the input signals but more importantly it is the coordinate from which the axon, the output of the neuron, exits the cell. The fact that the location of the exiting axon determines the neuron's shape was at the center of Cajal's axopetal polarity theory. In the cortex, most long-range axons project toward the white matter away from the pial surface. We would therefore predict a stereotypic polarity of pyramidal cell morphology: Basal dendrites of pyramidal cells should be on the inside closer to the white matter, whereas the apical dendrites should be on the pial side. This indeed is the case. At the example of the pyramidal cell dendrite I showed that it is possible to predict both their DDF and their precise branching structure by making assumptions about the input axon distribution. In this way it might for example be possible to link regionalized specializations in pyramidal cell dendrite shape (Elston, 2003) with differences in local connectivity. To summarize, I have shown that the DDF is a promising attribute of dendrite shape which enables direct conclusions on the arrangement of a neuron's axonal inputs.

METHODS

The methods presented here have been discussed in depth in previous reports (Cuntz et al., 2007, 2008, 2010, 2011) and the corresponding code is available at www.treestoolbox.org.

EXTENSION TO THE MST ALGORITHM

The original MST algorithm was implemented as an iterative process which connects unconnected target points one at a time to an existing tree structure following the wiring costs mentioned in the text (**Figure 1A**; see Cuntz et al., 2007). The algorithm was adapted to allow labeling of groups of target points. When a target point is connected to the tree, the remaining target points in the same group become unavailable for the algorithm in the further process. Target input axons were then implemented as labeled groups of target points distributed in close intervals along the trajectory of the respective axons. This was tested in **Figures 2B–D** on simple parallel axon trajectories including a slight spatial jitter in **Figure 2C** (50 axons) and 2D (100 axons). The resulting MST dendrite grown to connect a set of parallel axons was flat in all cases (**Figure 2D**).

GRANULE CELL MORPHOLOGICAL MODEL

For the dentate gyrus granule cell model in **Figures 2E,F**, the set of axons was generated by randomly selecting X and Y coordinates and a random angle for each axon within a 1.5-mm × 1.5-mm plane and drawing straight lines with these coordinates. Three hundred axons were generated in this way and a random Z-value between 0 and 250 µm was associated to each axon. The starting point for the dendrite was located 25 µm below the axonal layer and in the center of the XY plane. Only axons passing in 125 µm of the center of the axonal layer were selected resulting on average in a set of around 60 axons. Target points were distributed every 50 µm along the axons. The resulting synthetic granule cells had an average of 20 branch points.

PYRAMIDAL CELL MORPHOLOGICAL MODEL

For the pyramidal cell basal dendrite in **Figure 2G**, the procedure for **Figures 2E,F** was reproduced after moving the starting point to the center of the axonal layer. For the complete pyramidal cell model in **Figure 2H–J**, two layers similar to the granule cell axonal layer from **Figures 2E,F** were generated with 200 axons each. Around 30–40 axons were selected by the same 125 µm sharp cutoff criterion. The starting point for the dendrite was located in the center of the lower axonal layer.

ACKNOWLEDGMENTS

I am grateful to Alexander Borst, Alexandre Mathy, and Arnd Roth for their helpful discussions and comments on the manuscript.

REFERENCES

Branco, T., Clark, B. A., and Häusser, M. (2010). Dendritic discrimination of temporal input sequences in cortical neurons. *Science* 329, 1671–1675.

Budd, J. M. L., Kovács, K., Ferecskó, A. S., Buzás, P., Eysel, U. T., and Kisvárday, Z. F. (2010). Neocortical axon arbors trade-off material and conduction delay conservation. *PLoS Comput. Biol.* 6, e1000711. doi:10.1371/journal.pcbi.1000711

Chklovskii, D. B. (2004). Synaptic connectivity and neuronal morphology: two sides of the same coin. *Neuron* 43, 609–617.

Chklovskii, D. B., Mel, B. W., and Svoboda, K. (2004). Cortical rewiring and information storage. *Nature* 431, 782–788.

Cuntz, H., Borst, A., and Segev, I. (2007). Optimization principles of dendritic structure. *Theor. Biol. Med. Model.* 4, 21.

Cuntz, H., Forstner, F., Borst, A., and Häusser, M. (2010). One rule to grow them all: a general theory of neuronal branching and its practical application. *PLoS Comput. Biol.* 6, e1000877. doi: 10.1371/journal.pcbi.1000877

Cuntz, H., Forstner, F., Borst, A., and Häusser, M. (2011). The TREES toolbox probing the basis of axonal and dendritic branching. *Neuroinformatics* 9, 91–96.

Cuntz, H., Forstner, F., Haag, J., and Borst, A. (2008). The morphological identity of insect dendrites. *PLoS Comput. Biol.* 4, e1000251. doi:10.1371/journal.pcbi.1000251

DeFelipe, J., Elston, G. N., Fujita, I., Fuster, J., Harrison, K. H., Hof, P. R., Kawaguchi, Y., Martin, K. A., Rockland, K. S., Thomson, A. M., Wang, S. S., White, E. L., and Yuste, R. (2002). Neocortical circuits: evolutionary aspects and specificity versus non-specificity of synaptic connections. Remarks, main conclusions and general comments and discussion. *J. Neurocytol.* 31, 387–416.

Douglas, R. J., and Martin, K. A. C. (2004). Neuronal circuits of the neocortex. *Annu. Rev. Neurosci.* 27, 419–451.

Elston, G. N. (2003). Cortex, cognition and the cell: new insights into the pyramidal neuron and prefrontal function. *Cereb. Cortex* 13, 1124–1138.

Fares, T., and Stepanyants, A. (2009). Cooperative synapse formation in the neocortex. *Proc. Natl. Acad. Sci. U.S.A.* 106, 16463–16468.

Horton, J. C., and Adams, D. L. (2005). The cortical column: a structure without a function. *Philos. Trans. R. Soc. Lond. B Biol. Sci.* 360, 837–862.

Hubel, D. H., and Wiesel, T. N. (1962). Receptive fields, binocular interaction and functional architecture in the cat's visual cortex. *J. Pysiol.* 160, 106–154.

Kalisman, N., Silberberg, G., and Markram, H. (2005). The neocortical microcircuit as a tabula rasa. *Proc. Natl. Acad. Sci. U.S.A.* 102, 880–885.

Koene, R. A., Tijms, B., vanHees, P., Postma, F., deRidder, A., Ramakers, G. J. A., van Pelt, J., and van Ooyen, A. (2009). NETMORPH: a framework for the stochastic generation of large scale neuronal networks with realistic neuron morphologies. *Neuroinformatics* 7, 195–210.

Kubota, Y., Karube, F., Nomura, M., Gulledge, A. T., Mochizuki, A., Schertel, A., and Kawaguchi, Y. (2011). Conserved properties of dendritic trees in four cortical interneuron subtypes. *Sci. Rep.* 1, 89.

Lübke, J., and Feldmeyer, D. (2007). Excitatory signal flow and connectivity in a cortical column: focus on barrel cortex. *Brain Struct. Funct.* 212, 3–17.

Lübke, J., Roth, A., Feldmeyer, D., and Sakmann, B. (2003). Morphometric analysis of the columnar innervation domain of neurons connecting layer 4 and layer 2/3 of juvenile rat barrel cortex. *Cereb. Cortex* 13, 1051–1063.

Malach, R. (1994). Cortical columns as devices for maximizing neuronal diversity. *Trends Neurosci.* 17, 101–104.

Mountcastle, V. B. (1957). Modality and topographic properties of single neurons of cat's somatic sensory cortex. *J. Neurophysiol.* 20, 408–434.

Polsky, A., Mel, B. W., and Schiller, J. (2004). Computational subunits in thin dendrites of pyramidal cells. *Nat. Neurosci.* 7, 621–627.

Prinz, A. A., Billimoria, C. P., and Marder, E. (2003). Alternative to hand-tuning conductance-based models: construction and analysis of databases of model neurons. *J. Neurophysiol.* 90, 3998–4015.

Ramón y Cajal, S. (1909). *Histologie du système nerveux de l'homme et des vertébrés.* Paris: Maloine. [Quote: from engl. translation by Swanson N. and Swanson L. W. (1995). Histology of the nervous system of man and vertebrates. Oxford University Press. Vol. 1, Chap. 5, p. 116].

Rihn, L. L., and Claiborne, B. J. (1990). Dendritic growth and regression in rat dentate granule cells during late postnatal development. *Brain Res. Dev. Brain Res.* 54, 115–124.

Shepherd, G. M. G., Stepanyants, A., Bureau, I., Chklovskii, D. B., and Svoboda, K. (2005). Geometric and functional organization of cortical circuits. *Nat. Neurosci.* 8, 782–790.

Sjöström, P. J., and Häusser, M. (2006). A cooperative switch determines the sign of synaptic plasticity in distal dendrites of neocortical pyramidal neurons. *Neuron* 51, 227–238.

Snider, J., Pillai, A., and Stevens, C. F. (2010). A universal property of axonal and dendritic arbors. *Neuron* 66, 45–56.

Song, S., Sjöström, P. J., Reigl, M., Nelson, S., and Chklovskii, D. B. (2005). Highly nonrandom features of synaptic connectivity in local cortical circuits. *PLoS Biol.* 3, e68. doi:10.1371/journal.pbio.0030068

Stepanyants, A., and Chklovskii, D. B. (2005). Neurogeometry and potential synaptic connectivity. *Trends Neurosci.* 28, 387–394.

Stepanyants, A., Hof, P. R., and Chklovskii, D. B. (2002). Geometry and structural plasticity of synaptic connectivity. *Neuron* 34, 175–288.

Stepanyants, A., Tamás, G., and Chklovskii, D. B. (2004). Class-specific features of neuronal wiring. *Neuron* 43, 251–259.

Szentágothai, J. (1975). The "module-concept" in cerebral cortex architecture. *Brain Res.* 95, 475–496.

Teeter, C. M., and Stevens, C. F. (2011). A general principle of neural arbor branch density. *Curr. Biol.* 21, 2105–2108.

van Pelt, J., Carnell, A., de Ridder, S., Mansvelder, H. D., and van Ooyen, A. (2010). An algorithm for finding candidate synaptic sites in computer generated networks of neurons with realistic morphologies. *Front. Comput. Neurosci.* 4:148. doi:10.3389/fncom.2010.00148

Vetter, P., Roth, A., and Häusser, M. (2001). Propagation of action potentials in dendrites depends on dendritic morphology. *J. Neurophysiol.* 85, 926–937.

Wang, Y., Gupta, A., Toledo-Rodriguez, M., Wu, C. Z., and Markram, H. (2002). Anatomical, physiological, molecular and circuit properties of nest basket cells in the developing somatosensory cortex. *Cereb. Cortex* 12, 395–410.

Wen, Q., and Chklovskii, D. B. (2008). A cost-benefit analysis of neuronal morphology. *J. Neurophysiol.* 99, 2620–2328.

Wen, Q., Stepanyants, A., Elston, G. N., Grosberg, A. Y., and Chklovskii, D. B. (2009). Maximization of the connectivity repertoire as a statistical principle governing the shapes of dendritic arbors. *Proc. Natl. Acad. Sci. U.S.A.* 106, 12536–12441.

Conflict of Interest Statement: The author declares that the research was conducted in the absence of any commercial or financial relationships that could be construed as a potential conflict of interest.

Received: 29 September 2011; accepted: 11 January 2012; published online: 01 February 2012.

Citation: Cuntz H (2012) The dendritic density field of a cortical pyramidal cell. Front. Neuroanat. ***6****:2. doi: 10.3389/fnana.2012.00002*

frontiers in
NEUROANATOMY

REVIEW ARTICLE
published: 11 July 2012
doi: 10.3389/fnana.2012.00024

Excitatory neuronal connectivity in the barrel cortex

Dirk Feldmeyer[1,2]*

[1] Institute of Neuroscience and Medicine, INM-2, Research Centre Jülich, Jülich, Germany
[2] Department of Psychiatry, Psychotherapy, and Psychosomatics, RWTH Aachen University, and Jülich-Aachen Research Alliance-Brain, Translational Brain Medicine, Aachen, Germany

Edited by:
Julian Budd, University of Sussex, UK

Reviewed by:
Idan Segev, The Hebrew University of Jerusalem, Israel
Heiko J. Luhmann, Institut für Physiologie und Pathophysiologie, Germany
Randy M. Bruno, Columbia University, USA

***Correspondence:**
Dirk Feldmeyer, Institute of Neuroscience and Medicine (INM-2), Research Centre Jülich, D-52425 Jülich, Germany.
e-mail: d.feldmeyer@fz-juelich.de

Neocortical areas are believed to be organized into vertical modules, the cortical columns, and the horizontal layers 1–6. In the somatosensory barrel cortex these columns are defined by the readily discernible barrel structure in layer 4. Information processing in the neocortex occurs along vertical and horizontal axes, thereby linking individual barrel-related columns via axons running through the different cortical layers of the barrel cortex. Long-range signaling occurs within the neocortical layers but also through axons projecting through the white matter to other neocortical areas and subcortical brain regions. Because of the ease of identification of barrel-related columns, the rodent barrel cortex has become a prototypical system to study the interactions between different neuronal connections within a sensory cortical area and between this area and other cortical as well subcortical regions. Such interactions will be discussed specifically for the feed-forward and feedback loops between the somatosensory and the somatomotor cortices as well as the different thalamic nuclei. In addition, recent advances concerning the morphological characteristics of excitatory neurons and their impact on the synaptic connectivity patterns and signaling properties of neuronal microcircuits in the whisker-related somatosensory cortex will be reviewed. In this context, their relationship between the structural properties of barrel-related columns and their function as a module in vertical synaptic signaling in the whisker-related cortical areas will be discussed.

Keywords: barrel cortex, cortical column, excitatory connections, long-range collaterals, pyramidal cell, somatosensory cortex, spiny stellate cell

INTRODUCTION

In the 1950s, Vernon Mountcastle (Mountcastle, 1957, 1997, 2003) introduced the expression "cortical column" for the concept of vertical information processing in the somatosensory cortex, an idea that was later adopted by David Hubel and Torsten Wiesel (Hubel and Wiesel, 1959, 1963) for the visual cortex. However, in recent years the existence of such vertical modules of cortical signal processing has become a matter of scientific debate. Some reviews and/or commentaries have proposed that the "cortical column" is "a structure without function" (Horton and Adams, 2005) and obituaries for cortical columns have also been written (da Costa and Martin, 2010; but see Rockland, 2010).

The ground-breaking work by Woolsey and Van der Loos (Woolsey and Van der Loos, 1970) showed that the vibrissae on the rodents' snout are topographically represented in the contralateral somatosensory cortex by distinct cytoarchitectonic units in layer 4. These cytoarchitectonic units have therefore been coined "barrels" to describe their structure and the cortical region in which they are located as "barrel field." Already in 1922, Lorente de Nó (Lorente de Nó, 1922; for a translation see Lorente de Nó, 1992) showed such barrel-like structures (see Figures 5–8 in Lorente de Nó, 1922, 1992) which he assumed were located in the acoustic cortex.

Here, aggregations of somata of small spiny neurons exist that surround a "hollow" center. In the mouse and many other rodents "hollows" are clearly visible for every barrel (Woolsey et al., 1975a) while in the rat such hollows are only discernible in the anterolateral, large barrels (Welker and Woolsey, 1974; Land and Erickson, 2005). The cell density in the barrel hollows is lower than in the barrel borders; barrel hollows contain a large fraction of the thalamocortical and intracortical axons, dendrites, the somata of some L4 neurons and possibly also glia (see e.g., Woolsey et al., 1975a; Lübke et al., 2000). Barrels are separated by narrow septa (Woolsey and Van der Loos, 1970; Welker and Woolsey, 1974) which are narrower in mice than in rats (Woolsey et al., 1975b). Distinct cortical microcircuits have been proposed for barrel- and septum-related excitatory neurons (see e.g., Alloway, 2008). However, since the intracortical microcircuits of septum-related spiny neurons are not known they will not be discussed in detail in this review.

Barrel- and septum-related cortical columns (from layer 1–6) are defined by the barrel and septum borders in layer 4, in the framework of which the synaptic connectivity will be discussed here. For the different cortical layers the following definitions will be used: Layer 1 (L1), layer 2/3 (L2/3) with a distinction between layer 2 (L2) and 3 (L3), layer 4 (L4), layer 5 (L5) with its sublaminae 5A (L5A) and 5B (L5A) and layer 6 (L6) with the sublaminae

6A (L6A) and 6B (L6B). This terminology has been introduced by Lorente de Nó (Lorente de Nó, 1922) for the mouse and adopted by Valverde (Valverde et al., 1989) for the rat and has been used in many other publications. I will also use this nomenclature for the discussion of synaptic connectivity patterns in the somatosensory barrel cortex.

It should be noted, however, that the boundaries of the different layers are often not very sharp and dependent on the type of staining and observation method used. Several different characteristics can be used in combination to define the cortical lamination. The density and distribution of excitatory neurons are clearly one of them and have been used already in early publications on the organization of the neocortex (Ramón y Cajal, 1904; Lorente de Nó, 1922). However, the changes in cell density between the cortical layers are generally gradual, particular those between layer 5 and 5B as well as 6A and 6B (for the barrel cortex see Meyer et al., 2010b). Nevertheless, some layers are readily identifiable such a cortical layers 1 and 4 because of their low and high cell density, respectively; this feature is even visible in unstained neocortical slices (e.g., Marx et al., 2012). At some layer borders neuronal cell types change abruptly, for example at the border between layer 4 and 5A: while layer 4 contains only spiny stellate cells and star pyramids, exclusively slender-tufted pyramidal cells are found immediately below the layer border (e.g., Lübke et al., 2000).

Another feature that helps to delineate cortical layers in the barrel cortex is the projection pattern of the afferents from the ventroposterior medial (VPM) and the posteromedial (POm) thalamic nuclei, which have distinct and generally no-overlapping target regions (for a qualitative analysis in the barrel cortex see Meyer et al., 2010a; for a review see Ahissar and Staiger, 2010). In addition, the distribution of cortical interneurons differs also markedly between layer (see below) and can help to define cortical lamination.

According to a very recent study on rat barrel cortex, about 88–89% of the 19,000 neurons in a barrel-related column are excitatory neurons while only 11–12% are GABAergic interneuron; thus there are about 2200 interneurons per barrel column. The relative fraction of interneurons differed between cortical layers and sublaminae but was for all layers significantly lower than previously estimated (Meyer et al., 2010b, 2011). The highest fraction of interneurons was found in layers 2 and 5A. In mouse barrel cortex, the total number of neurons in a barrel-related column is only about a third of the value observed for the rat (∼6500 neurons) of which 11% are inhibitory interneuron (Lefort et al., 2009), a fraction similar to that found for the rat.

Somatotopic representations of peripheral sensory receptors analogous to those in the rodent barrel cortex have also been identified for other animals. A very prominent example is the star-nosed mole [(Catania et al., 1993; Catania and Kaas, 1995) see also (Fox, 2008) for a comprehensive overview] in which the arrangement of the somatosensory receptors on the animal's nose are reflected in their neocortical representation. However, rodents are much more readily available as experimental animals. For this reason, the barrel cortex has become a model system to study the structural and functional characteristics of cortical neuronal microcircuits. Because of their almost cylindrical arrangement, layer 4 barrel columns are now considered to be "prototypical" cortical columns. Here, I will discuss how the intracortical, thalamocortical, and corticothalamic connectivity patterns in barrel-related cortical columns govern and modulate neuronal signaling.

VERTICAL ORGANIZATION OF THALAMOCORTICAL PROJECTIONS IN THE BARREL CORTEX

Sensory signals from the whiskers on the rodent's snout reach the somatosensory "barrel" cortex *via* several distinct pathways (**Table 1**). Neurons of the trigeminal ganglion innervate whisker follicles in the skin of the rodent's snout and project to four different trigeminal nuclei in the brainstem. In the brainstem trigeminal complex, rod-shaped cytoarchitectonic units termed "barrelettes" have been identified that show a somatotopic arrangement reflecting that of the whiskers on the animal's snout (Ma, 1991). All barrel-related trigeminal nuclei receive input from the whiskers *via* the trigeminal nerve. Evidence accumulated over the past 15 years has demonstrated that at least three distinct axonal pathways project to different regions of the somatosensory thalamic nuclei and from there to the primary and secondary somatosensory (S1 and S2) barrel cortex (Jensen and Killackey, 1987; Deschênes et al., 1996; Pinault and Deschênes, 1998; Pierret et al., 2000; Veinante et al., 2000a; Arnold et al., 2001; Furuta et al., 2009; Wimmer et al., 2010; Oberlaender et al., 2011b; for reviews see Deschênes et al., 1998; Alloway, 2008; Fox, 2008; Deschênes, 2009; Bosman et al., 2011). These pathways have been termed lemniscal, extralemniscal, and paralemniscal pathway and they differ in their brain stem origin, their thalamic relay stations and their neocortical target structures/layers (**Table 1**); a brief description of them is given below (see also **Table 1** and **Figure 2**).

The ***lemniscal pathway*** relays whisker signals through the principal trigeminal nucleus (PrV) and projects from there to the dorsal medial region of VPM nucleus (VPMdm) of the thalamus. Here, the axons from a specific "barrelette" in the trigeminal nucleus contact neurons in the corresponding contralateral thalamic "barreloid," a cytoarchitectonic structure which is a curved, tapering rod with an oblique orientation (Hoogland et al., 1987; Land et al., 1995; Haidarliu and Ahissar, 2001; Varga et al., 2002). The lemniscal pathway can be subdivided into two separate branches depending on the target region in the VPM barreloid (**Table 1**, **Figure 2**). The so-called "lemniscal (1)" branch innervates the core region of the VPM barreloid while the "lemniscal (2)" branch project to its head region. Axons arising from VPM neurons in the barreloid core innervate predominantly layer 4 and 6A of the corresponding S1 barrel column and to a lesser extent also layer 3 and 5B (Bureau et al., 2006; Cruikshank et al., 2010; Oberlaender et al., 2011b) and have single-whisker receptive fields (Ito, 1988; Simons and Carvell, 1989; Armstrong-James and Callahan, 1991; Diamond et al., 1992; Brecht and Sakmann, 2002b). A small fraction of VPM neurons may have larger receptive fields but their exact location in the barreloid was not determined (Minnery et al., 2003). In marked contrast, afferents arising from the head of the VPM barreloid [i.e., those in the lemniscal (2) branch] innervate exclusively neurons located in the L4 "septa" and have multi-whisker

Table 1 | Pathways in the whisker-to-barrel cortex system.

Pathway	Brainstem (trigeminal nuclei)	Thalamus (*contralateral*)	Neocortex (main target regions are italicized and bold)	Response type
Lemniscal (1)	N. principalis	VPMdm core barreloid	S1 Layer 3 *S1 Layer 4 barrels* S1 Layer 5B *S1 Layer 6A*	Single whisker
Lemniscal (2)	N. principalis	VPMdm head barreloid	*S1 Layer 4 septa*	Single whisker Multiple whisker
Extralemniscal	N. interpolaris (caudal)	VPMvl No clear barreloid detectable	S1 Layer 3 dysgranular S1 Layer 4 dysgranular S1 Layer 6A dysgranular *S2 Layer 4* *S2 Layer 6*	Multiple whisker
Paralemniscal	N. interpolaris (rostral)	POm	S1 Layer 1 barrels and septa *S1 Layer 4 septa* *S1 Layer 5A barrels and septa* S2	Multiple whisker

Pathways from the brain stem to the barrel cortex indicating the name of the pathway, the brainstem relay, the thalamic relay station, the target regions in the primary and secondary somatosensory cortices and whether the neuronal response is elicited only by a single or by several (multiple) whiskers.

receptive fields (Urbain and Deschênes, 2007; Furuta et al., 2009).

The majority of the lemniscal thalamic afferents, in particular those arising from the core VPM barreloids, show a clear barrel-column related axonal projection with profuse branching at the level of a single barrel in layer 4 (**Figures 1**, **3A**; Jensen and Killackey, 1987; Chmielowska et al., 1989; Lu and Lin, 1993; Pierret et al., 2000; Arnold et al., 2001; Meyer et al., 2010a,b; Oberlaender et al., 2011b). However, some VPM neurons possess axons that bifurcate in layer 6 or 5 to innervate two or more barrel columns; these may arise from other regions, e.g., the barreloid head (Pierret et al., 2000). This structural feature may contribute to the relatively large subthreshold whisker-related receptive fields (as defined by EPSP recordings) in layer 4 that have been observed in *in vivo* studies (Brecht and Sakmann, 2002a). Nevertheless, even these bifurcating thalamocortical axons showed a clear preference for a barrel-related columns (Arnold et al., 2001).

The ***paralemniscal pathway*** originates from neurons located in the rostral (oral) section of the interpolar spinal trigeminal nucleus (SpV; Veinante et al., 2000a); the SpV lies posterior to the PrV. This section shows no "barrelette"-like subdivisons; neurons in this structure show multi-whisker responses (Erzurumlu and Killackey, 1980; Peschanski, 1984; Williams et al., 1994; Veinante and Deschênes, 1999). Their axons terminate in the POm nucleus of the thalamus (Lavallée et al., 2005) that does not show "barreloid"-like cytoarchitectonic units like the VPM nucleus. From there, the thalamic afferents project to both S1 and S2 whisker-related cortex. In S1 cortex, the main target regions of POm afferents are neurons in layer 1, and 5A and the septum-related but not barrel-related layer 4 neurons (**Table 1**, **Figure 2** and Herkenham, 1980; Chmielowska et al., 1989; Lu and Lin, 1993; Bureau et al., 2006; Wimmer et al., 2010; but see Furuta et al., 2009). Axon fibers from neurons in the anterior part of POm target preferentially layer 5A of S1 while those from neurons in the posterior part were predominantly found in layer 1 (Ohno et al., 2011). The fact that the target regions of the—predominantly lemniscal—VPM afferents and the paralemniscal POm afferents show a largely complementary distribution (**Table 1** and **Figures 1**, **2** and Koralek et al., 1988; Alloway, 2008; Wimmer et al., 2010) has lead to the hypothesis that there are distinct streams of whisker information processing in rodent barrel cortex. In the cortex itself, these streams are represented by barrel and septal circuits, which are involved in sensory analysis (both barrel and septal circuits) and the modulation of whisking behavior (septal circuits only; for details see Alloway et al., 2004; Alloway, 2008; Chakrabarti and Alloway, 2009). However, these two circuits may not be entirely separate. Septal L4 neurons receive also input from the lemniscal (2) pathway (**Table 1**; see Furuta et al., 2009); neurons in this region are therefore in a position to integrate the lemniscal and paralemniscal streams to the neocortex at a very early stage. Septal neurons are therefore not simply elements of an intracortical "paralemniscal" pathway as previously suggested (Bureau et al., 2006).

Like the paralemniscal pathway, the ***extralemniscal pathway*** also relays signals through the caudal region of the interpolar SpV which shows a "barrelette"-like organization—in contrast to the oral part of the interpolar SpV which is a relay station in the paralemniscal pathway. It reaches the somatosensory cortex through the ventral-lateral region of the VPM (VPMvl), the tail region of the barreloids. In contrast to VPMdm, the VPMvl region of the somatosensory thalamus shows no clear subdivision into barreloids or similar neuron clusters. Extralemniscal afferents target to a moderate degree the dysgranular regions of layers 3, 4, and 6 of S1 barrel cortex and densely neurons in layers 4 and 6 of S2 cortex (**Table 1** and Pierret et al., 2000; Bokor et al., 2008).

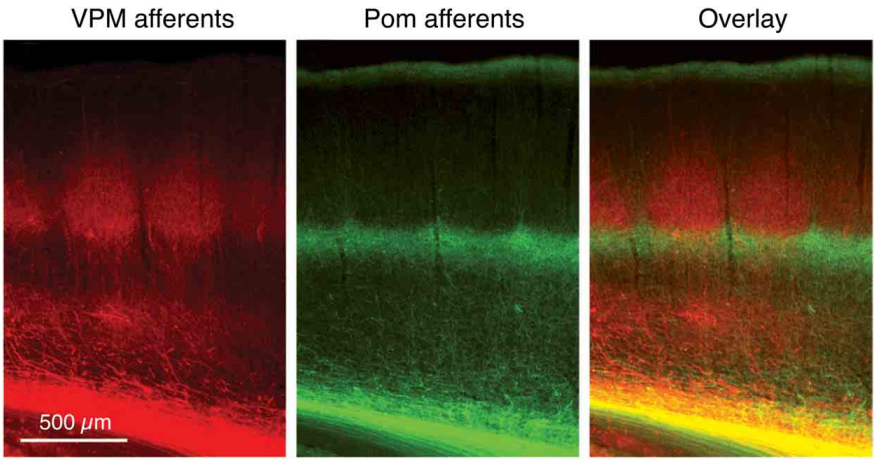

FIGURE 1 | Dual labeling of axons projecting from the VPM and POm axons. Labeling of VPM and POm axons in the same animal by adeno-associated virus-mediated expression of different fluorescent proteins. **VPM afferents** (red) in a thalamocortical barrel cortex slice. **POm afferents** (green). **Overlay** of VPM and POm labeled thalamocortical axons illustrating afferent sparse zones of low fluorescence (i.e., low thalamocortical innervation). There is potential overlay of VPM and POm afferents in the deeper portion of barrels (yellow). Modified from Wimmer et al. (2010), with permission of the Society for Neuroscience.

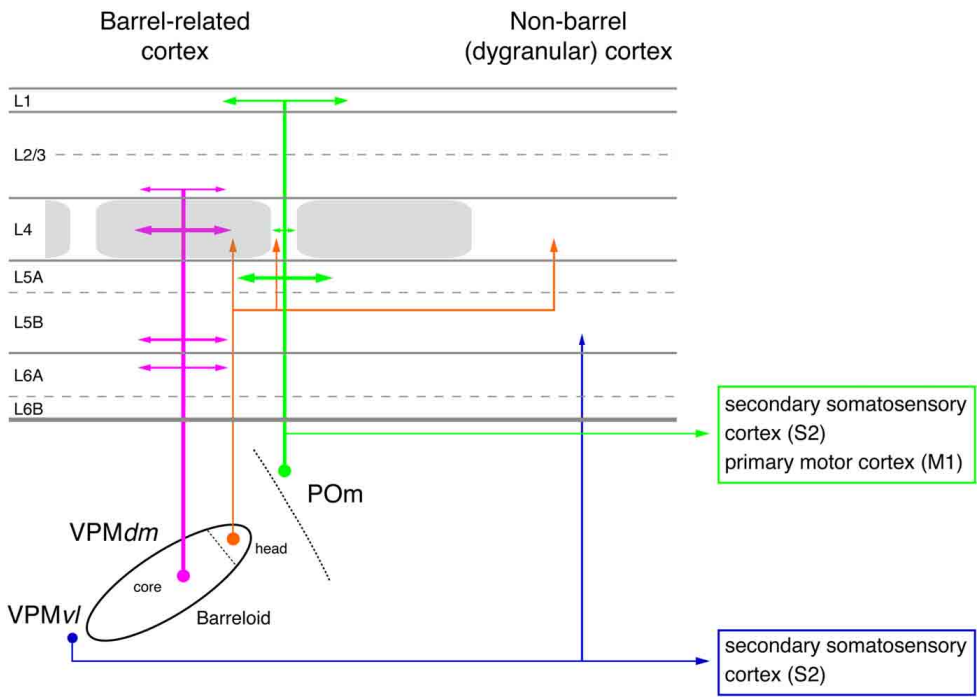

FIGURE 2 | Pathways from thalamus to the primary somatosensory cortex (S1). The figure shows the section of the four different whisker-related pathways from the thalamus to the primary somatosensory cortex. The thalamus is represented by a single barreloid in VPM; the border between POm and VPM by a dashed line. The input stations in the brainstem nuclei have been omitted in this diagram. Magenta: lemniscal (1) pathway; orange: lemniscal (2) pathway; green: paralemniscal pathway; blue: extralemniscal pathway. The term "dysgranular cortex" in S1 defines the region in and around the barrel field in which layer 4 shows no clear barrel structure. Abbreviations: VPMvl, ventrolateral portion of a barreloid in the ventroposterior medial nucleus of the thalamus; VPMdm, dorsomedial portion of a barreloid in the VPM.

Nevertheless, even here a distinct vertical projection pattern can be observed. It has been suggested that the distinct whisker-to-barrel cortex pathways are associated with specific sensory modalities (Yu et al., 2006). The lemniscal pathway has been associated with a combined whisking-touch signal while the extralemniscal pathway is hypothesized to mediate only the contact signal and the paralemniscal pathway only the sensor motion (whisking) signal.

CORTICAL SIGNAL PROCESSING IN THE BARREL-RELATED COLUMN

During the past 10–15 years significant advances in the study of signal processing in a barrel-related cortical column have been made using anterograde or retrograde axonal labeling, paired electrophysiological recording, and connectivity mapping experiments using either caged glutamate release or—more recently—light activation of neurons that are selectively manipulated to selectively express the light-sensitve bacterial ion channel "channelrhodopsin 2" (ChR2; Petreanu et al., 2007; Zhang et al., 2007; Scanziani and Häusser, 2009).

INPUT TO THE NEOCORTEX

Virtually all cortical layers of the whisker-related S1 cortex receive thalamic input from either the VPM or POm neurons as mentioned above. This input shows a clear vertical organization (**Figures 1**, **2A**). The highest density of thalamocortical axon collaterals can be found in cortical layer 4 (Bernardo and Woolsey, 1987; Jensen and Killackey, 1987; Chmielowska et al., 1989; Senft and Woolsey, 1991; Pierret et al., 2000; Wimmer et al., 2010; Oberlaender et al., 2011b) which can therefore be regarded as the major input layer of the barrel and also of other sensory cortices. As can be seen in **Figure 3A**, the lemniscal VPM afferents show many bifurcations at the level of a single barrel in layer 4; in addition, lower layer 3 and layers 5B and 6 are also innervated by axons from the VPM neurons; neurons in layer 2 receive only sparse innervation by thalamic axons, while those in layer 6B receive almost none (Meyer et al., 2010a; Oberlaender et al., 2011b). In layer 4 as well as other cortical layers the lemniscal afferents target both excitatory neurons and inhibitory interneurons (Hersch and White, 1981; White et al., 1984; Porter et al., 2001; Beierlein et al., 2003). The majority of VPM afferents form synaptic connection with excitatory neurons because these outnumber L4 interneurons by far. However, they show also a strong convergence onto L4 interneurons (Bruno and Simons, 2002; Cruikshank et al., 2007). Thus, layer 4 is the major and dominant input layer in a barrel-related column in which the bouton density of VPM axons is higher than in any other cortical layers; most of theset boutons form synapses with L4 spiny stellate cells and star pyramidal neurons (Bruno and Sakmann, 2006; Oberlaender et al., 2011b). It should be noted, however, that synaptic contacts established by the thalamocortical afferents are only about 10–20% of the total number of synaptic contacts in layer 4 (White and Rock, 1979; Benshalom and White, 1986) and are therefore considerably outnumbered by intracortical synaptic connections. *In vivo* during anaesthesia, the monosynaptic thalamocortical (VPM-L4) EPSP is about 1 mV in amplitude; during mild sedation this amplitude drops even further, suggesting a relatively low synaptic efficacy. Because synaptic inputs from VPM onto L4 neurons are both relatively frequent and show a high degree of synchronous activity amplification *via* intralaminar L4 synaptic connections is nevertheless not required to drive the intracortical signal flow (Brumberg et al., 1999; Miller et al., 2001; Bruno and Sakmann, 2006).

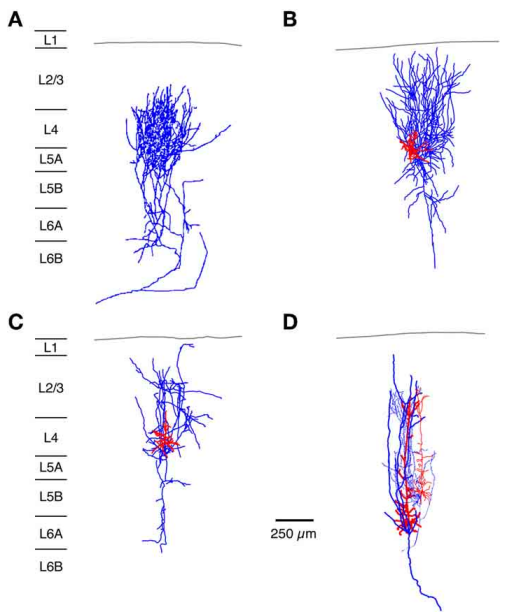

FIGURE 3 | Neuronal elements in the S1 barrel cortex with a predominantly vertical axonal organization. The figure shows four types of axonal projections (blue) with a predominantly vertical axonal projection that is largely confined to a barrel column in the whisker-related S1 cortex. **(A)** Most thalamic afferents from VPM nucleus of the thalamus arborize extensively in layer 4 in a barrel-restricted fashion, **(B)** L4 spiny stellate cell, **(C)** L4 star pyramidal cell, **(D)** corticothalamically projecting L6A pyramidal cell. The dendritic domain of intracortical neurons is given in red. (Modified from Oberlaender et al. (2011b) **(A)**, from Feldmeyer et al. (1999) **(B,C)**, from Zhang and Deschênes **(D)** with permission of John Wiley and sons on behalf of The Physiological Society, the Society for Neuroscience and Oxford Journals).

It has been proposed that barrels in layer 4 can be functionally classified into "mini"-columns containing neurons that are preferentially activated by whisker deflections at a specific angle. Such "angular tuning" domains are formed by convergent synaptic inputs from thalamocortical neurons with corresponding angular preferences. Processing within such domains may depend on local connectivity among vertically aligned barrel neurons (Bruno et al., 2003; Andermann and Moore, 2006; Furuta et al., 2011) which have been reported to be organized in clusters (Feldmeyer et al., 1999; Lübke et al., 2000). In addition, cytoarchitectonic subbarrel domains have been identified in large but not small barrels in mouse S1 cortex that are enriched in thalamocortical axon terminals (Land and Erickson, 2005). It is tempting to speculate that sub-barrels are the morphological correlates of functional "angular tuning" domains. "Angular tuning" domains similar to those observed at the level of layer 4 have also been confirmed for layer 2/3 in rat whisker-related S1 cortex (Andermann and Moore, 2006; Kremer et al., 2011).

INTRACORTICAL EXCITATION

Within a defined cortical area such as the barrel cortex, neuronal connections can be subdivided into three major groups: local, intralaminar connections, translaminar connections, and connections between cortical columns; in addition there are also long-range synaptic connections that link neurons to other cortical areas and subcortical target regions. The barrel cortex is ideal

to investigate the functional and structural properties of such connections because of its clearly visible somatosensory topography, which relates the sensory periphery to the cortical signal processing area (Fox, 2008; Bosman et al., 2011). Because individual synaptic connections have mainly been characterized for the S1 cortex, the review concentrates on this type of connections.

LAYER 4 SERVES TO DISTRIBUTE INTRACORTICAL EXCITATION

The neuronal targets of thalamocortical afferents in layer 4 are spiny stellate cells, star pyramids, and L4 pyramidal neurons (Brecht and Sakmann, 2002a; Staiger et al., 2004; Bruno and Sakmann, 2006). However, the latter type of neurons has not been identified in other studies (Lübke et al., 2000; Egger et al., 2008). Major functional differences have not been reported for excitatory L4 neurons (Feldmeyer et al., 1999; Lübke et al., 2000; but see Cowan and Stricker, 2004; Staiger et al., 2004). The two different types of excitatory L4 neurons may differ in their synaptic connectivity: Star pyramids have been reported to receive weak and sparse synaptic input from other cortical layers in the home column while spiny stellate cells do not (Schubert et al., 2003).

The axonal and dendritic domain of spiny stellate cells and star pyramids show a column-related topology but differ in the fine structure of the dendritic and axonal projections (Lübke et al., 2000; Egger et al., 2008). The dendritic domain of L4 spiny neurons remains largely within a barrel in layer 4 (with the exception of the apical dendrite of star pyramids) while their axonal domain is largely columnar with a very high density of axon collaterals in layers 4 and 2/3 (**Figures 3** and **4A** and Feldmeyer et al., 1999; Lübke et al., 2000; Brecht and Sakmann, 2002a; Lübke et al., 2003; Bruno and Sakmann, 2006; Egger et al., 2008). This columnar topography is developmentally regulated: during early postnatal stages (postnatal day (P) 4 to 10) the axon projects over the borders of the home barrel column while it is largely confined to it by the end of the third to fourth postnatal week (Bender et al., 2003; Radnikow et al., 2010). In another study such a developmental regulation was not observed; however, this study used a much narrower age range (P8–16; Bureau et al., 2004). Other neurons in the neocortex such as the corticothalamically projecting L6A pyramidal cells show a similar columnar organization of their axon (**Figures 3** and **7A**; Zhang and Deschênes, 1997; Kumar and Ohana, 2008).

A small fraction of L4 spiny neuron axons projects into neighboring barrel-related columns where they branch profusely in the neighboring barrel but still obey column borders (Egger et al., 2008). These neurons may serve in interbarrel signaling and could enlarge the subthreshold receptive fields of L4 spiny neurons. Furthermore, some L4 star pyramids exhibit long-range projections over several barrel-columns or rows, both in layer 4 and in infragranular layers (Lübke et al., 2000; Brecht and Sakmann, 2002a; Egger et al., 2008).

In rodent barrel cortex, L4 spiny neurons form cell clusters in which they are highly interconnected. Reported connectivity ratios range from 25 to 36% (about 20–30% of which are reciprocal) and are thus the highest reported for excitatory neocortical synapses (Feldmeyer et al., 1999; Petersen and Sakmann, 2000; Lefort et al., 2009). The presynaptic excitatory L4 neuron forms between two and five synaptic contacts on the dendrites

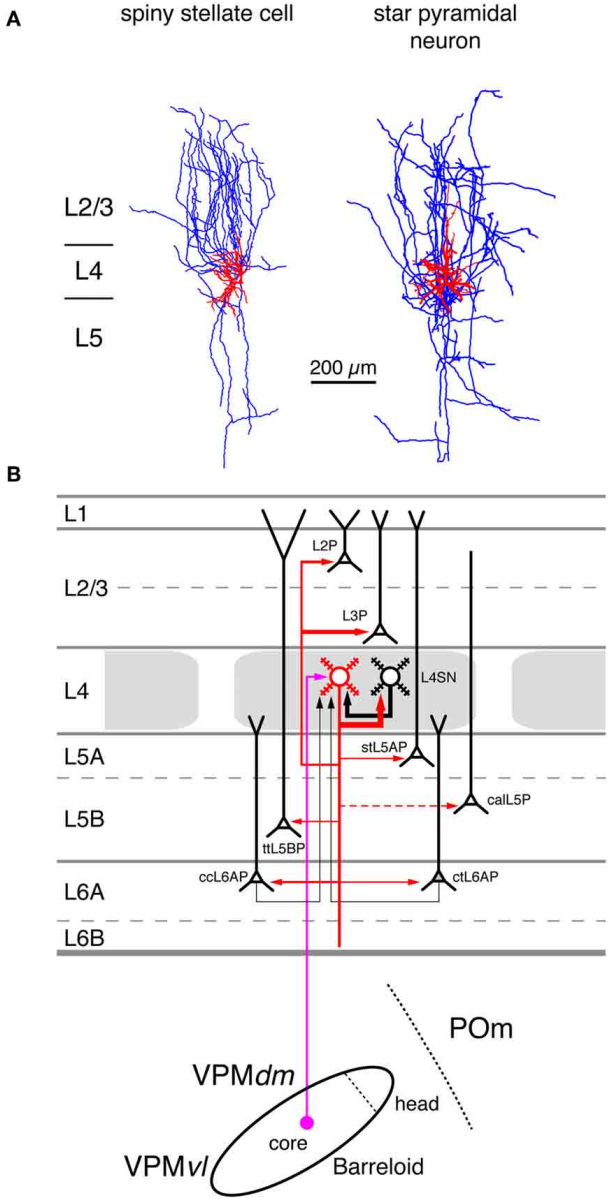

FIGURE 4 | Excitatory synaptic input–output relationship in layer 4 of the S1 barrel cortex. (A) Reconstructions of a L4 spiny stellate cell (left) and a L4 star pyramidal neuron (right) in rat barrel cortex (Feldmeyer et al., 1999). Modified with permission of John Wiley and Sons on behalf of The Physiological Society. **(B)** Diagram of the excitatory synaptic connections of and onto L4 spiny neurons (red neuron with blue axon) in the barrel cortex. Although layer 4 contains both spiny stellate and star pyramidal neurons and a few pyramidal cells only spiny stellate cells are shown for simplicity. Note that L4 spiny neurons provide synaptic output to virtually all layers in a barrel column. For detailed information on the location of synaptic contacts and differences in the connectivity of the three different excitatory L4 neurons see text. The thalamic region is represented by a single barreloid in the VPM nucleus of the thalamus; the VPM/POm border is marked by a dashed line. **Red neuron**; Dendrites and axon of the neuron for which the input–output relationship is described in this figure. Different cortical layers as indicated on the left. The thickness of the red arrows pointing to a postsynaptic (black) neurons indicates the connection probability between this and the black neurons as well as cortical and subcortical areas.

(Continued)

FIGURE 4 | Continued.
The dashed red arrow in layer 5 marks a likely but not yet verified synaptic connection onto a corticocallosal L5 pyramidal cell. It should be noted that **Black neurons**: Dendrites and axon of neurons sending to and receiving synaptic input from to the red neuron. The thickness of the black arrows pointing to the red neuron indicates the connection probability between these neurons and the red neuron. **Light blue arrows**: Excitatory synaptic input from cortical regions outside the S1 barrel cortex. **Magenta arrow**: Synaptic input from the VPM (lemniscal (1) pathway. **Green arrow**: Synaptic input from the POm (paralemniscal pathway). However, for L4 spiny neurons synaptic input from outside thhe barrel cortex originates almost exclusively from the core of the barreloid in the dorsomedial part of the VPM. **Abbreviations**: VPM, ventroposterior medial nucleus of the thalamus; dm, dorsomedial part; vl, ventrolateral part; POm, posterior medial nucleus of the thalamus; L2P, L2 pyramidal cell; L3P, L3 pyramidal cell; L4SN, L4 spiny neuron; stL5P, slender-tufted L5A pyramidal cell; ttL5BP, thick-tufted L5B pyramidal cell; calL5P, corticocallosal L5 pyramidal cell; ccL6AP, corticocortical L6A pyramidal cell; ctL6AP, corticothalamic L6A pyramidal cell.

of the postsynaptic neuron at an average geometric distance of ∼70 μm. Monosynaptic connections between L4 spiny neurons are relatively efficacious (mean unitary EPSP (uEPSP) amplitude: 1.6 mV) and highly reliable, indicative of a high release probability. In a few L4-L4 connections, single uEPSPs were found to be sufficiently large to evoke action potentials (Feldmeyer et al., 1999). The L4-L4 connection is almost the only intracortical synaptic input L4 spiny neurons receive (**Figure 4B**). The connectivity ratios with excitatory neurons in all other layers of S1 barrel cortex are extremely low, often below 1% (Lefort et al., 2009). However, it is likely that a connections between L4 spiny neurons and L6 pyramidal neurons exist as the the strong axonal arborization of the L6 axon suggests (Pichon et al., 2012).

From layer 4 the incoming thalamocortical excitation spreads to other cortical layers, most prominently to layer 2/3 which shows also a high density of L4 spiny neuron axon collaterals (Lübke et al., 2000, 2003). L2/3 pyramidal cells are strongly innervated by L4 spiny neurons in the home barrel-related column; the connectivity ratio ranges between 10 and 15% (Feldmeyer et al., 2002; Silver et al., 2003; Lefort et al., 2009). The presynaptic L4 axons form synaptic contacts mainly with the basal dendritic arbor of the postsynaptic L2/3 pyramidal cell at an average distance of ∼70 μm, i.e., close to the soma. The number of synaptic contacts varies between four and five. Despite their relatively large axonal distance (200–400 μm), synaptic connections between L4 spiny neurons and L2/3 pyramidal cells have a surprisingly high connectivity ratio, are efficacious (uEPSP amplitudes ranging from 0.6 to 1.0 mV) and of a relatively high release probability ($P_r \sim 0.8$; Feldmeyer et al., 2002; Silver et al., 2003; Sarid et al., 2007; Lefort et al., 2009).

In contrast to the intralaminar L4-L4 connection, L4-L2/3 connections are never reciprocal (Feldmeyer et al., 2002) and connections between presynaptic L2/3 pyramidal cells and L4 spiny neurons are extremely rare (Lefort et al., 2009). In studies on rat neocortex using laser scanning photo-release of caged glutamate in brain slices it has been shown that L4 spiny neurons in a cortical barrel are the most dominant input to barrel-related L2/3 pyramidal neurons (located above a barrel in layer 2/3) while this is not the case for septum-related L2/3 pyramids (i.e., those above a septum in layer 4; Shepherd et al., 2005; Shepherd and Svoboda, 2005). For murine barrel cortex, however, the same group has proposed a different connectivity. Barrel-related pyramidal neurons in lower layer 2/3 (often referred to as layer 3) receive strong input from layer 4 while those in upper layer 2/3 (i.e., layer 2) Septum-related L2 and L3 pyramids, are only weakly innervated by barrel- and septum-related L4 neurons (Bureau et al., 2006). This view is not supported by paired recording studies in both mouse and rat barrel cortex which report comparable connectivity ratios between L4 spiny neurons and pyramidal cells in deep and superficial layer 2/3 (Feldmeyer et al., 2002; Lübke et al., 2003; Lefort et al., 2009). Nevertheless, a decrease in the connectivity with increasing axonal path length is likely because of the reduction in axonal density (and hence the probability of forming synaptic contacts; Lübke et al., 2003).

As discussed above, L4 spiny neurons in a cortical barrel target preferentially other L4 spiny neurons and pyramidal neurons in layer 2/3 of the same barrel-related column. However, they have also been demonstrated to innervate L5A, L5B, and L6A pyramidal cells suggesting the existence of a direct, monosynaptic signal transformation from layer 4 to infragranular layers (in addition to the indirect, disynaptic connection from layer 4 via layer 2/3 to layer 5; see below). The connectivity of L4 spiny neurons with L5A and L5B pyramidal cells is also relatively high with a connectivity ratio of about 10%, but of a lower efficacy (mean uEPSP amplitude of ∼0.6 mV) than that of other L4 connections (Schubert et al., 2001, 2006; Feldmeyer et al., 2005; Lefort et al., 2009; Petreanu et al., 2009; Hooks et al., 2011). Synaptic contacts on infragranular neurons are mainly established on the basal dendrites of the L5 pyramidal cells (Markram et al., 1997; Feldmeyer et al., 2005; Petreanu et al., 2009); the distribution of these contacts overlaps to a significant degree with that proposed for thalamocortical synaptic contacts (Petreanu et al., 2009; Meyer et al., 2010a,b; Oberlaender et al., 2011b). In addition to pyramidal cells of layer 5A and 5B, L4 spiny neurons target also pyramidal cells in layer 6, although the observed connectivity ratio was very low (Lefort et al., 2009; Qi and Feldmeyer, 2010; Tanaka et al., 2011). However, synaptic connections between L4 spiny neurons and L6A pyramidal cells exhibit a synaptic target region specificity not found for other L4 connections: L4 spiny stellate cells innervate exclusively the apical tuft of L6A pyramidal cell and show slow EPSPs with rise times exceeding 3 ms. On the other hand, L4 star pyramids target predominantly—but not exclusively—basal and deep apical oblique dendrites of L6A pyramidal cells and give mainly rise to fast EPSPs (Qi and Feldmeyer, 2010).

From the available data it appears that cortical layer 4 acts as a "hub" of intracolumnar information processing because neurons of this layer signal to all other cortical layers in the same barrel-related column with the possible exception of layer 1. Although L4 spiny neurons do not project outside the barrel cortex and are largely confined to a barrel column they are an integral part of many neuronal subnetworks that are involved in both feedforward signaling within the S1 cortex and to S2 and the primary motor (M1) cortices (*via* L2/3 and corticocortically projecting L5 and L6 pyramidal neurons, see below) and feedback signaling to

structures such as the thalamus (*via* corticothalamic L5 and L6 pyramidal neurons, see below).

VERTICAL AND HORIZONTAL SPREAD OF SYNAPTIC SIGNALING IN LAYER 2/3 OF THE BARREL CORTEX

The spread of excitation from the thalamus to layer 4 and from there to layer 2/3 is mostly vertical and largely confined to the barrel-related column (Petersen and Sakmann, 2001; Feldmeyer et al., 2002; Laaris and Keller, 2002; Lübke et al., 2003; Shepherd et al., 2003, 2005; Shepherd and Svoboda, 2005). In addition, L3 pyramidal neurons (**Figure 5A**, right neuron) also receive (Jensen and Killackey, 1987; Arnold et al., 2001; Meyer et al., 2010b; Oberlaender et al., 2011b) intput from the VPM nucleus of the thalamus (**Figure 5C**).

L2 Pyramidal cells (**Figure 5A**, left neuron) have short apical dendrites with relatively large tufts in layer 1 while L3 pyramids have longer apical dendrites with more slender tufts (Lübke et al., 2003; Shepherd and Svoboda, 2005; Feldmeyer et al., 2006; Oberlaender et al., 2011b). It is conceivable that the different types of apical tufts of L2 and L3 pyramids is the structural basis of a differential POm input (*via* layer 1, see **Figure 5B**) to these neurons: large tufts are in a position to form more synaptic contacts because of the number of dendrites in this layer. However, this has not been demonstrated directly.

Most pyramidal neurons in layer 2/3 have axonal domains that exhibit a "butterfly" appearance: a long stem axon that runs down into the white matter and has several long-range collaterals projecting horizontally mainly in layers 2/3 and 5 over the entire barrel field in S1 and into the ipsilateral S2 and M1 cortex while sparing layer 4 almost completely (**Figure 5A**; Feldmeyer et al., 2006; Larsen and Callaway, 2006; Bruno et al., 2009; Aronoff et al., 2010, see also below). Apart from these, a few L3 pyramidal cells have been identified that exhibit some collateralization in layer 4 (Larsen and Callaway, 2006; Bruno et al., 2009) and have a much narrower axonal field in supra- and infragranular cortical layers (and a high axonal density in the barrel column). Both types of neurons were found above barrels. All these functional data suggest an heterogeneity in the neuronal make-up of layer 2/3. How

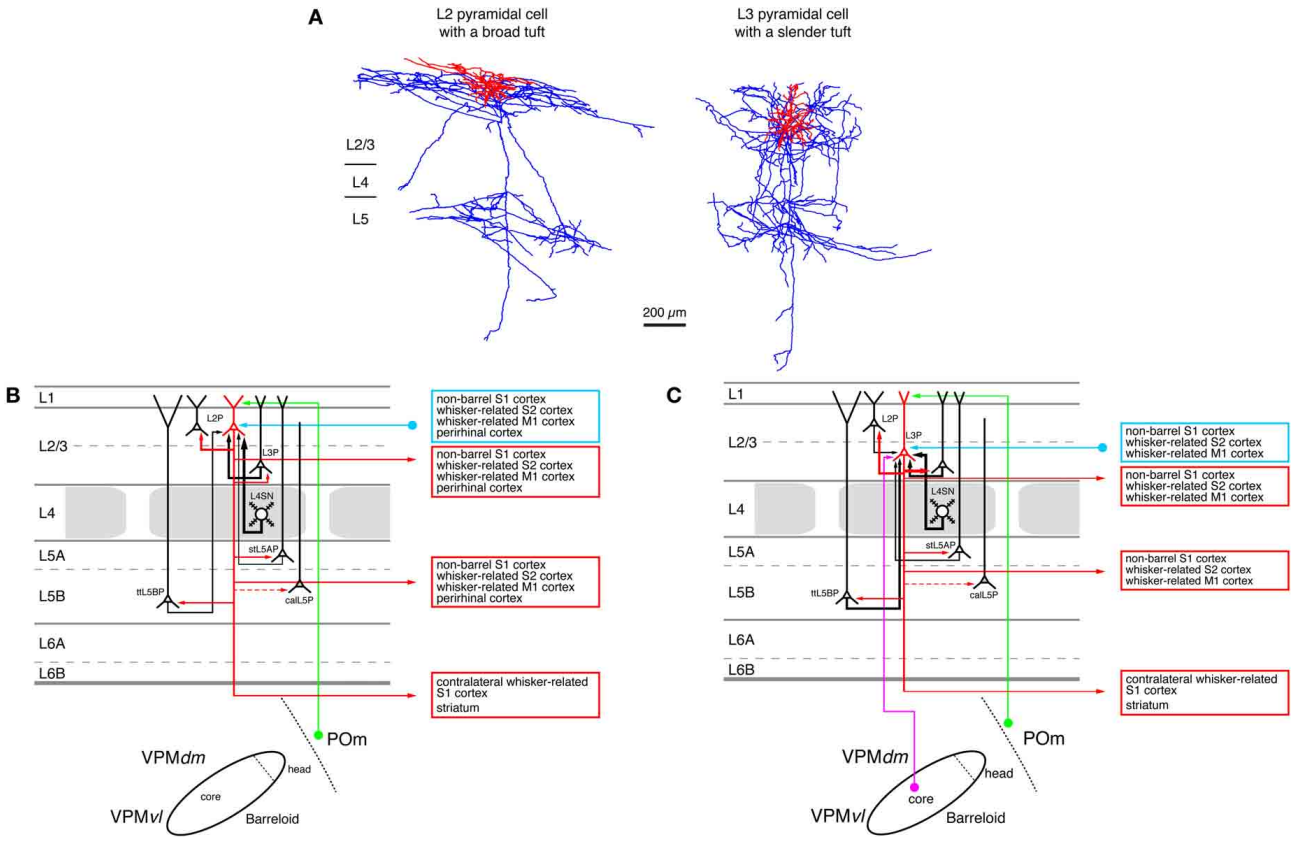

FIGURE 5 | Excitatory synaptic input–output relationship in layer 2/3 of the S1 barrel cortex. (A) Reconstructions of a pyramidal cell located in the upper half of layer 2/3 (L2 pyramidal cell, left) and a pyramidal cell located in the lower half of layer 2/3 (L3 pyramidal cell, left) of rat barrel cortex (Bruno et al., 2009); modified with permission of the Society of Neuroscience. Note that the apical tuft of the L2 pyramidal cell is substantially larger than the basal dendritic tree of that neuron while L3 pyramidal cells have slender apical tufts. Modified with permission from the Society of Neuroscience. **(B)** Diagram of the excitatory synaptic connections of and onto L2 pyramidal cells (red neuron with blue axon) in the barrel cortex. Only synaptic input from neurons and regions relevant for L2 pyramidal cells is shown in this graph. For detailed information on the location of synaptic contacts and possible subtypes of L2 pyramidal cells see text. **(C)** Diagram of the excitatory synaptic connections of and onto L3 pyramidal cells (red neuron with blue axon) in the barrel cortex. Only synaptic input from neurons and regions relevant for L3 pyramidal cells is shown in this graph. For detailed information on the location of synaptic contacts and possible subtypes of L3 pyramidal cells see text. Color coding and abbreviations as in **Figure 4**.

this is related to the functional role of this layer remains to be determined.

Studies using photo-release of caged glutamate to stimulate synaptic connections onto L2/3 pyramidal cells (Shepherd et al., 2005; Shepherd and Svoboda, 2005; Schubert et al., 2006) revealed that these neurons show differential excitation pattern depending on their location in relation to the barrel field. In these studies it was found that both L2 and L3 pyramidal neurons above a barrel are strongly excited by the subjacent L4 neurons (see above) while L2 pyramidal neurons above a septum between barrels are more excited by L5A pyramidal neurons. Septal L3 pyramidal are only weakly excited by L5A neurons although the somatic distance between pre- and post-synaptic neurons is shorter for this connection type. Because L4 neurons are the major target neurons of the lemniscal (1) thalamic afferents and L5A pyramidal cells targets of the paralemniscal afferents, the authors suggested that the L4-L2/3 (barrel) pathway and the L5A-L2 (septal) pathway represent intracortical continuations of the lemniscal and paralemniscal pathways, respectively. These two pathways have been suggested to converge in layer 2 because L2 pyramidal cells receive input from L3 pyramidal cells that are targeted by both L4 barrel neurons and VPM (lemniscal) thalamic axons (**Figures 3B,C**; Shepherd et al., 2005; Shepherd and Svoboda, 2005; Bureau et al., 2006). However, layer 2 is not the only cortical layer where the lemniscal and paralemniscal pathway converge: pyramidal neurons in layer 5A receive anddirect input from POm neurons in the paralemniscal pathway and indirect lemniscal input *via* L4 spiny neurons and L3 pyramidal cells (Feldmeyer et al., 2005; Lefort et al., 2009). In addition, the septa between the barrels in layer 4 are innervated by both lemniscal (2) (Furuta et al., 2009) and paralemniscal afferents (Koralek et al., 1988; Alloway, 2008; Wimmer et al., 2010) and thus constitute a third region in which these pathways converge (see above). Finally, pyramidal neurons in layer 5B receive input from the—largely lemniscal—VPM nucleus of the thalamus (Wimmer et al., 2010; Oberlaender et al., 2011b) but project back to the—paralemniscal—POm were they synapse onto thalamic relay neurons (Hoogland et al., 1987, 1991; Groh et al., 2008). All this data indicates that lemniscal and paralemniscal pathways cross-talk at multiple stations. It is therefore questionable whether separate lemniscal and paralemniscal pathways exist in the neocortex.

When pyramidal cells in layer 2/3 are depolarized above the action potential threshold intracortical signaling spreads *locally* to neighboring L2/3 pyramidal cells (Egger et al., 1999; Holmgren et al., 2003; Feldmeyer et al., 2006; Lefort et al., 2009; Hardingham et al., 2010) and *vertically* to deeper cortical layers (and here mainly to L5A and L5B pyramidal neurons; Reyes and Sakmann, 1999; Lefort et al., 2009; Petreanu et al., 2009; Hardingham et al., 2010; Hooks et al., 2011) but also *horizontally* across several barrel columns both within layer 2/3 and 5 (Adesnik and Scanziani, 2010); L2/3 pyramidal cells are thus in a position to integrate the activity of several columns surrounding their home barrel column.

Local synaptic connections between pairs of L2/3 pyramidal cells have a connectivity rate of 10–20%. Their mean uEPSP amplitude is about 0.4–1.0 mV with a release probability ($P_r \sim 0.7$–0.8), a value comparable to that observed for excitatory L4-L2/3 connections. They establish between two and four synaptic contacts at a mean geometric distance ∼90 μm from the postsynaptic L2/3 pyramidal cell soma; the majority of these synaptic contacts can be found on basal dendrites with a few contacts being formed with proximal apical oblique dendrites (Feldmeyer et al., 2006). Synaptic connectivity ratios are, however, far from fixed: For L2/3 pyramids in S1 barrel cortex it has been shown that sensory deprivation affects the local (i.e., L2/3-L2/3 pyramidal cell) connectivity and connection strength (Cheetham et al., 2007). In the deprived region the connectivity is reduced without concomitant changes in synaptic efficacy while in the spared region connections are strengthened with an otherwise unaltered connectivity. This indicates an experience-dependent regulation of connectivity in the neuronal microcircuitry that serves to expand the representation of the spared, sensory active cortex into the deprived regions. Similar mechanisms may work for other cortical connections.

A substantial fraction of L2/3 pyramidal cell axons descend to *deeper* cortical layers where they arborize extensively, in particular in layer 5A and 5B. Here L2/3 pyramidal neurons establish synaptic contacts predominantly with the basal dendrites of L5A and L5B pyramidal neurons (Reyes and Sakmann, 1999; Schubert et al., 2006; Lefort et al., 2009; Petreanu et al., 2009). One study suggests that L2/3 pyramidal cells are more strongly connected to L5 pyramidal cells when they are located above barrel walls (Dodt et al., 2003). Synaptic connections of L2/3 pyramids onto L5 pyramids are of relatively low efficacy (0.1 mV at postnatal day 28) and display short-term facilitation, indicative of a low release probability (Reyes and Sakmann, 1999). L2/3 pyramidal cells connect with a higher probability to subnetworks of interconnected L5 pyramids while L5 pyramids are more likely to integrate inputs from L2/3 pyramids that are not connected (Kampa et al., 2006). Synaptic signaling from different L2/3 subnetworks thus converges onto specific L5 subnetwork thereby integrating different streams of sensory input.

Besides the vertical signal transformation within the home column of the pyramidal neurons, axons collaterals of L2/3 pyramidal cells expand also substantially *horizontally* in particular within layer 2/3 and 5 to contact surrounding cortical domains ("barrel"-related columns). They are therefore in a position to coordinate synaptic activity in their home column with respect to the neighboring cortical columns in the same cortical hemisphere. Furthermore, L2/3 pyramidal cells are also connected to neurons in the contralateral whisker-related S1 cortex *via* the corpus callosum (White and Czeiger, 1991; Petreanu et al., 2007) and may thus integrate the activity of the two cortical hemispheres. In a separate section below I will describe the structural and functional properties of long-range intracortical connections.

LAYER 5 AS THE MAIN CORTICAL OUTPUT LAYER

Similar to other sensory cortices, layer 5 is the main output layer of the whisker-related S1 cortex. It contains at least two, possibly three main excitatory cell types. These are pyramidal neurons with a slender apical tuft with only few axonal collaterals in layer 1 (**Figure 6A**, left neuron), those with apical dendrites exhibiting thick, elaborate terminal tufts (**Figure 6A**, middle neuron) or

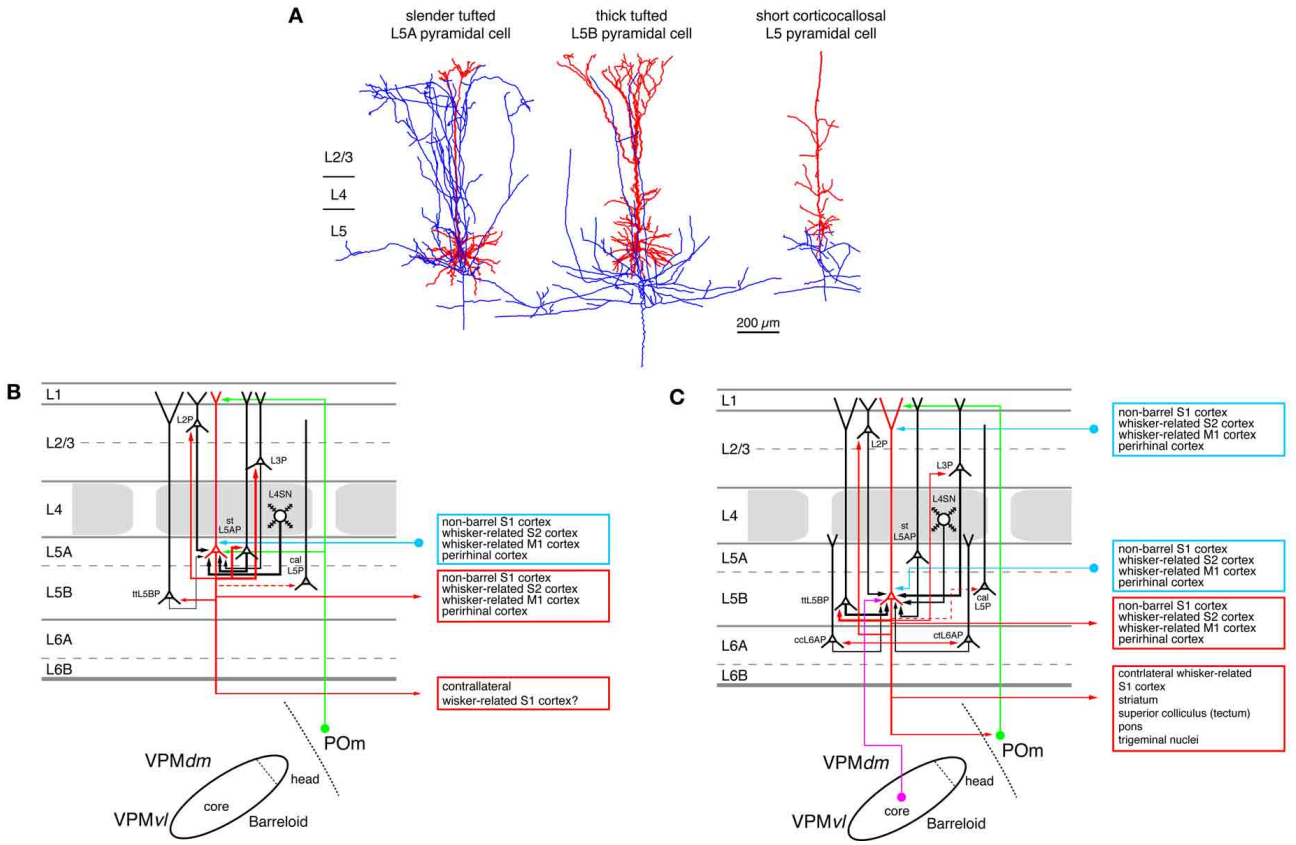

FIGURE 6 | Excitatory synaptic input–output relationship in layer 5 of the S1 barrel cortex. (A) Reconstructions of three types of pyramidal cells in layer 5 of the barrel cortex. Slender-tufted pyramidal cells (left) are predominantly located in sublamina 5A (Feldmeyer et al., 2005) while thick-tufted pyramidal cells (middle) are mostly found in sublamina 5B (Lübke and Feldmeyer, 2007). Corticocallosal L5 pyramidal cells (right) are found throughout layer 5. They are characterized by a very diminutive or even absent apical tuft (Le Bé et al., 2007). Modified with permission of the Society of Neuroscience, Springer and Oxford Journals, respectively. **(B)** Diagram of the excitatory synaptic connections of and onto slender-tufted L5A pyramidal cells (red neuron with blue axon) in the barrel cortex. Only synaptic input from neurons and regions relevant for slender-tufted L5A pyramidal cells is shown in this graph. For detailed information on the location of synaptic contacts and possible subtypes of slender-tufted L5A pyramidal cells see text. **(C)** Diagram of the excitatory synaptic connections of and onto thick-tufted L5B pyramidal cells (red neuron with blue axon) in the barrel cortex. Only synaptic input from neurons and regions relevant for thick-tufted L5B pyramidal cells is shown in this graph. Note that thick-tufted L5B pyramidal cells receive synaptic input from virtually all cortical layers. For detailed information on the location of synaptic contacts and possible subtypes of thick-tufted L5B pyramidal cells see text. Color coding and abbreviations as in **Figure 4**.

those that have only short, virtually untufted apical dendrites (**Figure 6A**, right neuron). The majority of the slender-tufted pyramidal neurons is located in sublayer 5A (Manns et al., 2004; Feldmeyer et al., 2005; Schubert et al., 2006; de Kock et al., 2007; Hooks et al., 2011; Oberlaender et al., 2011b), although some of them are also present in sublayer 5B. In contrast, thick-tufted pyramidal cells are mainly found in sublamina B of layer 5 where also most of the untufted pyramidal cells are found (Larsen and Callaway, 2006). Both slender- and thick-tufted pyramidal cells in layer 5 have been shown to receive synaptic input from the thalamus (Petreanu et al., 2009; Meyer et al., 2010b; Oberlaender et al., 2011b). The slender-tufted L5A neurons receive afferents from the POm nucleus of the thalamus on their basal dendrites and apical tufts (**Figure 6B**). The thick-tufted L5B pyramidal cells receive VPM thalamic afferents also predominantly on the basal dendrites; however, a few synaptic contacts are also formed with the apical oblique and the terminal tuft dendrites (**Figure 6C**). Thus, synaptic inputs from the somatosensory thalamic nuclei to L5 pyramidal neurons largely overlap with their main intracortical synaptic inputs from layers 4 (in the case of the L5A pyramids) and 2/3 (in the case of the L5B pyramids).

Short L5 pyramidal cells have extensive axonal projections predominantly to super-granular layers 2/3, in particular to the deeper portion sof this layer. In layer 5 the axon density is considerably lower (not shown in **Figure 6A** but see Larsen and Callaway, 2006). At least a subset of the short L5 pyramidal cell has axonal projections via the corpus callosum to the contralateral (S1) cortex (Larsen et al., 2007; Le Bé et al., 2007) like the short L5 pyramids in visual and auditory cortex (e.g., Games and Winer, 1988; Hübener and Bolz, 1988; Hübener et al., 1990; Koester and O'Leary, 1992).

Slender-tufted L5A pyramidal cells possess characteristic extensive and dense axons with many ascending collaterals that innervate predominantly the supragranular layers 2/3. Here the axon collaterals cover a wide area of the barrel field and project both within and outside the home barrel column, in fashion reminiscent of short L5 pyramids (Shepherd et al., 2005; Larsen and Callaway, 2006; Hattox and Nelson, 2007; Larsen et al., 2007; Oberlaender et al., 2011a). The infragranular portion of their axon is significantly less elaborate. *In vivo* labeling of these neurons shows that their total intracortical axonal length exceeds that of thick-tufted pyramidal cells in sublamina B of layer 5 by more than a factor of two (Oberlaender et al., 2011a) with a substantial fraction projecting outside the barrel cortex proper. Slender-tufted L5A pyramids project also to ipsilateral cortical areas such as the whisker-related M1 cortex (Mao et al., 2011) and, like the short L5 pyramids, to the contralateral S1 cortex (**Figure 6B**; Larsen et al., 2007).

The majority of the intracortical axonal collaterals of thick-tufted L5B pyramidal cells (∼60%) resides in layer 5; the fraction of supragranular axonal collaterals is markedly lower than that of the slender-tufted or untufted L5 pyramids. Thick-tufted L5 pyramidal cells project to various subcortical target regions such as the thalamic nuclei, the superior colliculus (the tectum), the striatum, and the trigeminal nuclei (**Figure 6C**; Veinante et al., 2000b; Kozloski et al., 2001; Larsen et al., 2007; Brown and Hestrin, 2009b; Mao et al., 2011). Based on these different target regions further subtypes of thick-tufted (L5B) pyramidal neurons have been proposed (e.g., Hattox and Nelson, 2007; Brown and Hestrin, 2009b; for a review see Brown and Hestrin, 2009a). These L5B pyramid subtypes differ in their passive electrical membrane and their action potential firing characteristics as has been shown for mouse S1 cortex (Hattox and Nelson, 2007); they are therefore likely to process incoming synaptic activity differently. Gene and protein expression profiles can be used for further classification of L5 pyramidal neurons. Studies in recent years have revealed a large degree of diversity in these features (Hevner et al., 2003; Molnár and Cheung, 2006; Nelson et al., 2006; Chen et al., 2008; Groh et al., 2010). Different types of L5 pyramidal cells may form distinct, synaptically connected neuronal subnetworks. For example, Brown and Hestrin (Brown and Hestrin, 2009b) were able to demonstrate that in visual cortex the frequency of monosynaptic connections among corticostriatal L5 pyramidal cells is with 18% significantly higher than among corticocortical or corticotectal pyramids (for which the authors report values of 5 and 7%, respectively). Similar differences were also observed for heterologous L5 pyramidal cell pairs, i.e., of which pre- and post-synaptic neuron belonged to different subclasses (Brown and Hestrin, 2009b). A comparable functional and structural differentiation of L5 pyramidal neurons based on the axonal projection targets has also been observed for rat frontal cortex (Morishima and Kawaguchi, 2006; Morishima et al., 2011; Otsuka and Kawaguchi, 2011) and mouse motor cortex (Anderson et al., 2010). Here, it was found that the synaptic connectivity was higher between neurons with the same subcortical target region (homologous neuron types) than between those with different target regions.

The fact that the probability of finding a synaptic connection as well as its functional properties depend on the identity of both the presynaptic and postsynaptic L5 pyramidal cells support the idea that different neuronal subnetworks exist also in the whisker-related S1 cortex. The local, intralaminar connectivity of slender-tufted (L5A) pyramidal neurons is ∼20%, 15% of which are reciprocal connections. Cell bodies and apical dendrites of connected L5A pyramidal cells were located at the border between barrel and septal columns with a clear tendency toward vertical clustering (Frick et al., 2008). Such an organization is consistent with the concept that slender-tufted L5A pyramids belong to a "septal processing" system. This system is recruited by paralemniscal thalamic input from POm and may be involved in the modulation of whisking behavior (Alloway, 2008). Between one and six synaptic contacts are formed between L5A pyramidal cell pairs, mainly on the basal dendrites. These contacts had a low failure rate and an average uEPSP amplitude of 0.3–0.6 mV (Frick et al., 2008; Lefort et al., 2009).

Data from *in vitro* paired recordings demonstrated that L5A pyramidal neurons are more frequently connected to pyramidal neurons in layer 2 and 3 (connectivity ratio 2–4%, respectively; Lefort et al., 2009) than the thick-tufted (L5B) pyramidal neurons (connectivity ratio 1–2%, respectively; Lefort et al., 2009), a finding that is in agreement with the higher axonal density in layer 2/3 found for these neurons (Oberlaender et al., 2011a). This predominant innervation of more superficial L2/3 pyramidal neurons has also been revealed in studies using laser-scanning photo-stimulation by glutamate uncaging or ChR2 activation (Shepherd et al., 2005; Shepherd and Svoboda, 2005; Bureau et al., 2006; Petreanu et al., 2009) although some of these studies note a preferential innervation of L2 pyramidal neurons above the barrel septa.

Figure 6C shows the input output relationship of thick-tufted (L5B) pyramidal neurons Their local connection probability is with 5–20% relatively high (depending on the distance between neuronal cell bodies) with some showing reciprocal connectivity; (Markram et al., 1997; Reyes and Sakmann, 1999; Le Bé et al., 2007; Lefort et al., 2009; Perin et al., 2011). Connections tend to cluster and are thus highly non-random (Song et al., 2005). The L5B-L5B connection probability is lower than that of L5A pyramidal cell pairs but the number of synaptic contacts is larger: between 4 and 8 contacts are established on both basal and apical oblique dendrites at an average geometric distance of 150 μm. In both rat and mouse, L5B-L5B connections are also quite efficacious with reported mean uEPSP amplitudes of 0.7–1.3 mV (Markram et al., 1997; Le Bé et al., 2007; Lefort et al., 2009). While the thick-tufted (L5B) pyramidal cells are to some degree innervated by descending axon collaterals of L5A pyramidal cells, ascending connections from layer 5B to 5A appear to be rare, suggesting a directed signal flow between the two sublaminae (Lefort et al., 2009).

L5A and L5B pyramidal neurons may interact in the following way according to a hypothesis put forward by Oberlaender and coworkers (Oberlaender et al., 2011a): Slender-tufted (L5A) pyramidal neurons have been shown to carry information on the motion and phase of the vibrissae during active whisking but show little if any action potential firing activity after passive touch (Curtis and Kleinfeld, 2009; de Kock and Sakmann, 2009). With their long-range collaterals the slender-tufted (L5A) pyramidal

neurons may integrate the barrel-column activity and phase-lock the membrane potential in the dendrites of L2/3 pyramidal neurons to the whisking cycle through their dense axonal collaterals in this layer. They will also recruit thick-tufted pyramidal neurons but to a significantly lesser degree. In contrast, it has been demonstrated that thick-tufted (L5B) pyramidal cells reliably increase action potential firing after *passive* whisker touch (de Kock et al., 2007), possibly through direct synaptic input *via* the VPM thalamic afferents (Bureau et al., 2006; Yu et al., 2006; Petreanu et al., 2009; Meyer et al., 2010a,b; Oberlaender et al., 2011b). In addition, when the slender-tufter (L5A) pyramidal cells and the VPM afferents are activated almost simultaneously during exploratory (sensory-motor) behavior such as during object location, the thick-tufted (L5B) pyramidal cells may be depolarized at both basal dendrites (*via* the VPM afferents) and the apical dendritic tuft (*via* the extensive axon collaterals of the slender-tufted neurons and possibly also *via* afferents from the POm running through layer 1). This will then result in increased neuronal firing, which is subsequently conveyed to other intracortical but also to other subcortical targets.

A subset of thick-tufted L5B pyramidal neurons—which have already been introduced above—receives thalamic input from the VPM and projects back to the POm nucleus of the thalamus (see also the section on long-range connection below). These connections, which may be the cortical relay of a thalamocorticothalamic feedback loop, have been characterized in more detail: Thalamocortically projecting L5B pyramidal cells form giant large diameter (2–8 μm) presynaptic terminals and establish glutamatergic synapses (containing Ca^{2+}-permeable AMPA and NMDA receptors) with POm relay neurons (Hoogland et al., 1987, 1991; Bourassa et al., 1995; Groh et al., 2008; Liao et al., 2010). However, it has also ben hypothesized that this connection may be an integral element of a sequential, feed-forward signal transfer from VPM via layer 5B in S1 cortex to POm and from there to other S1 laminae and other cortical areas (i.e., a transthalamic signaling process) such as the S2 or the M1 cortex [see.e.g., (Killackey and Sherman, 2003; Guillery and Sherman, 2011)]. However, this point remains still an open question. It is also possible that L5B pyramidal cells are elements in both the feedforward and the feed-back pathways described above.

The L5B-POm synapses have a high release probability ($P_r \sim 0.8$) and are sufficiently strong to elicit multiple action potentials in the POm neurons. However, spontaneous *in vivo* activity of the L5B pyramids counteracts this "driving" action through a strong short-term synaptic depression and hence results in a depression of action potential transfer. The L5B-POm giant synapse may therefore have two modes of action: During *high* spontaneous activity, the synapse is suppressed and only synchronous activity of several inputs—possibly arising from multi-whisker deflections—will cause the postsynaptic POm neuron to spike: the synapse acts as a coincidence detector. In contrast, when the spontaneous activity is *low*—e.g., during active whisking or cortical silence—a single, asynchronous input will result in the firing of the POm neuron. Thus, depending on the rate of spontaneous activity, the L5B-POm giant synapse operates either as a detector of neuronal synchrony or cortical silence (Groh et al., 2008).

Synaptic connections between short, corticocallosally projecting L5 pyramidal neurons (**Figure 6A**, right neuron) in somatosensory cortex are quite distinct from those between other L5 pyramidal neuron types in a number of features (Le Bé et al., 2007). Their connectivity ratio was with 3% considerably lower than for the other types of L5 pyramidal neuron. The release probability at this synaptic connection was with 0.4 also exceptionally low; however, the average uEPSP amplitude was comparable to that of other pyramidal neuron connections in the barrel cortex. Corticocallosally projecting L5 pyramidal neuron pairs formed between one and six synaptic contacts, mainly on the basal dendritic tree at an average distance of ∼130 μm. The likely connections (based on the axonal projection pattern; see above and Larsen and Callaway, 2006) between short L5 pyramidal cells and those in layer 2/3 (based on the axon projection pattern of the short L5 have not yet been characterized).

Figures 6B and **C** summarize what is presently known about the intra- and extracortical connectivity pattern of slender- and thick-tufted pyramidal cells. It should be noted that thick-tufted L5B pyramidal cells receive synaptic input from virtually all cortical layers and project to numerous intra- and subcortical target regions. However, the schematic diagram shown here cannot cover the emerging structural and functional diversity as well as the differential connectivity of L5B pyramidal cells (Brown and Hestrin, 2009a,b). Therefore, this picture is likely to change in the near future.

THE ROLE OF CORTICAL LAYER 6

Throughout the neocortex layer 6A has been proposed to be the preeminent source of corticothalamic projections (Jones, 1984; Deschênes et al., 1998; Douglas et al., 2004; Sherman, 2005; Shipp, 2007; Fox, 2008; Thomson, 2010). In sensory cortices, corticothalamic projections are generally considered to be elements of a feed-back loop that modulates the response of thalamic relay neurons to peripheral stimuli. In the somatosensory cortex of rodents the relative thickness of infragranular layers in rodents is significantly larger than that of supragranular layers; the thickness of layer 6 is almost equal to that of layer 5 (Ren et al., 1992; Hutsler et al., 2005). The structure of layer 6 reflects its mixed origin with sublamina 6A being derived from the cortical plate (like layer 2–5) while sublamina 6B is a heterogeneous layer that contains neurons that have developed—at least to some extent—from the subplate but may also hold neurons that have migrated there from the cortical plate (Marín-Padilla, 1978). Sublamina 6B contains several distinct types of neurons with highly diverse dendritic domains; their functional role and even their synaptic connectivity has only received little attention to date (Tömböl et al., 1975; Tömböl, 1984; Miller, 1988; Bueno-Lopez et al., 1991; Chen et al., 2009). In contrast, sublamina 6A contains mainly pyramidal neurons with vertically oriented, untufted or sparsely tufted apical dendrites that terminate in lower layer 3–5A. Furthermore, a few neurons with inverted or obliquely oriented dendrites have also been described (Zhang and Deschênes, 1997; Chen et al., 2009). Like L5 pyramidal cells those in layer 6A can be subdivided into at least two different groups with respect to their axonal projection pattern: both groups are equally large groups and consist of pyramidal neurons the axons of which project either predominantly

intracortically or corticothalamically to the somatosensory thalamus (**Figure 7**; Zhang and Deschênes, 1997; Groh et al., 2008; Kumar and Ohana, 2008; Oberlaender et al., 2011b; Tanaka et al., 2011; Pichon et al., 2012); a small group of local circuit neurons (which comprises about 10% of the excitatory L6A neurons) may also exist.

A further subdivision of L6 pyramidal cells can be made on the basis of their axonal projection targets. L6A pyramids that project exclusively to the VPM nucleus of the thalamus have intracortical axon collaterals that show a columnar distribution with most of the collaterals ascending to layer 4 of the home barrel column where they terminate (**Figure 7A**, left neuron; Zhang and Deschênes, 1997; Kumar and Ohana, 2008). The majority of these neurons are located in the upper to middle portion of sublamina 6A (Bourassa et al., 1995; Killackey and Sherman, 2003). L6A pyramidal cells that target both neurons in the VPM and the POm nucleus have also been identified by Zhang and Dêschenes (**Figure 7A**, middle neuron; Zhang and Deschênes, 1997) A recent study (Pichon et al., 2012) demonstrated that a subset of L6A pyramidal cells has an extensive axonal domain with many ascending collaterals terminating largely in layer 4 but also in layer 5. Their axon collaterals innervate several barrels ramifying profusely. These neurons may correspond to the corticothalamic, both VPM and POm targeting L6A pyramidal cells. Only few corticothalamic L6A pyramids that target exclusively POm have been described today; these are located in the lower portion of sublamina 6A (Bourassa et al., 1995; Zhang and Deschênes, 1997) and possess relatively short apical dendrites terminating in layer 5. Their intracortical axon collaterals reside mainly in layer 6 with a few branches reaching into lower layer 5B (Zhang and Deschênes, 1997). In addition, another group of L6A neurons has been found in both whisker-related S1 cortex (as well as in S2) that targets the VPMvl, the origin of the extralemniscal pathway (Bokor et al., 2008). The functional role of these corticothalamic L6A neurons may be to provide direct (through layer 6) and indirect (though input from layer 4

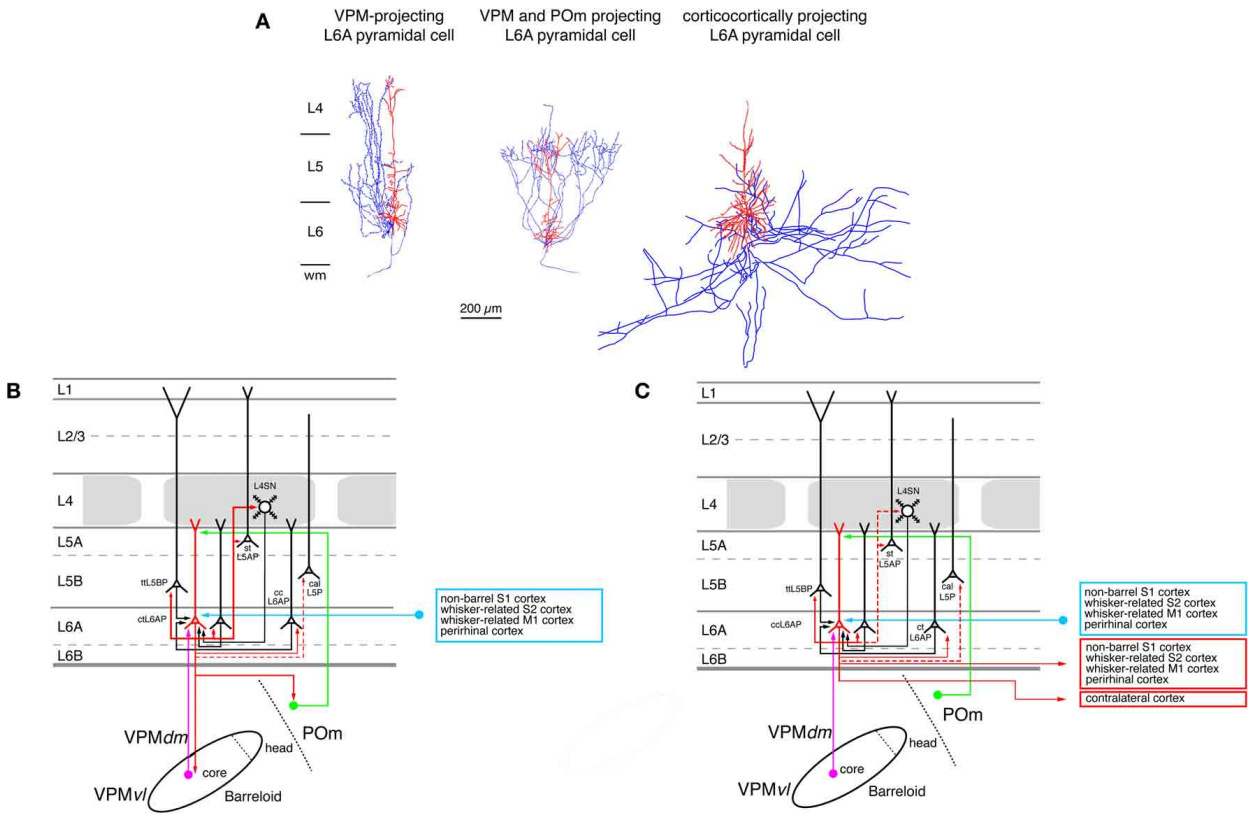

FIGURE 7 | Excitatory synaptic input–output relationship in layer 6 of the S1 barrel cortex. (A) Reconstructions of three types of pyramidal cells in sublamina A of layer 6 in the rat barrel cortex (Zhang and Deschênes, 1997); modiefied with permission of the Society for Neuroscience. L6A pyramidal cell projecting exclusively back to the VPM nucleus of the thalamus (left), L6A pyramidal neuron projecting to both the VPM and the POm nuclei of the somatosensory thalamus (middle) and a corticocortical L6A pyramidal cell. The apical trees of L6A pyramidal cells terminate between upper layer 5 and lower layer 3 and have very small or even no tuft. Modified with permission from the Society for Neuroscience. **(B)** Diagram of the excitatory synaptic connections of and onto corticothalamic L6A pyramidal cells (red neuron with blue axon) in the barrel cortex. Only synaptic input from neurons and regions relevant for corticothalamic L6A pyramidal cells is shown in this graph. For detailed information on the location of synaptic contacts and possible subtypes of corticothalamic L6A pyramidal cells see text. **(C)** Diagram of the excitatory synaptic connections of and onto corticocortical L6A pyramidal cells (red neuron with blue axon) in the barrel cortex. Only synaptic input from neurons and regions relevant for corticocortical L6A pyramidal cells is shown in this graph. For detailed information on the location of synaptic contacts and possible subtypes of corticocortical L6A pyramidal cells see text. Color coding and abbreviations as in **Figure 4**.

and 5B, see below) feed-back modulation of the thalamic activity in the different thalamocortical pathways. They may also be involved in feedforward signaling from the S1 cortex to S2 or M1 cortex.

In contrast to corticothalamic L6A pyramidal neurons, the axons of corticocortical L6A pyramidal cells remain mainly within layer 5 and 6 of the S1 cortex (**Figure 7A**, right neuron; Zhang and Deschênes, 1997). They project over many barrel columns thus mediating transcolumnar interactions in the infragranular layers of the barrel cortex. The majority of their axonal branches remain within the S1 cortex with some long-range collaterals projecting to the S2 and/or M1 cortex (**Figure 7C**); they have no obvious subcortical target. It has been suggested that different subtypes of corticocortical L6A pyramids exist, which can be differentiated on the basis of their dendritic and axonal arborization but the exact functional roles of these neurons remain unclear at present (Zhang and Deschênes, 1997; Kumar and Ohana, 2008; Pichon et al., 2012).

Only few studies on the intracortical connectivity of L6A pyramidal neurons in the barrel cortex are currently available and virtually nothing is known about synaptic connections between L6B excitatory neurons. The knowm input–output relationships of corticothalamic and corticocortical L6A pyramids are shown in **Figures 7A** and **B**. L6A pyramidal neurons receive input from L5A, L5B, and L6A pyramidal neurons. Homologous L6A connections (i.e., pairs between two corticocortical or corticothalamic L6A neurons) are more frequent than heterologous ones. Both corticocortical and corticothalamic L6 neurons are also presynaptic to L5B pyramids (Mercer et al., 2005; Lefort et al., 2009; Hooks et al., 2011; Tanaka et al., 2011). Corticothalamic L6A pyramidal cells receive a strong and focussed excitatory synaptic input from L4 neurons in their home column, indicating that neurons in this layer are involved in shaping the cortical modulation of the activity in the somatosensory thalamus (Tanaka et al., 2011). Connections with layer 4 were also observed for postsynaptic corticocortical L6A neurones (Qi and Feldmeyer, 2010). Inputs from layer 4 show a distinct sender neuron specificity: spiny stellate neurons contact exclusively the apical tufts of both types of L6A pyramidal cells, while star pyramidal neurons target predominantly the basal dendritic domain and deep apical oblique dendrites This suggests different computational roles for the two types of L4 excitatory neurons in the L4-L6A excitatory synaptic pathway.

Excitatory neurons in sublamina 6B of the barrel cortex have very heterogeneous dendritic morphologies, ranging from short, untufted pyramids with apical dendrites that terminate in layer 5, those with atypically oriented (oblique, horizontal or inverted) "apical" dendrites to multipolar neurons without a clear apical dendrite (Andjelic et al., 2009; Chen et al., 2009). This is in accordance with the description of L6B neurons located in other cortical areas (Tömböl et al., 1975; Tömböl, 1984; Clancy and Cauller, 1999). Few if any studies are available describing the axonal projection pattern of identified L6B neurons. For S1 barrel cortex it has been shown that—like L5B pyramids (see above)—L6B neurons located in both barrel and non-barrel (i.e., septal) cortex innervate POm (Killackey and Sherman, 2003). Furthermore, at least a subset of L6B neurons send also axons to layer 1 [(Mitchell and Cauller, 2001); in this paper layer 6B was termed layer 7]. Future studies are needed to elucidate the morphological and functional properties of the distinct excitatory L6B neuron types.

LONG-RANGE CONNECTIONS WITHIN THE S1 BARREL CORTEX AND TO OTHER CORTICAL AND SUBCORTICAL REGIONS

As already indicated in the preceding paragraphs excitatory pyramidal neurons of the rodent barrel cortex project to distant cortical and subcortical target regions and receive afferent input from them. In a recent review, the overall connectivity with these target regions has been described in detail (Bosman et al., 2011). Therefore, the main focus here will be on connections from identified neurons in S1 barrel cortex to other cortical and subcortical regions and their possible function.

Long-range axonal projections were first investigated by anterograde and retrograde transport using classical tracer substances and more recently by viral vectors coupled to fluorescent markers (which can also be used as anatomical tracers). In addition, studies using electrophysiological or optical stimulation (i.e., photo-activation of caged glutamate or ChR2) and optical recording (calcium or voltage-sensitive dye imaging) have revealed the functional synaptic connectivity between these brain regions, which exists often in loops between brain regions.

Within the S1 cortex, L2/3, L5 and a subset of L6 pyramidal neurons in the barrel field possess long-range horizontal axon collaterals. These projections run predominantly along the barrel rows and less along the barrel arcs (Bruno et al., 2009; Adesnik and Scanziani, 2010), i.e., they show a certain direction preference. Long-range projections in S1 cortex may play a role in the modulation of the home column activity with respect to its neighbors. For example, activation of L2/3 pyramidal neurons (Adesnik and Scanziani, 2010) generated rhythmic oscillation in the activity of L2/3 and L5 excitatory (and inhibitory) neurons in the gamma frequency range (∼40 Hz) in the home and adjacent barrel columns. On the cellular level, activation of L2/3 pyramids resulted in a lateral suppression of spiking in L2/3 pyramidal cells of neighboring barrel columns but feedforward facilitation of action potential firing in L5 pyramidal cells with very similar spatial profiles. Since layer 2/3 provides the dominant input to layer 5 and this layer is the prominent cortical output, (see above) L2/3 pyramidal cells can drive the output to neighboring barrel-related columns *via* the L5 axons while inhibiting their inputs by depressing L2/3 neuronal activity. In consequence, this coordinated modulation of L2/3 and L5 neurons may result in the lateral expansion of the activity of the principal barrel-related column. Thus, at a given point in time the most active barrel-related column may dominate the output of the S1 cortex at the expense of the adjacent, less active cortical domains.

In addition to the aforementioned horizontal axon collaterals *within* the S1 cortex, L2/3, L5, and L6 neurons project also outside S1. The most prominent connections between whisker-related cortical areas have been reported for S1 and S2 cortex and S1 and M1 cortex; in addition connections to the insular and the perirhinal cortex have been identified (White and DeAmicis, 1977; Welker et al., 1988; Fabri and Burton, 1991; Cauller et al.,

1998; Zhang and Deschênes, 1998; Hoffer et al., 2003; Aronoff et al., 2010).

Axonal projections from S1 barrel cortex to the ipsilateral S2 cortex are topographic. The connections between the two whisker-related cortical areas are strong and reciprocal (Carvell and Simons, 1987; Aronoff et al., 2010) and emanate from pyramidal neurons in layers 2/3, 5 (mostly sublamina A) and (to a lesser degree) 6 from neurons in both the barrel and septal columns of the S1 cortex (Koralek et al., 1990; Zhang and Deschênes, 1998; Kim and Ebner, 1999; Chakrabarti and Alloway, 2006). The general connectivity pattern in both cortices is rather similar [see (Hooks et al., 2011) for details] despite some minor differences. Sensory processing in the S2 cortex is likely to be parallel to that in the S1 cortex because whisker signals reach S2 *via* the extralemniscal pathway through the ventrolateral section of the VPM nucleus (Pierret et al., 2000; Bokor et al., 2008) and the POm nucleus (Carvell and Simons, 1987; Spreafico et al., 1987; Alloway et al., 2000; Theyel et al., 2010). This suggests that synaptic input to S2 occurs at virtually the same time as it does in S1.

Because somatosensation in rodents depends on the active movement of their whiskers and the deflection from the free whisker trajectory by an object, an interaction between motor and somatosensory cortex is important not only for object location and recognition but also to modulate and coordinate the whisker movement. Monosynaptic connections between the ipsilateral, whisker-related S1, and M1 cortices have been identified structurally and functionally (White and DeAmicis, 1977; Porter and White, 1983; Miyashita et al., 1994; Izraeli and Porter, 1995; Farkas et al., 1999; Veinante and Deschênes, 2003; Chakrabarti and Alloway, 2006; Ferezou et al., 2007; Petreanu et al., 2009; Aronoff et al., 2010; Sato and Svoboda, 2010; Mao et al., 2011) and are also somatotopically arranged. These projections from the whisker-related S1 to M1 motor cortex arise from a subset of L2/3 and L5A pyramidal neurons in S1 barrel cortex, run through both deep and superficial cortical layers and target L2/3 and L5A neurons in M1 cortex (Porter and White, 1983; Koralek et al., 1990; Miyashita et al., 1994; Aronoff et al., 2010; Sato and Svoboda, 2010; Mao et al., 2011); the majority of these neurons have been suggested to originate in septal columns (Crandall et al., 1986; Alloway et al., 2004; Chakrabarti et al., 2008) and are as such elements of the septal circuits that are hypothesized to modulate whisker motion (Alloway, 2008). M1 neurons receiving input from S1 project directly back to this region thus forming a strong feedback loop. In addition, a small percentage of L6 neurons in S1 also projects to M1 (Mao et al., 2011).

Conversely, ipsilateral M1-to-S1 connections innervate L2/3 and L5 pyramidal neurons *via* axon collaterals that ramify in both layer 5 and 6 as well as layer 1 (Cauller et al., 1998; Veinante and Deschênes, 2003; Petreanu et al., 2009; Matyas et al., 2010; Mao et al., 2011). Specifically, it has been demonstrated that connection from layer 1 in the M1 cortex innervates the apical tufts of L2/3 and L5 pyramidal cells in S1 cortex (Cauller and Connors, 1994; Larkum et al., 1999; Larkum and Zhu, 2002; Zhu and Zhu, 2004; Rubio-Garrido et al., 2009). These neurons receive also direct input from the POm neurons via layer 1 (see above; Wimmer et al., 2010; Ohno et al., 2011) POm neurons are believed to code signals related to whisker position (Yu et al., 2006) while the whisker-related M1 cortex is involved in the voluntary whisker control (Berg and Kleinfeld, 2003). It is therefore conceivable that synapses in layer 1 established between POm and M1 axons and the apical tuft of L2/3 and L5 pyramidal cells serve to integrate signals related to whisker movement and position. This may involve the activation of Ca^{2+} action potential in the apical tufts of the pyramidal cells (Larkum et al., 1999; Larkum and Zhu, 2002).

Finally, the barrel-related M1 cortices in the two brain hemispheres are interconnected *via* the claustrum (Smith and Alloway, 2010) and L6 pyramidal cells in this cortex project back to the contralateral ventromedial and the ventrolateral nuclei of the thalamus (Alloway et al., 2008), suggesting a modulatory role of M1 cortex in S1 signaling and in the bilateral coordination of whisker movement.

In addition to their role in sensory perception, it has recently been shown that M1 and S1 cortex have different and independent roles in whisker motion (Matyas et al., 2010). While M1 drives whisker protraction *via* the brainstem reticular formation and the facial nucleus, the S1 cortex induces the retraction of the whisker *via* the SpV trigeminal nucleus and also the facial nucleus. This finding argues for a strong parallel processing of both sensory and motor signals in the somatosensory barrel cortex.

Future experiments with higher cellular resolution are necessary to characterize the distinct structural and functional properties of neuronal subclasses in the different layers of the barrel-related cortices. In particular, it will be important to determine which neuron types in layers 2/3, 5, and 6 of S1 form synaptic connections with which target neuron types in layer S2 or M1 and *vice versa*.

Pyramidal neurons in layer 2/3 and 5 target the contralateral S1 cortex *via* dense callosal axon projections (Olavarria et al., 1984; Larsen et al., 2007; Petreanu et al., 2007; Aronoff et al., 2010). Callosal projections also preferentially target septal rather than barrel areas (Olavarria et al., 1984). A ChR2-assisted circuit mapping study showed that L2/3 pyramids target predominantly L2/3, L5A, and L5B pyramids in the contralateral S1 cortex; only few connection with L6 neurons were found (Petreanu et al., 2007). Functional interactions between S1 cortices in the two hemispheres have been demonstrated because a chronic suppression of the activity in one hemisphere down-regulates sensory responses in the contralateral S1 barrel cortex (Li et al., 2005). However, it remains to be determined whether these interactions occur *via* corticocortical connections or involve subcortical regions.

Furthermore, there are also connections from S1 barrel cortex to the ventral orbital and the ipsi- and contralateral perirhinal cortex, a cortical region that is a crucial link between the neo- and the allocortex (Deacon et al., 1983) and thus contribute to the processing of tactile information in the hippocampus (Pereira et al., 2007). However, these connections occur at a much weaker density than those targeting the whisker-related M1 and S2 cortices (Welker et al., 1988; Aronoff et al., 2010). Neurons in both the ventral orbital and the perirhinal cortex project also back to the S1 cortex (Aronoff et al., 2010).

In particular pyramidal cells in layers 5 and 6 have been demonstrated to send axonal projections back to the thalamus (see above and Bourassa et al., 1995; Zhang and Deschênes, 1997, 1998; Veinante et al., 2000b; Alloway et al., 2003; Killackey and Sherman, 2003; Groh et al., 2008; Liao et al., 2010; Theyel et al., 2010). Because these neurons receive input from either the VPM or POm nucleus of the thalamus (or both) they may be elements of thalamocorticothalamic feedback loops; but see (Guillery and Sherman, 2011). While some of them target the same thalamic nucleus from which they receive synaptic input (e.g., L6A pyramids) others interdigitate different thalamic nuclei, e.g., L5B pyramids that receive VPM input and project to the dorsal part of POm. This connection is also involved in the interaction of S1 and S2 cortex (Theyel et al., 2010): action potentials in corticothalamic L5B pyramidal cells result in the efficient recruitment of POm relay neurons (*via* their giant presynaptic terminals; Groh et al., 2008) which in turn activate L4 neurons in the higher-order S2 cortex (Carvell and Simons, 1987; Spreafico et al., 1987; Alloway et al., 2000; Theyel et al., 2010). This stimulation was eliminated following an inhibition of the thalamic nucleus (Theyel et al., 2010) suggesting a corticothalamocortical pathway via layer 5B from S1 cortex to higher-order sensory cortices such as the S2 cortex. This could run in parallel to the corticocortical signal flow but the exact functional characteristics of and difference between these two pathways are so far unkown.

L6B pyramids may also be involved in this process because they innervate POm (Killackey and Sherman, 2003) and are likely to receive synaptic input from VPM *via* L6A pyramids. Thus, the whisker-related S1 and S2 cortex are interconnected by at least two different routes: a direct feedforward route from thalamus to S1 and from there to S2 *via* long-range axon collaterals of S1 neurons and through a corticothalamocortical feedback involving the POm. The exact cellular identity of the neurons involved in these pathways remains to be determined.

Besides the thalamus, excitatory neurons in the barrel-related S1 cortex project also to other subcortical targets such as the striatum (and through this region the basal ganglia) (Donoghue and Kitai, 1981; Welker et al., 1988; Gerfen, 1989; Cowan and Wilson, 1994; Alloway et al., 1998, 1999, 2006; Wright et al., 1999; Hoover et al., 2003; Aronoff et al., 2010), the superior colliculus (tectum) (Wise and Jones, 1977; Welker et al., 1988; Hoffer et al., 2005; Cohen et al., 2008; Aronoff et al., 2010; Cohen and Castro-Alamancos, 2010) and the pons (Welker et al., 1988; Legg et al., 1989; Leergaard et al., 2000, 2004; Schwarz and Möck, 2001; Aronoff et al., 2010), all of which are involved in the integration of motor performance, sensation and general behavior. Most of the neurons targeting these regions reside in the infragranular layers of the ipsilateral S1 cortex and here mostly in layer 5B; however, a small population of corticostriatally projecting supragranular pyramidal cells appears to exist (Gerfen, 1989; Wright et al., 1999). In addition to these subcortical target regions, there are also direct projections of axons originating in S1 cortex back to the ipsilateral PrV and the contralateral SpV trigeminal nuclei (Welker et al., 1988; Jacquin et al., 1990; Aronoff et al., 2010) suggesting that neurons in these first relay stations of the whisker-to-cortex pathway are under a very direct feedback modulation of the S1 barrel cortex. How these different regions in the whisker system are interconnected with one another (e.g., the thalamic nuclei with the striatum), to which other brain regions involved in somatosensation project. How they integrate and coordinate sensory and motor signals is not a subject this but of other excellent reviews (see Alloway, 2008; Fox, 2008; Bosman et al., 2011).

CONCLUSION

On the basis of the available studies it can be stated that the barrel cortex has a very prominent vertical organization with a pronounced and spatially confined thalamocortical input and signal transformation to supragranular and to a lesser degree also to infragranular layers. This vertical organization is clearly visible, more so than in other sensory cortices. The readily discernible barrel structure and the largely vertical axonal projection of several of several neuronal cell types in the barrel-related column serves as evidence for this fact. In addition, thalamic afferents from VPM and POm have a barrel or septal-related projection into the S1 barrel cortex. All these structural features support the concept of vertical modules in cortical signal processing.

A barrel-related column is not a separate unit. Synaptic mechanisms such as the coordinated modulation of L2/3 and L5 pyramidal cells by the long-range collaterals of L2/3 pyramidal cells may serve to enhance the output of the most active barrel column. In addition, many interactions between cortical output neurons and neurons in other cortical and subcortical target regions show somatotopic arrangements suggesting a specific interaction between cortical columns in different cortical areas, particular the M1 and S2 cortex. Therefore, it is likely that there is a link between the structure and function of the S1 barrel column and other cortical areas. Thus, a cortical column is not merely a structural unit but may be the prerequisite of vertical signal transfer. Some functional properties of the barrel cortex such as the angular tuning have even been assigned to substructures such as sub-barrel domains.

The barrel cortex and its barrel-related columns show many interactions with cortical and subcortical brain regions. First of all, the available data on the neuronal connectivity suggests that signal processing in the S1 barrel cortex is far from being a purely serial and hierarchical process. Rather, neuronal connections in the S1 barrel cortex represent a distributed network that includes many parallel steps at which subcortical (thalamic) input occurs and which has many feedback controls (most notably through monosynaptic thalamocorticothalamic connections). This is also true for the different cortical areas such as the barrel-related M1 and S2 cortices that are involved in—often reciprocal—synaptic signaling. Not only do they receive direct input *from* neurons in S1 but also from subcortical structures via corticothalamocortical feed-foward circuits. In return, neurons in M1 and S2 cortices influence the activity of S1 cortex both directly through corticocortical or indirectly through cortico-thalamo-cortical axonal projections. While this does not necessarily negate the importance of vertical signal transformation it suggests that neurons in a barrel column show a large degree of interaction with neurons in other cortical and subcortical areas. Such synaptic interactions are not necessarily organized in vertical modules. Future studies are required to define the connectivity and function of the pre- and postsynaptic neurons in these pathways. Such studies will be

essential in identifying the different functional roles of cortical columns in the barrel cortex of rodents.

Furthermore, the elucidation of the excitatory cortical connectivity is largely dependent on the knowledge of the types of excitatory neurons. In recent years (see above) it has become increasingly more evident that there is a large degree of diversity in excitatory neurons of the neocortex (in addition to the well-known diversity of inhibitory interneurons, see e.g., Ascoli et al., 2008) and that these different types of excitatory neurons have very distinct properties and functional roles in the cortical microcircuitry. For example in their target region and neuron specificity. We are just beginning to unravel this diversity and much more work needs to be done to understand how it impacts on our view on cortical connectivity not only in the barrel cortex but also with other cortical regions.

Finally, the synaptic activity in the barrel cortex (and those in other cortical areas) is highly dynamic because it fluctuates slowly between depolarized "up" states and hyperpolarized "down" states (Steriade et al., 1993; Cowan and Wilson, 1994; Petersen et al., 2003; Brecht et al., 2004; Haider et al., 2006; Waters and Helmchen, 2006; for reviews see Destexhe et al., 2003; Buzsaki and Draguhn, 2004); a point that has not been discussed here. These fluctuations are under the control of neuromodulators such as acetylcholine and noradrenaline, (Eggermann and Feldmeyer, 2009; Constantinople and Bruno, 2011) which are released during different behavioral states such as sleep, arousal, and attention. Neuromodulators show a cell-specific effect on neuronal cell types and synaptic connections (e.g., Eggermann and Feldmeyer, 2009), for example with respect to the release probability and synaptic efficacy. Synaptic networks in the barrel cortex and other cortical areas are therefore not stable but highly dynamic and the synaptic weight in cortical microcircuits may change considerably. For future studies of cortical connectivity such connection-specific changes should be taken into account if one wants to understand the cellular correlates during different behavioral states.

ACKNOWLEDGMENTS

I would like to thank Dr. Ted Abel for reading a previous version of the manuscript. Furthermore, I would also like to thank Dr. Gabriele Radnikow for many helpful suggestions and careful reading of the final version of this manuscript. This work was supported by the Helmholtz Foundation and project grants from the Helmholtz Alliance on Systems Biology and the DFG Research Group "Barrel Cortex Function."

REFERENCES

Adesnik, H., and Scanziani, M. (2010). Lateral competition for cortical space by layer-specific horizontal circuits. *Nature* 464, 1155–1160.

Ahissar, E., and Staiger, J. F. (2010). S1 laminar specialization. *Scholarpedia* 5, 7457.

Alloway, K. D. (2008). Information processing streams in rodent barrel cortex: the differential functions of barrel and septal circuits. *Cereb. Cortex* 18, 979–989.

Alloway, K. D., Crist, J., Mutic, J. J., and Roy, S. A. (1999). Corticostriatal projections from rat barrel cortex have an anisotropic organization that correlates with vibrissal whisking behavior. *J. Neurosci.* 19, 10908–10922.

Alloway, K. D., Hoffer, Z. S., and Hoover, J. E. (2003). Quantitative comparisons of corticothalamic topography within the ventrobasal complex and the posterior nucleus of the rodent thalamus. *Brain Res.* 968, 54–68.

Alloway, K. D., Lou, L., Nwabueze-Ogbo, F., and Chakrabarti, S. (2006). Topography of cortical projections to the dorsolateral neostriatum in rats: multiple overlapping sensorimotor pathways. *J. Comp. Neurol.* 499, 33–48.

Alloway, K. D., Mutic, J. J., Hoffer, Z. S., and Hoover, J. E. (2000). Overlapping corticostriatal projections from the rodent vibrissal representations in primary and secondary somatosensory cortex. *J. Comp. Neurol.* 428, 51–67.

Alloway, K. D., Mutic, J. J., and Hoover, J. E. (1998). Divergent corticostriatal projections from a single cortical column in the somatosensory cortex of rats. *Brain Res.* 785, 341–346.

Alloway, K. D., Olson, M. L., and Smith, J. B. (2008). Contralateral corticothalamic projections from MI whisker cortex: potential route for modulating hemispheric interactions. *J. Comp. Neurol.* 510, 100–116.

Alloway, K. D., Zhang, M., and Chakrabarti, S. (2004). Septal columns in rodent barrel cortex: functional circuits for modulating whisking behavior. *J. Comp. Neurol.* 480, 299–309.

Andermann, M. L., and Moore, C. I. (2006). A somatotopic map of vibrissa motion direction within a barrel column. *Nat. Neurosci.* 9, 543–551.

Anderson, C. T., Sheets, P. L., Kiritani, T., and Shepherd, G. M. (2010). Sublayer-specific microcircuits of corticospinal and corticostriatal neurons in motor cortex. *Nat. Neurosci.* 13, 739–744.

Andjelic, S., Gallopin, T., Cauli, B., Hill, E. L., Roux, L., Badr, S., Hu, E., Tamas, G., and Lambolez, B. (2009). Glutamatergic nonpyramidal neurons from neocortical layer VI and their comparison with pyramidal and spiny stellate neurons. *J. Neurophysiol.* 101, 641–654.

Armstrong-James, M., and Callahan, C. A. (1991). Thalamo-cortical processing of vibrissal information in the rat. II. Spatiotemporal convergence in the thalamic ventroposterior medial nucleus (VPm) and its relevance to generation of receptive fields of S1 cortical "barrel" neurones. *J. Comp. Neurol.* 303, 211–224.

Arnold, P. B., Li, C. X., and Waters, R. S. (2001). Thalamocortical arbors extend beyond single cortical barrels: an *in vivo* intracellular tracing study in rat. *Exp. Brain Res.* 136, 152–168.

Aronoff, R., Matyas, F., Mateo, C., Ciron, C., Schneider, B., and Petersen, C. C. (2010). Long-range connectivity of mouse primary somatosensory barrel cortex. *Eur. J. Neurosci.* 31, 2221–2233.

Ascoli, G. A., Alonso-Nanclares, L., Anderson, S. A., Barrionuevo, G., Benavides-Piccione, R., Burkhalter, A., Buzsaki, G., Cauli, B., DeFelipe, J., Fairén, A., Feldmeyer, D., Fishell, G., Fregnac, Y., Freund, T. F., Gardner, D., Gardner, E. P., Goldberg, J. H., Helmstaedter, M., Hestrin, S., Karube, F., Kisvárday, Z. F., Lambolez, B., Lewis, D. A., Marin, O., Markram, H., Munoz, A., Packer, A., Petersen, C. C., Rockland, K. S., Rossier, J., Rudy, B., Somogyi, P., Staiger, J. F., Tamas, G., Thomson, A. M., Toledo-Rodriguez, M., Wang, Y., West, D. C., and Yuste, R. (2008). Petilla terminology: nomenclature of features of GABAergic interneurons of the cerebral cortex. *Nat. Rev. Neurosci.* 9, 557–568.

Beierlein, M., Gibson, J. R., and Connors, B. W. (2003). Two dynamically distinct inhibitory networks in layer 4 of the neocortex. *J. Neurophysiol.* 90, 2987–3000.

Bender, K. J., Rangel, J., and Feldman, D. E. (2003). Development of columnar topography in the excitatory layer 4 to layer 2/3 projection in rat barrel cortex. *J. Neurosci.* 23, 8759–8770.

Benshalom, G., and White, E. L. (1986). Quantification of thalamocortical synapses with spiny stellate neurons in layer IV of mouse somatosensory cortex. *J. Comp. Neurol.* 253, 303–314.

Berg, R. W., and Kleinfeld, D. (2003). Vibrissa movement elicited by rhythmic electrical microstimulation to motor cortex in the aroused rat mimics exploratory whisking. *J. Neurophysiol.* 90, 2950–2963.

Bernardo, K. L., and Woolsey, T. A. (1987). Axonal trajectories between mouse somatosensory thalamus and cortex. *J. Comp. Neurol.* 258, 542–564.

Binzegger, T., Douglas, R. J., and Martin, K. A. (2004). A quantitative map of the circuit of cat primary visual cortex. *J. Neurosci.* 24, 8441–8453.

Bokor, H., Acsády, L., and Deschênes, M. (2008). Vibrissal responses of thalamic cells that project to the septal columns of the barrel cortex and to the second somatosensory area. *J. Neurosci.* 28, 5169–5177.

Bosman, L. W., Houweling, A. R., Owens, C. B., Tanke, N., Shevchouk, O. T., Rahmati, N., Teunissen, W. H., Ju, C., Gong, W., Koekkoek, S. K., and De Zeeuw, C. I. (2011). Anatomical pathways involved in generating and sensing rhythmic whisker movements. *Front. Integr. Neurosci.* 5:53. doi: 10.3389/fnint.2011.00053

Bourassa, J., Pinault, D., and Deschênes, M. (1995). Corticothalamic projections from the cortical barrel field to the somatosensory thalamus in rats: a single-fibre study using biocytin as an anterograde tracer. *Eur. J. Neurosci.* 7, 19–30.

Brecht, M., and Sakmann, B. (2002a). Dynamic representation of whisker deflection by synaptic potentials in spiny stellate and pyramidal cells in the barrels and septa of layer 4 rat somatosensory cortex. *J. Physiol.* 543, 49–70.

Brecht, M., and Sakmann, B. (2002b). Whisker maps of neuronal subclasses of the rat ventral posterior medial thalamus, identified by whole-cell voltage recording and morphological reconstruction. *J. Physiol.* 538, 495–515.

Brecht, M., Schneider, M., Sakmann, B., and Margrie, T. W. (2004). Whisker movements evoked by stimulation of single pyramidal cells in rat motor cortex. *Nature* 427, 704–710.

Brown, S. P., and Hestrin, S. (2009a). Cell-type identity: a key to unlocking the function of neocortical circuits. *Curr. Opin. Neurobiol.* 19, 415–421.

Brown, S. P., and Hestrin, S. (2009b). Intracortical circuits of pyramidal neurons reflect their long-range axonal targets. *Nature* 457, 1133–1136.

Brumberg, J. C., Pinto, D. J., and Simons, D. J. (1999). Cortical columnar processing in the rat whisker-to-barrel system. *J. Neurophysiol.* 82, 1808–1817.

Bruno, R. M., Hahn, T. T., Wallace, D. J., de Kock, C. P., and Sakmann, B. (2009). Sensory experience alters specific branches of individual corticocortical axons during development. *J. Neurosci.* 29, 3172–3181.

Bruno, R. M., Khatri, V., Land, P. W., and Simons, D. J. (2003). Thalamocortical angular tuning domains within individual barrels of rat somatosensory cortex. *J. Neurosci.* 23, 9565–9574.

Bruno, R. M., and Simons, D. J. (2002). Feedforward mechanisms of excitatory and inhibitory cortical receptive fields. *J. Neurosci.* 22, 10966–10975.

Bruno, R. M., and Sakmann, B. (2006). Cortex is driven by weak but synchronously active thalamocortical synapses. *Science* 312, 1622–1627.

Bueno-Lopez, J. L., Reblet, C., Lopez-Medina, A., Gomez-Urquijo, S. M., Grandes, P., Gondra, J., and Hennequet, L. (1991). Targets and laminar distribution of projection neurons with 'inverted' morphology in rabbit cortex. *Eur. J. Neurosci.* 3, 713.

Bureau, I., Shepherd, G. M., and Svoboda, K. (2004). Precise development of functional and anatomical columns in the neocortex. *Neuron* 42, 789–801.

Bureau, I., von Saint Paul, F., and Svoboda, K. (2006). Interdigitated paralemniscal and lemniscal pathways in the mouse barrel cortex. *PLoS Biol.* 4:e382. doi: 10.1371/journal.pbio.0040382

Buzsaki, G., and Draguhn, A. (2004). Neuronal oscillations in cortical networks. *Science* 304, 1926–1929.

Carvell, G. E., and Simons, D. J. (1987). Thalamic and corticocortical connections of the second somatic sensory area of the mouse. *J. Comp. Neurol.* 265, 409–427.

Catania, K. C., and Kaas, J. H. (1995). Organization of the somatosensory cortex of the star-nosed mole. *J. Comp. Neurol.* 351, 549–567.

Catania, K. C., Northcutt, R. G., Kaas, J. H., and Beck, P. D. (1993). Nose stars and brain stripes. *Nature* 364, 493.

Cauller, L. J., Clancy, B., and Connors, B. W. (1998). Backward cortical projections to primary somatosensory cortex in rats extend long horizontal axons in layer I. *J. Comp. Neurol.* 390, 297–310.

Cauller, L. J., and Connors, B. W. (1994). Synaptic physiology of horizontal afferents to layer I in slices of rat SI neocortex. *J. Neurosci.* 14, 751–762.

Chakrabarti, S., and Alloway, K. D. (2006). Differential origin of projections from SI barrel cortex to the whisker representations in SII and MI. *J. Comp. Neurol.* 498, 624–636.

Chakrabarti, S., and Alloway, K. D. (2009). Differential response patterns in the SI barrel and septal compartments during mechanical whisker stimulation. *J. Neurophysiol.* 102, 1632–1646.

Chakrabarti, S., Zhang, M., and Alloway, K. D. (2008). MI neuronal responses to peripheral whisker stimulation: relationship to neuronal activity in SI barrels and septa. *J. Neurophysiol.* 100, 50–63.

Cheetham, C. E., Hammond, M. S., Edwards, C. E., and Finnerty, G. T. (2007). Sensory experience alters cortical connectivity and synaptic function site specifically. *J. Neurosci.* 27, 3456–3465.

Chen, B., Wang, S. S., Hattox, A. M., Rayburn, H., Nelson, S. B., and McConnell, S. K. (2008). The Fezf2-Ctip2 genetic pathway regulates the fate choice of subcortical projection neurons in the developing cerebral cortex. *Proc. Natl. Acad. Sci. U.S.A.* 105, 11382–11387.

Chen, C. C., Abrams, S., Pinhas, A., and Brumberg, J. C. (2009). Morphological heterogeneity of layer VI neurons in mouse barrel cortex. *J. Comp. Neurol.* 512, 726–746.

Chmielowska, J., Carvell, G. E., and Simons, D. J. (1989). Spatial organization of thalamocortical and corticothalamic projection systems in the rat SmI barrel cortex. *J. Comp. Neurol.* 285, 325–338.

Clancy, B., and Cauller, L. J. (1999). Widespread projections from subgriseal neurons (layer VII) to layer I in adult rat cortex. *J. Comp. Neurol.* 407, 275–286.

Cohen, J. D., and Castro-Alamancos, M. A. (2010). Behavioral state dependency of neural activity and sensory (whisker) responses in superior colliculus. *J. Neurophysiol.* 104, 1661–1672.

Cohen, J. D., Hirata, A., and Castro-Alamancos, M. A. (2008). Vibrissa sensation in superior colliculus: wide-field sensitivity and state-dependent cortical feedback. *J. Neurosci.* 28, 11205–11220.

Constantinople, C. M., and Bruno, R. M. (2011). Effects and mechanisms of wakefulness on local cortical networks. *Neuron* 69, 1061–1068.

Cowan, A. I., and Stricker, C. (2004). Functional connectivity in layer IV local excitatory circuits of rat somatosensory cortex. *J. Neurophysiol.* 92, 2137–2150.

Cowan, R. L., and Wilson, C. J. (1994). Spontaneous firing patterns and axonal projections of single corticostriatal neurons in the rat medial agranular cortex. *J. Neurophysiol.* 71, 17–32.

Crandall, J. E., Korde, M., and Caviness, V. S. Jr. (1986). Somata of layer V projection neurons in the mouse barrelfield cortex are in preferential register with the sides and septa of the barrels. *Neurosci. Lett.* 67, 19–24.

Cruikshank, S. J., Lewis, T. J., and Connors, B. W. (2007). Synaptic basis for intense thalamocortical activation of feedforward inhibitory cells in neocortex. *Nat. Neurosci.* 10, 462–468.

Cruikshank, S. J., Urabe, H., Nurmikko, A. V., and Connors, B. W. (2010). Pathway-specific feedforward circuits between thalamus and neocortex revealed by selective optical stimulation of axons. *Neuron* 65, 230–245.

Curtis, J. C., and Kleinfeld, D. (2009). Phase-to-rate transformations encode touch in cortical neurons of a scanning sensorimotor system. *Nat. Neurosci.* 12, 492–501.

da Costa, N. M., and Martin, K. A. (2010). Whose cortical column would that be? *Front. Neuroanat.* 4:16. doi: 10.3389/fnana.2010.00016

Deacon, T. W., Eichenbaum, H., Rosenberg, P., and Eckmann, K. W. (1983). Afferent connections of the perirhinal cortex in the rat. *J. Comp. Neurol.* 220, 168–190.

de Kock, C. P., Bruno, R. M., Spors, H., and Sakmann, B. (2007). Layer- and cell-type-specific suprathreshold stimulus representation in rat primary somatosensory cortex. *J. Physiol.* 581, 139–154.

de Kock, C. P., and Sakmann, B. (2009). Spiking in primary somatosensory cortex during natural whisking in awake head-restrained rats is cell-type specific. *Proc. Natl. Acad. Sci. U.S.A.* 106, 16446–16450.

Deschênes, M. (2009). Vibrissal afferents from trigeminus to cortices. *Scholarpedia* 4, 7454.

Deschênes, M., Bourassa, J., Doan, V. D., and Parent, A. (1996). A single-cell study of the axonal projections arising from the posterior intralaminar thalamic nuclei in the rat. *Eur. J. Neurosci.* 8, 329–343.

Deschênes, M., Veinante, P., and Zhang, Z. W. (1998). The organization of corticothalamic projections: reciprocity versus parity. *Brain Res. Brain Res. Rev.* 28, 286–308.

Destexhe, A., Rudolph, M., and Pare, D. (2003). The high-conductance state of neocortical neurons *in vivo*. *Nat. Rev. Neurosci.* 4, 739–751.

Diamond, M. E., Armstrong-James, M., Budway, M. J., and Ebner, F. F. (1992). Somatic sensory responses in the rostral sector of the posterior group (POm) and in the ventral posterior medial nucleus (VPM) of the rat thalamus: dependence on the barrel field cortex. *J. Comp. Neurol.* 319, 66–84.

Dodt, H. U., Schierloh, A., Eder, M., and Zieglgänsberger, W. (2003). Circuitry of rat barrel cortex

investigated by infrared-guided laser stimulation. *Neuroreport* 14, 623–627.

Donoghue, J. P., and Kitai, S. T. (1981). A collateral pathway to the neostriatum from corticofugal neurons of the rat sensory-motor cortex: an intracellular HRP study. *J. Comp. Neurol.* 201, 1–13.

Douglas, R., Markram, H., and Martin, K. (2004). "Neocortex," in *The Synaptic Organization of the Brain*, 5th Edn. ed G. M. Shepherd (New York, NY: Oxford University Press), 499–558.

Douglas, R. J., and Martin, K. A. (1991). A functional microcircuit for cat visual cortex. *J. Physiol.* 440, 735–769.

Egger, V., Feldmeyer, D., and Sakmann, B. (1999). Coincidence detection and changes of synaptic efficacy in spiny stellate neurons in rat barrel cortex. *Nat. Neurosci.* 2, 1098–1105.

Egger, V., Nevian, T., and Bruno, R. M. (2008). Subcolumnar dendritic and axonal organization of spiny stellate and star pyramid neurons within a barrel in rat somatosensory cortex. *Cereb. Cortex* 18, 876–889.

Eggermann, E., and Feldmeyer, D. (2009). Cholinergic filtering in the recurrent excitatory microcircuit of cortical layer 4. *Proc. Natl. Acad. Sci. U.S.A.* 106, 11753–11758.

Erzurumlu, R. S., and Killackey, H. P. (1980). Diencephalic projections of the subnucleus interpolaris of the brainstem trigeminal complex in the rat. *Neuroscience* 5, 1891–1901.

Fabri, M., and Burton, H. (1991). Ipsilateral cortical connections of primary somatic sensory cortex in rats. *J. Comp. Neurol.* 311, 405–424.

Farkas, T., Kis, Z., Toldi, J., and Wolff, J. R. (1999). Activation of the primary motor cortex by somatosensory stimulation in adult rats is mediated mainly by associational connections from the somatosensory cortex. *Neuroscience* 90, 353–361.

Feldmeyer, D., Egger, V., Lübke, J., and Sakmann, B. (1999). Reliable synaptic connections between pairs of excitatory layer 4 neurones within a single 'barrel' of developing rat somatosensory cortex. *J. Physiol.* 521(Pt 1), 169–190.

Feldmeyer, D., Lübke, J., and Sakmann, B. (2006). Efficacy and connectivity of intracolumnar pairs of layer 2/3 pyramidal cells in the barrel cortex of juvenile rats. *J. Physiol.* 575, 583–602.

Feldmeyer, D., Lübke, J., Silver, R. A., and Sakmann, B. (2002). Synaptic connections between layer 4 spiny neurone-layer 2/3 pyramidal cell pairs in juvenile rat barrel cortex: physiology and anatomy of interlaminar signalling within a cortical column. *J. Physiol.* 538, 803–822.

Feldmeyer, D., Roth, A., and Sakmann, B. (2005). Monosynaptic connections between pairs of spiny stellate cells in layer 4 and pyramidal cells in layer 5A indicate that lemniscal and paralemniscal afferent pathways converge in the infragranular somatosensory cortex. *J. Neurosci.* 25, 3423–3431.

Ferezou, I., Haiss, F., Gentet, L. J., Aronoff, R., Weber, B., and Petersen, C. C. (2007). Spatiotemporal dynamics of cortical sensorimotor integration in behaving mice. *Neuron* 56, 907–923.

Fox, K. D. (2008). *Barrel Cortex,* 1st Edn. Cambridge, UK: Cambridge University Press.

Frick, A., Feldmeyer, D., Helmstaedter, M., and Sakmann, B. (2008). Monosynaptic connections between pairs of L5A pyramidal neurons in columns of juvenile rat somatosensory cortex. *Cereb. Cortex* 18, 397–406.

Furuta, T., Deschênes, M., and Kaneko, T. (2011). Anisotropic distribution of thalamocortical boutons in barrels. *J. Neurosci.* 31, 6432–6439.

Furuta, T., Kaneko, T., and Deschênes, M. (2009). Septal neurons in barrel cortex derive their receptive field input from the lemniscal pathway. *J. Neurosci.* 29, 4089–4095.

Games, K. D., and Winer, J. A. (1988). Layer V in rat auditory cortex: projections to the inferior colliculus and contralateral cortex. *Hear. Res.* 34, 1–25.

Gerfen, C. R. (1989). The neostriatal mosaic: striatal patch-matrix organization is related to cortical lamination. *Science* 246, 385–388.

Groh, A., de Kock, C. P., Wimmer, V. C., Sakmann, B., and Kuner, T. (2008). Driver or coincidence detector: modal switch of a corticothalamic giant synapse controlled by spontaneous activity and short-term depression. *J. Neurosci.* 28, 9652–9663.

Groh, A., Meyer, H. S., Schmidt, E. F., Heintz, N., Sakmann, B., and Krieger, P. (2010). Cell-type specific properties of pyramidal neurons in neocortex underlying a layout that is modifiable depending on the cortical area. *Cereb. Cortex* 20, 826–836.

Guillery, R. W., and Sherman, S. M. (2011). Branched thalamic afferents: what are the messages that they relay to the cortex? *Brain Res. Brain Res. Rev.* 66, 205–219.

Haidarliu, S., and Ahissar, E. (2001). Size gradients of barreloids in the rat thalamus. *J. Comp. Neurol.* 429, 372–387.

Haider, B., Duque, A., Hasenstaub, A. R., and McCormick, D. A. (2006). Neocortical network activity *in vivo* is generated through a dynamic balance of excitation and inhibition. *J. Neurosci.* 26, 4535–4545.

Hardingham, N. R., Read, J. C., Trevelyan, A. J., Nelson, J. C., Jack, J. J., and Bannister, N. J. (2010). Quantal analysis reveals a functional correlation between presynaptic and postsynaptic efficacy in excitatory connections from rat neocortex. *J. Neurosci.* 30, 1441–1451.

Hattox, A. M., and Nelson, S. B. (2007). Layer V neurons in mouse cortex projecting to different targets have distinct physiological properties. *J. Neurophysiol.* 98, 3330–3340.

Herkenham, M. (1980). Laminar organization of thalamic projections to the rat neocortex. *Science* 207, 532–535.

Hersch, S. M., and White, E. L. (1981). Thalamocortical synapses involving identified neurons in mouse primary somatosensory cortex: a terminal degeneration and golgi/EM study. *J. Comp. Neurol.* 195, 253–263.

Hevner, R. F., Daza, R. A., Rubenstein, J. L., Stunnenberg, H., Olavarria, J. F., and Englund, C. (2003). Beyond laminar fate: toward a molecular classification of cortical projection/pyramidal neurons. *Dev. Neurosci.* 25, 139–151.

Hoffer, Z. S., Arantes, H. B., Roth, R. L., and Alloway, K. D. (2005). Functional circuits mediating sensorimotor integration: quantitative comparisons of projections from rodent barrel cortex to primary motor cortex, neostriatum, superior colliculus, and the pons. *J. Comp. Neurol.* 488, 82–100.

Hoffer, Z. S., Hoover, J. E., and Alloway, K. D. (2003). Sensorimotor corticocortical projections from rat barrel cortex have an anisotropic organization that facilitates integration of inputs from whiskers in the same row. *J. Comp. Neurol.* 466, 525–544.

Holmgren, C., Harkany, T., Svennenfors, B., and Zilberter, Y. (2003). Pyramidal cell communication within local networks in layer 2/3 of rat neocortex. *J. Physiol.* 551, 139–153.

Hoogland, P. V., Welker, E., and van der Loos, H. (1987). Organization of the projections from barrel cortex to thalamus in mice studied with *Phaseolus vulgaris*-leucoagglutinin and HRP. *Exp. Brain Res.* 68, 73–87.

Hoogland, P. V., Wouterlood, F. G., Welker, E., and van der Loos, H. (1991). Ultrastructure of giant and small thalamic terminals of cortical origin: a study of the projections from the barrel cortex in mice using *Phaseolus vulgaris* leucoagglutinin (PHA-L). *Exp. Brain Res.* 87, 159–172.

Hooks, B. M., Hires, S. A., Zhang, Y. X., Huber, D., Petreanu, L., Svoboda, K., and Shepherd, G. M. (2011). Laminar analysis of excitatory local circuits in vibrissal motor and sensory cortical areas. *PLoS Biol.* 9:e1000572. doi: 10.1371/journal.pbio.1000572

Hoover, J. E., Hoffer, Z. S., and Alloway, K. D. (2003). Projections from primary somatosensory cortex to the neostriatum: the role of somatotopic continuity in corticostriatal convergence. *J. Neurophysiol.* 89, 1576–1587.

Horton, J. C., and Adams, D. L. (2005). The cortical column: a structure without a function. *Philos. Trans. R. Soc. Lond. B Biol. Sci.* 360, 837–862.

Hubel, D. H., and Wiesel, T. N. (1959). Receptive fields of single neurones in the cat's striate cortex. *J. Physiol.* 148, 574–591.

Hubel, D. H., and Wiesel, T. N. (1963). Shape and arrangement of columns in cat's striate cortex. *J. Physiol.* 165, 559–568.

Hübener, M., and Bolz, J. (1988). Morphology of identified projection neurons in layer 5 of rat visual cortex. *Neurosci. Lett.* 94, 76–81.

Hübener, M., Schwarz, C., and Bolz, J. (1990). Morphological types of projection neurons in layer 5 of cat visual cortex. *J. Comp. Neurol.* 301, 655–674.

Hutsler, J. J., Lee, D. G., and Porter, K. K. (2005). Comparative analysis of cortical layering and supragranular layer enlargement in rodent carnivore and primate species. *Brain Res.* 1052, 71–81.

Ito, M. (1988). Response properties and topography of vibrissa-sensitive VPM neurons in the rat. *J. Neurophysiol.* 60, 1181–1197.

Izraeli, R., and Porter, L. L. (1995). Vibrissal motor cortex in the rat: connections with the barrel field. *Exp. Brain Res.* 104, 41–54.

Jacquin, M. F., Wiegand, M. R., and Renehan, W. E. (1990). Structure-function relationships in rat brain stem subnucleus interpolaris. VIII. Cortical inputs. *J. Neurophysiol.* 64, 3–27.

Jensen, K. F., and Killackey, H. P. (1987). Terminal arbors of axons projecting to the somatosensory cortex of the adult rat. I. The

normal morphology of specific thalamocortical afferents. *J. Neurosci.* 7, 3529–3543.

Jones, E. G. (1984). "Laminar distribution of cortical efferent cells," in *Cerebral Cortex, Vol. 1, Cellular Components of the Cerebral Cortex,* eds A. Peters and E. G. Jones (New York, NY: Plenum Press), 521–533.

Kampa, B. M., Letzkus, J. J., and Stuart, G. J. (2006). Cortical feedforward networks for binding different streams of sensory information. *Nat. Neurosci.* 9, 1472–1473.

Killackey, H. P., and Sherman, S. M. (2003). Corticothalamic projections from the rat primary somatosensory cortex. *J. Neurosci.* 23, 7381–7384.

Kim, U., and Ebner, F. F. (1999). Barrels and septa: separate circuits in rat barrels field cortex. *J. Comp. Neurol.* 408, 489–505.

Koester, S. E., and O'Leary, D. D. (1992). Functional classes of cortical projection neurons develop dendritic distinctions by class-specific sculpting of an early common pattern. *J. Neurosci.* 12, 1382–1393.

Koralek, K. A., Jensen, K. F., and Killackey, H. P. (1988). Evidence for two complementary patterns of thalamic input to the rat somatosensory cortex. *Brain Res.* 463, 346–351.

Koralek, K. A., Olavarria, J., and Killackey, H. P. (1990). Areal and laminar organization of corticocortical projections in the rat somatosensory cortex. *J. Comp. Neurol.* 299, 133–150.

Kozloski, J., Hamzei-Sichani, F., and Yuste, R. (2001). Stereotyped position of local synaptic targets in neocortex. *Science* 293, 868–872.

Kremer, Y., Leger, J. F., Goodman, D., Brette, R., and Bourdieu, L. (2011). Late emergence of the vibrissa direction selectivity map in the rat barrel cortex. *J. Neurosci.* 31, 10689–10700.

Kumar, P., and Ohana, O. (2008). Inter- and intralaminar subcircuits of excitatory and inhibitory neurons in layer 6a of the rat barrel cortex. *J. Neurophysiol.* 100, 1909–1922.

Laaris, N., and Keller, A. (2002). Functional independence of layer IV barrels. *J. Neurophysiol.* 87, 1028–1034.

Land, P. W., Buffer, S. A. Jr., and Yaskosky, J. D. (1995). Barreloids in adult rat thalamus: three-dimensional architecture and relationship to somatosensory cortical barrels. *J. Comp. Neurol.* 355, 573–588.

Land, P. W., and Erickson, S. L. (2005). Subbarrel domains in rat somatosensory (S1) cortex. *J. Comp. Neurol.* 490, 414–426.

Larkum, M. E., and Zhu, J. J. (2002). Signaling of layer 1 and whisker-evoked Ca2+ and Na+ action potentials in distal and terminal dendrites of rat neocortical pyramidal neurons *in vitro* and *in vivo*. *J. Neurosci.* 22, 6991–7005.

Larkum, M. E., Zhu, J. J., and Sakmann, B. (1999). A new cellular mechanism for coupling inputs arriving at different cortical layers. *Nature* 398, 338–341.

Larsen, D. D., and Callaway, E. M. (2006). Development of layer-specific axonal arborizations in mouse primary somatosensory cortex. *J. Comp. Neurol.* 494, 398–414.

Larsen, D. D., Wickersham, I. R., and Callaway, E. M. (2007). Retrograde tracing with recombinant rabies virus reveals correlations between projection targets and dendritic architecture in layer 5 of mouse barrel cortex. *Front. Neural circuits* 1:5. doi: 10.3389/neuro.04.005.2007

Lavallée, P., Urbain, N., Dufresne, C., Bokor, H., Acsády, L., and Deschênes, M. (2005). Feedforward inhibitory control of sensory information in higher-order thalamic nuclei. *J. Neurosci.* 25, 7489–7498.

Le Bé, J. V., Silberberg, G., Wang, Y., and Markram, H. (2007). Morphological, electrophysiological, and synaptic properties of corticocallosal pyramidal cells in the neonatal rat neocortex. *Cereb. Cortex* 17, 2204–2213.

Leergaard, T. B., Alloway, K. D., Mutic, J. J., and Bjaalie, J. G. (2000). Three-dimensional topography of corticopontine projections from rat barrel cortex: correlations with corticostriatal organization. *J. Neurosci.* 20, 8474–8484.

Leergaard, T. B., Alloway, K. D., Pham, T. A., Bolstad, I., Hoffer, Z. S., Pettersen, C., and Bjaalie, J. G. (2004). Three-dimensional topography of corticopontine projections from rat sensorimotor cortex: comparisons with corticostriatal projections reveal diverse integrative organization. *J. Comp. Neurol.* 478, 306–322.

Lefort, S., Tomm, C., Floyd Sarria, J. C., and Petersen, C. C. (2009). The excitatory neuronal network of the C2 barrel column in mouse primary somatosensory cortex. *Neuron* 61, 301–316.

Legg, C. R., Mercier, B., and Glickstein, M. (1989). Corticopontine projection in the rat: the distribution of labelled cortical cells after large injections of horseradish peroxidase in the pontine nuclei. *J. Comp. Neurol.* 286, 427–441.

Li, L., Rema, V., and Ebner, F. F. (2005). Chronic suppression of activity in barrel field cortex downregulates sensory responses in contralateral barrel field cortex. *J. Neurophysiol.* 94, 3342–3356.

Liao, C. C., Chen, R. F., Lai, W. S., Lin, R. C., and Yen, C. T. (2010). Distribution of large terminal inputs from the primary and secondary somatosensory cortices to the dorsal thalamus in the rodent. *J. Comp. Neurol.* 518, 2592–2611.

Lorente de Nó, R. (1922). "La corteza cerebral de ratón (Primera contribución – La corteza acústica)," *Trabajos del Laboratorio de Investigaciones Biologicas de la Universidad de Madrid,* 20, 41–78.

Lorente de Nó, R. (1992). The cerebral cortex of the mouse (a first contribution–the "acoustic" cortex). *Somatosens. Mot. Res.* 9, 3–36.

Lübke, J., Egger, V., Sakmann, B., and Feldmeyer, D. (2000). Columnar organization of dendrites and axons of single and synaptically coupled excitatory spiny neurons in layer 4 of the rat barrel cortex. *J. Neurosci.* 20, 5300–5311.

Lübke, J., and Feldmeyer, D. (2007). Excitatory signal flow and connectivity in a cortical column: focus on barrel cortex. *Brain Struct. Funct.* 212, 3–17.

Lübke, J., Roth, A., Feldmeyer, D., and Sakmann, B. (2003). Morphometric analysis of the columnar innervation domain of neurons connecting layer 4 and layer 2/3 of juvenile rat barrel cortex. *Cereb. Cortex* 13, 1051–1063.

Lu, S. M., and Lin, R. C. (1993). Thalamic afferents of the rat barrel cortex: a light- and electron-microscopic study using *Phaseolus vulgaris* leucoagglutinin as an anterograde tracer. *Somatosens. Mot. Res.* 10, 1–16.

Ma, P. M. (1991). The barrelettes–architectonic vibrissal representations in the brainstem trigeminal complex of the mouse. I. Normal structural organization. *J. Comp. Neurol.* 309, 161–199.

Manns, I. D., Sakmann, B., and Brecht, M. (2004). Sub- and suprathreshold receptive field properties of pyramidal neurones in layers 5A and 5B of rat somatosensory barrel cortex. *J. Physiol.* 556, 601–622.

Mao, T., Kusefoglu, D., Hooks, B. M., Huber, D., Petreanu, L., and Svoboda, K. (2011). Long-range neuronal circuits underlying the interaction between sensory and motor cortex. *Neuron* 72, 111–123.

Marín-Padilla, M. (1978). Dual origin of the mammalian neocortex and evolution of the cortical plate. *Anat. Embryol. (Berl.)* 152, 109–126.

Markram, H., Lübke, J., Frotscher, M., Roth, A., and Sakmann, B. (1997). Physiology and anatomy of synaptic connections between thick tufted pyramidal neurones in the developing rat neocortex. *J. Physiol.* 500(Pt 2), 409–440.

Marx, M., Günter, R. H., Hucko, W., Radnikow, G., and Feldmeyer, D. (2012). Improved biocytin labeling and neuronal 3D reconstruction. *Nat. Protoc.* 7, 394–407.

Matyas, F., Sreenivasan, V., Marbach, F., Wacongne, C., Barsy, B., Mateo, C., Aronoff, R., and Petersen, C. C. (2010). Motor control by sensory cortex. *Science* 330, 1240–1243.

Mercer, A., West, D. C., Morris, O. T., Kirchhecker, S., Kerkhoff, J. E., and Thomson, A. M. (2005). Excitatory connections made by presynaptic cortico-cortical pyramidal cells in layer 6 of the neocortex. *Cereb. Cortex* 15, 1485–1496.

Meyer, H. S., Schwarz, D., Wimmer, V. C., Schmitt, A. C., Kerr, J. N., Sakmann, B., and Helmstaedter, M. (2011). Inhibitory interneurons in a cortical column form hot zones of inhibition in layers 2 and 5A. *Proc. Natl. Acad. Sci. U.S.A.* 108, 16807–16812.

Meyer, H. S., Wimmer, V. C., Hemberger, M., Bruno, R. M., de Kock, C. P., Frick, A., Sakmann, B., and Helmstaedter, M. (2010a). Cell type-specific thalamic innervation in a column of rat vibrissal cortex. *Cereb. Cortex* 20, 2287–2303.

Meyer, H. S., Wimmer, V. C., Oberlaender, M., de Kock, C. P., Sakmann, B., and Helmstaedter, M. (2010b). Number and laminar distribution of neurons in a thalamocortical projection column of rat vibrissal cortex. *Cereb. Cortex* 20, 2277–2286.

Miller, K. D., Pinto, D. J., and Simons, D. J. (2001). Processing in layer 4 of the neocortical circuit: new insights from visual and somatosensory cortex. *Curr. Opin. Neurobiol.* 11, 488–497.

Miller, M. W. (1988). Maturation of rat visual cortex: IV. The generation, migration, morphogenesis, and connectivity of atypically oriented pyramidal neurons. *J. Comp. Neurol.* 274, 387–405.

Minnery, B. S., Bruno, R. M., and Simons, D. J. (2003). Response transformation and receptive-field synthesis in the lemniscal trigeminothalamic circuit. *J. Neurophysiol.* 90, 1556–1570.

Mitchell, B. D., and Cauller, L. J. (2001). Corticocortical and thalamocortical projections to layer I of the frontal neocortex in rats. *Brain Res.* 921, 68–77.

Miyashita, E., Keller, A., and Asanuma, H. (1994). Input-output organization of the rat vibrissal motor cortex. *Exp. Brain Res.* 99, 223–232.

Molnár, Z., and Cheung, A. F. (2006). Towards the classification of subpopulations of layer V pyramidal projection neurons. *Neurosci. Res.* 55, 105–115.

Morishima, M., and Kawaguchi, Y. (2006). Recurrent connection patterns of corticostriatal pyramidal cells in frontal cortex. *J. Neurosci.* 26, 4394–4405.

Morishima, M., Morita, K., Kubota, Y., and Kawaguchi, Y. (2011). Highly differentiated projection-specific cortical subnetworks. *J. Neurosci.* 31, 10380–10391.

Mountcastle, V. B. (1957). Modality and topographic properties of single neurons of cat's somatic sensory cortex. *J. Neurophysiol.* 20, 408–434.

Mountcastle, V. B. (1997). The columnar organization of the neocortex. *Brain* 120(Pt 4), 701–722.

Mountcastle, V. B. (2003). Introduction. Computation in cortical columns. *Cereb. Cortex* 13, 2–4.

Nelson, S. B., Hempel, C., and Sugino, K. (2006). Probing the transcriptome of neuronal cell types. *Curr. Opin. Neurobiol.* 16, 571–576.

Oberlaender, M., Boudewijns, Z. S., Kleele, T., Mansvelder, H. D., Sakmann, B., and de Kock, C. P. (2011a). Three-dimensional axon morphologies of individual layer 5 neurons indicate cell type-specific intracortical pathways for whisker motion and touch. *Proc. Natl. Acad. Sci. U.S.A.* 108, 4188–4193.

Oberlaender, M., de Kock, C. P. J., Bruno, R. M., Ramirez, A., Meyer, H. S., Dercksen, V. J., Helmstaedter, M., and Sakmann, B. (2011b). Cell type-specific three-dimensional structure of thalamocortical circuits in a column of rat vibrissal cortex. *Cereb. Cortex*. doi: 10.1093/cercor/bhr317. [Epub ahead of print].

Ohno, S., Kuramoto, E., Furuta, T., Hioki, H., Tanaka, Y. R., Fujiyama, F., Sonomura, T., Uemura, M., Sugiyama, K., and Kaneko, T. (2011). A morphological analysis of thalamocortical axon fibers of rat posterior thalamic nuclei: a single neuron tracing study with viral vectors. *Cereb. Cortex*. doi: 10.1093/cercor/bhr356. [Epub ahead of print].

Olavarria, J., Van Sluyters, R. C., and Killackey, H. P. (1984). Evidence for the complementary organization of callosal and thalamic connections within rat somatosensory cortex. *Brain Res.* 291, 364–368.

Otsuka, T., and Kawaguchi, Y. (2011). Cell diversity and connection specificity between callosal projection neurons in the frontal cortex. *J. Neurosci.* 31, 3862–3870.

Pereira, A., Ribeiro, S., Wiest, M., Moore, L. C., Pantoja, J., Lin, S. C., and Nicolelis, M. A. (2007). Processing of tactile information by the hippocampus. *Proc. Natl. Acad. Sci. U.S.A.* 104, 18286–18291.

Perin, R., Berger, T. K., and Markram, H. (2011). A synaptic organizing principle for cortical neuronal groups. *Proc. Natl. Acad. Sci. U.S.A.* 108, 5419–5424.

Peschanski, M. (1984). Trigeminal afferents to the diencephalon in the rat. *Neuroscience* 12, 465–487.

Petersen, C. C., Hahn, T. T., Mehta, M., Grinvald, A., and Sakmann, B. (2003). Interaction of sensory responses with spontaneous depolarization in layer 2/3 barrel cortex. *Proc. Natl. Acad. Sci. U.S.A.* 100, 13638–13643.

Petersen, C. C., and Sakmann, B. (2000). The excitatory neuronal network of rat layer 4 barrel cortex. *J. Neurosci.* 20, 7579–7586.

Petersen, C. C., and Sakmann, B. (2001). Functionally independent columns of rat somatosensory barrel cortex revealed with voltage-sensitive dye imaging. *J. Neurosci.* 21, 8435–8446.

Petreanu, L., Huber, D., Sobczyk, A., and Svoboda, K. (2007). Channelrhodopsin-2-assisted circuit mapping of long-range callosal projections. *Nat. Neurosci.* 10, 663–668.

Petreanu, L., Mao, T., Sternson, S. M., and Svoboda, K. (2009). The subcellular organization of neocortical excitatory connections. *Nature* 457, 1142–1145.

Pichon, F., Nikonenko, I., Kraftsik, R., and Welker, E. (2012). Intracortical connectivity of layer VI pyramidal neurons in the somatosensory cortex of normal and barrelless mice. *Eur. J. Neurosci.* 35, 855–869.

Pierret, T., Lavallée, P., and Deschênes, M. (2000). Parallel streams for the relay of vibrissal information through thalamic barreloids. *J. Neurosci.* 20, 7455–7462.

Pinault, D., and Deschênes, M. (1998). Projection and innervation patterns of individual thalamic reticular axons in the thalamus of the adult rat: a three-dimensional, graphic, and morphometric analysis. *J. Comp. Neurol.* 391, 180–203.

Porter, J. T., Johnson, C. K., and Agmon, A. (2001). Diverse types of interneurons generate thalamus-evoked feedforward inhibition in the mouse barrel cortex. *J. Neurosci.* 21, 2699–2710.

Porter, L. L., and White, E. L. (1983). Afferent and efferent pathways of the vibrissal region of primary motor cortex in the mouse. *J. Comp. Neurol.* 214, 279–289.

Qi, G., and Feldmeyer, D. (2010). Cell type-specific excitatory synaptic connections from layer 4 to layer 6A in rat barrel cortex. *Acta Physiol.* 198, 90.

Radnikow, G., Lübke, J. R., and Feldmeyer, D. (2010). Developmental changes in synaptic transmission between layer 4 spiny neurons in rat barrel cortex. *Acta Physiol.* 198, 179.

Ramón y Cajal, S., (1904). *Textura Del Sistema Nervioso Del Hombre y De Los Vertebrados*. Madrid: Imprenta de Nicolás Moya.

Ren, J. Q., Aika, Y., Heizmann, C. W., and Kosaka, T. (1992). Quantitative analysis of neurons and glial cells in the rat somatosensory cortex, with special reference to GABAergic neurons and parvalbumin-containing neurons. *Exp. Brain Res.* 92, 1–14.

Reyes, A., and Sakmann, B. (1999). Developmental switch in the short-term modification of unitary EPSPs evoked in layer 2/3 and layer 5 pyramidal neurons of rat neocortex. *J. Neurosci.* 19, 3827–3835.

Rockland, K. S. (2010). Five points on columns. *Front. Neuroanat.* 4:22. doi: 10.3389/fnana.2010.00022

Rubio-Garrido, P., Pérez-de-Manzo, F., Porrero, C., Galazo, M. J., and Clascá, F. (2009). Thalamic input to distal apical dendrites in neocortical layer 1 is massive and highly convergent. *Cereb. Cortex* 19, 2380–2395.

Sarid, L., Bruno, R., Sakmann, B., Segev, I., and Feldmeyer, D. (2007). Modeling a layer 4-to-layer 2/3 module of a single column in rat neocortex: interweaving *in vitro* and *in vivo* experimental observations. *Proc. Natl. Acad. Sci. U.S.A.* 104, 16353–16358.

Sato, T. R., and Svoboda, K. (2010). The functional properties of barrel cortex neurons projecting to the primary motor cortex. *J. Neurosci.* 30, 4256–4260.

Scanziani, M., and Häusser, M. (2009). Electrophysiology in the age of light. *Nature* 461, 930–939.

Schubert, D., Kötter, R., Luhmann, H. J., and Staiger, J. F. (2006). Morphology, electrophysiology and functional input connectivity of pyramidal neurons characterizes a genuine layer Va in the primary somatosensory cortex. *Cereb. Cortex* 16, 223–236.

Schubert, D., Kötter, R., Zilles, K., Luhmann, H. J., and Staiger, J. F. (2003). Cell type-specific circuits of cortical layer IV spiny neurons. *J. Neurosci.* 23, 2961–2970.

Schubert, D., Staiger, J. F., Cho, N., Kötter, R., Zilles, K., and Luhmann, H. J. (2001). Layer-specific intracolumnar and transcolumnar functional connectivity of layer V pyramidal cells in rat barrel cortex. *J. Neurosci.* 21, 3580–3592.

Schwarz, C., and Möck, M. (2001). Spatial arrangement of cerebropontine terminals. *J. Comp. Neurol.* 435, 418–432.

Senft, S. L., and Woolsey, T. A. (1991). Growth of thalamic afferents into mouse barrel cortex. *Cereb. Cortex* 1, 308–335.

Shepherd, G. M., Pologruto, T. A., and Svoboda, K. (2003). Circuit analysis of experience-dependent plasticity in the developing rat barrel cortex. *Neuron* 38, 277–289.

Shepherd, G. M., Stepanyants, A., Bureau, I., Chklovskii, D., and Svoboda, K. (2005). Geometric and functional organization of cortical circuits. *Nat. Neurosci.* 8, 782–790.

Shepherd, G. M., and Svoboda, K. (2005). Laminar and columnar organization of ascending excitatory projections to layer 2/3 pyramidal neurons in rat barrel cortex. *J. Neurosci.* 25, 5670–5679.

Sherman, S. M. (2005). Thalamic relays and cortical functioning. *Prog. Brain Res.* 149, 107–126.

Shipp, S. (2007). Structure and function of the cerebral cortex. *Curr. Biol.* 17, R443–R449.

Silver, R. A., Lübke, J., Sakmann, B., and Feldmeyer, D. (2003). High-probability uniquantal transmission at excitatory synapses in barrel cortex. *Science* 302, 1981–1984.

Simons, D. J., and Carvell, G. E. (1989). Thalamocortical response transformation in the rat vibrissa/barrel system. *J. Neurophysiol.* 61, 311–330.

Smith, J. B., and Alloway, K. D. (2010). Functional specificity of claustrum connections in the rat: interhemispheric communication between specific parts of motor cortex. *J. Neurosci.* 30, 16832–16844.

Song, S., Sjöström, P. J., Reigl, M., Nelson, S., and Chklovskii, D. B. (2005). Highly nonrandom features of synaptic connectivity in local cortical circuits. *PLoS Biol.* 3:e68. doi: 10.1371/journal.pbio.0030068

Spreafico, R., Barbaresi, P., Weinberg, R. J., and Rustioni, A. (1987).

SII-projecting neurons in the rat thalamus: a single- and double-retrograde-tracing study. *Somatosens. Res.* 4, 359–375.

Staiger, J. F., Flagmeyer, I., Schubert, D., Zilles, K., Kötter, R., and Luhmann, H. J. (2004). Functional diversity of layer IV spiny neurons in rat somatosensory cortex: quantitative morphology of electrophysiologically characterized and biocytin labeled cells. *Cereb. Cortex* 14, 690–701.

Steriade, M., McCormick, D. A., and Sejnowski, T. J. (1993). Thalamocortical oscillations in the sleeping and aroused brain. *Science* 262, 679–685.

Tanaka, Y. R., Tanaka, Y. H., Konno, M., Fujiyama, F., Sonomura, T., Okamoto-Furuta, K., Kameda, H., Hioki, H., Furuta, T., Nakamura, K. C., and Kaneko, T. (2011). Local connections of excitatory neurons to corticothalamic neurons in the rat barrel cortex. *J. Neurosci.* 31, 18223–18236.

Theyel, B. B., Llano, D. A., and Sherman, S. M. (2010). The corticothalamocortical circuit drives higher-order cortex in the mouse. *Nat. Neurosci.* 13, 84–88.

Thomson, A. M. (2010). Neocortical layer 6, a review. *Front. Neuroanat.* 4:13. doi: 10.3389/fnana.2010.00013

Tömböl, T. (1984). "Layer VI cells," in *Cerebral Cortex*, eds A. Peters and E. G. Jones (New York, London: Plenum Press), 479–519.

Tömböl, T., Hajdu, F., and Somogyi, G. (1975). Identification of the Golgi picture of the layer VI corticogeniculate projection neurons. *Exp. Brain Res.* 24, 107–110.

Urbain, N., and Deschênes, M. (2007). A new thalamic pathway of vibrissal information modulated by the motor cortex. *J. Neurosci.* 27, 12407–12412.

Valverde, F., Facal-Valverde, M. V., Santacana, M., and Heredia, M. (1989). Development and differentiation of early generated cells of sublayer VIb in the somatosensory cortex of the rat: a correlated Golgi and autoradiographic study. *J. Comp. Neurol.* 290, 118–140.

Varga, C., Sik, A., Lavallée, P., and Deschênes, M. (2002). Dendroarchitecture of relay cells in thalamic barreloids: a substrate for cross-whisker modulation. *J. Neurosci.* 22, 6186–6194.

Veinante, P., and Deschênes, M. (1999). Single- and multi-whisker channels in the ascending projections from the principal trigeminal nucleus in the rat. *J. Neurosci.* 19, 5085–5095.

Veinante, P., and Deschênes, M. (2003). Single-cell study of motor cortex projections to the barrel field in rats. *J. Comp. Neurol.* 464, 98–103.

Veinante, P., Jacquin, M. F., and Deschênes, M. (2000a). Thalamic projections from the whisker-sensitive regions of the spinal trigeminal complex in the rat. *J. Comp. Neurol.* 420, 233–243.

Veinante, P., Lavallée, P., and Deschênes, M. (2000b). Corticothalamic projections from layer 5 of the vibrissal barrel cortex in the rat. *J. Comp. Neurol.* 424, 197–204.

Waters, J., and Helmchen, F. (2006). Background synaptic activity is sparse in neocortex. *J. Neurosci.* 26, 8267–8277.

Welker, C., and Woolsey, T. A. (1974). Structure of layer IV in the somatosensory neocortex of the rat: description and comparison with the mouse. *J. Comp. Neurol.* 158, 437–453.

Welker, E., Hoogland, P. V., and Van der Loos, H. (1988). Organization of feedback and feedforward projections of the barrel cortex: a PHA-L study in the mouse. *Exp. Brain Res.* 73, 411–435.

White, E. L., Benshalom, G., and Hersch, S. M. (1984). Thalamocortical and other synapses involving nonspiny multipolar cells of mouse SmI cortex. *J. Comp. Neurol.* 229, 311–320.

White, E. L., and Czeiger, D. (1991). Synapses made by axons of callosal projection neurons in mouse somatosensory cortex: emphasis on intrinsic connections. *J. Comp. Neurol.* 303, 233–244.

White, E. L., and DeAmicis, R. A. (1977). Afferent and efferent projections of the region in mouse SmI cortex which contains the posteromedial barrel subfield. *J. Comp. Neurol.* 175, 455–482.

White, E. L., and Rock, M. P. (1979). Distribution of thalamic input to different dendrites of a spiny stellate cell in mouse sensorimotor cortex. *Neurosci. Lett.* 15, 115–119.

Williams, M. N., Zahm, D. S., and Jacquin, M. F. (1994). Differential foci and synaptic organization of the principal and spinal trigeminal projections to the thalamus in the rat. *Eur. J. Neurosci.* 6, 429–453.

Wimmer, V. C., Bruno, R. M., de Kock, C. P., Kuner, T., and Sakmann, B. (2010). Dimensions of a projection column and architecture of VPM and POm Axons in rat vibrissal cortex. *Cereb. Cortex* 20, 2265–2276.

Wise, S. P., and Jones, E. G. (1977). Somatotopic and columnar organization in the corticotectal projection of the rat somatic sensory cortex. *Brain Res.* 133, 223–235.

Woolsey, T. A., Dierker, and M. L., Wann, D. F. (1975a). Mouse SmI cortex: qualitative and quantitative classification of golgi-impregnated barrel neurons. *Proc. Natl. Acad. Sci. U.S.A.* 72, 2165–2169.

Woolsey, T. A., Welker, C., and Schwartz, R. H. (1975b). Comparative anatomical studies of the SmI face cortex with special reference to the occurrence of "barrels" in layer IV. *J. Comp. Neurol.* 164, 79–94.

Woolsey, T. A., and Van der Loos, H. (1970). The structural organization of layer IV in the somatosensory region (SI) of mouse cerebral cortex. The description of a cortical field composed of discrete cytoarchitectonic units. *Brain Res.* 17, 205–242.

Wright, A. K., Norrie, L., Ingham, C. A., Hutton, E. A., and Arbuthnott, G. W. (1999). Double anterograde tracing of outputs from adjacent "barrel columns" of rat somatosensory cortex. Neostriatal projection patterns and terminal ultrastructure. *Neuroscience* 88, 119–133.

Yu, C., Derdikman, D., Haidarliu, S., and Ahissar, E. (2006). Parallel thalamic pathways for whisking and touch signals in the rat. *PLoS Biol.* 4:e124. doi: 10.1371/journal.pbio.0040124

Zhang, F., Aravanis, A. M., Adamantidis, A., de Lecea, L., and Deisseroth, K. (2007). Circuit-breakers: optical technologies for probing neural signals and systems. *Nat. Rev. Neurosci.* 8, 577–581.

Zhang, Z. W., and Deschênes, M. (1997). Intracortical axonal projections of lamina VI cells of the primary somatosensory cortex in the rat: a single-cell labeling study. *J. Neurosci.* 17, 6365–6379.

Zhang, Z. W., and Deschênes, M. (1998). Projections to layer VI of the posteromedial barrel field in the rat: a reappraisal of the role of corticothalamic pathways. *Cereb. Cortex* 8, 428–436.

Zhu, Y., and Zhu, J. J. (2004). Rapid arrival and integration of ascending sensory information in layer 1 nonpyramidal neurons and tuft dendrites of layer 5 pyramidal neurons of the neocortex. *J. Neurosci.* 24, 1272–1279.

Conflict of Interest Statement: The author declares that the research was conducted in the absence of any commercial or financial relationships that could be construed as a potential conflict of interest.

Received: 02 February 2012; accepted: 15 June 2012; published online: 11 July 2012.

*Citation: Feldmeyer D (2012) Excitatory neuronal connectivity in the barrel cortex. Front. Neuroanat. **6**:24. doi: 10.3389/fnana.2012.00024*

frontiers in
NEUROANATOMY

REVIEW ARTICLE
published: 10 January 2012
doi: 10.3389/fnana.2011.00069

Small-scale module of the rat granular retrosplenial cortex: an example of the minicolumn-like structure of the cerebral cortex

Noritaka Ichinohe*

Department of Ultrastructural Research, National Institute of Neuroscience, National Center of Neurology and Psychiatry, Kodaira, Tokyo, Japan

Edited by:
Zoltan F. Kisvarday, University of Debrecen, Hungary

Reviewed by:
Antonio Pereira, Federal University of Rio Grande do Norte, Brazil
Toshio Terashima, Kobe University School of Medicine, Japan

****Correspondence:***
Noritaka Ichinohe, Department of Ultrastructural Research, National Institute of Neuroscience, National Center of Neurology and Psychiatry, 4-1-1 Ogawa-Higashi, Kodaira, Tokyo 187-8502, Japan.
e-mail: nichino@ncnp.go.jp

Structures associated with the small-scale module called "minicolumn" can be observed frequently in the cerebral cortex. However, the description of functional characteristics remains obscure. A significant confounding factor is the marked variability both in the definition of a minicolumn and in the diagnostic markers for identifying a minicolumn (see for review, Jones, 2000; DeFelipe et al., 2002; Rockland and Ichinohe, 2004). Within a minicolumn, cell columns are easily visualized by conventional Nissl staining. Dendritic bundles were first discovered with Golgi methods, but are more easily seen with microtubule-associated protein 2 immunohistochemistry. Myelinated axon bundles can be seen by Tau immunohistochemistry or myelin staining. Axon bundles of double bouquet cell can be seen by calbindin immunohistochemistry. The spatial interrelationship among these morphological elements is more complex than expected and is neither clear nor unanimously agreed upon. In this review, I would like to focus first on the minicolumnar structure found in layers 1 and 2 of the rat granular retrosplenial cortex. This modular structure was first discovered as a combination of prominent apical dendritic bundles from layer 2 pyramidal neurons and spatially matched thalamocortical patchy inputs (Wyss et al., 1990). Further examination showed more intricate components of this modular structure, which will be reviewed in this paper. Second, the postnatal development of this structure and potential molecular players for its formation will be reviewed. Thirdly, I will discuss how this modular organization is transformed in mutant rodents with a disorganized layer structure in the cerebral cortex (i.e., reeler mouse and shaking rat Kawasaki). Lastly, the potential significance of this type of module will be discussed.

Keywords: cortical modular organization, dendritic bundle, input and recipient matching, thalamocortical, cortico-cortical

INTRODUCTION

Morphologic small-scale modules or "minicolumn" structures can be observed frequently in the cerebral cortex. Functional minicolumns have also been identified, but the relationship between morphologic and functional minicolumns is ambiguous. Although morphologic minicolumn structures can be observed frequently, there is a marked variability in the definition of minicolumns, as well as in the diagnostic markers used for identifying these minicolumns (for review see Jones, 2000; DeFelipe et al., 2002; Rockland and Ichinohe, 2004). For example, the cell column is visualized by conventional Nissl staining. Dendritic bundles were first discovered using Golgi methods, but these structures can today be more easily seen using microtubule-associated protein 2 (MAP2) immunohistochemistry. Myelinated axon bundles can be visualized using Tau immunohistochemistry or conventional myelin staining, and axon bundles of double bouquet cell can be seen using calbindin immunohistochemistry. The spatial interrelationship between these differently identified morphologic minicolumns is more complex than originally expected, and is neither clear nor unanimously defined.

In this review, I will focus on a well-examined small module exiting in layers 1 and 2 of the rat granular retrosplenial (GRS) cortex. This modular structure was first described as a module consisting of a combination of prominent apical dendritic bundles from layer 2 pyramidal neurons and thalamocortical patchy inputs, which are spatially matched with the dendritic bundles (Wyss et al., 1990). Further examination showed more intricate components of this modular structure, which will be reviewed first in this paper. Second, the postnatal development of this structure and potential molecular mechanisms underlying the formation of this module will be reviewed. Thirdly, I will describe the way in which this modular organization in wild-type rodents is transformed in mutant rodents, which have a disorganized layer structure in the cerebral cortex (i.e., the reeler mouse and shaking rat Kawasaki, SRK). Lastly, the potential significance of this type of module will be discussed.

STRUCTURAL AND CHEMICAL ORGANIZATION OF MODULAR STRUCTURES IN LAYERS 1 AND 2 OF THE ADULT RAT GRS

The modular GRS organization was first discovered by Wyss et al. (1990) by injecting the retrograde tracer Fluoro-Gold into the contralateral rat GRS. The well-filled dendrites of callosally projecting layer 2 pyramidal neurons were found to group together in discrete bundles, as they ascend toward the pial surface (**Figure 1**).

Following this initial discovery, these prominent dendritic bundles have been demonstrated by several other methods. Most recently, molecular techniques have been used for visualizing fluorescent protein-filled layer 2 pyramidal neurons (**Figure 2A**; Miyashita et al., 2010; Zgraggen et al., 2011). As shown in **Figure 1**, the dendritic bundles in layer 1b/c are tighter than those in other layers, with a reported width of 30–100 μm and a distance between bundles of approximately 30–200 μm (Wyss et al., 1990; Ichinohe and Rockland, 2002). Near the layer 1b/1a interface, the dendritic tufts diverge and spread out in layer 1a to occupy the entire width of the layer (**Figure 2A**). The extension range of these tufts is about the same range as the distance between dendritic bundles (i.e., 30–200 μm; Wyss et al., 1990; Ichinohe and Rockland, 2002).

Immunohistofluorescence for MAP2 has been a convenient method for visualizing these dendritic modules (**Figure 2B**; Ichinohe and Rockland, 2002; Ichinohe et al., 2003b; Miró-Bernié et al., 2006). Using double/triple-immunofluorescence with a combination of appropriate antibodies, including antibodies against MAP2, the spatial relationship between dendritic modules and other structures labeled by the different antibodies can be easily examined (summarized in **Figure 1**). One interesting example is that double-immunofluorescence for MAP2 and parvalbumin (PV), a marker for a subpopulation of GABAergic neurons, reveals that PV-positive dendrites co-localize with apical dendritic bundles (**Figures 1** and **2B–D**). This intricate structure may be related to feedforward inhibition, as characterized by electrophysiologic studies in other thalamocortical systems (Swadlow and Gusev, 2000). That is, these PV-positive neurons, activated by thalamic inputs, may inhibit layer 2 pyramidal neurons receiving the same thalamic inputs. Another possibility is

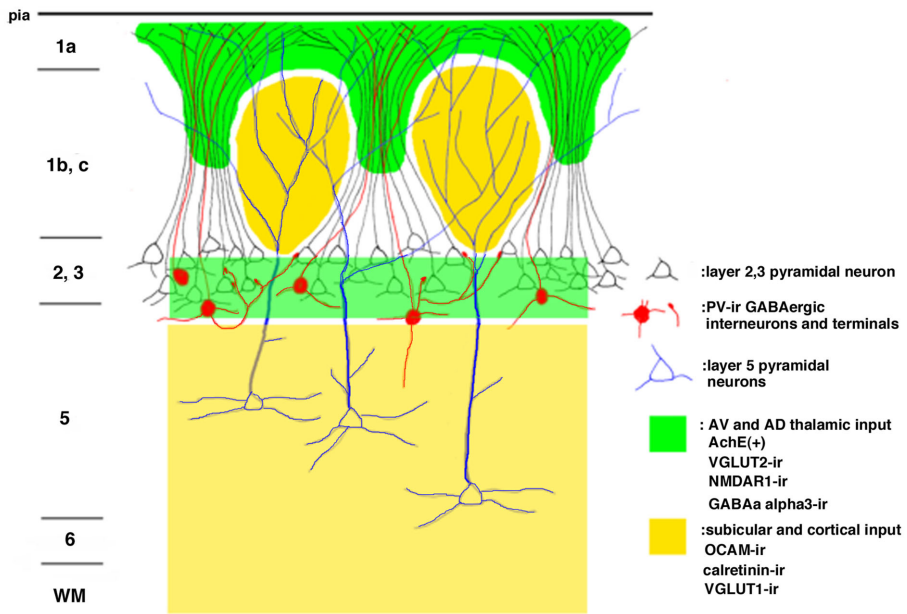

FIGURE 1 | Schematic drawing of the modular organization of the layer 1 granular retrosplenial cortex (GRS). Arabic numbers represent layer numbers. ir, immunoreactive.

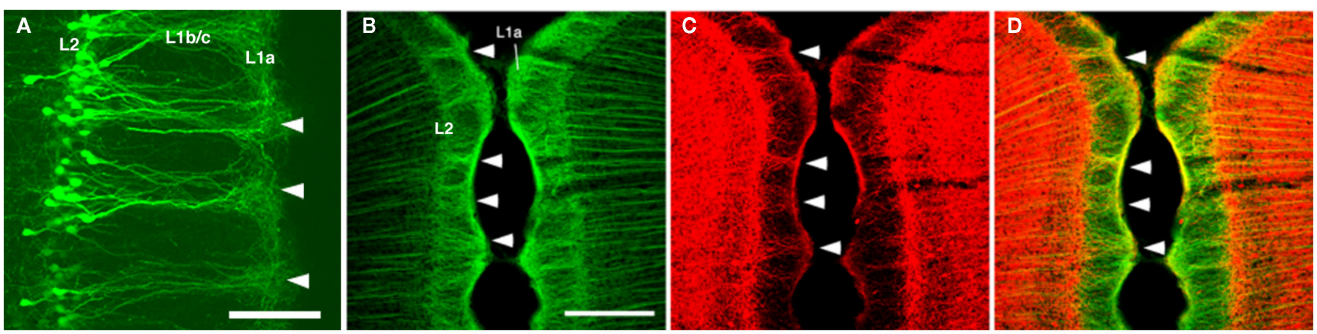

FIGURE 2 | (A) Dendritic bundles in layer 1 [postnatal day (P) 10], visualized by electroporation of enhanced green fluorescence protein (EGFP) at embryonic day (E) 18. **(B–D)** Confocal micrographs of layer 1 of the rat GRS stained by double-immunofluorescence for microtubule-associated protein 2 (MAP2; green) and parvalbumin (PV; red). Coronal sections. Scale bar: **(A)**, 50 μm; **(B–D)**, 200 μm.

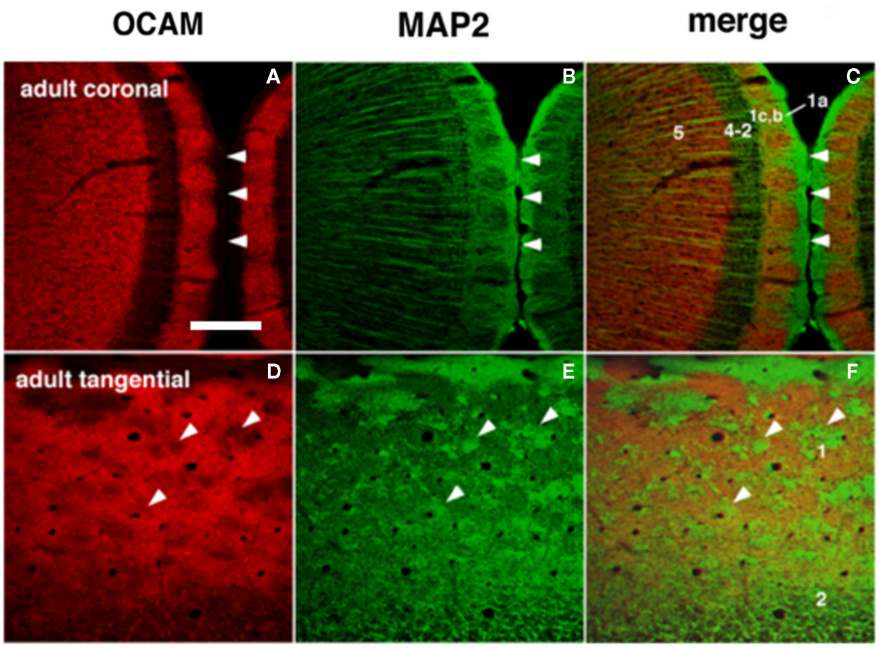

FIGURE 3 | Dendritic modules in layer 1 are visualized by OCAM-immunoreactive (ir) and MAP2-ir in adults. The right column shows merged images where patches of OCAM-ir and MAP2-ir are seen to interdigitate. **(A–C)** Coronal sections. **(D–F)** Semi-tangential sections. Arrowheads point to corresponding locations in two sets consisting of three figures **(A–F)**. Arabic numbers indicate layers. Scale bar: 200 μm.

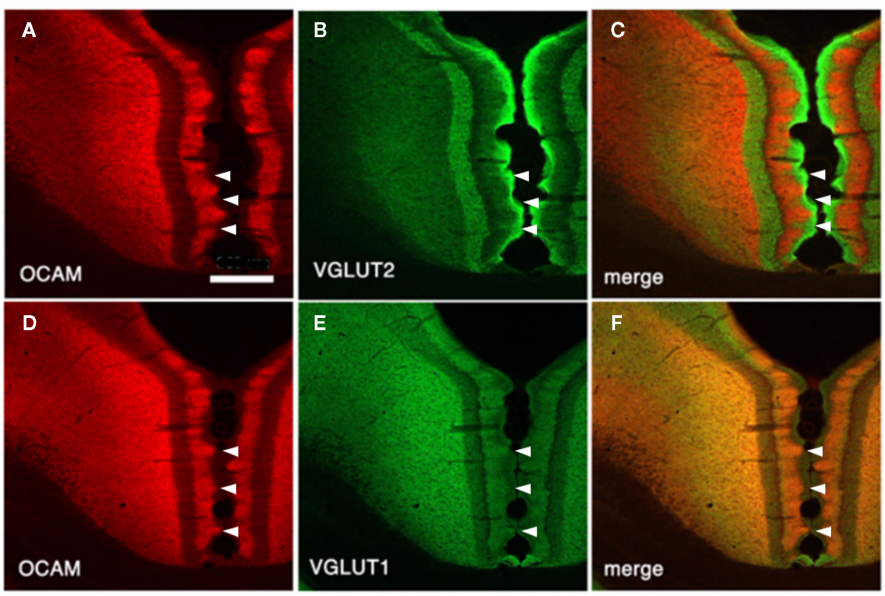

FIGURE 4 | Architectonics of the rat GRS, visualized by immunohistochemistry for OCAM and vesicular glutamate transporter 1 (VGLUT2; presumptive thalamocortical terminations) or VGLUT1 (presumptive corticocortical terminations). (A–C) Coronal sections reacted for OCAM and VGLUT2. OCAM-ir in the wild-type rat **(A)** is bistratified, with one superficial band in layers 1b and c and another, deeper band in layers 5 and 6. Note the notch-like appearance of layer 1. Similarly, VGLUT2 concentrates are seen in two bands, but these correspond to layer 1a and layers 3 and 4 **(B)**. Double-immunofluorescence for OCAM and VGLUT2 directly demonstrates this complementary relationship **(C)**. Layer 2 has low levels of both OCAM and VGLUT2. **(D–F)** Coronal sections reacted for OCAM and VGLUT2. Scale bar: 300 μm.

that, since some PV-positive neurons have laterally widespread axonal fields (Kisvárday et al., 2002), these PV-positive neurons can inhibit intricate combinations of pyramidal neurons within different modules, which receive thalamic inputs different from inputs

to these PV-positive interneurons. This potential organization may work as a substrate for lateral inhibition between modules.

Immunohistochemistry using OCAM, a cell adhesion molecule, has revealed patchy structures in layer 1 of the GRS (**Figures 1** and **3A,D**). The patches of OCAM-positive and MAP2-positive areas can be seen to interdigitate (**Figure 3**). To identify OCAM-positive structures in layer 1, electron microscopy was used. This shows that OCAM-positive structures are composed mostly of dendrites (Ichinohe et al., 2003b). *In situ* hybridization for the *OCAM* gene shows that expression of the gene occurs in layer 5/6 pyramidal neurons (Ichinohe et al., 2008). Thus, the OCAM-positive patches in layer 1 appear to constitute an aggregation of apical dendritic tufts of layer 5 pyramidal neurons (**Figure 1**). OCAM is associated with the fasciculation of subsets of olfactory and vomeronasal axons (Yoshihara et al., 1997) and the accurate segregation of odorant receptor-specific axons (Alenius and Bohm, 2003). Moreover, recent studies in olfactory glomeruli have shown that OCAM is required for establishing or maintaining the compartmental organization and segregation of axodendritic and dendrodendritic synapses within glomeruli (Walz et al., 2006), and is important for the synchrony of mitral cell activity in olfactory glomeruli (Borisovska et al., 2011). In the dendritic module in GRS layer 1, OCAM may be also involved in the maintenance of compartmental organization (i.e., segregation of MAP2-positive dendritic bundles from layer 2 pyramidal neurons and the complementary aggregation of OCAM-positive apical dendrites from layer 5 pyramidal neurons).

Vesicular glutamate transporter 1 (VGLUT1) and VGLUT2 are convenient markers for corticocortical and thalamocortical terminals in the cerebral cortex, respectively (Fujiyama et al., 2001). Double-immunofluorescence for OCAM and VGLUT1 or VGLUT2 has shown that OCAM- and VGLUT1-positive modules are co-localized and that OCAM- and VGLUT2-positive modules are interdigitated in layer 1 (**Figures 1** and **4**). These results underscore the notion that OCAM-negative (i.e., MAP2-positive) apical dendritic bundles from layer 2 pyramidal neurons are targeted by thalamocortical terminals and that OCAM-positive aggregations of apical dendritic tufts of layer 5 pyramidal neurons are targeted by corticocortical inputs (Shibata, 1993; Van Groen and Wyss, 1995, 2003; Miró-Bernié et al., 2006; Ichinohe et al., 2008). These results indicate that not only different types of dendrites but also different kinds of axon terminals are aggregated and segregated in this module. That is, specific combinations of dendritic modules ("recipients") and axon terminal modules ("inputs") are co-localized. This type of co-localization of recipient and input modules has previously been described in other cortical areas and layers (e.g., the rodent barrel cortex and the honeycomb-like structure at the border of layers 1 and 2 of the cerebral cortex; Datwani et al., 2002; Ichinohe et al., 2003a; Ichinohe and Rockland, 2004).

POSTNATAL DEVELOPMENT OF THE MODULAR ORGANIZATION IN THE GRS

The developmental time-course of the dendritic bundles in the GRS has been investigated using immunohistochemistry for MAP2 and glutamate receptor subunits 2/3 (GluR2/3; Ichinohe et al., 2003b). Bundles in layer 1 are apparent as early as postnatal day (P) 5, first using GluR2/3 immunohistochemistry and then, from P14, using MAP2 immunohistochemistry. As a step toward understanding the mechanisms underlying dendritic aggregation, we further investigated the ontogeny of expression of the cell adhesion molecule OCAM. OCAM exhibits a patchy distribution in layer 1 from P3 to adulthood, and the regions of weak OCAM immunoreactivity selectively correspond to the dendritic bundles (using GluR2/3 and MAP2 immunohistochemistry). The periodic geometry of OCAM-positive regions, the time-course of their appearance, and their distinct localization, complementary to the bundles, support the possibility that OCAM significantly contributes to the establishment and maintenance of dendritic modules. More specifically, the interdigitating relationship between regions of high OCAM immunoreactivity and the dendritic bundles in layer 1 suggests that OCAM may have a repellent influence on the formation of these bundles (see also above section).

In order to identify molecules other than OCAM that are involved in the formation of the GRS layer 1 bundles from layer 2 pyramidal neurons, microarray techniques have been used (Miyashita et al., 2010). Several genes, including that for *neurotrophin-3* (*NT-3*), have been found to be highly and specifically expressed in GRS layer 2 at P3 versus P12 (i.e., before and after bundle formation). Specificity was inferred by comparisons with GRS layer 5 at P3 and with barrel cortex layer 2 at P3. In barrel cortex (with low *NT-3* expression), layer 2 pyramidal neurons do not form prominent apical dendritic bundles. To examine whether NT-3-mediated events are causally involved in bundle formation, we used *in utero* electroporation to overexpress *NT-3* in other cortical areas. This overexpression succeeded in producing prominent bundles of dendrites originating from layer 2 neurons in the barrel field cortex, where layer 2 bundles are normally absent (**Figure 5**). The controlled ectopic induction of dendritic bundles identifies a new role for NT-3 and a new *in vivo* model for investigating dendritic bundles and their formation.

TRANSFORMATION OF THE GRS ARCHITECTURE FROM WILD-TYPE RODENTS TO MUTANT RODENTS

To further investigate the distinctive compartmental organization in the GRS, we examined reelin-deficient mutant rodents; namely,

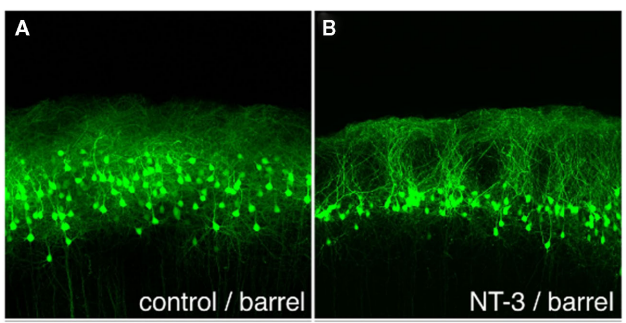

FIGURE 5 | Ectopically expressed neurotrophin-3 (NT-3) induces dendritic bundles in neocortical layer 1. (A) EGFP-expressing layer 2 pyramidal neurons at P20, after electroporation of *EGFP* alone at E18. Note the uniform distribution of cells and dendrites, without bundles. **(B)** Electroporation of *EGFP* and *NT-3* at E18 induces distinct dendritic bundles in the barrel cortex. Scale bar: 100 μm.

the reeler mouse and SRK. In these animals, the normal GRS lamination is conspicuously disrupted, and dendrites are mal-positioned (Lambert de Rouvroit and Goffinet, 1998; Kikkawa et al., 2003). To understand these abnormalities in more detailed level, it is necessary to examine how the highly organized laminar and modular architecture of the GRS in the wild-type rodent is transformed in these mutant rodents (Ichinohe et al., 2008).

In both the SRK and reeler GRS, immunohistochemistry for OCAM revealed a patch and matrix-like mosaic, with large OCAM-negative patches, in the middle of the cortical thickness, embedded in an OCAM-positive matrix (**Figure 6**). Steindler et al. (1994) also reported a similar patch-matrix pattern in the reeler visual cortex using acetylcholinesterase staining; however, the visual cortex described in their study may actually have been the GRS, as discussed by Ichinohe et al. (2008). It is difficult to conclude that the patch-matrix organization in mutant rodents is comparable to the micromodularity of layer 1 in wild-type rodents. Nevertheless, it may be significant that the discontinuous appearance of both features is strikingly similar between mutant and wild-type rodents. Moreover, the thalamic and cortical afferents in mutant rodents maintain the same relationship in the patch-matrix configuration as in wild-type rodents (**Figure 4**); namely, OCAM-positive areas match VGLUT1 (corticocortical input)-rich areas and OCAM-negative areas match VGLUT2 (thalamocortical input)-rich areas. Further, by filling neurons with Lucifer Yellow in fixed slices of the reeler GRS, we ascertained that these neurons can be grouped into two populations, with dendrites showing preference to either OCAM-negative patches (**Figure 7A**) or the OCAM-positive matrix (**Figures 7B–E**; Ichinohe et al., 2008). From additional *in situ* hybridization and electron microscopy results, we conclude that the OCAM-positive matrix in mutant rodents is filled with aggregated dendrites of neurons, comparable to layer 5 neurons in wild-type, and OCMA-negative patch in mutant rodents with aggregated dendrites of layer 2 neurons. Thus, even in the disrupted laminar cortex of the reeler mouse and SRK, OCAM may exert dendritic population-dependent homophilic or repellent effects. Further, these results suggest that, even though layer formation (and subsequently the position of the cell bodies) is disorganized in mutant rodents, recipient dendrites, and specific inputs aggregate appropriately and probably maintain proper synaptic connectivity, sufficient for maintaining relatively normal cortical function in these mutant animals (Simmons and Pearlman, 1983).

POTENTIAL SIGNIFICANCE OF GRS SMALL-SCALE MODULAR ORGANIZATION

The GRS in rats is implicated in a wide range of behaviors, including visual and vestibular integration, path integration, and spatial

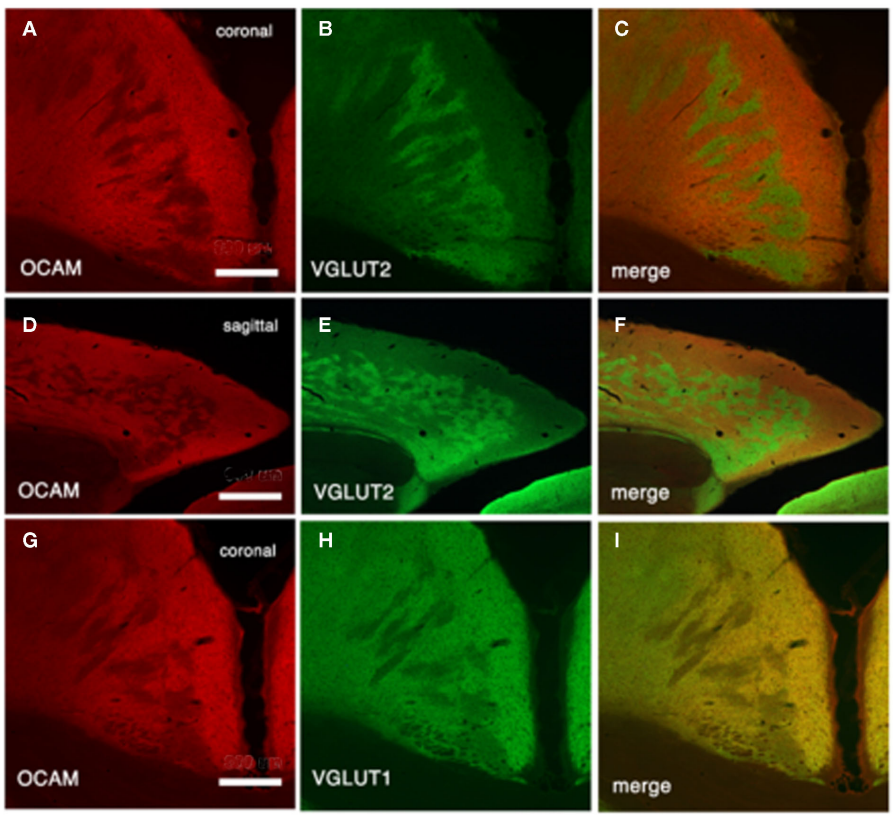

FIGURE 6 | Architectonics of mutant GRS, visualized by immunohistochemistry for OCAM and VGLUT2 (presumptive thalamocortical terminations) or VGLUT1 (presumptive corticocortical terminations). (A–C) Coronal sections reacted for OCAM and VGLUT2 from shaking rat Kawasaki. **(D–F)** Tangential sections. **(G–I)** Coronal sections reacted for OCAM and VGLUT1. Scale bar: **(A–C,G–I)**, 300 μm; **(D–F)**, 600 μm.

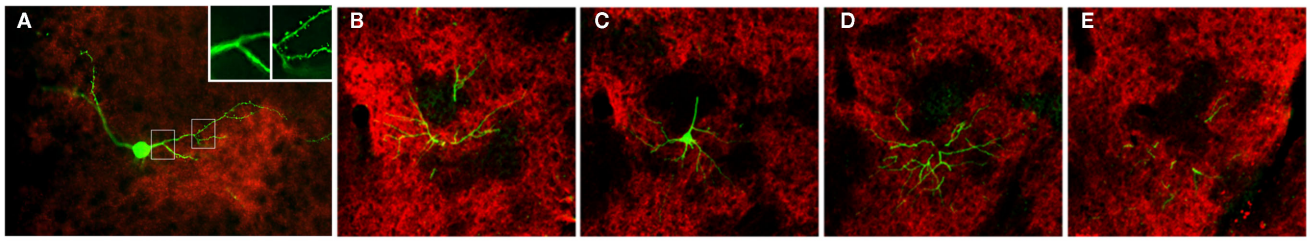

FIGURE 7 | Pyramidal cell dendrites preferentially arborize in either patch or matrix compartments in reeler GRS. (A) Coronal section reacted for VGLUT2 (red), with a Lucifer yellow (LY)-filled neuron (green). This LY-filled neuron has a soma located in a zone of low VGLUT2-ir (presumably equivalent to the OCAM-positive matrix) and many dendrite branches within a VGLUT2-dense patch (presumably equivalent to an OCAM-negative patch). These dendritic portions within VGLUT2-dense patches have spines [arrowheads in **(A″)**], but not the portions outside the VGLUT2-dense region **(A′)**. Insets in **(A)** [i.e., **(A′,A″)**] show a higher magnification of the images in the white boxes [**(A′)** from left box and **(A″)** from right box]. **(B–E)** Serial sections of a LY-filled neuron (green), double reacted for OCAM (red). The cell body is located within the OCAM-positive matrix **(C)**. An apical dendrite-like process gives off an oblique dendrite proximally, before entering an OCAM-negative patch. An apical tuft branches just at the border between patch and matrix compartments **(C)**. The basal dendrites tend, like the cell body, to stay within the OCAM-dense matrix. Scale bar: **(A–E)**, 50 μm; **(A′,A″)**, 20 μm.

navigation, as well as certain aspects of learning and memory (Cooper et al., 2001; Garden et al., 2009; Vann et al., 2009; Aggleton, 2010). The GRS is part of a heavily interconnected limbic circuit, including the anterior thalamic nuclei and subiculum. The underlying substrates involved in GRS functioning and the true significance of upper layer modular organization are undoubtedly complex. More anatomical and physiological studies will obviously be necessary (see recent anatomical study by Odagiri et al., 2011).

Prominent characteristics of the modular organization of the rat GRS in layer 1 include (1) the aggregation or segregation of apical dendrites ("recipients") of the same or different types of pyramidal neurons, respectively, and (2) the fact that certain types of terminals ("inputs") either match or interdigitate with a particular type of dendritic aggregation. As mentioned above, this type of recipient and input matching also occurs in other small-scale modular organizations in the neocortex (i.e., honeycomb-like organization in the uppermost layers: Ichinohe et al., 2003a; Ichinohe and Rockland, 2004). Modular aggregations consisting of appropriate types of recipients and inputs, such as those seen in the rat GRS, may help to achieve efficient and quick synaptic wiring changes, such as occur in the context of learning and memory.

ACKNOWLEDGMENTS

This study was supported by a Grant-in-Aid for Scientific Research on Innovative Areas, "Face perception and recognition," by the Ministry of Education, Science, Sports and Culture, Japan.

REFERENCES

Aggleton, J. P. (2010). Understanding retrosplenial amnesia: insights from animal studies. *Neuropsychologia* 48, 2328–2338.

Alenius, M., and Bohm, S. (2003). Differential function of RNCAM isoforms in precise target selection of olfactory sensory neurons. *Development* 130, 917–927.

Borisovska, M., McGinley, M. J., Bensen, A., and Westbrook, G. L. (2011). Loss of olfactory cell adhesion molecule reduces the synchrony of mitral cell activity in olfactory glomeruli. *J. Physiol.* 589, 1927–1941.

Cooper, B. G., Manka, T. F., and Mizumori, S. J. (2001). Finding your way in the dark: the retrosplenial cortex contributes to spatial memory and navigation without visual cues. *Behav. Neurosci.* 115, 1012–1028.

Datwani, A., Iwasato, T., Itohara, S., and Erzurumlu, R. S. (2002). NMDA receptor-dependent pattern transfer from afferents to postsynaptic cells and dendritic differentiation in the barrel cortex. *Mol. Cell. Neurosci.* 21, 477–492.

DeFelipe, J., Alonso-Nanclares, L., and Arellano, J. I. (2002).Microstructure of the neocortex: comparative aspects. *J. Neurocytol.* 31, 299–316.

Fujiyama, F., Furuta, T., and Kaneko, T. (2001). Immunocytochemical localization of candidates for vesicular glutamate transporters in the rat cerebral cortex. *J. Comp. Neurol.* 435, 379–387.

Garden, D. L., Massey, P. V., Caruana, D. A., Johnson, B., Warburton, E. C., Aggleton, J. P., and Bashir, Z. I. (2009). Anterior thalamic lesions stop synaptic plasticity in retrosplenial cortex slices: expanding the pathology of diencephalic amnesia. *Brain* 132, 1847–1857.

Ichinohe, N., Fujiyama, F., Kaneko, T., and Rockland, K. S. (2003a). Honeycomb-like mosaic at the border of layers 1 and 2 in the cerebral cortex. *J. Neurosci.* 23, 1372–1382.

Ichinohe, N., Yoshihara, Y., Hashikawa, T., and Rockland, K. S. (2003b). Developmental study of dendritic bundles in layer 1 of the rat granular retrosplenial cortex with special reference to a cell adhesion molecule, OCAM. *Eur. J. Neurosci.* 18, 1764–1774.

Ichinohe, N., Knight, A., Ogawa, M., Ohshima, T., Mikoshiba, K., Yoshihara, Y., Terashima, T., and Rockland, K. S. (2008). Unusual patch-matrix organization in the retrosplenial cortex of the reeler mouse and shaking rat Kawasaki. *Cereb. Cortex* 18, 1125–1138.

Ichinohe, N., and Rockland, K. S. (2002). Parvalbumin positive dendrites co-localize with apical dendritic bundles in rat retrosplenial cortex. *Neuroreport* 13, 757–761.

Ichinohe, N., and Rockland, K. S. (2004). Region specific micromodularity in the uppermost layers in primate cerebral cortex. *Cereb. Cortex* 14, 1173–1184.

Jones, E. G. (2000). Microcolumns in the cerebral cortex. *Proc. Natl. Acad. Sci. U.S.A.* 97, 5019–5021.

Kikkawa, S., Yamamoto, T., Misaki, K., Ikeda, Y., Okado, H., Ogawa, M., Woodhams, P. L., and Terashima, T. (2003). Missplicing resulting from a short deletion in the reelin gene causes reeler-like neuronal disorders in the mutant shaking rat Kawasaki. *J. Comp. Neurol.* 463, 303–315.

Kisvárday, Z. F., Ferecskó, A. S., Kovács, K., Buzás, P., Budd, J. M., and Eysel, U. T. (2002). One axon-multiple functions: specificity of lateral inhibitory connections by large basket cells. *J. Neurocytol.* 31, 255–364.

Lambert de Rouvroit, C., and Goffinet, A. M. (1998). The reeler mouse as a model of brain development. *Adv. Anat. Embryol. Cell Biol.* 150, 1–106.

Miró-Bernié, N., Ichinohe, N., Pérez-Clausell, J., and Rockland, K. S. (2006). Zinc-rich transient vertical modules in the rat retrosplenial cortex during postnatal development. *Neuroscience* 138, 523–535.

Miyashita, T., Wintzer, M., Kurotani, T., Konishi, T., Ichinohe, N., and Rockland, K. S. (2010). Neurotrophin-3 is involved in the formation of apical dendritic bundles in cortical layer 2 of the rat. *Cereb. Cortex* 20, 229–240.

Odagiri, S., Meguro, R., Asano, Y., Tani, T., and Ichinohe, N. (2011). Single axon branching analysis in rat thalamocortical projection from the anteroventral thalamus to the granular retrosplenial cortex. *Front. Neuroanat.* 5, 63. doi: 10.3389/fnana.2011.00063

Rockland, K. S., and Ichinohe, N. (2004). Some thoughts on cortical minicolumns. *Exp. Brain Res.* 158, 265–277.

Shibata, H. (1993). Efferent projections from the anterior thalamic nuclei to the cingulate cortex in the rat. *J. Comp. Neurol.* 330, 533–542.

Simmons, P. A., and Pearlman, A. L. (1983). Receptive-field properties of transcallosal visual cortical neurons in the normal and reeler mouse. *J. Neurophysiol.* 50, 838–848.

Steindler, D. A., Faissner, A., and Harrington, K. L. (1994). A unique mosaic in the visual cortex of the reeler mutant mouse. *Cereb. Cortex* 4, 129–137.

Swadlow, H. A., and Gusev, A. G. (2000). The influence of single VB thalamocortical impulses on barrel columns of rabbit somatosensory cortex. *J. Neurophysiol.* 83, 2802–2813.

Van Groen, T., and Wyss, J. M. (1995). Projections from the anterodorsal and anteroventral nucleus of the thalamus to the limbic cortex in the rat. *J. Comp. Neurol.* 358, 584–604.

Van Groen, T., and Wyss, J. M. (2003). Connections of the retrosplenial granular b cortex in the rat. *J. Comp. Neurol.* 463, 249–263.

Vann, S. D., Aggleton, J. P., and Maguire, E. A. (2009). What does the retrosplenial cortex do? *Nat. Rev. Neurosci.* 10, 792–802.

Walz, A., Mombaerts, P., Greer, C. A., and Treloar, H. B. (2006). Disrupted compartmental organization of axons and dendrites within olfactory glomeruli of mice deficient in the olfactory cell adhesion molecule, OCAM. *Mol. Cell. Neurosci.* 32, 1–14.

Wyss, J. M., Van Groen, T., and Sripanidkulchai, K. (1990). Dendritic bundling in layer I of granular retrosplenial cortex: intracellular labeling and selectivity of innervation. *J. Comp. Neurol.* 295, 33–42.

Yoshihara, Y., Kawasaki, M., Tamada, A., Fujita, H., Hayashi, H., Kagamiyama, H., and Mori, K. (1997). OCAM: a new member of the neural cell adhesion molecule family related to zone-to-zone projection of olfactory and vomeronasal axons. *J. Neurosci.* 17, 5830–5842.

Zgraggen, E., Boitard, M., Roman, I., Kanemitsu, M., Potter, G., Salmon, P., Vutskits, L., Dayer, A. G., and Kiss, J. Z. (2011). Early postnatal migration and development of layer II pyramidal neurons in the rodent cingulate/retrosplenial cortex. *Cereb. Cortex* 22, 144–157.

Conflict of Interest Statement: The author declares that the research was conducted in the absence of any commercial or financial relationships that could be construed as a potential conflict of interest.

Received: 13 September 2011; paper pending published: 02 November 2011; accepted: 28 December 2011; published online: 10 January 2012.

*Citation: Ichinohe N (2012) Small-scale module of the rat granular retrosplenial cortex: an example of the minicolumn-like structure of the cerebral cortex. Front. Neuroanat. **5**:69. doi: 10.3389/fnana.2011.00069*

frontiers in
NEUROANATOMY

REVIEW ARTICLE
published: 28 September 2011
doi: 10.3389/fnana.2011.00062

Signaling mechanisms in cortical axon growth, guidance, and branching

***Katherine Kalil*[1,2]*, *Li Li*[1,3] *and B. Ian Hutchins*[1,4]**

[1] *Neuroscience Training Program, University of Wisconsin-Madison, Madison, WI, USA*
[2] *Department of Neuroscience, University of Wisconsin-Madison, Madison, WI, USA*
[3] *Pfizer, Inc., Groton, CT, USA*
[4] *National institute of Neurological Disorders and Stroke, National Institutes of Health, Bethesda, MD, USA*

Edited by:
Julian Budd, University of Sussex, UK

Reviewed by:
Carol Mason, Columbia University Medical Center, USA
Sarah L. Pallas, Georgia State University, USA
Susana Cohen-Cory, University of California, USA

***Correspondence:**
Katherine Kalil, Department of Neuroscience, University of Wisconsin-Madison, 1300 University Avenue, Madison, WI 53706, USA.
e-mail: kakalil@facstaff.wisc.edu

Precise wiring of cortical circuits during development depends upon axon extension, guidance, and branching to appropriate targets. Motile growth cones at axon tips navigate through the nervous system by responding to molecular cues, which modulate signaling pathways within axonal growth cones. Intracellular calcium signaling has emerged as a major transducer of guidance cues but exactly how calcium signaling pathways modify the actin and microtubule cytoskeleton to evoke growth cone behaviors and axon branching is still mysterious. Axons must often pause their extension in tracts while their branches extend into targets. Some evidence suggests a competition between growth of axons and branches but the mechanisms are poorly understood. Since it is difficult to study growing axons deep within the mammalian brain, much of what we know about signaling pathways and cytoskeletal dynamics of growth cones comes from tissue culture studies, in many cases, of non-mammalian species. Consequently it is not well understood how guidance cues relevant to mammalian neural development *in vivo* signal to the growth cone cytoskeleton during axon outgrowth and guidance. In this review we describe our recent work in dissociated cultures of developing rodent sensorimotor cortex in the context of the current literature on molecular guidance cues, calcium signaling pathways, and cytoskeletal dynamics that regulate growth cone behaviors. A major challenge is to relate findings in tissue culture to mechanisms of cortical development *in vivo*. Toward this goal, we describe our recent work in cortical slices, which preserve the complex cellular and molecular environment of the mammalian brain but allow direct visualization of growth cone behaviors and calcium signaling. Findings from this work suggest that mechanisms regulating axon growth and guidance in dissociated culture neurons also underlie development of cortical connectivity *in vivo*.

Keywords: axon outgrowth, axon guidance, axon branching, calcium signaling, Wnt5a, CaMKII, corpus callosum, microtubules

INTRODUCTION

The development of appropriate connections is essential for the nervous system to function correctly. To achieve this motile growth cones at axon tips guide growing axons along appropriate pathways and into targets by responding to environmental guidance cues (Dickson, 2002). Thus intense interest has focused on the signaling mechanisms within the growth cone that link activation of surface guidance cue receptors to the actin and microtubule cytoskeleton that regulates growth cone motility and guidance behaviors (Dent and Gertler, 2003; Lowery and Van Vactor, 2009). It is well established, particularly in the mammalian central nervous system, that axons establish connections not only by activity of their growth cones but also by extending collateral branches from the shaft of the primary axon into the target (Kalil et al., 2000). This mechanism of interstitial branching (O'Leary et al., 1990) is especially important for the wiring of the cerebral cortex to distant targets in the spinal cord and contralateral cortex by efferent corticospinal and callosal axons. In cortical slice preparations direct visualization of cortical axons branching within the corpus callosum (Halloran and Kalil, 1994) and corticopontine tract (Bastmeyer and O'Leary, 1996) revealed that interstitial branching occurs from the axon shaft after the growth cone has extended past the target. Defining the signaling mechanisms that regulate axon growth, guidance, and branching is essential for understanding how the cerebral cortex becomes wired to appropriate targets during development. To address this question our laboratory used *in vitro* preparations of developing hamster sensorimotor cortex, which, *in vivo*, gives rise to the major efferent corticospinal and callosal pathways that contribute to motor, sensory, and cognitive functions. We identified guidance cues that promote cortical axon outgrowth, guidance, and branching, the intracellular calcium signaling pathways that evoke these axonal responses and the cytoskeletal mechanisms that regulate them. This review will focus on recent work from our laboratory and others showing how these cellular mechanisms shape the wiring of cortical connectivity during development.

GUIDANCE CUES PROMOTE OR INHIBIT CORTICAL AXON BRANCHING BY CYTOSKELETAL REORGANIZATION

Cortical axons navigate over long distances by responses of their motile growth cones to attractive and inhibitory guidance cues in their environment. However, the growth cone at the tip of the primary axon does not typically grow directly into cortical and spinal targets. Instead branches arise interstitially from the axon shaft and then enter targets where they then form terminal arbors. Axon branching may be mechanistically linked to pausing behaviors of growth cones, which leave behind remnants on the axon at sites of future branching (Kalil et al., 2000; Dent et al., 2003). Growth cones consist of a central region which contains bundled microtubules and a thin expanded peripheral region dominated by actin filaments that form a meshwork in veil-like lamellipodia and bundles in fingerlike filopodia that protrude from highly motile lamellipodia (**Figure 1**). The growth cone responds to attractive cues by turning toward the source of the positive guidance cue whereas inhibitory guidance cues repel axons away from the repulsive guidance cue (Huber et al., 2003).

Guidance cues influence growth cone behaviors through cytoskeletal reorganization (Dent and Gertler, 2003; Kalil and Dent, 2005). Netrins, such as netrin-1, promote outgrowth of a wide variety of axons (Manitt and Kennedy, 2002) and attract growing cortical axons in explant cocultures (Metin et al., 1997; Richards et al., 1997). In contrast semaphorin 3A repels cortical axons *in vitro* (Bagnard et al., 1998; Polleux et al., 1998, 2000). However, little is known about effects of these attractive and repulsive guidance cues on cortical axon branching or the underlying cytoskeletal mechanisms. We therefore investigated effects of netrin-1 and semaphorin 3A on axon branching of cortical neurons in dissociated culture (Dent et al., 2004) and found that netrin-1 increased branching by almost 60%. Branches began as filopodia that grew to form stable branches within a few hours. Thus the effect of netrin-1 was to accelerate and increase branch formation. Local application of netrin-1 pulsed onto cortical axons evoked branching *de novo* from the axon shaft within minutes but had no effect on outgrowth of the primary axon, suggesting that axon outgrowth and branching are differentially regulated. Semaphorin 3A had opposing effects, reducing axon branching and branch length without affecting axon length. Using live cell imaging of cortical neurons microinjected with fluorescent markers for actin filaments or microtubules, we investigated the cytoskeletal mechanisms underlying increased branching by netrin-1 or decreased branching by semaphorin 3A. In growth cones and at branch points along the axon shaft of cortical neurons interactions between dynamic microtubules (i.e., those able to grow and shrink in dynamic instability) and actin filaments are necessary for branch formation (Dent and Kalil, 2001). Netrin-1 increased actin filament bundles in the growth cone and axon shaft thereby increasing the number of filopodia along the axon shaft. Dynamic splayed microtubules interacted with the newly polymerized actin bundles to initiate new directions of growth by axon branches. In growth cones treated with semaphorin 3A bundled actin filaments in the growth cone depolymerized, which reduced the motility and protrusion of filopodia and decreased microtubule exploration in the growth cone periphery. In collateral branches semaphorin 3A caused collapse of splayed microtubules and disappearance of actin bundles leading to a decrease in cortical axon branching. These results demonstrate that axon outgrowth and branching may in some cases be differentially regulated since netrin-1 and semaphorin 3A increased or decreased cortical axon branching respectively without affecting axon length. Moreover, development of axon branches involves changes at the growth cone as well as the axon shaft in cytoskeletal organization and dynamics. When actin/microtubule interactions are inhibited by guidance cues that depolymerize the cytoskeleton or inhibit their dynamics growth cones collapse and branching is inhibited.

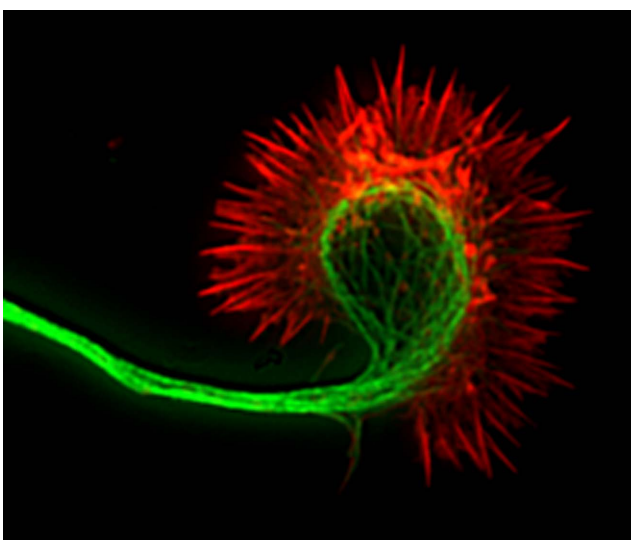

FIGURE 1 | Fluorescence image of a cortical axon and its growth cone. Actin filaments (indicated in red) are stained with phalloidin and occupy the lamellipodium and the spiky filopodia that protrude from its periphery. Microtubules (indicated in green) are stained with anti-tubulin antibodies and occupy the axon and central region of the growth cone. Dynamic microtubules can extend from the central region into the growth cone periphery to interact with actin filaments.

CALCIUM SIGNALING PATHWAYS MEDIATE NETRIN-1 INDUCED CORTICAL AXON BRANCHING

The intracellular mechanisms that regulate axon branching independent of axon outgrowth are not well understood. Calcium is an essential second messenger that transduces axon guidance signals to regulate growth cone motility and pathfinding (Gomez and Zheng, 2006; Wen and Zheng, 2006; Zheng and Poo, 2007). In cortical neurons spontaneous global calcium (Ca^{2+}) fluctuations (transients) regulate axon outgrowth in a frequency dependent manner (Tang et al., 2003). Since netrin-1 induces extensive axon branching (Dent et al., 2004) and elevates Ca^{2+} levels in growth cones during steering events (Hong et al., 2000; Ming et al., 2002) we hypothesized that netrin-1 might promote axon branching through Ca^{2+} signaling events in the axon. Activation of specific signaling components is related to frequencies of Ca^{2+} transients. For example, calcium/calmodulin-dependent protein kinase II (CaMKII) functions as a spike-frequency detector (Hudmon and Schulman, 2002) and mitogen activated protein kinases (MAPKs) are also sensitive to intracellular Ca^{2+} changes

(Cullen and Lockyer, 2002). Thus if repetitive Ca^{2+} transients are indeed involved in axon branching, CaMKII and MAPKs are likely candidates as downstream targets of Ca^{2+} signaling.

We investigated the role of calcium signaling in netrin-1 induced axon branching (Tang and Kalil, 2005) by loading cortical neurons with the membrane permeable calcium indicator dye Fluo-4AM, which detects changes in Ca^{2+} activity by changes in fluorescence intensity. Bath applied netrin-1 increased the average frequency of calcium transients fourfold either locally or globally in the axon. When netrin was withdrawn, Ca^{2+} activity declined to baseline levels. Reducing Ca^{2+} activity by blocking IP_3 receptors on the endoplasmic reticulum to inhibit Ca^{2+} release from intracellular stores severely reduced branching. Local application of netrin-1 to the axon elicited large changes in Ca^{2+} in local regions of the axon. Remarkably, within minutes branches often protruded *de novo* from these regions of netrin-1 induced Ca^{2+} activity. Increased frequency of calcium transients by netrin-1 was strongly correlated with activation of CaMKII (as shown by increased phosphorylation). Whereas CaMKII inhibitors reduced cortical axon branching in the presence of netrin-1 and also reduced axon outgrowth, over expression of αCaMKII increased axon branching. Conversely, RNAi knockdown of αCaMKII prevented netrin-1 induced axon branching. MAPK over expression increased axon branching whereas MAPK inhibition prevented netrin-1 induced branching but did not affect axon length. These results demonstrate for the first time that the axon guidance cue netrin-1 evokes rapid cortical axon branching through repetitive Ca^{2+} transients that activate the downstream kinases CaMKII and MAPK, which are sensitive to changes in the frequency of Ca^{2+} transients.

How are these findings relevant to cortical axon branching by netrin-1 *in vivo*? Netrin-1 is not expressed in the developing rodent cortical plate. Instead, the DCC ligand netrin-4 (Qin et al., 2007) is expressed in sensorimotor cortex at P6 (Takemoto et al., 2011) when mouse layer 2–3 axons are first extending branches into this region (Wang et al., 2007). Strong netrin-1 expression is observed in the cortical plate of the developing human fetus by 14 weeks of gestation (Harter et al., 2010), the time when callosal axons cross the midline and project to the contralateral cortex (Ren et al., 2006). This suggests that netrin-1 may have a larger role in human cortical development compared to rodents. In addition, DCC-expressing cortical axons extend collateral branches into the striatum (Sheth et al., 1998), which expresses netrin-1 at high levels throughout development (Livesey and Hunt, 1997; Takemoto et al., 2011). Taken together with our results on netrin-1 induced axon branching (Dent et al., 2004; Tang and Kalil, 2005), these data strongly suggest that during embryonic development netrins may direct the extension of collateral branches into the targets of cortical projection neurons.

CALCIUM TRANSIENTS DIFFERENTIALLY REGULATE CORTICAL AXON OUTGROWTH AND BRANCHING

In vivo and *in vitro* outgrowth of axons and the extension of branches are independently regulated such that branches can extend while their axons stall or retract (Luo and O'Leary, 2005). Thus, during the formation of corticospinal and callosal branches, axons have already completed their extension into efferent pathways (reviewed in Kalil et al., 2000). The mechanisms that regulate differential rates of outgrowth by axons and branches are poorly understood. One possibility, a competitive activity-dependent mechanism, regulates synaptic innervation at target sites. For example (Uesaka et al., 2006) in organotypic cocultures of thalamus and cortex neural activity enhanced the branch dynamics of thalamocortical axons that were biased toward more branch addition and elongation of branches in specific cortical target layers. The importance of electrical activity was further demonstrated *in vivo* where reducing neuronal activity in cortical neurons inhibited their morphological maturation including neurite elongation and branch development (Cancedda et al., 2007). Competition among neighboring axon arbors for synaptic space in the zebra fish visual system also favored arbors with higher levels of neural activity (Hua et al., 2005). Since electrical activity is reflected by changes in intracellular Ca^{2+} (Spitzer, 2006), we hypothesized that differences in levels of Ca^{2+} activity could also be a mechanism for regulating the differential growth of several processes of the same axon. This idea is supported by experiments with sympathetic neurons grown in divided chambers (Singh and Miller, 2005) which showed that one axon branch depolarized to increase Ca^{2+} activity grew longer at the expense of unstimulated branches in another chamber. This competition was dependent on calcium influx and downstream activation of CaMKII. However, these experiments could not distinguish between branches vs. axons from another cell and further investigation (Singh et al., 2008) suggested the involvement of neighboring axons.

To determine whether cortical neurons regulate axon outgrowth and branching by different levels of Ca^{2+} activity we measured spontaneous activity or manipulated calcium levels in an axon and its branches (Hutchins and Kalil, 2008). The frequencies of spontaneous Ca^{2+} transients were often different in a region of an axon vs. a branch or in one branch vs. another branch of the same axon (**Figure 2**). Higher frequency Ca^{2+} transients were correlated with more rapid outgrowth. Interestingly, differences in rates of outgrowth between processes of the same axon were dependent on relative differences in their Ca^{2+} transient frequencies. Processes with higher frequency transients were favored for growth while those with lower frequencies not only grew more slowly but retracted, suggesting a competitive effect. Moreover, the greatest differences in rates of outgrowth of two different processes of the same axon occurred when differences in frequencies were the highest. Global transients contributed relatively little to differential process outgrowth. To induce Ca^{2+} transients we applied BayK, which opens L-type voltage gated Ca^{2+} channels. BayK evoked localized calcium transients in cortical axons, which exhibited significant differences in outgrowth of processes belonging to the same axon. Over a 24-h time course both extension and retraction occurred in axons and their branches (**Figure 3**). Ca^{2+} imaging during the last 10–15 min revealed that higher frequency Ca^{2+} transients were associated with increased rates of outgrowth vs. association of lower frequency Ca^{2+} transients with retraction or slower rates of outgrowth. We also used photolysis of caged calcium to evoke repetitive transients in restricted regions of axons and their branches (Hutchins and Kalil, 2008). This approach releases caged calcium in a region restricted to a small spot (12–50 μm) and permits the choice of an optimal Ca^{2+} transient frequency by repetitive pulses of UV light. In most cases

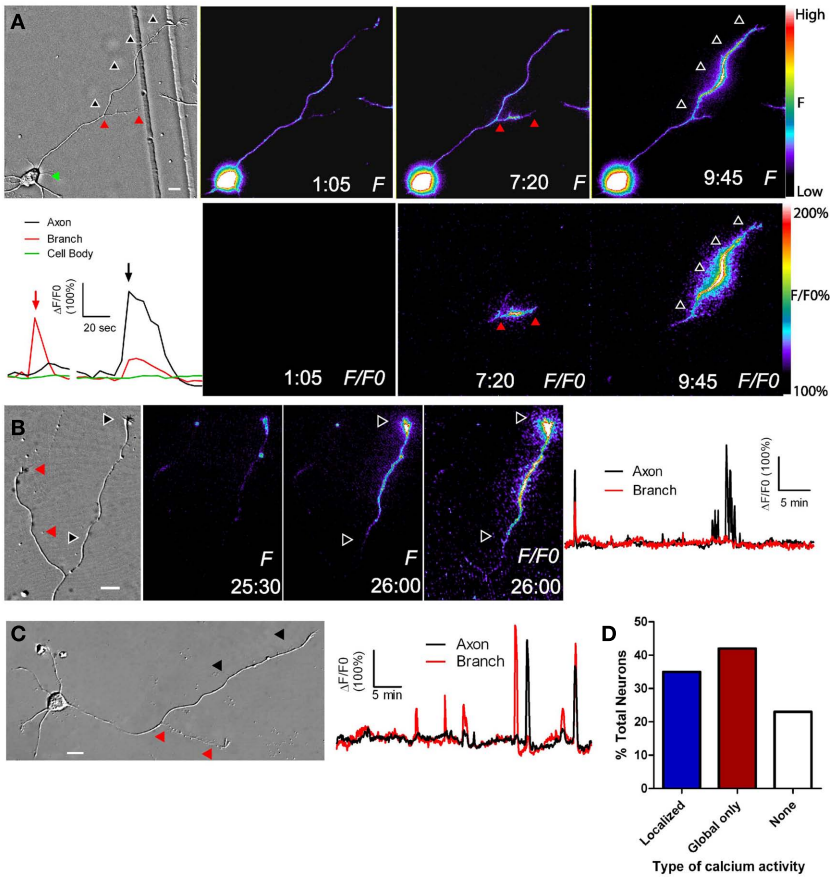

FIGURE 2 | Localized calcium transients occur in restricted regions of primary axons or their collateral branches. (A) DIC image at left and fluorescence images of calcium activity in a cortical neuron in which calcium transients are localized to the primary axon (at 9:45) or its collateral branch (7:20). At 1:05 there is no calcium activity. Black and red arrowheads correspond to regions of localized calcium activity. Panels *F/FO* show fluorescence change from baseline rather than raw fluorescence (lower panels). Pseudocolor calibration bars for images of raw fluorescence (*F*) and fluorescence normalized to baseline (*F/FO*) are shown at right. The graph at left shows calcium activity in the primary axon (black), branch (red), and cell body (green) during calcium transients shown in the fluorescence images at 7:20 (red arrow) and 9:45 (black arrow). **(B)** DIC image (left) and fluorescence images of localized calcium activity indicated by black arrowheads in the primary axon of a cortical neuron (right panels). As shown in the graph of calcium activity (far right), localized calcium transients occurred only in the primary axon (black), and not in the branch (red). One global calcium transient occurred at the beginning of the imaging session. **(C)** Both the primary axon (black arrowheads) and branch (red arrowheads) show localized calcium transients but the branch has a higher frequency (graph at right). **(D)** Distribution of total cortical neurons with different types of calcium activity. Times are in minutes and seconds. Scale bar, 10 μm. (Reprinted from Hutchins and Kalil, 2008; with permission from the Society for Neuroscience).

the stimulated process was favored for growth while unstimulated processes often retracted. Thus results from spontaneous and induced Ca^{2+} activity revealed similar competitive effects on the growth of one axonal process at the expense of another by differential frequencies of Ca^{2+} transients.

How do results from these *in vitro* experiments shed light on mechanisms of cortical axon branching *in vivo*? Cortical axons in pathways such as the corpus callosum vs. their branches projecting into cortical target regions could encounter different guidance cues such as netrin-1 at varying concentrations that evoke different levels of Ca^{2+} activity. This could lead to competition among different processes of the same axon for growth such that the primary axon could stall or retract while a branch of the same axon could extend into targets. In living cortical slices (Halloran and Kalil, 1994), we observed these events directly in the developing corpus callosum. Different frequencies of Ca^{2+} transients could regulate the differential outgrowth of an axon vs. its branch by activation of calcium frequency dependent effectors such as CaMKII and MAPK in each axonal process. Effectors such as CaMKI and CaMKII promote neurite outgrowth (Borodinsky et al., 2003; Wayman et al., 2004, 2006) and CaMKII is preferentially activated in cortical axon branches with higher frequency Ca^{2+} transients (Tang and Kalil, 2005). CaMKIIβ binds to actin filaments and increases filopodial dynamics (Fink et al., 2003), consistent with the observation that direct elevation of Ca^{2+} activity by photolysis of caged calcium can rapidly evoke protrusion of new axonal filopodia by actin filament polymerization (Lau et al., 1999). Calcium transients of different frequencies may target different kinases and phosphatases such as CaMKII and calcineurin in the cytoplasm to evoke different cellular responses (Tomida et al., 2003). Events, such as extension and

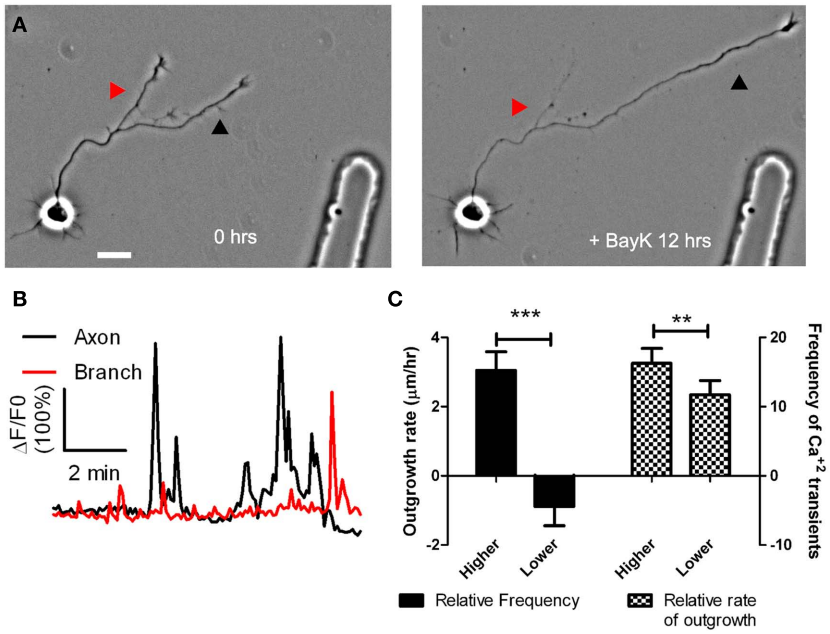

FIGURE 3 | BayK induced calcium transients, which persist throughout long term treatments, are correlated in their frequencies with process outgrowth. (A) Phase images of a cortical neuron treated with BayK in the bath for 12 h. At the end of the imaging session the process at right (black arrowhead) had extended, whereas the process at left (red arrowhead) retracted. **(B)** After phase imaging, cortical neurons were loaded with Fluo-4 and calcium activity was measured. The extending process in **(A)** (black) showed high levels of calcium activity compared with the retracting process (red). **(C)** Quantifications from 16 experiments imaging calcium activity after long term BayK treatments revealed correlations between BayK induced differential calcium activity and process outgrowth. At left comparisons between processes from the same axon showed that those with higher frequency calcium transients had higher rates of outgrowth, whereas those with lower frequencies retracted ($n = 22$ comparisons; $^{***}p < 0.001$, paired t test). At right processes that extended faster had higher frequencies of calcium transients ($n = 26$ comparisons; $^{**}p < 0.01$, paired t test). Scale bar, 20 μm. (Reprinted from Hutchins and Kalil, 2008; with permission from the Society for Neuroscience).

retraction of axonal processes, may be regulated by Ca^{2+} transients at optimal frequencies (Eshete and Fields, 2001). For rapid extension of cortical axons and branches the optimal frequencies of spontaneous and induced localized Ca^{2+} transients were similar across experiments (Hutchins and Kalil, 2008). Thus, one role for localized Ca^{2+} signaling may be to restrict Ca^{2+} transients at optimal frequencies to local regions of the axon. Local Ca^{2+} signaling would thereby regulate extension and retraction of axonal processes in response to environmental growth and guidance cues.

Although competition between different branches of a single axon has now been well-documented (Ruthel and Banker, 1999; Singh and Miller, 2005; Hutchins and Kalil, 2008), the competitive signaling mechanisms initiated by localized calcium activity remain mysterious. An early hypothesis of the mechanism of competitive axon growth proposed that actin ruffles flowing distally along the axon mediated competition among axonal processes (Ruthel and Banker, 1999). These actin-rich axon waves are important in promoting axon outgrowth and branching (Flynn et al., 2009). However, while disrupting actin dynamics with cytochalasin reduced rates of axon growth, the competition between processes remained intact (Ruthel and Hollenbeck, 2000). An alternative hypothesis that branches compete for mitochondria transported along the axon arose from the observation that mitochondria selectively invade axons showing robust growth (Morris and Hollenbeck, 1993). However, subsequent investigation showed that mitochondria follow, rather than precede, competitive outgrowth among axonal processes (Ruthel and Hollenbeck, 2003). More recently, it was shown that cAMP and cGMP promote or inhibit, respectively, axon formation and that these signals mutually inhibit one another (Shelly et al., 2010). This cAMP signaling in one neurite initiates a long-distance cGMP signal that hydrolyzes cAMP in all other neurites, leading to competition and the establishment of a single axon. Since calcium signaling can activate cAMP signaling (Gorbunova and Spitzer, 2002), one possibility is that the localized calcium transients that initiate competition among axonal processes (Hutchins and Kalil, 2008) do so through long-distance cyclic nucleotide signals. Supporting this possibility, recent experiments demonstrated that netrin-evoked calcium transients, of the type that promote growth cone advance, drive cAMP signals in the growth cone center (Nicol et al., 2011). Despite this promising avenue of research, it is still not known how such long-distance signals propagate or whether competitive outgrowth reflects competition for scarce resources or a purely signaling-based mechanism for restricting growth to certain branches. One possible mechanism for propagating long-distance signals is an inhibitory autocrine signal similar to that which mediates competition between neighboring axons (Singh et al., 2008). This mechanism could lead to signaling-based competition through mutual inhibition of growth between different branches from the same axon (Hutchins, 2010). However, another

possibility is that these signaling events direct the transport of rate-limiting resources such as tubulin to the "winning" branch and thereby deprive other branches of the opportunity to grow (Butz et al., 2009; van Ooyen, 2011). The selective growth and retraction of branches is a fundamental mechanism of establishing connectivity in the mammalian CNS (McLaughlin and O'Leary, 2005). Elucidating the mechanisms of competitive axon growth will therefore be crucial for our understanding of the wiring principles of the cerebral cortex.

Wnt5a PROMOTES CORTICAL AXON OUTGROWTH AND REPULSION BY DIFFERENTIAL SIGNALING

In addition to positive guidance cues that attract cortical axons and promote their branching, repulsive guidance cues that repel growing axons are equally important in shaping the formation of cortical connections. Recently, the morphogen Wnt5a was identified as an axon guidance cue (Salinas and Zou, 2008) that repels growing cortical axons during development (Zou and Lyuksyutova, 2007). Wnts play important roles in embryogenesis such as determination of cell fate, patterning, migration, and differentiation (Ciani and Salinas, 2005). Wnt5 was first identified in Drosophila as a repulsive guidance cue for commissural axons (Yoshikawa et al., 2003). In the mouse corticospinal pathway a high to low gradient of Wnt5a *in vivo* acts as a repulsive cue for cortical axons (Liu et al., 2005) through the Wnt5a receptor Ryk (an atypical tyrosine kinase receptor). *In vitro* a source of secreted Wnt5a inhibited axon outgrowth from cortical explants facing a Wnt5a gradient. Since Wnt5a is expressed in a high to low gradient surrounding the corticospinal tract, these results (Liu et al., 2005) suggested that cortical axons must navigate down the spinal cord through a high to low inhibitory Wnt5a gradient. In the embryonic mouse corpus callosum Keeble et al. (2006) also demonstrated the repulsive effects of Wnt5a on cortical axon outgrowth. *In vitro* axons extending from cortical explants were repelled away from a source of Wnt5a but this repulsive effect was abolished in cortex from mutant mice lacking the Ryk receptor. *In vivo* the corpus callosum is surrounded by a gradient of Wnt5a secreted by midline glial structures, the indusium griseum, and glial wedge (Keeble et al., 2006; Lindwall et al., 2007). In Ryk knockout mice callosal axons, which normally express Ryk receptors during development, were able to cross the midline but became misrouted after the midline and were thus unable to project away from it and formed abnormal bundles on the contralateral side. How a repulsive axon guidance cue could promote the growth of cortical axons down the spinal cord and across the corpus callosum was still a mystery.

To elucidate the mechanisms by which Wnt5a could regulate axon outgrowth of developing cortical pathways (Li et al., 2009) we bath applied Wnt5a to dissociated cortical neurons. This doubled axon outgrowth rates over 3 day in culture and in 1 h increased axon outgrowth fourfold. To determine whether a point source of Wnt5a could repel cortical axons, we used a turning assay in which axons were exposed to a gradient of Wnt5a. Control axons in BSA gradients showed no preference in turning toward or away from the BSA source. In contrast (**Figure 4**), axons consistently turned away from a source of Wnt5a by reorienting their growth cones in as little as 20 min. However, growth cones remained motile with no obvious collapse. Surprisingly, axons turning away from the Wnt5a source also increased their growth rates by 50%. This simultaneous repulsion and increased axon outgrowth in response to Wnt5a could explain how a Wnt5a gradient *in vivo* propels the extension of cortical axons by a repulsive mechanism.

What signaling pathways mediate responses of cortical axons to Wnt5a? Wnts exert their effects through both Ryk and Frizzled (Fz) receptors (Salinas and Zou, 2008) which are expressed on developing hamster cortical neurons (Li et al., 2009) at P0–P3 when axons are projecting into corticospinal and callosal pathways (Reh and Kalil, 1981; Norris and Kalil, 1992). Early postnatal mouse cerebral cortex also expresses seven different Fz receptors (Shimogori et al., 2004). In Fz3 knockout mice cortical axon tracts including the corpus callosum and corticospinal pathway failed to develop (Wang et al., 2002) providing the first evidence that Fz signaling plays an important role in cortical axon development. We blocked or knocked down Ryk receptors which prevented increased cortical axon outgrowth by Wnt5a (Li et al., 2009). In contrast, blocking Wnt/Fz interactions (Rodriguez et al., 2005), did not prevent increased axon outgrowth (**Figure 5**). These results showed that Wnt5a increases in axon outgrowth are mediated by Ryk but not Fz receptors whereas knocking down Ryk and blocking Fz receptors prevents Wnt5a repulsive turning (**Figure 5**). Thus both Ryk and Fz receptors mediate repulsive cortical axon guidance by Wnt5a. Fz receptors are involved in Wnt/calcium signaling during morphogenic events and in cell motility (Kohn and Moon, 2005) but the involvement of Wnt/calcium signaling in axon growth and guidance are unknown. Further, the downstream components of Ryk signaling have not been identified. Wnt5a induced global or local Ca^{2+} transients involving both Ryk and Fz receptor types (Li et al., 2009). The source of intracellular calcium is important for its function (Henley and Poo, 2004; Gomez and Zheng, 2006) and Ca^{2+} release from intracellular stores regulates axon growth and guidance (Ooashi et al., 2005; Jacques-Fricke et al., 2006). To determine the role of this Ca^{2+} signaling mechanism in effects of Wnt5a we blocked IP_3 receptors on the endoplasmic reticulum which blocked calcium release from intracellular stores. This partially attenuated Wnt5a induced Ca^{2+} activity. Calcium influx through TRP (transient receptor potential) channels also plays an important role during axon growth and guidance (Li et al., 2005; Shim et al., 2005; Wang and Poo, 2005). We therefore blocked TRP channels, which also partially inhibited Wnt5a induced calcium activity. Simultaneously blocking calcium release from stores and calcium influx through TRP channels virtually silenced Wnt5a induced calcium activity. Blocking Ca^{2+} release from stores prevented Wnt5a induced increase in axon outgrowth but the same axons showed repulsive turning away from the source of Wnt5a (Li et al., 2009). In contrast, blocking TRP channels prevented both increased axon outgrowth and repulsion by Wnt5a. As in netrin-1 calcium signaling (Tang and Kalil, 2005) CaMKII is an essential downstream component of Wnt5a/calcium signaling. These results suggest a model (**Figure 6**) in which increased axon outgrowth induced by Wnt5a involves activation of Ryk receptors, calcium release from intracellular stores and activation of CaMKII signaling. Growth cone repulsion by a gradient of Wnt5a is mediated by both Ryk and Fz receptors and requires calcium entry through TRP channels but not calcium release from intracellular stores. In support of our results that different calcium

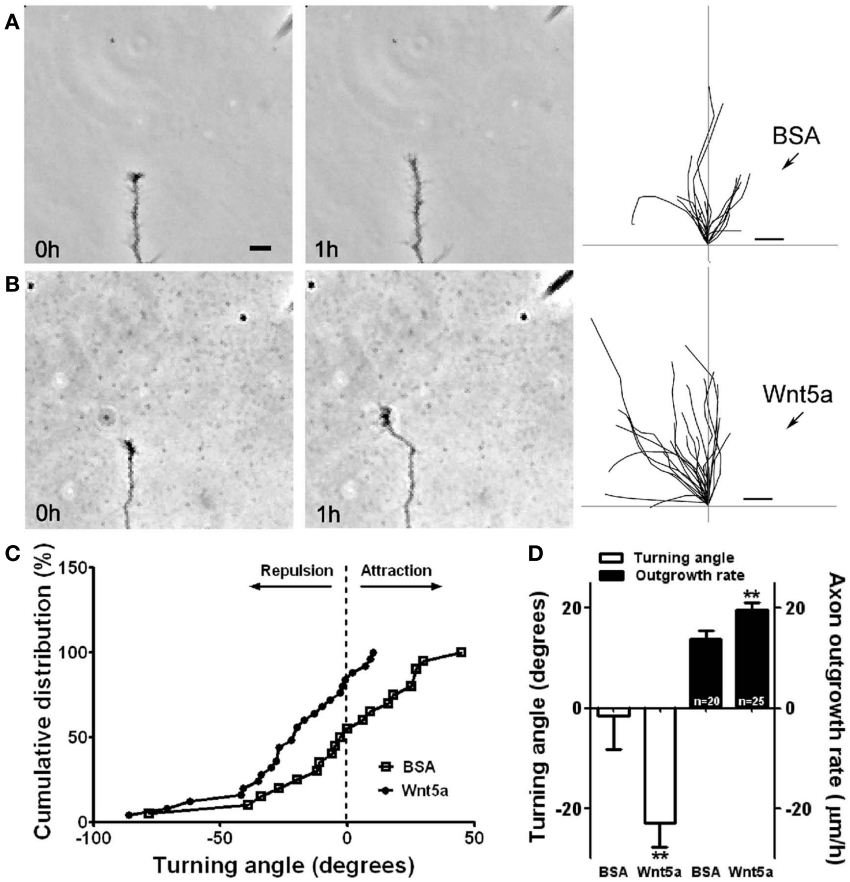

FIGURE 4 | Wnt5a gradients simultaneously increase axon outgrowth and induce repulsive axon turning. (A,B) Time lapse images of a cortical axon and its growth cone at the beginning and end of a 1-h exposure to a point source of BSA (control) **(A)** or 10 μg/ml Wnt5a **(B)** emitted by the pipette at right. The axon extends straight in the BSA gradient but is repelled by the Wnt5a gradient. Right, tracings of trajectories of individual axons extending during 1 h exposure to BSA ($n = 20$ axons) or Wnt5a gradients ($n = 25$ axons) showing random turning in the presence of BSA and repulsive turning in response to Wnt5a. Note that axons repelled by Wnt5a are also significantly longer. **(C)** Cumulative distribution of turning angles of axons showing random turning in BSA and repulsive turning in Wnt5a gradients. **(D)** Bar graphs comparing average turning angles and average axon outgrowth rates in BSA and Wnt5a. In all experiments, neurons were obtained from P2 pups and cultured for 2–3 day before the turning assays. Scale bar, 5 μm. In all histograms, $^{**}p < 0.01$. (Reprinted from Li et al., 2009; with permission from the Society for Neuroscience).

signaling mechanisms (perhaps in different regions of the growth cone) mediate Wnt5a axon growth vs. guidance behaviors, a recent study (Nicol et al., 2011) showed that in *Xenopus* spinal neurons different calcium and cyclic AMP signaling localized to central vs. filopodial growth cone regions mediate netrin-1 evoked axon outgrowth vs. steering. Thus Wnt5a can simultaneously activate different receptors and different calcium signaling pathways at the growth cone to elicit growth and guidance behaviors required for wiring of cortical circuits during development.

AXON GROWTH AND GUIDANCE IN THE CORPUS CALLOSUM IS REGULATED BY Wnt/CALCIUM SIGNALING

Thus far we have discussed mechanisms of axon growth and guidance in dissociated cortical neurons. However, it is important to test the relevance of these mechanisms in a more complex cellular environment that mimics development *in vivo*. For example, in dissociated cultures knocking down CaMKI decreased hippocampal and cortical axon elongation (Ageta-Ishihara et al., 2009; Davare et al., 2009; Neal et al., 2010) whereas knockdown of CaMKI *in vivo* during activity-dependent cortical wiring decreased callosal axon branching into cortex without affecting rates of callosal axon elongation (Ageta-Ishihara et al., 2009). To test the *in vivo* function of Wnt/calcium signaling mechanisms we used living slices of developing hamster sensorimotor cortex that contained the entire callosal pathway (Hutchins et al., 2011). This permitted live cell imaging of intact callosal axons extending along their entire trajectory (Halloran and Kalil, 1994). We electroporated plasmids, encoding the cytoplasmic fluorescent marker DsRed2, into one hemisphere of cortical slices from P0 brains and after 48 h used confocal microscopy to image fluorescently labeled callosal axons (**Figure 7**), which exhibited continual growth cone motility and forward advance during the 90-min imaging sessions. Importantly, axons before the midline (precrossing) advanced more slowly than those that have crossed the midline (postcrossing). To determine whether callosal axons expressed Ca^{2+} transients correlated with rates of

axon outgrowth we electroporated a genetically encoded calcium indicator (GCaMP2) into one hemisphere and measured frequencies of Ca^{2+} transients in pre- and post-crossing axons for up to 30 min. (**Figure 8**). Calcium transients were expressed in axons and growth cones (**Figure 8**) in frequencies closely related to rates of callosal axon outgrowth. Thus higher frequencies of Ca^{2+} transients are well correlated with higher rates of callosal axon outgrowth, similar to our results for dissociated cortical neurons (Hutchins and Kalil, 2008).

The corpus callosum is surrounded by a Wnt5a gradient secreted by midline glial structures (Keeble et al., 2006). Since callosal axons express Ca^{2+} transients correlating with rates of axon outgrowth we reasoned that in the corpus callosum the Wnt5a gradient could mediate axon growth and guidance by calcium signaling mechanisms. To determine whether Ca^{2+} release from

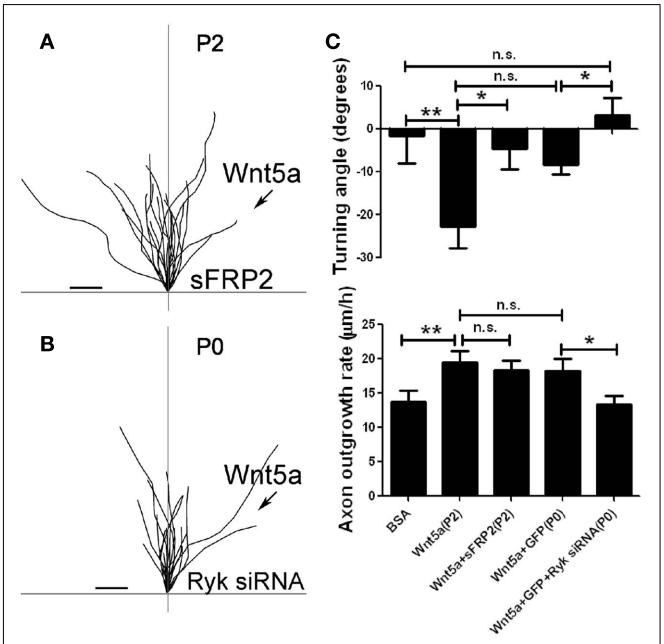

FIGURE 5 | Fz receptors mediate Wnt5a induced axon repulsion but not outgrowth, but Ryk receptors mediate both outgrowth and repulsion. **(A)** Tracings of trajectories of axons exposed to Wnt5a gradients in the presence of sFRP2 showing increased axon outgrowth but not repulsion. **(B)** Tracings of trajectories of P0 axons exposed to Wnt5a gradients following Ryk knockdown, which prevents increased axon outgrowth as well as repulsion by Wnt5a. **(C)** Bar graphs quantifying turning angles (top) and outgrowth rates (bottom) of axons in **(A)** and **(B)**. Scale bar, 5 μm. In all histograms $*p < 0.05$, $**p < 0.01$; n.s., not significant. (Reprinted from Li et al., 2009; with permission from the Society for Neuroscience).

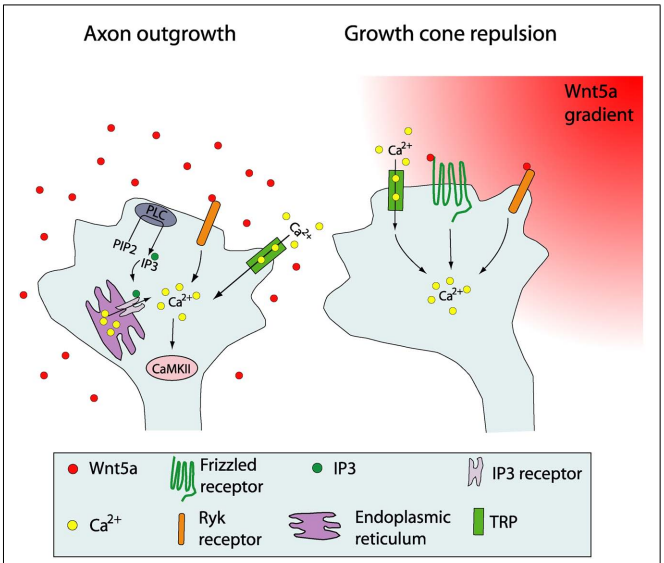

FIGURE 6 | Schematic summary showing Wnt receptors and calcium signaling components involved in cortical growth cone behaviors in response to Wnt5a. At left, increased cortical axon outgrowth is induced by Wnt5a, which involves activation of Ryk receptors, calcium entry through TRP channels, calcium release from intracellular stores via IP3 receptors on the endoplasmic reticulum, and activation of PLC and CaMKII signaling. At right, growth cone repulsion by a Wnt5a gradient is mediated by both Ryk and Fz receptors and requires calcium entry through TRP channels. Symbols in the growth cone are shown in the box. (Reprinted from Li et al., 2009; with permission from the Society for Neuroscience).

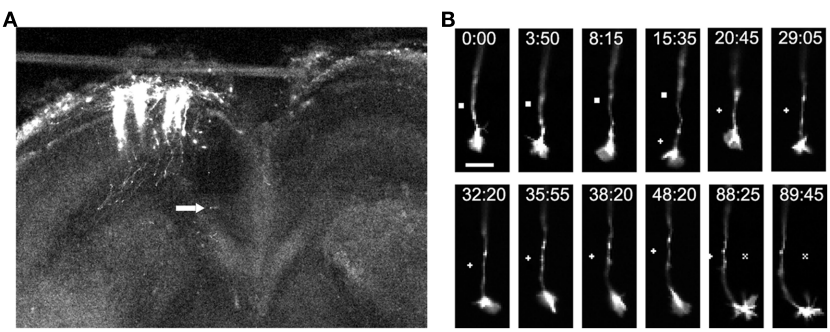

FIGURE 7 | Imaging of individual callosal axons and their growth cones extending through the corpus callosum. **(A)** A low power confocal image of a cortical slice at 3DIV, after electroporation of cortical neurons with DsRed2 in the slice from P0 sensorimotor hamster cortex. Individual efferent axons are clearly visible. Arrow indicates location of the cortical growth cone imaged at higher power in the time lapse sequence in **(B)** which shows filopodia and lamellipodia of growth cones during outgrowth and turning. Times are in minutes and seconds. Scale bar, 10 μm. Symbols show reference points. (Reprinted from Hutchins et al., 2011).

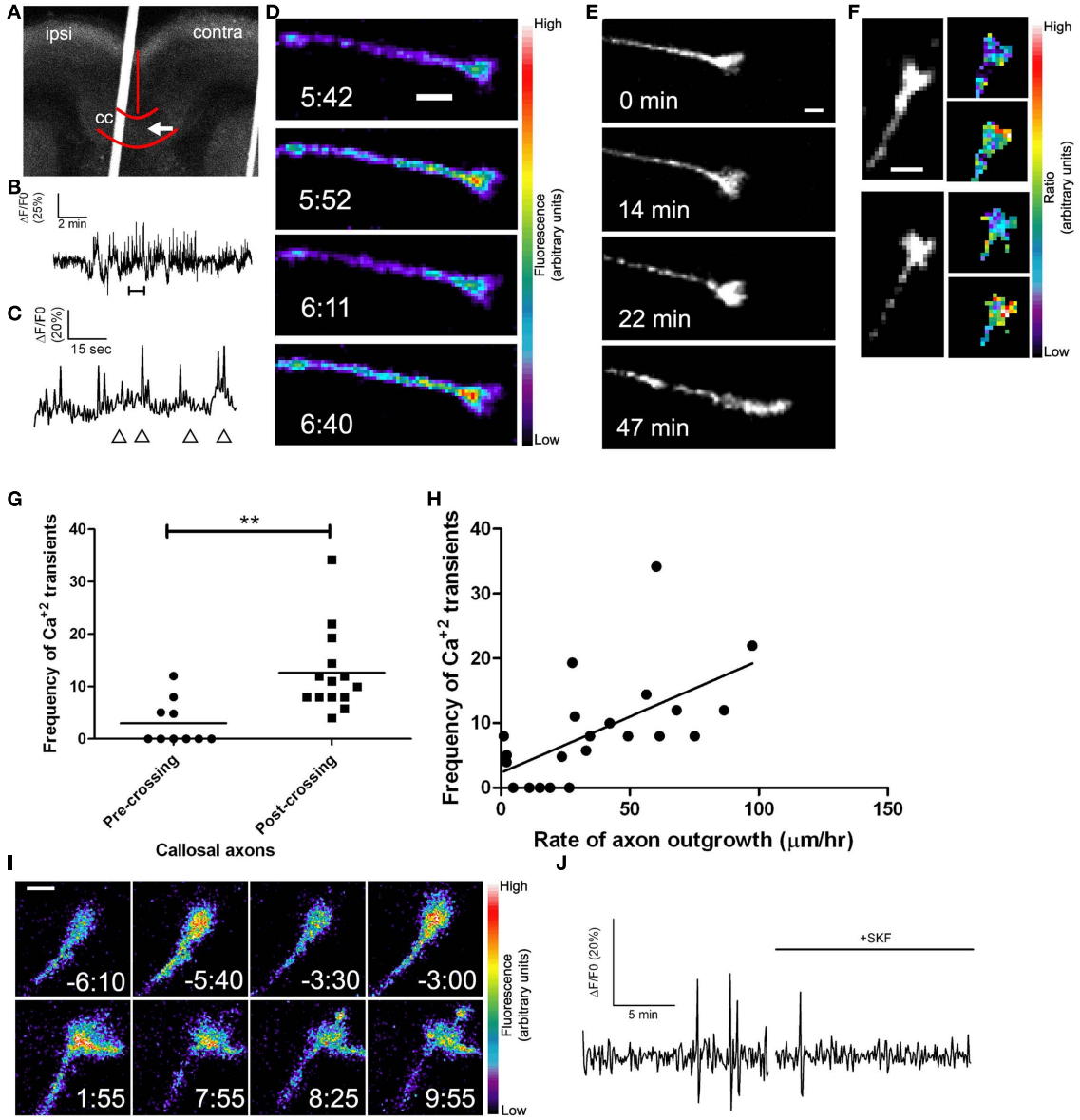

FIGURE 8 | Callosal axons express spontaneous calcium transients positively correlated with rates of axon outgrowth. (A) A coronal cortical slice electroporated with GCaMP2 plasmids into the left cortex. Arrow indicates postcrossing (contra) position of the growth cone imaged in **(D)**. Borders of the callosum (cc) and the midline are outlined in red. **(B)** Tracing of calcium activity measured by changes in GCaMP2 fluorescence over baseline. Calcium activity increases after a few min. **(C)** Tracing of calcium activity from **(B)** zoomed in to the time shown in the bracket. **(D)** Fluorescence images of the growth cone measured in **(B,C)** at time points indicated by the arrowheads in **(C)**. **(E)** Within 20 min of the onset of calcium activity shown in **(B)** the axon begins to advance rapidly through the contralateral callosum. **(F)** Examples of single calcium transients measured by ratiometric imaging of growth cones co-expressing DsRed2 and GCaMP2. **(G)** Plot of frequencies of calcium transients in pre- or post-crossing callosal axons, $^{**}p < 0.01$, *t* test. All frequencies are in transients/h. **(H)** Scatter plot of the frequency of calcium transients vs. the rate of axon outgrowth in individual callosal axons. The line represents the least-squares linear regression (slope significantly non-zero, $p < 0.01$). **(I)** An example of spontaneous calcium transients (top row) which are attenuated by application of SKF at time 0.00 (bottom row). **(J)** Tracing of calcium activity in the growth cone shown in **(I)** before and after application of SKF. Scale bars 10 μm except **(I)** which is 5 μm. Pseudocolor calibration bars indicate fluorescence intensity **(D)** or ratio of GCaMP2 to DsRed2 fluorescence intensities **(F)** in arbitrary units. (Reprinted from Hutchins et al., 2011).

stores plays a role in regulating callosal axon outgrowth we blocked IP_3 receptors (on the endoplasmic reticulum) pharmacologically to inhibit calcium release from stores. Using live cell imaging, we measured growth of postcrossing axons since a recent study (Wang et al., 2007) showed that *in vivo* suppression of spontaneous electrical activity in mouse callosal axons decreased rates of axon outgrowth on the postcrossing but not the precrossing side of the callosum. Treatment with blockers to IP_3 receptors slowed

axon outgrowth of postcrossing axons but their normal rates were restored after washout of the blocking reagent. However, blocking Ca^{2+} release from stores had no effect on guidance of callosal axons whose trajectories (measured from images obtained at the beginning and end of the 3-h experiments) after crossing the midline were similar to those of untreated controls. In contrast, pharmacologically blocking Ca^{2+} entry through TRP channels not only slowed axon outgrowth but also severely misrouted postcrossing callosal axons, which turned prematurely toward the cortical plate or turned ventrally toward the septum. We verified the involvement of calcium activity by blocking TRP channels and then measuring effects on Ca^{2+} transients in individual postcrossing callosal axons. As shown in **Figure 8I**, blocking TRP channels attenuated frequencies of Ca^{2+} transients to about 3 h compared with 12 h for controls, showing directly that the growth and guidance defects resulted from decreased Ca^{2+} activity. Furthermore, as we found in dissociated cultures, calcium signaling by store release or by Ca^{2+} entry through TRP channels respectively mediates axon outgrowth or both axon outgrowth and guidance in the corpus callosum.

Although these results demonstrate the requirement for calcium signaling in outgrowth and guidance of callosal axons, it was important to show the specific involvement of Wnt5a signaling. *In vivo* knockout mice lacking the Wnt5a Ryk receptor showed guidance errors in callosal axons only after they crossed the midline (Keeble et al., 2006). This is consistent with the finding that mouse callosal axons do not respond to Wnt5a until the age when they cross the midline (E 16) and begin to express the Ryk receptor (Keeble et al., 2006). However, these experiments did not address signaling mechanisms downstream of Ryk receptors. Therefore, we knocked down the Ryk receptor by electroporation of Ryk siRNA in a small number of axons and then analyzed effects on DsRed2 labeled callosal axons in living cortical slices (Hutchins et al., 2011). Ryk knockdown slowed the growth rate of postcrossing callosal axons to half their normal growth rate, but had no effect on precrossing axon growth rates, consistent with Ryk expression on callosal axons only after they cross the midline (Keeble et al., 2006). Importantly, Ryk knockdown also caused severe guidance errors in about a third of labeled postcrossing axons that deviated inappropriately toward the septum or prematurely turned toward the overlying cortex. Since we found previously (Li et al., 2009) that knocking down the Ryk receptor reduced the proportion of neurons expressing Ca^{2+} transients in response to Wnt5a, we asked whether growth and guidance defects in callosal axons in which Ryk was knocked down resulted from interference with Wnt5a evoked calcium signaling. To address this question we coelectroporated the calcium biosensor GCaMP2 with Ryk siRNA to measure calcium activity in neurons in which RyK/Wnt signaling was disrupted. In such neurons frequencies of Ca^{2+} transients were reduced fourfold in postcrossing axons. Remarkably, in growth cones projecting aberrantly toward the septum, Ca^{2+} transients were undetectable. Taken together, these results suggest that callosal axon growth and guidance errors caused by Ryk knockdown result from attenuation of calcium activity. Since CaMKII is also a component of the Wnt/calcium signaling pathway (Li et al., 2009), we investigated its role in callosal axon growth and guidance by cortical transfection of plasmids encoding an inhibitory CaMKII protein (Tang and Kalil, 2005). For postcrossing but not precrossing axons, this treatment slowed axon outgrowth by about half and caused dramatic axon guidance errors in which some axons projected aberrantly while others looped backward in the corpus callosum. Do these defects represent a failure of axon repulsion mechanisms mediated by Wnt5a? Using turning assays in which dissociated neurons were exposed to Wnt5a gradients, we found that neurons transfected with the CaMKII inhibitor were unable to increase their growth rates or show repulsive turning. These results suggest that CaMKII, downstream of Wnt/calcium signaling, is necessary for the outgrowth and repulsive guidance mechanisms by which Wnt5a regulates development of callosal axons.

Taken together these results, summarized in a cortical slice model of the developing corpus callosum (**Figure 9**), show that Wnt/calcium signaling pathways are essential for regulating callosal axon outgrowth and guidance. Nevertheless, additional growth and guidance factors are known to regulate development of the corpus callosum (Lindwall et al., 2007). For example, in addition to Wnt5a, sources of netrins, semaphorins, and Slit 2 surround the corpus callosum and their role in callosal axon guidance across the midline has been well characterized (Shu and Richards, 2001; Shu et al., 2003; Niquille et al., 2009; Piper et al., 2009). Although direct evidence for netrins in guiding callosal axons to the midline is lacking, callosal axons express the netrin-1 receptor DCC and netrin-1 knockout mice lack all forebrain commissural projections (Serafini et al., 1996). Slits are chemorepellent proteins expressed in glial structures adjacent to the callosal midline in a pattern similar to that of Wnt5a. Knockout mice lacking the Slit receptor Robo 1 display aberrant projections of callosal axons that are misdirected at the midline, suggesting that Slits may channel callosal axons into the correct pathway (Lindwall et al., 2007). Mutant mice whose axons are unable to bind semaphorins also show callosal malformations. However, our finding that inhibiting calcium signaling only affected growth of axons after but not before the midline suggests the involvement of Wnt5a signaling because cortical axons do not respond to Wnt5a until the age at which they cross the midline (Keeble et al., 2006). Although Slit 2 affects both pre- and post-crossing axons (Shu and Richards, 2001; Shu et al., 2003) our results show that interfering with Wnt/calcium/CaMKII signaling only affects postcrossing axon outgrowth.

MICROTUBULE DYNAMICS REGULATE Wnt5a EVOKED AXON OUTGROWTH AND GUIDANCE

Growth cone behaviors are regulated by reorganization and dynamics of the actin and microtubule (MT) cytoskeleton (Dent and Gertler, 2003; Lowery and Van Vactor, 2009), which can be modulated by extracellular guidance cues (Luo, 2002; Huber et al., 2003; Kalil and Dent, 2005). Stable microtubules occupy the central region of the growth cone while dynamic MTs that grow and shrink in dynamic instability actively explore the periphery (Dent et al., 1999; Dent and Kalil, 2001; Schaefer et al., 2002, 2008; Lowery and Van Vactor, 2009). Inhibiting MT dynamics can abolish growth cone turning and localized MT stabilization and de-stabilization can induce attractive turning and repulsion (Buck and Zheng, 2002), suggesting an instructive role for MTs in axon guidance. Wnt signaling increases MT stability and Wnt3a

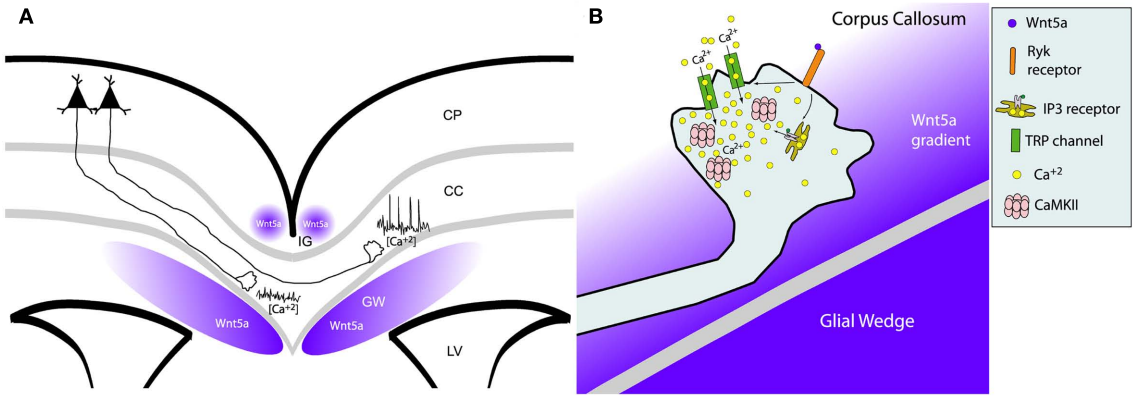

FIGURE 9 | Wnt/calcium signaling guides axon growth through the corpus callosum. (A) Schematic of a cortical slice showing cortical axons extending through the corpus callosum (cc) surrounded by Wnt5a secreted by the indusium griseum (IG) and glial wedge (GW). Axons in the contralateral callosum have high frequencies of calcium transients evoked by Wnt5a signaling, which accelerates rates of axon outgrowth. In contrast, ipsilateral axons not yet responsive to Wnt5a, have low levels of calcium activity and thus grow more slowly. LV, lateral ventricle; CP, cortical plate. **(B)** Schematic of intracellular signaling in the postcrossing axon from **(A)** showing that Wnt5a gradient from the glial wedge activates RyK receptors to open IP3 receptors and TRP channels causing release of calcium from intracellular stores and calcium influx through the plasma membrane. These calcium transients activate CaMKII to accelerate axon extension and repel growth cones away from the glial wedge toward the contralateral cortex. (Reprinted from Hutchins et al., 2011).

and Wnt7a specifically decrease axon length and increase growth cone size of DRG and cerebellar mossy fiber terminals (Lucas and Salinas, 1997; Hall et al., 2000) by reorganization of MTs into stable loops (Ciani and Salinas, 2005; Salinas, 2007; Purro et al., 2008). This occurs through changes in MT directionality across the growth cone rather than toward the leading edge (Purro et al., 2008). In contrast we showed that Wnt5a increases cortical axon outgrowth and induces growth cone repulsion (Li et al., 2009) but the cytoskeletal mechanisms are unknown. Our preliminary results (Li et al., unpublished observations) suggest that reorganization of dynamic MTs plays a major role in increased axon outgrowth and repulsive growth cone turning induced by Wnt5a.

We first confirmed that dynamic MTs are required for the growth promoting and guidance effects of Wnt5a by applying nocodazole, an inhibitor of MT dynamics (Dent and Kalil, 2001), which prevented Wnt5a induced increases in axon outgrowth and repulsive turning in Wnt5a gradients. To determine the relationship between directionality of MTs and the direction of growth cone advance induced by Wnt5a, we used high resolution fluorescence (total internal reflection fluorescence, TIRF) microscopy to image growth cones of early postnatal cortical neurons transfected with an EGFP-EB3 construct to label dynamic MT plus ends and DsRed2 to label the cytoplasm. EB3 is a +TIP protein that binds to the growing plus ends of MTs (Nakagawa et al., 2000) and EGFP-EB3 has been used to image MT dynamics in neurons (Stepanova et al., 2003). Dynamic growing MT tips were visualized as EB3 "comets" in cortical growth cones before and after bath application of Wnt5a. Wnt5a oriented dynamic MTs in the direction of axon elongation, suggesting that increased axon outgrowth by Wnt5a occurs by reorientation of dynamic MTs. We then applied Wnt5a as a gradient to investigate the possible redistribution of dynamic MTs in growth cones during repulsive turning behaviors. Preliminary results (**Figure 10**) showed that before application of Wnt5a

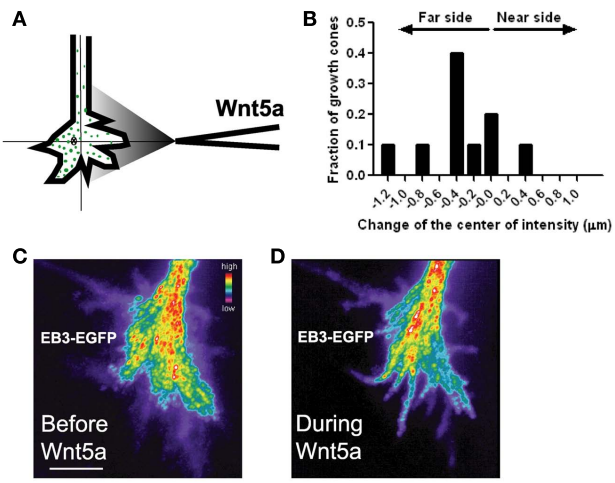

FIGURE 10 | Wnt5a gradients induce redistribution and reorganization of dynamic microtubules (MTs) in growth cones. (A) Schematic of measurement of the distribution of EB3 comets on MT plus ends in the presence of a pipette gradient of Wnt5a locally applied at the right side of the growth cone. Individual EB3 comets are detected by fluorescence (green dots) and their center of intensity (cross) is determined. **(B)** Localization of the center of intensity of EB3 comets evoked by a Wnt5a gradient in 10 growth cones in independent experiments including the growth cone shown in **(C,D)**. Negative numbers indicate EB3 localization to the side of the growth cone farthest from the Wnt5a source. Change of the center of intensity = $-0.35 \pm 0.14\,\mu m$ ($p < 0.05$, Wilcoxon signed rank test). **(C,D)** Composite images of the same growth cone showing redistribution of EB3 comets over time 30 min before and during 30 min of application of the Wnt5a gradient ($n = 601$ images before Wnt5a and 601 images during Wnt5a application). The maximum intensity was computed for each pixel from the entire image stack by using algorithms in Metamorph. Using these values stacks of all images were superimposed and pixels assigned values in pseudocolor to indicate fluorescence intensity.

EB3 comets were randomly distributed throughout the growth cone but during 30 min exposure of growth cones to Wnt5a gradients EB3 comets redistributed to the far side of the growth cone away from the Wnt5a source. These results suggest that in Wnt5a gradients asymmetric redistribution of dynamic MTs may be a first step in repulsive turning.

Gradients of guidance cues can evoke asymmetries in calcium activity (Gomez and Zheng, 2006) that are typically highest on the side of the growth cone facing a source of either an attractive or repulsive guidance cue gradient. Thus it was surprising to find that Wnt5a can evoke Ca^{2+} transients localized to the far side of the growth cone facing away from the Wnt5a source. The coincidence of MT and Ca^{2+} asymmetries led us to investigate a possible relationship between asymmetries in Ca^{2+} transients and the redistribution of dynamic MTs in growth cones exposed to Wnt5a gradients. One candidate link is the MT associated protein tau which binds to MTs to increase their stability (Dehmelt and Halpain, 2005). CaMKII phosphorylates tau at the MT binding site (Litersky et al., 1996; Sironi et al., 1998). This leads to detachment of tau from MTs and thus decreased MT stability and increased MT dynamics (Biernat et al., 1993). Furthermore, Wnt5a is known to activate CaMKII (Kuhl et al., 2000). Together these findings led us to investigate tau as a possible link between calcium signaling and dynamic MTs. To determine whether tau is required for the growth promoting effects of Wnt5a on cortical axons, we knocked down tau with siRNAs which prevented Wnt5a from increasing rates of cortical axon outgrowth. Importantly, this treatment also prevented growth cone repulsion in Wnt5a gradients. We then co-transfected cortical neurons with EGFP-EB3 and tau siRNA, and imaged dynamic MTs by following EB3 comets in growth cones. Remarkably, we found that tau knockdown prevented the redistribution of dynamic MTs toward the far side of the growth cone facing away from the Wnt5a gradient. As shown in **Figure 11** dynamic MTs remain randomly distributed throughout the growth cones as in untreated controls. Since calcium activity is required for the growth and guidance effects of Wnt5a on cortical axons *in vitro* (Li et al., 2009) and within the corpus callosum (Hutchins et al., 2011) these results suggest a relationship, possibly mediated by tau, between Wnt5a evoked calcium signaling and the redistribution of dynamic MTs during Wnt5a evoked cortical growth cone repulsion.

FUTURE DIRECTIONS

This review has emphasized the central role of intracellular calcium signaling in transducing the effects of guidance molecules on growth and guidance of cortical axons during development. However, many questions remain unanswered. First, the mechanisms by which guidance cues evoke calcium transients localized to small regions of axons and growth cones are not well understood. Second, how competitive mechanisms, mediated by calcium signaling, favor the growth of one cortical axon process over another requires further study. Third, the relationship between calcium activity and cytoskeletal dynamics leading to cortical axon branching, outgrowth and guidance remains obscure. Fourth, effects of guidance cues on cytoskeletal reorganization leading to specific growth cone behaviors are only beginning to be addressed. Finally, it is not always clear that axon growth and guidance mechanisms identified in tissue culture are applicable to development *in vivo*. Thus a major challenge will be to elucidate how axons of neurons in the complex *in vivo* environment of the cerebral cortex can integrate multiple extracellular guidance cues and intracellular signaling pathways necessary for appropriate axon outgrowth, guidance, and branching during wiring of cortical circuits.

ACKNOWLEDGMENTS

The work from our laboratory was funded by National Institutes of Health Grant NSO14428 and grants from the Whitehall

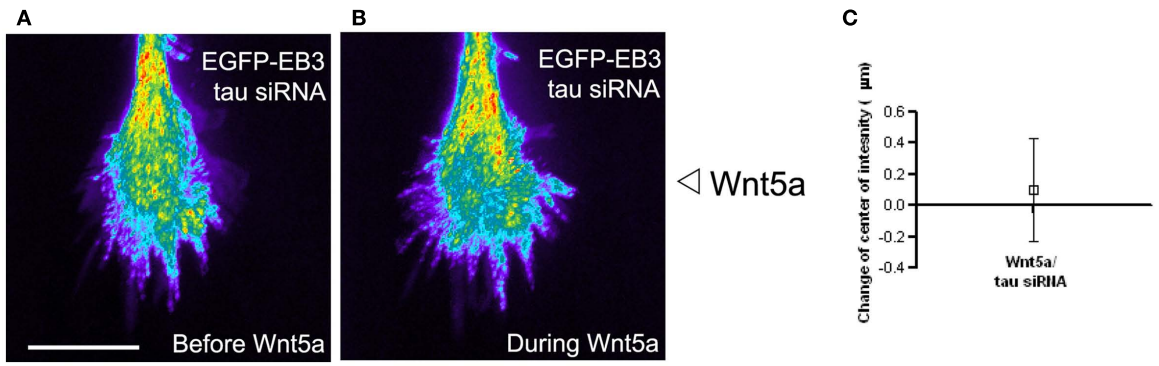

FIGURE 11 | The microtubule associated protein tau is required for Wnt5a induced redistribution of dynamic MTs in growth cones. (A,B) Composite images showing the redistribution of EB3 comets in the same growth cone over time 30 min before and during 30 min of application of the Wnt5a gradient ($n = 361$ images before Wnt5a and 601 images during Wnt5a application). The maximum intensity was computed for each pixel from the entire image stack by using algorithms in Metamorph. Using these values stacks of all images were superimposed and pixels assigned values in pseudocolor to indicate fluorescence intensity. Wnt5a was locally applied as a gradient at the right side of the growth cone. In this growth cone tau was knocked down with siRNA, which prevented the asymmetric redistribution of EB3 comets during exposure of the growth cone to Wnt5a gradients. **(C)** Localization of the center of intensity of EB3 comets evoked by Wnt5a gradients in four growth cones in independent experiments including the growth cone shown in **(A,B)**. Quantitative analysis shows that Wnt5a fails to induce redistribution of EB3 comets to the far side of the growth cone after tau knockdown with siRNA (change in center of intensity not different from 0. $p > 0.05$, Wilcoxon signed rank test).

Foundation and the University of Wisconsin Graduate School (to Katherine Kalil), a Herman Shapiro fellowship (to Li Li), and National Research Service Award GM801642 (to Bruce Ian Hutchins). Bruce Ian Hutchins is currently supported by the Intramural Research Program of NINDS and the Pharmacology Research Associate Program of NIGMS.

REFERENCES

Ageta-Ishihara, N., Takemoto-Kimura, S., Nonaka, M., Adachi-Morishima, A., Suzuki, K., Kamijo, S., Fujii, H., Mano, T., Blaeser, F., Chatila, T. A., Mizuno, H., Hirano, T., Tagawa, Y., Okuno, H., and Bito, H. (2009). Control of cortical axon elongation by a GABA-driven Ca2+/calmodulin-dependent protein kinase cascade. *J. Neurosci.* 29, 13720–13729.

Bagnard, D., Lohrum, M., Uziel, D., Puschel, A. W., and Bolz, J. (1998). Semaphorins act as attractive and repulsive guidance signals during the development of cortical projections. *Development* 125, 5043–5053.

Bastmeyer, M., and O'Leary, D. D. (1996). Dynamics of target recognition by interstitial axon branching along developing cortical axons. *J. Neurosci.* 16, 1450–1459.

Biernat, J., Gustke, N., Drewes, G., Mandelkow, E. M., and Mandelkow, E. (1993). Phosphorylation of Ser262 strongly reduces binding of tau to microtubules: distinction between PHF-like immunoreactivity and microtubule binding. *Neuron* 11, 153–163.

Borodinsky, L. N., O'Leary, D., Neale, J. H., Vicini, S., Coso, O. A., and Fiszman, M. L. (2003). GABA-induced neurite outgrowth of cerebellar granule cells is mediated by GABA(A) receptor activation, calcium influx and CaMKII and erk1/2 pathways. *J. Neurochem.* 84, 1411–1420.

Buck, K. B., and Zheng, J. Q. (2002). Growth cone turning induced by direct local modification of microtubule dynamics. *J. Neurosci.* 22, 9358–9367.

Butz, M., Worgotter, F., and van Ooyen, A. (2009). Activity-dependent structural plasticity. *Brain Res. Rev.* 60, 287–305.

Cancedda, L., Fiumelli, H., Chen, K., and Poo, M. M. (2007). Excitatory GABA action is essential for morphological maturation of cortical neurons in vivo. *J. Neurosci.* 27, 5224–5235.

Ciani, L., and Salinas, P. C. (2005). WNTs in the vertebrate nervous system: from patterning to neuronal connectivity. *Nat. Rev. Neurosci.* 6, 351–362.

Cullen, P. J., and Lockyer, P. J. (2002). Integration of calcium and Ras signaling. *Nat. Rev. Mol. Cell Biol.* 3, 339–348.

Davare, M. A., Fortin, D. A., Saneyoshi, T., Nygaard, S., Kaech, S., Banker, G., Soderling, T. R., and Wayman, G. A. (2009). Transient receptor potential canonical 5 channels activate Ca2+/calmodulin kinase Igamma to promote axon formation in hippocampal neurons. *J. Neurosci.* 29, 9794–9808.

Dehmelt, L., and Halpain, S. (2005). The MAP2/Tau family of microtubule-associated proteins. *Genome Biol.* 6, 204.

Dent, E. W., Barnes, A. M., Tang, F., and Kalil, K. (2004). Netrin-1 and semaphorin 3A promote or inhibit cortical axon branching, respectively, by reorganization of the cytoskeleton. *J. Neurosci.* 24, 3002–3012.

Dent, E. W., Callaway, J. L., Szebenyi, G., Baas, P. W., and Kalil, K. (1999). Reorganization and movement of microtubules in axonal growth cones and developing interstitial branches. *J. Neurosci.* 19, 8894–8908.

Dent, E. W., and Gertler, F. B. (2003). Cytoskeletal dynamics and transport in growth cone motility and axon guidance. *Neuron* 40, 209–227.

Dent, E. W., and Kalil, K. (2001). Axon branching requires interactions between dynamic microtubules and actin filaments. *J. Neurosci.* 21, 9757–9769.

Dent, E. W., Tang, F., and Kalil, K. (2003). Axon guidance by growth cones and branches: common cytoskeletal and signaling mechanisms. *Neuroscientist* 9, 343–353.

Dickson, B. J. (2002). Molecular mechanisms of axon guidance. *Science* 298, 1959–1964.

Eshete, F., and Fields, R. D. (2001). Spike frequency decoding and autonomous activation of Ca2+-calmodulin-dependent protein kinase II in dorsal root ganglion neurons. *J. Neurosci.* 21, 6694–6705.

Fink, C. C., Bayer, K. U., Myers, J. W., Ferrell, J. E. Jr., Schulman, H., and Meyer, T. (2003). Selective regulation of neurite extension and synapse formation by the beta but not the alpha isoform of CaMKII. *Neuron* 39, 283–297.

Flynn, K. C., Pak, C. W., Shaw, A. E., Bradke, F., and Bamburg, J. R. (2009). Growth cone-like waves transport actin and promote axonogenesis and neurite branching. *Dev. Neurobiol.* 69, 761–779.

Gomez, T. M., and Zheng, J. Q. (2006). The molecular basis for calcium-dependent axon pathfinding. *Nat. Rev. Neurosci.* 7, 115–125.

Gorbunova, Y. V., and Spitzer, N. C. (2002). Dynamic interactions of cyclic AMP transients and spontaneous Ca(2+) spikes. *Nature* 418, 93–96.

Hall, A. C., Lucas, F. R., and Salinas, P. C. (2000). Axonal remodeling and synaptic differentiation in the cerebellum is regulated by WNT-7a signaling. *Cell* 100, 525–535.

Halloran, M. C., and Kalil, K. (1994). Dynamic behaviors of growth cones extending in the corpus callosum of living cortical brain slices observed with video microscopy. *J. Neurosci.* 14, 2161–2177.

Harter, P. N., Bunz, B., Dietz, K., Hoffmann, K., Meyermann, R., and Mittelbronn, M. (2010). Spatiotemporal deleted in colorectal cancer (DCC) and netrin-1 expression in human foetal brain development. *Neuropathol. Appl. Neurobiol.* 36, 623–635.

Henley, J., and Poo, M. M. (2004). Guiding neuronal growth cones using Ca2+ signals. *Trends Cell Biol.* 14, 320–330.

Hong, K., Nishiyama, M., Henley, J., Tessier-Lavigne, M., and Poo, M. (2000). Calcium signaling in the guidance of nerve growth by netrin-1. *Nature* 403, 93–98.

Hua, J. Y., Smear, M. C., Baier, H., and Smith, S. J. (2005). Regulation of axon growth in vivo by activity-based competition. *Nature* 434, 1022–1026.

Huber, A. B., Kolodkin, A. L., Ginty, D. D., and Cloutier, J. F. (2003). Signaling at the growth cone: ligand-receptor complexes and the control of axon growth and guidance. *Annu. Rev. Neurosci.* 26, 509–563.

Hudmon, A., and Schulman, H. (2002). Neuronal CA2+/calmodulin-dependent protein kinase II: the role of structure and autoregulation in cellular function. *Annu. Rev. Biochem.* 71, 473–510.

Hutchins, B. I. (2010). Competitive outgrowth of neural processes arising from long-distance cAMP signaling. *Sci. Signal.* 3, jc1.

Hutchins, B. I., and Kalil, K. (2008). Differential outgrowth of axons and their branches is regulated by localized calcium transients. *J. Neurosci.* 28, 143–153.

Hutchins, B. I., Li, L., and Kalil, K. (2011). Wnt/calcium signaling mediates axon growth and guidance in the developing corpus callosum. *Dev. Neurobiol.* 71, 269–283.

Jacques-Fricke, B. T., Seow, Y., Gottlieb, P. A., Sachs, F., and Gomez, T. M. (2006). Ca2+ influx through mechanosensitive channels inhibits neurite outgrowth in opposition to other influx pathways and release from intracellular stores. *J. Neurosci.* 26, 5656–5664.

Kalil, K., and Dent, E. W. (2005). Touch and go: guidance cues signal to the growth cone cytoskeleton. *Curr. Opin. Neurobiol.* 15, 521–526.

Kalil, K., Szebenyi, G., and Dent, E. W. (2000). Common mechanisms underlying growth cone guidance and axon branching. *J. Neurobiol.* 44, 145–158.

Keeble, T. R., Halford, M. M., Seaman, C., Kee, N., Macheda, M., Anderson, R. B., Stacker, S. A., and Cooper, H. M. (2006). The Wnt receptor Ryk is required for Wnt5a-mediated axon guidance on the contralateral side of the corpus callosum. *J. Neurosci.* 26, 5840–5848.

Kohn, A. D., and Moon, R. T. (2005). Wnt and calcium signaling: beta-catenin-independent pathways. *Cell Calcium* 38, 439–446.

Kuhl, M., Sheldahl, L. C., Malbon, C. C., and Moon, R. T. (2000). Ca(2+)/calmodulin-dependent protein kinase II is stimulated by Wnt and Frizzled homologs and promotes ventral cell fates in Xenopus. *J. Biol. Chem.* 275, 12701–12711.

Lau, P. M., Zucker, R. S., and Bentley, D. (1999). Induction of filopodia by direct local elevation of intracellular calcium ion concentration. *J. Cell Biol.* 145, 1265–1275.

Li, L., Hutchins, B. I., and Kalil, K. (2009). Wnt5a induces simultaneous cortical axon outgrowth and repulsive axon guidance through distinct signaling mechanisms. *J. Neurosci.* 29, 5873–5883.

Li, Y., Jia, Y. C., Cui, K., Li, N., Zheng, Z. Y., Wang, Y. Z., and Yuan, X. B. (2005). Essential role of TRPC channels in the guidance of nerve growth cones by brain-derived neurotrophic factor. *Nature* 434, 894–898.

Lindwall, C., Fothergill, T., and Richards, L. J. (2007). Commissure formation in the mammalian forebrain. *Curr. Opin. Neurobiol.* 17, 3–14.

Litersky, J. M., Johnson, G. V., Jakes, R., Goedert, M., Lee, M., and Seubert, P. (1996). Tau protein is phosphorylated by cyclic AMP-dependent protein kinase and calcium/calmodulin-dependent protein kinase II within its microtubule-binding domains at Ser-262 and Ser-356. *Biochem. J.* 316(Pt 2), 655–660.

Liu, Y., Shi, J., Lu, C. C., Wang, Z. B., Lyuksyutova, A. I., Song, X. J., and Zou, Y. (2005). Ryk-mediated Wnt repulsion regulates posterior-directed growth of corticospinal tract. *Nat. Neurosci.* 8, 1151–1159.

Livesey, F. J., and Hunt, S. P. (1997). Netrin and netrin receptor expression in the embryonic mammalian nervous system suggests roles in retinal, striatal, nigral, and cerebellar development. *Mol. Cell. Neurosci.* 8, 417–429.

Lowery, L. A., and Van Vactor, D. (2009). The trip of the tip: understanding the growth cone machinery. *Nat. Rev. Mol. Cell Biol.* 10, 332–343.

Lucas, F. R., and Salinas, P. C. (1997). WNT-7a induces axonal remodeling and increases synapsin I levels in cerebellar neurons. *Dev. Biol.* 192, 31–44.

Luo, L. (2002). Actin cytoskeleton regulation in neuronal morphogenesis and structural plasticity. *Annu. Rev. Cell Dev. Biol.* 18, 601–635.

Luo, L., and O'Leary, D. D. (2005). Axon retraction and degeneration in development and disease. *Annu. Rev. Neurosci.* 28, 127–156.

Manitt, C., and Kennedy, T. E. (2002). Where the rubber meets the road: netrin expression and function in developing and adult nervous systems. *Prog. Brain Res.* 137, 425–442.

McLaughlin, T., and O'Leary, D. D. (2005). Molecular gradients and development of retinotopic maps. *Annu. Rev. Neurosci.* 28, 327–355.

Metin, C., Deleglise, D., Serafini, T., Kennedy, T. E., and Tessier-Lavigne, M. (1997). A role for netrin-1 in the guidance of cortical efferents. *Development* 124, 5063–5074.

Ming, G. L., Wong, S. T., Henley, J., Yuan, X. B., Song, H. J., Spitzer, N. C., and Poo, M. M. (2002). Adaptation in the chemotactic guidance of nerve growth cones. *Nature* 417, 411–418.

Morris, R. L., and Hollenbeck, P. J. (1993). The regulation of bidirectional mitochondrial transport is coordinated with axonal outgrowth. *J. Cell Sci.* 104(Pt 3), 917–927.

Nakagawa, H., Koyama, K., Murata, Y., Morito, M., Akiyama, T., and Nakamura, Y. (2000). EB3, a novel member of the EB1 family preferentially expressed in the central nervous system, binds to a CNS-specific APC homologue. *Oncogene* 19, 210–216.

Neal, A. P., Molina-Campos, E., Marrero-Rosado, B., Bradford, A. B., Fox, S. M., Kovalova, N., and Hannon, H. E. (2010). CaMKK-CaMKI signaling pathways differentially control axon and dendrite elongation in cortical neurons. *J. Neurosci.* 30, 2807–2809.

Nicol, X., Hong, K. P., and Spitzer, N. C. (2011). Spatial and temporal second messenger codes for growth cone turning. *Proc. Natl. Acad. Sci. U.S.A.* 108, 13776–13781.

Niquille, M., Garel, S., Mann, F., Hornung, J. P., Otsmane, B., Chevalley, S., Parras, C., Guillemot, F., Gaspar, P., Yanagawa, Y., and Lebrand, C. (2009). Transient neuronal populations are required to guide callosal axons: a role for semaphorin 3C. *PLoS Biol.* 7, e1000230. doi:10.1371/journal.pbio.1000230

Norris, C. R., and Kalil, K. (1992). Development of callosal connections in the sensorimotor cortex of the hamster. *J. Comp. Neurol.* 326, 121–132.

O'Leary, D. D., Bicknese, A. R., De Carlos, J. A., Heffner, C. D., Koester, S. E., Kutka, L. J., and Terashima, T. (1990). Target selection by cortical axons: alternative mechanisms to establish axonal connections in the developing brain. *Cold Spring Harb. Symp. Quant. Biol.* 55, 453–468.

Ooashi, N., Futatsugi, A., Yoshihara, F., Mikoshiba, K., and Kamiguchi, H. (2005). Cell adhesion molecules regulate Ca2+-mediated steering of growth cones via cyclic AMP and ryanodine receptor type 3. *J. Cell Biol.* 170, 1159–1167.

Piper, M., Plachez, C., Zalucki, O., Fothergill, T., Goudreau, G., Erzurumlu, R., Gu, C., and Richards, L. J. (2009). Neuropilin 1-Sema signaling regulates crossing of cingulate pioneering axons during development of the corpus callosum. *Cereb. Cortex* 19(Suppl. 1), i11–i21.

Polleux, F., Giger, R. J., Ginty, D. D., Kolodkin, A. L., and Ghosh, A. (1998). Patterning of cortical efferent projections by semaphorin-neuropilin interactions. *Science* 282, 1904–1906.

Polleux, F., Morrow, T., and Ghosh, A. (2000). Semaphorin 3A is a chemoattractant for cortical apical dendrites. *Nature* 404, 567–573.

Purro, S. A., Ciani, L., Hoyos-Flight, M., Stamatakou, E., Siomou, E., and Salinas, P. C. (2008). Wnt regulates axon behavior through changes in microtubule growth directionality: a new role for adenomatous polyposis coli. *J. Neurosci.* 28, 8644–8654.

Qin, S., Yu, L., Gao, Y., Zhou, R., and Zhang, C. (2007). Characterization of the receptors for axon guidance factor netrin-4 and identification of the binding domains. *Mol. Cell. Neurosci.* 34, 243–250.

Reh, T., and Kalil, K. (1981). Development of the pyramidal tract in the hamster. I. A light microscopic study. *J. Comp. Neurol.* 200, 55–67.

Ren, T., Anderson, A., Shen, W. B., Huang, H., Plachez, C., Zhang, J., Mori, S., Kinsman, S. L., and Richards, L. J. (2006). Imaging, anatomical, and molecular analysis of callosal formation in the developing human fetal brain. *Anat. Rec. A Discov. Mol. Cell. Evol. Biol.* 288, 191–204.

Richards, L. J., Koester, S. E., Tuttle, R., and O'Leary, D. D. (1997). Directed growth of early cortical axons is influenced by a chemoattractant released from an intermediate target. *J. Neurosci.* 17, 2445–2458.

Rodriguez, J., Esteve, P., Weinl, C., Ruiz, J. M., Fermin, Y., Trousse, F., Dwivedy, A., Holt, C., and Bovolenta, P. (2005). SFRP1 regulates the growth of retinal ganglion cell axons through the Fz2 receptor. *Nat. Neurosci.* 8, 1301–1309.

Ruthel, G., and Banker, G. (1999). Role of moving growth cone-like "wave" structures in the outgrowth of cultured hippocampal axons and dendrites. *J. Neurobiol.* 39, 97–106.

Ruthel, G., and Hollenbeck, P. J. (2000). Growth cones are not required for initial establishment of polarity or differential axon branch growth in cultured hippocampal neurons. *J. Neurosci.* 20, 2266–2274.

Ruthel, G., and Hollenbeck, P. J. (2003). Response of mitochondrial traffic to axon determination and differential branch growth. *J. Neurosci.* 23, 8618–8624.

Salinas, P. C. (2007). Modulation of the microtubule cytoskeleton: a role for a divergent canonical Wnt pathway. *Trends Cell Biol.* 17, 333–342.

Salinas, P. C., and Zou, Y. (2008). Wnt signaling in neural circuit assembly. *Annu. Rev. Neurosci.* 31, 339–358.

Schaefer, A. W., Kabir, N., and Forscher, P. (2002). Filopodia and actin arcs guide the assembly and transport of two populations of microtubules with unique dynamic parameters in neuronal growth cones. *J. Cell Biol.* 158, 139–152.

Schaefer, A. W., Schoonderwoert, V. T., Ji, L., Mederios, N., Danuser, G., and Forscher, P. (2008). Coordination of actin filament and microtubule dynamics during neurite outgrowth. *Dev. Cell* 15, 146–162.

Serafini, T., Colamarino, S. A., Leonardo, E. D., Wang, H., Beddington, R., Skarnes, W. C., and Tessier-Lavigne, M. (1996). Netrin-1 is required for commissural axon guidance in the developing vertebrate nervous system. *Cell* 87, 1001–1014.

Shelly, M., Lim, B. K., Cancedda, L., Heilshorn, S. C., Gao, H., and Poo, M. M. (2010). Local and long-range reciprocal regulation of cAMP and cGMP in axon/dendrite formation. *Science* 327, 547–552.

Sheth, A. N., McKee, M. L., and Bhide, P. G. (1998). The sequence of formation and development of corticostriate connections in mice. *Dev. Neurosci.* 20, 98–112.

Shim, S., Goh, E. L., Ge, S., Sailor, K., Yuan, J. P., Roderick, H. L., Bootman, M. D., Worley, P. F., Song, H., and Ming, G. L. (2005). XTRPC1-dependent chemotropic guidance of neuronal growth cones. *Nat. Neurosci.* 8, 730–735.

Shimogori, T., VanSant, J., Paik, E., and Grove, E. A. (2004). Members of the Wnt, Fz, and Frp gene families expressed in postnatal mouse cerebral cortex. *J. Comp. Neurol.* 473, 496–510.

Shu, T., and Richards, L. J. (2001). Cortical axon guidance by the glial wedge during the development of the corpus callosum. *J. Neurosci.* 21, 2749–2758.

Shu, T., Sundaresan, V., McCarthy, M. M., and Richards, L. J. (2003). Slit2 guides both precrossing and postcrossing callosal axons at the midline in vivo. *J. Neurosci.* 23, 8176–8184.

Singh, K. K., and Miller, F. D. (2005). Activity regulates positive and negative neurotrophin-derived signals to determine axon competition. *Neuron* 45, 837–845.

Singh, K. K., Park, K. J., Hong, E. J., Kramer, B. M., Greenberg, M. E., Kaplan, D. R., and Miller, F. D. (2008). Developmental axon pruning mediated by BDNF-p75NTR-dependent axon degeneration. *Nat. Neurosci.* 11, 649–658.

Sironi, J. J., Yen, S. H., Gondal, J. A., Wu, Q., Grundke-Iqbal, I., and Iqbal, K. (1998). Ser-262 in human recombinant tau protein is a markedly more favorable site for phosphorylation by CaMKII than PKA or PhK. *FEBS Lett.* 436, 471–475.

Spitzer, N. C. (2006). Electrical activity in early neuronal development. *Nature* 444, 707–712.

Stepanova, T., Slemmer, J., Hoogenraad, C. C., Lansbergen, G., Dortland, B., De Zeeuw, C. I., Grosveld, F., van Cappellen, G., Akhmanova, A., and Galjart, N. (2003). Visualization of microtubule growth in cultured neurons via the use of EB3-GFP (end-binding protein 3-green fluorescent protein). *J. Neurosci.* 23, 2655–2664.

Takemoto, M., Hattori, Y., Zhao, H., Sato, H., Tamada, A., Sasaki, S., Nakajima, K., and Yamamoto, N. (2011). Laminar and areal expression of unc5d and its role in cortical cell survival. *Cereb. Cortex* 21, 1925–1934.

Tang, F., Dent, E. W., and Kalil, K. (2003). Spontaneous calcium transients in developing cortical neurons regulate axon outgrowth. *J. Neurosci.* 23, 927–936.

Tang, F., and Kalil, K. (2005). Netrin-1 induces axon branching in developing cortical neurons by frequency-dependent calcium signaling pathways. *J. Neurosci.* 25, 6702–6715.

Tomida, T., Hirose, K., Takizawa, A., Shibasaki, F., and Iino, M. (2003). NFAT functions as a working memory of Ca2+ signals in decoding Ca2+ oscillation. *EMBO J.* 22, 3825–3832.

Uesaka, N., Ruthazer, E. S., and Yamamoto, N. (2006). The role of neural activity in cortical axon branching. *Neuroscientist* 12, 102–106.

van Ooyen, A. (2011). Using theoretical models to analyse neural development. *Nat. Rev. Neurosci.* 12, 311–326.

Wang, C. L., Zhang, L., Zhou, Y., Zhou, J., Yang, X. J., Duan, S. M., Xiong, Z. Q., and Ding, Y. Q. (2007). Activity-dependent development of callosal projections in the somatosensory cortex. *J. Neurosci.* 27, 11334–11342.

Wang, G. X., and Poo, M. M. (2005). Requirement of TRPC channels in netrin-1-induced chemotropic turning of nerve growth cones. *Nature* 434, 898–904.

Wang, Y., Thekdi, N., Smallwood, P. M., Macke, J. P., and Nathans, J. (2002). Frizzled-3 is required for the development of major fiber tracts in the rostral CNS. *J. Neurosci.* 22, 8563–8573.

Wayman, G. A., Impey, S., Marks, D., Saneyoshi, T., Grant, W. F., Derkach, V., and Soderling, T. R. (2006). Activity-dependent dendritic arborization mediated by CaM-kinase I activation and enhanced CREB-dependent transcription of Wnt-2. *Neuron* 50, 897–909.

Wayman, G. A., Kaech, S., Grant, W. F., Davare, M., Impey, S., Tokumitsu, H., Nozaki, N., Banker, G., and Soderling, T. R. (2004). Regulation of axonal extension and growth cone motility by calmodulin-dependent protein kinase I. *J. Neurosci.* 24, 3786–3794.

Wen, Z., and Zheng, J. Q. (2006). Directional guidance of nerve growth cones. *Curr. Opin. Neurobiol.* 16, 52–58.

Yoshikawa, S., McKinnon, R. D., Kokel, M., and Thomas, J. B. (2003). Wnt-mediated axon guidance via the Drosophila Derailed receptor. *Nature* 422, 583–588.

Zheng, J. Q., and Poo, M. M. (2007). Calcium signaling in neuronal motility. *Annu. Rev. Cell Dev. Biol.* 23, 375–404.

Zou, Y., and Lyuksyutova, A. I. (2007). Morphogens as conserved axon guidance cues. *Curr. Opin. Neurobiol.* 17, 22–28.

Conflict of Interest Statement: The authors declare that the research was conducted in the absence of any commercial or financial relationships that could be construed as a potential conflict of interest.

Received: 20 June 2011; accepted: 08 September 2011; published online: 28 September 2011.

Citation: Kalil K, Li L and Hutchins BI (2011) Signaling mechanisms in cortical axon growth, guidance, and branching. Front. Neuroanat. ***5****:62. doi: 10.3389/fnana.2011.00062*

frontiers in
NEUROANATOMY

REVIEW ARTICLE
published: 28 July 2011
doi: 10.3389/fnana.2011.00046

Wiring of divergent networks in the central auditory system

Charles C. Lee[1]*†, Amar U. Kishan[2]† and Jeffery A. Winer[3]

[1] *Department of Comparative Biomedical Sciences, School of Veterinary Medicine, Louisiana State University, Baton Rouge, LA, USA*
[2] *Harvard Medical School, Boston, MA, USA*
[3] *Division of Neurobiology, Department of Molecular and Cell Biology, University of California, Berkeley, CA, USA*

Edited by:
Julian Budd, University of Sussex, UK

Reviewed by:
Sarah L. Pallas, Georgia State University, USA
Hisayuki Ojima, Tokyo Medical and Dental University, Japan

****Correspondence:***
Charles C. Lee, Department of Comparative Biomedical Sciences, School of Veterinary Medicine, Louisiana State University, Skip Bertman Drive, Baton Rouge, LA 70803, USA.
e-mail: cclee@lsu.edu

†Charles C. Lee and Amar U. Kishan have contributed equally to this work.

Divergent axonal projections are found throughout the central auditory system. Here, we evaluate these branched projections in terms of their types, distribution, and putative physiological roles. In general, three patterns of axon collateralization are found: intricate local branching, long-distance collaterals, and branched axons (BAs) involved in feedback-control loops. Local collaterals in the auditory cortex may be involved in local processing and modulation of neuronal firing, while long-range collaterals are optimized for wide-dissemination of information. Rarely do axons branch to both ascending and descending targets. Branched projections to two or more widely separated nuclei or areas are numerically sparse but widespread. Finally, branching to contralateral targets is evident at multiple levels of the auditory pathway and may enhance binaural computations for sound localization. These patterns of axonal branching are comparable to those observed in other modalities. We conclude that the operations served by BAs are area- and nucleus-specific and may complement the divergent unbranched projections of local neuronal populations.

Keywords: branched axon, auditory system, collaterals, cortical, thalamocortical, brainstem

INTRODUCTION

A cardinal feature of axons is their divergent projections, which range from sparse branching in the thalamic input to different auditory cortex (AC) areas (Morel and Imig, 1987; Lee et al., 2004a; Kishan et al., 2008) to the many collaterals and thousand of boutons of single spiral Ia cochlear ganglion axons (Brown, 1981). Branched axons (BAs) are present throughout the auditory system (Fekete et al., 1984; Willard and Martin, 1984; Ojima, 1994; Hazama et al., 2004; Coomes et al., 2005; Kimura et al., 2005; Lee and Winer, 2008a,b,c) and can take many forms, from local (Brown et al., 1988a,b) to very distant (Hashikawa et al., 1995; Cetas et al., 1999; Huang and Winer, 2000), presumably allowing neurons to synchronize remote events or form multiple feature-specific representations.

Different patterns of axonal branching prevail at different levels of the auditory system (**Figures 1–3**). For instance, branching between different nuclei is common in the pathways to and from the medial nucleus of the trapezoid body (MTB; Morest, 1968; Spirou et al., 1990; Kuwabara and Zook, 1991, 1992; Kuwabara et al., 1991; Smith et al., 1991), while thalamocortical axons rarely project to different cortical fields, such as the primary auditory cortex (AI) and the anterior auditory field (AAF; Morel and Imig, 1987; Lee et al., 2004a,b). Other axons have both descending and ascending projections, e.g., from MTB cell axons projecting to the cochlear nucleus (CoN) and the inferior colliculus (IC), <1% project to both (Schofield, 1994).

In discussing the wide variety of branching patterns present in the auditory system, it is imperative to acknowledge that various methods allow the detection of different patterns of axonal branching, and that these different methods have inherent limitations in terms of the conclusions that can be drawn from their use. Thus, we review the technical considerations inherent in assessing axonal branching. An especially important caveat to establish at the outset, however, is that dual retrograde injections can only ascertain axonal branching to the specific regions within the nuclei injected; conclusions cannot be drawn about other forms of axonal branching from these studies. Nonetheless, the use of dual retrograde tracing has been useful in formulating hypotheses about neural function.

Abbreviations: AAF, anterior auditory field; AC, auditory cortex; AI, primary auditory area; AII, second auditory cortex; AVCN, anteroventral cochlear nucleus; BA, branched axon; CF, characteristic frequency; CN, central nucleus of the IC; CoN, cochlear nucleus; CT, corticothalamic; CTβ, cholera toxin β fragment; CTβG, cholera toxin β fragment, gold conjugated; DCoN, dorsal CoN; DL, double-labeled neuron; DLL, dorsal nucleus of the lateral lemniscus; DlP, dorsolateral periolivary area; DmP, DMPO, dorsomedial periolivary area; DZ, dorsal auditory zone; ED, dorsal posterior ectosylvian area; EE, excitatory–excitatory band; EI, excitatory–inhibitory response band; EI, intermediate posterior ectosylvian area; EV, ventral posterior ectosylvian area; IC, inferior colliculus; II, V, VI, auditory cortex layers; In, insular cortex; IL, intermediate nucleus of the lateral lemniscus; LA, lateral amygdaloid nucleus; La, lateral nucleus of the IC; LOC, lateral olivocochlear neurons; LSO, lateral superior olive; LT, LTB, lateral nucleus of the trapezoid body; MG, medial geniculate body; MGBd, MGd, dorsal division of the MG; MGBv, MGv, ventral division of the MGv; MGm, medial division of the MG; MOC, medial olivocochlear system; MSO, medial superior olive; MTB, medial nucleus of the trapezoid body; NA, nucleus angularis; NL, nucleus laminaris; NM, nucleus magnocellularis; P, posterior auditory area; PDL, percentage of double-labeled neurons; PIN, posterior intralaminar nucleus; PON, periolivary nuclei; PRh, perirhinal area; PVCN, posteroventral cochlear nucleus; RC, radiate multipolar cell; RP, rostral pole of the MG; SC, superior colliculus; SOC, superior olivary complex; SPN, superior paraolivary nucleus; TC, thalamocortical; Te, temporal cortex; Te3, third area of temporal cortex; TRN, thalamic reticular nucleus; VCN, ventral CoN; Ve, ventral auditory area; VIII, auditory nerve; VNLL, VL, ventral nucleus of the lateral lemniscus; VPO, ventral periolivary nucleus; VTB, ventral nucleus of the trapezoid body.

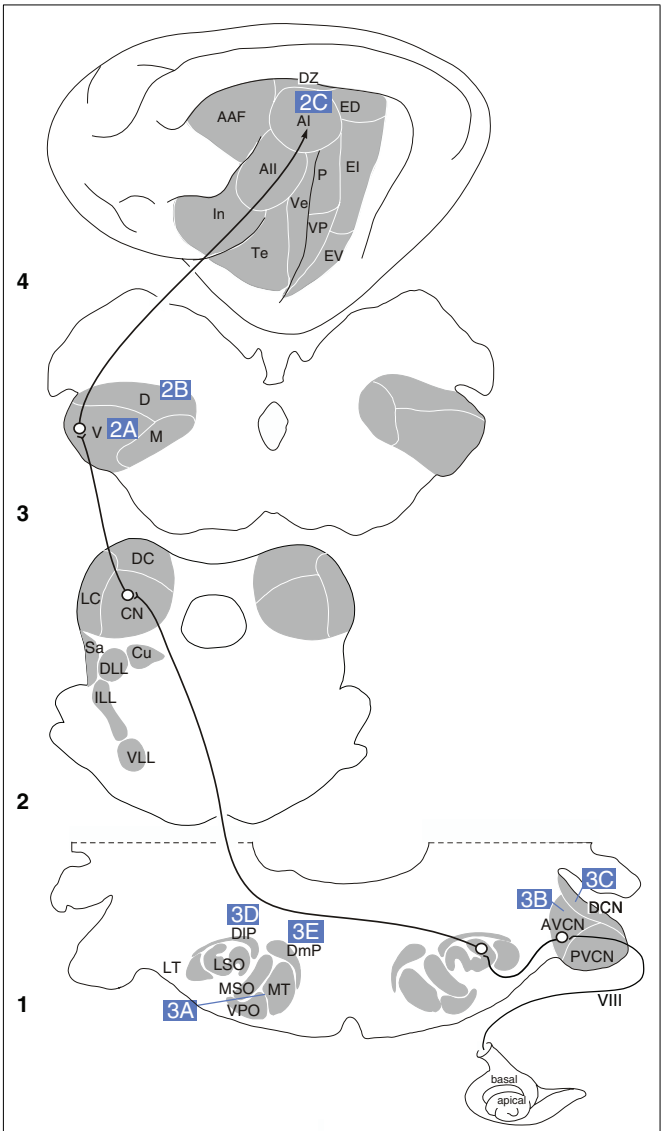

FIGURE 1 | The central auditory pathway. Key nuclei in the feline auditory system and elements of the lemniscal pathway from the medulla (1), midbrain (2), thalamus (3), and auditory cortex (4). Letters in blue boxes indicate the pathways depicted in **Figures 2** and **3**.

Although the functional implications of BAs are numerous (Morest, 1968; Kuwabara et al., 1991; Ojima et al., 1991, 1992; Li and Mizuno, 1997a,b; Kuwabara and Zook, 1999; Ye et al., 2000; Mulders and Robertson, 2002, 2003; Mulders et al., 2007), we are treating the function of BAs from the perspective of general organizational principles.

In the first two sections (see Branched Axons in the Auditory Cortical System, Branched Axons in the Auditory Brainstem and Midbrain), we review the existence, magnitude, and possible functions of BAs in the auditory cortex and thalamus as compared with those at earlier levels of the auditory system. These initial sections review the specifics of axonal branching in the auditory system, which the general reader may wish to skim in favor of the final sections (see Technical Considerations, Thematic Perspective, Alternatives to Collateralization in the Auditory Cortex, Collaterals in Other Modalities, and Summary), where we examine principles of axonal branching and evaluate the technical difficulties inherent in detecting BAs.

BRANCHED AXONS IN THE AUDITORY CORTICAL SYSTEM

THALAMOCORTICAL SYSTEM

All regions of the auditory cortex (AC) receive an input from the thalamus (Lee and Winer, 2008a). The principal source of auditory thalamocortical (TC) input, the medial geniculate body (MG), has tonotopic ventral (MGv) and rostral pole (RP) divisions, and non-tonotopic dorsal (MGd) and medial (MGm) divisions, which project in varying degrees to each of the 13 auditory cortical (AC) areas in the cat (Huang and Winer, 2000). Although focal regions within a thalamic nucleus can project broadly to multiple cortical areas based on anterograde tracing studies (Huang and Winer, 2000), axonal divergence of single neurons beyond a few millimeters is quite rare based on retrograde double labeling studies (Kishan et al., 2008). Thus, axonal branching in the auditory thalamocortical system is highly local, but with unique topographical features.

One of these features is the patchy distribution of TC BAs, which extend over 300–500 μm in layers IIIb and IV of the primate AC core (Hashikawa et al., 1995). In the lateral and posteromedial auditory cortical areas, larger (1000–1500 μm) patches arise from the MG anterodorsal and/or posterodorsal nuclei. In the rabbit, TC BAs form patches 1–2 mm apart in AI layers III and IV, with tangential layer I BAs up to 7 mm long (Cetas et al., 1999; **Figure 2A**). In the cat, similar patches are seen in AI, AAF, ventral, and the posterior AC (P) following injections of anterograde tracers into the MGv (Huang and Winer, 2000). More divergence occurs after similar MGd and MGm deposits, though not explicitly from BAs. Thick MGm axons in AC layer Ia project laterally across wide expanses, and vertical branches in layers II, IVb, and Va have fewer lateral BAs (Huang and Winer, 2000). Axons in layer IIIb also have many local BAs shorter than those in layers Ia and VIb.

The patchy distribution of MG afferents in AC may correlate with parvalbumin immunoreactivity and perhaps with modules of broadly and narrowly tuned neurons (Read et al., 2008) or binaural excitatory–excitatory/inhibitory (EE, EI) modules, though physiological–anatomical studies suggest that EE and EI columns are not linked by BAs (Middlebrooks and Zook, 1983). Similar patchy distributions in AC areas ostensibly lacking a binaural columnar arrangement imply that BAs are unrelated to binaurality. Intraareal BAs linking EE or EI columns are also sparse (Middlebrooks and Zook, 1983, but see Brandner and Redies, 1990).

Another canonical feature of the primary auditory cortical areas is the orderly spatial arrangement of neurons according to characteristic frequency (CF), i.e., tonotopy. A question that naturally arises is whether TC BAs contribute to the creation of the multiple AC CF maps (Morel and Imig, 1987) from the two representations in the MG (Imig and Morel, 1985a,b, 1985a,b)? Based on retrograde studies where different tracers are placed into matched isofrequency loci in different primary cortical areas, few double-labeled thalamic neurons are found (Morel and Imig,

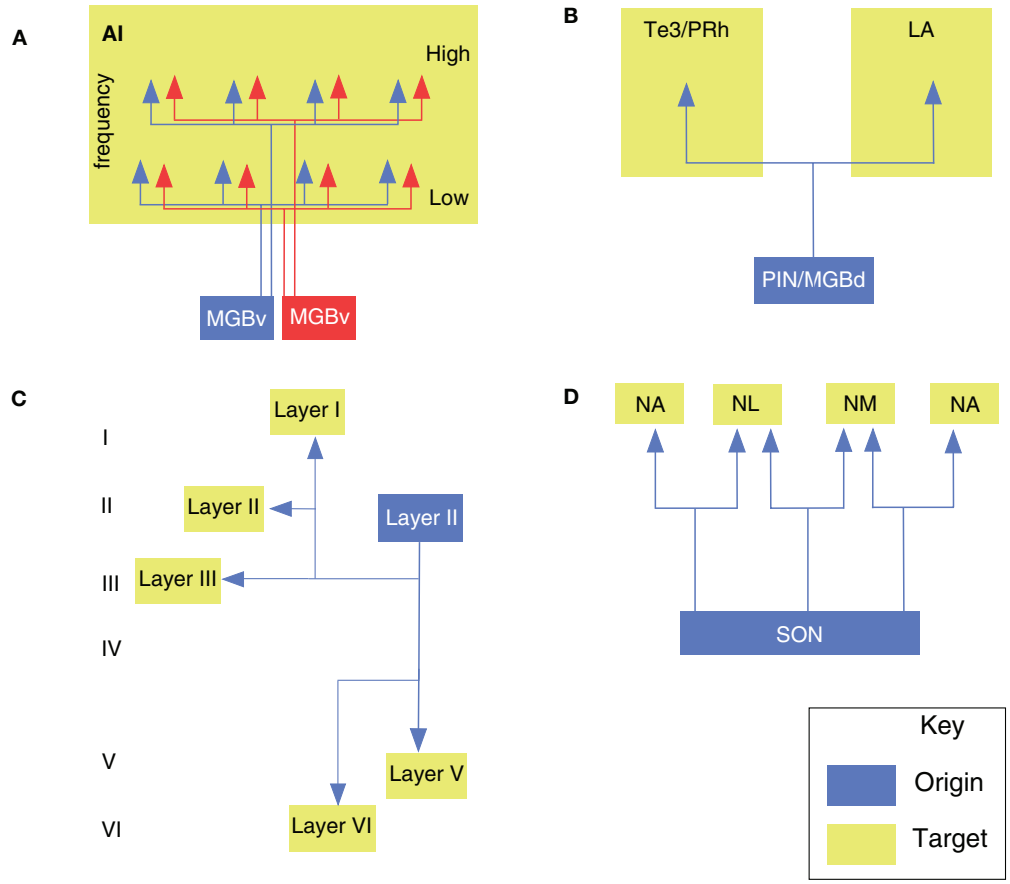

FIGURE 2 | Branched axonal projections in the auditory forebrain. (A) Clustered and periodic thalamocortical projections from medial geniculate body subdivisions to area AI (Velenovsky et al., 2003). **(B)** Posterior intralaminar (PIN) and dorsal division of the medial geniculate body branched projections to the non-primary auditory cortex (Te3/PRh) and lateral amygdala (LA; Doron and LeDoux, 2000). **(C)** Local, interlaminar, and collateral projections of an intracellularly labeled layer II pyramidal cell in AI (Ojima et al., 1991). **(D)** Avian olivary (SON) branched input to the laminaris (NL) and angularis (NA) nuclei (Burger et al., 2005).

1987), with some differences among the MGv and RP (Lee et al., 2004a; Kishan et al., 2008). Due to the paucity of double labeling in such studies, it appears that TC BAs do not create multiple CF maps in these areas.

Finally, the MG and intralaminar nuclei also project widely to non-auditory cortex. Thalamic BAs targeting both the lateral amygdaloid nucleus and the perirhinal or primary AC could influence autonomic and affective responses to auditory and multisensory stimuli (Namura et al., 1997). BAs may link some intralaminar nuclei with the dorsal (and, less so) ventral perirhinal cortex, and rarely arise from MGd/m neurons, though up to 17% of MGm cells project to perirhinal cortex and to the lateral amygdaloid nucleus (**Figure 2B**; **Table 1**). Although MGd cells project to both the frontal cortex and primary/non-primary AC, these originate from unbranched sources (Kurokawa and Saito, 1995). Thus, these TC parts of the auditory and motor pathways are segregated, despite extensive interdigitation of the projection cells. Overall, the few studies and diversity of relevant pathways make it difficult to specify the role of BAs in TC projections to non-auditory cortex.

CORTICOCORTICAL SYSTEM

Every area of the auditory cortex receives extensive input from local intrinsic cortical connections and extrinsic connections from other cortical areas in both hemispheres (Winer and Lee, 2007; Lee and Winer, 2008b,c), which provide ∼95% of the total input to an area (Lee et al., 2004a; Lee and Winer, 2011). As with the thalamocortical system, anterograde, axon-filling, and retrograde studies each provide complementary evidence about BAs in the corticocortical system.

On a local level, neurons in the auditory cortex branch within an area to create extensive divergent laminar circuits. In particular, layer II and III pyramidal cell axons branch proximally and distally to the cell body (Ojima et al., 1991; **Figure 2C**), forming an axonal network that extends across layers I–V, with two-to-five thick collaterals in layer III or V in addition to the main axon descending to the white matter for other cortical targets (Ojima et al., 1992). The horizontal branches in layer III or V run parallel to the pia for 500–2500 μm and emit, at a few distant points, local plexuses of secondary branches extending to upper and lower layers. This collateralization as a whole forms

a columnar terminal field in layers I through V with a branch-sparse gap in layer IV (**Figure 2C**). Each neuron has a number of vertical branches distributing around its cell body, forming a columnar terminal field, which is similar to that formed at distant points. Some non-projecting pyramidal neurons have thick, bifurcated axons with recurrent oblique or horizontal BAs; the latter extend 1–2 mm in layer V, and oblique branches project heavily in layers II–IV, with weaker input to layers I or II. Such cells may interact with those producing the synchronized oscillations arising in layer V (Silva et al., 1991). Several long-range dorsoventrally oriented BAs may link or segregate AI isofrequency loci in the cat (Read et al., 2001). Alternatively, they may synchronize cells with similar CF response properties, analogously to pyramidal neurons in visual cortex (Gray and Singer, 1989; Gray et al., 1989). Perhaps TC BAs complement these rich, local periodic projections.

As with the thalamocortical system, branched corticocortical projections that link similar CF regions are sparse, comprising <1% of AI and AAF cells projecting to matched CF regions (Lee et al., 2004a), although earlier studies using anterograde methods found extensive interconnections among matched CF regions (Imig and Reale, 1980), perhaps accounted for by neuronal populations that project in an unbranched manner to matched CF regions in different areas. Thus, long-range cortical BAs may be more rare than axon filling studies suggest. This implies that cortical BAs do not contribute significantly to spectral maps in different AC areas and illustrates a fundamental difference between the auditory forebrain and the brainstem, where axons subdivide profusely to innervate many different targets (Irvine, 1986). Intrinsic intraareal BAs across frequency laminae are also rare (Kishan et al., 2008), but may be more prevalent along an isofrequency contour.

Commissural AI axons may also target disparate areas, with homo- and hetero-topic terminal sites; a dual retrograde study found that some rat BAs target both sites (Rüttgers et al., 1990). However, <1% of AI or AAF neurons project commissurally to frequency-matched loci in both fields, and <4% of non-primary (AII, Te, and In) neurons project to two loci in their contralateral counterparts (Kishan et al., 2008).

CORTICOFUGAL PROJECTIONS

The auditory corticofugal system targets many thalamic, midbrain, and brainstem nuclei (Winer, 2006). Of these, the corticothalamic (CT) system is massive, with each major MG division receiving input from four or more AC areas (Winer et al., 2001). Two types of terminals arise from AI: small endings from thin axons of layer VI pyramidal neurons and large boutons from thick axons of layer V pyramidal neurons (Ojima, 1994; Winer et al., 1999; Llano and Sherman, 2008). Layer VI CT neurons typically project in a feedback manner to the thalamic nucleus from which they receives their major TC input, while layer V CT neurons project in a feedforward manner to a higher order thalamic nucleus (Winer et al., 2001; Sherman and Guillery, 2006).

Layer V CT pyramidal cell targets include MGm, MGd, and ventrolateral MGv, with thick horizontal BAs occurring in cortical layers V and VI forming heterogeneous en passant and spine-like boutons, and thin vertical axons ending above layer IV (Ojima et al., 1992), and with no BAs to the contralateral AI (Wong and Kelly, 1981), reserving collateralization to the ipsilateral AC. BAs crossing the cortical CF axis may enhance inhibition at other CFs, while those parallel to the isofrequency contours could have local roles (Ojima et al., 1991; Song et al., 2006).

Layer VI CT neurons branch extensively in both thalamus and cortex. Some layer VI CT cells have recurrent branches in cortical layer VI, then ascend to layers III and IV, where their processes form a dense plexus. In the thalamus, thin fiber BAs form dorsoventrally elongated bands parallel to MGv CF laminae (Rouiller and de Ribaupierre, 1990). Layer VI CT cells may activate local columnar neurons, while layer V CT neurons target more remote columns at the same or different CF. In addition, anterograde tracer deposits at separate frequency loci in the cat label terminals segregated in the MG, suggesting that microtopography complements BAs (Takayanagi and Ojima, 2006).

Corticothalamic projections include BAs to the thalamic reticular nucleus (TRN; Lam and Sherman, 2010). Layer V or VI axons traverse the TRN (Hazama et al., 2004); forming elongated slabs; these may be BAs of cells targeting the MGv. High- and low-CF loci in rat primary and non-primary AC areas converge in the MGv and target different TRN regions (Kimura et al., 2005). The TRN has inhibitory input to much of the MG, and some TRN neurons project to both the ventrolateral MGv and MGd, or to both the MGv *pars ovoidea* and MGm (Crabtree, 1998). This branching pattern might enable two AC tonotopic areas to convergently excite one MG region via direct CT projections, while divergently inhibiting separate MG regions via indirect reticulothalamic projections (Kimura et al., 2005). The AC also targets the midbrain, medulla, and striatum (Winer, 2006), and these corticofugal cells may also have intracortical BAs. Layer V corticostriatal neurons have vertical and short-range horizontal BAs. The vertical BAs form a dense network of terminal arbors in layers III and IV, perhaps reinforcing supragranular, reciprocal connections between AC CF loci projecting to similar striatal targets.

The corticocollicular system is also a rich substrate for axonal branching (Winer et al., 1998; Winer, 2006). Rat corticocollicular cells project to the caudal striatum (Moriizumi and Hattori, 1991b), and some corticofugal cells target the superior olivary complex (SOC) and IC, or the IC and the CoN, via BAs (Doucet et al., 2002, 2003). Some corticocollicular cells send BAs to the nucleus of the brachium of the IC (Saldaña et al., 1996). Retrograde experiments indicate that ∼5% of layer V neurons project to both IC (Willard and Martin, 1984; Coomes et al., 2005). Almost half of contralaterally projecting corticocollicular cells project bilaterally. Given the conservative estimates provided by retrograde tracers, all contralaterally projecting cells may target both ICs (Coomes et al., 2005), though no neurons appear to have BAs targeting both the IC and MG (Wong and Kelly, 1981).

BRANCHED AXONS IN THE AUDITORY BRAINSTEM AND MIDBRAIN

BRAINSTEM PROJECTIONS

Now, we consider the axonal branching patterns observed in the auditory brainstem and midbrain, in comparison with those of the auditory cortical systems described previously. Do similar branching patterns and principles apply across multiple stages of the auditory pathway? The numerous connections among brainstem

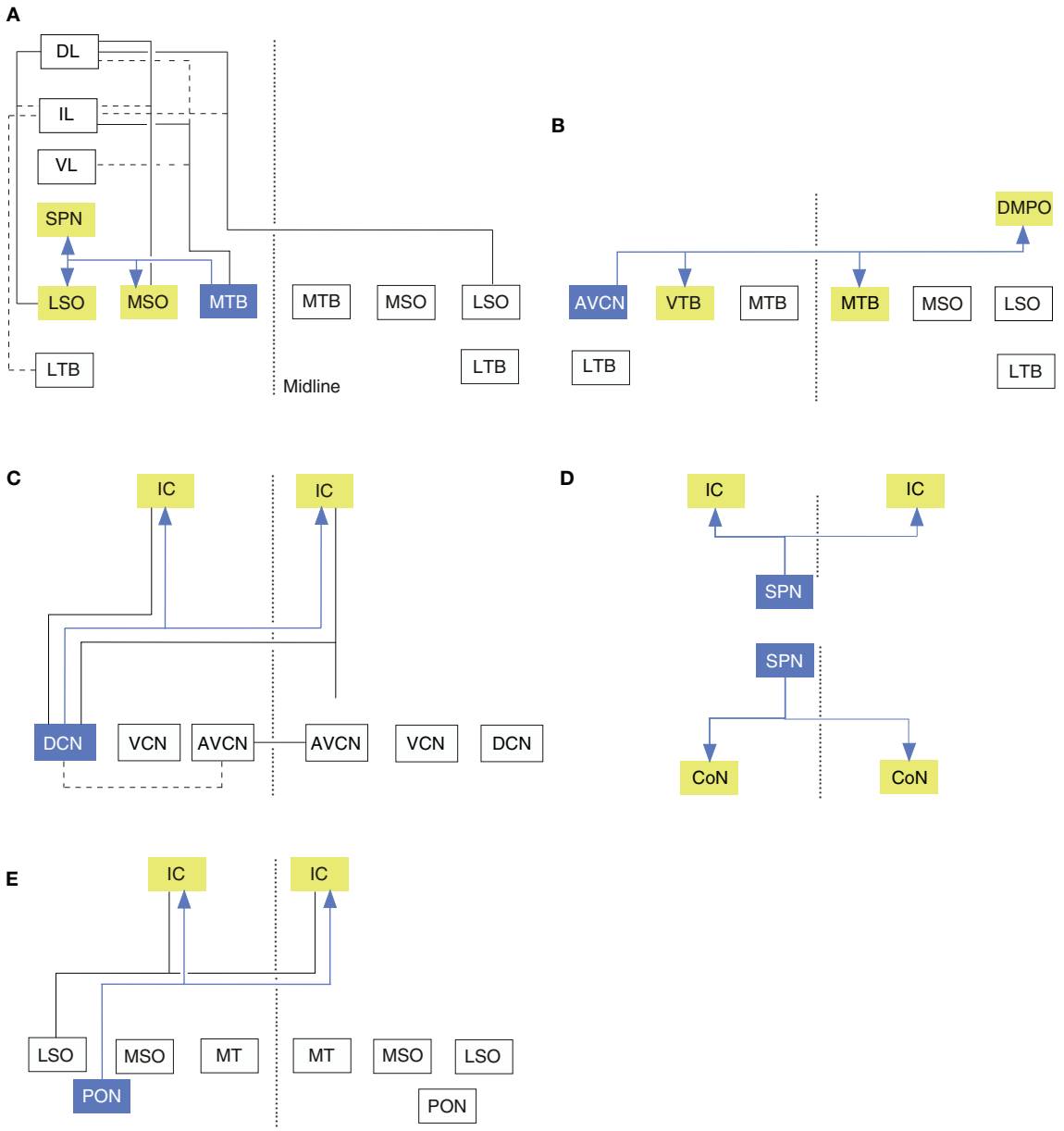

FIGURE 3 | Branched axonal projections in the auditory brainstem and midbrain. (A) Collateral projections from the medial nucleus of the trapezoid body to olivary and lateral lemniscal targets (Kuwabara and Zook, 1992). **(B)** Anteroventral cochlear nucleus collateral input to the ventral nucleus of the trapezoid body (VTB) and dorsomedial periolivary nucleus (Smith et al., 1991). **(C)** Cochlear nucleus branched projections to the inferior colliculus (IC; Schofield and Cant, 1996a; Schofield, 2002). **(D)** Branched ascending and descending projections from the superior paraolivary nucleus to the cochlear nucleus (CoN) and IC (Schofield, 1995). **(E)** Periolivary (PON) projections to the inferior colliculus (IC) and CoN. Dashed line in all panels represents the midline.

and midbrain nuclei might suggest different patterns of axonal branching exist at these stages. As noted in morphological studies, auditory BAs begin in the periphery (Lorente de Nó, 1981). At the earliest levels, type I auditory nerve fibers branch extensively in the CoN (Fekete et al., 1984). One main branch targets the ventral cochlear nucleus (VCoN) and the other ends in the dorsal cochlear nucleus (DCoN). Near this bifurcation, the parent trunk has few collaterals at low CFs, while axons at higher CFs have more numerous and complex axonal branches. Descending axons have 14–30 collaterals and, in the DCoN, the main trunk often makes parallel branches ending within 100 μm. Many BAs end in simple, en passant swellings, and others terminate diffusely in the neuropil. BAs

have regional morphologic variations, e.g., in the posteroventral cochlear nucleus, some have en passant swellings, while in the central part of the nucleus, fibers with a CF >4 kHz have many BAs that extend for hundreds of microns. These are parallel to octopus cell primary dendrites and could enhance the sharpness of tuning near the intensity threshold and broaden tuning at higher intensities. The ascending branch has 4–16 collaterals and ends in calyces of Held. These collaterals form complex, endbulb-like endings or en passant swellings and often remain within 100 μm of the parent branch, though one-third end in the anteroventral CoN. Small branches from high- and low-CF fiber may create heterotopic high frequency response zones in the VCoN (Fekete et al., 1984).

Cochlear nucleus afferents also branch. VCoN neurons send branches to matching frequency loci in the cat IC and contralateral DCoN (Adams, 1983a). Planar and radiate multipolar cells (T- and D-stellate cells, respectively) in the anterior VCoN branch to the DCoN and posterior VCoN, mainly to the multipolar cell area (Oertel et al., 1990). Radiate multipolar cells project to both the ipsilateral DCoN and the contralateral CoN (Doucet and Ryugo, 2006). Up to half the cells projecting to CoN also target the thalamic ventrobasal complex and may provide information about head and body position useful in sound localization or for somatic sensory–auditory interactions (Li and Mizuno, 1997a).

A prominent CoN target is the contralateral MTB (Morest, 1968), whose principal cells provide glycinergic input to the ipsilateral lateral superior olive (LSO) for interaural intensity difference computations (Smith et al., 1998). CoN projections form calyces of Held endings on MTB principal cells (Smith et al., 1991) and collateralize ipsilateral to the CoN of origin, targeting the lateral nucleus of the trapezoid body (LTB), posterior periolivary nucleus, or ventrolateral periolivary nucleus and end in large terminal swellings of variable shapes (**Figure 3B**; Spirou et al., 1990). En passant swellings are rare.

Most CoN BAs are precalycine. These traverse the MTB and ventral nucleus of the trapezoid body (VTB) toward the lateral lemniscus, forming branches in the anterolateral periolivary nucleus, the rostral LTB, and the VTB. Some fibers form collaterals at their branch point near the abducens nerve root, and branch sparsely before ending in the nucleus paragigantocellularis lateralis. Other precalycine collaterals target the dorsomedial and ventral periolivary nuclei and branch repeatedly within it (Kuwabara et al., 1991). About 40% of ipsilateral calyciferous branches end axosomatically in the ventral periolivary nucleus (VPO), 20% in the LTB and LSO, and 7% near the MTB in an area associated with the medial olivocochlear system (MOC). All axons have extensive BAs within the MTB, perhaps contributing to lateral inhibition. Other BAs end diffusely in the adjacent periolivary nuclei, the LTB, and the LSO, and 25% reach the lateral lemniscus (**Figure 3A**). Of the calycine collaterals, all terminate 20–80 μm from their origin in varicosities. Thus, ascending input to the MTB reaches parts of the ipsilateral lateral and medial olivocochlear system and diverse contralateral brain stem nuclei. MOC BAs to the CoN often converge with type II auditory nerve fiber endings (Benson and Brown, 2004), and areas targeted by such axons also project to the MOC, forming another prospective feedback-gain loop (Ye et al., 2000).

Perhaps unsurprisingly for brainstem projections, MTB axons are also collateralized (**Figure 3A**; Morest, 1968; Kuwabara et al., 1991). Principal cell axons send 2–6 BAs to the periolivary nuclei, superior paraolivary nucleus (SPN; the rodent homolog of the cat dorsomedial periolivary nucleus), and the VTB. Half of these axons also branch to the medial superior olive (MSO), and 25% branch to the lateral lemniscus. Recurrent MTB collaterals are also seen. The main axon often ends in a cascade of terminal BAs in the LSO; sometimes forming 1–2 thick perpendicular branches and then arborizing in the neuropil. MTB branches to the MSO are tonotopically organized (Smith et al., 1998).

Many brain stem neurons sample both the outputs of the MTB as well as collaterals bifurcating from input to the MTB, perhaps for monitoring or instructing gain control (Morest, 1968; Kuwabara et al., 1991). LSO-projecting neurons from the LTB also have collaterals to MSO (except in big brown bats), which, like MTB BAs, have axosomatic input on bipolar cells (Kuwabara and Zook, 1992). These inhibitory inputs may complement excitatory CoN afferents, perhaps preceding excitatory inputs because the contralateral calyciferous axons are much thicker than the CoN axons directly projecting to the contralateral MSO. Cell filling experiments in gerbil brain stem slices demonstrate that the MSO input to the SPN is highly branched, with >40% of thick, ascending MSO axons having one or more short BAs from their main trunk that ramify sparsely in the SPN (Kuwabara and Zook, 1999).

Not all brain stem projections have BAs. While some CoN efferent axons in the guinea pig target both CoN-projecting and IC-projecting cells in the SPN, their BAs may not be extensive (Schofield, 1995). Further, <1% of MTB neurons project to both the IC and CoN ipsilaterally, contralaterally, or have one ipsilateral and one contralateral target (Schofield, 1994).

PROJECTIONS OF THE INFERIOR COLLICULUS

The IC is the midbrain target for auditory input arising from earlier brainstem sources, e.g., the CoN, SOC, lateral lemniscal nuclei, AC, and many other non-auditory structures. The tonotopic central nucleus of the IC (CN) contains narrowly tuned neurons, while the cells in the dorsal cortex and lateral cortex (La) have broader frequency-tuning and multisensory properties. The IC projects to the MG, CoN, SOC, dorsal column nuclei, superior colliculi (SC), and other nuclei (for review see Winer and Schreiner, 2005).

The projection from the ventral nucleus of the lateral lemniscus to the CN has few BAs to different high- and low-frequency regions in the rat CN (Merchán and Berbel, 1996).

Such tonotopic precision is implicit in the narrow frequency tuning of anteroventral CoN cells (Bourk et al., 1981). In addition, in the rat lateral lemniscal nuclei, no neurons project to both the IC and the SC, or to both SCs, though cells in the dorsal nucleus of the lateral lemniscus may project to the SC deep layers for acoustic motor reflexes and head orientation (Tanaka et al., 1985).

The proportion of brainstem afferents that target both ICs via BAs may be species specific. In the cat IC, only 2% of LSO olivocollicular neurons project to both IC, while surprisingly, in the opossum, 20–25% of LSO olivocollicular neurons and almost all MSO olivocollicular cells project to both (Willard and Martin, 1984). Similar work in the guinea pig finds no branched projections in the LSO, MSO, or VCoN, but in the DCoN, 68% of ipsilateral

Table 1 | Retrograde studies of auditory branched projections.

System	Study and species	Method	Results
Thalamocortical	Middlebrooks and Zook (1983), Cat	EI band in AI: NY	MGv: none mentioned ($n = 3$)
		EE band in AI: PI (same CF)	
		Middle EE band in AI: NY	MGv: no%, but reported ($n = 1$)
		Ventral EE band in AI: PI (same CF)	
	Morel and Imig (1987), Cat	AI: HRP	MGv: 6.5 ($n = 5$, 6 sections)
		AAF: ^{3}H-BSA	RP: 6.0 ($n = 6$, 5 sections)
			MGv: 6.4 ($n = 1$, 2 sections)
		AI: ^{3}H-HRP	
		P: BSA	
	Brandner and Redies (1990), Cat	Dorsal AI: NY	MGv: no %, mentioned in one case ($n = 4$)
		Ventral and/or central AI: Bb	
		NY and Bb along AI isofrequency contour	MGv: none mentioned ($n = 2$)
	Kurokawa and Saito (1995), Rat	Te3: FG	MGd: 0 ($n = 6$)
		Fr1: FB	MGd: 0 ($n = 6$)
		Te1: NY	
		Fr1: FB	
	Namura et al. (1997), Rat	Dorsal perirhinal: DY	PIN: 3.3
		Lateral amygdaloid nucleus: FB	MGd[1]: 5
			SPFp: 11.3
			SPFm: 6.0
			MGm: 1.2 ($n = 1$)
		Ventral perirhinal: DY	PIN: 1.7
		Lateral amygdaloid nucleus: FB	MGd: 2.1
			SPFp: 3.7
			SPFm: 0
			MGm: 0 ($n = 1$)
		Te1: DY	0 ($n = 7$)
		Lateral amygdaloid nucleus: FB	
		Perirhinal: DY	0 ($n = 3$)
		Central amygdaloid nucleus: FB	
	Kishan et al. (2008), Cat	AI: CTβ	MGd: 1.5
		AAF: CTβG	MGm: 2.1
		Injected in frequency – matched loci	MGv: 1.4
			RP: 2.8 ($n = 4$)
		AI	MGd: 1.2
		Injected CTβ, CTβG at sites 3.3 mm apart	MGm: 2.8
			MGv: 0.6
			RP: 0 ($n = 1$)
		AII	MGd: 2.2
		Injected CTβ, CTβG at sites 3.3 mm apart	MGm: 3.9
			MGv: 2.1
			RP: 4.5 ($n = 1$)
		Te	MGd: 6.7
		Injected CTβ, CTβG at sites 1.7 mm apart	MGm: 4.9
			MGv: 5.8
			RP: 0.00 ($n = 1$)
		In	MGd: 3.9
		Injected CTβ, CTβG at sites 3.3 mm apart	MGm: 5.1
			MGv: 1.4
			RP: 0.00 ($n = 1$)

(Continued)

Table 1 | Continued

System	Study and species	Method	Results
Corticocortical	Rüttgers et al. (1990), Rat	DY and FB in regions of terminations of homotopic and heterotopic commissural projections	AI: no %, but reported
	Kishan et al. (2008), Cat	AI: CTβ AAF: CTβG Injected in frequency – matched loci	AI (i): 0.8 AAF (i): 0.6 AI (c): 0.8 AAF (c): 0.6 ($n=4$)
		AI Injected CTβ, CTβG at sites 3.3 mm apart from each other	AI (i): 0.1 AI (c): 1.4 ($n=1$)
		AII Injected CTβ, CTβG at sites 3.3 mm apart from each other	AII (i): 1.5 AII (c): 3.7 ($n=1$)
		Te Injected CTβ, CTβG at sites 1.7 mm apart from each other	Te (i): 1.3 Te (c): 1.8 ($n=1$)
		In Injected CTβ, CTβG at sites 3.3 mm apart from each other	In (i): 0.6 In (c): 1.1 ($n=1$)
Corticofugal	Wong and Kelly (1981), Cat	MG: HRP or NY Contra AI: NY or HRP	AI, layer V: 0 ($n=12$)
		IC: HRP or NY MG: NY or HRP	AI, layer V: 0 ($n=4$)
	Crabtree (1998), Cat	MGv, ventrolateral: FB or NY MGd: FB or NY	TRN: no %, always saw DLs ($n=3$)
		MGv, pars ovoidea: FB or NY MGm: FB or NY	TRN: no %, always saw DLs ($n=3$)
	Moriizumi and Hattori, 1991a, Rat	IC: TB Caudal striatum: DY	AI, layer V: 6.4% of IC projecting cells ($n=4$, pooled)
	Doucet et al. (2002), Rat	CoN: FB SOC: DY	AI: <10% ($n=2$, pooled)
	Doucet et al. (2003), Rat	CoN: FB IC: DY	AI: 10–20 ($n=4$)
		SOC: FB IC: DY	AI: 10–20 ($n=3$)
	Coomes et al. (2005), Guinea pig	Various combinations of FB, FG, red/green beads into both IC	Layer V of AC: 5.2 ($n=5$)
Brain stem	Adams (1983b), Cat	DCoN (c): EB or NY IC: HRP or EB (frequency matched with anatomical position)	VCoN (i): no %, but reported ($n=2$)
	Schofield (1994), Guinea pig	Various combinations of FB, FG, green beads into CoN and IC	MTB: <1% ($n=3$)
		CoN (i), IC (c) or CoN (c), IC (i) (same tracers)	MTB: <1% ($n=13$)
	Li and Mizuno (1997a), Rat	CoN: FG VB (c): TMRDA	Dorsal column (i): 50.7% of CoN-projecting STN: 30% of CoN-projecting ($n=1$, from figure)
	Doucet and Ryugo (2006), Rat	DCoN: BDA CoN (c): DY (large)	VCoN: 3.6% of planar multipolar No % for RC-multipolar, but reported ($n=3$)
IC afferents	Glendenning and Masterton (1983), Cat	Various combinations of DB, NY, Bb, PI, and DPD into both IC	LSO: 2% ($n=18$)
	Tanaka et al. (1985), Rat	DAPI and PI into both IC IC: PI or DAPI SC: DAPI or PI	LL: no %, but reported ($n=3$) LL: 0 ($n=3$)

(Continued)

Table 1 | Continued

System	Study and species	Method	Results
	Willard and Martin (1984), Opossum	TB and NY into both IC	AC: 6 CoN: <3% Dorsal columns: 6.67–12 DLL: <5 LSO core: 20–25% MSO: 100% ($n=8$)
	Moriizumi and Hattori (1991), Rat	AC (widely): TB IC: DY	Caudal globus pallidus: 0 ($n=2$)
	Schofield (1991), Guinea pig	Various combinations of FB, FG, green beads into CoN and IC	SPN: 1.7% of IC-projecting 3.3% of CoN-projecting ($n=3$)
	Schofield and Cant (1992), Guinea pig	CoN (i), IC (c) or CoN (c), IC (i) (same tracers) Various combinations of FB, FG, green beads into both IC	SPN: 0 ($n=4$ each) DLPO, LTB: <1% LSO, MSO: 0 ($n=4$)
	Schofield and Cant (1996a), Guinea pig	Various combinations of FB, FG, red/green beads into CoN (c) and IC	DCoN: 68.4% to IC (i) also project to IC (c) VCoN: 0
	Merchán and Berbel (1996), Rat	High frequency CNIC: HRP Low frequency CNIC: Biocytin	VLL: no %, very few reported
	Li and Mizuno (1997b), Rat	VB: TMRDA La: FG	Dorsal column nuclei and STN: no %, many reported ($n=8$)
	Li and Mizuno (1997a), Rat	CoN (i): FG IC (c): TMRDA CoN (c): FG IC (c): TMRDA	Gr: 60% of CoN-projecting Cu: 72.4% of CoN-projecting STN: 42.9% of CoN-projecting ($n=1$, from figure) Gr: 60% of CoN-projecting Cu: 61.5% of CoN-projecting STN: 36.4% of CoN-projecting ($n=1$, from figure)
IC efferents	Hashikawa (1983), Cat	CoN: PI, NY, Pr, or Bb MG: PI, NY, Pr, or Bb CoN: PI, NY, Pr, or Bb MG (c): PI, NY, Pr, or Bb PN: PI, NY, Pr, or Bb SC: PI, NY, Pr, or Bb	IC: 0 ($n=1$) IC: 0 ($n=1$) IC: <1% ($n=1$)
	González-Hernández et al. (1991), Rat	IC (c): NY MG: FB	IC: 5–10% of tectothalamic ($n=7$)
	Schofield (2001), Guinea pig	Various combinations of FB, FG, red/green beads into both CoN	IC: <1% ($n=12$)
	Coomes and Schofield (2004), Guinea pig	Various combinations of FB, FD, FG, FR, red/green beads into CoN, MG CoN (c), MG (i) (same tracers) CoN (i), MG (c) (same tracers) CoN (c), MG (c) (same tracers) CoN (c), MG (c) (same tracers)	IC: <1% ($n=6$) IC: <1% ($n=5$) IC: <1% ($n=3$) IC: 0 ($n=4$) IC: 0 ($n=4$)
	Okoyama et al. (2006), Rat	FG and FR into MG and CoN FG and FR into IC (c), MG FG and FR into CoN, IC (c)	IC: 0 ($n=11$) IC: <1% ($n=8$) IC: 0 ($n=10$)

(Continued)

Table 1 | Continued

System	Study and species	Method	Results
		FG and FR into both CoN	IC: 0 ($n = 6$)
		FG and FR into CoN (c), SOC	IC: 0 ($n = 3$)

[1]Originally counted as being part of the supragenicular nucleus, which is considered as part of the MGd; c, contralateral; i, ipsilateral; [3]H-BSA, tritiated bovine serum albumin; AAF, anterior auditory field; AC, auditory cortex; AI, primary auditory area; AII, second auditory cortex; Bb, bisbenzimide; BSA, bovine serum albumin; CoN, cochlear nucleus; CN, central nucleus of the IC; CTβ, β subunit of cholera toxin; CTβG, gold conjugate of CTβ; Cu, cuneate nucleus; DCoN, dorsal CN; DLPO, dorsolateral periolivary nucleus; DNLL, dorsal nucleus of the LL; DY, diamidino yellow; EB, Evans blue; EE, excitatory–excitatory band; EI, excitatory–inhibitory response band; FB, fast blue; FD, fluorescein–dextran; FG, fluorogold; FR, fluororuby; Fr1, frontal cortex; Gr, gracile nucleus; HRP, horseradish peroxidase; IC, inferior colliculus; La, lateral nucleus of the IC; In, insular cortex; LL, lateral lemniscus; LTB, lateral nucleus of the trapezoid body; LOC, lateral olivocochlear neurons; LSO, lateral superior olive; MG, medial geniculate body; MGd, dorsal division of the MG; MGm, medial division of the MG; MGv, ventral division of the MGv; MTB, medial nucleus of the trapezoid body; MOC, medial olivocochlear system; MSO, medial superior olive; NY, nuclear yellow; PI, propidium iodide; PIN, posterior intralaminar nucleus; PN, pontine nuclei; Pr, primulin; RC-multipolar, radiate multipolar cells projecting contralaterally; RP, rostral pole of the MG; SC, superior colliculus; SOC, superior olivary complex; SPFm, medial portion of the subparafascicular nucleus; SPFp, posterior portion of the subparafascicular nucleus; STN, spinal trigeminal nucleus; TB, true blue; Te, temporal cortex; Te1, primary auditory area; Te3, non-auditory temporal cortex; TMRDA, tetramethylrhodamine–dextran amine; TRN, thalamic reticular nucleus; VCN, ventral CN; VNLL, ventral nucleus of the LL.

IC-projecting cells have BAs to the contralateral IC (**Figure 3C**; Schofield and Cant, 1996b). Compared with the corticofugal system (see above), in both the guinea pig and the opossum, ∼6% of AC neurons project bilaterally to the IC.

Branched brainstem projections to the IC and other targets are also rare. In the SPN, ∼2% of IC-projecting cells branch to the CoN (**Figure 3D**; Schofield, 1991). Similarly, in the guinea pig SOC, only 1% of IC-projecting neurons send axons to the CoN (**Figure 3E**; Schofield, 2002). These few branched projections originate in the ventral periolivary region, including the anteroventral periolivary nucleus and the VTB, but no cells project to both targets contralaterally, or to one ipsilaterally – and the other contralaterally. In addition, some non-auditory afferents also have BAs (Moriizumi and Hattori, 1991a,b; Li and Mizuno, 1997a,b).

Within the IC itself, local connections are highly collateralized as revealed by intracellular filling studies in the cat (Oliver et al., 1991). These intrinsic BAs sometimes parallel the dendrites, extending for hundreds of microns (as in the CoN), while other IC neurons have non-oriented CN BAs. This diversity suggests extensive IC computational roles for local BAs and interneurons (Oliver et al., 1991). Axons of these cells extend toward the brachium of the IC, and many likely project to the MG (Winer et al., 1996). Some of these tectothalamic neurons are inhibitory (Winer et al., 1996; Peruzzi et al., 1997; Bartlett and Smith, 2002; Lee and Sherman, 2010), providing a source of feedforward inhibition that is unique to the auditory system.

However, most long-range IC projections have few BAs. Few colliculobulbar neurons target both CoNs in the guinea pig (Schofield, 2001) and rat (Okoyama et al., 2006). Instead, the IC may exert descending divergent influence disynaptically through contact with cells that projecting bilaterally to the CoN, particularly in the VTB and anteroventral periolivary nucleus (Schofield and Cant, 1999). As in the brain stem, IC neurons with ascending and descending projections are rare, with reports suggesting that no or few cells project to both the CoN and the MG in the cat (Hashikawa, 1983), rat (Okoyama et al., 2006), and guinea pig (Coomes and Schofield, 2004), and <1% project to both the SC and the pontine nuclei (Hashikawa, 1983). IC neurons branching to the MG and the contralateral IC also target the contralateral CoN, and comprise 1–10% of all tectothalamic cells (González-Hernández et al., 1991; Okoyama et al., 2006). Similarly, few axons target both the contralateral IC and the SOC or CoN.

TECHNICAL CONSIDERATIONS

Many approaches have been used to characterize BAs. Dual retrograde tract tracing (Hayes and Rustioni, 1979; Kuypers et al., 1980; Jones, 1983) can provide a profile of BA projections, as the many labeled cells permit quantitative analyses (**Table 1**). However, these studies presume equivalent uptake affinity, injection site size and efficacy, visualization methods, the interaction of damage with uptake, and transport rate (Schofield et al., 2007). To label significant numbers of cells, sufficiently large deposits can complicate the collection of quantitative data. Thus, for example, injections restricted to a single binaural response bands may be too small to label sufficient cells to provide reliable statistically appropriate estimates of double-labeled cells (DLs; Kishan et al., 2008).

Negative results are also problematic. Few DLs suggest that the injected regions do not receive BAs, though other areas might, or that the tracers were neither equivalent spatially nor equally likely to be transported. If BAs are oriented selectively, and the injections are not aligned appropriately, DL estimates would be spurious. Finally, dual retrograde tracing methods are limited since BAs to only a few sites can be detected, even if multiple targets are present. Thus, dual retrograde tracing likely underestimates the divergence of axonal projections.

In comparison, focal anterograde injections may overestimate the degree of single axon divergence by labeling fibers-of-passage or filling closely apposed neurons that project to separate loci. However, both anterograde and axon filling studies can demonstrate recurrent, local, and distant BAs. Some BAs are too near their source to be detected reliably by retrograde means (Winer, 1986), and anterograde or filling approaches do not require a precise or systematic injection orientation to reveal them. Anterograde studies may not reveal the full range of targets since incomplete filling of fine or long processes or insufficient transport time may confound estimates.

Intracellular filling studies are highly constrained by sample size (Fekete et al., 1984; Ojima et al., 1991). While a few axons may have collaterals (or, alternatively, lack branches), it is uncertain whether these are representative. As in anterograde studies, incomplete staining or insufficient transport time can constrain firm conclusions or population values except when many axons can be filled and their targets visualized (Brown, 1981; Humphrey et al., 1985).

THEMATIC PERSPECTIVE

Branched axons are common in the auditory cortical system, as well as in the auditory midbrain and brainstem. However, several general principles are evident from a comparison across processing levels. First, most axons branch according to one of three patterns: intricate local BAs, long-distance collaterals, and BAs involved in feedback-control loops. Second, cells rarely project to both ascending and descending targets, suggesting that these streams are well segregated and that descending projections play specific roles rather than merely feedback or modulatory ones (Guinan, 2006; Winer, 2006). Third, some neurons have both ascending and contralateral targets, e.g., CoN neurons projecting to the IC and the contralateral CoN (Adams, 1983b), and IC neurons targeting the MG and the contralateral IC (González-Hernández et al., 1991). Most projections are contra- or ipsi-lateral because of the acoustic chiasm (Glendenning and Masterton, 1983); thus, these BAs may enhance binaural computations for sound localization or otherwise modulate ascending input from an ear with contralateral influence. This may not pertain to descending projections since corticothalamic neurons are not commissural (Wong and Kelly, 1981). Fourth, bilateral projection neurons are part of at least the corticofugal and olivocochlear streams, with ∼5% of corticocollicular neurons projecting to both IC (Willard and Martin, 1984; Coomes and Schofield, 2004), and a similar proportion of MOC cells targeting both cochleae (Thompson and Thompson, 1986; Robertson et al., 1987a,1987a,b; Aschoff and Ostwald, 1988). Such bilaterally projecting neurons in ascending pathways are differentially distributed in various nuclei.

ALTERNATIVES TO COLLATERALIZATION IN THE AUDITORY CORTEX

In the auditory cortex, one might predict that BAs would be an ideal way to create multiple independent representations of frequency, aurality, amplitopy, or other dimensions required for computation (Ehret, 1997). It is somewhat unexpected that BAs to matched frequency regions are comparatively rare, especially in the forebrain (Lee et al., 2004a), where the emergence of multiple CF maps (Reale and Imig, 1980) suggest that they might be more common.

A robust alternative mechanism is provided by heterotopic projections that arise from interleaved thalamic and cortical neurons situated in close proximity and serving presumably similar physiologic roles but whose targets are separated widely (Lee et al., 2004b; Lee and Winer, 2005). Three obvious advantages accrue to this arrangement. First, precise branching to multiple targets is unnecessary, and neurons that target multiple cortical areas can migrate as a group and assemble their connectivity with comparative ease relative to the precision required by multiple branches that must terminate in exact register in different targets. Second, and perhaps most critically, heterotopic arrangements enable easy coordination of activity across large spatial territories, a prospectively problematic issue when coordinating diverse spatiotemporal patterns across vast expanses of brain (Lee et al., 2004b; Winer et al., 2004). Third, they provide a simple mechanism enabling the precise coordination of discharge patterns among resident thalamic or cortical neurons, either via local circuit neurons or, in their absence (Winer and Larue, 1996), via the BAs of excitatory neurons.

A second alternative is that the terminal plexus of many axons is highly divergent, and can span wide arrays, as in the TC axons in visual (Ferster and LeVay, 1978), somatic sensory (Landry and Deschênes, 1981), and auditory (Velenovsky et al., 2003) cortex. Such axons engage large areas and could readily initiate or sustain parallel intracortical and corticocortical modularity (DeFelipe et al., 1986) in networks larger than the comparatively finer scale of interneuronal projections (Kisvárday et al., 1994). The complexity of these axons belies point-to-point models of connectivity (Brandner and Redies, 1990).

COLLATERALS IN OTHER MODALITIES

Comparable, and perhaps even more extensive, collaterals systems exist in other modalities. The complexity of the subcortical auditory pathway frustrates direct comparisons with the visual, somatic sensory, or autonomic systems. Nonetheless, some comparisons can be drawn. For example, primary phrenic afferents send BAs to different spinal cord laminae (Goshgarian and Roubal, 1986), as do Ia muscle spindle (Brown and Fyffe, 1978), and Ib Golgi tendon organ (Brown and Fyffe, 1978) afferents. Many cuneate nucleus inputs are collateralized (Weinberg et al., 1990), resembling type I ganglion cell axons near the CoN. Retinofugal fibers to the lateral geniculate nucleus (LGN) ramify within the LGN (Conley and Fitzpatrick, 1989), resembling type I ganglion axons within the CoN.

Forebrain connections are compared more readily. The visual TC system may have more interareal BAs and intraareal BAs to matched functional domains than the somatic sensory or auditory systems. Retinotopically matched deposits in areas 17 and 18 double label 3–16% of neurons in the LGN A lamina (Bullier, 1984; Birnbacher and Albus, 1987; Salin et al., 1989), while matched somatotopic injections (SI) in the primary and secondary somatosensory areas only double label 2.3% of cells (Fisher et al., 1983).

Horizontal BAs are also present in all modalities. In the visual system, extensive lateral collaterals, similar to those seen in AI link loci with similar functional properties (Gilbert and Wiesel, 1979; Michalski et al., 1983; LeVay, 1988). There are also horizontal connections in higher-level areas such as the macaque inferior temporal cortex (Tanigawa et al., 2005), and long-range horizontal collaterals from SI pyramidal cells may target neurons in other fields (DeFelipe et al., 1986).

As in AI, some rat SI CT cells have local collaterals to neurons in the same column, while others project remotely (Zhang and Deschênes, 1997). Mirroring the absence of AI corticofugal BAs to diverse targets, <2% of SI cells have BAs to the corticostriatal, corticorubral, corticopontine, and corticospinal pathways

(Akintunde and Buxton, 1992). In the somatic sensory (Bourassa et al., 1995) and visual (Bourassa and Deschênes, 1995) systems, the CT fibers arising from axons of layer V neurons in V1 or SI were collaterals of corticotectal or corticopontine axons, unlike the auditory CT system. This suggests modality specific rules for BAs, whose ontogeny and functional specificity remain for further investigation.

SUMMARY

The floridness of axonal branching throughout the central auditory system, and other modalities, is indicative of the functional importance of divergent processing in sensory systems. Such branching ranges across scales, from intrinsic branches that modulate firing in local circuits, to long-range collaterals that widely disseminate information. Yet, it remains an open question whether BAs as a wiring principle is more efficient from an ontological and developmental standpoint, compared with the targeting of separate loci by unbranched neuronal ensembles. In addition, the degree to which separate branches have similar synaptic properties and efficacy in terms of transmitting auditory information remains to be investigated. Indeed, widely varying synaptic properties at separate axonal branches would have profound effects on the divergent dissemination of auditory information. Thus, defining the functional role of axonal divergence will require a convergence of future theory and experiments.

ACKNOWLEDGMENTS

This work is dedicated to the late Jeffery A. Winer, who served as a mentor and inspirational figure for innumerable students, colleagues, and friends, and without whom this work would not have reached fruition. The void left by his absence testifies to the breadth and depth of his scholarship, friendship, and humanity. Jeff, we miss you greatly. We also thank David T. Larue for helpful discussions and assistance with the figures. This work was supported by NIH Grants R03 DC 11361 (Charles C. Lee) and R01 DC 2319 (Jeffery A. Winer).

REFERENCES

Adams, J. C. (1983a). Cytology of periolivary cells and the organization of their projections in the cat. *J. Comp. Neurol.* 215, 275–289.

Adams, J. C. (1983b). Multipolar cells in the ventral cochlear nucleus project to the dorsal cochlear nucleus and the inferior colliculus. *Neurosci. Lett.* 37, 205–208.

Akintunde, A., and Buxton, D. F. (1992). Origins and collateralization of corticospinal, corticopontine, corticorubral and corticostriatal tracts: a multiple retrograde fluorescent tracing study. *Brain Res.* 586, 208–218.

Aschoff, A., and Ostwald, J. (1988). Different origins of cochlear efferents in some bat species, rats, and guinea pigs. *J. Comp. Neurol.* 264, 56–72.

Bartlett, E. L., and Smith, P. H. (2002). Effects of paired-pulse and repetitive stimulation on neurons in the rat medial geniculate body. *Neuroscience* 113, 957–974.

Benson, T. E., and Brown, M. C. (2004). Postsynaptic targets of type II auditory nerve fibers in the cochlear nucleus. *J. Assoc. Res. Otolaryngol.* 5, 111–125.

Birnbacher, D., and Albus, K. (1987). Divergence of single axons in afferent projections to the cat's visual cortical areas 17, 18, and 19: a parametric study. *J. Comp. Neurol.* 261, 543–561.

Bourassa, J., and Deschênes, M. (1995). Corticothalamic projections from the primary visual cortex in rats: a single fiber study using biocytin as an anterograde tracer. *Neuroscience* 66, 253–263.

Bourassa, J., Pinault, D., and Deschênes, M. (1995). Corticothalamic projections from the cortical barrel field to the somatosensory thalamus in rats: a single-fibre study using biocytin as an anterograde tracer. *Eur. J. Neurosci.* 7, 19–30.

Bourk, T. R., Mielcarz, J. P., and Norris, B. E. (1981). Tonotopic organization of the anteroventral cochlear nucleus of the cat. *Hear. Res.* 4, 215–241.

Brandner, S., and Redies, H. (1990). The projection of the medial geniculate body to field AI: organization in the isofrequency dimension. *J. Neurosci.* 10, 50–61.

Brown, A. G. (1981). *Organization in the Spinal Cord.* Berlin: Springer-Verlag.

Brown, A. G., and Fyffe, R. W. (1978). The morphology of group Ia muscle afferent fibre collaterals. *J. Physiol. (Lond.)* 278, 111–127.

Brown, M. C., Berglund, A. M., Kiang, N. Y. S., and Ryugo, D. K. (1988a). Central trajectories of type II spiral ganglion cells. *J. Comp. Neurol.* 278, 581–590.

Brown, M. C., Liberman, M. C., Benson, T. E., and Ryugo, D. K. (1988b). Brainstem branches from olivocochlear axons in cats and rodents. *J. Comp. Neurol.* 278, 591–603.

Bullier, J. (1984). "Axonal bifurcation in the afferents to cortical areas of the visual system," in *Visual Neuroscience*, eds J. D. Pettigrew, K. J. Sanderson, and W. R. Levick (London: Cambridge University Press), 239–259.

Burger, R. M., Cramer, K. S., Pfeiffer, J. D., and Rubel, E. W. (2005). Avian superior olivary nucleus provides divergent inhibitory input to parallel auditory pathways. *J. Comp. Neurol.* 481, 6–18.

Cetas, J. S., de Venecia, R. K., and McMullen, N. T. (1999). Thalamocortical afferents of Lorente de Nó: medial geniculate axons that project to primary auditory cortex have collateral branches to layer I. *Brain Res.* 830, 203–208.

Conley, M., and Fitzpatrick, D. (1989). Morphology of retinogeniculate axons in the macaque. *Vis. Neurosci.* 2, 287–296.

Coomes, D. L., and Schofield, B. R. (2004). Separate projections from the inferior colliculus to the cochlear nucleus and thalamus in guinea pigs. *Hear. Res.* 191, 67–78.

Coomes, D. L., Schofield, R. M., and Schofield, B. R. (2005). Unilateral and bilateral projections from cortical cells to the inferior colliculus in guinea pigs. *Brain Res.* 1042, 62–72.

Crabtree, J. W. (1998). Organization in the auditory sector of the cat's thalamic reticular nucleus. *J. Comp. Neurol.* 390, 167–182.

DeFelipe, J., Conley, M., and Jones, E. G. (1986). Long-range focal collateralization of axons arising from corticocortical cells in monkey sensory-motor cortex. *J. Neurosci.* 6, 3749–3766.

Doron, N. N., and LeDoux, J. E. (2000). Cells in the posterior thalamus project to both amygdala and temporal cortex: a quantitative retrograde double-labeling study in the rat. *J. Comp. Neurol.* 425, 257–274.

Doucet, J. R., Molavi, D. L., and Ryugo, D. K. (2003). The source of corticocollicular and corticobulbar projections in area Te1 of the rat. *Exp. Brain Res.* 153, 477–485.

Doucet, J. R., Rose, L., and Ryugo, D. K. (2002). The cellular origin of corticofugal projections to the superior olivary complex in the rat. *Brain Res.* 925, 28–41.

Doucet, J. R., and Ryugo, D. K. (2006). Structural and functional classes of multipolar cells in the ventral cochlear nucleus. *Anat. Rec.* 288, 331–344.

Ehret, G. (1997). The auditory cortex. *J. Comp. Physiol. A* 181, 547–557.

Fekete, D. M., Rouiller, E. M., Liberman, M. C., and Ryugo, D. K. (1984). The central projections of intracellularly labeled auditory nerve fibers in cats. *J. Comp. Neurol.* 229, 432–450.

Ferster, D., and LeVay, S. (1978). The axonal arborizations of lateral geniculate neurons in the striate cortex of the cat. *J. Comp. Neurol.* 182, 923–944.

Fisher, G. R., Freeman, B., and Rowe, M. J. (1983). Organization of parallel projections from Pacinian afferent fibers to somatosensory cortical areas I and II in the cat. *J. Neurophysiol.* 49, 75–97.

Gilbert, C. D., and Wiesel, T. N. (1979). Morphology and intracortical projections of functionally characterised neurones in the cat visual cortex. *Nature* 280, 120–125.

Glendenning, K. K., and Masterton, R. B. (1983). Acoustic chiasm: efferent projections of the lateral superior olive. *J. Neurosci.* 3, 1521–1537.

González-Hernández, T. H., Galindo-Mireles, D., Castañeyra-Perdomo, A., and Ferres-Torres, R. (1991). Divergent projections of projecting neurons of the inferior colliculus to the medial geniculate body and the contralateral inferior colliculus in the rat. *Hear. Res.* 52, 17–22.

Goshgarian, H. G., and Roubal, P. J. (1986). Origin and distribution of phrenic primary afferent nerve fibers in the spinal cord of the adult rat. *Exp. Neurol.* 92, 624–638.

Gray, C. M., Konig, P., Engel, A. K., and Singer, W. (1989). Oscillatory responses in cat visual cortex exhibit inter-columnar synchronization which reflects global stimulus properties. *Nature* 338, 334–338.

Gray, C. M., and Singer, W. (1989). Stimulus-specific neuronal oscillations in orientation columns of cat visual cortex. *Proc. Natl. Acad. Sci. U.S.A.* 86, 1698–1702.

Guinan, J. J. (2006). Olivocochlear efferents: anatomy, physiology, function, and the measurement of efferent effects. *Ear Hear.* 27, 589–607.

Hashikawa, T. (1983). The inferior colliculopontine neurons of the cat in relation to other collicular descending neurons. *J. Comp. Neurol.* 219, 241–249.

Hashikawa, T., Molinari, M., Rausell, E., and Jones, E. G. (1995). Patchy and laminar terminations of medial geniculate axons in monkey auditory cortex. *J. Comp. Neurol.* 362, 195–208.

Hayes, N. L., and Rustioni, A. (1979). Dual projections of single neurons are visualized simultaneously: use of enzymatically inactive [3]HRP. *Brain Res.* 165, 321–326.

Hazama, M., Kimura, A., Donishi, T., Sakoda, T., and Tamai, Y. (2004). Topography of corticothalamic projections from the auditory cortex of the rat. *Neuroscience* 124, 655–667.

Huang, C. L., and Winer, J. A. (2000). Auditory thalamocortical projections in the cat: laminar and areal patterns of input. *J. Comp. Neurol.* 427, 302–331.

Humphrey, A. L., Sur, M., Uhlrich, D. J., and Sherman, S. M. (1985). Projection patterns of individual X- and Y-cell axons from the lateral geniculate nucleus to cortical area 17 in the cat. *J. Comp. Neurol.* 233, 159–189.

Imig, T. J., and Morel, A. (1985a). Tonotopic organization in ventral nucleus of medial geniculate body in the cat. *J. Neurophysiol.* 53, 309–340.

Imig, T. J., and Morel, A. (1985b). Tonotopic organization in lateral part of posterior group of thalamic nuclei in the cat. *J. Neurophysiol.* 53, 836–851.

Imig, T. J., and Reale, R. A. (1980). Patterns of cortico-cortical connections related to tonotopic maps in cat auditory cortex. *J. Comp. Neurol.* 192, 293–332.

Irvine, D. R. F. (1986). "The auditory brainstem. A review of the structure and function of auditory brainstem processing mechanisms," in *Progress in Sensory Physiology*, eds H. Autrum, D. Ottoson, E. R. Perl, R. F. Schmidt, H. Shimazu, and W. D. Willis (Berlin: Springer-Verlag), 1–279.

Jones, E. G. (1983). Lack of collateral thalamocortical projections to fields of the first somatic sensory cortex in monkeys. *Exp. Brain Res.* 52, 375–384.

Kimura, A., Donishi, T., Okamoto, K., and Tamai, Y. (2005). Topography of projections from the primary and non-primary auditory cortical areas to the medial geniculate body and thalamic reticular nucleus in the rat. *Neuroscience* 135, 1325–1342.

Kishan, A. U., Lee, C. C., and Winer, J. A. (2008). Branched projections in the auditory thalamocortical and corticocortical systems. *Neuroscience* 154, 283–293.

Kisvárday, Z. F., Kim, D.-S., Eysel, U. T., and Bonhoeffer, T. (1994). Relationship between lateral inhibitory connections and the topography of the orientation map in cat visual cortex. *Eur. J. Neurosci.* 6, 1619–1632.

Kurokawa, T., and Saito, H. (1995). Retrograde axonal transport of different fluorescent tracers from the neocortex to the suprageniculate nucleus in the rat. *Hear. Res.* 85, 103–108.

Kuwabara, N., DiCaprio, R. A., and Zook, J. M. (1991). Afferents to the medial nucleus of the trapezoid body and their collateral projections. *J. Comp. Neurol.* 314, 684–706.

Kuwabara, N., and Zook, J. M. (1991). Classification of the principal cells of the medial nucleus of the trapezoid body. *J. Comp. Neurol.* 314, 707–720.

Kuwabara, N., and Zook, J. M. (1992). Projections to the medial superior olive from the medial and lateral nuclei of the trapezoid body in rodents and bats. *J. Comp. Neurol.* 324, 522–538.

Kuwabara, N., and Zook, J. M. (1999). Local collateral projections from the medial superior olive to the superior paraolivary nucleus in the gerbil. *Brain Res.* 846, 59–71.

Kuypers, H. G. J. M., Bentivoglio, M., Catsman-Berrevoets, C. E., and Bharos, A. T. (1980). Double retrograde labeling through divergent axons collaterals, using two fluorescent tracers with the same excitation wavelength which label different features of the cell. *Exp. Brain Res.* 40, 383–392.

Lam, Y. W., and Sherman, S. M. (2010). Functional organization of the somatosensory cortical layer 6 feedback to the thalamus. *Cereb. Cortex* 20, 13–24.

Landry, P., and Deschênes, M. (1981). Intracortical arborizations and receptive fields of identified ventrobasal thalamocortical afferents to the primary somatic sensory cortex in the cat. *J. Comp. Neurol.* 199, 345–372.

Lee, C. C., Imaizumi, K., Schreiner, C. E., and Winer, J. A. (2004a). Concurrent tonotopic processing streams in auditory cortex. *Cereb. Cortex* 14, 441–451.

Lee, C. C., Schreiner, C. E., Imaizumi, K., and Winer, J. A. (2004b). Tonotopic and heterotopic projection systems in physiologically defined auditory cortex. *Neuroscience* 128, 871–887.

Lee, C. C., and Sherman, S. M. (2010). Topography and physiology of ascending streams in the auditory tectothalamic pathway. *Proc. Natl. Acad. Sci. U.S.A.* 107, 372–377.

Lee, C. C., and Winer, J. A. (2005). Principles governing auditory forebrain connections. *Cereb. Cortex* 15, 1804–1814.

Lee, C. C., and Winer, J. A. (2008a). Connections of cat auditory cortex: I. Thalamocortical system. *J. Comp. Neurol.* 507, 1879–1900.

Lee, C. C., and Winer, J. A. (2008b). Connections of cat auditory cortex: II. Commissural system. *J. Comp. Neurol.* 507, 1901–1919.

Lee, C. C., and Winer, J. A. (2008c). Connections of cat auditory cortex: III. Corticocortical system. *J. Comp. Neurol.* 507, 1920–1943.

Lee, C. C., and Winer, J. A. (2011). Convergence of thalamic and cortical pathways in cat auditory cortex. *Hear. Res.* 274, 85–94.

LeVay, S. (1988). The patchy intrinsic projections of visual cortex. *Prog. Brain Res.* 75, 147–161.

Li, H., and Mizuno, N. (1997a). Collateral projections from single neurons in the dorsal column nuclei to the inferior colliculus and the ventrobasal thalamus: a retrograde double-labeling study in the rat. *Neurosci. Lett.* 225, 21–24.

Li, H., and Mizuno, N. (1997b). Direct projections from nucleus X to the external cortex of the inferior colliculus in the rat. *Brain Res.* 774, 200–206.

Llano, D. A., and Sherman, S. M. (2008). Evidence for non-reciprocal organization of the mouse auditory thalamocortical-corticothalamic projection systems. *J. Comp. Neurol.* 507, 1209–1227.

Lorente de Nó, R. (1981). *The Primary Acoustic Nuclei.* New York: Raven Press.

Merchán, M. A., and Berbel, P. (1996). Anatomy of the ventral nucleus of the lateral lemniscus in rats: a nucleus with a concentric laminar organization. *J. Comp. Neurol.* 372, 245–263.

Michalski, A., Gerstein, G. L., Czarkowska, J., and Tarnecki, R. (1983). Interactions between cat striate cortex neurons. *Exp. Brain Res.* 51, 97–107.

Middlebrooks, J. C., and Zook, J. M. (1983). Intrinsic organization of the cat's medial geniculate body identified by projections to binaural response-specific bands in the primary auditory cortex. *J. Neurosci.* 3, 203–225.

Morel, A., and Imig, T. J. (1987). Thalamic projections to fields A, AI, P, and VP in the cat auditory cortex. *J. Comp. Neurol.* 265, 119–144.

Morest, D. K. (1968). The collateral system of the medial nucleus of the trapezoid body of the cat, its neuronal architecture and relation to the olivo-cochlear bundle. *Brain Res.* 9, 288–311.

Moriizumi, T., and Hattori, T. (1991a). Non-dopaminergic projection from the subparafascicular area to the temporal cortex in the rat. *Neurosci. Lett.* 129, 127–130.

Moriizumi, T., and Hattori, T. (1991b). Pyramidal cells in rat temporoauditory cortex project to both striatum and inferior colliculus. *Brain Res. Bull.* 27, 141–144.

Mulders, W. H. A. M., Harvey, A. R., and Robertson, D. (2007). Electrically evoked responses in onset chopper neurons in guinea pig cochlear nucleus. *J. Neurophysiol.* 97, 3288–3297.

Mulders, W. H. A. M., and Robertson, D. (2002). Inputs from the cochlea and the inferior colliculus converge on olivocochlear neurones. *Hear. Res.* 167, 206–213.

Mulders, W. H. A. M., and Robertson, D. (2003). Olivocochlear collaterals evoke excitatory effects in onset neurones of the rat cochlear nucleus. *Hear. Res.* 176, 113–121.

Namura, S., Takada, M., Kikuchi, H., and Mizuno, N. (1997). Collateral projections of single neurons in the posterior thalamic region to both the temporal cortex and the amygdala: a fluorescent retrograde double-labeling study in the rat. *J. Comp. Neurol.* 384, 59–70.

Oertel, D., Wu, S. H., Garb, M. W., and Dizack, C. (1990). Morphology and physiology of cells in slice preparations of the posteroventral cochlear nucleus of mice. *J. Comp. Neurol.* 295, 136–154.

Ojima, H. (1994). Terminal morphology and distribution of corticothalamic fibers originating from layers 5 and 6 of cat primary auditory cortex. *Cereb. Cortex* 6, 646–663.

Ojima, H., Honda, C. N., and Jones, E. G. (1991). Patterns of axon collateralization of identified supragranular pyramidal neurons in the cat auditory cortex. *Cereb. Cortex* 1, 80–94.

Ojima, H., Honda, C. N., and Jones, E. G. (1992). Characteristics of intracellularly injected infragranular pyramidal neurons in cat primary auditory cortex. *Cereb. Cortex* 2, 197–216.

Okoyama, S., Ohbayashi, M., Ito, M., and Harada, S. (2006). Neuronal organization of the rat inferior colliculus participating in four major auditory pathways. *Hear. Res.* 218, 72–80.

Oliver, D. L., Kuwada, S., Yin, T. C. T., Haberly, L. B., and Henkel, C. K. (1991). Dendritic and axonal morphology of HRP-injected neurons in the inferior colliculus of the cat. *J. Comp. Neurol.* 303, 75–100.

Peruzzi, D., Bartlett, E., Smith, P. H., and Oliver, D. L. (1997). A monosynaptic GABAergic input from the inferior colliculus to the medial geniculate body in rat. *J. Neurosci.* 17, 3766–3777.

Read, H. L., Miller, L. M., Schreiner, C. E., and Winer, J. A. (2008). Two thalamic pathways to primary auditory cortex. *Neuroscience* 152, 151–159.

Read, H. L., Winer, J. A., and Schreiner, C. E. (2001). Modular organization of intrinsic connections associated with spectral tuning in cat auditory cortex. *Proc. Natl. Acad. Sci. U.S.A.* 98, 8042–8047.

Reale, R. A., and Imig, T. J. (1980). Tonotopic organization in auditory cortex of the cat. *J. Comp. Neurol.* 192, 265–291.

Robertson, D., Anderson, C. J., and Cole, K. S. (1987a). Segregation of efferent projections to different turns of the guinea pig cochlea. *Hear. Res.* 25, 69–76.

Robertson, D., Cole, K. S., and Corbett, K. (1987b). Quantitative estimates of bilaterally projecting medial olivocochlear neurones in the guinea pig brainstem. *Hear. Res.* 27, 177–181.

Rouiller, E. M., and de Ribaupierre, F. (1990). Arborization of corticothalamic axons in the auditory thalamus of the cat: a PHA-L tracing study. *Neurosci. Lett.* 108, 29–35.

Rüttgers, K., Aschoff, A., and Friauf, E. (1990). Commissural connections between the auditory cortices of the rat. *Brain Res.* 509, 71–79.

Saldaña, E., Feliciano, M., and Mugnaini, E. (1996). Distribution of descending projections from primary auditory neocortex to inferior colliculus mimics the topography of intracollicular projections. *J. Comp. Neurol.* 371, 15–40.

Salin, P. A., Bullier, J., and Kennedy, H. (1989). Convergence and divergence in the afferent projections to cat area 17. *J. Comp. Neurol.* 283, 486–512.

Schofield, B. R. (1991). Superior paraolivary nucleus in the pigmented guinea pig: separate classes of neurons project to the inferior colliculus and the cochlear nucleus. *J. Comp. Neurol.* 312, 68–76.

Schofield, B. R. (1994). Projections to the cochlear nuclei from principal cells in the medial nucleus of the trapezoid body in guinea pigs. *J. Comp. Neurol.* 344, 83–100.

Schofield, B. R. (1995). Projections from the cochlear nucleus to the superior paraolivary nucleus in guinea pigs. *J. Comp. Neurol.* 360, 135–149.

Schofield, B. R. (2001). Origins of projections from the inferior colliculus to the cochlear nucleus in guinea pigs. *J. Comp. Neurol.* 429, 206–220.

Schofield, B. R. (2002). Ascending and descending projections from the superior olivary complex in guinea pigs: different cells project to the cochlear nucleus and the inferior colliculus. *J. Comp. Neurol.* 453, 217–225.

Schofield, B. R., and Cant, N. B. (1992). Organization of the superior olivary complex in the guinea pig: II. Patterns of projection from the periolivary nuclei to the inferior colliculus. *J. Comp. Neurol.* 317, 438–455.

Schofield, B. R., and Cant, N. B. (1996a). Projections from the ventral cochlear nucleus to the inferior colliculus and the contralateral cochlear nucleus in guinea pigs. *Hear. Res.* 102, 1–14.

Schofield, B. R., and Cant, N. B. (1996b). Origins and targets of commissural connections between cochlear nuclei in guinea pigs. *J. Comp. Neurol.* 375, 128–146.

Schofield, B. R., and Cant, N. B. (1999). Descending auditory pathways: projections from the inferior colliculus contact superior olivary cells that project bilaterally to the cochlear nuclei. *J. Comp. Neurol.* 409, 210–223.

Schofield, B. R., Schofield, R. M., Sorensen, K. A., and Motts, S. D. (2007). On the use of retrograde tracers for identification of axon collaterals with multiple fluorescent retrograde tracers. *Neuroscience* 146, 773–783.

Sherman, S. M., and Guillery, R. W. (2006). Exploring the Thalamus and Its Role in Cortical Function. MIT Press, Cambridge.

Silva, L. R., Amitai, Y., and Connors, B. W. (1991). Intrinsic oscillations of neocortex generated by layer 5 pyramidal neurons. *Science* 251, 432–435.

Smith, P. H., Joris, P. X., Carney, L. H., and Yin, T. C. T. (1991). Projections of physiologically characterized globular bushy cell axons from the cochlear nucleus of the cat. *J. Comp. Neurol.* 304, 387–407.

Smith, P. H., Joris, P. X., and Yin, T. C. T. (1998). Anatomy and physiology of principal cells of the medial nucleus of the trapezoid body (MNTB) of the cat. *J. Neurophysiol.* 79, 3127–3142.

Song, W.-J., Kawaguchi, H., Totoki, S., Inoue, Y., Katura, T., Maeda, S., Inagaki, S., Shirasawa, H., and Nishimura, M. (2006). Cortical intrinsic circuits can support activity propagation through an isofrequency strip of the guinea pig primary auditory cortex. *Cereb. Cortex* 16, 718–729.

Spirou, G. A., Brownell, W. E., and Zidanic, M. (1990). Recordings from cat trapezoid body and HRP labeling of globular bushy cell axons. *J. Neurophysiol.* 63, 1169–1190.

Takayanagi, M., and Ojima, H. (2006). Microtopography of the dual corticothalamic projections originating from domains along the frequency axis of the cat primary auditory cortex. *Neuroscience* 142, 769–780.

Tanaka, K., Katsumi, O., Tokunaga, A., and Sugita, S. (1985). The organization of neurons in the nucleus of the lateral lemniscus projecting to the superior and inferior colliculi in the rat. *Brain Res.* 341, 252–260.

Tanigawa, H., Wang, Q., and Fujita, I. (2005). Organization of horizontal axons in the inferior temporal cortex and primary visual cortex of the macaque monkey. *Cereb. Cortex* 15, 1887–1899.

Thompson, G. C., and Thompson, A. M. (1986). Olivocochlear neurons in the squirrel monkey brainstem. *J. Comp. Neurol.* 254, 246–258.

Velenovsky, D. S., Cetas, J. S., Price, R. O., Sinex, D. G., and McMullen, N. T. (2003). Functional subregions in primary auditory cortex defined by thalamocortical terminal arbors: an electrophysiological and anterograde labeling study. *J. Neurosci.* 23, 308–316.

Weinberg, R., Pierce, J., and Rustioni, A. (1990). Single fiber studies of ascending input to the cuneate nucleus of cats: I. Morphometry of primary afferent fibers. *J. Comp. Neurol.* 300, 113–133.

Willard, F. H., and Martin, G. F. (1984). Collateral innervation of the inferior colliculus in the North American opossum: a study using fluorescent markers in the double-labeling paradigm. *Brain Res.* 303, 171–182.

Winer, J. A. (1986). Neurons accumulating [^{3}H]gamma-aminobutyric acid (GABA) in supragranular layers of cat primary auditory cortex (AI). *Neuroscience* 19, 771–793.

Winer, J. A. (2006). Decoding the auditory corticofugal systems. *Hear. Res.* 212, 1–8.

Winer, J. A., Diehl, J. J., and Larue, D. T. (2001). Projections of auditory cortex to the medial geniculate body of the cat. *J. Comp. Neurol.* 430, 27–55.

Winer, J. A., and Larue, D. T. (1996). Evolution of GABAergic circuitry in the mammalian medial geniculate body. *Proc. Natl. Acad. Sci. U.S.A.* 93, 3083–3087.

Winer, J. A., Larue, D. T., Diehl, J. J., and Hefti, B. J. (1998). Auditory cortical projections to the cat inferior colliculus. *J. Comp. Neurol.* 400, 147–174.

Winer, J. A., Larue, D. T., and Huang, C. L. (1999). Two systems of giant axon terminals in the cat medial geniculate body: convergence of cortical and GABAergic inputs. *J. Comp. Neurol.* 413, 181–197.

Winer, J. A., and Lee, C. C. (2007). The distributed auditory cortex. *Hear. Res.* 229, 3–13.

Winer, J. A., Lee, C. C., Imaizumi, K., and Schreiner, C. E. (2004). "Challenges to a theory of neuroanatomical theory of forebrain auditory plasticity," in *Plasticity and Signal Representation in the Auditory System*, eds J. Syka and M. M. Merzenich (New York: Kluwer/Academic Plenum Publishers), 99–107.

Winer, J. A., Saint Marie, R. L., Larue, D. T., and Oliver, D. L. (1996).

GABAergic feedforward projections from the inferior colliculus to the medial geniculate body. *Proc. Natl. Acad. Sci. U.S.A.* 93, 8005–8010.

Winer, J. A., and Schreiner, C. E. (2005). "The central auditory system: a functional analysis," in *The Inferior Colliculus*, eds J. A. Winer and C. E. Schreiner (New York: Springer-Verlag), 1–68.

Wong, D., and Kelly, J. P. (1981). Differentially projecting cells in individual layers of the auditory cortex: a double-labeling study. *Brain Res.* 230, 362–366.

Ye, Y., Machado, D. G., and Kim, D. O. (2000). Projection of the marginal shell of the anteroventral cochlear nucleus to olivocochlear neurons in the cat. *J. Comp. Neurol.* 420, 127–138.

Zhang, Z. W., and Deschênes, M. (1997). Intracortical axonal projections of lamina VI cells of the primary somatosensory cortex in the rat: a single-cell labeling study. *J. Neurosci.* 17, 6365–6379.

Conflict of Interest Statement: The authors declare that the research was conducted in the absence of any commercial or financial relationships that could be construed as a potential conflict of interest.

Received: 12 May 2011; accepted: 09 July 2011; published online: 28 July 2011.

Citation: Lee CC, Kishan AU and Winer JA (2011) Wiring of divergent networks in the central auditory system. Front. Neuroanat. ***5****:46. doi: 10.3389/fnana.2011.00046*

frontiers in
NEUROANATOMY

HYPOTHESIS AND THEORY ARTICLE
published: 02 February 2012
doi: 10.3389/fnana.2012.00003

How the cortex gets its folds: an inside-out, connectivity-driven model for the scaling of mammalian cortical folding

Bruno Mota*[1,2] *and Suzana Herculano-Houzel*[1,2]

[1] *Instituto de Ciências Biomédicas, Universidade Federal do Rio de Janeiro, Rio de Janeiro, Brazil*
[2] *Instituto Nacional de Neurociência Translacional, São Paulo, Brazil*

Edited by:
Julian Budd, University of Sussex, UK

Reviewed by:
Charles F. Stevens, The Salk Institute for Biological Studies, USA
David C. Van Essen, Washington University in St. Louis, USA

***Correspondence:**
Suzana Herculano-Houzel, Instituto de Ciências Biomédicas, Universidade Federal do Rio de Janeiro, Av. Brigadeiro Trompowski, s/n, Ilha do Fundão, Rio de Janeiro, Rio de Janeiro 21941-590, Brazil.
e-mail: suzanahh@gmail.com

Larger mammalian cerebral cortices tend to have increasingly folded surfaces, often considered to result from the lateral expansion of the gray matter (GM), which, in a volume constrained by the cranium, causes mechanical compression that is relieved by inward folding of the white matter (WM), or to result from differential expansion of cortical layers. Across species, thinner cortices, presumably more pliable, would offer less resistance and hence become more folded than thicker cortices of a same size. However, such models do not acknowledge evidence in favor of a tension-based pull onto the GM from the inside, holding it in place even when the constraint imposed by the cranium is removed. Here we propose a testable, quantitative model of cortical folding driven by tension along the length of axons in the WM that assumes that connections through the WM are formed early in development, at the same time as the GM becomes folded, and considers that axonal connections through the WM generate tension that leads to inward folding of the WM surface, which pulls the GM surface inward. As an important necessary simplifying hypothesis, we assume that axons leaving or entering the WM do so approximately perpendicularly to the WM–GM interface. Cortical folding is thus driven by WM connectivity, and is a function of the fraction of cortical neurons connected through the WM, the average length, and the average cross-sectional area of the axons in the WM. Our model predicts that the different scaling of cortical folding across mammalian orders corresponds to different combinations of scaling of connectivity, axonal cross-sectional area, and tension along WM axons, instead of being a simple function of the number of GM neurons. Our model also explains variations in average cortical thickness as a result of the factors that lead to cortical folding, rather than as a determinant of folding; predicts that for a same tension, folding increases with connectivity through the WM and increased axonal cross-section; and that, for a same number of neurons, higher connectivity through the WM leads to a higher degree of folding as well as an on average thinner GM across species.

Keywords: allometry, brain size, evolution, white matter, cortical folding, connectivity, axon caliber, cortical thickness

INTRODUCTION

Across different mammalian orders and species, adult brain cerebral cortices vary over several orders of magnitude in size, becoming more folded as their size increases. Already in the late eighteenth century, Franz Gall acknowledged that cortical folding, and thus the non-isometrical expansion of the cerebral cortical gray matter (GM), allowed a faster increase in number of neurons than would be granted by increased cranial volume alone if the cortical surface expanded isometrically, or simply as a balloon would (Gross, 1999). Later, His (1874) considered that cerebral shape could be explained by unequal growth, competing volume demands, and resulting tension of different brain structures.

Cortical folding has since been considered to increase with brain size as the GM expands laterally and supposedly pushes inward the underlying white matter (WM; Le Gros Clark, 1945), specially given the constraint imposed by the skull (Welker, 1990). Because the distribution of neurons beneath the cortical surface has traditionally been considered to be constant across species (Rockel et al., 1980), cortical folding would thus be a direct function of the number of neurons in the cortex. This is in line with the

Abbreviations: a, average cross-section area of myelinated axons in WM; A_E, Exposed surface area of cerebral cortex; A_T, Total surface area of cerebral cortex; A_W, White–gray matter interface surface area; C, Cortical estimated computational capacity; $F_G = A_T/A_E$, Cortical folding index; $F_W = A_I/4\pi R_W{}^2$, white matter folding index; GM, cerebral cortical gray matter; l, average length of myelinated axons in WM; $L = l\ n{\cdot}N_N$, total length of myelinated axons in WM; M_G, mass of cerebral cortex GM; M_W, mass of cerebral cortex subcortical WM; n, GM connectivity through the WM, defined as the fraction of neurons in GM with myelinated axon in WM; N, Number of neurons in GM; O, number of other (non-neuronal) cells in WM; $R_W(3V_W/4\pi)^{1/3}$, WM "radius" (or, more properly, length scale); $T = V_G/A_T$, average thickness of cerebral cortex GM; V, volume of cerebral cortex (GM + WM); V_G, volume of cerebral cortex gray matter (GM); V_W, volume of cerebral cortex white matter (WM); WM, subcortical white matter.

usual expectation that elephants and large cetaceans, with larger brains than humans, have larger numbers of cortical neurons in their more folded cortices than humans do.

Contrary to these traditional views, however, we have recently shown that cortical size is not a uniform function of the number of cortical neurons across mammals. Using the isotropic fractionator to determine numbers of brain neurons (Herculano-Houzel and Lent, 2005), we find that cortical mass increases much faster in rodents than in primates as the cerebral cortex gains neurons across species (Herculano-Houzel et al., 2006, 2007, 2011; Gabi et al., 2010), which is due to an increase in average neuronal cell size in larger-brained rodents while there is barely any increase in average neuronal cell size in larger-brained primates (Herculano-Houzel, 2011). As a result, neuronal densities are larger in primate cortices than in rodent cortices of a comparable size (Herculano-Houzel, 2011). Moreover, we recently showed that the number of neurons beneath the cortical surface is not constant across primate species as previously thought (Herculano-Houzel et al., 2008), and is also not constant across rodents, actually decreasing in larger brains (Ventura, Mota, and Herculano-Houzel, to be submitted), which means that there is not a single relationship that applies between cortical surface area and number of cortical neurons across mammals. The combination of these findings leaves one no longer any reason to expect cortical folding to be a simple, homogeneous function of increased numbers of cortical neurons across mammals. For instance, although large cetacean and artiodactyla brains have more folded cerebral cortices than similar sized primate brains, they probably have not more but rather far fewer neurons in the cortex than primates, due to their very low neuronal densities (Tower, 1954; Herculano-Houzel, 2009; and our unpublished observations).

This is not to say, however, that cortical folding is not driven by a shared, conserved mechanism across mammalian species. In fact, our recent work on the scaling of the subcortical WM in primates as a function of their numbers of cerebral cortical neurons unexpectedly led us to realize that cortical folding can be universally predicted as a function of not simply the total number of cortical neurons, but of the number of cortical neurons that are connected through the WM compounded with the average caliber of their axons in the WM and the tension in these axons (Herculano-Houzel et al., 2010). Cortical folding, according to this view, would not be driven by the GM, but rather primarily by tension in the WM.

A qualitative, tension-based theory of cortical morphogenesis was first proposed by Van Essen (1997), taking into consideration the patterns of connectivity between cortical areas. His connectivity-driven hypothesis for the placement of cortical folds accounts for the consistent formation of convolutions in a species-specific pattern. It does not, however, explain the increased cortical folding that accompanies increasing cortical size across species; Van Essen himself still resorted to a GM driven mechanism to account for that. There are, however, a number of other evidences against a GM driven mechanism of cortical folding. Partial removal of the skull during development does not have a dramatic effect on the fissure pattern, and lesion experiments suggest that cortical folding is not primarily dependent on a disproportionate growth between cortical and subcortical structures (reviewed in Kaas, 2009). Thus, the primary source of fissure formation must be sought in factors within the cortex itself – or underneath it.

Based on our findings on the scaling of cortical connectivity and WM volume in primates (Herculano-Houzel et al., 2010), we proposed in that paper an extension of Van Essen's qualitative tension-based theory of cortical folding to explain quantitatively how increased folding accompanies increasing cortical size across primate species. According to our model, rather than *driving* the folding of the WM surface, the folding of the external surface of the GM *results* from folding of the WM surface, which, in turn, results from increased tension within the WM due to increased numbers of axons composing the WM depending on their physical properties of caliber and tension. Our model is quantitative; acknowledges that the cortex scales differently in size across mammalian orders as different power functions of its number of neurons; is therefore applicable, in principle, to all mammalian species; and makes easily testable predictions for all of them. The following is a description of the model, its assumptions, and a discussion of its implications and predictions, and how they can be tested.

ASSUMPTIONS AND RATIONALE

So far, we have found the size of the different brain structures, the numbers of cells that compose them, and their average densities, and therefore average cell size, to be parameters related to one another by power functions (Herculano-Houzel et al., 2006, 2007, 2011; Sarko et al., 2009; Gabi et al., 2010). Generically, one should expect brain and cortical allometric scaling rules that are valid over several orders of magnitude across species within a particular mammalian order to take the form of power laws (i.e., relating measurable quantities "x" and "y" by $y = kx^a$). This is because relations which are expected to remain valid over many orders of magnitude should not be given in terms of parameters that specify a particular size scale, that is, they should be scale-independent. As can be easily demonstrated, a one-variable function is scale-independent if and only if it is a power law. We therefore expect to find the scaling rules that determine cortical folding to also be scale-invariant, and therefore power laws.

Even more importantly, we assume that the number of neuronal cells is the main free parameter that coordinates the scaling of every other quantity of interest, measurable, or estimated. There are several reasons for this assumption. First, neurons, rather than glia, are the first cells to populate the developing brain in large numbers, and their connectivity begins to be established at the same time as convolutions begin to form, even before the final neuronal complement is in place (Goldman-Rakic, 1980; Goldman-Rakic and Rakic, 1984). Therefore, and in contrast to most earlier studies on brain allometry that implicitly or explicitly regarded the number of neurons as a consequence of brain size, we believe instead that any biologically plausible model of brain allometry must consider brain size, in all its aspects, to be a *consequence* of its number of neurons, according to scaling laws that may vary across different phyla. Second, we have found that, in contrast to the order- and structure-specific neuronal scaling rules, the scaling of different brain structures seems to occur as a universally shared function of their numbers of glial cells, both across orders and

structures (Herculano-Houzel, 2011). This result, combined with the late onset of gliogenesis in post-natal development (Sauvageot and Stiles, 2002), suggests that we can assume that cortical composition is determined essentially by the number of neurons and their average mass (which is itself closely related to the number of neurons by an order-specific power law); after neurogenesis, nearly invariant glia will then infiltrate the intraneuronal space in proportion to the total neuronal mass (Herculano-Houzel, 2011). The development of an adult mammalian cortex can then be viewed as a process whereby total numbers of neurons, numbers of neurons connected through the WM, their size (which includes the soma, all dendrites, and an axon of a particular caliber), and cortical folding vary in lockstep, over an invariant background of glia.

Our model thus assumes that all parameters related to cortical scaling and folding can be described as power functions of the total number of cortical neurons. Note that the fact that general allometric rules exist for cortical morphology in each order, expressible as power laws of their number of neurons, does not mean that the latter is the only significant degree of freedom in brain or cortical evolution. Rather, the power laws tell us that any other significant degrees of freedom must be present either at a substructure level, thus being erased by measurements that average over the entire structure, or at the microscopic level of detailed connectivity, which is not accessible to our methods, but also not relevant to the model at hand.

Our model, as presented for cross-species comparisons, considers total cortical volumes and areas, and average values of neuronal density and cortical thickness for the whole cortex, in line with the empirical studies that generated the numerical data used here (Herculano-Houzel et al., 2006, 2007, 2010, 2011; Sarko et al., 2009). Neuronal density is now known to vary across the cortical surface within primate species (Collins et al., 2010), and it is known that cortical thickness and gyrification also vary across the cortex (Zilles et al., 1988; Toro et al., 2008). However, comparative studies on the scaling of cortical gyrification traditionally analyze whole-brain patterns (Hofman, 1985; Pillay and Manger, 2007), and attempts to understand the scaling of cortical gyrification have similarly been directed toward whole-brain comparisons. We therefore developed our model based on average values for whole cortex that can be compared across orders, but predict that the scaling rules proposed here to govern gyrification at the level of the whole cortex might also be applicable at the local level across cortical areas.

White matter is largely composed of axons connecting neurons in the GM, mostly with each other but also with subcortical structures, along with the glial cells that support their function. The volume of each axon is simply its cross-sectional area multiplied by its length. If there is no significant correlation between these two latter quantities (which can be proven mathematically that will be the case when axon bundle volume is constrained and average signal propagation time is minimized), then the total axonal volume is the product of average axon cross-section area *a*, the average axonal length *l*, and the total number of axons present in the WM. We can assume further that the volume of the intra-axonal space, including in particular the myelin sheath and the myelinating oligodendrocytes, is proportional to axonal volume, given the experimental support for a linear relation between axon diameter and myelin sheath diameter (Sadahiro et al., 2000). Using the common assumption of a linear relation between total number of oligodendrocytes and the total axon length (Barres and Raff, 1994, 1999), then the total volume of the WM can be written to scale with the product of the total axon length (or total number of oligodendrocytes) and average axonal cross-sectional area.

We also assume that WM axons intersect the surface of the WM–GM interface in a perpendicular direction. This is a simplifying assumption, since it can observed from direct imagery that multiple fiber orientations can be present very close to each other even at the WM–GM interface. However, we believe on theoretical grounds that this is a reasonable if imperfect approximation of a somewhat more complex anatomical reality. Indeed, axons typically cross this interface in parallel bundles (Mori et al., 2002), which are the most volume-economical way of building such surface; in a growing cortex the combination of axonal longitudinal tension, WM hydrostatic pressure, and WM–GM interface surface tension should align most bundles very close to perpendicularly to the interface. We must make this assumption because we are unfortunately aware of no systematic studies of the distribution axonal incidence angles in the literature, although published diffusion tensor imaging tracing studies show a clear (but unquantified) preference for perpendicular angles of incidence (for instance, Mori et al., 2002). A systematic variation in the average incidence angle across species would alter our results somewhat, but not appreciably except for a very large range of values[1].

Finally, our model assumes that connections through the WM are formed early in development, at the same time as the GM becomes folded, an assumption that is supported by experimental evidence (reviewed in Welker, 1990); that most axons in mammalian cortical WM are myelinated (Olivares et al., 2001); and that most of the WM volume amounts to myelinated axons (Wang et al., 2008), thus neglecting the contribution to the volume of (small) non-myelinated fibers in the WM.

THE MODEL

We consider that the surface of the WM–GM interface, with total area A_W, is crossed nearly perpendicularly by most axons leaving or entering the WM, of an average cross-sectional area *a*, and which, together with the ensheathing glial cells, comprise the entirety of the WM surface. A_W can thus be quantified as the product of the number of cortical neurons, *N*; the fraction *n* of these neurons that are connected through the WM; and their cross-sectional area, *a* (**Figure 1**). Thus,

$$A_W \sim \gamma^{-1} n\, N\, a,$$

where γ is the average cosine of the incidence angle of axons at the WM–GM interface. The value of γ is of course 1 in the simplified

[1] A deviation from perpendicular incidence would be reflected on a proportional discrepancy in the estimation of axonal lengths; but only a systematic variation (with *N*) of incidence angle would alter the calculated power law coefficients. Unfortunately we cannot at this point rule out or numerically constraint such variation, and must therefore recognize this fact as a limitation of our model as it stands.

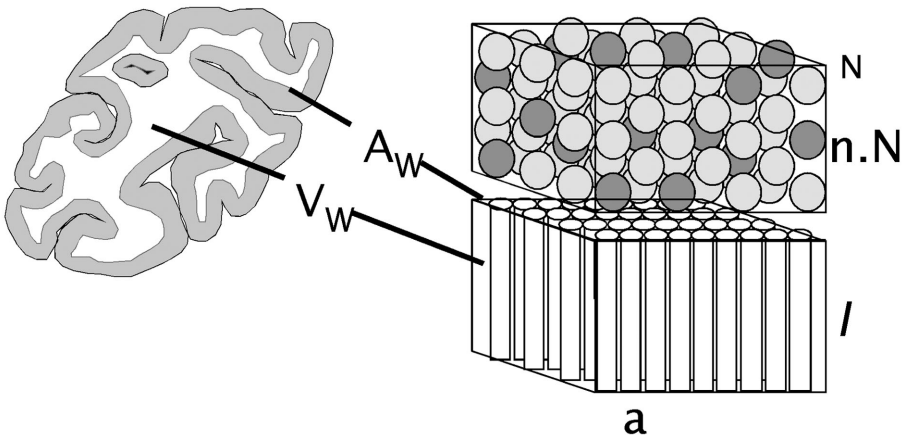

FIGURE 1 | Schematic of the cortical layout used in the model. The two volumes on the right illustrate the cortical gray matter (top) and white matter (bottom). The gray matter is composed of an *N* number of neurons, a fraction *n* of which are connected through the white matter (darker gray), either sending or receiving axons (of an average cross-sectional area *a*) through it. Glial cells, which have been found to be distributed at a fairly constant density across species (Herculano-Houzel, 2011), are not shown. The surface area of the interface between the gray and white matter, A_W, is given as the product *nNa*, and the volume of the white matter, V_W, is proportional to the product of A_W and the average axonal length in the white matter, *l*.

case of perfectly orthogonal incidence, and presumably close to 1 in reality. The WM volume V_W is the sum total of the volumes of all fibers and is thus equal to one half of the product of A_W and the average axonal length in the WM, *l*, such that

$$V_W \sim n\ N\ a\ l.$$

Note that the average value of axonal length is given by $l = 2V_w/\gamma A_w$. A direct measurement of γ would provide us with a direct measurement of *l* for each species. Assuming $\gamma = 1$, then *l* can be obtained from the existing measurements of V_w and A_w. Strictly speaking, these quantities are only lower bounds on the average axonal lengths; if however $\gamma \approx 1$ as we postulate, they can be taken as good approximations of their actual values.

If the WM scales under tension, the cubic root of its volume should increase more slowly than the square root of its surface area, leading to deformation of the latter, that is, to folding of the GM–WM surface. To quantify the extent of WM folding, we define a folding index F_W, which is the ratio between the actual WM surface, A_W, and the exposed surface expected from its volume $(9\pi/2)^{1/3}\ V_W{}^{2/3}$.

$$F_W = (2/9\pi)^{1/3}\ \ (n\ Na) \Big/ (nNa\ l)^{2/3}$$

Thus, a F_W value of exactly one implies a spherical WM, and larger values imply more convoluted forms. Importantly, notice that it is not necessary to model the cerebrum as a sphere for the 2/3 scaling relationship between its surface area and volume to hold; a volume of any shape that scaled isometrically would have the same scaling relationship of 2/3. In this case of isometric growth, which would ensue if the WM did not scale under tension, then we would expect F_W to be invariant as function of *N*.

Now, considering that *a*, *n*, and *l* are themselves related to *N* as power functions such that $a \sim N^{\alpha}$, $n \sim N^{c}$, and $l \sim N^{\lambda}$, the relationships above can be entirely rewritten as power functions of *N*:

$$A_W \sim N^C N\ N^{\alpha} \sim N^{c+1+\alpha}$$
$$V_W \sim N^C N\ N^{\alpha} N^{\lambda} \sim N^{c+1+\alpha+\lambda}$$
$$F_W \sim N^{(1+c+\alpha-2\lambda)/3}$$

Note that if we took into account a systematic variation of the incidence angle of fibers at the GM–WM interface as a power law of *N*, we would have to introduce a (non-zero) new coefficient at the expression for A_w. There is unfortunately currently no experimental way of estimating the value of such coefficient. We have assumed throughout that it is small enough to be disregarded, but should it prove to be otherwise we will have to recalculate the other coefficients accordingly, and revisit the conclusion obtained.

Simultaneously, for cortices with average GM thickness T much smaller than the cortical characteristic length so that the internal and external areas of GM scale linearly (that is, $A_G \propto A_W$), T can be defined as simply the ratio between the volume of the GM, V_G, and area of the GM–WM interface, A_W. Given that V_G scales as a power function of *N*, with N^{ν}, then

$$T \sim N^{\nu} \Big/ N^{c+1+\alpha}$$

and therefore cortical thickness T scales with N^t, such that

$$t = \nu - c - 1 - \alpha.$$

Instead of ν, we can use a more biologically meaningful parameter *d*, which is the exponent relating neuronal density D in the GM to *N*, given that $V_G = N \cdot D^{-1}$ and that $D \sim N^{d}$. Because $V_G \sim N^{1-d}$, then $\nu = 1 - d$, and the equation above becomes

$$t = -d - c - \alpha.$$

Average cortical thickness, therefore, scales a function of a GM-related variable (the scaling of neuronal density with N), and two WM-related variables that, together with N, determine WM folding (the scaling of connectivity and of axonal cross-sectional area with N). Remarkably, cortical thickness is therefore not itself a function of N, but rather of how exponents d, c, and α are interrelated.

Finally, the extent of GM folding, F_G, can be expressed as the ratio between its actual surface, A_G (which can be written as proportional to V_G/T, or N^{1-d-t}), and the exposed surface expected from the total volume $(V_G + V_W)^{2/3}$:

$$F_G = N^{1-d-t}/(N^{-d} + N^{c+1+\alpha+\lambda})^{2/3}$$

Note that although this equation is not an exact power law, it can in practice be well approximated by one since V_W and V_G scale in fairly similar ways with N. Another way to express F_G, now as an exact power law, is by writing the total volume $V_T = V_G + V_W$ itself as a measurable power function of N, varying with N^z. In this case, F_G becomes

$$F_G = N^{1-d-t}/(N^Z)^{2/3}$$

Returning to the first equation of F_G, and recalling that $t = -d-c-\alpha$, GM folding is thus a combined function of the number of cortical neurons; the fraction of these neurons that are connected through the WM; and the average cross-section area of the axons in the WM. Further, the thickness of the GM is thus a consequence of some of the same parameters that determine how the cortex folds, and not a determinant of it. A schematic of the model is depicted in **Figure 2**.

PREDICTIONS FROM THE MODEL

Useful mathematical models are those that lead to a number of testable predictions. This is one major advantage of our model: it allows us to derive not only testable qualitative insights on the scaling of cortical folding, but also quantitative predictions that can be tested experimentally.

QUALITATIVE PREDICTIONS ABOUT CORTICAL FOLDING

Our model predicts that the folding of the GM is related to the folding of the WM, and the scaling of the former across species depends on the scaling of the latter. We predict that WM folding scales across mammalian species with the number of cortical neurons; the fraction of these neurons that are interconnected through the WM; the average length of the myelinated fibers in the WM; and their average cross-sectional area. GM folding then scales depending, additionally, on the scaling of the GM thickness, which in turn is determined by the scaling of neuronal density

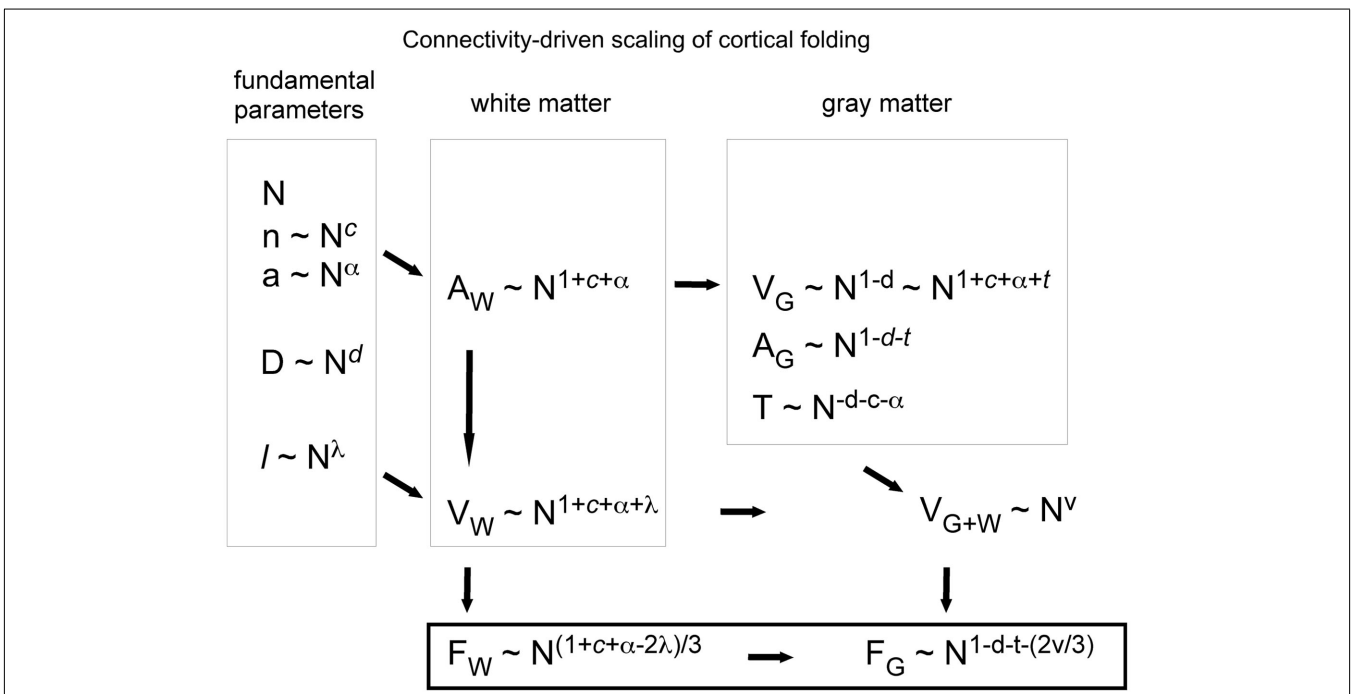

FIGURE 2 | Schematic of our connectivity-driven model of the scaling of cortical folding with increasing numbers of cortical neurons *(N)*. To the left are shown what we propose to be the fundamental parameters determining cortical folding, probably determined genetically, and which we postulate to vary alometrically with N: the fraction of cortical neurons connected through the gray matter (n), the average cross-sectional area of the axons in the white matter (a), the average neuronal density in the gray matter (D, which is approximately proportional to the inverse of average neuronal cell volume in the gray matter), and the average axonal length in the white matter (l). Next, white matter surface (A_W) and volume (V_W) are organized as shown, depending on N and the scaling exponents, and thus determine the folding of the white matter surface (F_W). On top of A_W, the gray matter becomes organized depending on the average size of its neurons, which, combined to a and n, determine cortical thickness, T. The degree of folding of the gray matter, F_G, is thus a consequence of the folding of the white matter, which is in turn dependent on how the parameters determining cortical connectivity (c, a, and l) scale with N.

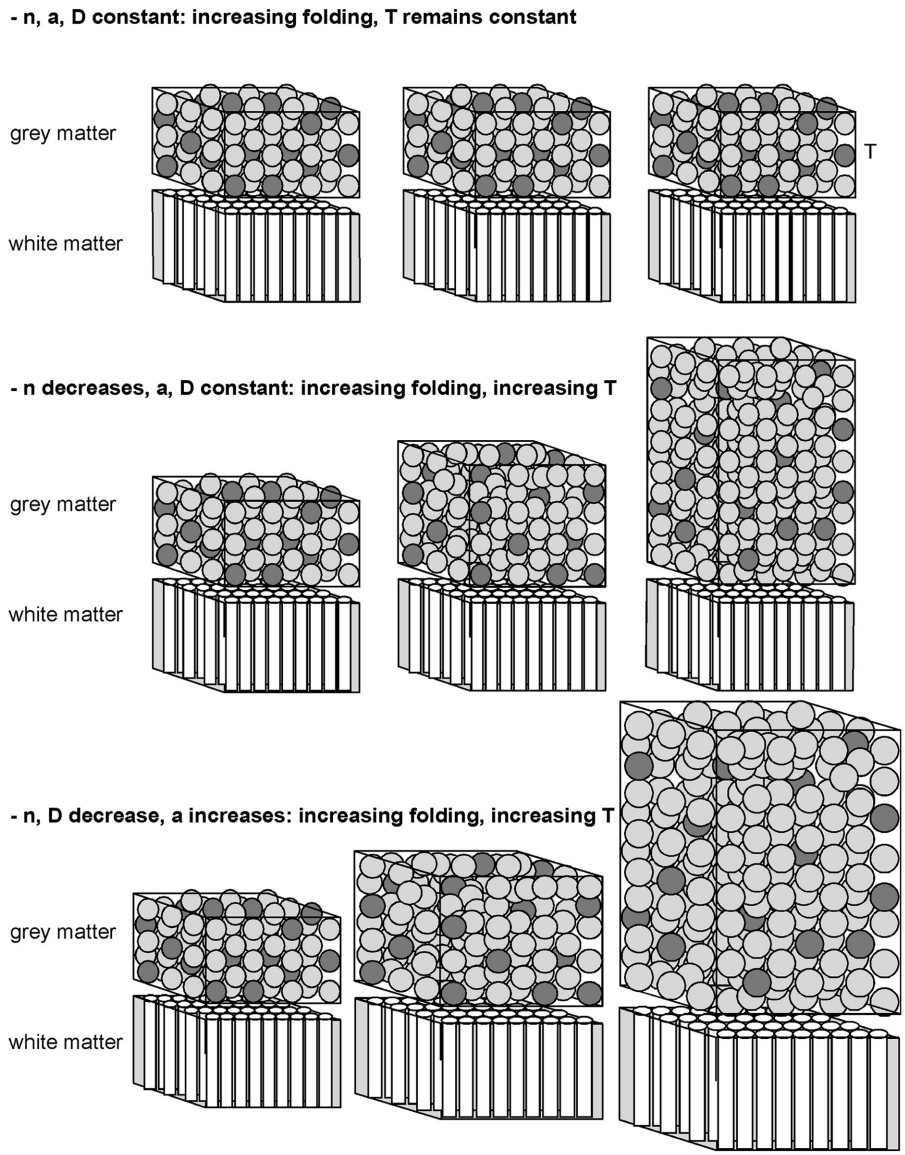

FIGURE 3 | Schematics of various manners of cortical scaling (and folding, not shown) depending on the interplay between the scaling parameters and how they vary with the number of cortical neurons as it increases (left to right). In all three scenarios, axons in the white matter grow under enough tension to lead to cortical folding, fulfilling the condition that $\lambda < (c+1+\alpha)/2$. In the *top scenario*, in which the connectivity fraction is unchanged (indicated by the dark gray "neurons" in the gray matter), $c = \alpha = 0$; therefore $\lambda < 0.5$, and the cortex folds more and more with an unchanging thickness given that, in this scenario, d is also 0. In the *middle scenario*, in which the connectivity fraction decreases but $\alpha = d = 0$, cortical folding will increase, with an accompanying increase in thickness that scales with N^{-c} (from $t = -c-d-\alpha$). In the *bottom scenario*, in which the connectivity fraction decreases ($c < 0$) and both average neuronal size in the gray matter and axonal cross-sectional area in the white matter increase with N (that is, $d < 0$ and $\alpha > 0$), cortical folding increases with a rapid increase in thickness that scales with $N^{-c-d-\alpha}$.

in the GM (besides the scaling of connectivity and average axonal cross-sectional area in the WM). **Figure 3** illustrates how the interplay across the scaling of these parameters determines cortical morphology and folding.

One remarkable characteristic of our model is that, in principle, it applies universally across mammalian orders (and therefore describes the scaling of cortical folding universally), even though relationships such as those among folding index, cortical thickness, and cortical size are different across orders (Pillay and Manger, 2007). In fact, we can predict that these relationships will be different across orders depending on the particular defining exponents that apply to each order; order-specific characteristics of the scaling of cortical folding will result from combinations of these exponents. Thus, it is conceivable that cortical folding increases in larger brains with no change in connectivity and no change in the average cross-sectional area of the axons in the WM; with decreasing connectivity and increasing average cross-sectional area of the WM; and so forth.

Indeed, one of the strengths of the model is that one can predict how the different scaling exponents will be related. Because folding of the WM scales with $N^{(1+c+\alpha-2\lambda)/3}$, then larger cortices in a mammalian order will only be increasingly folded when $(1+c+\alpha-2\lambda)/3 > 0$. This condition imposes constraints on the combinations of values of c, α, and λ that will lead to increased folding in larger cortices (that is, as N increases).

For instance, supposing that cortical scaling occurs in an order with a fixed λ of 0.5, then $c+\alpha > 0$, which implies that if folding increases in larger cortices, then any decrease in connectivity (that is, a negative value of c), or even a constant connectivity (that is, $c=0$) is necessarily surpassed by a positive scaling of average axonal cross-section in the WM. In these circumstances, the thickness of the GM, which scales with $t=-d-c-\alpha$, will depend on the scaling of neuronal density minus the positive sum of $c+\alpha$; as a consequence, the number of neurons underneath a given cortical surface will not be constant (a condition that is only met when $t=-d$).

By the same token, if cortical scaling occurs in an order with increasing folding in the presence of fixed connectivity (that is, with $c=0$), then necessarily $\alpha > 2\lambda - 1$. In these circumstances, the average axonal cross-sectional area in the WM will increase in larger-brained cortices for any value of $\lambda \geq 0.5$. Consequently, the thickness of the GM will scale depending on the value of $-d-\alpha$.

Likewise, it is possible for cortical scaling to occur with increased cortical folding within an order with fixed connectivity and unchanging average axonal cross-sectional area in the WM, as long as $\lambda < 0.5$. In these conditions, it can be predicted that the thickness of the GM will scale depending on the scaling of neuronal density alone, and thus occur indeed with a constant number of neurons beneath the cortical surface, as intended in some models (Rockel et al., 1980).

CORTICAL THICKNESS

Thinner mammalian cortices are usually found to be more folded than thicker cortices of a similar size (Hofman, 1985; Pillay and Manger, 2007). This finding has been attributed to thinner cortices being supposedly more pliable than thicker cortices, which would render the former less resistant to being folded (Pillay and Manger, 2007). In contrast, our model predicts that cortical thickness is actually determined by two WM-related factors that also determine the degree of cortical folding (connectivity and average axonal cross-sectional area in the WM), and a third, GM-related variable (neuronal density). Remarkably, the scaling of cortical thickness is therefore not simply a function of N, but rather of how d, c, and α are interrelated; if neuronal density, connectivity, and average axonal cross-sectional area are unchanging in a mammalian order, then larger cortices, with larger N, would be expected to have an unchanging thickness as well. In another scenario, even if neuronal densities in the GM were still constant across species in an order, cortical thickness would still increase with N as long as $c+\alpha < 0$, which would be the case, for instance, if connectivity decreased ($c<0$) and average axonal cross-sectional area did not change ($\alpha=0$).

CORTICAL UNIFORMITY

Remarkably, the relationship between cortical thickness, connectivity, neuronal density, and axonal cross-sectional area predicts that a uniform number of neurons underneath a cortical surface area will only be found across species (Rockel et al., 1980) when a very specific condition is met. Given that $V_G = A_W\ T = N/D$, then the ratio N/A_W will only be constant when the product $D \cdot T$ is constant. Written as a function of N, and remembering that D varies with N^d, and T with $N^{-d-c-\alpha}$, then this condition is met only when $d+(-d-c-\alpha)=0$, that is, when the sum of the exponents c and α is zero, or, alternatively, when cortical connectivity through the WM remains constant and simultaneously the average axonal cross-section in the WM does not scale (that is, both c and α are zero). In all other cases, the number of neurons underneath a cortical surface will scale with a non-zero combination of d and t. Notice that this prediction is valid both for the scaling of the entire cerebral cortex and for different cortical areas.

SCALING OF WM WITH GM

Because V_G can be defined as the product of A_W and T, and therefore varies with $N^{c+1+\alpha}\ N^t$, or $N^{c+1+\alpha+t}$, then the ratio V_W/V_G varies with $N^{c+1+\alpha+\lambda}/N^{c+1+\alpha+t} = N^{\lambda-t}$, that is, depending on which is steeper: the scaling of axonal length reduction (faster with smaller values of l) or of cortical thickening (faster with larger value of t) as a function of N. Ratios larger than 0 mean that axons shorten relative to isometry more *slowly* than the cortex thickens as it gains neurons. The implication here is that the ratio V_W/V_G will be constant across mammalian species when $\lambda = t$ and that it will increase when $\lambda > t$; and may even scale similarly across orders when they share a similar relationship between λ and t. Note that a similar scaling of the V_W/V_G relationship across orders does not imply similar values of λ or of t, but only a similar difference between them across orders. The increase in the ratio V_W/V_G in larger cortices (Zhang and Sejnowski, 2000) can thus be predicted to be a consequence of a slower minimization of average axonal length relative to isometry than the thickening of the GM as a function of N.

PROPAGATION TIME

Another way of thinking about F_W is to express it in terms of the average axon length l and the WM characteristic length R_W (defined as the radius of a sphere with volume V_W). This relationship can be written as $F_W = 2R_W/3l$, where the WM folding index is simply proportional to the ratio between the characteristic size of the WM and the average axonal length. Thus, the more axonal tension curtails the growth of l, the greater the F_W and the more convoluted the WM becomes. Compared to a smooth WM surface, folding the WM results in axons having to travel shorter distances to connect GM neurons. A more folded WM will have shorter axons, as a fraction of its characteristic size.

Since the whole purpose of the axons in WM is to transmit signals, it makes sense to quantify how well and quickly they do it, in terms of the scaling rules obtained above. It is well known that an action potential impulse propagates along a myelinated axon in a time proportional to the axon length and inversely proportional to the square root of axon cross-sectional area. The average impulse propagation time should then be given by $\bar{t}\ \alpha\ l/a^{1/2}$.

Since $l = 2V_W/A_W \propto N^{\lambda}$, $A_W \sim N^{c+1+\alpha+\lambda}$, and $V_W \sim N^{c+1+\alpha+\lambda}$, we can combine the three equations to describe how the average propagation time scales with N:

$$\bar{t} \propto \frac{l}{a^{1/2}} \propto \frac{2V_W}{A_W N^{\alpha/2}} \propto N^{\tau}$$
$$\tau = \lambda - \tfrac{\alpha}{2}$$

From the equation above, it is clear that, with all else being equal, increasing axonal thickness would result in smaller propagation times. However, if all axons in the WM were to grow thicker by the same factor, then a tightly packed WM would also have to expand to accommodate the extra volume. But a larger WM would mean that GM neurons would be further apart, and axons would have to be longer to connect them.

For the sake of argument, let us considering an isometric doubling of all the lengths and diameters (i.e., a fourfold increase in average cross-sectional areas) of all axons in the WM, such that the overall shape of the WM does not change. According to the formula given above, the average axon impulse propagation time in this isometrically scaled up WM would also be unchanged. Signals have to propagate further due to the doubling of l, but the propagation speed is proportionally faster due to the quadrupling of a. Thus, as far as average propagation times in the WM are concerned, there is no difference between scaled up or scaled down isometric versions of the WM. In contrast, the hypometric scaling of axonal length in the WM has the obvious consequence of decreasing propagation time: the smaller the value of l, the smaller the increase in axonal cross-sectional area required to maintain a constant average propagation time as the cortex gains neurons interconnected through the WM.

With the realization that average propagation time scales with N raised to an exponent of $\lambda - \alpha/2$, then the folding of the WM can be written to scale as

$$F_W \sim N^{(1+c+\alpha-2\lambda)/3} \sim N^{(1+c-2\tau)/3}$$

Thus, the WM folding index can be expressed in such a way as to depend on only two quantities: The total number of axons in WM (which scales with N^{c+1}), and the inverse of the square of the average axonal signal propagation time (which scales as $N^{\lambda-\alpha/2}$). This means that cortices in which connectivity through the WM and average propagation time scale similarly will have folding indices that also scale similarly. This also means that, for a given value of c, a faster upscaling of WM folding will be accompanied by a slower increase in propagation times. Increasing cortical folding in larger brains is thus associated with the advantage of a diminished increase in the average propagation time that would otherwise be expected if the WM grew isometrically.

COMPUTATIONAL CAPACITY

Signal propagation times tell us how fast a cortex computes information, but not how effectively. To quantify computational capacity in a simple way, consider a simple neuronal circuit composed of a few neurons connected by axons passing through the WM. A discrete "operation" in such a circuit consists of a set number of signals being passed back and forth among the neurons (for instance in response to a specific external input). A typical such operation is memory retrieval: The circuit receives as input an incomplete pattern that is a partial match to a stored pattern. After a few cycles over its feedback loops, the circuit's output eventually converges to the stored pattern. Clearly, each such computational cycle (which can be as simple as two neurons with reciprocal connections) is completed in the time it takes for a signal to propagate along the axons of its interconnected, constituting neurons. Thus, in general terms, and assuming that all propagation times in the circuit scale up similarly, then the time needed to perform one operation in this circuit is proportional to the average propagation time along its axons; conversely, the number of operations it can perform per unit time is inversely proportional to the average impulse propagation time of the circuit's axons. In this case, C, the number of operations involving WM fibers (i.e., non-local operations) that a cortex would be able to perform per unit time, a very simple proxy for its overall computational capacity, is then proportional to the number of "circuits," or the number of axons, and inversely proportional to the average propagation time.

$$C \propto \frac{nN}{\tau} = \frac{O^{\frac{1}{2}} A_W^2}{V_W^{\frac{3}{2}}} \propto N^{\theta}$$
$$\theta = 1 + c - \tau = 1 + c - \lambda + \tfrac{\alpha}{2}$$

Note that, like the WM folding index, the scaling of C depends only on the number of axons crossing the WM, and on the coefficient τ for the scaling of average propagation time.

We can also define a volumetric computational efficiency, that is, computational capacity per unit of WM cortical volume, $C^{ef} = C/V_W$,

$$C^{ef} \propto \frac{nN}{V_W \tau} = \frac{N_O^{\frac{1}{2}} A_W^2}{V_W^{\frac{5}{2}}} \propto N^{\varepsilon}$$
$$\varepsilon = -2\lambda - \tfrac{\alpha}{2}.$$

The computational efficiency of the WM is thus predicted to scale with $N^{-2\lambda-(\alpha/2)}$. Note that C^{ef} is highly dependent on the scaling of axonal length, but only weakly so on the scaling of axonal cross-sectional area.

WHEN SHOULD THE CORTEX FOLD?

If the WM scales isometrically, that is, without folding, then the average axonal length l will scale with ${V_W}^{1/3}$, or with ${A_W}^{1/2}$. If on the contrary the WM scales under tension, with a smaller increase in V_W than expected, that implies that l is scaling more slowly than expected. Assuming that $A_W \sim nNa$ and that a, n, and l are themselves related to N as power functions such that $a \sim N^{\alpha}$, $n \sim N^{\varepsilon}$, and $l \sim N^{\lambda}$, then, in the case of isometric scaling of V_W,

$$l \sim N^{\lambda} \sim (n\ N\ a)^{1/2} \sim N^{(c+1+\alpha)/2}$$

so $\lambda = (c + 1 + \alpha)/2$ if the WM scales isometrically.

In all scenarios where $\lambda < (c + 1 + \alpha)/2$, the WM will become convoluted as it increases in size, and one can therefore expect

the cortical GM to also become more and more folded at the same time. Qualitatively, this means that, due to increasing WM folding, axons do not grow in direct proportion to the characteristic length of the brain (R_W), but rather much more slowly; with cortical growth, connections become relatively shorter, as if axons resisted being "stretched" to accommodate more and more connections through the WM. As we have seen, this results in average propagation times increasing more slowly with the addition of more axons in WM.

Finally, in these scenarios where $\lambda < (c+1+\alpha)/2$ and the WM becomes increasingly folded in larger cortices, it can also be predicted that $\tau < (c+1)/2$ (by substituting $\tau = \lambda - \alpha/2$ in the equation), which implies that there is an upper limit to the scaling exponent of propagation time in the WM determined by the connectivity fraction. This leads to the interesting realization that decreasing the fraction of cortical neurons connected through the WM (that is, more negative values of c) minimizes the upscaling of propagation times in larger cortices.

TESTING THE MODEL

There are two main ways in which our model can be tested: by designing experiments to address the prediction that cortical connectivity through the WM affects the establishment of cortical folds; and by testing the quantitative relationships predicted by the model. While we have not yet had the opportunity to design experiments specifically to test this model, earlier experiments showing that cortical folding is altered after disrupting cortical connectivity but not after partial removal of the skull during development (reviewed in Kaas, 2009) do support our proposal that cortical folding is driven by pulling on the inside of the cortex, rather than from the cortex pushing inward.

Testing the numerical relationships predicted by the current model requires quantifying, across different mammalian species, their numbers of neurons in the GM, numbers of other cells in the WM; obtaining surface and volume measurements for the GM and WM; and determining, from the scaling across these parameters, whether the exponents thus calculated match the predictions from the model. Here we discuss how the scaling exponents can be obtained; in the next section, we will address how well the model's predictions are matched by experimental data available so far from rodents and primates.

MEASURING *l* AND λ

We showed above how, given that $l = 2V_W/A_W \propto N^{\lambda}$, the allometric exponent λ for scaling of l with N can be determined experimentally from the relationship between the ratio between the measureable values V_W/A_W and N. Additionally, the same relationship also allows the average value of l to be estimated for each species, as the quotient $2V_W/A_W$. The factor of 2 is due to the fact that we expect the vast majority of fibers in the WM to be cortico-cortical (Braitenberg and Schüz, 1998) and thus cross the WM–GM interface twice, coming in and out of the WM as they connect different areas of the cortical GM. Notice that because any deviation of the true factor will be in the direction of being smaller than 2, the value of l thus determined can be considered an upper limit of the average axon length in the WM for that species; moreover, deviations from this value of 2 do not affect the exponent, λ.

DETERMINING *c* AND α

Experimentally, one can obtain the sum $c+\alpha$ from plotting A_W as a function of N, but not the individual values of these exponents. A simple, well-fundamented assumption, however, allows the exponents c and α to be determined empirically using the isotropic fractionator (Herculano-Houzel and Lent, 2005) to count the number of non-neuronal (other) cells in WM, O, most of which are oligodendrocytes myelinating neighboring axons. According to Barres and Raff (1994, 1999), it is reasonable to assume that the total length L of all axons in WM, given by $L = n{\cdot}N{\cdot}l$, is proportional to the total number of oligodendrocytes found in the WM. Thus, $O \sim L$.

Now, because V_W amounts to total axon length L multiplied by a, then $V_W \sim O{\cdot}a$. Because the power law relating O to N, $O \sim N^{\omega}$, can be determined empirically (Herculano-Houzel et al., 2010), V_W may be rewritten as

$$V_W \sim N^{\omega}N^{\alpha}.$$

This is a power function that allows the exponent α to be determined, given that ω is known. The exponent c can next be calculated simply from the scaling relationship above between A_W and N, now that has been determined.

TESTING THE PREDICTIONS

Once the values of exponents λ, c, and α are obtained from the measurements of V_W, A_W, N, and O, it becomes possible to predict if the WM should become increasingly folded in larger brains from the comparison between λ and $(c+1+\alpha)/2$. If these quantities are equal, then the WM should scale isometrically. If, on the other hand, $\lambda < (c+1+\alpha)/2$, the WM will become convoluted as it increases in size, and one can therefore expect the cortical GM to also become more and more folded at the same time.

The actual folding of the WM, F_W, is easily determined experimentally for each species as being proportional to $A_W/{V_W}^{2/3}$; the exponent of the experimentally obtained scaling of F_W with N can thus be compared to the predicted exponent given by $F_W \sim N^{(1+c+\alpha-2\lambda)/3}$.

Next, once the average thickness of the GM is determined for each species as the ratio V_G/A_W, the exponent t of its scaling with N can be determined experimentally, as can the exponent d of the scaling relationship between neuronal density and number of cortical neurons. Once these exponents are available, it can be tested whether, as predicted, $t = -d-c-\alpha$; and whether the extent of GM folding, F_G, expressed as the ratio $A_G/(V_G+V_W)^{2/3}$, scales as predicted, with

$$F_G = N^{1-d-t}/\left(N^{-d} + N^{C+1+\alpha+\lambda}\right)^{2/3}$$

EXPERIMENTAL FINDINGS

This model has so far been applied to a primate dataset containing 11 species, including humans (Herculano-Houzel et al., 2010),

and more recently to a dataset of 5 rodent species (Ventura, Mota, and Herculano-Houzel, to be submitted). Experimentally, we find that the average cross-section area remains nearly invariant in primates as a function of *N*, while it increases sharply with *N* across rodents. This is qualitatively very similar to what happens with average neuron size in both orders: It increases significantly with *N* in rodents, but increases very slowly with *N* across primate species (Herculano-Houzel, 2011), suggesting there is a connection between average neuron size and axon caliber.

As for the fraction of GM neurons projecting axons through the WM, we find that it decreases with *N* in both orders, but at a rate that is more pronounced in primates than in rodents. As a result, the WM becomes increasingly folded in larger primate brains, but less rapidly in larger rodent brains.

Using the experimental method described above to determine the values of the scaling exponents that appear in the model, we obtained, in rodents and in primates, the values listed in **Table 1**.

In both orders, *l* scales sublinearly with *N*, which is a significant finding given that any increase in average axon length implies an increase in volumetric and propagation time costs. However, while the rodent λ closely matches the value of 0.689 expected in case of isometric scaling of V_W of $\lambda = (c + 1 + \alpha)/2$, the primate $\lambda = 0.207$ is significantly smaller than the value of 0.436 expected in the case of isometric scaling of the WM. This is a strong indication that in primates, the increase in distance between interconnected cortical regions is minimized by effective shortening of the axons, as would be expected to happen if they grew under longitudinal tension (Van Essen, 1997).

As a consequence of these exponents, the folding of the WM is predicted to scale as the cortex gains neurons with $N^{0.153}$ in primates, which matches precisely the observed scaling of the WM calculated as $A_W/{V_W}^{2/3}$; and is predicted to scale with N^0, that is, not to increase in larger rodents cortices. Notice that this prediction apparently contradicts the finding that large rodent cortices, such as those of the agouti and capybara, are indeed folded. We believe, however, that the apparent failure of the model to predict the folding of large rodent cortices is due to the fact that in our sample, three of the five species (mouse, rat, and guinea pig) are small-brained and practically lissencephalic. Thus, rodent cortices seem to scale without becoming folded only up to a certain point, beyond which larger cortices do become increasingly folded. This is actually circumstantial evidence in favor of the push–pull model that we propose, in which the WM only begins to fold once the traction that it exerts upon the GM exceeds the resistance of the latter to becoming folded inward.

Table 1 | Experimentally determined exponents for, respectively, the scaling of average axonal length in the WM (*l*), average axonal cross-sectional area in the WM (*a*), fraction of GM neurons connected through the WM (*n*), average GM thickness (*t*), and neuronal density in the GM (*d*) as power functions of the number of cortical neurons (*N*).

Order	λ	α	*c*	*t*	*d*
Primates	0.207	0.085	−0.212	0.127	0*
Rodents	0.699	0.466	−0.088	0.427	−0.640

*Note that the values in the table value slightly from the values reported in Herculano-Houzel et al. (2010) because here they are estimated for values of V_W, which are not available for human brains in our dataset, while in that study, they were estimated for values of M_W, which are available for humans, although A_W is not. Because of the lack of all values for human brains, we chose to recalculate the exponents here for only those species for which V_W and A_W are available. *Neuronal density in the GM was not found to scale with N in the original study where λ, α, c, and t were estimated (Herculano-Houzel et al., 2010), but in a later review of a large dataset was found to scale with d = −0.168 (Herculano-Houzel, 2011). Again, we chose to report the value that applies to the current dataset, for consistency.*

NUMBER OF CORTICAL NEURONS CONNECTED THROUGH THE WM

Our model predicts that GM connectivity *n* (the fraction of GM neurons that sends an axon through the WM) decreases as the GM gains neurons, in a manner that we estimate in primates as $n \propto N^{-0.212}$. Although we do not dispose of estimates of the actual number of cortical neurons connected through the WM, it is illuminating to consider the following exercise scenario. Supposing, for the sake of argument, that 50% of all cortical neurons were connected through the WM in the marmoset, then a scaling of *n* with $N^{-0.212}$ would imply that in a monkey-sized cortex with 10 times more neurons than the marmoset, WM connectivity would fall to $10^{-0.212} = 0.61 \times 50\% = 30\%$ of all neurons; and a human-sized cortex with about 100 times more neurons than a marmoset would have only 19% of its neurons interconnected through the WM.

Note that decreased connectivity occurs in the face of an increased total number of axons in the WM, which is proportional to $n{\cdot}N$, or N^{1+c}. In the exercise scenario above, the total number of axons in the WM would increase from about 122 million in the marmoset, to 510 million in the macaque, to 3.0 billion in the human cortex. Larger primate cortices, therefore, increase in size proportionally to N^1 neurons in the GM, of which a number proportional to $N^{0.788}$ send axons into the WM.

A CONSTANT NUMBER OF NEURONS BENEATH THE CORTICAL SURFACE?

As observed above, our model predicts that the ratio N/A_G will only be constant, as assumed in several models (e.g., Prothero, 1997; Zhang and Sejnowski, 2000), under particular circumstances, when $d = -t$, that is, when both *c* or α are zero, or so is their sum. Indeed, we have recently found that the ratio N/A_G (which is similar to the ratio N/A_W), far from being constant across primate species, varies threefold across primate species, and actually scales with variations in neuronal density across the species (Herculano-Houzel et al., 2008).

In primates, the predicted value of $t = 0.127$ agrees nicely with a measured value of 0.109 ± 0.025 SE. In rodents, the predicted value of $t = 0.262$ is well below the measured value of 0.427 ± 0.048, possibly because our current estimate of *d* for the GM is not as accurate as in primates for methodological reasons (Ventura, Mota, and Herculano-Houzel, to be submitted). In both cases, however, cortical thickness clearly does not scale as the inverse of neuronal density (because either *c* or α or both are significantly different from zero, and non-canceling), thus

explaining why the number of neurons underneath a given cortical surface does not remain constant as cortical size varies (Herculano-Houzel et al., 2008; Ventura, Mota, and Herculano-Houzel, to be submitted).

SCALING OF V_W/V_G

It has been proposed that larger cortices scale with a ratio between the volumes of the WM and GM that increases homogeneously across all mammalian species, with V_W scaling with ${V_G}^{1.22}$ to ${V_G}^{1.33}$ depending on the study (reviewed in Zhang and Sejnowski, 2000). We find that V_W scales with ${V_G}^{1.184\pm0.054}$ in primates, and with ${V_G}^{1.250\pm0.057}$ in rodents. Thus, V_W appears to scale as not significantly different functions of V_G across the two orders.

These volume relationships, however, mask the finding that the ratio V_W/V_G increases much more rapidly in rodents than in primates as their cortices gain neurons, varying experimentally with $N^{0.421\pm0.087}$ in the former and with $N^{0.162\pm0.057}$ in the latter. Remembering that V_W/V_G varies with $N^{c+1+\alpha+\lambda}/N^{c+1+\alpha+t} = N^{\lambda - t}$, the scaling exponents above 0 indicate that in both rodents and primates, $\lambda > \tau$. The increase in the ratio V_W/V_G in larger cortices can thus be explained by the slower minimization of average axonal length relative to isometry than the rate of thickening of the GM as a function of N – but with axonal length minimization lagging behind cortical thickening more pronouncedly in rodents than in primates.

PROPAGATION TIMES

As detailed above, the average propagation time in WM axons can be described to scale proportionally to average axon length and inversely proportionally to the square root of the average axonal cross-sectional area, varying as a function of N^{τ} where $\tau = \lambda - \alpha/2$. Given the values of λ and α found for rodents and primates (above), we have that

$$\tau_{rodent} = 0.466$$
$$\tau_{primate} = 0.165$$

This suggests that average signal propagation time through the WM increases far more steeply with N in rodent brains than in primate brains. Indeed, a recent study of the corpus callosum in primates suggested that the expected conduction delays between the hemispheres for different cortical areas doubles from macaque to man (Caminiti et al., 2009). Interestingly, although propagation time could in theory scale similarly across orders (which would offer evidence of a common trend toward minimization of propagation time in brain evolution), our initial results suggest that it not only increases in larger primate cortices, but it also increases faster in rodents than in primates. The faster scaling of WM folding in primate than in rodent brains, which we propose to result from the stronger minimization of axonal lengths under tension in the former, thus bestows upon primate cortices the advantage over rodents of gaining neurons without having signal propagation through the WM slowed down as much.

COMPUTATIONAL CAPACITY

As described above, the computational capacity of the WM (the number of operations involving WM axons that a cortex would be able to perform per unit time) is proportional to the number of axons in the WM, and inversely proportional to the average propagation time. In this manner, computational capacity through the WM scales with N raised to the power of $\theta = 1 + c - \tau$. Given the values of c and α calculated above, then we can estimate

$$\theta_{rodent} = 0.446$$
$$\theta_{primate} = 0.623$$

Like for propagation times, we find that the total computational capacity of the cortex through the WM also scales faster in primates than in rodents, although increasing more slowly than the rate at which the cortex gains neurons.

Finally, the computational efficiency of the WM, predicted to scale with $N^{-2\lambda - (\alpha/2)}$, is thus estimated to scale with $N^{-1.631}$ in rodents, and with $N^{-0.584}$ in primates. In both orders, thus, the increase in number of cerebral cortical neurons is accompanied by a decrease in the computational efficiency of the WM – a decrease that is faster in rodents than in primates.

COMPARISON WITH OTHER MODELS

OUTSIDE-IN OR INSIDE-OUT?

One influential hypothesis for the formation of cortical folds is the differential growth hypothesis, which considers that the faster growth of the outer cortical layers compared to the inner layers cause the cortical GM to fold (Richman et al., 1975). That hypothesis, however, assumes that cortical GM is much stiffer (by an unrealistic factor of 10) than the underlying WM. Our model, in contrast, is aligned with the opposite view that cortical folding is driven by tension generated by axonal connectivity in the WM (Van Essen, 1997), which posits that differences in cortical growth might be a result, and not the cause of cortical folding (Hilgetag and Barbas, 2005).

Another previous model of cortical folding acknowledged a radial pull on the cortical GM by elastic axonal fibers in the WM (Toro and Burnod, 2005). That model, however, attributed the source of cortical folding to a growing cortical surface, depending simply on cortical thickness and mechanical properties of the cortical GM. Although the model showed cortical convolutions to form as a natural consequence of cortical growth, it was largely descriptive, not predictive, since cortical thickness does not appear as an independent parameter; did not take numbers of neurons, of fibers in the WM, nor neuronal size into consideration; nor did it acknowledge that the cerebral cortex may scale as different functions of its number of neurons and connectivity across mammalian groups.

Recently, a study of the distribution of stress in the subcortical WM of the developing ferret brain found that axons are indeed under tension, although the majority of them are located circumferentially in the WM, radially in the subplate, and in the cores of outward folds (Xu et al., 2010). While the authors took this distribution as evidence against Van Essen's tension-driven model of cortical folding (because of the failure to find tension across the walls of gyri), we believe that it actually provides direct evidence that confirms that the WM grows under considerable axonal tension, which should make its growth deviate from allometry and thus, according to our model, suffice to cause its surface to fold.

Evidence that induced, abnormal cortical growth induces convolutions in the normally lissencephalic mouse brain (Haydar et al., 1999; Chenn and Walsh, 2002; Kingsbury et al., 2003) seems to favor models of cortical folding driven by cortical growth like that of Toro and Burnod (2005). However, our model, which attributes no major determinant role to the thickness of the WM, also predicts increased folding as a consequence of a larger number of cortical neurons, depending simply on there being enough internal tension in the WM, even if cortical connectivity remains unchanged. One of the key features of our connectivity-based model, then, is that it shows that changes in the properties of the GM are not necessarily a factor driving cortical folding; rather, they may occur as a consequence of WM folding, depending on other, possibly unrelated factors such as the average neuronal size, number of neurons in the GM and the fraction connected through the WM, determining for instance the resulting average cortical thickness. Note that, according to our model, local variations in cortical thickness do not affect the WM volume and folding index. Such variations in thickness across the cortical surface, which are known to be exist, may however in some cases create discrepancies between our expected and observed values of the GM folding.

Notice that our model does not predict where cortical folds should occur. Gyral placement might be directed by tension patterns (Van Essen, 1997) and/or by differential GM growth patterns (Richman et al., 1975; Xu et al., 2010). Our model does not deny the influence of differential growth in cortical patterning; it simply predicts that the extent of these folds should scale as the cortex gains neurons depending on the connectivity fraction, the average cross-sectional area of the axons in the WM, and their tension.

In the end, we envision cortical patterning as the result of a mechanical phenomenon, probably involving a tug-of-war or push–pull effect of GM and WM on each other during development – maybe as the GM is nudged into curving by its expanding outer layers, at the same time as the WM pulls onto it. The organization (anisotropy) of the WM seems to come into being via stretch growth, in which it is pulled outward as the diameter of the growing cortex increases (Smith, 2009) – and, therefore, as it necessarily resists this outward pull, due to intrinsic tension (or axons would continue to grow in a disorganized fashion). In culture, stretch growth transforms random axonal projections formed via outgrowth from central nervous system explants into uniform parallel fascicles (Smith et al., 2001; Pfister et al., 2004). The same process is likely to occur in the brain, as the expanding ensemble of the growing cortex physically pulls the WM into long organized tracts during development. Our finding that the volume of the WM grows hypometrically relative to its surface (Herculano-Houzel et al., 2010) provides strong evidence that the axons composing the WM not only resist towing, but also produce a net opposite force on the GM, which we propose that contributes to folding the GM into gyri – and determines the increasing folding of the cortical surface in larger brains across species.

CORTICAL THICKNESS: CAUSE OR CONSEQUENCE?

Qualitatively, thinner cerebral cortices are usually found in more convoluted brains, whether across species or in pathological conditions. In schizophrenia, for example, the cortex may be found to be thinner than usual, with a reduced volume of the superficial layers, and also more folded (Sallet et al., 2003); lissencephalic cortices, on the contrary, are often found to be thicker than normal (Olson and Walsh, 2002). These findings are often interpreted as evidence of a thicker cortex resisting buckling. Our model, however, offers an alternative interpretation: that cortical thickness increases as a consequence of a smaller fraction of neurons connected through the WM, in combination or not to an increased average neuronal size in the WM. This can be intuitively understood as the stacking of a larger number of neurons on top of the GM/WM interface when smaller proportions of cortical neurons send or receive axons from the WM; combined to a thinner spreading of cortical neurons over the GM/WM interface when the average axonal cross-sectional area leaving or entering the WM is larger (**Figure 3**). According to our model, then, more highly folded cortices are those that have larger connectivity fractions and/or larger average axonal cross-sectional areas, which for the said reasons lead to a thinner cortex. Similarly, the thicker lissencephalic cortex is predicted to be a result of abnormal (insufficient) cortical connectivity through the WM, possibly due to abnormal neuronal migration (Olson and Walsh, 2002), and not simply a cortex that became too thick to be folded.

CORTICAL FOLDING AND NUMBER OF CORTICAL NEURONS

One last and very important aspect of cortical folding is that is has often been considered a means of making more neurons fit into a space-limited brain, as the larger-than-expected cortical surface supposedly allows a larger-than-expected number of neurons for a given cranial volume. However, this would only be the case if cortical expansion occurred mostly laterally, and with a homogeneous number of neurons per surface area. In contrast, as we have shown previously, cortical expansion can no longer be considered to occur homogeneously across species, nor with a homogeneous number of neurons beneath a unit surface area. This means that it is no longer necessarily true that more convoluted cortices have more neurons than less convoluted cortices. Indeed, the elephant cortex, which has a larger surface area and is more convoluted than the human brain, has been estimated to have fewer neurons than the letter (Roth and Dicke, 2005; Herculano-Houzel, 2009).

CONCLUSION

Here we show that cortical folding in mammals can be predicted to happen as a consequence of the folding of the underlying WM under tension of its axons, and not as a simple, linear function of its number of neurons. Moreover, we show that the scaling of cortical folding with larger numbers of cortical neurons can be predicted, and possibly determined, in different groups of mammals by the scaling of a small number of parameters: (1) the fraction of cortical neurons connected through the WM; (2) the average cross-sectional area of axons in the WM; and (3) the shrinkage, under tension, of average axonal length relative to isometry. Just one further parameter, the scaling of (4) neuronal density, is required next to predict, or determine, both how the thickness of the GM varies, and how the folding of the GM itself scales. This of course assumes near perpendicular (or at least invariant across species) incidence of axonal fibers at the WM–GM interface. This is a plausible hypothesis for fibers under longitudinal tension; but the lack of actual systematic measurement of incidence angles that could confirm this hypothesis must be takes as a limitation of the present

work. Such a measurement would be most welcome, allowing us extend our model by introducing another measured coefficient (relating the average incidence angle as a power law of N), to recalculate the values of the various coefficients with a source of uncertainty removed, and to independently test our underlying hypothesis (since we expect a cortex grown subject to axonal longitudinal tensions to show a marked tendency toward orthogonal incidence).

Importantly, while the model is potentially universal, applying across the different orders of mammals, it does not at all imply that there is a single way for the cortex to scale. Rather, we show that, according to the same model, there are many possible combinations of exponents c, α, and λ that lead to cortices that become increasingly folded as they gain neurons – as long as $\lambda < (c + 1 + \alpha)/2$. Again, our model predicts that cortical thickness is not a determinant of cortical folding, but rather a consequence, depending on the scaling of neuronal density as well as of the connectivity fraction and average cross-sectional area of the axons in the WM.

Even in the case that experimental testing eventually shows that causality in cortical folding is not as proposed in our model without the introduction of further variables, the latter has the enormous advantage of allowing one to deduce the scaling of cortical connectivity, axonal length, cross-sectional area, and thus to infer propagation time and computational capability and efficacy, from readily measurable values of A_W, V_W, N, O_W, and D_N.

ACKNOWLEDGMENTS

Suzana Herculano-Houzel is supported by FAPERJ-Cientista do Nosso Estado, CNPq – Edital Universal, INNT/MCT, and the James McDonnell Foundation; Bruno Mota is supported by a FAPERJ/CAPES postdoctoral grant.

REFERENCES

Barres, B. A., and Raff, M. C. (1994). Control of oligodendrocyte number in the developing rat optic nerve. *Neuron* 12, 935–942.

Barres, B. A., and Raff, M. C. (1999). Axonal control of oligodendrocyte development. *J. Cell Biol.* 147, 1123–1128.

Braitenberg, V., and Schüz, A. (1998). *Cortex: Statistics and Geometry of Neuronal Connectivity*, 2nd Edn. Berlin: Springer Verlag.

Caminiti, R., Ghaziri, H., Galuske, R., Hof, P. R., and Innocenti, G. M. (2009). Evolution amplified processing with temporally dispersed slow neuronal connectivity in primates. *Proc. Natl. Acad. Sci. U.S.A.* 106, 19551–19556.

Chenn, A., and Walsh, C. (2002). Regulation of cerebral cortical size by control of cell cycle exit in neural precursos. *Science* 297, 365–369.

Collins, C. E., Airey, D. C., Young, N. A., Leitch, D. B., and Kaas, J. H. (2010). Neuron densities vary across and within cortical areas in primates. *Proc. Natl. Acad. Sci. U.S.A.* 107, 15927–15932.

Gabi, M., Collins, C. E., Wong, P., Kaas, J. H., and Herculano-Houzel, S. (2010). Cellular scaling rules for the brain of an extended number of primate species. *Brain Behav. Evol.* 76, 32–44.

Goldman-Rakic, P. (1980). Morphological consequences of prenatal injury to the primate brain. *Prog. Brain Res.* 53, 3–19.

Goldman-Rakic, P., and Rakic, P. (1984). "Experimental modification of gyral patterns," in *Cerebral Dominance: The Biological Foundation*, eds N. Geschwind and A. Galaburda (Cambridge: Harvard University Press), 179–192.

Gross, C. G. (1999). *Brain, Vision, Memory: Tales in the History of Neuroscience.* Cambridge: MIT Press.

Haydar, T., Kuan, C., Flavell, R., and Rakic, P. (1999). The role of cell death in regulating the size and shape of the mammalian forebrain. *Cereb. Cortex* 9, 621–626.

Herculano-Houzel, S. (2009). The human brain in numbers: a linearly scaled-up primate brain. *Front. Hum. Neurosci.* 3:31. doi:10.3389/neuro.09.031.2009

Herculano-Houzel, S. (2011). Not all brains are made the same: new views on brain scaling in evolution. *Brain Behav. Evol.* 78, 22–36.

Herculano-Houzel, S., Collins, C. E., Wong, P., and Kaas, J. H. (2007). Cellular scaling rules for primate brains. *Proc. Natl. Acad. Sci. U.S.A.* 104, 3562–3567.

Herculano-Houzel, S., Collins, C. E., Wong, P., Kaas, J. H., and Lent, R. (2008). The basic non-uniformity of the cerebral cortex. *Proc. Natl. Acad. Sci. U.S.A.* 105, 12593–12598.

Herculano-Houzel, S., and Lent, R. (2005). Isotropic fractionator: a simple, rapid method for the quantification of total cell and neuron numbers in the brain. *J. Neurosci.* 25, 2518–2521.

Herculano-Houzel, S., Mota, B., and Lent, R. (2006). Cellular scaling rules for rodent brains. *Proc. Natl. Acad. Sci. U.S.A.* 103, 12138–12143.

Herculano-Houzel, S., Mota, B., Wong, P., and Kaas, J. H. (2010). Connectivity-driven white matter scaling and folding in primate cerebral cortex. *Proc. Natl. Acad. Sci. U.S.A.* 107, 19008–19013.

Herculano-Houzel, S., Ribeiro, P. F. M., Campos, L., da Silva, A. V., Torres, L. B., Catania, K., and Kaas, J. H. (2011). Updated neuronal scaling rules for the brains of Glires (rodents/lagomorphs). *Brain Behav. Evol.* 78, 302–314.

Hilgetag, C. C., and Barbas, H. (2005). Developmental mechanics of the primate cerebral cortex. *Anat. Embryol.* 210, 411–417.

His, W. (1874). *Unsere Körperform und das physiologische Problem ihrer Enstellung.* Leipzig: FCW Vogel.

Hofman, M. (1985). Size and shape of the cerebral cortex in mammals. I. The cortical surface. *Brain Behav. Evol.* 27, 28–40.

Kaas, J. H. (2009). *Encyclopedia of Neuroscience.* Amsterdam: Elsevier, 793–800.

Kingsbury, M., Rehen, S., Contos, J., Higgins, C., and Chun, J. (2003). Non-proliferative effects of lysophosphatidic acid enhance cortical growth and folding. *Nat. Neurosci.* 6, 1292–1299.

Le Gros Clark, W. (1945). "Deformation patterns on the cerebral cortex," in *Essays on Growth and Form*, eds. W. Le Gros Clark and P. B. Medawar. (Oxford: Oxford University Press), 1–23.

Mori, S., Kaufmann, W. E., Davatzikos, C., Stieltjes, B., Amodei, L., Fredericksen, K., Pearlson, G. D., Melhem, E. R., Solaiyappan, M., Raymond, G. V., Moser, H. W., and van Sizj, P. C. (2002). Imaging cortical association tracts in the human brain using diffusion-tensor-based axonal tracking. *Magn. Reson. Med.* 47, 215–223.

Olivares, R., Montiel, J., and Aboitiz, F. (2001). Species differences and similarities in the fine structure of the mammalian corpus callosum. *Brain Behav. Evol.* 57, 98–105.

Olson, E. C., and Walsh, C. A. (2002). Smooth, rough and upside-down neocortical development. *Curr. Opin. Genet. Dev.* 12, 320–327.

Pfister, B. J., Iwata, A., Meaney, D. F., and Smith, D. H. (2004). Extreme stretch growth of integrated axons. *J. Neurosci.* 24, 7978–7983.

Pillay, P., and Manger, P. R. (2007). Order-specific quantitative patterns of cortical gyrification. *Eur. J. Neurosci.* 25, 2705–2712.

Prothero, J. (1997). Scaling of cortical neuron density and white matter volume in mammals. *J. Hirnforsch.* 38, 513–524.

Richman, D., Stewart, R., Hutchunson, J., and Caviness, V. Jr. (1975). Mechanical model of brain convolution development. *Science* 189, 18–21.

Rockel, A. J., Hiorns, R. W., and Powell, T. P. S. (1980). The basic uniformity in the structure of the neocortex. *Brain* 103, 221–244.

Roth, G., and Dicke, U. (2005). Evolution of the brain and intelligence. *Trends Cogn. Sci. (Regul. Ed.)* 9, 250–257.

Sadahiro, S., Yoshikawa, H., Yagi, N., Yamamoto, Y., Yanagihara, T., Kimura, M., and Sakoda, S. (2000). Morphometric analysis of the myelin-associated oligodendrocytic basic protein-deficient mouse reveals a possible role for myelin-associated oligodendrocytic basic protein in regulating axonal diameter. *Neuroscience* 98, 361–367.

Sallet, P. C., Elkis, H., Oliveira, J. R., Sassi, E., de Castro, C. C., Busatto, G. F., and Gattaz, W. F. (2003). Reduced cortical folding in schizophrenia: an MRI morphometric study. *J. Anat. Physiol.* 36, 309–319.

Sarko, D. K., Catania, K. C., Leitch, D. B., Kaas, J. H., and Herculano-Houzel, S. (2009). Cellular scaling rules of insectivore brains. *Front. Neuroanat.* 3:8. doi:10.3389/neuro.05.008.2009

Sauvageot, C. M., and Stiles, C. D. (2002). Molecular mechanisms controlling cortical gliogenesis. *Curr. Opin. Neurobiol.* 12, 244–249.

Tower, D. B. (1954). Structural and functional organization of mammalian cerebral cortex; the correlation of neurone density with brain size; cortical neurone density in the fin whale (*Baleanoptera physalus L.*) with a note on the cortical neurone density in the Indian elephant. *J. Comp. Neurol.* 101, 19–51.

Smith, D. H. (2009). Stretch growth of integrated axon tracts: extremes and exploitations. *Prog. Neurobiol.* 89, 231–239.

Smith, D. H., Wolf, J. A., and Meaney, D. F. (2001). A new strategy to produce sustained growth of central nervous system axons: continuous mechanical tension. *Tissue Eng.* 7, 131–139.

Toro, R., and Burnod, Y. (2005). A morphogenetic model for the development of cortical convolutions. *Cereb. Cortex* 15, 1900–1913.

Toro, R., Perron, M., Pike, B., Richer, L., Veillette, S., Pausova, Z., and Paus, T. (2008). Brain size and folding of the human cerebral cortex. *Cereb. Cortex* 18, 2352–2357.

Van Essen, D. C. (1997). A tension-based theory of morphogenesis and compact wiring in the central nervous system. *Nature* 385, 313–318.

Wang, S. S. H., Shultz, J. R., Burish, M. J., Harrison, K. H., Hof, P. R., Towns, L. C., Wagers, M. W., and Wyatt, K. D. (2008). Functional trade-offs in white matter axonal scaling. *J. Neurosci.* 28, 4047–4056.

Welker, W. (1990). "Why does cerebral cortex fissure and fold? A review of determinants of gyri and sulci," in *Cerebral Cortex Vol. 8B, Comparative Structure and Evolution of Cerebral Cortex, Part II*, eds E. G. Jones and A. Peters (New York: Plenum Press), 3–136.

Xu, G., Knutsen, A. K., Dikranian, K., Kroenke, C. D., Bayly, P. V., and Taber, L. A. (2010). Axons pull on the brain, but tension does not drive cortical folding. *J. Biomech. Eng.* 132, 071013–71011.

Zhang, K., and Sejnowski, T. J. (2000). A universal scaling law between gray matter and white matter of cerebral cortex. *Proc. Natl. Acad. Sci. U.S.A.* 97, 5621–5626.

Zilles, K., Armstrong, E., Schleicher, A., and Kretschmann, H. J. (1988). The human pattern of gyrification in the cerebral cortex. *Anat. Embryol.* 179, 173–179.

Conflict of Interest Statement: The authors declare that the research was conducted in the absence of any commercial or financial relationships that could be construed as a potential conflict of interest.

Received: 02 August 2011; accepted: 15 January 2012; published online: 02 February 2012.

Citation: Mota B and Herculano-Houzel S (2012) How the cortex gets its folds: an inside-out, connectivity-driven model for the scaling of mammalian cortical folding. Front. Neuroanat. ***6****:3. doi: 10.3389/fnana.2012.00003*

frontiers in
NEUROANATOMY

ORIGINAL RESEARCH ARTICLE
published: 19 February 2013
doi: 10.3389/fnana.2013.00001

Computing the size and number of neuronal clusters in local circuits

Rodrigo Perin, Martin Telefont and Henry Markram*

Brain Mind Institute, Ecole Polytechnique Fédérale de Lausanne, Lausanne, Switzerland

Edited by:
Zoltan F. Kisvarday, University of Debrecen, Hungary

Reviewed by:
Kathleen S. Rockland, Massachusetts Institute of Technology, USA
Armen Stepanyants, Northeastern University, USA
Julian Budd, University of Sussex, UK

****Correspondence:***
Henry Markram, Brain Mind Institute, Ecole Polytechnique Fédérale de Lausanne, Station 15, CH-1015 Lausanne, Switzerland.
e-mail: henry.markram@epfl.ch

The organization of connectivity in neuronal networks is fundamental to understanding the activity and function of neural networks and information processing in the brain. Recent studies show that the neocortex is not only organized in columns and layers but also, within these, into synaptically connected clusters of neurons (Ko et al., 2011; Perin et al., 2011). The recently discovered common neighbor rule, according to which the probability of any two neurons being synaptically connected grows with the number of their common neighbors, is an organizing principle for this local clustering. Here we investigated the theoretical constraints for how the spatial extent of neuronal axonal and dendritic arborization, heretofore described by morphological reach, the density of neurons and the size of the network determine cluster size and numbers within neural networks constructed according to the common neighbor rule. In the formulation we developed, morphological reach, cell density, and network size are sufficient to estimate how many neurons, on average, occur in a cluster and how many clusters exist in a given network. We find that cluster sizes do not grow indefinitely as network parameters increase, but tend to characteristic limiting values.

Keywords: data driven modeling, neuronal assemblies, layer 5 pyramidal cell, layer 2 pyramidal cell, clustering

INTRODUCTION

Network theory is increasingly applied to better understand the principles of how neurons are interconnected and hence to unravel the networking and topologic mysteries of the brain (Honey et al., 2007, 2010; Sporns et al., 2007; Sporns, 2010). Much of this work has been focused on macroscopic network principles such as those connecting brain regions. Increased interest in mesoscopic neuroanatomical connectivity also grew considerably over the years (Bohland et al., 2009). Recently, the discovery of clusters of synaptically connected neurons has opened up investigations of the microscopic network principles. The expression of a number of cellular level motifs of synaptic connectivity was first reported by Song et al. (2005). Subsequent publications on the rat (Perin et al., 2011) and mouse (Ko et al., 2011), hint at a theme shared by different species.

A number of cortical networks that have been described are based on cells with large somata, which are easy to distinguish in electrophysiological experiments. The cell of choice in the neocortex has been the large thick tufted layer 5 pyramidal cell (TTL5-PCs) which, thanks to its size and shape, can be isolated and recorded reliably (Markram et al., 1997). In a multi-electrode patch-clamp setup it is possible to record from many such cells simultaneously, determine their synaptic connectivity and, after staining, also obtain their morphological properties. In order to simulate different expanses of axonal and dendritic arborization (**Figures 1A,B**) we developed the concept of "morphological reach," denoted *r*, a proportionality factor applied to the decay in connection probability as a function of distance. Our reference, the TTL5-PC (Oberlaender et al., 2011), is assigned a morphological reach of 1. Other cell types, in our simulations, are assigned proportional morphological reaches indicative of the extent of their basal dendritic arborizations as measured using the sum of all branch intersections in Sholl Analyses (**Figures 1C,D**). TTL5 pyramidal cells have broad dendritic arborization (Markram et al., 1997) and form clusters that may constitute elementary units of information processing within a brain region (medium/regional projections) and between brain regions (long/interregional projections). In previous work we identified a rule, the common neighbor rule, governing the connectivity of these groups of neurons (Perin et al., 2011). The common neighbor rule describes a directly proportional relationship between the connection probability between any two neurons and the number of other neurons in the network connected to both neurons in this pair. In this case the term connected indicates neurons that project to as well as neurons receiving synaptic appositions from the neurons in the pair. When applied, the common neighbor rule produces complex clustered networks that lie between completely random networks (Erdös–Reni-type) (Erdõs and Rényi, 1960) and highly clustered networks with hubs (Barabási-type) (Barabási and Albert, 1999) resembling more closely a Watts-Strogatz-type network (Watts and Strogatz, 1998). A key distinguishing feature between macro-clustering in the brain (between brain regions) and micro-clustering (between neurons of a local microcircuit) is that there are no hubs at the micro (local) network level within a given cell-type. In other words, each neuron of a given type makes contact with and receives contacts from about the same number of neurons of the same type—in fact a pre-requisite for the occurrence of hubs is that the number of boutons and spines per neuron within the population span some orders of magnitude so that the degree

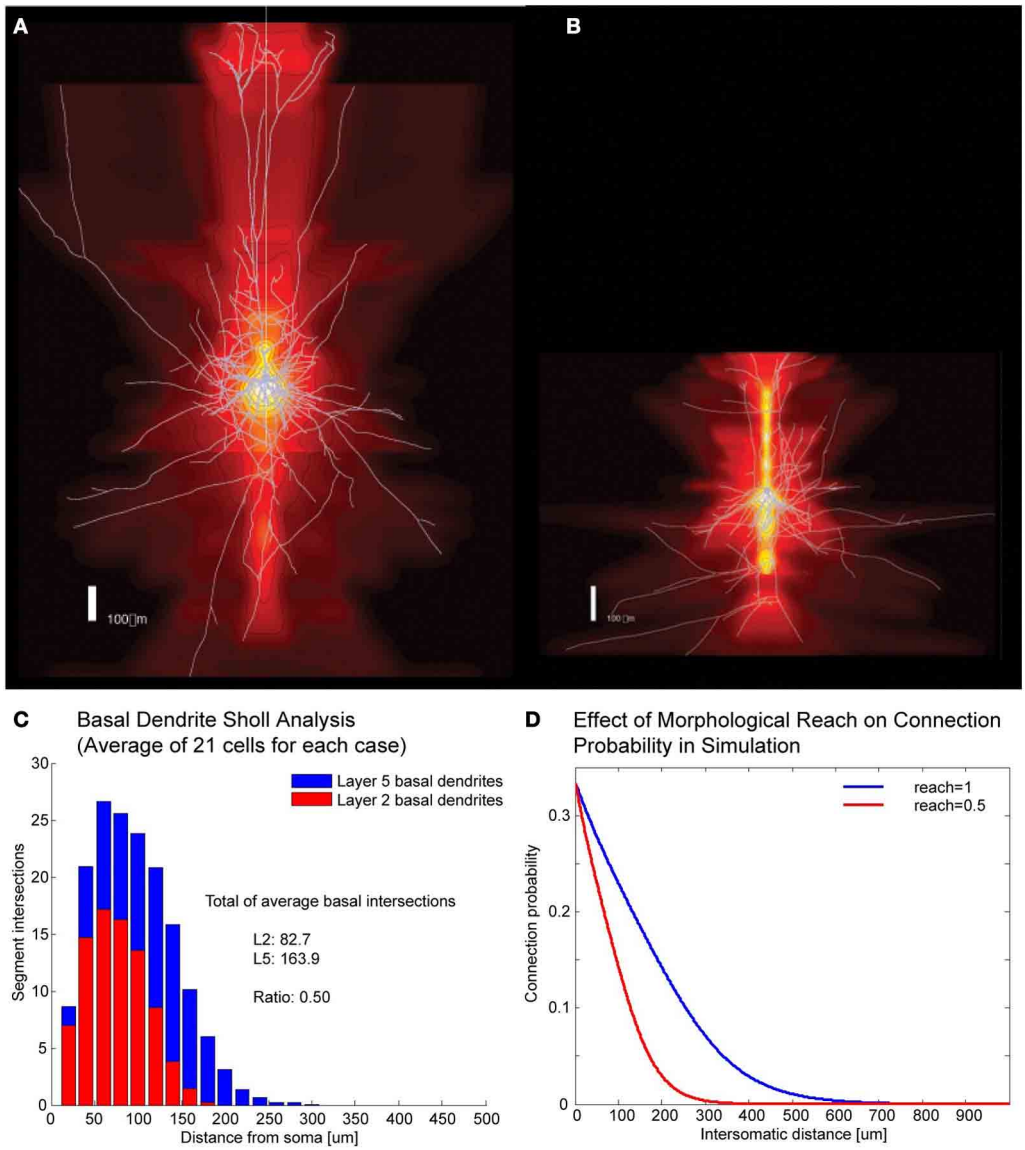

FIGURE 1 | Correlates of different cell types. (A,B) Example of Layer V Pyramidal Cell and Layer II/III Pyramidal Cell morphologies, respectively, superposed on intensity maps representing the average density of morphological processes around the soma. **(C)** Sholl analysis of the basal dendrites of Layer V and Layer II/III. **(D)** Illustration of how morphological reach is used to modify connection probabilities as a function of inter-somatic distance in simulations.

of connectivity might vary accordingly. This form of clustering is quite exceptional amongst biological and social networks in that it contains no hubs and has a degree of separation less than 2.

Since the common neighbor based clustering applies similarly across individuals of the same species, the neuronal groups formed would be quite similar. Bootstrap analysis, in which different subsets of the connectivity data originating from different individuals are used, consistently captures the common neighbor rule (**Figures A1**, **A2**). This has led to the suggestion that these clusters are in fact innate (genetically preprogrammed to develop) holding innate knowledge of elementary forms of information processing. These posited innate groups likely require some general activity, rather than experience-dependent activity, during development to form.

It may therefore be of special interest to understand the sizes and numbers of such clusters in a brain region. We therefore constructed networks by applying the common neighbor rule and derived the relationships between cluster sizes and numbers as a function of morphological reach, neuronal density, and network size.

METHODS

Point neurons were placed in a cubic tridimensional lattice arrangement with regular spacing that assumed the values of 18,

19, 21, 23, 25, 28, and 36 μm in different simulations, yielding the corresponding cell densities of 171470, 145790, 107980, 82190, 64000, 45554, and 21433 neurons/mm^3 (**Figure 2A**) covering the range of experimentally observed densities in a neocortical column (Meyer et al., 2010). Uniformly random jitter was then added to each position in three dimensions with amplitude equal to the grid spacing between neurons (**Figure 2B**). Since point neurons are used no compensation for extreme proximity between neurons is applied. The simulations used network sizes of 512, 1000, 1728, 3375, 4096, and 5832 cells

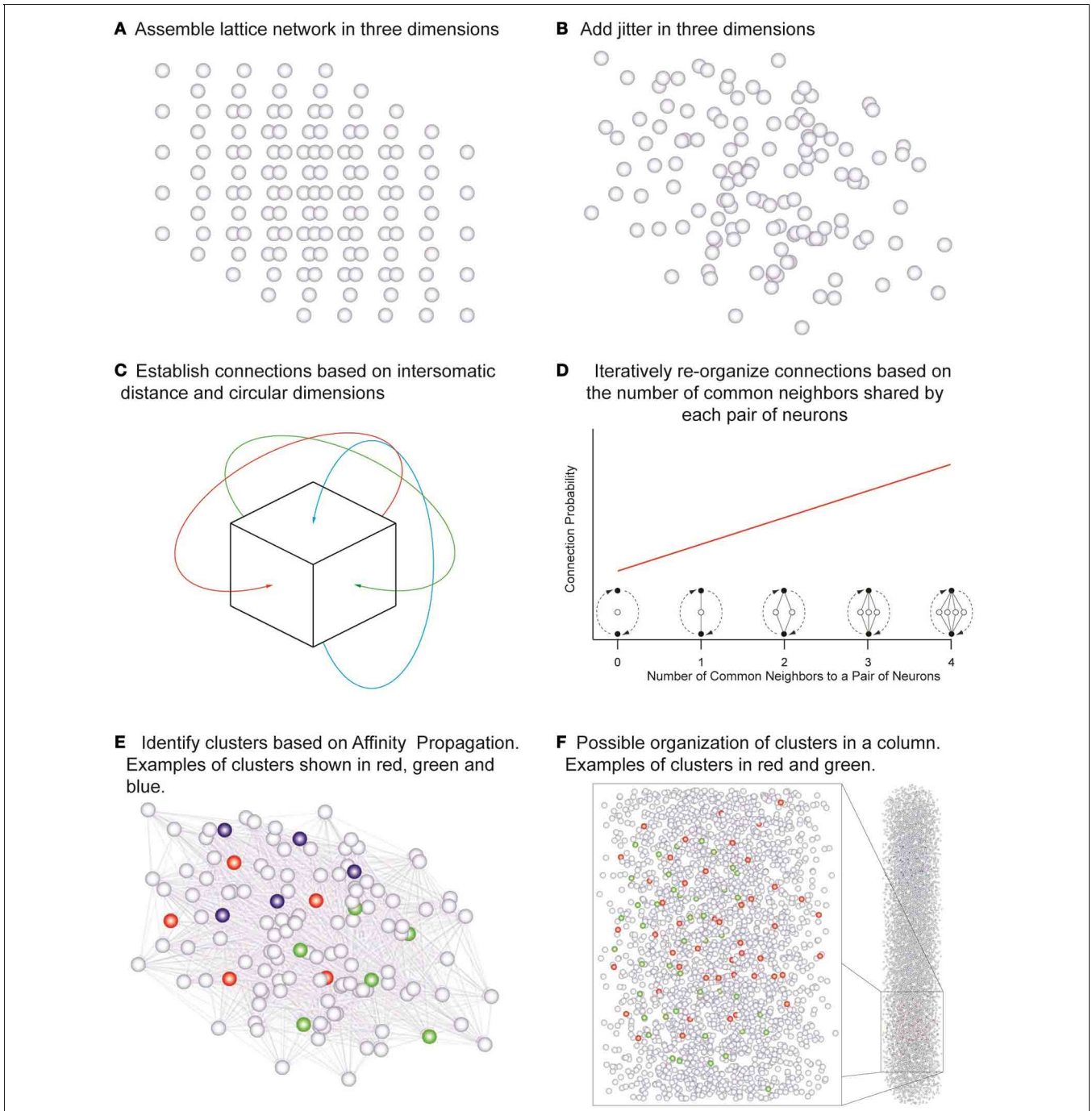

FIGURE 2 | The network assembly and reorganization of connections. **(A)** Initial lattice arrangement of somas. **(B)** Jitter added in three dimensions to the lattice arrangement. **(C)** Connections assigned according to intersomatic distance probability profiles in circular dimensions in order to eliminate boundary effects. **(D)** Iterative reorganization of connections based on numbers of common neighbors. **(E)** Cluster identification based on affinity propagation. **(F)** Possible organization of clusters in a column with examples of clusters sharing the same space.

in cubic arrangements. Each of the three dimensions in this model was made circular so that neurons close to one edge were considered to be close to neurons on the opposite edge of the network (**Figure 2C**). Edge effects were countered in this way and every neuron was exposed to a similar number of neighbors and could potentially form the same number of connections.

In order to investigate the influence of morphology on clustering, the morphological reach of TTL5 pyramidal cells was multiplied by factors of 0.5, 0.667, 0.8, 1, 1.333, and 2 in networks containing 4096 neurons. We defined a neuron's neighbors as those cells that form synaptic connections onto or that receive synaptic connections from the neuron in question. In our model, the small world clustering of layer 5 pyramidal cells is made directly proportional to the number of common neighbors (**Figure 2D**) (Perin et al., 2011). To achieve this goal the connections in the initial network were assigned pseudo-randomly according to inter-somatic distance profiles observed experimentally (Perin et al., 2011) (see also **Figure A3**). While morphological reconstructions indicate a degree of anisotropy in process arborization such observations indicate that a purely distance-based connection probability function still can capture the trend in connectivity patterns. In the simulations where we were interested in simulating different arborizations we linearly extended or shortened such profiles by dividing the actual distance supplied to these profiles by the "morphological reach" factor. The initial connectivity was then modified according to the number of common neighbors. The pair of neurons sharing the maximal number of common neighbors was assigned a probability of connection of 1. Pairs of neurons sharing no common neighbors we assigned a connection probability of 0. Pairs of neurons sharing intermediate numbers of common neighbors were assigned linearly interpolated connection probability values. This process was iterated until the clustering coefficient of the whole network no longer increased (see **Figure A4**). The observed clusters consist of a few dozen neurons typically distributed 100–150 μm apart. Based on this study (Perin et al., 2011) we decided to investigate the effects of different network sizes and cell densities as well as the impact of different extents of morphological arborization on the clustering properties of networks. Clusters were identified using the affinity propagation algorithm (Frey and Dueck, 2007) at the end of the simulation and providing the number of common neighbors as the similarity measure (**Figure 2E**). Similarity was defined exclusively for connected neuron pairs, being set to zero in pairs that were not connected in any way.

Sets of 10 simulations were performed for each parameter combination. The average numbers of clusters and average cluster sizes were plotted and the data points were fitted with surface fits using the MatLab curve fitting tool.

RESULTS

The goal of our modeling was to better understand the relationship between the different network parameters and the network clustering properties. Six basic relationships were investigated by varying three parameters—network size, cell density, and morphological reach—and analyzing the effects on the two clustering properties—the average number of clusters and the average number of cells contained in clusters (cluster size). From these results we also calculated the number of clusters per unit volume.

NETWORK SIZE AND DENSITY

To investigate the impact of network size on the number and size of clusters we constructed networks ranging from 512 to 5832 neurons. These networks were based on TTL5 Pyramidal Cells and ranged in density from 45554 to 455170 cells/mm^3. Networks containing different numbers of neurons display different clustering properties. A relatively simple linear relationship exists between the network size and the number of clusters. Simply put, larger networks fit more clusters of similar size (**Figure 3A**) as can observed in the curve that fits the surface that describes the number of cluster as a function of networks size and density:

$$NC = 21.54 - \frac{3.90}{10000}d + \frac{6.42}{100}s$$

where NC stands for the number of clusters, s for network size in number of cells and d for network density in cells/mm^3.

A mild decay in the number of clusters occurs as the network density increases. This is because higher densities lead to larger average cluster sizes (**Figure 3B**). Cluster size as a function of network size follows a lognormal profile, first increasing then decreasing. This is a particular feature of networks without boundaries. The fitted surface for cluster sizes as a function of network size and density can be expressed as

$$CS = 13.23 + \frac{d}{10000}e^{-\left(\log\left(\frac{s}{1300+\frac{3d}{1000}}\right)\right)^2}$$

where CS stands for cluster size, s for network size in number of cells and d for network density in cells/mm^3. Goodness of fit for the resulting surfaces according to Adjusted R-square values were 0.97 for average number of clusters as a function of network density and size, 0.95 for average cluster sizes as a function of network density and size. The number of clusters per unit volume grows with cell density and displays an inverted relationship to cluster size as a function of network size (**Figure 3C**).

NETWORK DENSITY AND MORPHOLOGICAL REACH

Morphological reach is a parameter that reflects the extent of neuronal arborization (**Figures 1A,B**). The more extensive the arborization the more connections a neuron is likely to form (**Figure 1C**). We attribute the value of 1 to the morphological reach characteristic of TTL5 Pyramidal Cells. Cells with more restricted arborization display, therefore, morphological reaches corresponding to some fractional value (**Figure 1D**).

The density of neurons in a local network, in the following simulations involving 4096 neurons, strongly influences the number of clusters formed, particularly very low densities which cause neurons to be more isolated thus yielding numerous clusters involving few neurons (**Figures 3D**, **A5**). As neuronal densities increase the number of clusters quickly becomes less dependent on this parameter reaching a plateau before decreasing again due to increasing cluster sizes (**Figures 3D,E**). The relationship between the number of clusters in a network and the

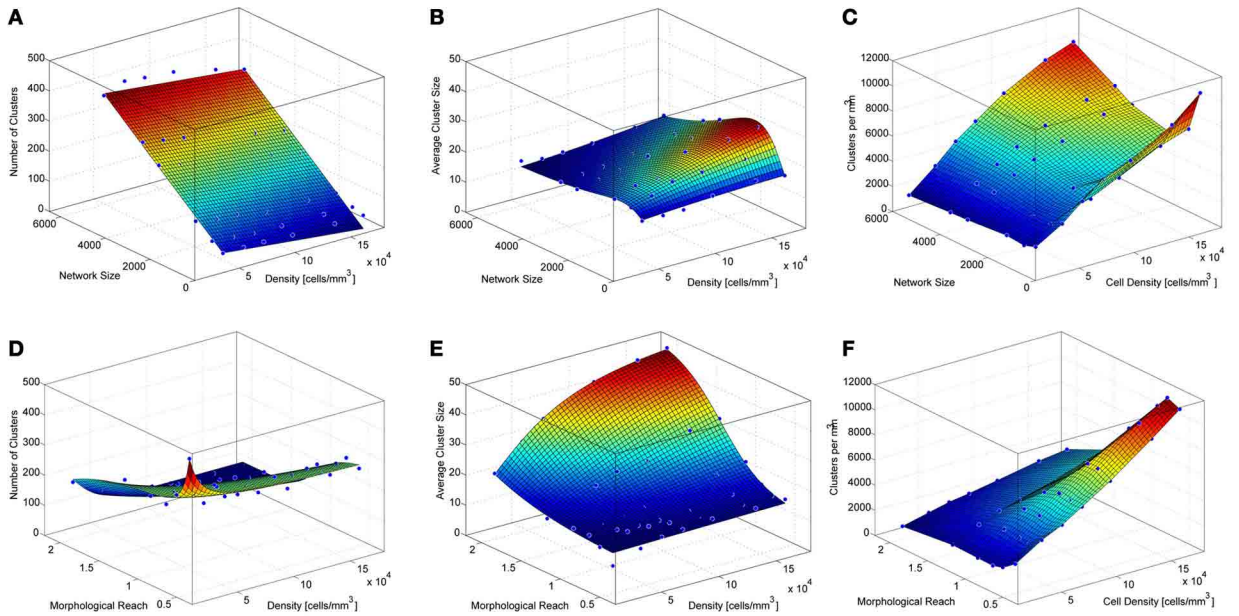

FIGURE 3 | Properties of simulated cortical network clustering. **(A)** Average number of clusters observed in the different simulations as a function of network size and density. Each data point corresponds to the average of 10 simulations. **(B)** Average cluster size for the same simulations show in **A**. **(C)** Number of clusters per mm^3 calculated from **A** and **B**. **(D)** Average number of clusters observed in the different simulations as a function of network density and morphological reach. Each green data point corresponds to the average of 10 simulations. **(E)** Average cluster size for the same simulations show in **D**. **(F)** Number of clusters per mm^3 calculated from **D** and **E**.

morphological reach of the cells that form this network follows a similar trend, also forming a plateau before further decreasing.

$$NC = 100.70 + \frac{210.60}{1 + e^{-(1.57 - dr^3/1e5)/0.97}} + \frac{1.23e9}{(dr^3)^2}$$

where NC stands for the number of clusters, r for morphological reach and d for network density in cells/mm^3. Morphological reach, similarly to density, has little effect on the number of clusters in a network except in the case of extremely low values, which lead to nearly isolated neurons (**Figure 3D**). Within the physiological range of 0.5–1, growth in morphological reach leads to approximately linear and relatively mild increases in cluster sizes. Increases in morphological reach above 1 tend to have larger effects, especially in the case of networks with large cell density but eventually tend to saturation at extreme values of both. Changes in reach and density led to different cluster sizes (**Figure 3E**) according to a sigmoidal:

$$CS = -13.78 + \frac{62.37}{1 + e^{\frac{8.36e4 - dr^3}{3.23e5}}}$$

where CS stands for cluster size, d for network density in cells/mm^3 and r for morphological reach. It is important to capture variations in morphological reach and cell density since the combination of both is necessary in order to estimate clustering properties.

Goodness of fit for the resulting surfaces according to Adjusted R-square values was 0.97 for average number of clusters as a function of network density and morphological reach, 0.98 for average cluster sizes as a function of network density and morphological reach. The number of clusters per unit volume grows approximately linearly with both cell density and morphological reach (**Figure 3F**).

DISCUSSION

The most abundant neuronal type in the mammal neocortex, the pyramidal cell can be found in five of the six neocortical layers and with varying spatial reach of their arbors. This cell retains a remarkable stereotypical shape from mice to man and varies mainly in the length of its axonal and dendritic arbors (Peters and Yilmaz, 1993). Thick tufted layer 5 pyramidal cells are among the largest neurons in the brain and provide the output from the neocortex to subcortical structures and distant brain regions to drive behavior (Morishima and Kawaguchi, 2006). We previously found that these pyramidal cells are networked according to a simple synaptic organization rule; neurons that share more common neighbors are also more likely to be connected (Perin et al., 2011). This rule results in stereotypical clusters of synaptically connected neurons and therefore do not seem to be uniquely shaped by experience. In fact, the synaptic weights of the connections between neurons in these clusters are also on average saturated, which is not ideal for acquired memory storage. We therefore propose that forming synaptic connections according to common neighbors is a pre-programmed rule that drives stereotypical neuronal clustering during development. These clusters may therefore express elementary units of innate knowledge that are combined in an experience-dependent manner to form acquired memories while preserving fundamental perceptual mechanisms. It is likely that at its origin, cluster formation

may be linked to the fact that sister cells (i.e., cells that originated from the same progenitor radial glial cell) are more likely to develop strong electrical coupling which in turn favors chemical synapse formation (Yu et al., 2009, 2012). These preferentially connected sets of neurons may associate to form larger ensembles as those involved in orientation selectivity in the visual cortex (Ko et al., 2011).

The common neighbor rule also makes it possible to prespecify the underlying synaptic connectivity in a network of such neurons even before learning rules come into play. The influence from common input leading to greater connection probabilities between neurons, which constituted the central mechanism explored in the current work, seems to apply not only for local but also long-range projections (Otsuka and Kawaguchi, 2008; Brown and Hestrin, 2009). The question we focused on, however, is how the structural features of neuronal arborization further influence the local synaptic connectivity organization. The common neighbor rule, which ensures that important features of synaptic organization are respected, was therefore imposed on the connectivity between neurons with different morphological reach and cell densities. From these networks we derived relationships between morphological reach, cell density and number of cells in a network, in order to determine how many neurons make up the clusters and how many clusters can potentially be formed under different conditions.

Experimental evidence from juvenile rat somatosensory cortex (Perin et al., 2011) as well as adult visual, (Ohki et al., 2005; Yoshimura et al., 2005) and auditory (Rothschild et al., 2010) and mouse frontal cortices (Otsuka and Kawaguchi, 2011) supports the occurrence of clusters of excitatory cells in Layers II/III through V, overlapped and interlaced in space, rather than tiled next to each other (**Figures 2E,F**). This not only allows the packing of many clusters of neurons in the same space but also enables monosynaptic connections between clusters to be adjusted and regulate the relationship between clusters.

Future investigations into this topic should also take into consideration the effects of network boundaries and interactions between different cell types, both constituting factors that further influence cluster formation.

ACKNOWLEDGMENTS

We would like to thank Michael Reimann for help with the volume renderings in **Figure 1**.

REFERENCES

Barabási, A.-L., and Albert, R. (1999). Emergence of scaling in random networks. *Science* 286, 509–512.

Bohland, J. W., Wu, C., Barbas, H., Bokil, H., Bota, M., Breiter, H. C., et al. (2009). A proposal for a coordinated effort for the determination of brainwide neuroanatomical connectivity in model organisms at a mesoscopic scale. *PLoS Comput. Biol.* 5:e1000334. doi: 10.1371/journal.pcbi.1000334

Brown, S. P., and Hestrin, S. (2009). Intracortical circuits of pyramidal neurons reflect their long-range axonal targets. *Nature* 457, 1133–1136.

Erdōs, P., and Rényi, A. (1960). On the evolution of random graphs. *Publ. Math. Inst. Hung. Acad. Sci.* 5, 17–61.

Frey, B. J., and Dueck, D. (2007). Clustering by passing messages between data points. *Science* 315, 972–976.

Honey, C. J., Kötter, R., Breakspear, M., and Sporns, O. (2007). Network structure of cerebral cortex shapes functional connectivity on multiple time scales. *Proc. Natl. Acad. Sci. U.S.A.* 104, 10240–10245.

Honey, C. J., Thivierge, J.-P., and Sporns, O. (2010). Can structure predict function in the human brain? *Neuroimage* 52, 766–776.

Ko, H., Hofer, S. B., Pichler, B., Buchanan, K. A., Sjöström P. J., and Mrsic-Flogel, T. D. (2011). Functional specificity of local synaptic connections in neocortical networks. *Nature* 473, 87–91.

Markram, H., Lübke, J., Frotscher, M., Roth, A., and Sakmann, B. (1997). Physiology and anatomy of synaptic connections between thick tufted pyramidal neurones in the developing rat neocortex. *J. Physiol.* 500, 409–440.

Meyer, H. S., Wimmer, V. C., Oberlaender, M., de Kock, C. P. J., Sakmann, B., and Helmstaedter, M. (2010). Number and laminar distribution of neurons in a thalamocortical projection column of rat vibrissal cortex. *Cereb. Cortex* 20, 2277–2286.

Morishima, M., and Kawaguchi, Y. (2006). Recurrent connection patterns of corticostriatal pyramidal cells in frontal cortex. *J. Neurosci.* 26, 4394–4405.

Oberlaender, M., Boudewijns, Z. S. R. M., Kleele, T., Mansvelder, H. D., Sakmann, B., and de Kock, C. P. J. (2011). Three-dimensional axon morphologies of individual layer 5 neurons indicate cell type-specific intracortical pathways for whisker motion and touch. *Proc. Natl. Acad. Sci. U.S.A.* 108, 4188–4193.

Ohki, K., Chung, S., Ch'ng, Y. H., Kara, P., and Reid, R. C. (2005). Functional imaging with cellular resolution reveals precise micro-architecture in visual cortex. *Nature* 433, 597–603.

Otsuka, T., and Kawaguchi, Y. (2008). Firing-pattern-dependent specificity of cortical excitatory feed-forward subnetworks. *J. Neurosci.* 28, 11186–11195.

Otsuka, T., and Kawaguchi, Y. (2011). Cell diversity and connection specificity between callosal projection neurons in the frontal cortex. *J. Neurosci.* 31, 3862–3870.

Perin, R., Berger, T. K., and Markram, H. (2011). A synaptic organizing principle for cortical neuronal groups. *Proc. Natl. Acad. Sci. U.S.A.* 108, 5419–5424.

Peters, A., and Yilmaz, E. (1993). Neuronal organization in area 17 of cat visual cortex. *Cereb. Cortex* 3, 49–68.

Rothschild, G., Nelken, I., and Mizrahi, A. (2010). Functional organization and population dynamics in the mouse primary auditory cortex. *Nat. Neurosci.* 13, 353–360.

Song, S., Sjöström, P. J., Reigl, M., Nelson, S., and Chklovskii, D. B. (2005). Highly nonrandom features of synaptic connectivity in local cortical circuits. *PLoS Biol.* 3:e68. doi: 10.1371/journal.pbio.0030068

Sporns, O. (2010). *Networks of the Brain*. Cambridge, MA: The MIT Press.

Sporns, O., Honey, C. J., and Kötter, R. (2007). Identification and classification of hubs in brain networks. *PLoS ONE* 2:e1049. doi: 10.1371/journal.pone.0001049

Watts, D. J., and Strogatz, S. H. (1998). Collective dynamics of /'small-world/' networks. *Nature* 393, 440–442.

Yoshimura, Y., Dantzker, J. L. M., and Callaway, E. M. (2005). Excitatory cortical neurons form fine-scale functional networks. *Nature* 433, 868–873.

Yu, Y.-C., Bultje, R. S., Wang, X., and Shi, S.-H. (2009). Specific synapses develop preferentially among sister excitatory neurons in the neocortex. *Nature* 458, 501–504.

Yu, Y.-C., He, S., Chen, S., Fu, Y., Brown, K. N., Yao, X.-H., et al. (2012). Preferential electrical coupling regulates neocortical lineage-dependent microcircuit assembly. *Nature* 486, 113–117.

Conflict of Interest Statement: The authors declare that the research was conducted in the absence of any commercial or financial relationships that could be construed as a potential conflict of interest.

Received: 09 December 2011; accepted: 31 January 2013; published online: 19 February 2013.

Citation: Perin R, Telefont M and Markram H (2013) Computing the size and number of neuronal clusters in local circuits. Front. Neuroanat. 7:1. doi: 10.3389/fnana.2013.00001

APPENDIX

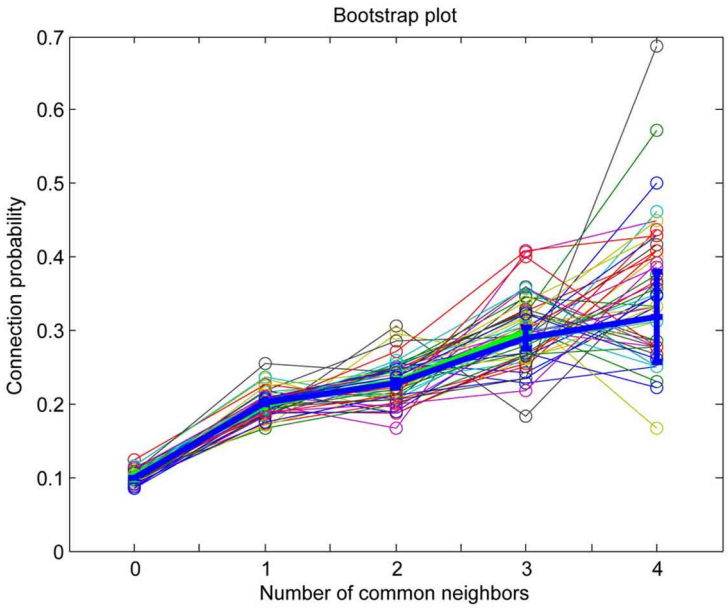

FIGURE A1 | MatLab bootstrap analysis of connection probability as a function of the number of common neighbors (thin lines in various colors) with original data mean and standard error of the mean superposed for reference (thick blue line).

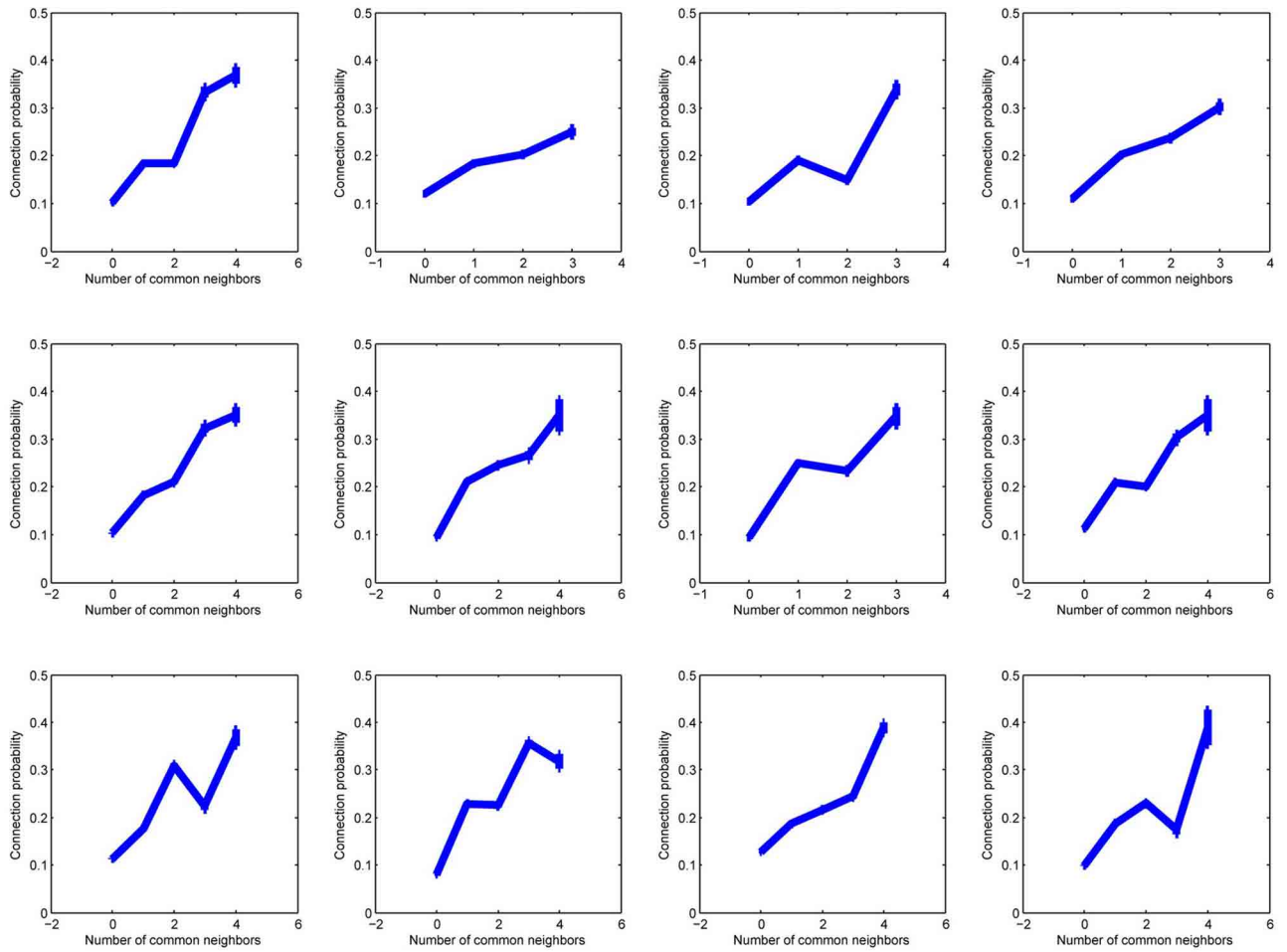

FIGURE A2 | Twelve plots of connection probability as a function of the number of common neighbors in subsets of 20 experiments, each experiment from a different individual.

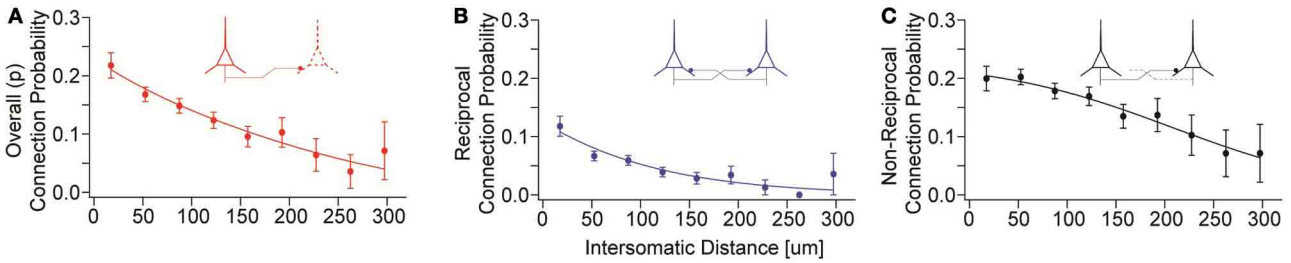

D Cell positions (rounded)

	X	Y	Z
Cell 1	40	31	36
Cell 2	34	66	40
Cell 3	54	45	50
Cell 4	66	68	34

E Inter-somatic distances (rounded)

	Cell 1	Cell 2	Cell 3	Cell 4
Cell 1	0	36	24	45
Cell 2	36	0	31	33
Cell 3	24	31	0	30
Cell 4	45	33	30	0

F Adjust profiles in a,b and c by multiplying distance in profiles by the value of morphological reach.
For example, panels a-c would cover a range of 150μm instead of 300μm for a morphological reach of 0.5.

G Overall Connection Probabilities p(i,j) from **a**

	Cell 1	Cell 2	Cell 3	Cell 4
Cell 1	0.00	0.29	0.31	0.28
Cell 2	0.29	0.00	0.30	0.30
Cell 3	0.31	0.30	0.00	0.30
Cell 4	0.28	0.30	0.30	0.00

H Non-reciprocal Connection Probabilities pnr(i,j) from **b**

	Cell 1	Cell 2	Cell 3	Cell 4
Cell 1	0.00	0.20	0.20	0.20
Cell 2	0.20	0.00	0.20	0.20
Cell 3	0.20	0.20	0.00	0.20
Cell 4	0.20	0.20	0.20	0.00

I Reciprocal Connection Probabilities pr(i,j) from **c**

	Cell 1	Cell 2	Cell 3	Cell 4
Cell 1	0.00	0.09	0.10	0.09
Cell 2	0.09	0.00	0.10	0.09
Cell 3	0.10	0.10	0.00	0.10
Cell 4	0.09	0.09	0.10	0.00

J Generate random numbers

	Cell 1	Cell 2	Cell 3	Cell 4
Cell 1	1.00	0.13	0.28	0.59
Cell 2	1.00	1.00	0.98	0.74
Cell 3	1.00	1.00	1.00	0.07
Cell 4	1.00	1.00	1.00	1.00

K

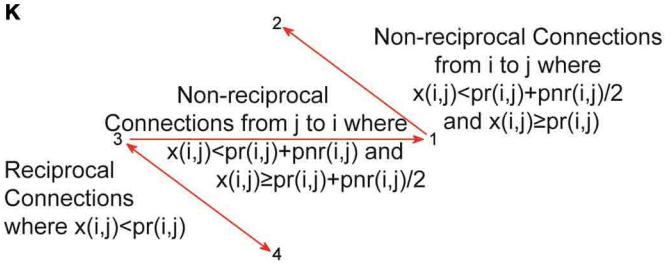

FIGURE A3 | Process illustrating assembly of pseudo-random networks that respect the overall connection probability as a function of distance as well as the non-reciprocal and reciprocal connection probabilities as a function of distance. (A–C) Experimentally observed connection probability profiles and fitted functions (sigmoids). **(D)** Example of cell positions generated by grid plus random jitter. **(E)** Calculated intersomatic distances from **D**. **(F)** Apply morphological reach as a factor in the connection probability profile. **(G–I)** Connection probabilities, given a morphological reach of 1, used for the remainder of the example. **(J)** Generate random numbers $x(i, j)$ once for each pair of neurons i and j. **(K)** Determine presence and direction of connections based on random numbers that were generated. Reciprocal connections occur where $x(i, j) < \mathrm{pr}(i, j)$. Non-reciprocal connections from neuron i to neuron j occur where $x(i, j) \geq \mathrm{pr}(i, j)$ and $x(i, j) < \mathrm{pr}(i, j) + \mathrm{pnr}(i, j)/2$. Non-reciprocal connections occur from neuron j to neuron i where $x(i, j) \geq \mathrm{pr}(i, j) + \mathrm{pnr}(i, j)/2$ and $x(i, j) < \mathrm{pr}(i, j) + \mathrm{pnr}(i, j)$. No connections are formed when $x(i, j) \geq \mathrm{pr}(i, j) + \mathrm{pnr}(i, j)$. The overall probability of connection p always respects its distance profile and the equation $p(i, j) = \mathrm{pr}(i, j) + \mathrm{pnr}(i, j)/2$.

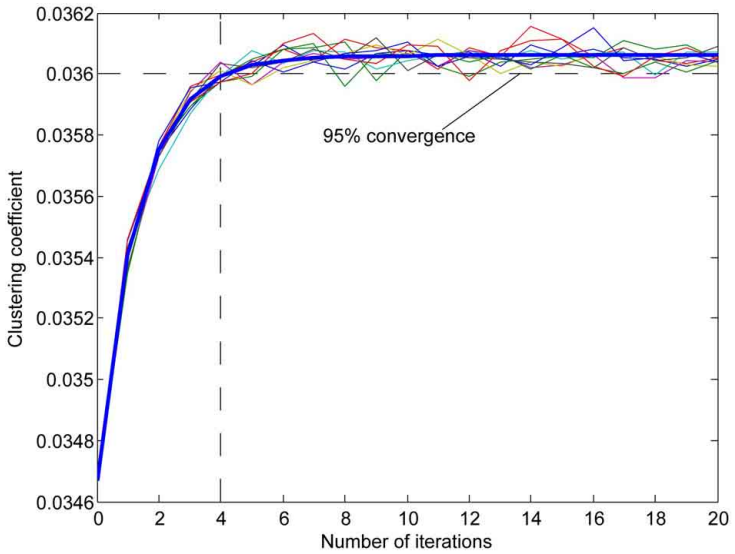

FIGURE A4 | Examples of the effect of reorganization on clustering coefficient of a network (multiple thin lines) with a fitted exponential curve (thick blue line). Since the computation of the clustering coefficient is time-consuming we used the number of iterations that best approximated 95% percent convergence to the value projected after infinite iterations (from fitted data). The clustering coefficient is the measure of the probability of connection among each neuron's neighbors calculated for each neuron in the network.

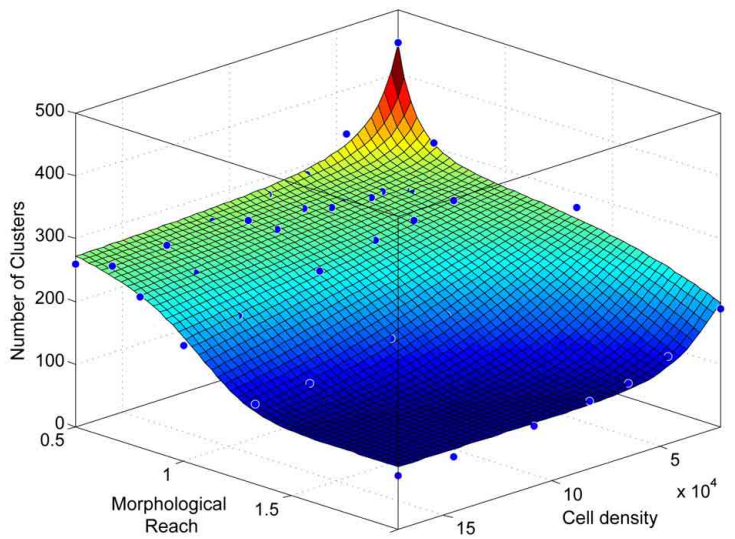

FIGURE A5 | Number of clusters as a function of network density and morphological reach as in Figure 3D, viewed from a different angle.

frontiers in
NEUROANATOMY

REVIEW ARTICLE
published: 20 December 2011
doi: 10.3389/fnana.2011.00065

Cognitive consilience: primate non-primary neuroanatomical circuits underlying cognition

Soren Van Hout Solari [1,2] **** and Rich Stoner*** [3] *******

[1] *Simigence Inc., Solana Beach, Cardiff, CA, USA*
[2] *Department of Mechanical and Aerospace Engineering, University of California San Diego, La Jolla, CA, USA*
[3] *Department of Neurosciences, Autism Center of Excellence, University of California San Diego, La Jolla, CA, USA*

Edited by:
Julian Budd, University of Sussex, UK

Reviewed by:
Trygve B. Leergaard, University of Oslo, Norway
Giorgio Innocenti, Karolinska Institutet, Sweden
Hugo Merchant, Universidad Nacional Autónoma de México, Mexico

****Correspondence:***
Soren Van Hout Solari, Simigence Inc., 201 Lomas Santa Fe Suite 490, Solana Beach, CA 92075, USA.
e-mail: sorensolari@gmail.com;
Rich Stoner, Department of Neurosciences, Autism Center of Excellence, University of California San Diego, 8110 La Jolla Shores Road, Suite 200, La Jolla, CA 92037, USA.
e-mail: rstoner@ucsd.edu

Interactions between the cerebral cortex, thalamus, and basal ganglia form the basis of cognitive information processing in the mammalian brain. Understanding the principles of neuroanatomical organization in these structures is critical to understanding the functions they perform and ultimately how the human brain works. We have manually distilled and synthesized hundreds of primate neuroanatomy facts into a single interactive visualization. The resulting picture represents the fundamental neuroanatomical blueprint upon which cognitive functions must be implemented. Within this framework we hypothesize and detail 7 functional circuits corresponding to psychological perspectives on the brain: consolidated long-term declarative memory, short-term declarative memory, working memory/information processing, behavioral memory selection, behavioral memory output, cognitive control, and cortical information flow regulation. Each circuit is described in terms of distinguishable neuronal groups including the cerebral isocortex (9 pyramidal neuronal groups), parahippocampal gyrus and hippocampus, thalamus (4 neuronal groups), basal ganglia (7 neuronal groups), metencephalon, basal forebrain, and other subcortical nuclei. We focus on neuroanatomy related to primate non-primary cortical systems to elucidate the basis underlying the distinct homotypical cognitive architecture. To display the breadth of this review, we introduce a novel method of integrating and presenting data in multiple independent visualizations: an interactive website (http://www.frontiersin.org/files/cognitiveconsilience/index.html) and standalone iPhone and iPad applications. With these tools we present a unique, annotated view of neuroanatomical consilience (integration of knowledge).

Keywords: cerebral cortex, thalamus, basal ganglia, circuitry, consilience, isocortex, cognition

1. INTRODUCTION

At the turn of the twentieth century Cajal (1899, 2002) published what is considered now as the beginning of the modern anatomical understanding of the brain. Cajal's work, entirely dependent on the Golgi staining method, analyzed the neuroanatomical circuitry of complete brains in multiple species. His work stands out from 100 years of subsequent research as a single comprehensive examination across species and brain regions. Brodmann (1909) and von Economo (1929) respectively produced what are, surprisingly still today, the most comprehensive cytoarchitectonic maps of the human cerebral cortex. By the early 1970s, axonal tracing methods were introduced to study distant neuroanatomical projections (Graham and Karnovsky, 1966; Kristensson and Olsson, 1971). Tracing studies have continued to improve and produce detailed projection and connectivity data, but in so doing, fragment knowledge across species and brain regions (Zaborszky et al., 2006).

Forming an accurate mental view of brain circuitry is difficult, yet without one we cannot understand the function of the brain. Only with a comprehensive and cohesive picture can we make accurate inferences about the function of discrete neuroanatomical circuits. Each structure imposes dependencies and constraints on any theory that must be maintained for a working hypothesis of brain function. Several efforts are currently underway to reconcile the disparity between individual connectivity studies within a global scope. CoCoMac, a tool based on primate literature, represents the state of the art in mapping corticocortical interconnectivity between functional regions (Kotter, 2004). The Human Connectome Project (Marcus et al., 2011), along with other projects within the NIH Blueprint for Neuroscience Research, are using novel imaging methods to describe connectivity details for both primate and human brains (Stephan et al., 2000; Schmahmann et al., 2007; Hagmann et al., 2010). Unfortunately the resolution of external imaging methods is insufficient to elucidate neuroanatomical details underlying circuit organization.

This review is an attempt to form a comprehensive and cohesive understanding of the primate non-primary neuroanatomical circuitry through consilience (the integration of knowledge). Our first goal is to assemble a comprehensive neuroanatomical picture that is not *inconsistent* with known facts. We have produced an interactive visualization by synthesizing a vast number of fragmented studies into a single referenced framework that can be explored dynamically (**Figure 1**). We present this neuroanatomical picture as a detailed first-order approximation of

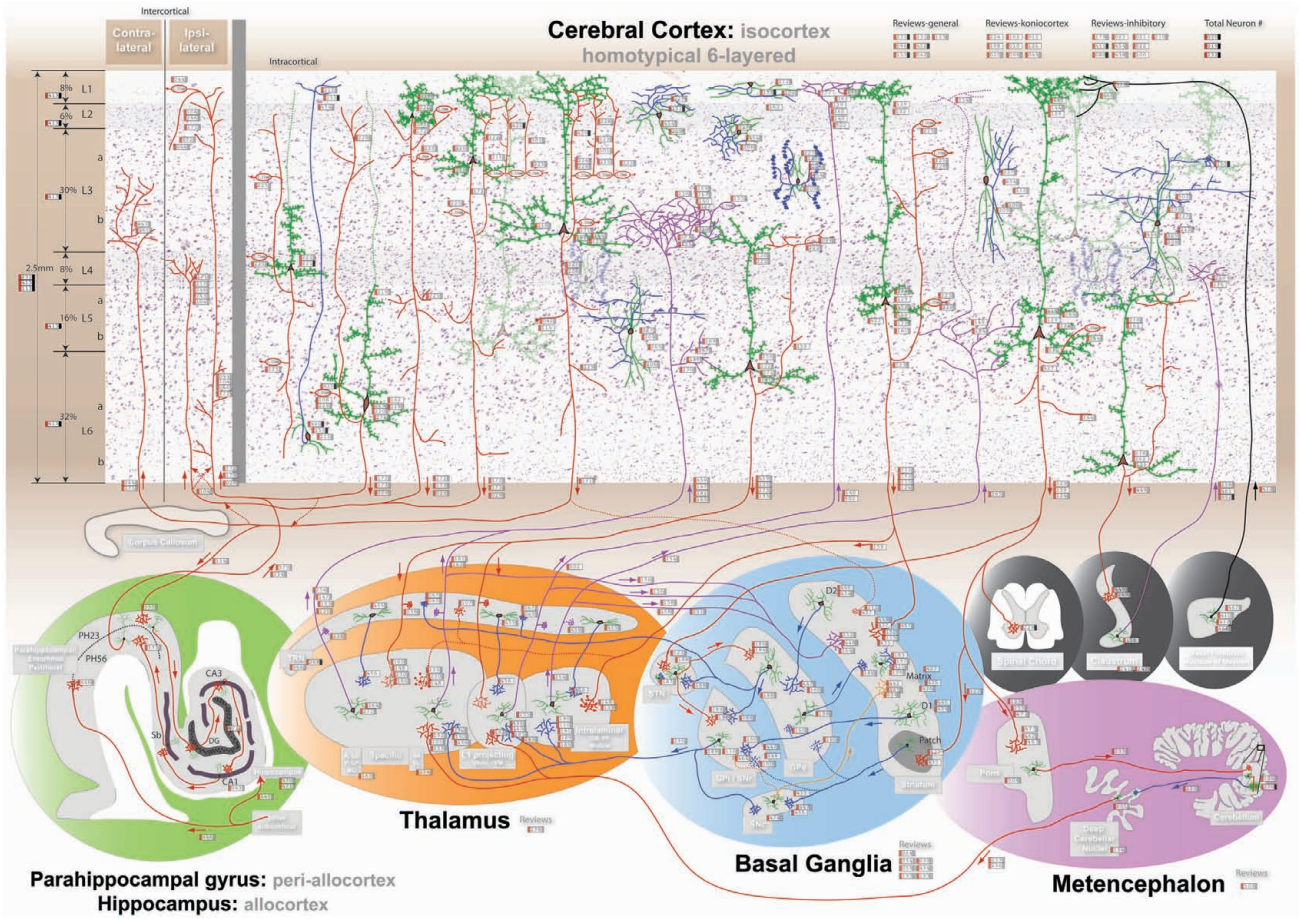

FIGURE 1 | The comprehensive neuroanatomical picture formed by synthesizing hundreds of original neuroanatomical studies into the homotypical blueprint underlying cognition. The interactive visualization can be experienced at http://www.frontiersin.org/files/cognitiveconsilience/index.html. The visualization is designed to be interactively zoomable, therefore details may not be clear in the above image. The 6-layered cerebral isocortex with 9 distinct pyramidal neurons and 8 cortical interneurons is presented at the top with a Nissl background. The parahippocampal gyrus including upper (PH23) and lower (PH56) layers and the hippocampus including the dentate gyrus (Dg), CA3 fields, CA1 fields, and subiculum (Sb; green). The thalamus is divided into 4 parts namely the specific, intralaminar, layer 1 projecting and thalamic reticular nucleus (Trn; orange). The basal ganglia includes the matrix (D1 and D2 receptors) and patch portions of the striatum, the external globus pallidus (Gpe), the internal globus pallidus (Gpi) and substantia nigra pars reticulata (Snr), the subthalamic nucleus (Stn), and the substantia nigra pars compacta (Snc; blue). The metencephalon includes the pons, cerebellum, and deep cerebellar nuclei (Dcn; purple). Finally the spinal chord, claustrum, and basal forebrain are shown in black.

cognitive circuitry in the primate brain for use as a skeleton upon which to hang additional knowledge. The visualizations should be viewed as information static "interactive figures" associated with the review. The re-application of the technology and framework as an interactive tool with evolving information is a desirable future endeavor.

Our second goal is to synthesize the facts and patterns in the established neuroanatomical picture into a detailed functional framework consisting of seven discrete circuits that correspond to psychological perspectives on the brain. While neuroanatomy is necessary to understand the function of a brain, it is not sufficient. The vast amount of additional information from electrophysiology to psychology must be integrated and explained. For each circuit we provide a brief hypothesis of cognitive circuitry development and information flow at the neuron level. We understand that our novel functional perspective may generate healthy conversation and debate. The technology we provide offers an easily accessible medium in which to question, challenge, and verify the information presented.

Ultimately, cognitive consilience is an attempt to establish a unified framework within which the vast majority of knowledge on the primate brain can be placed.

2. METHODS AND TECHNOLOGY: WEB, iPHONE, AND iPAD App

Methodologically, the interactive **Figure 1** was created by performing an extensive review of the non-primary primate literature, organizing the knowledge into a single framework, and selecting relevant reference data to include on the graphic. Non-primate data was utilized in occasions where primate data was insufficient or did not exist. In order to be placed on the graphic, reference data needed to contain sufficiently detailed location information

by identifying an afferent/efferent cortical layer or subcortical nuclei. The graphic contains 410 referenced data visualization points from 186 unique references. By no means does this visualization include the complete body of neuroanatomical literature, but rather creates a comprehensive basis as a starting point for reader investigation. Data from many high quality citations could not be included as the data (raw or processed) was provided with insufficient spatial context. In general, we can only be as precise as the data we are reviewing. The graphic was hand drawn and attempts to recreate a reasonably accurate visual feel for structures, neurons, and their connectivity. Prominent axonal pathways were then identified as circuits, shown in **Figure 4**, based on known correlates with psychological and neuroscience data to provided a theoretical framework within which to understand neuroanatomy.

The review is accompanied by the release of an interactive web application[1] and a portable application for the Apple iPad and iPhone (search: cognitive consilience), illustrated in **Figure 2**. The interactive figure was built around a Google Maps-like interface to enable a reader to rapidly locate relevant citations. Each functional circuit discussed in the following sections can be toggled on and off to refine the presentation of important citations. Neurons and projections are directly referenced with appropriate links to PubMed and NeuroLex[2]. The web application provides additional search tools, including citation filters by publication date, species, author last name, and keywords.

The interactive medium provides a means for readers to rapidly evaluate hypotheses made in this review and to construct new ideas from the organized citations. The technology is presented as an information static "interactive figure" accompanying this review. Source code for the web application and raw citation data are available upon request and source code for the iphone/ipad app is available through collaboration. A future version that incorporates data mining and interactive citation addition is at the planning stage.

The inclusion of a spatially referenced interactive visualization accompanying a scientific review is novel and establishes a desirable new feature for future presentations of neuroanatomical work.

3. PRIMATE NON-PRIMARY HOMOTYPICAL ARCHITECTURE

Our near exclusive focus on primate non-primary data is unique. Neuroscience literature is biased toward studying primary sensory cortex in non-primates. This bias is introduced by the cost of primate research combined with the desire to correlate anatomical findings with electrophysiology stimulus response experiments.

As described in this review, the non-primary primate brain appears to have a consistent homotypical organization. The non-primary isocortex contains important contrasting features not found in primary sensory koniocortex, yet general cortical organization, in nearly all neuroscience textbooks, is taught corresponding to koniocortical principles (Purves et al., 2004). Some examples of primate isocortical principles not found in koniocortex:

1. Specific thalamocortical projections target layer 3b often avoiding layer 4,
2. Lack of layer 4 spiny stellate cells,
3. Striatally projecting layer 5 neurons, and
4. Long corticocortical white matter projections including callosal projections.

If we are to understand the entire primate (human) brain, our understanding must be based on the correct neuroanatomy. In this paper, we focus on primate non-primary literature, and consciously avoid major discussion and citing of primary sensory literature. In so doing, we hope to establish a basis for the fundamental principles of brain circuit organization.

Brains follow general principles of development dictated by evolved gene expression patterns (Striedter, 2005; Watakabe et al., 2007); however, for any "rule" or general principle of organization, there can be found an exception to the rule. The described functional circuits are an attempt to elucidate the blueprint of the homotypical neuroanatomical architecture underlying cognition. When we refer to the blueprint of a homotypical architecture, we imply that the underlying neuronal organization and projection rules are the same across different regions of analogous nuclei. If a neuron type X sends its most dense projections to a target location Z and sends collateral projections to location Y, we would consider $X \rightarrow Z$ the first-order neuroanatomical architecture. In order to create a compact yet comprehensive picture, we focus on the homotypical first-order architecture of the cerebral cortex, thalamus, basal ganglia, and their interconnections. This first-order architecture creates a factually consistent starting point upon which to build.

If we assume that neuroanatomical organization defines function, then a homotypical architecture supports the conjecture that different locations of the same neuronal group, although processing different information modalities, processes the information in the similar manner. Our viewpoint is that the cerebral cortex, thalamus, and basal ganglia only perform a limited few cognitive information processing functions. Within a homotypical architecture, each functional circuit determines *how* information is processed while the differences between the afferent input of two analogous pathways define *what* information is processed.

4. NEUROANATOMICAL CIRCUITS

Seven hypothesized functional circuits are presented. The seven circuits described are consolidated long-term declarative memory, short-term declarative memory, working memory/information processing, behavioral memory selection, behavioral memory output, cognitive control, and cortical information flow regulation. Each circuit is described in terms of readily distinguishable neuronal groups including the cerebral isocortex (9 pyramidal neuronal groups), parahippocampal gyrus and hippocampus, thalamus (4 neuronal groups), basal ganglia (7 neuronal groups), metencephalon, claustrum, basal forebrain, and spinal chord.

For clarity, each major neuronal group represented in the graphic is placed into only one primary circuit for discussion. However, in a functioning brain, circuits interact, and a single neuronal group participates in multiple circuits. The anatomical details of each circuit, shown in **Figures 1** and **4**, are meant to be explored dynamically through the associated technology.

[1] http://www.frontiersin.org/files/cognitiveconsilience/index.html
[2] http://neurolex.org/

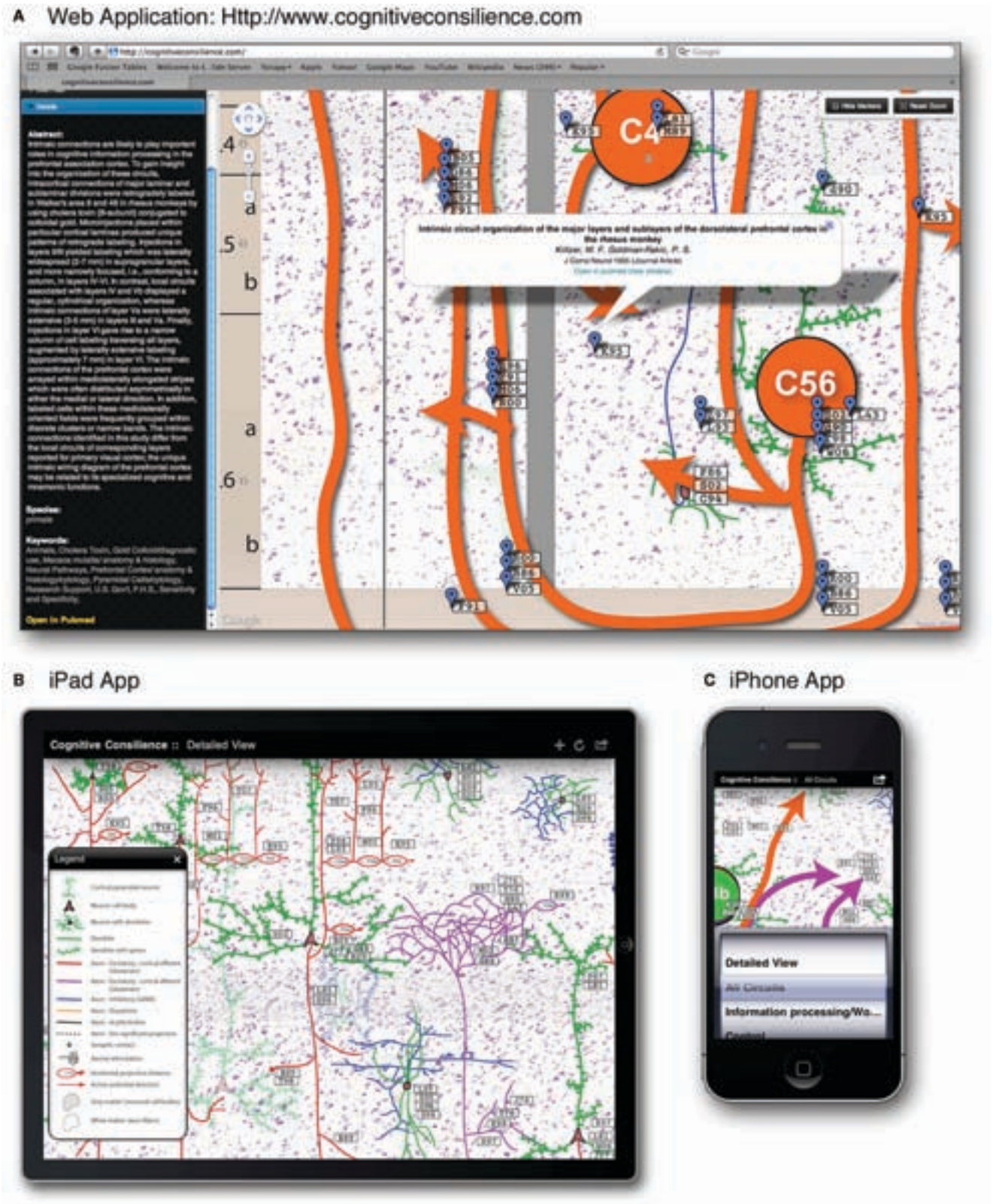

FIGURE 2 | Cognitive consilience visualization deployment across three technology platforms. The visualizations are identical and function similarly across platforms. **(A)** Interactive web application showing easy access to reference information throughout the visualization (http://www.frontiersin.org/files/cognitiveconsilience/index.html). **(B)** Deployment as an iPad App. **(C)** Deployment as an iPhone App.

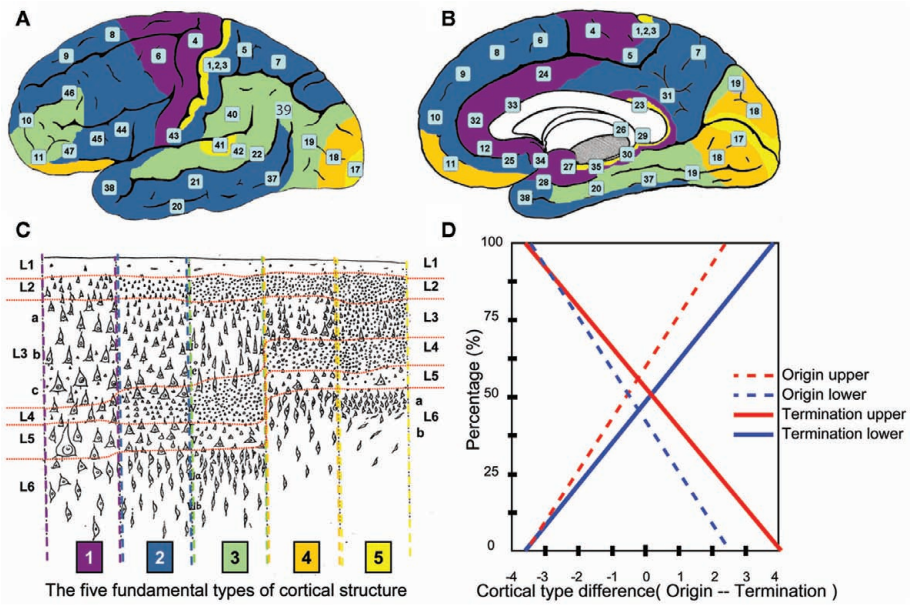

FIGURE 3 | Prediction of human laminar corticocortical projections. Synthesis of von Economo cortical laminar types and homotypical laminar corticocortical projections in the monkey. Lateral **(A)** and medial **(B)** view of human cortical regions colored to correspond to the five fundamental cortical types depicted in **(C)** with numbers corresponding to Brodmann's areas. **(C)** Von Economo's five fundamental human cortical lamination types (von Economo, 1929). 1 = purple, 2 = dark blue, 3 = green, 4 = orange, 5 = yellow. The laminar distribution in the human cerebral cortex can be identified along a smooth numerical gradient, where 5 corresponds to "input" granular koniocortex and 1 corresponds to "output" agranular cortex. Horizontal red lines highlight layer boundaries, with average human cortical thickness = 2.5 mm. **(D)** Rough prediction of human laminar corticocortical (origin/termination) projection percentages predicted by numerical difference of cortical types in **(C)**. Dotted red = % neurons originating in upper layers 2, 3. Dotted blue = % neurons originating in lower layers 5, 6, and lesser 4. Solid red = % synaptic terminations in layers 1, 2, and lesser 3. Solid blue = % synaptic terminations in mid/lower layers 4, 5, and lesser 6. In general, "feedforward" = (dotted red/solid blue), "feedback" = (solid red/dotted blue). Example: A type 2 (blue origin) projecting to a type 4 (orange target) would have a difference of -2(feedback), and predict roughly 25% of the projections from type 2 would originate from neurons in upper layers 2, 3, and roughly 20% of synaptic terminations in the type 3 cortical area would terminate in middle/lower layers.

The organization of the review follows a pattern to enable the reader to more clearly distinguish between neuroanatomical fact and the authors synthesized viewpoint. A subsection titled "perspective" concludes each circuit description and presents hypotheses and a more speculative synthesized viewpoint. All other sections attempt to conform to the unbiased presentation of important published information. We also include a concise summarized author's viewpoint on the function of each neuronal group following their neuroanatomical description indicated with "Viewpoint": Historical notes, indicated as such, are interjected to explain the current state of thinking and reinvigorate important concepts that seem faded in the literature.

4.1. CONSOLIDATED LONG-TERM DECLARATIVE MEMORY: CORTICOCORTICAL CIRCUIT

The identification of declarative memory is adopted from Squire as referring to "*the capacity for conscious recollection about facts and events*" (Squire, 2004). We define long-term memory as that which is stored semi-permanently in the isocortex. Lesions of the isocortex or of white matter fiber tracts produce a wide variety of stereotypical cognitive deficits (Geschwind, 1965b; Penfield and Rasmussen, 1968). Two distinct long-term memory deficits arise when comparing cortical gray matter lesions to corticocortical white matter lesions, although human lesions are rarely isolated (Geschwind, 1965a; Schmahmann et al., 2008). Localized gray matter lesions result in a reduced capacity to recall and process domain specific information, often manifesting as a form of agnosia (i.e., loss of the ability to recognize). For example, the inability of humans to recognize faces with lesions to the fusiform face area or recognize motion with lesions to cortical area MT. White matter lesions result in subtly different deficits representative of a disconnection of information shared between separate cortical areas. For example, lesions to the arcuate fasciculus disconnect Wernicke's area (speech comprehension) from Broca's area (speech production) and result in deficits in speech repetition (Damasio and Damasio, 1980). In essence, although speech comprehension and production both independently remain intact, the associations between them have been severed. These two distinct forms of long-term memory exist within the interconnectivity of the cerebral cortex.

4.1.1. Cerebral cortex

The human cerebral cortex is a 2.5-mm thick sheet of tissue approximately 2400 cm^2 (four 8.5 × 11 pieces of paper) in size folded up around the entire brain (Toro et al., 2008). The cerebral cortex consists of a homotypical six layer pattern of neuron density distribution (von Economo, 1929; Lorente de No, 1943). The cerebral cortex develops inside out, with neurons in the innermost

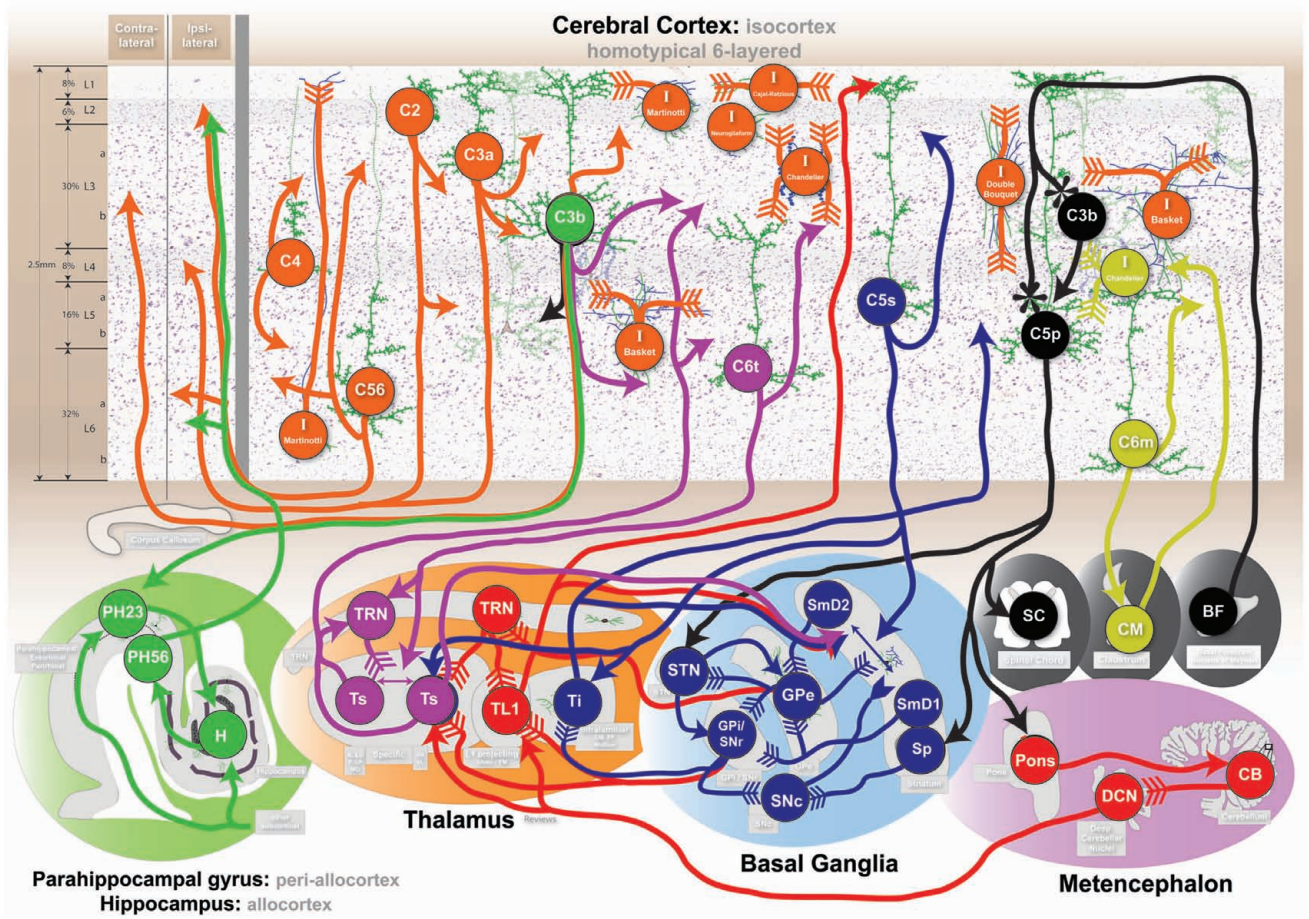

FIGURE 4 | Cognitive circuits as shown at http://www.frontiersin.org/files/cognitiveconsilience/index.html. Circuits from left to right. Orange: consolidated declarative long-term memory. Green: short-term declarative memory. Purple: working memory/Information processing. Blue: Behavioral memory action selection. Black: behavioral memory output. Red: cognitive control. Yellow: cortical information flow regulation. Arrow head type indicates neurotransmitter: solid arrow-glutamate, feather-GABA, flower-acetylcholine, reverse arrow-dopamine. See website and text for additional details.

layer (L6) migrating into place first and neurons in successive outer layers migrating into place later (Rakic, 1995). Cortical laminar differentiation lies along a very clear spectrum with *input* sensory cortex being the most laminated/granular and *output* motor cortex being the least laminated/granular (von Economo, 1929; see **Figure 3C**). The lamination gradient represents a major clue in functional organization. The cerebral cortex can be grouped into the isocortex (neocortex), allocortex (paleocortex), periallocortex, and koniocortex (primary vision, auditory, somatosensory, and granulous retrosplenial cortex) based on laminar differentiation and developmental origin. The koniocortices are based on the same underlying anatomical principles of six layers and have evolved additional structure for their more specific sensory roles (Northcutt and Kaas, 1995). The patterns of laminar differentiation have been used to parse the entire cerebral cortex into distinct areas often called Brodmann's areas (Brodmann, 1909; Triarhou, 2007). A large amount of experimental evidence on the cerebral cortex, from lesion studies to electrophysiology to FMRI, point to localized cortical information processing *modules* on the order of a few mm^2 (Szentagothai, 1975; Catani and ffytche, 2005). Each area appears to process a distinct type of information reflecting the external and internal perceptions/behaviors of the individual, such as visual objects, language, executive plans, or movements (Penfield and Rasmussen, 1968; Goldman-Rakic, 1996; Grafton et al., 1996; Tanaka, 2003). The *what* of cortical information processing is thus highly localized and modular. The neuroanatomical organization underlying these *what* regions follows a very homotypical blueprint, which drives a functional perspective that *how* information is processed throughout the cerebral cortex is the same.

4.1.2. *Intracortical circuit*

Intracortical projections are horizontal corticocortical projections traveling within the gray matter of the cerebral cortex (Kritzer and Goldman-Rakic, 1995). Although all pyramidal neurons have connections within the cerebral cortex, the prominent source of distant intracortical projections arise mainly from pyramidal neurons within layers 2 and 3, and a sub-set of neurons in layers 5 and 6. The intracortical terminations of C3a and C3b pyramidal neurons are not distributed uniformly, but form patchy or stripe-like patterns of termination which comprise areas up to 20 mm^2 in the monkey

(de Lima et al., 1990; Levitt et al., 1993; Fujita and Fujita, 1996; Pucak et al., 1996). Neurons in each layer appear to project horizontally, then the stripe-like terminations (spaced a few 100 μm apart) arise out of vertical collaterals. The laminar specificity and development of these corticocortical striped projections is largely activity dependent (Price et al., 2006). In the monkey, 50% of pyramidal neuron synaptic contacts, within its local stripe (roughly its dendritic tree size), are onto GABAergic inhibitory neurons, while more than 90% of synaptic contacts outside a pyramidal neurons local stripe are onto other pyramidal neurons (Melchitzky et al., 2001). The intracortical organization is suggestive that a *functional module* ($\sim$10s mm^2) in the isocortex is much larger than the traditional cortical minicolumn ($\sim$100s μm^2; Buxhoeveden and Casanova, 2002; Mountcastle, 2003; Rockland and Ichinohe, 2004).

Viewpoint: Neuroanatomically, an organization appears to exist where cell assemblies form intracortically in functional modules within select layers to encode perceptions.

4.1.3. Intercortical circuit

Intercortical circuits involve the large white matter corticocortical fiber tracts of the brain (Schmahmann and Pandya, 2006). Fiber tracts connect multiple distant cortical areas and subcortical nuclei with a great deal of specificity. The topology of corticocortical projections are the primary focus of the Human Connectome Project and CoCoMac (Kotter, 2004; Marcus et al., 2011). Contralateral corticocortical projections tend to connect the same spatial regions on opposite sides of the brain, while ipsilateral connections often connect distant areas on the same side (Barbas et al., 2005a). Different populations of pyramidal neurons tend to project contralaterally (lower layer 3b) as opposed to ipsilaterally (upper layer 3a and layers 5/6; Soloway et al., 2002).

We introduce a data-driven prediction for laminar projections between any two cortical areas in the human brain (**Figure 3**). Today, no safe experimental technique is capable of verifying laminar projections in the human. Yet by connecting and integrating previously unconnected research we arrive at very precise hypothesis with significant functional consequences in the human brain.

The cytoarchitectonics of the human cerebral cortex, as determined by von Economo, show the laminar pattern of a given area of cortex can generally fit within one of five fundamental types of cortical structure **Figure 3C** (von Economo, 1929; Walker, 1940). The pattern of projections between two cortical areas, as determined by Barbas in the monkey, shows a pattern of neuron layer origin and layer termination based on the difference between the two types of cortices as shown in **Figure 3D** (Barbas, 1986; Rockland, 1992; Barbas and Rempel-Clower, 1997; Rempel-Clower and Barbas, 2000; Barbas et al., 2005b; Van Essen, 2005; Medalla and Barbas, 2006). When von Economo and Barbas' research is aligned, as they are for the first time here, we arrive at rough laminar projection predictions between cortical areas in the human brain.

If a projection originates in a more granular (e.g., type 4, **Figure 3**-orange) cortical area and terminates in a less granular (e.g., type 3, **Figure 3**-green) cortical area, the cells of origin are predominantly in layer 3, while synaptic terminals are in layer 4 with collaterals in layers 5, 6 (feedforward projection). The majority of projections in the cerebral cortex are feedforward and originate in layers 2/3. If the projection is reversed, projection neurons reside mostly in layer 5, some in 6, and project to layers 1 and 2 with collaterals in layer 3 (feedback projection). In visual areas, this pattern of projections has been correlated with the functional hierarchy of the cortical area (Felleman and Van Essen, 1991). The neuroanatomical architecture of a given cortical region appears to be the predictor of its functional relationship to other cortical areas.

Historical note: Barbas does not mention or cite von Economo in her papers in conjunction with the five types of cortical laminar patterns. The five types of laminar patterns in the monkey originated in 1947 when von Bonin adopted/translated von Economo's human work into the monkey (von Bonin and Bailey, 1947). Since that time, the correlation between humans and monkeys appears to have been lost in the literature. **Figure 3** is designed to illustrate the correlation between the original von Economo human study and Barbas' monkey experiments performed 60 years later. The correlation adds additional significance to Barbas' original cortical projection research in the monkey (Barbas, 1986).

Viewpoint: Neuroanatomically, cell assembly to cell assembly associations form intercortically in a hierarchical layer dependent feedforward/feedback network.

4.1.4. Cortical pyramidal layer 4 cortically projecting – C4

Layer 4 is referred to as the inner granular layer, not for any particular cell type, but due to the visual appearance of small neurons stained in Nissl preparations. Layer 4, of all cortices, appears to be an input for feedforward type projections. In isocortex, layer 4 is the primary target of ipsilateral corticocortical feedforward cortical projections (**Figure 3**; DeFelipe et al., 1986; Felleman and Van Essen, 1991; Rockland, 1992; Barbas et al., 2005a; Medalla and Barbas, 2006). Since primary sensory koniocortex is the anatomically closest cortex to raw sensory input, other cortical areas can not provide feedforward input. Instead, in koniocortices, the specific thalamus provides the feedforward projection into layer 4. In primary motor cortex layer 4 is essentially non-existent, highlighting the diminished need for feedforward input to cortical areas involved in output behavior. The cortical pyramidal neurons in layer 4, C4, typically have a descending and an ascending axon that arborize locally (<1 mm; Kritzer and Goldman-Rakic, 1995). The ascending axon reaches all supragranular layers upward of layer 2. Descending axons do not prominently exit the cortex as with most other pyramidal cells.

Only in primary sensory areas, and especially in primary visual cortex, does layer 4 contain spiny stellate cells (Meyer et al., 1989). In all other parts of cortex, spiny stellate cells are non-existent or very rare, and instead small pyramidal cells along with interneurons compose the majority of cells in L4. Quoting Lund "*There are no spiny stellate neurons in V2 in contrast to area V1 where they are the main neuron types of lamina 4*" (Lund et al., 1981).

Viewpoint: Neuroanatomically, C4 appears to function as a corticocortical feedforward input system.

4.1.5. Cortical pyramidal layer 2 cortically projecting – C2

Layer 2 is referred to as the outer granular layer because of its similar granular structure as layer 4. The C2 neurons are small

pyramidal neurons with local horizontal projections mostly to layer 2 and to layer 3 (Tanigawa et al., 1998; Soloway et al., 2002; Barbas et al., 2005a). Layer 2 is a primary target of ipsilateral feedback type cortical projections (**Figure 3**). The granular similarity of layer 2 to layer 4 implies a similar input architecture for feedback projections. C2 receives feedback input and propagates information horizontally and down to C3a and C3b, with upper layer 5 being the focus of infragranular projections (Kritzer and Goldman-Rakic, 1995).

Viewpoint: Neuroanatomically, C2 appears to function as corticocortical feedback input system.

4.1.6. Cortical pyramidal layer 3a cortically projecting – C3a

C3a pyramidal neurons, of typical pyramidal shape, are distinguishable from layer 2 in isocortex because of their increased size and sparsity. In layer 3a the distance of intracortical horizontal projections increase into stripe-like patches (Lund et al., 1993; Fujita and Fujita, 1996; Melchitzky et al., 2001). C3a cells often have long horizontal projections in lower layer 3b (Kritzer and Goldman-Rakic, 1995). C3a cells are the dominant source of intercortical projections to layer 4 of ipsilateral cortices (**Figure 3**; DeFelipe et al., 1986; Rockland, 1992; Barbas et al., 2005a; Medalla and Barbas, 2006).

Viewpoint: Neuroanatomically, C3a appears to function as a corticocortical feedforward output system.

4.1.7. Cortical pyramidal layer 5/6 cortically projecting – C56

Neurons in the lower layers of the cerebral cortex are the most diverse, but are differentiable based on the targets of their projections. We use the term C56 to group the cortical neurons in the infragranular layers of the isocortex that dominantly project corticocortically (de Lima et al., 1990; Tanigawa et al., 1998; Soloway et al., 2002). The C56 neurons often have a spindle shape and appear to lack major dendritic tufts above layer 5a (de Lima et al., 1990). The intracortical supragranular projections appear more extensive in layers 2 and 3a (Levitt et al., 1993), with distant horizontal projections in layers 5/6 (Tardif et al., 2007). The C56 group are the dominant source of intercortical projections to layer 1 and 2 of ipsilateral cortices (**Figure 3**; Rockland and Drash, 1996; Barbas et al., 2005a; Medalla and Barbas, 2006).

Viewpoint: Neuroanatomically, C56 appears to function as corticocortical feedback output system.

4.1.8. Cortical interneurons

Cortical interneurons utilize gamma-Aminobutyric acid (GABA) as an inhibitory neurotransmitter and have axonal arbors that do not exit to the white matter. The increase in cortical interneuron number and complexity of organization has long been cited by neuroanatomists as a standard feature of phylogenetic evolution, humans having the greatest number and complexity (Cajal, 2002). Interneuron organization is complex, requiring attempts to standardize terminology (Ascoli et al., 2008). Interneurons are usually first characterized by their morphology, axonal arborization, and specificity of projections. Second, interneurons are often further differentiated by calcium binding protein staining (parvalbumin, calbindin, and calretinin) and their physiological firing properties. In the human, interneurons arise developmentally from two unique genetic expression patterns corresponding to the dorsal forebrain, a cerebral cortex precursor, and the ventral forebrain, a thalamic precursor (Letinic et al., 2002). Dendritic and axonal arborization of all inhibitory neurons are less than a few 100 μm in the monkey (Lund and Lewis, 1993). Inhibitory interneurons are the only known cortical neurons to form gap junctions and typically form gap junctions between the same type of interneuron (Gibson et al., 1999; Hestrin and Galarreta, 2005). Gap junctions have the property of spreading inhibition and synchronizing firing. In general, inhibitory GABAergic neurons are biased toward the upper layers of cortex. For conceptual simplicity, the dominant classes of interneurons are summarized in six neuroanatomical groupings:

1. *Basket* cells form the majority of interneurons, named for the basket like shape of synapses they form around the soma of pyramidal neurons (Cajal, 2002). Basket cells are typically fast spiking, parvalbumin staining, soma targeting, and have their highest densities between middle layer 3 and upper layer 5 (Lund and Lewis, 1993; Zaitsev et al., 2005). Basket cells are often further differentiated by the size and or curvature of their often long (∼100s μm) horizontal axonal arborization (Lund et al., 1993; Zaitsev et al., 2009).
2. *Chandelier* cells are a class of axoaxonic parvalbumin inhibitory neurons which provide exclusive terminations on the initial axon segment of pyramidal neurons found mostly between layers 3 and 5 (Lund and Lewis, 1993; Conde et al., 1994; Defelipe et al., 1999). Named for the vertical chandelier look alike synaptic boutons.
3. *Neurogliaform* cells are small, express calbindin, and are found throughout all layers, but biased toward superficial layers with a tight dense plexus of axons (Lund and Lewis, 1993; Gabbott and Bacon, 1996; Zaitsev et al., 2005).
4. *Martinotti* cells express calbindin and are unique in that they send a vertically projecting axon that arborizes horizontally in layer 1 (Conde et al., 1994; Zaitsev et al., 2009).
5. *Double bouquet* cells express calretinin and have vertically projecting dendrites and axons that span across layers that are direct sources of inter-layer feedforward or feedback projections (Lund and Lewis, 1993; Conde et al., 1994; Zaitsev et al., 2009). Bi-tufted neurons have similar dendritic and axonal organization.
6. *Cajal-Retzius* cells are horizontally projecting interneurons found exclusively in layer 1 of the cerebral cortex and are the only cells found in layer 1 (Conde et al., 1994; Gabbott and Bacon, 1996; Cajal, 2002).

Viewpoint: Neuroanatomically, interneurons appear to synchronize information processing and facilitate excitatory competition through localized vertical and horizontal inhibitory projections enabling cortical information processing.

4.1.9. Perspective on long-term declarative memory

Our neuroanatomical perspective is that long-term memory has two distinct components, namely *perceptions* and *associations* that correlate with psychological deficits related to gray matter (intracortical) vs white matter (intercortical) lesions respectively.

Perceptions are a form of encoding of information, while associations form relational interactions between perceptions.

Perceptions would be the result of the self-organization of different cell assemblies within a cortical module likely during prolonged (years in humans vs weeks in animals) developmental critical periods (Murphy et al., 2005). Hebb (1949) postulated that groups of neurons would form these single perceptual representations called cell assemblies. Some 56 years later, creative experiments are proving that true showing cell assembly formation in L2/3 of rat visual cortex (Yoshimura et al., 2005). The developmental temporal regulation of NMDA and GABA synaptic receptors appears to control plasticity and the formation of perceptual cell assembly representations in critical periods (Murphy et al., 2005). The long-term stability of these cell assemblies could be a direct result of the elimination of this plasticity, through for example the dramatic decrease in NMDA receptors. The spatial extent and laminar location of these cell assemblies would be defined by intracortical projections. Intracortical projections suggest that cell assemblies within a cortical module should form primarily between neurons in similar layers C3–C3, C56–C56 (Kritzer and Goldman-Rakic, 1995). Our locally distributed viewpoint of perceptions is consistent with electrophysiology evidence in the monkey (Tanaka, 2003; Tsao et al., 2006), but in direct competition with other distributed views of perceptual organization (Fuster, 2003).

The localized nature of inhibition in the cerebral cortex and the prominently local connections of excitatory pyramidal neurons onto inhibitory neurons creates an architecture sufficient for local cell assembly activity based competition. Cortical laminar organization should further aid in both the development and information processing regulation of input/output cell assembly functions.

Once perceptions stabilize within cortical modules, intercortical synaptic associations between those perceptions can form throughout life. The stability of an association would be determined by the direct corticocortical synaptic connections between the two perceptions. Presumably, if a direct corticocortical association is stable (say with fewer NMDA receptors) it would be very difficult or impossible to remove naturally. For example, the word "Brad" might exist as a stable representation in Wernicke's area, while the visual perception of facial features may exist in the fusiform face area. The simultaneous perceptions of "Brad" and "the face of Brad" could happen at any time in a persons life and may or may not be important to associate. As a consequence, the ability to temporarily store short-term associations for later consolidation to corticocortical long-term memory is necessary for the selection of stable associations. Short-term memory would presumably require an independent neuroanatomical architecture.

4.2. SHORT-TERM DECLARATIVE MEMORY: CORTICO-HIPPOCAMPAL-CORTICAL CIRCUIT

Psychological access to declarative memory occurs on different time-scales. Neuroanatomical evidence suggests the short-term memory system operates independently of the long-term memory system. Short-term declarative memory is defined as the declarative memory which requires the parahippocampal gyrus (periallocortex) and hippocampal (allocortex) formations for recollection (Squire, 2004). In humans, short-term memory takes weeks to years to consolidate from the periallocortex to the isocortex, wherein declarative memory is consolidated long-term (Squire and Alvarez, 1995). The localization of short-term memory to the hippocampal regions was demonstrated in patient H.M. who had no short-term memory, but retained long-term consolidated memory and behavioral/procedural memory. Due to surgical lesions, H.M. was essentially left with no allocortex or periallocortex (Milner, 2005). We can conclude that the periallocortical and hippocampal circuits are necessary neuroanatomical structures through which short-term memory is formed and later consolidated into corticocortical long-term memory (Squire and Zola, 1996; Eichenbaum, 2000; Squire, 2004).

4.2.1. Parahippocampal gyrus/periallocortex – PH

The parahippocampal gyrus, also called periallocortex because of its transitional laminar structure between isocortex and allocortex, consists of the entorhinal and perirhinal cortices. A reciprocal topographic connectivity exists between association isocortices and periallocortices that are well mapped, but the actual specificity of laminar projections remains vague at best (Witter et al., 1989; Burwell, 2000; Lavenex et al., 2002). The periallocortex contains intralayer connectivity similar to regular isocortex with less laminar differentiation. The periallocortex is the neuronal interface between the isocortex and the hippocampus, since the isocortex does not typically project directly to the hippocampus. The afferent input and efferent output of the periallocortex can grossly be split into upper (PH23) and lower (PH56) layers respectively based on its projections with the isocortex and allocortex. To a lesser degree, the periallocortex receives subcortical input from the amygdala, claustrum, basal forebrain, thalamus, hypothalamus, and brainstem (Insausti et al., 1987).

- PH23 is used to describe the upper layers in the periallocortex that receive afferent projections from the isocortex (typically C3b; Witter et al., 1989). Input to PH23 is topographically organized and dominated by multimodal association isocortex (Burwell, 2000). PH23 sends efferent projections to the hippocampus.
- PH56 is used to describe the lower layers in the periallocortex that send efferent projections to the isocortex with origin/target laminar distributions similar to intercortical association projections (**Figure 3**; Witter et al., 1989). PH56 generally projects back topographically in a reciprocal manner to multimodal association isocortex (Lavenex et al., 2002). PH56 receives afferent projections from the hippocampus.

The aggregate evidence suggests that C3b (and some C56) cells project to PH23 and receive reciprocal projections back from the PH56 regions to which they projected, but far more detailed studies are necessary.

Viewpoint: Neuroanatomically, the periallocortex appears to facilitate medium-term storage of associations, temporally acting between short-term and long-term memory, capable of mapping source C3b representations to target C3b representations in the isocortex.

4.2.2. Cortical pyramidal layer 3b cortically projecting – C3b

Lower layer 3b in the isocortex is centrally located to be the hub of perceptual information processing in the cerebral cortex. The large pyramidal neurons located in the lower part of layer 3, just above the granular layer 4 could be included in multiple circuits including long-term memory, working memory/information processing, and behavior output. The C3b cells have the classic pyramidal neuron shape and are usually the second largest pyramidal neuron group next to C5p (Jones and Wise, 1977; Rempel-Clower and Barbas, 2000; Barbas et al., 2005a). The C3b intracortical projections involve some of the longest (many millimeters) gray matter projections in the cerebral cortex (Kritzer and Goldman-Rakic, 1995; Fujita and Fujita, 1996; DeFelipe, 1997). The horizontal projections form stripe-like vertical patches and have all the same qualities described in the C3a group.

In the isocortex, different populations of pyramidal neurons tend to project contralaterally as opposed to ipsilaterally. The contralateral projections arise mostly from C3b cells and target the spatially analogous region of cortex on the other side of the brain, while ipsilateral projections mainly arise from C3a and C56 (Soloway et al., 2002). The same C3b and C56 cells appear to be the dominant source of isocortex → periallocortex projections (Witter et al., 1989; Burwell, 2000), responsible for communicating representations in the isocortex to the hippocampus for association.

The C3b cells appear to preferentially stain for acetylcholine with C5p cells (Voytko et al., 1992; Hackett et al., 2001), and have been shown to have preferential connections with C5p cells (Thomson and Bannister, 1998; Briggs and Callaway, 2005). In the agranular primary motor cortex, all layers visually look like a combination of C3b and C5p cells of various sizes.

Historical note: In 1949, Lorente de No referred to the large cells above the granular layer as "*star pyramids*" and called the location "*layer 4a*" (Lorente de No, 1943). Today, the same cells are typically referred to as large pyramidal neurons in layer 3b. The usage of the terms "star" and "layer 4" to describe these cells appears to have caused subtle confusion throughout the years, including the target layer of specific thalamocortical projections. The confusion arises due to the modern descriptions of "stellate" cells in "layer 4α" or "4β" of primary visual cortex.

Viewpoint: Neuroanatomically, C3b appears to function as stable invariant perceptual representations in the cerebral cortex that are associated in short-term memory.

4.2.3. Hippocampus/allocortex

The hippocampus proper, called allocortex due to its lack of lamination and different appearance from isocortex, is a full circuit in and of itself (Amaral and Witter, 1989). The hippocampus is functionally dominated by the dentate gyrus (DG), CA3 fields, CA1 fields, and subiculum (Sb). A simplified feedforward picture shows the projection circuit loop as: isocortex → PH23 → Dentate Gyrus → CA3 → CA1 → Subiculum → PH56 → isocortex. Multiple feedback connections exist within this path (Amaral and Witter, 1989). The DG and olfactory bulb/subventricular zone are the only widely accepted brain structures consistently shown to contain adult neurogenesis (the new production of neurons) in the non-damaged primate brain (Gould, 2007). Thehippocampus essentially receives all the same subcortical input as parahippocampal cortex described above (Amaral and Cowan, 1980).

Viewpoint: Neuroanatomically, the hippocampus appears to associate perceptions in the isocortex through mapped representations in periallocortex based upon emotional context.

4.2.4. Perspective on short-term declarative memory

Our neuroanatomical perspective on the perihippocampal cortex and hippocampus are that they function to temporarily store short-term associations between isocortical perceptions that can later be consolidated into direct corticocortical long-term memory associations. The subcortical input to the peri-/allocortex being part of the emotional system would imply that the creation of associations is largely influenced by emotional significance. The functional flow of short-term memory information would appear to involve (see also **Figures 4** and **5**):

- Association (cortical area A and B) – active C3b perceptions in area A and B → activation PH23 A and B → binding in hippocampus. Additionally, PH23 A and B → PH56 A and B activations.
- Recall – active C3b perception in area A → PH23 area A → unbinding in hippocampus → PH56 area B → active C3b perception area B.
- Alternate recall – active C3b perceptions in area A → PH23 area A → PH56 area B → active C3b perception area B.

The idea of stable perceptions in the isocortex being associated in the hippocampus is consistent with the hippocampal indexing theory of episodic memory (Teyler and Rudy, 2007). The consolidation of indirect hippocampal short-term memory associations into direct corticocortical long-term memory associations involves the reactivation of short-term memory associations during sleep (O'Neill et al., 2010).

Historical note: A curious, rarely talked about cortical region next to the periallocortex and allocortex is the granulous retrosplenial (Rsc) cortex [von Economo area LE; Brodmann area 29]. The Rsc has laminar differentiation representative of primary sensory koniocortex and significant reciprocal projections with allo-/periallocortex and prefrontal cortex (Kobayashi and Amaral, 2003, 2007). Thus, Rsc could potentially be viewed as "primary memory cortex."

4.3. WORKING MEMORY/INFORMATION PROCESSING: CORTICO-THALAMOCORTICAL CIRCUIT

The definition of working memory is adopted from Monsell as "*no more (or less) than a heterogeneous array of independent temporary storage capacities intrinsic to various subsystems specialized for processing in specific domains*" (Monsell, 1984). Working memory operates on the time-scale at which attention can be maintained, seconds to minutes (Baddeley, 1981; Monsell, 1984). Experiments typically require participants to hold digits, numbers, or words in memory for future recall and measure the number of elements capably held in working memory (usually between 4 and 7 items). Monsell's definition is consistent with a localized neuroanatomical information processing architecture. We use the term *information processing* to describe the dynamic activation of perceptions

described by Monsell's "independent. . .subsystems. . .processing in specific domains."

Exactly how information is processed in the brain is still an open question. However, information processing in the brain has been correlated with various brain wave oscillations (Buzsaki, 2006). Synchronized information processing across distributed regions of primate cortex has been correlated with low gamma (25–60 Hz; Knight, 2007). Cortical electrophysiology recordings of humans undergoing neurosurgery also include distinct localized high gamma (80–160 Hz) frequencies during speech tasks (Edwards et al., 2005; Canolty et al., 2006).

States of being awake or asleep are definitive indicators of information processing in the brain, and interactions in the thalamus are highly correlated in the transition from sleep to wakefulness, and for correlations between gamma and slower oscillations (Steriade, 2006).

The interactions between the thalamus and cerebral cortex are therefore essential in gaining understanding into working memory and information processing.

4.3.1. Thalamus

The thalamus has a uniform organization and highly stereotyped reciprocal projections with the cerebral cortex. For the interested reader, the thalamic bible written by the late Jones (2007) is unparalleled in its descriptive depth of the thalamus. The thalamus is composed of multiple nuclei that can be identified histologically and by the source/target of their afferent/efferent projections (Macchi and Jones, 1997). The general organization of the thalamus leads us to divide the thalamus into three homotypical types: specific (Ts), intralaminar (Ti), and layer 1 projecting (TL1). The division into three types of thalamic projections is novel and imparts a functional perspective to the target laminar location of thalamic neurons. Although thalamic neurons undoubtedly project to multiple layers, usually via collateral projections, the first-order homotypical architecture of thalamic laminar projections warrants a division into three distinct (source thalamus – target cortical layer) combinations: Ts – layers 3/4, Ti – layers 5/6, and TL1 – layer 1. For the present circuit we only discuss the Ts projection.

4.3.2. Specific thalamus – Ts

Specific thalamic neurons project to the mid layers in the cerebral cortex. Ts thalamocortical projections are to lower layer 3b in primate isocortex, often avoiding layer 4 (Jones and Burton, 1976; Trojanowski and Jacobson, 1976; Giguere and Goldman-Rakic, 1988; Romanski et al., 1997; Rockland et al., 1999; McFarland and Haber, 2002; Jones, 2007), while only koniocortical projections are to layer 4 (Callaway, 1998). The Ts thalamocortical projection is localized ($<$ a few mm^2) and topologically organized in the cerebral cortex in accordance with the temporal development of projections (Kievit and Kuypers, 1977; Goldman-Rakic and Porrino, 1985; Baleydier and Mauguiere, 1987; Vogt et al., 1987; Brysch et al., 1990; Hohl-Abrahao and Creutzfeldt, 1991).

Historical note: The early work by Cajal and Lorente de No, along with the disproportionate amount of research dedicated to primary sensory areas, appears to have ingrained layer 4 as the generally taught location of specific thalamocortical projections. The notion that the Ts thalamocortical projections terminate in layer 4 must be updated throughout the neuroscience world to differentiate between koniocortex layer 4 and isocortex layer 3b terminations. As Ted Jones says "*Outside these areas [koniocortex]. . . thalamic fibers tend to avoid layer IV and terminate almost completely in the deeper half of layer III.*" p. 95 (Jones, 2007).

The Ts is composed of multiple histologically identifiable subnuclei that can be further subdivided based on afferent/efferent projections. We functionally separate the non-primary Ts into two main groups and adhere to Jones (2007) terminology. The ventral group is composed of the ventral anterior (VA) and ventral lateral (VL) nuclei. VA and VL (having subdivisions themselves; Macchi and Jones, 1997) generally project to the behavioral parts of the brain related to thinking (frontal cortex) and movement (motor cortex) respectively. We separate the ventral group from other Ts nuclei because of the afferent projections from the basal ganglia (Sidibe et al., 1997; Parent and Parent, 2004) and cerebellum (Sakai et al., 1996; Hamani et al., 2006), both involved in controlling thinking and movement. The second non-primary Ts group of nuclei are composed of nuclei related to more sensory (as opposed to behavioral) regions of the brain. The pulvinar (P) and lateral posterior (LP) nuclei can be generally grouped (anatomically/functionally) and largely project to temporal and parietal isocortex. The anterior (A) and the lateral dorsal (LD) complex can be similarly grouped and are largely connected to cingular and retrosplenial cortex. Note the challenges in nuclei naming conventions, e.g., the lateral nuclei not being grouped together.

Viewpoint: Neuroanatomically, the specific thalamus appears to drive the convergent reentrant selection of C3b and C6t perceptual representations in cortico-thalamocortical oscillations.

4.3.3. Cortical pyramidal layer 6 thalamic projecting – C6t

Cortical C6t cells have a neuroanatomical organization highly linked to Ts projections. C6t cells send both apical dendrite and intracortical axon projections to layer 3b in the isocortex (Jones and Wise, 1977; Lund et al., 1981; Peters et al., 1997; Rockland and Ichinohe, 2004) and layer 4 in koniocortex (Briggs and Callaway, 2001). The C6t cell projections leaving the cortex target local regions of the Ts in a reciprocal manner (Trojanowski and Jacobson, 1977; Catsman-Berrevoets and Kuypers, 1978; Asanuma et al., 1985; Giguere and Goldman-Rakic, 1988; McFarland and Haber, 2002). Note the anatomical reentrant blueprint specifying that C6t intracortical axons/dendrites target the same cortical layer receiving Ts projections.

Viewpoint: Neuroanatomically, C6t appears to function in conjunction with C3b and Ts to facilitate cortico-thalamocortical oscillations.

4.3.4. Thalamic reticular nucleus – TRN

The TRN is a thin shell of GABAergic neurons surrounding the entire thalamus (Scheibel and Scheibel, 1966). The majority of TRN afferent connections arise from ascending Ts and descending C6t projections (Jones, 1975). Different sizes of axonal boutons (small and large) in the TRN have been correlated with source cortical topology and layer (L6 and L5) respectively (Zikopoulos and Barbas, 2006). The TRN then projects directly onto the Ts in an inhibitory manner (Scheibel and Scheibel, 1966; Velayos et al.,

1989). Other projections to the TRN include cholinergic projections from the brainstem as shown in the cat (Pare et al., 1988) and GABAergic projections from the basal ganglia GPe in the monkey targeting the ventral thalamic region (Asanuma, 1994).

Viewpoint: Neuroanatomically, the TRN appears to function in gating thalamocortical information to regulate cognitive states.

4.3.5. Perspective on working memory and information processing

Our neuroanatomical viewpoint is that working memory and associated gamma frequency information processing is the result of attentionality directed cortico-thalamocortical oscillations. We hypothesize that information processing involves the competitive selection (activation) of perceptions (cell assemblies) driven by the Ts → C3b → C6t → Ts circuit. Working memory would involve the maintenance of active perceptions in each localized thalamocortical loop, explaining both the distributed nature of working memory, the constraints on the number of items stored, the need for attention, and the competitive interaction between domain specific information. The source and mechanism of attentional control are highlighted in the control circuit.

Additional neuroanatomical evidence is consistent with our hypothesis. In the human, the distance between the cerebral cortex and the thalamus is approximately 20–50 mm (Nolte and Angevine, 2000). Typical conduction velocities throughout the brain might be regulated from 1 to 50 mm/ms depending on myelination (Kimura and Itami, 2009). Human thalamocortical conduction velocity has been estimated at 29 mm/ms (Kimura et al., 2008). The cortico-thalamocortical physical distances combined with conduction velocity and short delays in neuronal firing (1–8 ms) are consistent with a circuit level cortico-thalamocortical reentrant explanation for gamma frequency information processing oscillations in the brain. Spiking neuroanatomical models have been built supporting our hypothesis (Solari, 2009). This is in contrast to most other models of working memory that have focused on intrinsic properties of interneurons or intracortical activity without regard to the thalamus (Compte et al., 2000; Durstewitz et al., 2000; Brunel and Wang, 2001).

4.4. BEHAVIORAL MEMORY ACTION SELECTION: CORTICO-BASAL GANGLIA-THALAMOCORTICAL CIRCUIT

In contrast to declarative memory other psychological evidence highlights memory systems more highly involved in the learning of actions and behaviors. We utilize Squire's description that "*[procedural memory] is expressed through performance rather than recollection... the memories are revealed through reactivation of the systems within which the learning originally occurred*" (Squire, 2004). A distinguishing feature of procedural memory is that through practice and repetition, behavioral memories (i.e., actions) can be learned and executed without declarative recall of how the action was learned. Another term often used is skill learning. We use the term *behavioral memory* to include all behavioral actions generated by homotypical circuits including externally measurable procedural memory and internal procedural thought processes. Behavioral memory systems have been elucidated in patients like H.M., patients with Alzheimer's and in patients with Parkinson's and Huntington's disease (Heindel et al., 1989). For example, the behavioral effects of Parkinson's disease typically progress from motor movement rigidity, postural instability and tremor to cognitive apathy and diminished novelty seeking (Lauterbach, 2005). Huntington's disease on the other hand typically begins with chorea (initiated dance-like movements that flow from start to finish without stopping) and progress to cognitive dysfunctions impairing organizing, planning, or adapting alternatives (Walker, 2007). Parkinson's and Huntington's disease both involve degeneration of different parts of the basal ganglia, highlighting the role of the basal ganglia in behavior selection. The basal ganglia is highly involved in the action based reward system through increases and decreases in dopamine (Bromberg-Martin et al., 2010).

4.4.1. Basal ganglia

The basal ganglia is a structure that is essential for learning and coordination in movement and cognition (Doya, 1999; Benke et al., 2003; Lauterbach, 2005; Van Essen, 2005). The basal ganglia is composed of multiple subnuclei. The historical naming of the basal ganglia does not make the homotypical groupings intuitive. The striatum, containing GABAergic projection neurons, is the dominant input structure and is comprised of the putamen, caudate, and nucleus accumbens (also called the ventral striatum). The globus pallidus external segment (Gpe), referred to only as the globus pallidus in the mouse, dominates the internal circuitry of the basal ganglia. The globus pallidus internal segment (Gpi) and substantia nigra pars reticulata (Snr) form a spatially disjoint but functionally singular GABAergic output structure of the basal ganglia (Gpi/Snr). The subthalamic nucleus (Stn) provides glutamatergic excitatory input to multiple elements in the basal ganglia. The substantia nigra pars compacta (Snc) provides dopaminergic input to the striatum, the damage of which is the source of Parkinson disease. Huntington's disease involves the degeneration of the striatum progressing from motor (putamen) to cognitive (caudate) deficits (degeneration; Heindel et al., 1989). The same correlations between motor/cognitive deficits and putamen/caudate dysfunction is found in Parkinson's (Lauterbach, 2005).

The projections through the basal ganglia are organized into parallel, yet overlapped pathways from the entire isocortex (Smith et al., 1998, 2004) forming a homotypical architecture. Primary auditory and visual cortex are the only cortices that do not project to the basal ganglia in the monkey (Borgmann and Jurgens, 1999). Most nuclei in the basal ganglia rely on GABA as a neurotransmitter forming a consistent disinhibitory functional pathway. The GABAergic neurons in the basal ganglia are inherently tonically active and do not require input to continually fire action potentials. Based on neuron number, a significant amount of neural convergence occurs from input to output through the basal ganglia. The human and rat striatum have about 70 M and 2.8 M neurons respectively (Oorschot, 1996; Kreczmanski et al., 2007). In both species the number of neurons decrease approximately 50 to 1 (striatum → Gpe) and 2 to 1 (Gpe → Gpi/Snr; Oorschot, 1996; Hardman et al., 2002), resulting in a 100 to 1 neural convergence of basal ganglia input to output.

Several excellent reviews of the basal ganglia and dopamine system exist (Herrero et al., 2002; Haber, 2003; Lee and Tepper, 2009; Gerfen and Surmeier, 2010).

4.4.2. Striatum matrix and patch – Sm and Sp

The striatum can be divided into histologically defined compartments called the matrix (matrisome) and patch (striosome). Among other factors, the matrix compartments have high cholinesterase activity, while patches are enriched in enkephalin (i.e., endorphins; Gerfen, 1984). The striatum contains multiple interneurons containing both GABA and acetylcholine forming distinct intrastriatal networks (Kawaguchi et al., 1995).

The matrix compartments of the striatum receive projections from C5s neurons across the entire isocortex (Jones et al., 1977; Arikuni and Kubota, 1986; Kunishio and Haber, 1994; Yeterian and Pandya, 1994). The cortical projections are topographically mapped (Alexander et al., 1986). In general the striatum receives reciprocal projections back from the thalamic nuclei that it projects to. The intralaminar thalamus projects topographically onto the striatum with the rough order CM → putamen, PF → caudate, midline → ventral striatum (Sadikot et al., 1992a,b; Tande et al., 2006). The ventral thalamus also projects back onto the striatum (McFarland and Haber, 2001).

- SmD1 neurons are GABAergic spiny projection neurons found within the matrix portion of the striatum that express dopamine D1 receptors. The effect of dopamine on SmD1 neurons increases excitability (Surmeier et al., 2007). SmD1 is traditionally considered part of the *direct* pathway through the basal ganglia because of its projections to Gpi/Snr (Levesque and Parent, 2005b). The projection is topographically maintained from the striatum to Gpi/Snr (Haber et al., 1990).
- SmD2 neurons are GABAergic spiny projection neurons found within the matrix portion of the striatum that express dopamine D2 receptors. The effect of dopamine on SmD2 neurons decreases excitability (Surmeier et al., 2007). SmD2 is traditionally considered part of the *indirect* pathway through the basal ganglia because of its projections to the Gpe (Haber et al., 1990; Levesque and Parent, 2005b).
- Sp neurons are GABAergic spiny projection neurons found in the patches of the striatum and project prominently to the Snc (Haber et al., 1990; Fujiyama et al., 2011). The Sp send smaller numbers of axon collaterals into the Gpe and Gpi/Snr (Levesque and Parent, 2005b). In contrast to the matrix, the patch compartments receive their input from C5p neurons in the isocortex (Gerfen, 1984, 1989).

Viewpoint: Neuroanatomically, SmD1 appears as a C5s cortically evoked start action mapping through the disinhibitory direct pathway SmD1 → Gpi/Snr learned from positive dopamine reinforcement. SmD2 appears as a C5s cortically evoked stop action mapping through the dual disinhibitory-disinhibitory indirect pathway SmD2 → Gpe → Gpi/Snr or the feedback pathway SmD2 → Gpe → SmD1 learned from negative dopamine reinforcement. Sp appears as a C5p cortically evoked dopamine based learning signal via the Sp → Snc pathway in order to reinforce the two Sm pathways.

4.4.3. Globus pallidus external segment – Gpe

The Gpe neurons are GABAergic neurons that primarily receive inhibitory projections from the SmD2 portion of the striatum (Haber et al., 1990; Levesque and Parent, 2005b) and excitatory projections from the STN (Parent et al., 1989; Nambu et al., 2000). Gpe neurons project onto the Gpi/Snr, Stn, and send feedback connections onto the matrix portion of the striatum (Sato et al., 2000).

A potentially significant but rarely mentioned projection is the Gpe projection to the TRN of the ventral thalamus (Hazrati and Parent, 1991b; Gandia et al., 1993; Asanuma, 1994). Since the TRN provides inhibitory input to the thalamus, the Gpe projection to the TRN might be functionally analogous to the Gpe projection to the inhibitory Gpi/Snr that then projects onto the thalamus.

4.4.4. Globus pallidus internal segment/substantia nigra pars reticulata – Gpi/Snr

The Gpi/Snr is the source of the major GABAergic output from the basal ganglia. The Gpi and Snr are physically separated nuclei, with the Snr located adjacent to the Snc (hence the naming convention). However, from a neuroanatomical perspective these structures are functionally equivalent. The Gpi/Snr receives afferent input from all other basal ganglia nuclei, including the matrix striatum (Haber et al., 1990; Levesque and Parent, 2005b), the Gpe (Sato et al., 2000), the STN (Levesque and Parent, 2005a), and collateral projections from the Snc (Charara and Parent, 1994; Zhou et al., 2009).

The Gpi/Snr is tonically active (Zhou et al., 2009) and projects onto the intralaminar thalamus in a topographic pattern (Parent et al., 2001; Sidibe et al., 2002; Parent and Parent, 2004). The Gpi/Snr also send significant projections onto the ventral thalamus including TL1 (Hazrati and Parent, 1991a; Sidibe et al., 1997).

Viewpoint: Neuroanatomically, the Gpi/Snr appears to perform precise temporal action triggering in the intralaminar and ventral thalamus through disinhibition.

4.4.5. Subthalamic nucleus – STN

The STN is the only excitatory nucleus in the basal ganglia and utilizes glutamate as a neurotransmitter. The STN appears to receive an excitatory topographically mapped isocortical afferent input from C5p neurons (Nambu et al., 2000; Parent and Parent, 2006) as well as inhibitory input from the Gpe (Sato et al., 2000). The STN projects prominently onto the Gpi/Snr and to the Gpe (Parent et al., 1989; Nambu et al., 2000). The STN also contains inhibitory GABAergic interneurons (Levesque and Parent, 2005a).

Viewpoint: Neuroanatomically, the STN appears to provide a direct cortical mechanism to stop action triggering in the intralaminar thalamus through exciting the Gpi/Snr. A contrary hypothesis might suggest that the STN "prepares" desired output actions in Ti through increased inhibitory stimulation by the Gpi/Snr biasing future inhibitory rebound spikes.

4.4.6. Substantia nigra pars compacta – Snc

The Snc is the source of dopaminergic projections in the basal ganglia. The Snc receives its major afferent input from the patch compartments in the striatum (Gerfen, 1984; Fujiyama et al., 2011). The Snc is tonically active and receives additional inhibitory input from virtually all other structures in the basal ganglia (Lee and Tepper, 2009). The Snc projects onto the matrix compartment of the striatum (Langer and Graybiel, 1989; Matsuda et al., 2009; Gerfen and Surmeier, 2010).

Viewpoint: Neuroanatomically, the Snc appears to provide a differential dopamine reward signal to the striatum to learn start and stop action sequences.

4.4.7. Intralaminar thalamus – Ti

The intralaminar thalamus is composed of the center median (CM), parafascicular (PF), and midline nuclei (Jones, 2007). The midline nuclei are usually further subdivided into the central medial, paracentral, central lateral, and rhomboid nuclei. The intralaminar nuclei output topographic projections to both the striatum and to the lower layers of the isocortex (Brysch et al., 1984; Sadikot et al., 1992a,b; Tande et al., 2006). In a gross topographic organization, PF is associated with frontal cortex and the caudate, CM with motor cortex and the putamen, and midline with cingular cortex and the nucleus accumbens. Ti projects dominantly to lower layers 5/6 in the cerebral cortex (Herkenham, 1980). The most compelling evidence confirming this fact in primates comes from single-axon tracing studies in the monkey that undeniably demonstrate the majority of intralaminar (CM/PF) projections principally terminate in layers 5/6 with fewer collateral projections to layer 1 (Parent and Parent, 2005). The Ti nuclei projections are largely segregated into those that project exclusively to the cerebral cortex and those that project to the matrix portion of the striatum (Parent and Parent, 2005).

Historical note: The intralaminar nuclei of the thalamus were originally thought to provide the majority of the "non-specific" diffuse layer 1 input in the cerebral cortex identified by Lorente de No in the 1940s (Lorente de No, 1943). In the 1950s, research focused on understanding the cortical "recruiting response" due to intralaminar electrode stimulation (Hanbery and Jasper, 1953, 1954). The recruiting response (most studied in cats) requires pulsed thalamic stimulation of 3–10 Hz (Verzeano et al., 1953). After tens of milliseconds, strong surface negative wave potentials would appear across widespread cortical areas. The widespread nature of the recruiting response was attributed to the thalamocortical layer 1 projections described by Lorente de No. The measured recruiting response is more widespread than Ts stimulation but topographically organized, which is consistent with the intralaminar topographic projection. Today, a more anatomically consistent viewpoint is that the recruiting response involves Ti-C5s-basal ganglia-Ti and/or Ti-basal ganglia-Ti-cortical circuits that prominently involve the lower layers of the cerebral cortex rather than layer 1. Future experiments are necessary for any definitive conclusion.

Viewpoint: Neuroanatomically, the intralaminar thalamus appears to excite the behavioral output of the lower layers of the cerebral cortex to accurately select C5p output and drive cortically evoked behaviors.

4.4.8. Cortical pyramidal layer 5 striatally projecting – C5s

C5s are pyramidal neurons in the isocortex that principally project to the striatum. C5s pyramidal neurons are typically located in the upper portion of layer 5, L5a, with a prominent ascending dendrite that arborizes in L1 (Jones et al., 1977; Arikuni and Kubota, 1986; Yeterian and Pandya, 1994). C5s send projections to the matrix portion of the striatum (Jones and Wise, 1977; Gerfen, 1989; Parent and Parent, 2006). C5s neurons are likely the source of cortical projections to Ti that are distinct from C6t projections in the monkey (Catsman-Berrevoets and Kuypers, 1978) and cat (Kakei et al., 2001). C6t thalamic terminations are small and dense, while C5s synaptic terminals are large and sparse (Rouiller and Durif, 2004). The large terminals found in the TRN are likely a result of C5s collaterals (Zikopoulos and Barbas, 2006). In the rat, C5s and C5p neurons have been shown to be distinct populations (Levesque et al., 1996; Molnar and Cheung, 2006), with C5s having a higher probability of recurrent C5s → C5s connections (Morishima and Kawaguchi, 2006). L5a intracortical projections have distant ∼1–2 mm projections in layers 2/3a, and slightly longer projections within the same layer 5a (Levitt et al., 1993; Kritzer and Goldman-Rakic, 1995).

Viewpoint: Neuroanatomically, C5s appears to encode suggested action sequences within a cortical module for selection in the basal ganglia.

4.4.9. Perspective on behavioral memory action selection

The basal ganglia receives topographic projections from the entire isocortex, which has lead to the notion of separate functional loops through the basal ganglia (Smith et al., 1998, 2004; Haber, 2003). We differ in our assessment of the anatomical facts and hypothesize that the pathway through the basal ganglia has a single uniform function, with the only difference being the cortical source of information that is operated on. Functionally, the output from the Gpi/Snr to the thalamus is tonically inhibitory. Therefore, processing in the basal ganglia ultimately results in disinhibition of the thalamus for causal effect. One view of disinhibition is allowing target neurons to be excited. Another view of disinhibition is causing neurons to fire precise rebound spikes as a result of release from inhibition (Grenier et al., 1998). The evidence suggests that the basal ganglia is responsible for learning to select sequences of precise on/off action triggering (Bottjer, 2005). The evolution of the coordinated control of muscles and muscle groups in early ancestral vertebrates requires this exact on/off mechanism of learning. A hierarchical information structure, like the cerebral cortex and topographic striatal mapping, operating at different time-scales would enable enormous combinatorial flexibility of cognitive behavior just as with movement.

If the basal ganglia is responsible for action selection, then the near 100 to 1 neural convergence from the striatum to the Gpi/Snr complex implies a reduced set of output action possibilities compared to input action suggestions. The basal ganglia is likely capable of storing temporally sequenced actions (or cortical locations) through its internal circuitry. In this case, the 100 to 1 convergence may serve to encode temporal sequences of actions represented by C5s that are translated into disinhibition of singular actions in Ti in a sequential manner. The utilization of two prominent dopamine systems, D1 and D2, would serve to encode coupled starting and stopping actions respectively (Apicella, 2007). The increase (reward) or decrease (anti-reward) of dopamine would then serve to reinforce start and stop sequences.

The projection from the cerebral cortex C5p neurons to the patch portion of the striatum is significant because of the indirect effect on dopamine release via the Snc. The same C5p neurons appear to project to the STN, creating a significant path of primarily stopping actions (increased activity of STN), while simultaneously generating an anti-reward signal (increased inhibition of the Snc) to prevent that same future behavior.

4.5. BEHAVIORAL MEMORY OUTPUT: CORTICO-PONTINE (CORTICO-SUBCORTICAL) CIRCUIT

Behavior involves not only an organisms externally observable movement, but also its internal cognitive processes. During evolution, the same circuits that regulated muscles through the spinal chord in early vertebrates were re-directed to target internal brain structures (Striedter, 2005). We focus here on neuronal groups known to be involved in behavioral movement and their parallel internal connectivity presumably involved in behavioral cognitive processes.

In all vertebrates, motor neurons in the spinal chord project acetylcholine onto muscles to make them contract (Lieber, 2002; Striedter, 2005). In higher mammals projections from large neurons in lower layer 5 (C5p) of primary motor cortex directly target alpha-motor neurons in the spinal chord (Stanfield, 1992). Lesions to primary motor cortex in the human cause complete paralysis of the body associated with the cortical lesion (Penfield and Rasmussen, 1968).

To neuroanatomically understand behavioral output, we focus on the C5p neuron and the correlates to acetylcholine systems in the brain that appear to be phylogenetically involved in movement.

4.5.1. Cortical pyramidal layer 5 pons projecting – C5p

The C5p population refers to the collection of primarily pons (and other subcortically) projecting pyramidal cells found throughout the entire isocortex (Hackett et al., 2001; Watakabe et al., 2007). C5p neurons are located in layer 5b (Foster et al., 1981), have large dendritic tufts in layer 1, and are distinct from C5s neurons (Molnar and Cheung, 2006; Morishima and Kawaguchi, 2006). The C5p intracortical projections are not extensive, often restricted to short distances in layer 5 (Ghosh and Porter, 1988), however their dendritic arborization is quite large. Generally, the largest neurons in the isocortex are C5p neurons and in primary motor cortex C5p neurons are referred as large Betz cells (Braak and Braak, 1976). Since the majority of C5p neurons target the pons (relaying information to the cerebellum), we suggest that the cognitive function of C5p neurons may be inferred through analogy with Betz cells in primary motor cortex. The projections from C5p neurons in primary motor cortex synapse directly with the spinal chord causing physical movement (Stanfield, 1992). The direct projection to the spinal chord is weak in lower mammals, but becomes increasingly prominent in primates, and presumably dominates in humans, suggesting an increasingly more direct cortical involvement in behavior (Lemon and Griffiths, 2005). C5p projections from frontal cortex target the STN of the basal ganglia with collaterals to the striatum (Nambu et al., 2000; Parent and Parent, 2006). Evidence suggests that C5p striatal projections target the Sp patch (striosome) portion of the striatum that projects to the dopamine filled Snc (Gerfen, 1984, 1989).

The origin of C5p afferent input should provide a clue to the synaptic organization of cognitive and physical behavior memory output throughout the brain. A synaptic relationship exists between C3b and C5p neuronal groups because of a preference for direct synaptic connections from C3b to C5p neurons potentially related to basal forebrain acetylcholine activity (Thomson and Deuchars, 1997; Thomson and Bannister, 1998; Kaneko et al., 2000).

Viewpoint: Neuroanatomically, C5p neurons appear to form the physical and cognitive behavioral output of the cerebral cortex.

4.5.2. Basal forebrain – BF

Acetylcholine is found in primarily three populations of neurons in the brain: alpha-motor neurons, interneurons in the striatum, and the basal forebrain including the nucleus of Meynert (Satoh and Fibiger, 1985). Basal forebrain lesions "*abolish cortical plasticity associated with motor skill learning*" (Conner et al., 2003). Large lesions of the basal forebrain in the rat have resulted in deep coma consistent with the disruption of behavioral output (Fuller et al., 2011). Acetylcholinesterase staining typically stains layer 1 of most cortices, therefore the BF projection appears to primarily target layer 1 of most of the cortex (Bigl et al., 1982). In monkey and human cortex, C3b and C5p neurons appear to preferentially stain for acetylcholinesterase suggesting a prominent utilization of acetylcholine (Bravo and Karten, 1992; Voytko et al., 1992; Hackett et al., 2001).

Viewpoint: Neuroanatomically, the basal forebrain appears to provide cholinergic input to the cerebral cortex to learn and activate an output behavior mapping between C3b and C5p neurons.

4.5.3. Perspective on behavioral memory output

Within a homotypical cognitive architecture, if C5p neurons are a form of behavioral output in motor cortex they are a form of behavioral output in the rest of the isocortex. Similarly, if spinocerebellar signals communicate body movement/posture information states to the cerebellum, then C5p projections to the cerebellum through the pons may communicate analogous cognitive information states from brain (Doya, 1999). Combining the two analogies we hypothesize the C5p group provides a behavioral output *predicting* desired future coordinated behaviors. Motor cortex would communicate physical behaviors for the nervous system to operate on, while other isocortical regions would communicate cognitive or perceptual behaviors to various subcortical structures.

The neuroanatomical evidence suggests that acetylcholine delivered by the basal forebrain is critical for the activation and learning of a mapping between C3b and C5p neurons, and that this mapping is the source of cortically learned behavior output and/or skill learning. The relationship of C5p neurons to C3b populations is significant because the C3b population appears to be centrally located in nearly all circuits. Therefore a direct mapping, driven by acetylcholine projections, from stable C3b perceptions to C5p behavior output can be developed over time exclusively in the cerebral cortex.

4.6. COGNITIVE CONTROL: LAYER 1 THALAMOCORTICAL PROJECTION CIRCUIT

Nervous systems evolved to control muscles through structures like the basal ganglia and cerebellum (Striedter, 2005). Muscles are widely distributed throughout the body, but must be controlled in a coordinated manner. Human cognition, evolving from the same circuitry, is certainly controlled too. However, the neuroanatomical mechanism underlying cognitive control is still an open question.

Along with the basal ganglia, the cerebellum is another structure critical for smooth control of movement and cognition (Ramnani,

2006). Lesions to the cerebellum often produce dysmetria (lack of coordination of movement) and cerebellar cognitive dysfunction has been described as "*dysmetria of thought*" (Wolf et al., 2009). By psychological analogy movement and cognition appear to be functionally controlled in the same way.

4.6.1. Cortical layer 1 – L1

Layer 1 of the cerebral cortex, referred to as the molecular layer, lies closest to the pial surface of the brain. The only neurons in L1 are inhibitory Cajal-Retzius cells containing long horizontal axons (Conde et al., 1994; Gabbott and Bacon, 1996; Cajal, 2002). L1 is composed of a dense plexus of dendritic tufts of pyramidal neurons combined with axons from cortical and subcortical origin. Many non-glutamate neurotransmitters systems (serotoninergic, adrenergic, cholinergic) appear to target the lower portions of layer 1 (Eickhoff et al., 2007). The dense plexus of dendrites in L1 provides the opportunity for a given axon terminating in L1 to effect pyramidal neurons throughout all layers. The cortical pyramidal neurons consistently demonstrating prominent L1 apical dendritic tufts are C2, C3a, C3b, C5s, and C5p.

Viewpoint: Neuroanatomically, cortical layer 1 appears to be a plexus of dendrites and axons where a single-axon projection can easily influence or activate multiple pyramidal neurons in different cortical layers to control a functional module.

4.6.2. Thalamocortical layer 1 projections – TL1

Herkenham first described a localized region of the thalamus in the mouse, VM, that projected diffusely to layer 1 of nearly the entire cerebral cortex (Herkenham, 1979, 1980). The projection has a decreasing density gradient from frontal cortex (cognitive) to parietal cortex (sensory). Other studies in the rat definitively confirm the VM → L1 projection (Arbuthnott et al., 1990; Mitchell and Cauller, 2001). The ventral thalamus in the monkey has significant projections to layer 1 (Nakano et al., 1992; McFarland and Haber, 2002). However, a localized thalamic L1 projection nuclei has not been directly looked for in primates and we use the nuclei VAmc/VM to estimate the localized thalamic TL1 projection source occurring near the mammillothalamic tract that presumably exists in the primate (human). The VAmc/VM nuclei receive projections from the Gpi/Snr and the cerebellum (Sidibe et al., 1997; Parent et al., 2001; Francois et al., 2002) and send projections back to the striatum (McFarland and Haber, 2001). As part of the reticular activating system the ventral (and other thalamic nuclei) receive afferent cholinergic projections from the brainstem (Steriade et al., 1988). We include in the TL1 definition the more sparsely distributed layer 1 projecting *thalamic matrix* described by Jones (1998).

Historical Note: One of the most perplexing thalamic projections has been the non-specific thalamocortical layer 1 projection described by Lorente de No in the 1940s (Lorente de No, 1943). The intralaminar thalamic nuclei have long been thought to supply the layer 1 projection, but given the infragranular (L5/6) targets of Ti that appears unlikely today (Parent and Parent, 2005). Ironically, the discovery of the actual source of these layer 1 projections was surely, albeit unknowingly, discovered in the early electrophysiology intralaminar recruiting response experiments in cats (Hanbery and Jasper, 1953). Hanbery and Jaspers "*discovered a portion of the diffuse projection system which behaves quite differently from [the traditional recruiting response]. In. . .VA. . .we have obtained diffuse short latency cortical responses in response to a single shock. . .We seem to be stimulating here. . .a short latency diffuse projection system, which actually does not give true recruiting responses of the type presumably characteristic of the intralaminar system*" (Hanbery and Jasper, 1953). A focused experiment to directly test for this projection in the primate would be fruitful for neuroscience.

Viewpoint: Neuroanatomically, the layer 1 thalamic projection appears to provide short latency cortical stimulation across widespread areas to activate and control cortical information processing.

4.6.3. Metencephalon – pons, cerebellum

The metencephalon primarily includes the pons, cerebellum, and deep cerebellar nuclei. The pons receives nearly all its afferent projections from the isocortex and sends nearly all its efferent output to the cerebellum (Brodal and Bjaalie, 1992). This close relationship is demonstrated by the tight correlated volumetric evolution between the pons and cerebral cortex across species. The pons accounting for 6% of the brainstem in prosimians, 11–21% in monkeys and 37% in humans (Brodal and Bjaalie, 1992). As discussed, the pons receives its cortical projection from the C5p cells from nearly the entire cerebral cortex (Brodal, 1978; Leichnetz et al., 1984; Glickstein et al., 1985). A few prefrontal and temporal cortical regions in the primate do not appear to project to the pons (Schmahmann and Pandya, 1995). The pons then continues to project topographically onto the cerebellum (Kelly and Strick, 2003). The output of the cerebellum arises from inhibitory Purkinje cells that target the deep cerebellar nuclei (DCN; Ramnani, 2006). Therefore, like the basal ganglia, the cerebellum functions on the principle of disinhibition. A detailed cerebellum review is useful for understanding the internal cerebellar circuitry (Voogd, 2003). The output of the DCN is an excitatory glutamatergic projection targeting predominantly the ventral thalamus (Sakai et al., 1996). The cortico-cerebellar-thalamocortical circuit results in closed loop topographic projections to wide areas of the frontal, temporal, and parietal cortices (LeVay and Sherk, 1981; Kelly and Strick, 2003).

Viewpoint: Neuroanatomically, the pons integrates and transmits cortically evoked C5p output to the cerebellum. The cerebellum appears to be a control system for fine tuning and stabilizing sequences of movement and cognitive behaviors through the ventral thalamus.

4.6.4. Perspective on cognitive control

We present the hypothesis that cognition is fundamentally controlled via the TL1 thalamocortical projection system. We hypothesize all thalamocortical layer 1 projections have a similar functional role in cognitive control through the activation of cortical modules to drive cortico-thalamocortical information processing and working memory. While the VAmc/VM nuclei might be considered "centralized control," the matrix layer 1 projections from other distributed thalamic locations might be considered "local feedback control."

By analogy, if alpha-motor neurons activate individual muscles and TL1 projections activate individual cortical modules, then the TL1 projecting neurons might be considered "alpha-motor neurons of thought." If a cortical region like Brodmann's area 8 or 9 targets this region with cortico-thalamocortical C6t projections then that region might be considered "primary thought cortex." Human lesion studies to these areas resulting in the elimination of voluntary cognitive processes are consistent with this hypothesis (e.g., patient M.F.; Penfield and Rasmussen, 1968). Multiple experiments could be created to test this hypothesis in the primate, all beginning with first locating the exact thalamic region capable of exciting diffuse surface wave potentials described by Hanbery and Jasper (1953). With the region identified through electrophysiology, behavioral effects of stimulation or lesions can be tested, and the exact afferent/efferent cortical laminar projections can be determined through tracing studies.

4.7. CORTICAL INFORMATION FLOW REGULATION: CORTICO-CLAUSTRAL-CORTICO CIRCUIT

The claustrum and related circuitry is one of the least understood functionally. The most prominent ideas implicating the claustrum in the integration of conscious precepts (Crick and Koch, 2005).

4.7.1. Claustrum – CM

The claustrum is located midway between layer 6 of insular cortex (from which it breaks off early in brain development) and the striatum. Debate is ongoing on whether the claustrum's developmental origin is cortical, striatal, or a hybrid (Edelstein and Denaro, 2004).

Projections from the claustrum target nearly the entire brain, with little segregation of projections in the claustrum (Tanne-Gariepy et al., 2002). Claustrum projections travel through the external capsule and appear slightly biased to cognitive and cortical control centers of the brain (Molnar et al., 2006). The projections from the claustrum terminate mostly in layer 4 and appear to preferentially target inhibitory neurons, possibly chandelier cells with axoaxonic terminals (LeVay and Sherk, 1981; LeVay, 1986).

Viewpoint: Neuroanatomically, the claustrum appears to integrate cortical information from C6m neurons and provide feedforward excitatory input to inhibitory neurons in L4 of the cerebral cortex.

4.7.2. Cortical layer 6 claustrum projecting – C6m

The claustrum receives projections from virtually the entire cortex in a topographic, but largely overlapped fashion (Pearson et al., 1982). The projections from cortex originate from C6m neurons, which are distinct from C6t neurons in the cat (Katz, 1987). Apical dendrites of these neurons typically arborize directly below layer 4 in the upper part of layer 5 (Lorente de No, 1943; Soloway et al., 2002). Occasionally collaterals of C5s neurons are found in the claustrum (Parent and Parent, 2006).

Viewpoint: Neuroanatomically, C6m appears to function in coordination with C5s neurons to integrate action suggestions for transmission to the claustrum.

4.7.3. Perspective on the claustrum

The claustrum's functional connections are suited to regulate the flow of information between wide areas of the cortex, potentially through the excitation of inhibitory chandelier type cells. Activation of inhibitory chandelier cells would immediately prevent the transmission of action potentials from active neurons in layers 3–5 without reducing the excitation of the neuron. Notable is the C6m dendritic and axon projections to layer 5a containing C5s striatally projecting cells. The additional relationship of the claustrum to striatally projecting neurons further implies, through analogous function, selection and/or gating of information.

5. SUMMARY PERSPECTIVE ON NEUROANATOMICAL INFORMATION FLOW

Figure 5 shows the hypothesized organization of seven circuits viewable from two perspectives: circuit development and information flow. As a summary, we hypothesize a simplified but comprehensive cognitive framework mutually consistent with the summarized neuroanatomical facts. Rather than being exhaustive, **Figure 5** and each outline attempt to deliver the gist of information flow as a conceptual framework. All colors correspond to **Figure 5**. Each hypothesis is best viewed as a focused question of interest within the field of neuroanatomy and suitable for the topic of a graduate student's dissertation.

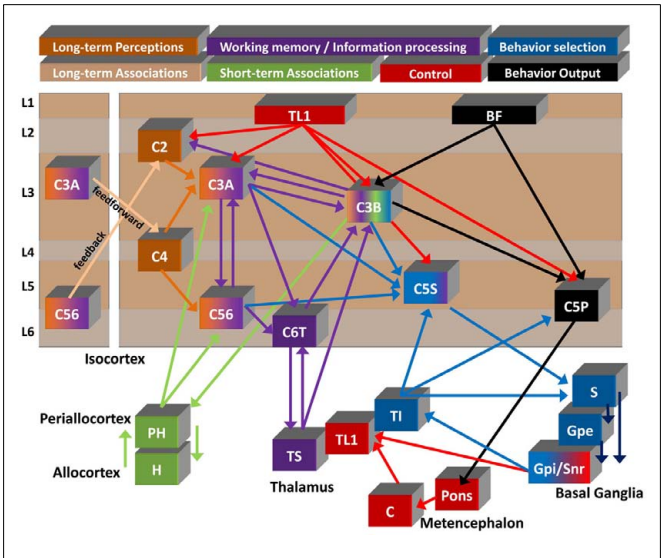

FIGURE 5 | Summary diagram of proposed flow of cognitive information. Seven of the circuits described in the text are shown to illustrate a summarized functional viewpoint of the hypothesized flow of information. Generally information flows from left to right through the color coded circuits. Circuit names and colors are represented at the top. Long-term memory is split into "perceptions" and "associations" as discussed in 4.1. Information flow details are describe in the text. Cortical neuron x (Cx), Parahippocampal gyrus (PH), Hippocampus (H), Specific thalamus (Ts), Layer 1 projecting thalamus (TL1), Intralaminar thalamus (Ti), Cerebellum (C), Striatum (S), External segment globus pallidus (Gpe), Internal segment globus pallidus (Gpi), Substantia nigra par reticulata (Snr), Basal forebrain (BF; note: the basal forebrain is placed in layer 1 to demonstrate the primary target of its projections).

5.1. PERSPECTIVE ON COGNITIVE DEVELOPMENT

We briefly hypothesize the development of the circuits in the maturing brain in relation to **Figure 5**.

- Layer 4 feedforward projections drive the formation of perceptual cell assemblies in C3a and C56 (orange).
- Critical periods first regulate the formation of cell assemblies within and between neuronal groups C3a and C56, followed by C3b and C6t (orange/purple).
- Stable invariant C3b representations are simultaneously formed through intercortical C4 feedforward and C2 feedback influence and C3a intracortical input (orange/purple/green).
- Stable C3b representations in different cortical modules are associated when temporally coactive in the hippocampus (green).
- During sleep cycles most behavioral selection (blue) and behavior output (black) circuits are shut down and working memory (purple) and short-term memory circuits (green) are active in order to consolidate short-term memory (green) into intercortical long-term memory (orange).
- Action representations (C5s) form to communicate cortical action behaviors to the basal ganglia (blue). The claustrum may be important in this development.
- Dopamine input to the striatum from the Snc is used to reward or anti-reward C5s action sequence selection, learning combinatorial sequences from the cortical modular hierarchy (blue).
- Ti projects upon the lower layers of the isocortex (C5s blue/C5p black) to aid in the selection of behaviors.
- Successful output behaviors, determined by cholinergic basal forebrain activity, reinforce the mapping between C3b and C5p for direct activation of learned behaviors (black).
- The cerebellum learns to aid in ventral thalamic control (red) in response to C5p cortical output.

5.2. PERSPECTIVE ON DEVELOPED COGNITIVE INFORMATION PROCESSING

We briefly hypothesize the utilization of the circuits in the matured brain in relation to **Figure 5**.

- Instigation of cognitive information processing begins with the layer 1 control projections (TL1 red) to the cerebral cortex. The cholinergic reticular activating system turns on thalamic nuclei.
- Control inputs drive cortico-thalamocortical information processing (purple) to select active C3b perceptions simultaneously in multiple cortical modules.
- Long-term memory associations (orange) and short-term memory (green) simultaneously bias the selection of C3b perceptions in target cortical modules.
- C5s cortical action suggestions are communicated to the basal ganglia for selection (blue).
- C3b perceptions trigger output C5p groups (black) that communicate cognitive output to the cerebellum (red) or directly cause physical behavior in motor cortex.
- Cognitive control via TL1 (red) is simultaneously driven by basal ganglia, cerebellar, and direct frontal cortex C6t input, resulting in ongoing "self-controlled thought."

6. CONCLUDING REMARKS

The causal function of any brain must ultimately be described in terms of a neuroanatomical description. Neuroanatomy must form the foundation of our understanding of the brain and experimental evidence should be explained in terms of neuroanatomical circuitry. The introduction of new experimental methods and the fragmentation of disciplines has scattered a vast numbers of anatomical puzzle pieces across the neuroscience information landscape. Cognitive consilience is a start to putting the puzzle pieces together. The picture is not perfect, but we have formed the beginning of a complete picture and re-introduced important neuroanatomical information that appears to have been lost in the literature. We have utilized technology to bring neuroanatomy literature and a synthesized picture of neuroanatomical circuits to anyone's fingertips and have put forth several novel and bold testable hypothesis on the neuroanatomical function of the brain.

The field of neuroanatomy is still in its infancy, the modern form beginning just over 100 years ago. Although modern technology has introduced novel experimental methods, huge gaps exist in our neuroanatomical knowledge for unexplained reasons. The last comprehensive Golgi staining assessment of a complete brain was published in 1899–1904 (Cajal, 2002). The last comprehensive histological Nissl staining study of a human brain was published in 1929 (von Economo, 1929). While these works were seminal and have lasted the test of time, the study by von Economo involves roughly 100 photographs of the human brain. Why not advance our understanding by redoing Cajal's seminal work or redoing von Economo's complete brain histology with twenty-first century capabilities?

A wealth of information and knowledge is piling up, while significantly more has been passed over. Consilience will ultimately be needed to arrive at our final understanding of the brain.

ACKNOWLEDGMENTS

The first author would like to acknowledge the initial support and encouragement of Robert Hecht-Nielsen in establishing the present research. The first author would also like to thank Glenn Northcutt and the late Ted Jones for their discussions, feedback, and encouragement to publish the research. The second author would like to acknowledge support from the UCSD Autism Center of Excellence, National Institutes of Health Grant 1-P50-MH081755, and the Simons Foundation for Autism Research Initiative (SFARI). The authors would like to thank SFARI for financial support to publish this work. Soren Solari was responsible for the neuroanatomical research and graphics and Rich Stoner was responsible for the technological integration and visualization.

REFERENCES

Alexander, G. E., DeLong, M. R., and Strick, P. L. (1986). Parallel organization of functionally segregated circuits linking basal ganglia and cortex. *Annu. Rev. Neurosci.* 9, 357–381.

Ascoli, G. A., Alonso-Nanclares, L., Anderson, S. A., Barrionuevo, G., Benavides-Piccione, R., Burkhalter, A., Buzsáki, G., Cauli, B., Defelipe, J., Fairén, A., Feldmeyer, D., Fishell, G., Fregnac, Y., Freund, T. F., Gardner, D., Gardner, E. P., Goldberg, J. H., Helmstaedter, M., Hestrin, S., Karube, F., Kisvárday, Z. F., Lambolez, B., Lewis, D. A., Marin, O., Markram, H., Muñoz, A., Packer, A., Petersen, C. C., Rockland, K. S., Rossier, J., Rudy, B., Somogyi, P.,

Staiger, J. F., Tamas, G., Thomson, A. M., Toledo-Rodriguez, M., Wang, Y., West, D. C., and Yuste, R. (2008). Petilla terminology: nomenclature of features of GABAergic interneurons of the cerebral cortex. *Nat. Rev. Neurosci.* 9, 557–568.

Amaral, D. G., and Cowan, W. M. (1980). Subcortical afferents to the hippocampal formation in the monkey. *J. Comp. Neurol.* 189, 573–591.

Amaral, D. G., and Witter, M. P. (1989). The three-dimensional organization of the hippocampal formation: a review of anatomical data. *Neuroscience* 31, 571–591.

Apicella, P. (2007). Leading tonically active neurons of the striatum from reward detection to context recognition. *Trends Neurosci.* 30, 299–306.

Arbuthnott, G. W., MacLeod, N. K., Maxwell, D. J., and Wright, A. K. (1990). Distribution and synaptic contacts of the cortical terminals arising from neurons in the rat ventromedial thalamic nucleus. *Neuroscience* 38, 47–60.

Arikuni, T., and Kubota, K. (1986). The organization of prefrontocaudate projections and their laminar origin in the macaque monkey: a retrograde study using hrp-gel. *J. Comp. Neurol.* 244, 492–510.

Asanuma, C. (1994). Gabaergic and pallidal terminals in the thalamic reticular nucleus of squirrel monkeys. *Exp. Brain Res.* 101, 439–451.

Asanuma, C., Andersen, R. A., and Cowan, W. M. (1985). The thalamic relations of the caudal inferior parietal lobule and the lateral prefrontal cortex in monkeys: divergent cortical projections from cell clusters in the medial pulvinar nucleus. *J. Comp. Neurol.* 241, 357–381.

Baddeley, A. (1981). The concept of working memory: a view of its current state and probable future development. *Cognition* 10, 17–23.

Baleydier, C., and Mauguiere, F. (1987). Network organization of the connectivity between parietal area 7, posterior cingulate cortex and medial pulvinar nucleus: a double fluorescent tracer study in monkey. *Exp. Brain Res.* 66, 385–393.

Barbas, H. (1986). Pattern in the laminar origin of corticocortical connections. *J. Comp. Neurol.* 252, 415–422.

Barbas, H., Hilgetag, C. C., Saha, S., Dermon, C. R., and Suski, J. L. (2005a). Parallel organization of contralateral and ipsilateral prefrontal cortical projections in the rhesus monkey. *BMC Neurosci.* 6, 32. doi:10.1186/1471-2202-6-32

Barbas, H., Medalla, M., Alade, O., Suski, J., Zikopoulos, B., and Lera, P. (2005b). Relationship of prefrontal connections to inhibitory systems in superior temporal areas in the rhesus monkey. *Cereb. Cortex* 15, 1356–1370.

Barbas, H., and Rempel-Clower, N. (1997). Cortical structure predicts the pattern of corticocortical connections. *Cereb. Cortex* 7, 635–646.

Benke, T., Delazer, M., Bartha, L., and Auer, A. (2003). Basal ganglia lesions and the theory of fronto-subcortical loops: neuropsychological findings in two patients with left caudate lesions. *Neurocase* 9, 70–85.

Bigl, V., Woolf, N. J., and Butcher, L. L. (1982). Cholinergic projections from the basal forebrain to frontal, parietal, temporal, occipital, and cingulate cortices: a combined fluorescent tracer and acetylcholinesterase analysis. *Brain Res. Bull.* 8, 727–749.

Borgmann, S., and Jurgens, U. (1999). Lack of cortico-striatal projections from the primary auditory cortex in the squirrel monkey. *Brain Res.* 836, 225–228.

Bottjer, S. W. (2005). Timing and prediction the code from basal ganglia to thalamus. *Neuron* 46, 4–7.

Braak, H., and Braak, E. (1976). The pyramidal cells of betz within the cingulate and precentral gigantopyramidal field in the human brain. A Golgi and pigmentarchitectonic study. *Cell Tissue Res.* 172, 103–119.

Bravo, H., and Karten, H. J. (1992). Pyramidal neurons of the rat cerebral cortex, immunoreactive to nicotinic acetylcholine receptors, project mainly to subcortical targets. *J. Comp. Neurol.* 320, 62–68.

Briggs, F., and Callaway, E. M. (2001). Layer-specific input to distinct cell types in layer 6 of monkey primary visual cortex. *J. Neurosci.* 21, 3600–3608.

Briggs, F., and Callaway, E. M. (2005). Laminar patterns of local excitatory input to layer 5 neurons in macaque primary visual cortex. *Cereb. Cortex* 15, 479–488.

Brodal, P. (1978). The corticopontine projection in the rhesus monkey. Origin and principles of organization. *Brain* 101, 251–283.

Brodal, P., and Bjaalie, J. G. (1992). Organization of the pontine nuclei. *Neurosci. Res.* 13, 83–118.

Brodmann, K. (1909). *Brodmann's "Localisation in the Cerebral Cortex."* London: Smith-Gordon.

Bromberg-Martin, E. S., Matsumoto, M., and Hikosaka, O. (2010). Dopamine in motivational control: rewarding, aversive, and alerting. *Neuron* 68, 815–834.

Brunel, N., and Wang, X. J. (2001). Effects of neuromodulation in a cortical network model of object working memory dominated by recurrent inhibition. *J. Comput. Neurosci.* 11, 63–85.

Brysch, I., Brysch, W., Creutzfeldt, O., Hayes, N. L., and Schlingensiepen, K. H. (1984). The second, intralaminar thalamo-cortical projection system. *Anat. Embryol.* 169, 111–118.

Brysch, W., Brysch, I., Creutzfeldt, O. D., Schlingensiepen, R., and Schlingensiepen, K. H. (1990). The topology of the thalamo-cortical projections in the marmoset monkey (*Callithrix jacchus*). *Exp. Brain Res.* 81, 1–17.

Burwell, R. D. (2000). The parahippocampal region: corticocortico connectivity. *Ann. N. Y. Acad. Sci.* 911, 25–42.

Buxhoeveden, D. P., and Casanova, M. F. (2002). The minicolumn hypothesis in neuroscience. *Brain* 125, 935–951.

Buzsaki, G. (2006). *Rhythms of the Brain.* New york: Oxford University Press.

Cajal, S. R. y. (1899). *Textura del sistema nervioso del hombre y de los vertebrados*, Vol. 1. Madrid: Imprenta y Librera de Nicols Moya.

Cajal, S. R. y. (2002). *Texture of the Nervous System of Man and the Vertebrates*, Vol. 3. New York: Springer-Verlag.

Callaway, E. M. (1998). Local circuits in primary visual cortex of the macaque monkey. *Annu. Rev. Neurosci.* 21, 47–74.

Canolty, R. T., Edwards, E., Dalal, S. S., Soltani, M., Nagarajan, S. S., Kirsch, H. E., Berger, M. S., Barbaro, N. M., and Knight, R. T. (2006). High gamma power is phase-locked to theta oscillations in human neocortex. *Science* 313, 1626–1628.

Catani, M., and ffytche, D. H. (2005). The rises and falls of disconnection syndromes. *Brain* 128, 2224–2239.

Catsman-Berrevoets, C. E., and Kuypers, H. G. (1978). Differential laminar distribution of corticothalamic neurons projecting to the vl and the center median. An hrp study in the cynomolgus monkey. *Brain Res.* 154, 359–365.

Charara, A., and Parent, A. (1994). Brainstem dopaminergic, cholinergic and serotoninergic afferents to the pallidum in the squirrel monkey. *Brain Res.* 640, 155–170.

Compte, A., Brunel, N., Goldman-Rakic, P. S., and Wang, X. J. (2000). Synaptic mechanisms and network dynamics underlying spatial working memory in a cortical network model. *Cereb. Cortex* 10, 910–923.

Conde, F., Lund, J. S., Jacobowitz, D. M., Baimbridge, K. G., and Lewis, D. A. (1994). Local circuit neurons immunoreactive for calretinin, calbindin d-28k or parvalbumin in monkey prefrontal cortex: distribution and morphology. *J. Comp. Neurol.* 341, 95–116.

Conner, J. M., Culberson, A., Packowski, C., Chiba, A. A., and Tuszynski, M. H. (2003). Lesions of the basal forebrain cholinergic system impair task acquisition and abolish cortical plasticity associated with motor skill learning. *Neuron* 38, 819–829.

Crick, F. C., and Koch, C. (2005). What is the function of the claustrum? *Philos. Trans. R. Soc. Lond. B Biol. Sci.* 360, 1271–1279.

Damasio, H., and Damasio, A. R. (1980). The anatomical basis of conduction aphasia. *Brain* 103, 337–350.

de Lima, A. D., Voigt, T., and Morrison, J. H. (1990). Morphology of the cells within the inferior temporal gyrus that project to the prefrontal cortex in the macaque monkey. *J. Comp. Neurol.* 296, 159–172.

DeFelipe, J. (1997). Types of neurons, synaptic connections and chemical characteristics of cells immunoreactive for calbindin-d28k, parvalbumin and calretinin in the neocortex. *J. Chem. Neuroanat.* 14, 1–19.

DeFelipe, J., Conley, M., and Jones, E. G. (1986). Long-range focal collateralization of axons arising from corticocortical cells in monkey sensory-motor cortex. *J. Neurosci.* 6, 3749–3766.

Defelipe, J., Gonzalez-Albo, M. C., Del Rio, M. R., and Elston, G. N. (1999). Distribution and patterns of connectivity of interneurons containing calbindin, calretinin, and parvalbumin in visual areas of the occipital and temporal lobes of the macaque monkey. *J. Comp. Neurol.* 412, 515–526.

Doya, K. (1999). What are the computations of the cerebellum, the basal ganglia and the cerebral cortex? *Neural Netw.* 12, 961–974.

Durstewitz, D., Seamans, J. K., and Sejnowski, T. J. (2000). Neurocomputational models of working memory. *Nat. Neurosci.* 3(Suppl.), 1184–1191.

Edelstein, L. R., and Denaro, F. J. (2004). The claustrum: a historical review of its anatomy, physiology, cytochemistry and functional significance. *Cell. Mol. Biol.* 50, 675–702.

Edwards, E., Soltani, M., Deouell, L. Y., Berger, M. S., and Knight, R. T. (2005). High gamma activity in response to deviant auditory stimuli recorded directly from human cortex. *J. Neurophysiol.* 94, 4269–4280.

Eichenbaum, H. (2000). A cortical-hippocampal system for declarative memory. *Nat. Rev. Neurosci.* 1, 41–50.

Eickhoff, S. B., Schleicher, A., Scheperjans, F., Palomero-Gallagher, N., and Zilles, K. (2007). Analysis of neurotransmitter receptor distribution patterns in the cerebral cortex. *Neuroimage* 34, 1317–1330.

Felleman, D. J., and Van Essen, D. C. (1991). Distributed hierarchical processing in the primate cerebral cortex. *Cereb. Cortex* 1, 1–47.

Foster, R. E., Donoghue, J. P., and Ebner, F. F. (1981). Laminar organization of efferent cells in the parietal cortex of the virginia opossum. *Exp. Brain Res.* 43, 330–336.

Francois, C., Tande, D., Yelnik, J., and Hirsch, E. C. (2002). Distribution and morphology of nigral axons projecting to the thalamus in primates. *J. Comp. Neurol.* 447, 249–260.

Fujita, I., and Fujita, T. (1996). Intrinsic connections in the macaque inferior temporal cortex. *J. Comp. Neurol.* 368, 467–486.

Fujiyama, F., Sohn, J., Nakano, T., Furuta, T., Nakamura, K. C., Matsuda, W., and Kaneko, T. (2011). Exclusive and common targets of neostriatofugal projections of rat striosome neurons: a single neuron-tracing study using a viral vector. *Eur. J. Neurosci.* 33, 668–677.

Fuller, P., Sherman, D., Pedersen, N. P., Saper, C. B., and Lu, J. (2011). Reassessment of the structural basis of the ascending arousal system. *J. Comp. Neurol.* 519, 933–956.

Fuster, J. M. (2003). *Cortex and Mind.* New York: Oxford University Press.

Gabbott, P. L., and Bacon, S. J. (1996). Local circuit neurons in the medial prefrontal cortex (areas 24a,b,c, 25 and 32) in the monkey: I. Cell morphology and morphometrics. *J. Comp. Neurol.* 364, 567–608.

Gandia, J. A., De Las Heras, S., Garcia, M., and Gimenez-Amaya, J. M. (1993). Afferent projections to the reticular thalamic nucleus from the globus pallidus and the substantia nigra in the rat. *Brain Res. Bull.* 32, 351–358.

Gerfen, C. R. (1984). The neostriatal mosaic: compartmentalization of corticostriatal input and striatonigral output systems. *Nature* 311, 461–464.

Gerfen, C. R. (1989). The neostriatal mosaic: striatal patch-matrix organization is related to cortical lamination. *Science* 246, 385–388.

Gerfen, C. R., and Surmeier, D. J. (2010). Modulation of striatal projection systems by dopamine. *Annu. Rev. Neurosci.* 34, 441–466.

Geschwind, N. (1965a). Disconnexion syndromes in animals and man. i. *Brain* 88, 237–294.

Geschwind, N. (1965b). Disconnexion syndromes in animals and man. ii. *Brain* 88, 585–644.

Ghosh, S., and Porter, R. (1988). Morphology of pyramidal neurones in monkey motor cortex and the synaptic actions of their intracortical axon collaterals. *J. Physiol. (Lond.)* 400, 593–615.

Gibson, J. R., Beierlein, M., and Connors, B. W. (1999). Two networks of electrically coupled inhibitory neurons in neocortex. *Nature* 402, 75–79.

Giguere, M., and Goldman-Rakic, P. S. (1988). Mediodorsal nucleus: areal, laminar, and tangential distribution of afferents and efferents in the frontal lobe of rhesus monkeys. *J. Comp. Neurol.* 277, 195–213.

Glickstein, M., May, J. G., and Mercier, B. E. (1985). Corticopontine projection in the macaque: the distribution of labelled cortical cells after large injections of horseradish peroxidase in the pontine nuclei. *J. Comp. Neurol.* 235, 343–359.

Goldman-Rakic, P. S. (1996). Regional and cellular fractionation of working memory. *Proc. Natl. Acad. Sci. U.S.A.* 93, 13473–13480.

Goldman-Rakic, P. S., and Porrino, L. J. (1985). The primate mediodorsal (md) nucleus and its projection to the frontal lobe. *J. Comp. Neurol.* 242, 535–560.

Gould, E. (2007). How widespread is adult neurogenesis in mammals? *Nat. Rev. Neurosci.* 8, 481–488.

Grafton, S. T., Arbib, M. A., Fadiga, L., and Rizzolatti, G. (1996). Localization of grasp representations in humans by positron emission tomography. *Exp. Brain Res.* 112, 103–111.

Graham, R. C. Jr., and Karnovsky, M. J. (1966). The early stages of absorption of injected horseradish peroxidase in the proximal tubules of mouse kidney: ultrastructural cytochemistry by a new technique. *J. Histochem. Cytochem.* 14, 291–302.

Grenier, F., Timofeev, I., and Steriade, M. (1998). Leading role of thalamic over cortical neurons during postinhibitory rebound excitation. *Proc. Natl. Acad. Sci. U.S.A.* 95, 13929–13934.

Haber, S. N. (2003). The primate basal ganglia: parallel and integrative networks. *J. Chem. Neuroanat.* 26, 317–330.

Haber, S. N., Lynd, E., Klein, C., and Groenewegen, H. J. (1990). Topographic organization of the ventral striatal efferent projections in the rhesus monkey: an anterograde tracing study. *J. Comp. Neurol.* 293, 282–298.

Hackett, T. A., Preuss, T. M., and Kaas, J. H. (2001). Architectonic identification of the core region in auditory cortex of macaques, chimpanzees, and humans. *J. Comp. Neurol.* 441, 197–222.

Hagmann, P., Cammoun, L., Gigandet, X., Gerhard, S., Grant, P. E., Wedeen, V., Meuli, R., Thiran, J. P., Honey, C. J., and Sporns, O. (2010). Mr connectomics: principles and challenges. *J. Neurosci. Methods* 194, 34–45.

Hamani, C., Dostrovsky, J. O., and Lozano, A. M. (2006). The motor thalamus in neurosurgery. *Neurosurgery* 58, 146–58; discussion 146–158.

Hanbery, J., and Jasper, H. (1953). Independence of diffuse thalamocortical projection system shown by specific nuclear destructions. *J. Neurophysiol.* 16, 252–271.

Hanbery, J., and Jasper, H. (1954). The non-specific thalamocortical projection system. *J. Neurosurg.* 11, 24–25.

Hardman, C. D., Henderson, J. M., Finkelstein, D. I., Horne, M. K., Paxinos, G., and Halliday, G. M. (2002). Comparison of the basal ganglia in rats, marmosets, macaques, baboons, and humans: volume and neuronal number for the output, internal relay, and striatal modulating nuclei. *J. Comp. Neurol.* 445, 238–255.

Hazrati, L. N., and Parent, A. (1991a). Contralateral pallidothalamic and pallidotegmental projections in primates: an anterograde and retrograde labeling study. *Brain Res.* 567, 212–223.

Hazrati, L. N., and Parent, A. (1991b). Projection from the external pallidum to the reticular thalamic nucleus in the squirrel monkey. *Brain Res.* 550, 142–146.

Hebb, D. O. (1949). *The Organization of Behavior: A Neuropsychological Theory*. New York: Lawrence Erlbaum Associates.

Heindel, W., Salmon, D., Shults, C., Walicke, P., and Butters, N. (1989). Neuropsychological evidence for multiple implicit memory systems: a comparison of Alzheimer's, Huntington's, and Parkinson's disease patients. *J. Neurosci.* 9, 582–587.

Herkenham, M. (1979). The afferent and efferent connections of the ventromedial thalamic nucleus in the rat. *J. Comp. Neurol.* 183, 487–517.

Herkenham, M. (1980). Laminar organization of thalamic projections to the rat neocortex. *Science* 207, 532–535.

Herrero, M. T., Barcia, C., and Navarro, J. M. (2002). Functional anatomy of thalamus and basal ganglia. *Childs Nerv. Syst.* 18, 386–404.

Hestrin, S., and Galarreta, M. (2005). Electrical synapses define networks of neocortical gabaergic neurons. *Trends Neurosci.* 28, 304–309.

Hohl-Abrahao, J. C., and Creutzfeldt, O. D. (1991). Topographical mapping of the thalamocortical projections in rodents and comparison with that in primates. *Exp. Brain Res.* 87, 283–294.

Insausti, R., Amaral, D. G., and Cowan, W. M. (1987). The entorhinal cortex of the monkey: Iii. Subcortical afferents. *J. Comp. Neurol.* 264, 396–408.

Jones, E. G. (1975). Some aspects of the organization of the thalamic reticular complex. *J. Comp. Neurol.* 162, 285–308.

Jones, E. G. (1998). Viewpoint: the core and matrix of thalamic organization. *Neuroscience* 85, 331–345.

Jones, E. G. (2007). *The Thalamus*, 2nd Edn, Vol. 1–2. Cambridge: Cambridge University Press.

Jones, E. G., and Burton, H. (1976). Areal differences in the laminar distribution of thalamic afferents in cortical fields of the insular, parietal and temporal regions of primates. *J. Comp. Neurol.* 168, 197–247.

Jones, E. G., Coulter, J. D., Burton, H., and Porter, R. (1977). Cells of origin and terminal distribution of corticostriatal fibers arising in the sensory-motor cortex of monkeys. *J. Comp. Neurol.* 173, 53–80.

Jones, E. G., and Wise, S. P. (1977). Size, laminar and columnar distribution of efferent cells in the sensory-motor cortex of monkeys. *J. Comp. Neurol.* 175, 391–438.

Kakei, S., Na, J., and Shinoda, Y. (2001). Thalamic terminal morphology and distribution of single corticothalamic axons originating from layers 5 and 6 of the cat motor cortex. *J. Comp. Neurol.* 437, 170–185.

Kaneko, T., Cho, R., Li, Y., Nomura, S., and Mizuno, N. (2000). Predominant information transfer from layer iii pyramidal neurons to corticospinal neurons. *J. Comp. Neurol.* 423, 52–65.

Katz, L. C. (1987). Local circuitry of identified projection neurons in cat visual cortex brain slices. *J. Neurosci.* 7, 1223–1249.

Kawaguchi, Y., Wilson, C. J., Augood, S. J., and Emson, P. C. (1995). Striatal interneurones: chemical, physiological and morphological characterization. *Trends Neurosci.* 18, 527–535.

Kelly, R. M., and Strick, P. L. (2003). Cerebellar loops with motor cortex and prefrontal cortex of a nonhuman primate. *J. Neurosci.* 23, 8432–8444.

Kievit, J., and Kuypers, H. G. (1977). Organization of the thalamocortical connexions to the frontal lobe in the rhesus monkey. *Exp. Brain Res.* 29, 299–322.

Kimura, F., and Itami, C. (2009). Myelination and isochronicity in neural networks. *Front. Neuroanat.* 3:12. doi:10.3389/neuro.05.012.2009

Kimura, T., Ozaki, I., and Hashimoto, I. (2008). Impulse propagation along thalamocortical fibers can be detected magnetically outside the human brain. *J. Neurosci.* 28, 12535–12538.

Knight, R. T. (2007). Neuroscience. Neural networks debunk phrenology. *Science* 316, 1578–1579.

Kobayashi, Y., and Amaral, D. G. (2003). Macaque monkey retrosplenial cortex: Ii. Cortical afferents. *J. Comp. Neurol.* 466, 48–79.

Kobayashi, Y., and Amaral, D. G. (2007). Macaque monkey retrosplenial cortex: Iii. Cortical efferents. *J. Comp. Neurol.* 502, 810–833.

Kotter, R. (2004). Online retrieval, processing, and visualization of primate connectivity data from the cocomac database. *Neuroinformatics* 2, 127–144.

Kreczmanski, P., Heinsen, H., Mantua, V., Woltersdorf, F., Masson, T., Ulfig, N., Schmidt-Kastner, R., Korr, H., Steinbusch, H. W., Hof, P. R., and Schmitz, C. (2007). Volume, neuron density and total neuron number in five subcortical regions in schizophrenia. *Brain* 130(Pt 3):678–692.

Kristensson, K., and Olsson, Y. (1971). Retrograde axonal transport of protein. *Brain Res.* 29, 363–365.

Kritzer, M. F., and Goldman-Rakic, P. S. (1995). Intrinsic circuit organization of the major layers and sublayers of the dorsolateral prefrontal cortex in the rhesus monkey. *J. Comp. Neurol.* 359, 131–143.

Kunishio, K., and Haber, S. N. (1994). Primate cingulostriatal projection: limbic striatal versus sensorimotor striatal input. *J. Comp. Neurol.* 350, 337–356.

Langer, L. F., and Graybiel, A. M. (1989). Distinct nigrostriatal projection systems innervate striosomes and matrix in the primate striatum. *Brain Res.* 498, 344–350.

Lauterbach, E. C. (2005). The neuropsychiatry of Parkinson's disease. *Minerva Med.* 96, 155–173.

Lavenex, P., Suzuki, W. A., and Amaral, D. G. (2002). Perirhinal and parahippocampal cortices of the macaque monkey: projections to the neocortex. *J. Comp. Neurol.* 447, 394–420.

Lee, C. R., and Tepper, J. M. (2009). Basal ganglia control of substantia nigra dopaminergic neurons. *J. Neural Transm. Suppl.* 73, 71–90.

Leichnetz, G. R., Smith, D. J., and Spencer, R. F. (1984). Cortical projections to the paramedian tegmental and basilar pons in the monkey. *J. Comp. Neurol.* 228, 388–408.

Lemon, R. N., and Griffiths, J. (2005). Comparing the function of the corticospinal system in different species: organizational differences for motor specialization? *Muscle Nerve* 32, 261–279.

Letinic, K., Zoncu, R., and Rakic, P. (2002). Origin of gabaergic neurons in the human neocortex. *Nature* 417, 645–649.

LeVay, S. (1986). Synaptic organization of claustral and geniculate afferents to the visual cortex of the cat. *J. Neurosci.* 6, 3564–3575.

LeVay, S., and Sherk, H. (1981). The visual claustrum of the cat. i. Structure and connections. *J. Neurosci.* 1, 956–980.

Levesque, J. C., and Parent, A. (2005a). Gabaergic interneurons in human subthalamic nucleus. *Mov. Disord.* 20, 574–584.

Levesque, M., and Parent, A. (2005b). The striatofugal fiber system in primates: a reevaluation of its organization based on single-axon tracing studies. *Proc. Natl. Acad. Sci. U.S.A.* 102, 11888–11893.

Levesque, M., Gagnon, S., Parent, A., and Deschenes, M. (1996). Axonal arborizations of corticostriatal and corticothalamic fibers arising from the second somatosensory area in the rat. *Cereb. Cortex* 6, 759–770.

Levitt, J. B., Lewis, D. A., Yoshioka, T., and Lund, J. S. (1993). Topography of pyramidal neuron intrinsic connections in macaque monkey prefrontal cortex (areas 9 and 46). *J. Comp. Neurol.* 338, 360–376.

Lieber, R. L. (2002). *Skeletal Muscle Structure, Function, and Plasticity*, 2nd Edn. Philadelphia: Lippincott Williams and Wilkins.

Lorente de No, R. (1943). "Cerebral cortex: architecture, intracortical connections, motor projections," in *Physiology of the Nervous System, Outlines of Physiology Series*, 2nd Edn, ed. J. Fulton (New York: Oxford University Press), 274–301.

Lund, J. S., Hendrickson, A. E., Ogren, M. P., and Tobin, E. A. (1981). Anatomical organization of primate visual cortex area vii. *J. Comp. Neurol.* 202, 19–45.

Lund, J. S., and Lewis, D. A. (1993). Local circuit neurons of developing and mature macaque prefrontal cortex: Golgi and immunocytochemical characteristics. *J. Comp. Neurol.* 328, 282–312.

Lund, J. S., Yoshioka, T., and Levitt, J. B. (1993). Comparison of intrinsic connectivity in different areas of macaque monkey cerebral cortex. *Cereb. Cortex* 3, 148–162.

Macchi, G., and Jones, E. G. (1997). Toward an agreement on terminology of nuclear and subnuclear divisions of the motor thalamus. *J. Neurosurg.* 86, 670–685.

Marcus, D. S., Harwell, J., Olsen, T., Hodge, M., Glasser, M. F., Prior, F., Jenkinson, M., Laumann, T., Curtiss, S. W., and Van Essen, D. C. (2011). Informatics and data mining tools and strategies for the human connectome project. *Front. Neuroinform.* 5:4. doi:10.3389/fninf.2011.00004

Matsuda, W., Furuta, T., Nakamura, K. C., Hioki, H., Fujiyama, F., Arai, R., and Kaneko, T. (2009). Single nigrostriatal dopaminergic neurons form widely spread and highly dense axonal arborizations in the neostriatum. *J. Neurosci.* 29, 444–453.

McFarland, N. R., and Haber, S. N. (2001). Organization of thalamostriatal terminals from the ventral motor nuclei in the macaque. *J. Comp. Neurol.* 429, 321–336.

McFarland, N. R., and Haber, S. N. (2002). Thalamic relay nuclei of the basal ganglia form both reciprocal and nonreciprocal cortical connections, linking multiple frontal cortical areas. *J. Neurosci.* 22, 8117–8132.

Medalla, M., and Barbas, H. (2006). Diversity of laminar connections linking periarcuate and lateral intraparietal areas depends on cortical structure. *Eur. J. Neurosci.* 23, 161–179.

Melchitzky, D. S., Gonzalez-Burgos, G., Barrionuevo, G., and Lewis, D. A. (2001). Synaptic targets of the intrinsic axon collaterals of supragranular pyramidal neurons in monkey prefrontal cortex. *J. Comp. Neurol.* 430, 209–221.

Meyer, G., Gonzalez-Hernandez, T. H., and Ferres-Torres, R. (1989). The spiny stellate neurons in layer iv of the human auditory cortex. A Golgi study. *Neuroscience* 33, 489–498.

Milner, B. (2005). The medial temporal-lobe amnesic syndrome. *Psychiatr. Clin. North Am.* 28, 599–611.

Mitchell, B. D., and Cauller, L. J. (2001). Corticocortical and thalamocortical projections to layer i of the frontal neocortex in rats. *Brain Res.* 921, 68–77.

Molnar, Z., and Cheung, A. F. (2006). Towards the classification of subpopulations of layer v pyramidal projection neurons. *Neurosci. Res.* 55, 105–115.

Molnar, Z., Metin, C., Stoykova, A., Tarabykin, V., Price, D. J., Francis, F., Meyer, G., Dehay, C., and Kennedy, H. (2006). Comparative aspects of cerebral cortical development. *Eur. J. Neurosci.* 23, 921–934.

Monsell, S. (1984). "Components of working memory underlying verbal skills: a 'distributed capacities' view," in *International Symposium on Attention and Performance X*, Vol. 10, eds H. Bouma and D. Bouwhuis (Hillsdale, NJ: Erlbaum), 327–350.

Morishima, M., and Kawaguchi, Y. (2006). Recurrent connection patterns of corticostriatal pyramidal cells in frontal cortex. *J. Neurosci.* 26, 4394–4405.

Mountcastle, V. B. (2003). Introduction. *Cereb. Cortex* 13, 2–4.

Murphy, K. M., Beston, B. R., Boley, P. M., and Jones, D. G. (2005). Development of human visual cortex: a balance between excitatory and inhibitory plasticity mechanisms. *Dev. Psychobiol.* 46, 209–221.

Nakano, K., Tokushige, A., Kohno, M., Hasegawa, Y., Kayahara, T., and Sasaki, K. (1992). An autoradiographic study of cortical projections from motor thalamic nuclei in the macaque monkey. *Neurosci. Res.* 13, 119–137.

Nambu, A., Tokuno, H., Hamada, I., Kita, H., Imanishi, M., Akazawa, T., Ikeuchi, Y., and Hasegawa, N. (2000). Excitatory cortical inputs to pallidal neurons via the subthalamic nucleus in the monkey. *J. Neurophysiol.* 84, 289–300.

Nolte, J., and Angevine, J. B. (2000). *The Human Brain in Pictures and Diagrams*, 2nd Edn. Philadelphia: Mosby.

Northcutt, R. G., and Kaas, J. H. (1995). The emergence and evolution of mammalian neocortex. *Trends Neurosci.* 18, 373–379.

O'Neill, J., Pleydell-Bouverie, B., Dupret, D., and Csicsvari, J. (2010). Play it again: reactivation of waking experience and memory. *Trends Neurosci.* 33, 220–229.

Oorschot, D. E. (1996). Total number of neurons in the neostriatal, pallidal, subthalamic, and substantia nigral nuclei of the rat basal ganglia: a stereological study using the cavalieri and optical disector methods. *J. Comp. Neurol.* 366, 580–599.

Pare, D., Smith, Y., Parent, A., and Steriade, M. (1988). Projections of brainstem core cholinergic and non-cholinergic neurons of cat to intralaminar and reticular thalamic nuclei. *Neuroscience* 25, 69–86.

Parent, A., Smith, Y., Filion, M., and Dumas, J. (1989). Distinct afferents to internal and external pallidal segments in the squirrel monkey. *Neurosci. Lett.* 96, 140–144.

Parent, M., Levesque, M., and Parent, A. (2001). Two types of projection neurons in the internal pallidum of primates: single-axon tracing and three-dimensional reconstruction. *J. Comp. Neurol.* 439, 162–175.

Parent, M., and Parent, A. (2004). The pallidofugal motor fiber system in primates. *Parkinsonism Relat. Disord.* 10, 203–211.

Parent, M., and Parent, A. (2005). Single-axon tracing and three-dimensional reconstruction of centre median-parafascicular thalamic neurons in primates. *J. Comp. Neurol.* 481, 127–144.

Parent, M., and Parent, A. (2006). Single-axon tracing study of corticostriatal projections arising from primary motor cortex in primates. *J. Comp. Neurol.* 496, 202–213.

Pearson, R. C., Brodal, P., Gatter, K. C., and Powell, T. P. (1982). The organization of the connections between the cortex and the claustrum in the monkey. *Brain Res.* 234, 435–441.

Penfield, W., and Rasmussen, T. (1968). *The Cerebral Cortex of Man: A Clinical Study of Localization of Function.* New York: Hafner Publishing Company.

Peters, A., Cifuentes, J. M., and Sethares, C. (1997). The organization of pyramidal cells in area 18 of the rhesus monkey. *Cereb. Cortex* 7, 405–421.

Price, D. J., Kennedy, H., Dehay, C., Zhou, L., Mercier, M., Jossin, Y., Goffinet, A. M., Tissir, F., Blakey, D., and Molnar, Z. (2006). The development of cortical connections. *Eur. J. Neurosci.* 23, 910–920.

Pucak, M. L., Levitt, J. B., Lund, J. S., and Lewis, D. A. (1996). Patterns of intrinsic and associational circuitry in monkey prefrontal cortex. *J. Comp. Neurol.* 376, 614–630.

Purves, D., Augustine, G. J., Fitzpatrick, D., Hall, W. C., Mantia, A.-S. L., McNamara, J. O., and Williams, S. M. (2004). *Neuroscience*, 3rd Edn. Sunderland: Sinauer Associates, Inc.

Rakic, P. (1995). A small step for the cell, a giant leap for mankind: a hypothesis of neocortical expansion during evolution. *Trends Neurosci.* 18, 383–388.

Ramnani, N. (2006). The primate cortico-cerebellar system: anatomy and function. *Nat. Rev. Neurosci.* 7, 511–522.

Rempel-Clower, N. L., and Barbas, H. (2000). The laminar pattern of connections between prefrontal and anterior temporal cortices in the rhesus monkey is related to cortical structure and function. *Cereb. Cortex* 10, 851–865.

Rockland, K. S. (1992). Configuration, in serial reconstruction, of individual axons projecting from area v2 to v4 in the macaque monkey. *Cereb. Cortex* 2, 353–374.

Rockland, K. S., Andresen, J., Cowie, R. J., and Robinson, D. L. (1999). Single axon analysis of pulvinocortical connections to several visual areas in the macaque. *J. Comp. Neurol.* 406, 221–250.

Rockland, K. S., and Drash, G. W. (1996). Collateralized divergent feedback connections that target multiple cortical areas. *J. Comp. Neurol.* 373, 529–548.

Rockland, K. S., and Ichinohe, N. (2004). Some thoughts on cortical minicolumns. *Exp. Brain Res.* 158, 265–277.

Romanski, L. M., Giguere, M., Bates, J. F., and Goldman-Rakic, P. S. (1997). Topographic organization of medial pulvinar connections with the prefrontal cortex in the rhesus monkey. *J. Comp. Neurol.* 379, 313–332.

Rouiller, E. M., and Durif, C. (2004). The dual pattern of corticothalamic projection of the primary auditory cortex in macaque monkey. *Neurosci. Lett.* 358, 49–52.

Sadikot, A. F., Parent, A., and Francois, C. (1992a). Efferent connections of the centromedian and parafascicular thalamic nuclei in the squirrel monkey: a pha-l study of subcortical projections. *J. Comp. Neurol.* 315, 137–159.

Sadikot, A. F., Parent, A., Smith, Y., and Bolam, J. P. (1992b). Efferent connections of the centromedian and parafascicular thalamic nuclei in the squirrel monkey: a light and electron microscopic study of the thalamostriatal projection in relation to striatal heterogeneity. *J. Comp. Neurol.* 320, 228–242.

Sakai, S. T., Inase, M., and Tanji, J. (1996). Comparison of cerebellothalamic and pallidothalamic projections in the monkey (*Macaca fuscata*): a double anterograde labeling study. *J. Comp. Neurol.* 368, 215–228.

Sato, F., Lavallee, P., Levesque, M., and Parent, A. (2000). Single-axon tracing study of neurons of the external segment of the globus pallidus in primate. *J. Comp. Neurol.* 417, 17–31.

Satoh, K., and Fibiger, H. C. (1985). Distribution of central cholinergic neurons in the baboon (*Papio papio*). i. General morphology. *J. Comp. Neurol.* 236, 197–214.

Scheibel, M. E., and Scheibel, A. B. (1966). The organization of the nucleus reticularis thalami: a Golgi study. *Brain Res.* 1, 43–62.

Schmahmann, J. D., and Pandya, D. N. (1995). Prefrontal cortex projections to the basilar pons in rhesus monkey: implications for the cerebellar contribution to higher function. *Neurosci. Lett.* 199, 175–178.

Schmahmann, J. D., and Pandya, D. N. (2006). *Fiber Pathways of the Brain.* New York: Oxford University Press.

Schmahmann, J. D., Pandya, D. N., Wang, R., Dai, G., D'Arceuil, H. E., de Crespigny, A. J., and Wedeen, V. J. (2007). Association fibre pathways of the brain: parallel observations from diffusion spectrum imaging and autoradiography. *Brain* 130(Pt 3), 630–653.

Schmahmann, J. D., Smith, E. E., Eichler, F. S., and Filley, C. M. (2008). Cerebral white matter: neuroanatomy, clinical neurology, and neurobehavioral correlates. *Ann. N. Y. Acad. Sci.* 1142, 266–309.

Sidibe, M., Bevan, M. D., Bolam, J. P., and Smith, Y. (1997). Efferent connections of the internal globus pallidus in the squirrel monkey: I. Topography and synaptic organization of the pallidothalamic projection. *J. Comp. Neurol.* 382, 323–347.

Sidibe, M., Pare, J. F., and Smith, Y. (2002). Nigral and pallidal inputs to functionally segregated thalamostriatal neurons in the centromedian/parafascicular intralaminar nuclear complex in monkey. *J. Comp. Neurol.* 447, 286–299.

Smith, Y., Bevan, M. D., Shink, E., and Bolam, J. P. (1998). Microcircuitry of the direct and indirect pathways of the basal ganglia. *Neuroscience* 86, 353–387.

Smith, Y., Raju, D. V., Pare, J. F., and Sidibe, M. (2004). The thalamostriatal system: a highly specific network of the basal ganglia circuitry. *Trends Neurosci.* 27, 520–527.

Solari, S. (2009). *A Unified Anatomical Theory and Computational Model of Cognitive Information Processing in the Mammalian Brain and the Introduction of DNA Reco Codes.* PhD thesis, University of California, San Diego.

Soloway, A. S., Pucak, M. L., Melchitzky, D. S., and Lewis, D. A. (2002). Dendritic morphology of callosal and ipsilateral projection neurons in monkey prefrontal cortex. *Neuroscience* 109, 461–471.

Squire, L. R. (2004). Memory systems of the brain: a brief history and current perspective. *Neurobiol. Learn. Mem.* 82, 171–177.

Squire, L. R., and Alvarez, P. (1995). Retrograde amnesia and memory consolidation: a neurobiological perspective. *Curr. Opin. Neurobiol.* 5, 169–177.

Squire, L. R., and Zola, S. M. (1996). Structure and function of declarative and nondeclarative memory systems. *Proc. Natl. Acad. Sci. U.S.A.* 93, 13515–13522.

Stanfield, B. B. (1992). The development of the corticospinal projection. *Prog. Neurobiol.* 38, 169–202.

Stephan, K. E., Hilgetag, C. C., Burns, G. A., O'Neill, M. A., Young, M. P., and Kotter, R. (2000). Computational analysis of functional connectivity between areas of primate cerebral cortex. *Philos. Trans. R. Soc. Lond. B Biol. Sci.* 355, 111–126.

Steriade, M. (2006). Grouping of brain rhythms in corticothalamic systems. *Neuroscience* 137, 1087–1106.

Steriade, M., Pare, D., Parent, A., and Smith, Y. (1988). Projections of cholinergic and non-cholinergic neurons of the brainstem core to relay and associational thalamic nuclei in the cat and macaque monkey. *Neuroscience* 25, 47–67.

Striedter, G. F. (2005). *Principles of Brain Evolution.* Sunderland: Sinauer Associates, Inc.

Surmeier, D. J., Ding, J., Day, M., Wang, Z., and Shen, W. (2007). D1 and d2 dopamine-receptor modulation of striatal glutamatergic signaling in striatal medium spiny neurons. *Trends Neurosci.* 30, 228–235.

Szentagothai, J. (1975). The "module-concept" in cerebral cortex architecture. *Brain Res.* 95, 475–496.

Tanaka, K. (2003). Columns for complex visual object features in the inferotemporal cortex: clustering of cells with similar but slightly different stimulus selectivities. *Cereb. Cortex* 13, 90–99.

Tande, D., Feger, J., Hirsch, E. C., and Francois, C. (2006). Parafascicular nucleus projection to the extrastriatal basal ganglia in monkeys. *Neuroreport* 17, 277–280.

Tanigawa, H., Fujita, I., Kato, M., and Ojima, H. (1998). Distribution, morphology, and gamma-aminobutyric acid immunoreactivity of horizontally projecting neurons in the macaque inferior temporal cortex. *J. Comp. Neurol.* 401, 129–143.

Tanne-Gariepy, J., Boussaoud, D., and Rouiller, E. M. (2002). Projections of the claustrum to the primary motor, premotor, and prefrontal cortices in the macaque monkey. *J. Comp. Neurol.* 454, 140–157.

Tardif, E., Probst, A., and Clarke, S. (2007). Laminar specificity of intrinsic connections in Broca's area. *Cereb. Cortex* 17, 2949–2960.

Teyler, T. J., and Rudy, J. W. (2007). The hippocampal indexing theory and episodic memory: updating the index. *Hippocampus* 17, 1158–1169.

Thomson, A. M., and Bannister, A. P. (1998). Postsynaptic pyramidal target selection by descending layer iii pyramidal axons: dual intracellular recordings and biocytin filling in slices of rat neocortex. *Neuroscience* 84, 669–683.

Thomson, A. M., and Deuchars, J. (1997). Synaptic interactions in neocortical local circuits: dual intracellular recordings in vitro. *Cereb. Cortex* 7, 510–522.

Toro, R., Perron, M., Pike, B., Richer, L., Veillette, S., Pausova, Z., and Paus, T. (2008). Brain size and folding of the human cerebral cortex. *Cereb. Cortex* 18, 2352–2357.

Triarhou, L. C. (2007). A proposed number system for the 107 cortical areas of economo and koskinas, and brodmann area correlations. *Stereotact. Funct. Neurosurg.* 85, 204–215.

Trojanowski, J. Q., and Jacobson, S. (1976). Areal and laminar distribution of some pulvinar cortical efferents in rhesus monkey. *J. Comp. Neurol.* 169, 371–392.

Trojanowski, J. Q., and Jacobson, S. (1977). The morphology and laminar distribution of cortico-pulvinar neurons in the rhesus monkey. *Exp. Brain Res.* 28, 51–62.

Tsao, D. Y., Freiwald, W. A., Tootell, R. B., and Livingstone, M. S. (2006). A cortical region consisting entirely of face-selective cells. *Science* 311, 670–674.

Van Essen, D. C. (2005). Corticocortical and thalamocortical information flow in the primate visual system. *Prog. Brain Res.* 149, 173–183.

Velayos, J. L., Jimenez-Castellanos, J. Jr., and Reinoso-Suarez, F. (1989). Topographical organization of the projections from the reticular thalamic nucleus to the intralaminar and medial thalamic nuclei in the cat. *J. Comp. Neurol.* 279, 457–469.

Verzeano, M., Lindsley, D. B., and Magoun, H. W. (1953). Nature of recruiting response. *J. Neurophysiol.* 16, 183–195.

Vogt, B. A., Pandya, D. N., and Rosene, D. L. (1987). Cingulate cortex of the rhesus monkey: I. Cytoarchitecture and thalamic afferents. *J. Comp. Neurol.* 262, 256–270.

von Bonin, G., and Bailey, P. (1947). *The Neocortex of Macaca mulatta.* Urbana: The University of Illinois Press.

von Economo, C. (1929). *The Cytoarchitectonics of the Human Cerebral Cortex.* London: Oxford University Press.

Voogd, J. (2003). The human cerebellum. *J. Chem. Neuroanat.* 26, 243–252.

Voytko, M. L., Kitt, C. A., and Price, D. L. (1992). Cholinergic immunoreactive fibers in monkey anterior temporal cortex. *Cereb. Cortex* 2, 48–55.

Walker, A. (1940). A cytoarchitectural study of the prefrontal area of the macaque monkey. *J. Comp. Neurol.* 73, 59–86.

Walker, F. O. (2007). Huntington's disease. *Lancet* 369, 218–228.

Watakabe, A., Ichinohe, N., Ohsawa, S., Hashikawa, T., Komatsu, Y., Rockland, K. S., and Yamamori, T. (2007). Comparative analysis of layer-specific genes in mammalian neocortex. *Cereb. Cortex* 17, 1918–1933.

Witter, M., Groenewegen, H., Silva, F. L. D., and Lohman, A. (1989). Functional organization of the extrinsic and intrinsic circuitry of the parahippocampal region. *Prog. Neurobiol.* 33, 161–253.

Wolf, U., Rapoport, M. J., and Schweizer, T. A. (2009). Evaluating the affective component of the cerebellar cognitive affective syndrome. *J. Neuropsychiatry Clin. Neurosci.* 21, 245–253.

Yeterian, E. H., and Pandya, D. N. (1994). Laminar origin of striatal and thalamic projections of the prefrontal cortex in rhesus monkeys. *Exp. Brain Res.* 99, 383–398.

Yoshimura, Y., Dantzker, J. L., and Callaway, E. M. (2005). Excitatory cortical neurons form fine-scale functional networks. *Nature* 433, 868–873.

Zaborszky, L., Wouterlood, F., and Lanciego, J. (2006). *Neuroanatomical Tract-Tracing 3: Molecules, Neurons, and Systems.* New York, NY: Springer.

Zaitsev, A. V., Gonzalez-Burgos, G., Povysheva, N. V., Kroner, S., Lewis, D. A., and Krimer, L. S. (2005). Localization of calcium-binding proteins in physiologically and morphologically characterized interneurons of monkey dorsolateral prefrontal cortex. *Cereb. Cortex* 15, 1178–1186.

Zaitsev, A. V., Povysheva, N. V., Gonzalez-Burgos, G., Rotaru, D., Fish, K. N., Krimer, L. S., and Lewis, D. A. (2009). Interneuron diversity in layers 2-3 of monkey prefrontal cortex. *Cereb. Cortex* 19, 1597–1615.

Zhou, F. W., Jin, Y., Matta, S. G., Xu, M., and Zhou, F. M. (2009). An ultra-short dopamine pathway regulates basal ganglia output. *J. Neurosci.* 29, 10424–10435.

Zikopoulos, B., and Barbas, H. (2006). Prefrontal projections to the thalamic reticular nucleus form a unique circuit for attentional mechanisms. *J. Neurosci.* 26, 7348–7361.

Conflict of Interest Statement: The authors declare that the research was conducted in the absence of any commercial or financial relationships that could be construed as a potential conflict of interest.

Received: 02 August 2011; accepted: 01 December 2011; published online: 20 December 2011.

*Citation: Solari SVH and Stoner R (2011) Cognitive consilience: primate non-primary neuroanatomical circuits underlying cognition. Front. Neuroanat. **5**:65. doi: 10.3389/fnana.2011.00065*